frontiers | Research Topics

Exploring volatile organic compounds in fruits and flowers: aroma, biosynthesis, and ecological impact

Edited by
Robin Joshi, Vikas Dadwal and Mariam Gaid

Coordinated by
Deepak Kumar Jha

Published in
Frontiers in Plant Science

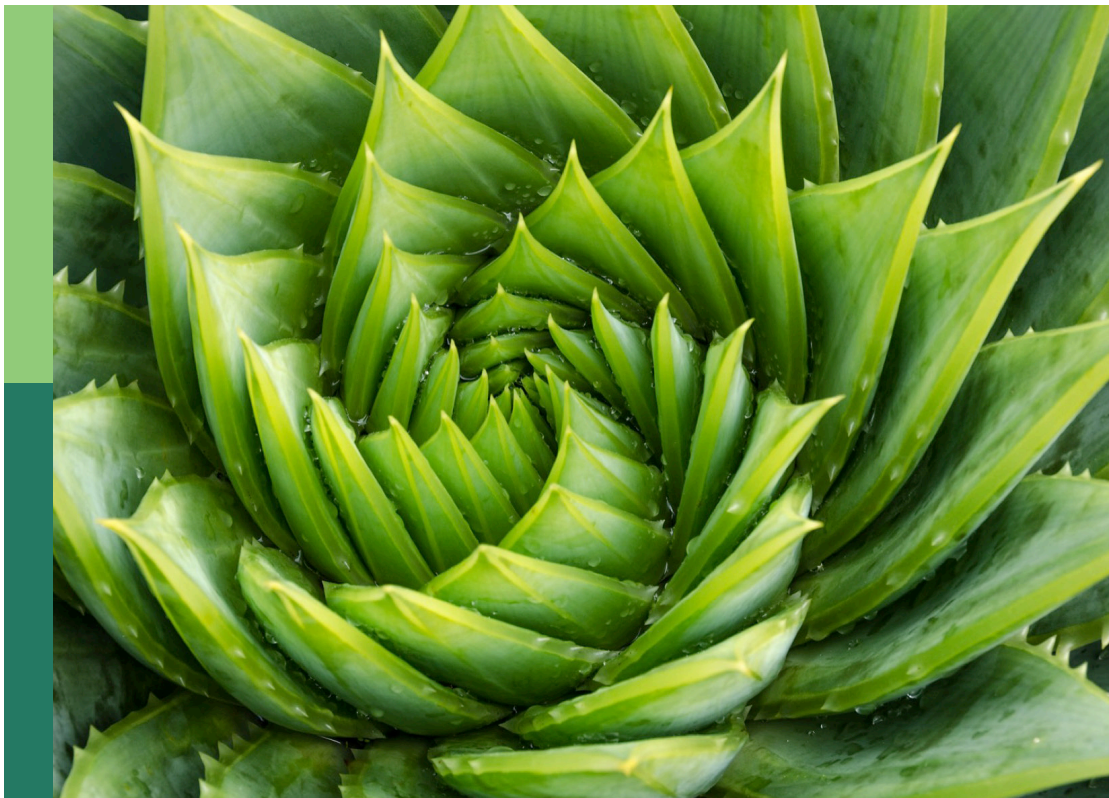

ISSN 1664-8714
ISBN 978-2-8325-6984-9
DOI 10.3389/978-2-8325-6984-9

Generative AI statement
Any alternative text (Alt text) provided alongside figures in the articles in this ebook has been generated by Frontiers with the support of artificial intelligence and reasonable efforts have been made to ensure accuracy, including review by the authors wherever possible. If you identify any issues, please contact us.

About Frontiers

Frontiers is more than just an open access publisher of scholarly articles: it is a pioneering approach to the world of academia, radically improving the way scholarly research is managed. The grand vision of Frontiers is a world where all people have an equal opportunity to seek, share and generate knowledge. Frontiers provides immediate and permanent online open access to all its publications, but this alone is not enough to realize our grand goals.

Frontiers journal series

The Frontiers journal series is a multi-tier and interdisciplinary set of open-access, online journals, promising a paradigm shift from the current review, selection and dissemination processes in academic publishing. All Frontiers journals are driven by researchers for researchers; therefore, they constitute a service to the scholarly community. At the same time, the *Frontiers journal series* operates on a revolutionary invention, the tiered publishing system, initially addressing specific communities of scholars, and gradually climbing up to broader public understanding, thus serving the interests of the lay society, too.

Dedication to quality

Each Frontiers article is a landmark of the highest quality, thanks to genuinely collaborative interactions between authors and review editors, who include some of the world's best academicians. Research must be certified by peers before entering a stream of knowledge that may eventually reach the public - and shape society; therefore, Frontiers only applies the most rigorous and unbiased reviews. Frontiers revolutionizes research publishing by freely delivering the most outstanding research, evaluated with no bias from both the academic and social point of view. By applying the most advanced information technologies, Frontiers is catapulting scholarly publishing into a new generation.

What are Frontiers Research Topics?

Frontiers Research Topics are very popular trademarks of the *Frontiers journals series*: they are collections of at least ten articles, all centered on a particular subject. With their unique mix of varied contributions from Original Research to Review Articles, Frontiers Research Topics unify the most influential researchers, the latest key findings and historical advances in a hot research area.

Find out more on how to host your own Frontiers Research Topic or contribute to one as an author by contacting the Frontiers editorial office: frontiersin.org/about/contact

Exploring volatile organic compounds in fruits and flowers: aroma, biosynthesis, and ecological impact

Topic editors
Robin Joshi — University of Pennsylvania, United States
Vikas Dadwal — Texas A and M University, United States
Mariam Gaid — Independent researcher, Braunschweig, Germany

Topic coordinator
Deepak Kumar Jha — Texas A and M University, United States

Citation
Joshi, R., Dadwal, V., Gaid, M., Jha, D. K., eds. (2025). *Exploring volatile organic compounds in fruits and flowers: aroma, biosynthesis, and ecological impact*. Lausanne: Frontiers Media SA. doi: 10.3389/978-2-8325-6984-9

Table of contents

frontiers | Frontiers in Plant Science

TYPE Editorial
PUBLISHED 26 September 2025
DOI 10.3389/fpls.2025.1701678

OPEN ACCESS

EDITED AND REVIEWED BY
Laigeng Li,
Chinese Academy of Sciences (CAS), China

*CORRESPONDENCE
Mariam Gaid
m.gaid@gmx.de
Robin Joshi
robinsjoshi@gmail.com;
robin.joshi@pennmedicine.upenn.edu

RECEIVED 08 September 2025
ACCEPTED 16 September 2025
PUBLISHED 26 September 2025

CITATION
Dadwal V, Jha DK, Gaid M and Joshi R (2025) Editorial: Exploring volatile organic compounds in fruits and flowers: aroma, biosynthesis, and ecological impact. *Front. Plant Sci.* 16:1701678. doi: 10.3389/fpls.2025.1701678

Editorial: Exploring volatile organic compounds in fruits and flowers: aroma, biosynthesis, and ecological impact

Vikas Dadwal[1], Deepak Kumar Jha[1], Mariam Gaid[2*] and Robin Joshi[3*]

[1]Vegetable and Fruit Improvement Center, United States Department of Agriculture (USDA) National Center of Excellence, Department of Horticultural Sciences, Texas A&M University, College Station, TX, United States, [2]Institute of Microbiology, University Greifswald, Greifswald, Germany, [3]Perelman School of Medicine, Institute of Translation Medicine for Therapeutics (ITMAT), University of Pennsylvania, Philadelphia, PA, United States

KEYWORDS

phenylpropanoids, fatty acid derivatives, metabolomics, volatilomics, transcriptomics, volatile organic compounds (VOCs), aroma

Editorial on the Research Topic
Exploring volatile organic compounds in fruits and flowers: aroma, biosynthesis, and ecological impact

Volatile organic compounds (VOCs) emitted by fruits and flowers play an important role in plant environment interaction through their distinctive aromas and signaling properties. These compounds, primarily terpenoids, phenylpropanoids, and fatty acid derivatives, are synthesized *via* complex metabolic pathways influenced by genetic, developmental, and environmental factors in fruits and flowers. Additionally, VOCs contribute significantly to plant reproductive success by attracting pollinators and seed dispersers, while also serving defensive roles against herbivores and pathogens. Metabolomics and other omics techniques offer a comprehensive approach to profiling and quantifying VOCs in plants and fruits, enabling deeper insights into their biosynthesis, regulation, and ecological functions. Understanding these VOCs not only supplements our understanding of plant biology but also has applications in agriculture, food science, and the fragrance industries. Therefore, invitations were sent to outstanding experts in this field to contribute their manuscripts to this Research Topic. An effort was undertaken to investigate metabolites, their diversity, and underlying regulatory mechanisms through an integrated omics approach. Finally, a total of 94 authors contributed, and 12 research articles were published in the present Research Topic.

Consumers' perception of longan fruit is heavily influenced by aroma, a key factor affecting flavor quality. In a recent study by Hu et al., a high-density linkage map was created through SNP genotyping, followed by QTL mapping to identify genes responsible for aromatic traits. Using the constructed high-density Bin map and validation through collinearity analysis, fifty-six QTLs were identified for nine aroma-related characteristics, including (E)-2-hexenal, ethyl acetate, ethyl butyrate, ethyl crotonate, and total ester content. Further analysis revealed that six candidate genes control ester biosynthesis.

This study offers valuable insights for breeders working on high-quality aromatic fruit crops. Besides genetic makeup, the fruit metabolome also plays a significant role in its flavor profile. A recent study by Li et al. demonstrated this through comprehensive metabolite analysis of kumquat fruits. Sucrose and limonin are key factors contributing to sweetness and bitterness, respectively. The red color of the fruit peel is linked to the upregulation of anthocyanins and carotenoids. Screening 1719 metabolites showed that the peel is rich in flavonoids, while the seeds contain bioactive triterpenoids like limonin. Considering health benefits, a study by Sonigra and Meena found that essential oils (EOs) from *Cymbopogon martinii* (Roxb.) Wats. have both aromatic and bioactive properties. Notably, EOs were analyzed at three developmental stages through hydro-distillation combined with GC-MS profiling. The analysis identified 59 compounds, with the highest amounts during the reproductive stage with an increased oil yield. This significant yield further demonstrated antibacterial and antifungal activities. Additionally, the post-reproductive stage showed higher antioxidant activity. This study effectively highlights the importance of harvesting time for maximizing the bioactive EO yield, which is crucial for future therapeutic and industrial applications.

In addition to being primary contributors to aroma, volatiles, particularly EOs, play key roles in plant defense and exhibit antimicrobial, antioxidant, antifungal, and insecticidal properties, making them valuable in food preservation, medicine, and pest management. Peng et al. explored the volatile diversity at different developmental stages and their potential antimicrobial roles. in *Zanthoxylum armatum*, an aromatic Rutaceae shrub, especially rich in bioactive EOs concentrated in its pericarp, showed strong antibacterial, antioxidant, and anti-inflammatory effects. The systematic analysis of *Z. armatum* fruits across seven growth stages and the resulting volatile fingerprint mapping, revealed stage-specific EO profiles dominated by linalool, D-limonene, and sabinene. Early stages accumulated simple monoterpenes, whereas alcohols and esters increased with maturation, with peak abundance in July–August, identified as the optimal harvest period. The bioassays of these EOs confirmed strong insect-repellent effects against *Tribolium castaneum* (without lethal toxicity) and significant antifungal activity against *Corynespora cassiicola*, particularly at the mid-July (mature) stage. Activities appeared driven by synergistic compound interactions rather than single constituents. Peng et al. findings provide the first systematic temporal profile of *Z. armatum* EOs, linking harvest stage to bioactivity and offering a basis for developing eco-friendly insect-repellent and antifungal agents.

Jujube flowers, abundant in diverse volatile compounds, enhance sensory appeal and stand out among aromatic plants. Ren et al. exhaustively performed sensory evaluation in jujube flowers across developmental stages and varieties, and compared with other aromatic plant flowers. A total of 65 VOCs were identified, and aroma fingerprinting revealed 24 distinct aromas, 14 of which intensified from bud stage to full bloom. Varieties such as Fuxiang, Dongzao, and Xingguang exhibited significantly stronger aromas at the flowering stage than others. Sensory evaluation further indicated a male preference for the fragrance of jujube flowers. Their finding, also highlighted the richness in volatile diversity and abundance, has potential for spice development, and could be a basis for future research on floral-derived spices.

While the effects of genetics, environment, and physiological status on crop volatile composition have been extensively studied, the contribution of microbial communities to shaping these volatile profiles has received far less recognition. Jia et al. integrated untargeted metabolomics and metagenomics to investigate the role of plant–microbe interactions in shaping the aroma profile of flue-cured tobacco leaves. Comparative analyses between light aromatic tobacco (LAT) and strong aromatic tobacco (SAT) detailed that LAT contained significantly higher sugar metabolites (e.g., sucrose, fructose, maltose), while SAT was enriched in acids and amino acids (e.g., xylonic acid, tartaric acid, L-phenylalanine). Metagenomic analyses demonstrated that LAT when dominated by *Methylorubrum*, *Pseudomonas*, and *Pseudokineococcus*, promoted sugar accumulation, whereas SAT when enriched in *Methylobacterium* and *Sphingomonas*, enhanced acid and amino acid metabolism but inhibited sugar accumulation. Redundancy analysis highlighted the bidirectional regulatory role of *Pseudokineococcus*, emphasizing complex microbe–metabolite interactions in shaping aroma profiles. It was worth noting that the conserved microbial functional traits modulate host metabolism, offering physiological guidance for tobacco aroma regulation and broader strategies for microbiome-mediated quality improvement in crops.

Recent advances highlight the complex metabolism and genetic regulation underlying volatile-mediated floral and fruit traits in grapes and pear. Darwish et al. provided the first comprehensive volatilomic characterization of *Muscadinia rotundifolia* flowers, identifying 150 volatiles across 16 genotypes. Multivariate analyses distinguished female and perfect flowers by 11 diagnostic terpenes. Perfect flowers emitted higher terpene quantities, aligning with greater pollinator attraction, while female flowers suffered from lower volatile emission and floral abnormalities, explaining reduced fruit set unless assisted by controlled pollination strategies. Similarly, Wu et al. characterized aroma diversity in six grape cultivars with contrasting aroma types. Muscat cultivars accumulated monoterpenes, the strawberry-type was defined by ester biosynthesis, and neutral types enriched C_6/C_9 compounds, preceded by the high expression of responsible genes in each case. Co-expression network analysis revealed distinct modules related to alcohols, carbonyls, fatty acids, and monoterpenes. Within the same context, aroma differentiation in pear was investigated by Wang et al. by integrating metabolite profiling with transcriptome analysis across three *Pyrus communis* cultivars rich in aroma and three *Pyrus pyrifolia* cultivars known to lack aroma. Among 510 identified volatiles, 16 ester and alcohol compounds were enriched in *Pyrus communis* relative to aroma-deficient *P.*

pyrifolia. The existence of these metabolites was linked to amino acid degradation pathways, where key differences could be attributed to the activity of related genes encoding monoacylglycerol lipase, threonine dehydratase, and acyl-CoA dehydrogenase. Collectively, these studies provide mechanistic insights into aroma and floral volatiles, offering targets for breeding and metabolic engineering to enhance aroma quality, pollination efficiency, and ultimately, crop quality. Wang et al. described the integrated volatile metabolite and transcriptome analyses, which provide insights into the warm aroma formation elicited by methyl jasmonate in carrot roots. The results identified 1,227 volatile organic compounds and 972 differentially accumulated metabolites, along with 4,787 differentially expressed genes. This study enabled an understanding of MeJA-mediated aroma formation in carrots. Qian et al. described the role of volatiles on insect behavior in *Aquilaria sinensis*. A total of 11 volatile compounds with electrophysiological activities were detected. These volatile components can be considered as an alternative to chemical insecticides in pest control. Another investigation by He et al. revealed the mechanism of volatile alterations during fruit development of 'Ehime 38' (*Citrus reticulata*) and its bud mutant. A total of 35 volatile compounds were identified in the pulps of both WT and MT across five developmental stages. Most of the genes in the MEP pathway showed a positive correlation with volatile levels, as determined by transcriptomic and RT-qPCR studies. A detailed metabolomics and transcriptomics study will be valuable for fruit flavor development in citrus.

In conclusion, the Research Topic exhaustively details the critical roles of volatile compounds in shaping the aroma, flavor, and bioactive properties of fruits, flowers, and other plant organs. It also highlights that the aroma profiles are influenced by a complex interplay of genetics, developmental stage, metabolite composition, and plant-microbe interactions, with specific volatiles such as monoterpenes, esters, and alcohols often driving sensory appeal, pollinator attraction, and defense responses. Integrative approach combining metabolomics, transcriptomics, and sensory evaluation revealed stage- and genotype-specific accumulation patterns, identified key biosynthetic genes, and linked volatiles to biological activities such as antimicrobial, antifungal, and insect-repellent effects. The insights in this Research Topic provide a foundation for breeding, metabolic engineering, and the development of eco-friendly plant-based products, ranging from high-quality aromatic fruits and floral spices to natural pest management and therapeutic agents.

Author contributions

VD: Writing – review & editing. DKJ: Writing – review & editing. MG: Writing – review & editing. RJ: Writing – original draft, Writing – review & editing.

Acknowledgments

VD, DKJ, MG, and RJ would like to thank all the contributing authors, reviewers, and editors for our Research Topic: Exploring Volatile Organic Compounds in Fruits and Flowers: Aroma, Biosynthesis, and Ecological Impact.

Conflict of interest

The authors declare that the research was conducted in the absence of any commercial or financial relationships that could be construed as a potential conflict of interest.

The author(s) declared that they were an editorial board member of Frontiers, at the time of submission. This had no impact on the peer review process and the final decision.

Generative AI statement

The author(s) declare that no Generative AI was used in the creation of this manuscript.

Any alternative text (alt text) provided alongside figures in this article has been generated by Frontiers with the support of artificial intelligence and reasonable efforts have been made to ensure accuracy, including review by the authors wherever possible. If you identify any issues, please contact us.

Publisher's note

frontiers | Frontiers in Plant Science

TYPE Original Research
PUBLISHED 26 June 2024
DOI 10.3389/fpls.2024.1430204

OPEN ACCESS

EDITED BY
Xue-Rong Zhou,
Commonwealth Scientific and Industrial Research Organization (CSIRO), Australia

REVIEWED BY
Thomas A. Colquhoun,
University of Florida, United States
Shouchuang Wang,
Hainan University, China

*CORRESPONDENCE
Zhihui Wang
wangzhihui318@sicau.edu.cn

†These authors have contributed equally to this work and share first authorship

RECEIVED 09 May 2024
ACCEPTED 10 June 2024
PUBLISHED 26 June 2024

CITATION
He J, Qin Z, Liu K, Li X, Kou Y, Jin Z, He R, Hong M, Xiong B, Liao L, Sun G, He S, Zhang M, Liang D, Lv X, Wang X and Wang Z (2024) Volatile metabolomics and transcriptomics analyses provide insights into the mechanism of volatile changes during fruit development of 'Ehime 38' (*Citrus reticulata*) and its bud mutant. *Front. Plant Sci.* 15:1430204. doi: 10.3389/fpls.2024.1430204

Volatile metabolomics and transcriptomics analyses provide insights into the mechanism of volatile changes during fruit development of 'Ehime 38' (*Citrus reticulata*) and its bud mutant

Jiaxian He[1†], Zeyu Qin[1†], Kexin Liu[1†], Xiangyi Li[1], Yiming Kou[1], Zhenghua Jin[1], Ruiyuan He[1], Min Hong[2], Bo Xiong[1], Ling Liao[1], Guochao Sun[1], Siya He[1], Mingfei Zhang[1], Dong Liang[1], Xiulan Lv[1], Xun Wang[1] and Zhihui Wang[1*]

[1]College of Horticulture, Sichuan Agricultural University, Chengdu, China, [2]Citrus Research Institute, Southwest University, Chongqing, China

Volatile compounds are important determinants affecting fruit flavor. Previous study has identified a bud mutant of 'Ehime 38' (*Citrus reticulata*) with different volatile profile. However, the volatile changes between WT and MT during fruit development and underlying mechanism remain elusive. In this study, a total of 35 volatile compounds were identified in the pulps of WT and MT at five developmental stages. Both varieties accumulated similar and the highest levels of volatiles at stage S1, and showed a downward trend as the fruit develops. However, the total volatile contents in the pulps of MT were 1.4–2.5 folds higher than those in WT at stages S2-S5, which was mainly due to the increase in the content of d-limonene. Transcriptomic and RT-qPCR analysis revealed that most genes in MEP pathway were positively correlated with the volatile contents, of which *DXS1* might mainly contribute to the elevated volatiles accumulation in MT by increasing the flux into the MEP pathway. Moreover, temporal expression analysis indicated that these MEP pathway genes functioned at different developmental stages. This study provided comprehensive volatile metabolomics and transcriptomics characterizations of a citrus mutant during fruit development, which is valuable for fruit flavor improvement in citrus.

KEYWORDS

citrus, bud mutant, volatile compounds, fruit development, MEP pathway

1 Introduction

Citrus is one of the most economically valuable fruit crops worldwide and is well-loved by consumers because of its unique flavor and high nutritive value (González-Molina et al., 2010; Wang et al., 2022). Aroma is an important indicator of fruit flavor, and it is an attractive and distinguishing characteristic of citrus fruits (Pan X. et al., 2023; Zhang et al., 2023). More than 300 volatile compounds have been characterized in citrus, mainly including terpenoids, esters, alcohols, aldehydes, ketones, and acids (Perez-Cacho and Rouseff, 2008; Zhang et al., 2017). These volatile compounds not only facilitate plants to resist pathogen and herbivorous insects, but also play important roles in human health (Sharma et al., 2017; Anandakumar et al., 2021; Zhou et al., 2022).

Different composition and concentration of volatiles contribute to the distinctive aroma of fruits among citrus varieties. Monoterpenes are the most abundant volatiles in most citrus fruits, of which d-limonene, a component with a pleasant lemon scent which is widely used as an aroma additive in perfumes, cosmetics and foods, constitutes 60%-95% of the total volatiles content (Lota et al., 2001; Gonzalez-Mas et al., 2011; Zhang et al., 2017; Anandakumar et al., 2021). However, sesquiterpenes are dominantly (~55%) accumulated in the peels of *C. ichangensis* 'Huaihua', and trans-β-ocimene is the major monoterpene (Zhang et al., 2017). Valencene is a sesquiterpene with citrus-like scent that is mainly identified in sweet orange (Shen et al., 2016; Zhang et al., 2017), while citral is highly accumulated in lemon compared with sweet orange and pummelo, contributing to a strong lemon fragrance (Liu et al., 2012). In addition, the volatile profile is also significantly affected by developmental factors. It has been found that the content of limonene in orange peels shows a dramatic increase from approximately 60 days post anthesis (DPA) to 150 DPA and remains high until fruit fully ripens (Rodríguez et al., 2011). In the juices of mandarins, most monoterpenes tend to decrease as fruit matures, while aldehydes, alcohols, and esters increase (Hijaz et al., 2020).

As the most prominent volatiles in citrus, terpenoids are synthesized through two independent pathways: the MEP (2-C-methyl-D-erythritol-4-phosphate) pathway in plastids and the MVA (mevalonic acid) pathway in cytosol (Nagegowda, 2010; Liao et al., 2016; Volke et al., 2019). The MEP pathway is initiated with the condensation of pyruvate and G3P (glyceraldehyde-3-phosphate) catalyzed by DXS (1-Deoxy-D-xylulose-5-phosphate synthase) enzyme, and generates C5 units IPP (isopentenyl diphosphate) and DMAPP (dimethylallyl diphosphate) for the biosynthesis of GPP (geranyl pyrophosphate). The MVA pathway is started by enzyme AACT (AcAc-CoA thiolase), providing these two same C5 units for the synthesis of FPP (farnesyl pyrophosphate). Terpene synthases (TPSs) are responsible for the conversion of precursors GPP from MEP pathway and FPP from MVA pathway into monoterpenes (C10) and sesquiterpenes (C15), respectively. There are 55 predicted functional TPSs in sweet orange genome (Alquézar et al., 2017), and the functions of few genes have been characterized. Transient overexpression assays showed that *CitTPS16* catalyzes the synthesis of E-geraniol, contributing to flavor of sweet orange (Li X. et al., 2017). *CsTPS21* encodes a β-ocimene synthase responding to methyl jasmonic acid (MeJA) treatment, and overexpressing *CsTPS21* upregulates JA biosynthetic genes expression and increases the resistance to Asian citrus psyllid (Bin et al., 2023). However, little is known about the function of these genes and their associated pathways in aroma formation during citrus fruits development.

Bud mutations generate many new citrus cultivars, providing excellent materials for understanding the molecular mechanism underlying key traits formation. In the stay-green mutant 'Green Ougan', CrMYB68 retards the transformation of α-carotene and β-carotene via repressing the expressions of *CrBCH2* and *CrNCED5* (Zhu et al., 2017). The 'Citrine Shiranui' mandarin is a yellowish bud mutant with low levels of phytoene, β-cryptoxanthin, and 9-*cis*-violaxanthin, which may be due to the low expression levels of *PSY* and *ZDS* (Wang X. et al., 2023). The mutations of *STAYGREEN* (*SGR*), which simultaneously functions in carotenoid and chlorophyll accumulation, result in the brown appearance of navel orange mutant (Zhu et al., 2021). Pollen abortion is a vital agronomic trait for breeding engineering, and researchers have found that excessive starch and sugar hydrolysis caused by the demethylation of carbohydrate genes is correlated with the pollen development in a seedless citrus mutant (Ye et al., 2020). In a wax-deficient 'Newhall' orange mutant, the enhanced resistance to fungal infections is attributed to the increased biosynthesis of JA (He et al., 2018).

Metabolites are the end products of cellular processes in response to internal and external factors, and various advanced techniques have been developed for metabolomics profiling in horticultural fruits, including tomato (Zhu et al., 2018; Yang et al., 2024), sand pear (Shi et al., 2021), and apple (Dadwal et al., 2023). In citrus, high-performance liquid chromatography-mass spectrometry (HPLC-MS)-based widely targeted and non-targeted metabolomics platforms are employed to detect the primary and secondary metabolites (sugar, amino acid, flavonoid and other bioactive components) in different fruit tissues and different species (Wang et al., 2016; Dadwal et al., 2022; Wang S. et al., 2023), and gas chromatography-mass spectrometry (GC-MS) combined with headspace solid-phase micro-extraction (HS-SPME) is convenient and effective for aroma analysis, especially in fruit pulps (Hou et al., 2020; Li et al., 2022; Hu et al., 2024).

Our previous study has identified a yellow mutant of 'Ehime 38' (*Citrus reticulata*) with a richer aroma in pulps relative to the wild type (Wang T. et al., 2023). However, the accumulation patterns of volatile compounds during fruit development in both varieties and molecular mechanism remain elusive. In the present study, the composition and content of volatiles in the pulps of WT and MT across five developmental stages were detected by HS-SPME-GC-MS, and transcriptome analysis was used to understand the underlying mechanism of volatile variations between WT and MT. This study will provide new insights into the molecular mechanism of volatiles accumulation in citrus fruits.

2 Materials and methods

2.1 Plant materials

'Ehime 38' (*Citrus reticulata*) and its bud mutant, which are referred to as 'WT' and 'MT' respectively, were grafted onto

different branches of the same rootstock 'red tangerine' (*Citrus reticulata*) in an orchard in Meishan city, Sichuan Province, China. Different developing fruits of WT and MT at 60, 90, 140, 170 and 210 days after full bloom (DAFB) were harvested, and fruit pulps were immediately separated and frozen in liquid nitrogen. Three biological replicates were performed for each sample, and one biological replicate contained three to ten fruits without mechanical injury and disease. All frozen pulps were stored at −80°C for further analysis.

2.2 Volatile compounds extraction and quantification

The extraction of volatiles was performed using solid phase micro extraction (SPME) according to previous study (Shen et al., 2016) with minor modifications. Frozen pulps were ground in liquid nitrogen and 0.5 g of powder was immediately transferred into a 20 mL headspace vial. The sample was incubated with 5 mL saturated sodium chloride solution and 50 μL 1-Hexanol (0.1%, v/v, used as an internal standard) at 42°C for 30 min. Then the SPME fiber coated with 50/30 μm divinylbenzene/carboxen/polydimethylsiloxane (Supelco, USA) was exposed to the headspace gases to extract the volatile compounds at 42°C for 30 min.

Volatile analysis was carried out on a gas chromatography (7890A, Agilent Technologies, Santa Clara) - mass spectrometry (Agilent 5975C) equipped with an HP-5MS column (30 m × 0.25 mm × 0.25 um, J&W Scientific, Folsom, CA, USA). The instrumental parameters were as follows: desorption in splitless mode at 250 °C for 5 min; oven temperature started at 40°C for 3 min, and gradually increased to 70°C at a rate of 3°C min^{-1}, to 130°C at 1°C min^{-1}, eventually to 230°C at 15°C min^{-1} and hod for 10 min; ion source, 230°C; electron energy, 70 eV; helium at 1.0 mL min^{-1}, and mass scanning range 35–500 m/z. Data were processed by the enhanced MSD ChemStation software (Agilent MSD Productivity Chemstation). Volatile identification was performed using the NIST/EPA/NIH Mass Spectrometry Library (NIST-14, USA) combing with the Retention Indes (RI). A C8-C20 n-alkane mixed standard was analyzed under the same GC-MS condition to calculate the RI of volatiles. Volatile compounds were relatively quantified using the peak area of the internal standard (1-hexanol).

2.3 RNA isolation and transcriptomic sequencing

Total RNA of all samples was extracted according to the instructions of RNAprep Pure Plant Kit (Tiangen, China). Of them, developing fruits of WT and MT at 90 and 140 DAFB were chosen for RNA-seq analysis with three biological replicates and six fruits per replicate. The RNA-seq libraries were constructed using Hieff NGS Ultima Dual-mode mRNA Library Prep Kit for Illumina (Yeasen Biotechnology (Shanghai) Co., Ltd.), and sequenced on an Illumina NovaSeq platform at Biomarker Technologies (Beijing, China). After removing the low-quality reads and adapter sequence reads, clean reads were mapped to sweet orange reference genome (http://citrus.hzau.edu.cn/index.php) using Hisat2 tools soft (Kim et al., 2019). The FPKM (fragments per kilobase of transcript per million mapped reads) was used to represent genes expression level. Differentially expressed genes (DEGs) of pairwise samples were identified using the DESeq2 with a threshold of p value < 0.05 and | log2 (fold change) | ≥ 1.

2.4 Weighted gene co-expression network analysis

The R package WGCNA (v1.71) was used to analyze the co-expression networks of gene expressions and volatiles contents. The co-expression modules were constructed using an unsigned type of topological overlap matrix (TOM) with the soft thresholding power of 6, branch merge cut height of 0.15 and minimal module size of 100.

2.5 Quantitative real-time polymerase chain reaction analysis

The pulps of WT and MT at five developmental stages (60, 90, 140, 170, and 210 DAF) were used to extract total RNA. Each sample included three biological replicates. The extracted RNA (1 mg) was reacted with HiScript IV RT SuperMix (Vazyme Biotech) to synthesize single-strand cDNA for further analysis. Real-time PCR reactions were performed on a 96-well plate using the 2 × SYBR Premix EsTaq (Mei5 Biotechnology Co. Ltd, China). The temperature program in a CFX96 instrument (Hercules, CA, USA) was as follows: 95°C for 2 min, 40 cycles at 95°C for 10 s, and 55°C for 30 s. The $2^{-\Delta\Delta Ct}$ method was adopted to calculate gene relative expression level and citrus *actin* gene (ID: Cs1g_pb000860) was used for reference. The gene-specific primers were provided in Supplementary Table S1.

2.6 Statistical analysis

Orthogonal partial least squares-discriminant analysis (OPLS-DA) was used to identify differentially accumulated volatiles (DAVs) between WT and MT during fruit development. Principal component analysis (PCA) was performed by R package factoextra. The significant difference between two samples was calculated using the two-tailed paired t-test (*, $p < 0.05$; **, $p < 0.01$).

3 Results

3.1 Identification of volatiles in the pulps of WT and MT during fruit development

To comprehensively investigate the volatile changes between WT and MT, different developing fruits were subjected to aroma profile analysis. Although MT was clearly distinguished from the orange-colored WT at ripening stages by its yellowish flavedo

(Wang T. et al., 2023), there was no visible difference in pulp color between the two varieties during fruit development (Figure 1A). HS-SPME-GC-MS was adopted to evaluate the differences in volatiles composition and content of pulps between WT and MT. A total of 35 volatiles, including 12 monoterpenes, 7 aldehydes, 5 alcohols, 5 ketones, 3 sesquiterpenes, 2 esters, and 1 other component were detected simultaneously in both varieties (Supplementary Table S2). Principal component analysis (PCA) was performed to compare the volatile profile of WT and MT at different growth stages. The first two components explained 88% of the total variability (PC1 = 55.9% and PC2 = 32.1%). In the score plot, the developing fruits from S1 to S4 stage were clearly separated, while the pulps between stages S4 and S5 showed no significant difference. Notably, MT was obviously differentiated from WT at stages S2 and S3 (Figure 1B).

Similar accumulation patterns of total volatiles were present in the pulps of WT and MT. Both varieties accumulated the highest content of approximately 4000 μg g^{-1} at early stage (S1) and showed a downward trend with fruit development (Figure 1C). In addition, monoterpenes as the most abundant components firstly decreased from 91% to 73% of the total volatiles from stage S1 to S2, and then gradually increased to a maximum of 98% in fully mature fruits (S5) of WT and MT (Figure 1D). It was noteworthy that MT showed a slow decreasing rate of total volatiles, and its content was 1.4 to 2.5 folds higher than WT at S2 to S5 stages (Figure 1C). These results indicated that the volatile profiles dynamically changed during fruit development, and MT showed significant differences in volatile profiles compared to WT.

3.2 Analysis of differentially accumulated volatiles between WT and MT during fruit development

To further reveal the volatiles difference between WT and MT during fruit development, orthogonal partial least-squares discrimination analysis (OPLS-DA) was performed. Among these comparisons, the OPLS-DA models of three groups (MT_S1 *vs* WT_S1, MT_S2 *vs* WT_S2 and MT_S3 *vs* WT_S3) generated values above 0.75 for both R2 and Q2, and their permutation test illustrated that the Y-permuted Q2 values were lower than the original Q2 points and that the Q2 regression line had a negative intercept (Supplementary Figure S1), indicating MT was clearly distinguished from WT at the early (S1 stage) and middle stages (S2 and S3 stages) of fruit development. Based on the thresholds of variable importance in project (VIP) > 1, p value < 0.05, and fold change (FC) ≥ 2 or ≤ 0.5, a total of 28 differentially accumulated volatiles (DAVs) were screened (Supplementary Table S3). These DAVs were grouped into three clusters by Mfuzz according to their accumulation trends in WT (Figure 2A). Meanwhile, the volatiles in developing MT fruits were normalized and present in accordance with the same clusters in WT (Figure 2B). The results indicated that some DAVs exhibited different accumulation trends between WT and MT during fruit development.

The relative change of DAVs between WT and MT was visualized by heatmaps (Figure 2C), which displayed the corresponding volatiles in the three clusters. Almost all DAVs in cluster 1, except for α-pinene, showed the highest content at stage

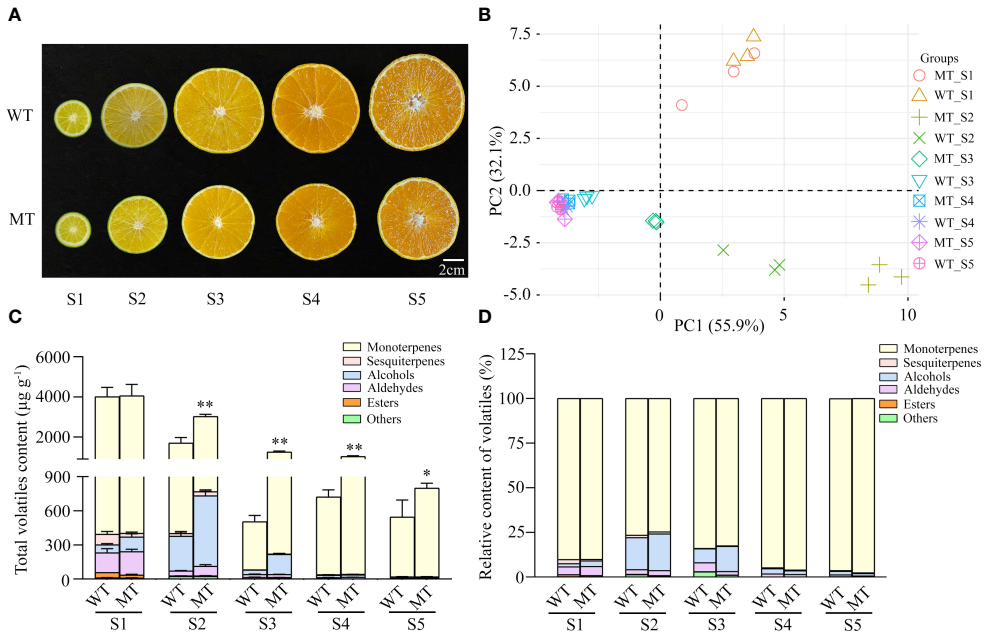

FIGURE 1
Phenotypes and total volatiles content in developing fruits of 'Ehime 38' (WT) and its bud mutant (MT). **(A)** Images of WT and MT at various developmental stages. Five stages from S1 to S5 refer to 60, 90, 140, 170, and 210 days after full bloom (DAFB), respectively. Bars = 2 cm. **(B)** PCA score of volatile profiles in the pulps of WT and MT during fruit development. **(C)** Total volatiles content in the pulps of WT and MT during fruit development. **(D)** Relative content of volatiles in the pulps of WT and MT during fruit development. Data were obtained from three biological replicates. Asterisks indicate statistically significant differences (two-tailed paired t-test, **p < 0.01; *p < 0.05).

10.3389/fpls.2024.1430204

S2 in both WT and MT. These DAVs mainly accumulated at first two stages in WT, but highly accumulated at first three stages in MT. The contents of 8 DAVs (cis-sabinene, α-terpinene, α-pinene, β-ocimene, γ-terpinene, α-terpineol, cis-dihydrocarvone and citral) were higher in MT compared with WT at stages S2 and S3. Among them, citral was a low abundance monoterpene aldehyde and showed a relatively small change in WT during fruit development. The citral content in MT was 5.8- and 7.2- fold higher than that in WT at stages S2 and S3, respectively (Supplementary Table S3). For cluster 2, all volatiles in WT showed a downward trend as the fruit develops, while α-terpinolene, trans-β-terpineol and (E)-β-famesene increased at first and then decreased in MT. D-limonene was the most abundant volatile, accounting for 61%-87% of the total volatile contents, and its content in MT was higher (1.5–2.4 folds) than that in WT during S2-S5 stages. A similar accumulation trend to d-limonene was found for β-myrcene (the second highest volatile at S1 stage, 3.8%) and 2,4-hexadienal. In contrast to perilla aldehyde, four DAVs (trans-β-terpineol, (E)-β-famesene, neryl acetate and 7-epi-sesquithujene) showed notably lower contents (< 0.6-fold) in MT than those in WT at stage S1 (Figure 2C). Cluster 3 contained two groups: Group 1, consisting of 8 DAVs (linalool, 1,3,8-p-menthatriene, 3-thujanone, p-mentha-2,8-diene-1-ol, terpinen-4-ol, d-carvone, p-mentha-1,8-dien-3-one, piperitenone) mainly accumulated at S2 and/or S3 stages, and their abundance in WT was less in comparison with MT at these two developmental stages; Group 2, consisting of o-cymene and p-cymenene, primarily accumulated at S2, S4 and S5 stages. Among them, linalool amount was only significantly lower to that of d-limonene and comprised 5.3%-13.1% of the total volatiles content at S2 and S3 stages, while o-cymene had the second highest content with 7.0%-18.2% at S4 and S5 stages. In addition, linalool as the richest component among monoterpene alcohols showed greater than 2-fold difference between WT and MT during the early and middle stages of fruit development (Supplementary Table S3).

3.3 Transcriptomic analysis of developing fruit pulps of WT and MT

Given the large difference of volatile profile between WT and MT at stages S2 and S3 (Supplementary Figure S1), transcriptome sequencing analysis was carried on the fruit pulps of the two varieties at these two stages. After removing the low-quality reads and adaptor sequence, a total of 268.7 million clean reads with Q30 scores greater than 91.99% were obtained (Supplementary Table S4). These reads were subsequently mapped to the reference genome of sweet orange (Wang et al., 2021) with the average

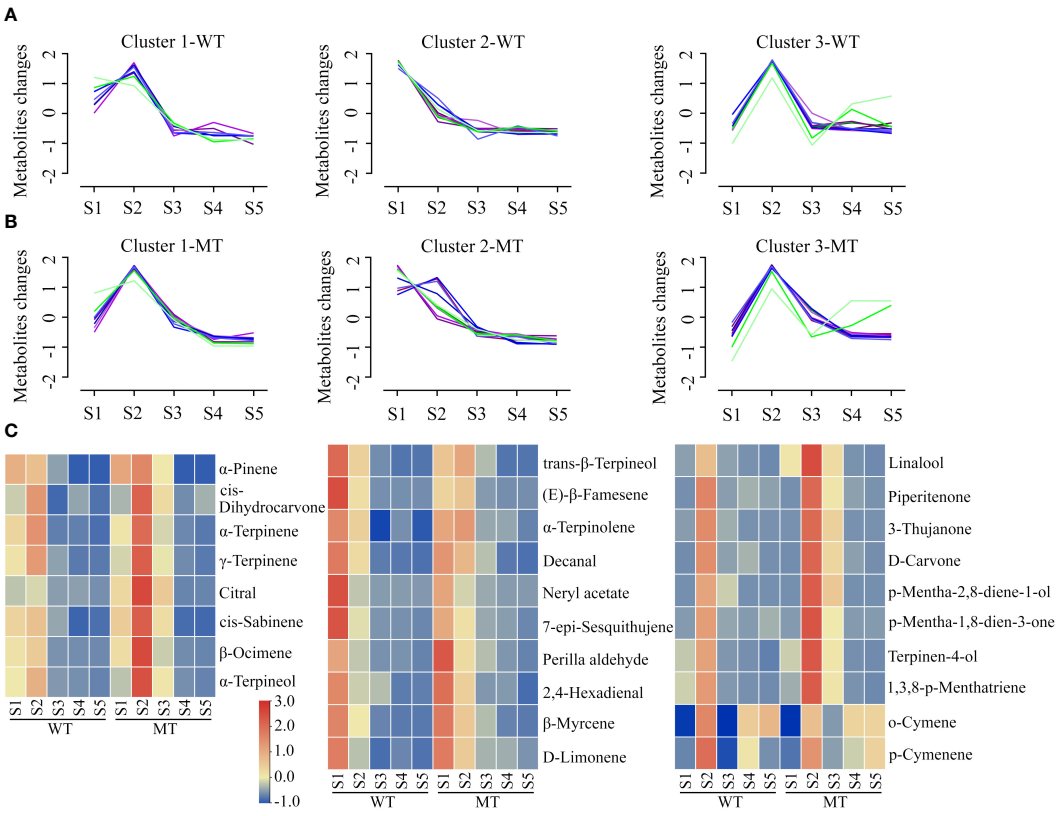

FIGURE 2
Analysis of differentially accumulated volatiles (DAVs) between WT and MT during fruit development. **(A)** Temporal accumulation patterns of DAVs in developing WT fruits. A total of 28 DAVs were grouped into three clusters by Mfuzz R package. **(B)** Accumulation trends of DAVs in developing MT fruits following the same clusters in WT. **(C)** Heatmaps of DAVs contents in the pulps of WT and MT during fruit development. The contents of DAVs were processed by in-row normalization, and a common scale was used for all heatmaps. These three heatmaps corresponded one-to-one with the Mfuzz clusters.

alignment rates of 91.08% (Supplementary Table S5). The correlations of 15 genes expression between qRT-PCR results and transcriptomic data were generally high (Supplementary Figure S2), indicating that the transcriptome sequencing data were reliable. Pairwise comparisons of transcriptomes with 4 groups were performed. The number of differentially expressed genes (DEGs) was largest in MT_S2 *vs* MT_S3 group with 2,371 upregulated and 2,802 downregulated genes, closely followed by 4,453 DEGs (2142 upregulations and 2311 downregulations) observed in WT_S2 *vs* WT_S3 group (Supplementary Figure S4). Only 688 and 699 DEGs were found in MT_S2 *vs* WT_S2 and MT_S3 *vs* WT_S3 comparison groups, respectively (Supplementary Figure S3).

Kyoto Encyclopedia of Genes and Genomes (KEGG) enrichment analysis was performed on these DEGs. In the groups comparing the developing fruits from WT or MT, the DEGs were individually significantly enriched into 52 and 57 KEGG pathways with 36 common pathways. In addition to the fruit growth and development-related metabolism processes, such as 'Amino sugar and nucleotide sugar metabolism', 'Photosynthesis proteins', 'Steroid hormone biosynthesis', and 'Fructose and mannose metabolism', the 36 common pathways also included 'Monoterpenoid biosynthesis', 'Linoleic acid metabolism', and 'Diterpenoid biosynthesis' that were associated with volatile compounds synthesis (Figures 3A, B). In the MT_S2 *vs* WT_S2 comparison group, the most significantly enriched pathways were 'Tyrosine metabolism', 'Cysteine and methionine metabolism' and 'Vitamin B6 metabolism' (Figure 3C). In the MT_S3 *vs* WT_S3 comparison group, the enriched pathways included 'Isoflavonoid biosynthesis', 'Linoleic acid metabolism', 'ABC transporters', 'Diterpenoid biosynthesis', and 'Limonene and pinene degradation' (Figure 3D). These KEGG enrichment results indicated that monoterpenoid metabolism, linoleic acid metabolism and isoflavonoid biosynthesis might play important roles in modulating the volatile profiles of WT and MT during fruit development.

3.4 Identification of genes correlated with volatiles accumulation

To explore the candidate genes involved in volatiles accumulation in WT and MT during fruit development, weighted gene co-expression network analysis (WGCNA) was performed to assess the correlations of genes and DAVs. After quality control, 17,344 genes were grouped into 18 modules (Figure 4A), which were marked with different colors. Among them, the turquoise module had the maximum number of genes (5,716), and the grey60 module had the lowest (114). It was shown that the turquoise and brown modules strongly negatively correlated with most of DAVs, while other three modules (purple, yellow, and blue modules) showed high positive correlations (Figure 4B). Given the similar results of correlation analysis of these DAVs, four representative DAVs (D-limonene, linalool, o-cymene and citral) were selected for screening candidate genes responsible for volatiles accumulation. There were 1,552 genes simultaneously well-correlated with the four volatiles ($|r| > 0.60$, $p < 0.05$) (Figure 4C). KEGG enrichment analysis of these common genes showed that they were mainly annotated in 'Metabolism' and 'Genetic information processing'

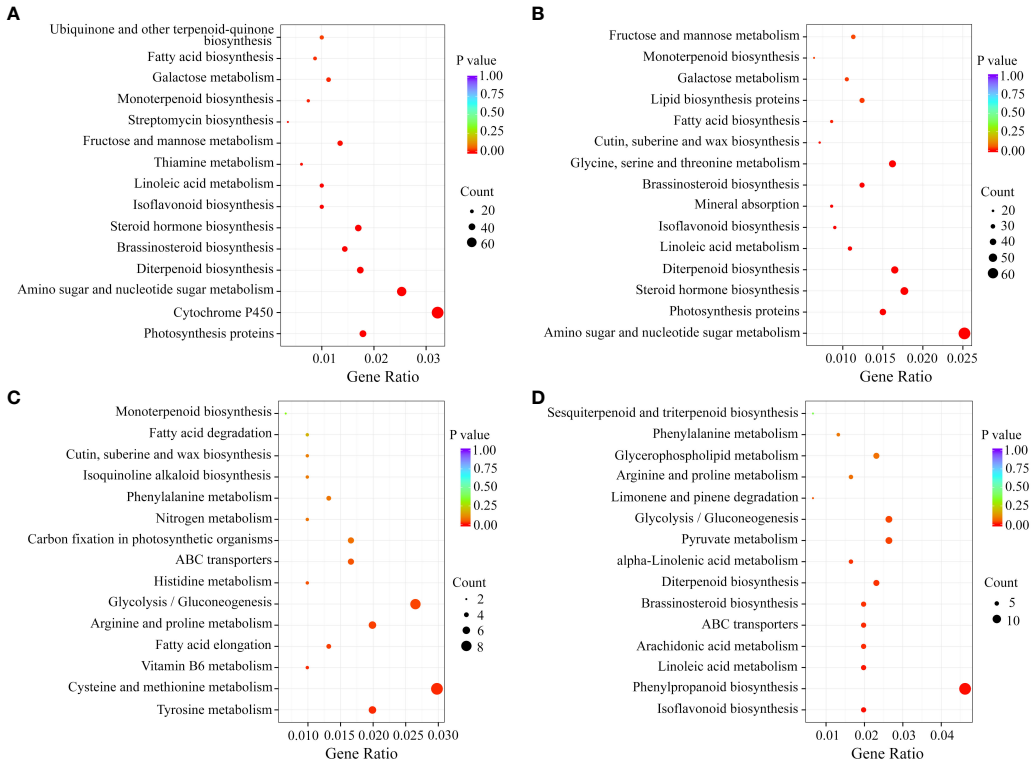

FIGURE 3
KEGG enrichment analysis of the DEGs in each comparison group. KEGG pathways of in comparison of WT_S3 and WT_S3 **(A)**, MT_S3 and MT_S3 **(B)**, MT_S2 and WT_S2 **(C)** and MT_S3 and WT_S3 **(D)**.

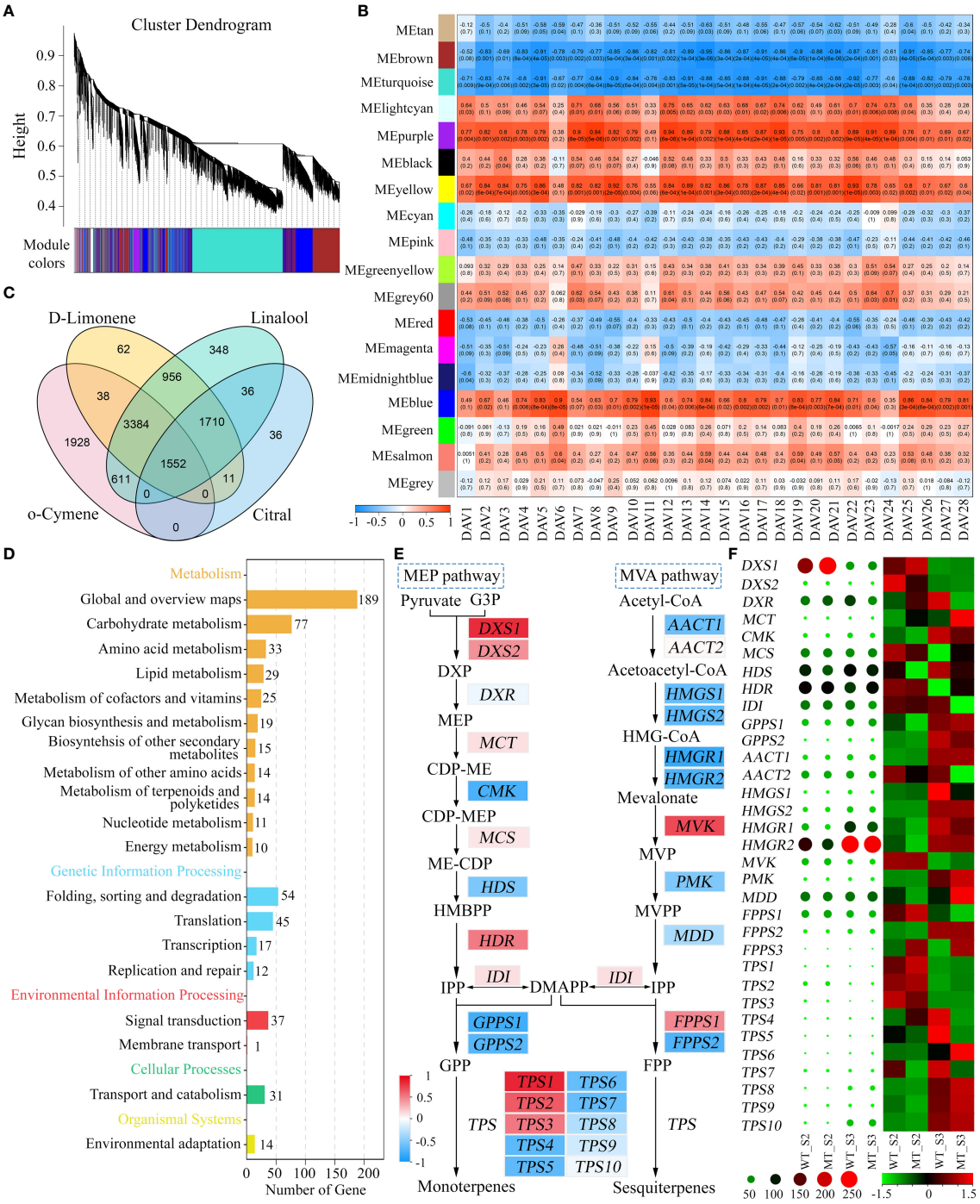

FIGURE 4
Identification of genes associated with DAVs accumulation in WT and MT. **(A)** Hierarchical clustering tree showing co-expression modules identified by WGCNA. **(B)** Correlations between DAVs and modules. The numbers in parentheses represent the significance, and the numbers above represent the correlation coefficient. **(C)** Venn diagram of candidate genes shared by d-limonene, linalool, o-cymene and citral. These genes were screened out from the turquoise, brown, purple, yellow, and blue modules of the four DAVs. **(D)** KEGG enrichment analysis of the common candidate genes. **(E)** Correlations of MEP and MVA pathway genes with d-limonene. D-limonene constituted the largest portion of total volatiles in both varieties, and it was chosen for representative of these DAVs. The background colors of genes represent the strength of the correlation. DXS, 1-deoxy-D-xylulose-5-phosphate synthase; DXR, 1-deoxy-D-xylulose-5-phosphate reductoisomerase; MCT, 2-C-methyl-D-erythritol 4-phosphate cytidylyltransferase; CMK, 4-(cytidine 50-diphospho)-2-C-methyl-D-erythritol kinase; MCS, 2-C-methyl-D-erythritol 2,4- cyclodiphosphate synthase; HDS, **(E)**-4-hydroxy-3-methylbut-2-enyl diphosphate synthase; HDR, **(E)**-4-hydroxy-3-methylbut-2-enyl diphosphate reductase; IDI, isopentenyl diphosphate isomerase; GPPS, geranyl diphosphate synthase; AACT, acetoacetyl-CoA thiolase; HMGS, 3-hydroxy-3-methylglutaryl-CoA synthase; HMGR, 3-hydroxy-3-methylglutaryl-CoA reductase; MVK, mevalonate kinase; PMK, phosphomevalonate kinase; MDD, mevalonate diphosphate decarboxylase; FPPS, farnesyl diphosphate synthase; TPS, terpene synthase. **(F)** Heatmaps of MEP and MVA pathway genes. The heatmap shown with circles was drawn based on the raw FPKM values, and that shown with rectangles was drawn based on the row-scaled FPKM values.

pathways (Figure 4D). Of them, the pathway 'Metabolism of terpenoids and polyketides' was of particular interest, which included *DXS*, *CMK* (*4-(cytidine 50-diphospho)-2-C-methyl-D-erythritol kinase*), *HMGR* (*3-hydroxy-3-methylglutaryl-CoA reductase*), and *TPS* genes involved in MEP pathway and MVA pathway. In addition, these structural genes also showed high correlations (| r | > 0.70) with 21 out of the remaining 24 DAVs (Supplementary Table S6), indicating their importance in volatiles accumulation in WT and MT.

Monoterpenes were the most abundant volatiles in the pulps of WT and MT during fruit development (Figure 1D), which were synthesized from the product (GPP) of MEP pathway (Nagegowda, 2010). Most of MEP pathway genes positively correlated with these DAVs (Supplementary Table S7), of which d-limonene was selected for presentation (Figure 4E). Among them, *DXS* that encoded the first enzyme controlling the flux into MEP pathway exhibited strong positive correlations. In contrast, the genes involved in MVA pathway that produce sesquiterpenes generally showed negative correlations (Figure 4E). Terpene synthases (TPS) catalyzed the formation of monoterpenes and sesquiterpenes from GPP and FPP, respectively, and there were 3 *TPSs* positively related and 7 *TPSs* negatively related. Interestingly, heatmap analysis of raw or scaled FPKM values showed that *DXS1* expressed at a substantially high level at stage S2, and its expression level in MT was significantly higher than that in WT (Figure 4F). In addition, the expression of *HDR* in MEP pathway also showed a decreasing trend from stage S2 to S3, while the expression of *HDS* significantly increased during the two periods. The genes in MVA pathway with high FPKM values such as *HMGR1*, *HMGR2* and *MDD* (*mevalonate diphosphate decarboxylase*) exhibited inconsistent trends with these DAVs (Figure 4F). These results indicated that the MEP pathway, especially *DXS1* gene, played important and positive roles in volatiles accumulation in WT and MT at stages S2 and S3.

3.5 Analysis of the critical genes related to volatiles metabolism in WT and MT throughout fruit development

To further evaluate the roles of MEP and MVA pathways in volatiles accumulation, the expression levels of structural genes in WT and MT across fruit development were analyzed. In MEP pathway, *DXS1* was consistently expressed at higher levels in MT than that in WT during fruit development (Figure 5A), indicating its critical role in determining the differential accumulation of volatiles between WT and MT. However, *DXS1* showed a very low expression level at S1, although this period had the highest total volatiles. Investigation of pathway genes indicated that the expression levels of *MCT*, *CMK*, and *HDR* were much higher at S1 than those at other four stages (Figure 5A). Comparing genes' expression between the two varieties, we found that *DXS1*, *DXS2*, and *MCT* expressed at higher levels in MT than WT at S2, and *DXS1*, *CMK*, and *GPPS2* expressed at higher levels in MT than WT at S3 (Figure 5A). These DEGs may be relevant to the variations of volatiles between WT and MT at S2 and S3 stages. In MVA pathway, the expression of *AACT1*, *HMGR1*, and *HMGR2* increased first, and then decreased and then increased, reaching the maximum at stage S5 (Figure 5B). The opposite was seen with *MVK*, it had the highest expression at S1 and showed a decreasing trend along fruit development (Figure 5B). In addition, *MVK* significantly differentially expressed between WT and MT. The results indicated that *MVK* might play important role in determining the accumulation of sesquiterpenes including 7-epi-sesquithujene and (E)-β-famesene in WT and MT.

In addition, we also analyzed the expression pattern of four *TPS* genes. All *TPS1*, *TPS2*, and *TPS3* positively correlated with the DAVs (Figure 4F), of which *TPS1* and *TPS3* was expressed the highest at stage S1, and *TPS2* exhibited the highest level at S2 (Figure 5C). Their expression trends were consistent with those observed in volatiles, as almost all DAVs showed the highest amount at stage S1 or S2 (Figure 2A). *TPS4* was the most negatively correlated with the DAVs (Figure 4F) and its expression level showed a clear upward trend as fruit develops (Figure 5C), thus this gene might be associated with the accumulation of the volatiles, such as valencene and o-cymene, which were highly accumulated at late stages.

4 Discussion

Volatile compounds not only are the important determinants of fruit quality perceived by consumers, but also are beneficial to human health (Liu et al., 2021; Pan X. et al., 2023). Citrus fruit has a strong aroma which is altered by developmental factors, thus analysis of volatile changes of citrus mutant during fruit development helps to better understand the mechanism of volatiles accumulation.

The volatile profiles of pulps in WT and MT at five developmental stages were determined. The composition of volatiles showed no difference between two varieties, and a total of 35 volatile compounds were detected in both varieties across fruit development, including terpenes, aldehydes, alcohols, ketones and esters. For total volatiles content, MT had significantly higher contents of total volatiles than WT at the stages S2-S5, although both of them were most abundant at stage S1 with a similar level. To better understand the difference between WT and MT, we performed OPLS-DA to identify differentially accumulated volatiles (DAVs) and analyzed their accumulation patterns during fruit development. Among these 28 DAVs, d-limonene was always the most dominant volatile throughout fruit development, which was similar to previous researches (Hou et al., 2020; Hu et al., 2024), and its average content in MT was 1.5–2.4 folds higher compared with WT during S2-S5 stages. Linalool was the richest component among monoterpene alcohols associated with typical sweet floral scent, exhibiting significant higher levels (2.3–4.4 folds) in MT than that in WT at S1-S3 stages. Other DAVs such as trans-β-terpineol, (E)-β-famesene, and α-terpinolene also showed different accumulation patterns between WT and MT. In addition to the differences between two varieties, there were also large changes in volatiles composition and content during fruit development. Valencene was specifically accumulated at the final two periods as previously reported (Shen et al., 2016; Hou et al., 2020), and octyl acetate was detected only in the first one period. In our study, the content of d-limonene in pulps decreased as the fruit develops,

10.3389/fpls.2024.1430204

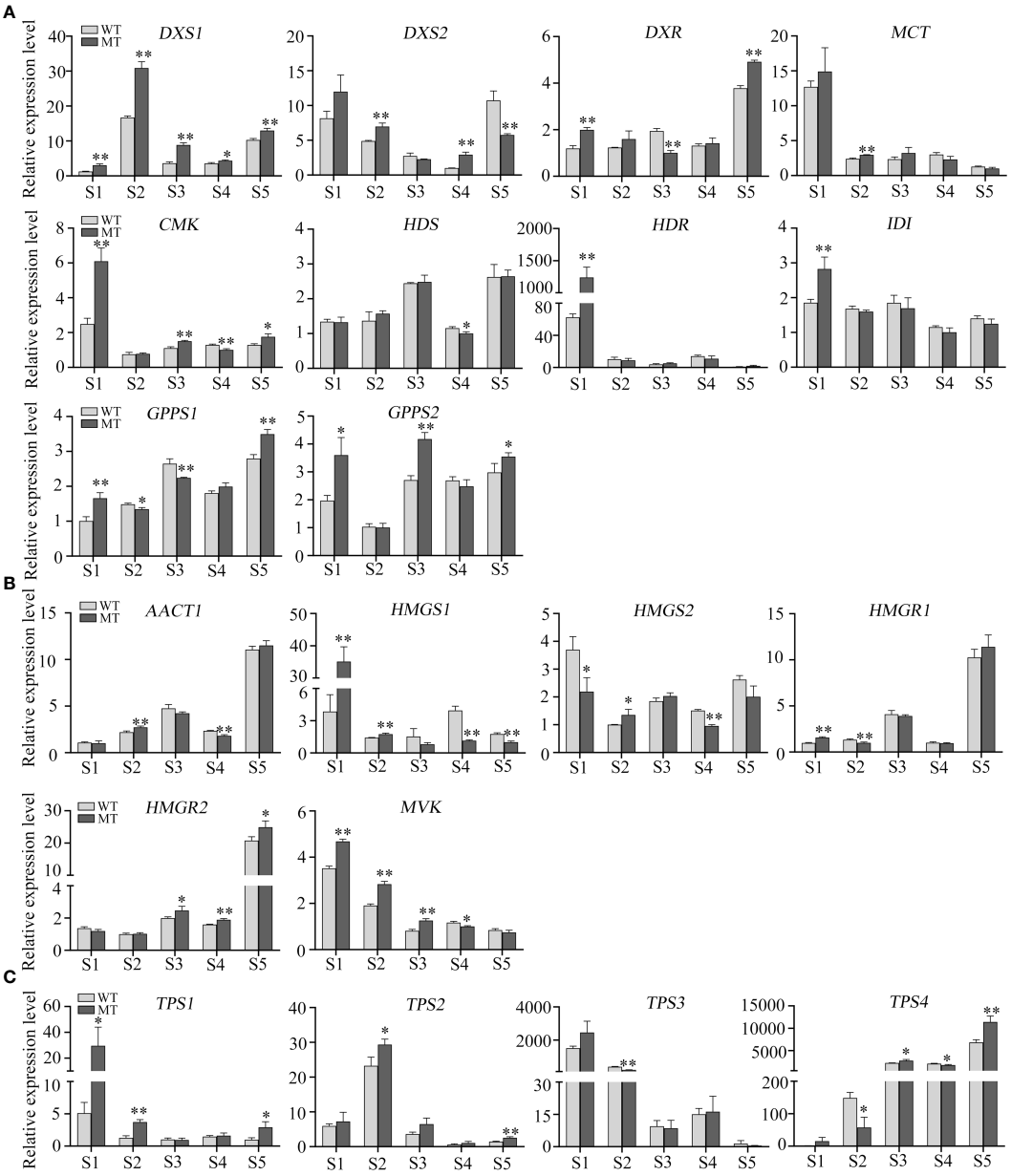

FIGURE 5
Relative expression levels of critical genes in WT and MT across fruit development. **(A)** Relative expression of MEP pathway genes in the pulps of WT and MT across fruit development. **(B)** Relative expression of MVA pathway genes. **(C)** Relative expression of *TPSs*. Data are expressed as means + SD, n = 3. Statistical analysis: Two-tailed paired t -test; *p < 0.05; **p < 0.01.

which was inconsistent with previous data (Hou et al., 2020; Kim et al., 2022). This may be due to that different citrus varieties were measured, or that our sampling time was earlier compared with previous studies. The latter speculation was supported by that the content of monoterpenes was much higher in the pulps of a very early-ripening pummelo 'LYZ' than that in other three pummelos (Pan T. et al., 2023).

Plant monoterpenes and sesquiterpenes are generally produced by the plastidial MEP pathway and the cytosolic MVA pathway, respectively (Nagegowda, 2010). It has been reported that the high expression levels of five genes in MVA pathway are associated with the high content of sesquiterpenes in the leaves of wild or semiwild citrus germplasms (Zhang et al., 2020). Monoterpenes constituted the largest portion of total volatiles in both WT and MT, and the expression of most genes in MEP pathway were positively correlated with the level of most DAVs (including d-limonene) and most genes in MVA pathway were negatively correlated. DXS is the first key rate-limiting enzyme in MEP pathway, and overexpressing *DXS* significantly enhances monoterpenes content in *Nicotiana benthamiana* (Nieuwenhuizen et al., 2015; Tian et al., 2022). In the pulps of MT, *DXS1* was consistently expressed at higher levels than that in WT during fruit development. Moreover, the higher expression levels of *DXS2*, *MCT*, *CMK*, and *GPPS2* in MT than those in WT might also contribute to the large variations between two varieties at S2 and S3 stages. A previous study indicated that the decreased volatiles contents were closely related

to the increased carotenoids contents in a red-flesh 'HJH' pummelo mutant (Zhu et al., 2022). In other citrus red-flesh mutants such as 'R-An', 'R-GX' and 'NRH', the total volatiles and carotenoids contents increased, and the ABA and/or limonoid aglycones contents decreased (Li W. et al., 2017; Liu et al., 2019). These researchers have proposed that the varied metabolites profiles are due to the flux balance of terpenoid metabolism rather than the increased flux into the isoprenoid pathway (Li W. et al., 2017; Liu et al., 2019; Zhu et al., 2022). In this study, MT had significantly higher expression levels of *DXS1* than WT, and the elevated volatiles accumulation in MT could be attributed mainly to the increased flux into MEP pathway. In addition, we found that *DXS2*, *MCT*, *CMK*, and *HDR* were active at S1, and *DXS1* was active at S2-S5 stages. These results indicated that different MEP pathway genes functioned at different stages of fruit development in WT and MT.

TPSs are key genes for terpene biosynthesis, few of which have been functionally characterized in citrus (Shen et al., 2016; Li X. et al., 2017; Bin et al., 2023). There were 3 *TPSs* and 7 *TPSs* positively and negatively correlated with the DAVs, respectively. Among them, *TPS4* was the most strongly negatively correlated with the DAVs. It has been reported that TPS4/VS mainly catalyzes the formation of valencene in navel orange (Hu et al., 2024). qRT-PCR assays showed that the expression of *TPS4* was increased gradually during fruit development in WT and MT, which was consistent with the accumulation pattern of valencene. Moreover, the expression trends of *TPS1*, *TPS2* and *TPS3* were similar to those observed in the DAVs during fruit development, and they were significantly differentially expressed between WT and MT at stage S2. These results indicated the important and positive roles of the three *TPSs* in volatiles accumulation of WT and MT, and this needs further functional validation.

5 Conclusions

A total of 35 volatile compounds were identified in the pulps of WT and MT during fruit development by HS-SPME-GC-MS, and differences in volatile profiles between both varieties at five developmental stages were analyzed by OPLS-DA. Compared with WT, the contents of total volatiles were significantly higher in MT at stages S2-S5, of which d-limonene was the most predominant volatile. Transcriptomic and qRT-PCR analysis revealed that the genes in MEP pathway, especially *DXS1*, played important and positive roles in the differential accumulation of volatiles accumulation in WT and MT during fruit development. These results could provide insights into the aroma characteristics of developing citrus fruit and the molecular mechanism underlying volatiles accumulation, which is of great importance in improving fruit flavor in citrus.

Data availability statement

The datasets presented in this study can be found in online repositories. The RNA-seq datasets can be found at: https://www.ncbi.nlm.nih.gov/, PRJNA1124587.

Author contributions

JH: Conceptualization, Data curation, Formal analysis, Funding acquisition, Methodology, Writing – original draft. ZQ: Conceptualization, Data curation, Formal analysis, Methodology, Resources, Writing – original draft. KL: Data curation, Methodology, Writing – original draft. XYL: Methodology, Writing – review & editing. YK: Methodology, Writing – review & editing. ZJ: Resources, Writing – review & editing. RH: Methodology, Writing – review & editing. MH: Methodology, Writing – review & editing. BX: Project administration, Resources, Writing – review & editing. LL: Project administration, Writing – original draft. GS: Project administration, Resources, Writing – original draft. SH: Project administration, Writing – original draft. MZ: Formal analysis, Project administration, Writing – review & editing. DL: Supervision, Writing – review & editing. XLL: Supervision, Writing – review & editing. XW: Supervision, Writing – review & editing. ZW: Funding acquisition, Project administration, Supervision, Writing – review & editing.

Funding

The author(s) declare financial support was received for the research, authorship, and/or publication of this article. This work was supported by China Postdoctoral Science Foundation (Grant No. 2023M742517), Science and Technology Department of Sichuan Province (Grant No. 2024NSFSC1305), the National Key Research and Development Program of China (Grant No. 2023YFD2300600), and Sichuan Central Guide Local Science and Technology Development Project (Grant No. 2023ZYD0293).

Conflict of interest

The authors declare that the research was conducted in the absence of any commercial or financial relationships that could be construed as a potential conflict of interest.

Publisher's note

Supplementary material

The Supplementary Material for this article can be found online at: https://www.frontiersin.org/articles/10.3389/fpls.2024.1430204/full#supplementary-material

References

Alquézar, B., Rodríguez, A., de la Peña, M., and Peña, L. (2017). Genomic analysis of terpene synthase family and functional characterization of seven sesquiterpene synthases from *Citrus sinensis*. *Front. Plant Sci.* 8. doi: 10.3389/fpls.2017.01481

Anandakumar, P., Kamaraj, S., and Vanitha, M. K. (2021). D-limonene: A multifunctional compound with potent therapeutic effects. *J. Food Biochem.* 45, e13566. doi: 10.1111/jfbc.13566

Bin, M., Peng, X., Yi, G., and Zhang, X. (2023). CsTPS21 encodes a jasmonate-responsive monoterpene synthase producing β-ocimene in citrus against Asian citrus psyllid. *Plant Physiol. Biochem.* 201, 107887. doi: 10.1016/j.plaphy.2023.107887

Dadwal, V., Joshi, R., and Gupta, M. (2022). A comparative metabolomic investigation in fruit sections of *Citrus medica* L. and *Citrus maxima* L. detecting potential bioactive metabolites using UHPLC-QTOF-IMS. *Food Res. Int.* 157, 111486. doi: 10.1016/j.foodres.2022.111486

Dadwal, V., Joshi, R., and Gupta, M. (2023). Comparative metabolomics of Himalayan crab apple (*Malus baccata*) with commercially utilized apple (*Malus domestica*) using UHPLC-QTOF-IMS coupled with multivariate analysis. *Food Chem.* 402, 134529. doi: 10.1016/j.foodchem.2022.134529

Gonzalez-Mas, M. C., Rambla, J. L., Alamar, M. C., Gutierrez, A., and Granell, A. (2011). Comparative analysis of the volatile fraction of fruit juice from different *Citrus* species. *PloS One* 6, e22016. doi: 10.1371/journal.pone.0022016

González-Molina, E., Domínguez-Perles, R., Moreno, D. A., and García-Viguera, C. (2010). Natural bioactive compounds of *Citrus limon* for food and health. *J. Pharm. Biomed. Anal.* 51, 327–345. doi: 10.1016/j.jpba.2009.07.027

He, Y., Han, J., Liu, R., Ding, Y., Wang, J., Sun, L., et al. (2018). Integrated transcriptomic and metabolomic analyses of a wax deficient citrus mutant exhibiting jasmonic acid-mediated defense against fungal pathogens. *Hortic. Res.* 5, 43. doi: 10.1038/s41438-018-0051-0

Hijaz, F., Gmitter, F. G., Bai, J., Baldwin, E., Biotteau, A., Leclair, C., et al. (2020). Effect of fruit maturity on volatiles and sensory descriptors of four mandarin hybrids. *J. Food Sci.* 85, 1548–1564. doi: 10.1111/1750-3841.15116

Hou, J., Liang, L., and Wang, Y. (2020). Volatile composition changes in navel orange at different growth stages by HS-SPME–GC–MS. *Food Res. Int.* 136, 109333. doi: 10.1016/j.foodres.2020.109333

Hu, Z., Chen, M., Zhu, K., Liu, Y., Wen, H., Kong, J., et al. (2024). Multiomics integrated with sensory evaluations to identify characteristic aromas and key genes in a novel brown navel orange (*Citrus sinensis*). *Food Chem.* 444, 138613. doi: 10.1016/j.foodchem.2024.138613

Kim, D., Paggi, J. M., Park, C., Bennett, C., and Salzberg, S. L. (2019). Graph-based genome alignment and genotyping with HISAT2 and HISAT-genotype. *Nat. Biotechnol.* 37, 907–915. doi: 10.1038/s41587-019-0201-4

Kim, S. S., Kim, H.-J., Park, K. J., Kang, S. B., Park, Y., Han, S.-G., et al. (2022). Metabolomic profiling of *Citrus unshiu* during different stages of fruit development. *Plants* 11, 967. doi: 10.3390/plants11070967

Li, C., Li, X., Liang, G., Xiang, S., and Han, G. (2022). Volatile composition changes in lemon during fruit maturation by HS-SPME-GC-MS. *J. Sci. Food Agric.* 102, 3599–3606. doi: 10.1002/jsfa.11706

Li, W., Liu, C., He, M., Li, J., Cai, Y., Ma, Y., et al. (2017). Largely different contents of terpenoids in beef red-flesh tangerine and its wild type. *BMC Plant Biol.* 17, 36. doi: 10.1186/s12870-017-0988-4

Li, X., Xu, Y., Shen, S., Yin, X., Klee, H., Zhang, B., et al. (2017). Transcription factor CitERF71 activates the terpene synthase gene CitTPS16 involved in the synthesis of E-geraniol in sweet orange fruit. *J. Exp. Bot.* 68, 4929–4938. doi: 10.1093/jxb/erx316

Liao, P., Hemmerlin, A., Bach, T. J., and Chye, M.-L. (2016). The potential of the mevalonate pathway for enhanced isoprenoid production. *Biotechnol. Adv.* 34, 697–713. doi: 10.1016/j.biotechadv.2016.03.005

Liu, C., Cheng, Y., Zhang, H., Deng, X., Chen, F., and Xu, J. (2012). Volatile constituents of wild citrus Mangshanyegan (*Citrus nobilis* Lauriro) peel oil. *J. Agric. Food Chem.* 60, 2617–2628. doi: 10.1021/jf2039197

Liu, C., He, M., Wang, Z., and Xu, J. (2019). Integrative analysis of terpenoid profiles and hormones from fruits of red-flesh citrus mutants and their wild types. *Molecules* 24, 3456. doi: 10.3390/molecules24193456

Liu, N., Li, X., Zhao, P., Zhang, X., Qiao, O., Huang, L., et al. (2021). A review of chemical constituents and health-promoting effects of citrus peels. *Food Chem.* 365, 130585. doi: 10.1016/j.foodchem.2021.130585

Lota, M., de Rocca Serra, D., Tomi, F., and Casanova, J. (2001). Chemical variability of peel and leaf essential oils of 15 species of mandarins. *Biochem. Syst. Ecol.* 29, 77–104. doi: 10.1016/S0305-1978(00)00029-6

Nagegowda, D. A. (2010). Plant volatile terpenoid metabolism: Biosynthetic genes, transcriptional regulation and subcellular compartmentation. *FEBS Lett.* 584, 2965–2973. doi: 10.1016/j.febslet.2010.05.045

Nieuwenhuizen, N. J., Chen, X., Wang, M. Y., Matich, A. J., Perez, R. L., Allan, A. C., et al. (2015). Natural variation in monoterpene synthesis in kiwifruit: Transcriptional regulation of terpene synthases by nac and ethylene-insensitive3-like transcription factors. *Plant Physiol.* 167, 1243–1258. doi: 10.1104/pp.114.254367

Pan, T., Kong, L., Zhang, X., Wang, Y., Zhou, J., Fu, Z., et al. (2023). Fruit quality and volatile constituents of a new very early-ripening pummelo (*Citrus maxima*) cultivar 'Liuyuezao'. *Front. Plant Sci.* 13. doi: 10.3389/fpls.2022.1089009

Pan, X., Bi, S., Lao, F., and Wu, J. (2023). Factors affecting aroma compounds in orange juice and their sensory perception: A review. *Food Res. Int.* 169, 112835. doi: 10.1016/j.foodres.2023.112835

Perez-Cacho, P. R., and Rouseff, R. L. (2008). Fresh squeezed orange juice odor: A review. *Crit. Rev. Food Sci. Nutr.* 48, 681–695. doi: 10.1080/10408390701638902

Rodríguez, A., San Andrés, V., Cervera, M., Redondo, A., Alquézar, B., Shimada, T., et al. (2011). Terpene down-regulation in orange reveals the role of fruit aromas in mediating interactions with insect herbivores and pathogens. *Plant Physiol.* 156, 793–802. doi: 10.1104/pp.111.176545

Sharma, E., Anand, G., and Kapoor, R. (2017). Terpenoids in plant and arbuscular mycorrhiza-reinforced defence against herbivorous insects. *Ann. Bot.* 119, 791–801. doi: 10.1093/aob/mcw263

Shen, S.-L., Yin, X.-R., Zhang, B., Xie, X.-L., Jiang, Q., Grierson, D., et al. (2016). CitAP2.10 activation of the terpene synthase CsTPS1 is associated with the synthesis of (+)-valencene in 'Newhall' orange. *J. Exp. Bot.* 67, 4105–4115. doi: 10.1093/jxb/erw189

Shi, C. H., Wang, X. Q., Xu, J. F., Zhang, Y. X., Qi, B., and Jun, L. (2021). Dissecting the molecular mechanism of russeting in sand pear (Pyrus pyrifolia Nakai) by metabolomics, transcriptomics, and proteomics. *Plant J.* 108, 1644–1661. doi: 10.1111/tpj.15532

Tian, L., Shi, J., Yang, L., and Wei, A. (2022). Molecular cloning and functional analysis of DXS and FPS genes from *Zanthoxylum bungeanum* Maxim. *Foods* 11, 1746. doi: 10.3390/foods11121746

Volke, D. C., Rohwer, J., Fischer, R., and Jennewein, S. (2019). Investigation of the methylerythritol 4-phosphate pathway for microbial terpenoid production through metabolic control analysis. *Microb. Cell. Fact.* 18, 192. doi: 10.1186/s12934-019-1235-5

Wang, L., Huang, Y., Liu, Z., He, J., Jiang, X., He, F., et al. (2021). Somatic variations led to the selection of acidic and acidless orange cultivars. *Nat. Plants* 7, 954–965. doi: 10.1038/s41477-021-00941-x

Wang, X., Huang, J., Yin, Z., Xu, K., Jiang, D., Lin, L., et al. (2023). Carotenoid components and their biosynthesis in a bud mutant of Shiranui mandarin (*Citrus reticulata* Blanco) with citrine flavedo. *J. Zhejiang University-SCIENCE B* 24, 94–100. doi: 10.1631/jzus.B2200431

Wang, Y., Liu, X. J., Chen, J. B., Cao, J. P., Li, X., and Sun, C. D. (2022). Citrus flavonoids and their antioxidant evaluation. *Crit. Rev. Food Sci. Nutr.* 62, 3833–3854. doi: 10.1080/10408398.2020.1870035

Wang, S., Shen, S., Wang, C., Wang, X., Yang, C., Zhou, S., et al. (2023). A metabolomics study in citrus provides insight into bioactive phenylpropanoid metabolism. *Hortic. Res.* 11, uhad267. doi: 10.1093/hr/uhad267

Wang, S., Tu, H., Wan, J., Chen, W., Liu, X., Luo, J., et al. (2016). Spatio-temporal distribution and natural variation of metabolites in citrus fruits. *Food Chem.* 199, 8–17. doi: 10.1016/j.foodchem.2015.11.113

Wang, T., Xiong, B., Zheng, Z., Qin, Z., Deng, L., Zheng, W., et al. (2023). Natural variation confers 'Aiyuan 38' citrus mutant a new color and unique flavor. *Int. J. Mol. Sci.* 24, 8816. doi: 10.3390/ijms24108816

Yang, J., Chen, R., Wang, C., Li, C., Ye, W., Zhang, Z., et al. (2024). A widely targeted metabolite modificomics strategy for modified metabolites identification in tomato. *J. Integr. Plant Biol.* 66, 810–823. doi: 10.1111/jipb.13629

Ye, L.-X., Gan, Z.-M., Wang, W.-F., Ai, X.-Y., Xie, Z.-Z., Hu, C.-G., et al. (2020). Comparative analysis of the transcriptome, methylome, and metabolome during pollen abortion of a seedless citrus mutant. *Plant Mol. Biol.* 104, 151–171. doi: 10.1007/s11103-020-01034-7

Zhang, H., Chen, M., Wen, H., Wang, Z., Chen, J., Fang, L., et al. (2020). Transcriptomic and metabolomic analyses provide insight into the volatile compounds of citrus leaves and flowers. *BMC Plant Biol.* 20, 7. doi: 10.1186/s12870-019-2222-z

Zhang, J., Wang, C., Wang, J., Yang, Y., Han, K., Bakpa, E. P., et al. (2023). Comprehensive fruit quality assessment and identification of aroma-active compounds in green pepper (*Capsicum annuum* L.). *Front. Nutr.* 9. doi: 10.3389/fnut.2022.1027605

Zhang, H., Xie, Y., Liu, C., Chen, S., Hu, S., Xie, Z., et al. (2017). Comprehensive comparative analysis of volatile compounds in citrus fruits of different species. *Food Chem.* 230, 316–326. doi: 10.1016/j.foodchem.2017.03.040

Zhou, S., Jander, G., and Ort, D. (2022). Molecular ecology of plant volatiles in interactions with insect herbivores. *J. Exp. Bot.* 73, 449–462. doi: 10.1093/jxb/erab413

Zhu, F., Luo, T., Liu, C., Wang, Y., Yang, H., Yang, W., et al. (2017). An R2R3-MYB transcription factor represses the transformation of α- and β-branch carotenoids by

negatively regulating expression of CrBCH2 and CrNCED5 in flavedo of *Citrus reticulate*. *New Phytol.* 216, 178–192. doi: 10.1111/nph.14684

Zhu, C., Peng, C., Qiu, D., and Zeng, J. (2022). Metabolic profiling and transcriptional analysis of carotenoid accumulation in a red-fleshed mutant of pummelo (*Citrus grandis*). *Molecules* 27, 4595. doi: 10.3390/molecules27144595

Zhu, G., Wang, S., Huang, Z., Zhang, S., Liao, Q., Zhang, C., et al. (2018). Rewiring of the fruit metabolome in tomato breeding. *Cell* 172, 249–261.e212. doi: 10.1016/j.cell.2017.12.019

Zhu, K., Zheng, X., Ye, J., Huang, Y., Chen, H., Mei, X., et al. (2021). Regulation of carotenoid and chlorophyll pools in hesperidia, anatomically unique fruits found only in *Citrus*. *Plant Physiol.* 187, 829–845. doi: 10.1093/plphys/kiab291

frontiers | Frontiers in Plant Science

TYPE Original Research
PUBLISHED 23 August 2024
DOI 10.3389/fpls.2024.1439087

OPEN ACCESS

EDITED BY
Wilhelm Boland,
Max Planck Institute for Chemical Ecology, Germany

REVIEWED BY
Yooichi Kainoh,
University of Tsukuba, Japan
Alfredo J. Ibáñez,
Pontificia Universidad Católica del Perú, Peru

*CORRESPONDENCE
Tao Ma
matao@scau.edu.cn

RECEIVED 27 May 2024
ACCEPTED 08 August 2024
PUBLISHED 23 August 2024

CITATION
Qian C, Xie W, Su Z, Wen X and Ma T (2024) Quantitative analysis and characterization of floral volatiles, and the role of active compounds on the behavior of *Heortia vitessoides*. *Front. Plant Sci.* 15:1439087. doi: 10.3389/fpls.2024.1439087

Quantitative analysis and characterization of floral volatiles, and the role of active compounds on the behavior of *Heortia vitessoides*

Chenyu Qian, Wenqi Xie, Zhongqi Su, Xiujun Wen and Tao Ma*

College of Forestry and Landscape Architecture, South China Agricultural University, Guangzhou, China

This study explores the role of floral volatile organic compounds (FVOCs) in insect behavior, focusing on *Aquilaria sinensis* (AS), a valuable tropical plant threatened by *Heortia vitessoides* Moore. Despite *H. vitessoides*' attraction to AS and non-host plants like *Elaeocarpus decipiens* (ED) and *Dalbergia odorifera* (DO), little is known about their chemical interactions. FVOCs from these plants were analyzed at 9:00 and 18:00 using GC×GC-QTOF-MS and HS-SPME. The results showed that ED exhibiting the highest concentration (92.340 ng/mg), followed by DO (75.167 ng/mg) and AS (64.450 ng/mg). Through GC-EAD and EAG, a total of 11 FVOC compounds with electrophysiological activates were identified. These compounds, except linalool, showed dose-dependent responses. Y-Tube bioassays confirmed phenylethyl alcohol or the mixture of EAD-active compounds produced positive chemotactic responses in both males and females. FVOCs have the potential to be used as a natural and sustainable alternative to chemical insecticides in pest control.

KEYWORDS

floral volatiles, Heortia vitessoides, HS-SPME, antennal response, olfactometer bioassay

1 Introduction

Aquilaria sinensis (Lour.) Gilg (Myrtales: Thymelaeaceae), the principal source of agarwood, is an economically plant that is primarily cultivated in tropical areas, such as South China, Vietnam, India, Malaysia, *etc* (Chen et al., 2016; Qiao et al., 2012), which has a long history of application in traditional medicines, religious ceremonies, and incense industries (Wang et al., 2021). However, the cultivation of *A. sinensis* forests is seriously threatened by *Heortia vitessoides* Moore (Lepidoptera: Crambidae), a severe and notorious pest (Cheng et al., 2019). The larvae of *H. vitessoides* feed on the leaves, causing weakening, defoliation and eventual death of *A. sinensis* trees. The widespread use of chemical insecticides to control *H. vitessoides* infestations in agriculture has resulted in the

development of resistance in these insects, leading to increased pesticide usage and severe environmental pollution. Chemical insecticides can enter water bodies, soil, and the atmosphere, affecting not only the target pests but also non-target organisms. Therefore, it is necessary to explore alternative strategies for *H. vitessoides* management that minimize the use of chemical insecticides and their associated environmental risks.

The floral fragrance is a blend of low-molecular-weight volatiles with various chemical functional groups, endogenously synthesized by plants (Dudareva and Negre, 2005). These volatiles serve as unique scent signals that attract specific visitor insects for successful reproduction and evolution (Zhang et al., 2022). Flowers emit aroma volatiles as chemical cues (Pichersky and Gershenzon, 2002), and offer nectar, pollen, or oil as rewards (Schiestl et al., 2011). Aroma volatiles also has adaptive roles as repellents and physiological protectors (Borg-Karlson et al., 1993; Kessler et al., 2008). Even plant species with different evolutionary histories might emit similar composition of floral scent when pollinated by the same moth species (Powers et al., 2020). Therefore, the temporal rhythms of nectar production and scent emission should be taken into consideration when investigating the chemical mechanism that flowers adapt to their pollinators (Balducci et al., 2020).

Headspace solid phase micro-extraction (HS-SPME) is a widely employed technique for extracting volatile organic compounds (VOCs) from various matrices (Rajhi et al., 2022; Oliveira et al., 2022; Muñoz-Redondo et al., 2022). HS-SPME is known for its simplicity and ease of use, requires minimal sample preparation, and the extraction process can be completed in a relatively short period of time (Marinaki et al., 2023). The method's high sensitivity and reliability make it a valuable tool for the analysis of complex mixtures found in environmental and biological samples (Domínguez et al., 2017; Issa et al., 2020). In general, HS-SPME's extraction efficiency is affected by experimental parameters such as sample amount, time and temperature of incubation, extraction, and desorption, which are therefore included in most of the optimization attempts (Muñoz-Redondo et al., 2020, 2022; Pati et al., 2021).

The pollinating *H. vitessoides* moths prefer *A. sinensis*, *Elaeocarpus decipiens* (Malvales: Elaeocarpaceae), and *Dalbergia odorifera* (Rosales: Fabaceae) as their primary and alternative hosts, respectively (Supplementary Figure 1), indicating that the attractance of flowers may be due to the present of some common FVOCs from these three plants. Yet, the extent of their attraction to these plants and the underlying mechanism are not fully understood. In this study, we aim to characterize the chemical composition of the floral fragrance emitted by these plants and assess their similarities and differences. The study also explored the temporal variations in volatile emissions in the morning and dusk. Simultaneously, the electroantennographic (EAG) and Y-tube olfactometer techniques were utilized to examine the antennal and behavioral reactions of *H. vitessoides* moths to the active compounds identified through gas chromatography-electroantennography detection (GC-EAD). By identifying FVOCs, it is possible to create a targeted approach to pest management that reduces the negative impact of chemical pesticides on the environment.

2 Materials and methods

2.1 Plant materials

The host plant *A. sinensis* (AS) flower was collected from Tianlu Lake Park (Guangzhou, China, 23°14′27″N, 113°24′48″E). Two non-host plants, *E. decipiens* (ED) and *D. odorifera* (DO) were harvested at South China Agricultural University (23°9′44″N, 113°21′21″E). The flower samples were all harvested in the early morning (9:00) and dusk (18:00), respectively. The phenotypic traits of the three flower species were shown in Supplementary Table 1.

2.2 Insect rear

The larvae in the fourth or fifth instar of *H. vitessoides* were also collected from Tianlu Lake Park. The larvae were maintained under environmental conditions of 26 ± 1°C and 80 ± 5% relative humidity (RH) under a 14:10 light: dark schedule. Fresh leaves of *A. sinensis* were added to feed larvae each day. The adults were kept in fine nylon mesh cages (50 × 50 × 50 cm) and supplied with 20% honey solution.

2.3 Chemicals

High-performance liquid chromatography (HPLC)-grade methanol was obtained from Baishi Chemical (Tianjin, China). Hexanal (>99%), benzaldehyde (>98%), 1-octen-3-ol (>96%), benzyl alcohol (>99%), heptanal (>96%), 3-octanol (>99%), nonanal (>98%), (*E*)-2-hexenal(>98%), and phenylacetaldehyde (>99%) were purchased from Cato Research Chemicals Inc (Oregon, U.S); Phenylethyl alcohol (≥98%), caryophyllene (>98%), geraniol (≥98%), linalool (>98%), nerol (≥97%), (*E*)-β-ocimene (>98%) were obtained from Macklin (Shanghai, China). A mixture of normal alkanes (C8-C25) was purchased from Sigma (St Louis, MO, USA).

2.4 Sample preparation

Flower samples were collected in liquid nitrogen and freeze-dried at -70°C (Alpha2-4 LD Plus; Christ, Osterode, German). Flowers were powdered and weighed into a 20-mL headspace vial (Agilent Technologies, Inc., Santa Clara, CA, USA). A 50/30 μm DVB/CAR/PDMS coated SPME fibers (Supelco-Aldrich, Bellefonte, PA, USA) was thermally cleaned and desorbed between samples. Extraction was performed at different temperatures and times considered for optimization in the next section. The SPME fiber was placed into the injector port at 250°C for 3 min. Each SPME process was repeated three times. Clean vials were used as controls. Quality control (QC) samples were created by mixing equal quantities of each type of sample (DO, AS, and ED flower collected at 9:00 and 18:00). The QC sample was used for validation of the SPME method. Each aliquot of flower sample was tested in triplicate.

2.5 Optimization of HS-SPME

The optimization of HS-SPME parameters was performed to ensure good chromatographic signals. The total peak area of extracted compounds was used to evaluate extraction efficiency. The optimization of the SPME parameters included low, medium, and high levels: sample weight (50, 125, and 200 mg), incubation temperature (30, 45, and 60°C), equilibration time (10, 20, and 30 min) and adsorption time (20, 40, and 60 min). Injections were made in triplicate.

2.6 GC × GC-QTOFMS

A comprehensive two-dimensional gas chromatography (GC×GC) system consisting of a GC gas chromatography (7890B, Agilent) and a quadrupole time-of-flight mass spectrometry (QTOFMS, 7250, Agilent) instrument was used. Samples were introduced by a split/splitless injector (SSL) system with a CTC autosampler (PAL RSI 120, Agilent). Helium carrier gas (99.999%) was set at a constant flow of 1 mL/min. The oven temperature was programmed from 50°C (held for 3 min) to 250°C at 5°C/min (held for 1 min), for a total running time of 44 min. A DB-Wax column (30 m × 250 μm, 0.25 μm film thickness; Agilent) and a DB-17 column (1.2 m × 180 μm, 0.18 μm film thickness; Agilent) were used for first and second-dimensional separation, respectively. A solid-state modulator (SSM 1800, J&X Technologies, Shanghai, China) was installed between the 1st and 2nd columns, and the cold zone temperature of the SSM was set at -50°C. The modulation period was 6 s. The transfer line temperature and ion source temperature of MS were 280°C and 200°C, respectively. Electron ionization (EI) mode was at 70 eV, and full-scan acquisition mode with a mass range of 40–450 m/z.

The raw data were processed with Canvas (J & X Technologies). The compounds were identified by comparing the gas chromatography-mass spectrometry spectra with standards, or tentatively identified by comparing mass spectrometry spectra with the data in the National Institute of Standards and Technology (NIST20) library. RI was calculated based on the retention times of *n*-alkanes (C_8-C_{25}) under the same conditions.

Quantification: The concentration of the identified major compounds was calculated by an external standard operating curves method. The standards were diluted respectively in methanol in a series of concentrations (0.5, 1, 5, 10, 50, and 100 μg/mL). For those components without corresponding standards, the curve of compounds that have similar chemical structures and the response signal were used to conduct semi-quantification (Zhou et al., 2020). The signal-to-noise ratio (S/N) of 3:1 and 10:1 was used for the LOD and LOQ, respectively. Precision was evaluated by calculating each QC sample's percent relative standard deviation (RSD) (n=3). The repeatability was accepted no more than RSD of 15% (Supplementary Table 2).

2.7 GC-EAD analysis

Flower compounds to which *H. vitessoides* moths responded were identified on an Agilent 7820A GC system with an HP-5MS capillary column and an EAD and flame ionization detector (FID). A mixture of all the VOCs (1 μL) was injected in splitless mode with injector and detector temperatures at 250 and 300°C, respectively. The effluent between FID and EAD was split at a 1:1 ratio with a glass Y splitter (Agilent). The experimental details were described by Ma et al. (2015). In brief, antenna of male or female moths was mounted onto an antenna holder for the EAG probe (PRG-2) and exposed to the GC effluent introduced into a glass transfer tube (15 mm ID) with purified and humidified air flow (100 mL/min). The constant airstream was supplied continuously from the EAD to the *H. vitessoides* antennae by an air stimulus controller (CS-55) (Syntech). The antennal signal was recorded simultaneously with the FID signal and considered active when it elicited antennal responses at least 5 times.

2.8 EAG test

The EAG system used to analyze *H. vitessoides* antennae responses to compound mixtures was modified from previous method (Magsi et al., 2021). The system consisted of a MP-15 probe/micromanipulator, an IDAC-2 data acquisition interface box, and a CS-55 air stimulus controller. The antenna was mounted on fork-shaped metal electrodes and fixed with electrode gel (Spectra 360, Parker Laboratory Inc., Orange, NJ, USA). Chemicals were dissolved in methanol at three concentrations (1, 10, and 100 μg/μL), with methanol as a control. Chemicals were applied to filter paper strip (1 × 2 cm) and inserted into a glass Pasteur pipet (15 cm long) in a mixing tube with moistened airflow (100 mL/min). The signal was analyzed using EAG Pro software (Syntech, Germany). Stimuli were delivered by puffing the humidified air for 0.3 s. The average EAG values of each chemical component were compared to methanol before and after stimulation.

2.9 Olfactometry bioassays

Behavioral bioassays were conducted using a Y-olfactometer consisting of a base tube (20 cm long × 4 cm diam.) with two 15 cm arms at 70° angles. Odor sources consisted of a 1 cm^2 piece of filter paper placed at the end of each arm. The test solutions were dissolved to the concentration of 10 μg/μL. The filter paper piece loaded with 10 μL of the corresponding standards was the test arm, and those loaded with 10 μL methanol were set as the control arm. Charcoal-filtered and moisten air was pumped into the system at 600 mL/min by using a gas sampling instrument. In each test, a single male or female moth was introduced into the base of the main olfactometer tube, and response to the corresponding stimulus was observed for 5 min. The observed behavior was recorded as follows:

(1) standard choice or control choice (entering the respective arm for more than 2 cm and remaining for at least 30 s); (2) no choice (do not reach or visit any arm). Each solution tested thirty females or males. During the assays, the position of each olfactometer arm was shifted every five tests.

2.9 Statistical analyses

The orthogonal partial least squares discriminant analysis (OPLS-DA) was carried out with SIMCA 14.0 software (Umetrics, Umea, Sweden). Venn graph was conducted online (http://jvenn.toulouse.inra.fr). An Independent sample t-test was conducted to compare the electrophysiological response values of *H. vitessoides* male and female moths in the EAG test by SAS 9.4 software (SAS Institute Inc., Cary, NC, USA). The choices made by moths in the bioassays were analyzed by the chi-square goodness-of-fit test (SAS 9.4). Origin 2022 (OriginLab Corporation, Northampton, MA) and GraphPad Prism 9 (GraphPad Software) were used for data visualization.

3 Results and discussion

3.1 Optimization of the HS-SPME conditions

3.1.1 Effect of sample amount

HS-SPME technology relies on a dynamic equilibrium process that balances analytes among the sample, headspace, and fiber coating (Ho et al., 2006). Therefore, the extraction efficiency depends on the amount of flower sample in the vial, which affects the ionic strength and vapor pressure of volatile compounds (Wei et al., 2020). Increasing the sample quantity from 50 mg to 125 mg doubled the efficiency of volatile compound extraction, but no further increase in extracted volatiles was observed with 200 mg (Supplementary Figure 2A). Additionally, the number of extracted compounds significantly decreased when the sample amount exceeded 200 mg. The results suggested that insufficient sample amounts might lead to low enrichment of trace compounds, while saturation of fiber sites prevented the collection of additional volatiles.

3.1.2 Effect of equilibration temperature

Increasing the equilibration temperature from 30 to 45°C led to an increase in the peak area of total volatile, reaching the highest performance at 45°C. To preserve natural volatiles, 60°C was chosen as the maximum temperature, but a further increase from 45 to 60°C decreased the peak areas and peak numbers (Supplementary Figure 2B). Due to the high-energy barriers that bind analytes to the matrix, the adsorption of volatile components is a slow process (Liang et al., 2022). Consecutive heating improves diffusion coefficients and analyte volatility (Wei et al., 2020). However, the incubation temperature above 50 °C may lead to the Millard reaction and Strecker degradation, leading to the adsorption of large weights volatiles and the desorption of small molecular weight volatiles (Mu et al., 2021). Additionally, the release and enrichment of analytes on the fiber are antagonistic energy phases (Zhang and Pawliszyn, 1993), indicating that higher temperatures may promote analyte release but inhibit fiber adsorption. Thus, 45°C was deemed an appropriate incubation temperature for further experiments. Under optimal temperature conditions, the total amount of absorbed compounds is highest, and the variety of compounds is most comprehensive.

3.1.3 Effect of equilibration and adsorption time

The SPME method combines extraction and pre-concentration into a single step, with equilibration and adsorption being dynamic processes that are closely related to the efficiency of HS-SPME (Piri-Moghadam et al., 2017). Equilibration time is critical for analyte release into the headspace and is typically necessary before extraction (Ma et al., 2013). Equilibrium time of 20 min and 30 min were tested and showed little difference, with 20 minutes selected as the optimal equilibrium time to balance efficiency and time cost (Supplementary Figure 2C). Subsequently, the extraction time was investigated. As shown in Supplementary Figure 2D, a maximum peak area and peak number was observed when the extraction time increased from 20 min to 40 min, followed by a decrease at 60 min due to the competitive adsorption of analytes on the fiber coating (Pawliszyn et al., 2010). Previous studies have suggested that longer extraction times do not significantly increase signal intensities (Pico et al., 2022). Therefore, 40 min was selected as the optimal adsorption time since longer extraction times do not continually facilitate extraction after the fiber is thoroughly occupied by volatile substances.

3.2 Volatile analysis

3.2.1 Floral volatile composition

The analysis of FVOCs revealed that the content of VOC varied among different flower cultivars, DO contained the most diverse range of compounds, whereas AS had the least. A total of 21 common FVOCs were identified. Additionally, the FVOCs were classified into various groups, including aldehydes, alcohols, terpenoids, *etc*. (Supplementary Table 3). Aldehydes and alcohols were the two most abundant groups in all three types of flowers, with concentrations ranging from 16.510 to 28.000 ng/mg and 10.724 to 26.321 ng/mg, respectively (Figure 1). Traces of esters (from 0 to 4.784 ng/mg), ketones (from 0 to 5.919 ng/mg) and heterocyclic compounds (from 0.033 to 3.091 ng/mg) were also detected. Hexanal was the most abundant VOC in DO flowers (from 7.135 ± 1.024 to 7.94 ± 0.182 ng/mg), while the concentration of 4-oxoisophorone was the highest in ED at 18:00 (11.26 ± 0.219 ng/mg). Furthermore, benzyl alcohol (ranging from 8.85 ± 0.141 to 10.277 ± 0.193 ng/mg) was the primary component of AS.

In accordance with the present results, these three plant species present pale petals and emit fragrant scents, providing a strong contrast to the darkness. Among those volatile compounds, linalool is a common component in floral aroma released by moth-pollinated flowers (Raguso and Pichersky, 1999; Knudsen et al., 2006), and has been shown to mediated a pollinator-plant association between the nocturnal moth *Manduca sexta* (Sphingidae) and *Datura wrightii*

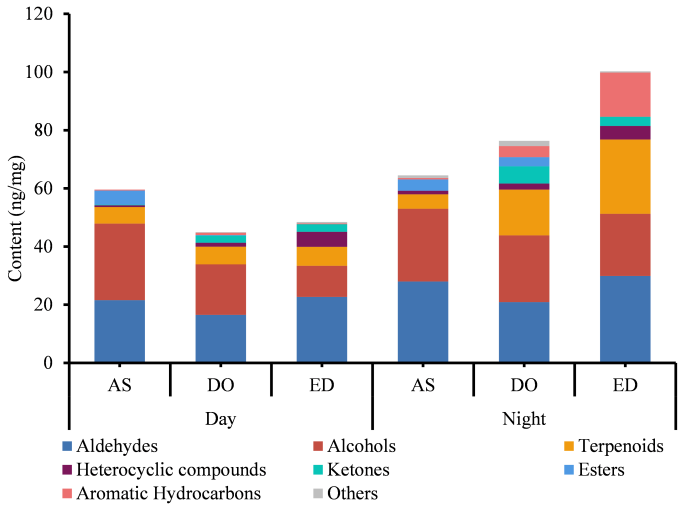

FIGURE 1
The analysis of VOCs of three tested flowers at day and night. DO, ED, and AS represent *Dalbergia odorifera*, *Elaeocarpus decipiens*, and *Aquilaria sinensis*, respectively.

(Solanaceae) (Reisenman et al., 2010). (*E*)-α-bergamotene emitted from the night-flowering *Nicotiana attenuata* (Solanaceae) also had positive effects on *M. sexta* moth-mediated pollination success (Zhou et al., 2017), indicating that different host/non-host plants might use unique compound to attract the same pollinator. In *Asclepias speciosa* (Apocynaceae), phenylacetaldehyde was used alone to attract *Synanthedon myopaeformis* (Sesiidae) moths, which induced the most frequent probosci's extension reflexes (Eby et al., 2013). The moth *Hadena bicruris* (Noctuidae) strongly preferred *Silene latifolia* (Caryophyllaceae) flowers over *S. dioica* (Bopp and Gottsberger, 2004), this preference could be attributed to the emission of lilac aldehydes and phenylacetaldehyde, which are known to be highly attractive to *H. bicruri* (Doetterl et al., 2009; Waelti et al., 2009). Thus, the VOCs profile of AS, ED, and DO may help explain the scent-mediated foraging behavior of *H. vitessoides* moths.

3.2.2 Day-night comparisons of FVOCs profiles

The analysis of three flowers harvested at two sampling periods showed that the variety of compounds extracted from flowers harvested at 18:00 was higher compared to those harvested at 9:00 (Figure 1). At 18:00, a total of 56 compounds were found in DO and ED, followed by AS (45). Except for AS, the compound identified in DO and ED at 18:00 was higher than those found at 9:00. In addition, four unique compounds were detected in both ED and AS harvested at 18:00, while three unique components were identified in AS flower at 9:00 (Figure 1). Four aromatic hydrocarbons were specific to ED at 18:00, including m-ethylcumene (7.651 ± 0.629 ng/mg), pentamethylbenzene (0.487 ± 0.065 ng/mg), and 1,3-diethyl-4-methylbenzene (0.387 ± 0.005 ng/mg). Quantitatively, the concentration of compounds in the same flower species varied considerably between the two time slots. At 18:00, ED showed the highest concentration (92.340 ng/mg), followed by DO (75.167 ng/mg) and AS (64.450 ng/mg). While AS, ED, and DO samples at 9:00 were only with a total concentration of 59.610 ng/mg, 48.521 ng/mg, and 44.955 ng/mg, respectively.

FVOCs are crucial cues in habitats with low light availability (Klatt et al., 2013). The timing of floral scent emission was often linked to pollinators activity, with emissions intensifying when pollinators are active (Dötterl et al., 2012; Powers et al., 2020). For example, the scent composition of *Platanthera chlorantha* (Asparagales: Orchidaceae) differed between day and night, with (*E*)-β-ocimene and linalool being the dominant compounds detected in larger amounts before sunset and at night, but only in trace amounts during the day, which positively related with the visition of *Sphinx pinastri* (Lepidoptera: Sphingidae) (Steen et al., 2019). Similarly, the strongest volatile emission of *Silene otites* (Caryophyllaceae) was found immediately after sunset, characterized by attractants such as phenylacetaldehyde, 2-phenylethanol, and lilac aldehyde for some moths (Dötterl et al., 2012). Although the scent compounds in various flower stages seem to have no difference from the evening of anthesis to the following morning, the content for each compound might be varied (Yan et al., 2016). A potential benefit of temporally regulating aroma emission is to reduce the cost associated with the consumption of energetically expensive aroma (van der Niet et al., 2015). Based on our field and indoor observations, *H. vitessoides* moth exhibits increased emergence, foraging (flower visiting), and mating activities post-dusk, with peak activity occurring during this period. Therefore, quantitative analyses revealed that three plant species released more abundant FVOCs after 18:00, corresponding with previous studies that illustrated that plants were expected to emit a stronger floral scent at night when pollinators were most active (Powers et al., 2020).

10.3389/fpls.2024.1439087

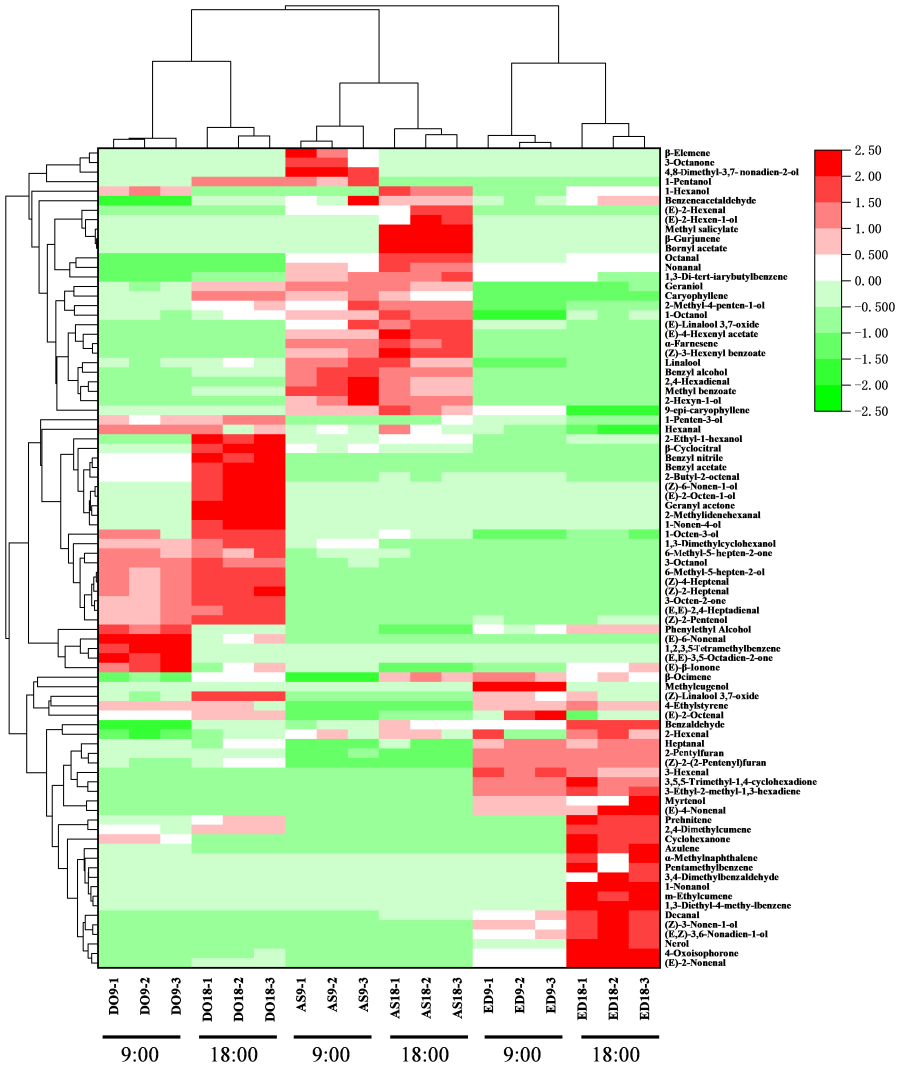

FIGURE 2
Hierarchical clustering and heatmap visualization of volatile compounds in three flower species. DO, ED, and AS represent *Dalbergia odorifera*, *Elaeocarpus decipiens*, and *Aquilaria sinensis*, respectively.

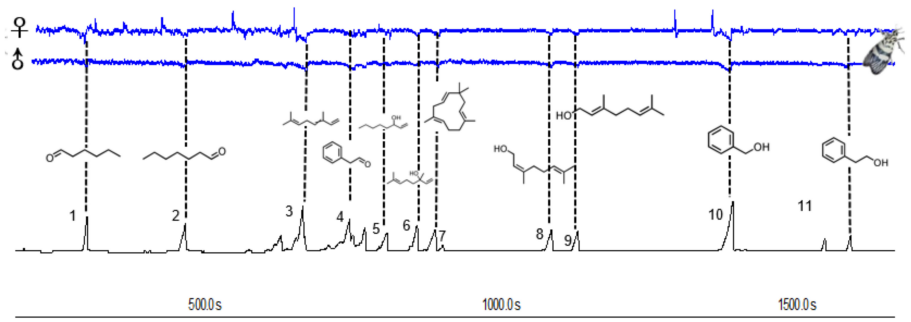

FIGURE 3
Responses of *Heortia vitessoides* female and male to volatiles detected by GC–EAD. The consistently EAD-active compounds in common floral volatile compounds were as follows: hexanal (1), heptanal (2), (*E*)-β-ocimene (3), benzaldehyde (4), 1-octen-3-ol (5), linalool (6), caryophyllene (7), nerol (8), geraniol (9), benzyl alcohol (10), phenylethyl alcohol (11) respectively.

10.3389/fpls.2024.1439087

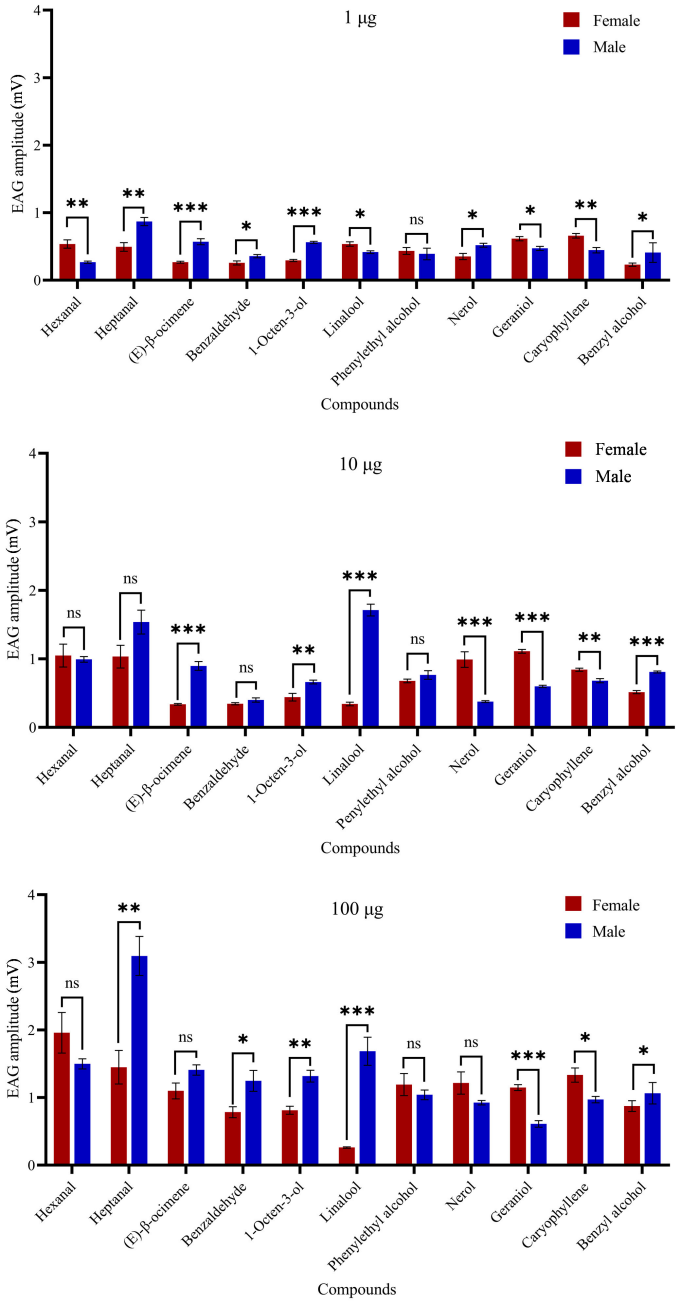

FIGURE 4
Electrophysiological response (means ± SE) values of *Heortia vitessoides* adult male and female moths to 11 floral volatiles at three different doses (1, 10, and 100 μg/μl). Significant differences between male and female EAG responses were analyzed by independent samples t-test (ns: not significant; *: $0.01 \leq p < 0.05$; **: $0.001 \leq p < 0.01$; ***: $p < 0.001$). N = 5 antennae per mean.

3.4 Hierarchical clustering analysis

To visualize and excavate the relationships among different flower species, hierarchical clustering analysis and a heat map were performed based on the content of volatile compounds detected by the GC × GC-QTOFMS method (Figure 2). The heat map graphically represented the differences in volatile abundance using a color scale, with the change from pink to green indicating a ranging from low to high content. The result showed that flowers of the same species were closely grouped, even when harvested at different times. According to HCA, the three flower species were divided into two groups. Base on the colors corresponding to volatile contents, DO and AS were classified into one group due to their similar volatile content, including myrtenol, 3,4-dimethylbenzene, nerol, *etc*. In contrast, the contents of the main compounds in ED were distinct from those in the other two species, particularly aldehydes like (*E*)-3-hexenal, decanal, and (*E*)-4-nonenal, *etc*. Thus, ED was categorized into the second group.

3.5 GC-EAD and EAG responses

The main common compounds were selected from the volatile components for electrophysiological testing. GC-EAD analyses revealed that the female and male antennae of *H. vitessoides* moths responded to all 11 compounds (Figure 3), which included 5 terpenoids, 3 alcohols, and 3 aldehydes, indicating that only a fraction of components were involved in the interaction between host/non-host flowers and the moths.

In electroantennogram test, the EAG responses of *H. vitessoides* moths to most volatiles were dose-dependent, with higher quantities triggering stronger responses. However, the response to benzyl alcohol appeared weaker with increasing dosage (Figure 4). Heptanal and hexanal elicited the largest EAG responses in males and females, respectively (Figure 4). Female moths appeared to be less sensitive to linalool than male moths (Supplementary Table 4; $P < 0.05$). Conversely, within each dose level, female antennal responses were significantly greater than males to geraniol and caryophyllene ($P < 0.05$). Thus, among the 11 chemical compounds tested, *H. vitessoides* moths only responded to certain FVOCs emitted by host/non-host plants.

3.6 Olfactometry bioassays

To further demonstrate the biological activity of these compounds, Y tube choice experiments were conducted on *H. vitessoides* moths. Behavior bioassays using selected standards as the odor source showed that both genders were attracted to phenylethyl alcohol (female, $\chi^2 = 5.5556$, df=1, P=0.0184; male, $\chi^2 = 4.8400$, df=1, P=0.0278) or mixture (female, $\chi^2 = 7.3478$, df=1, P=0.0067; male, $\chi^2 = 6.0000$, df=1, P=0.0143) (Figure 5). Additionally, compared to hexane, females significantly preferred benzaldehyde ($\chi^2 = 4.5455$, df=1, P=0.0330), while males were more attracted to caryophyllene ($\chi^2 = 6.0000$, df=1, P=0.0143), and no responses were observed for other compounds (Supplementary Table 5; $P > 0.05$). Hence, *H. vitessoides* moths exhibit different sensitivity and selectivity to particular volatiles. Previous research has indicated that phenylpropanoid/benzenoid compounds (e.g., phenethyl alcohol) and terpenes (e.g., linalool, caryophyllene) were known to attract lepidopterous insects and have positive effects on insect attraction (Andersson et al., 2002). The moths' preferences for specific volatile compounds potentially aid the pollinators in quickly locating valuable floral resources.

4 Conclusion

This study optimized an HS-SPME method for extracting volatiles from three flowers using single-factor optimization experiments. The optimal conditions were determined to be a sample quality of 125 mg, 45°C incubation temperature, 20 min equilibration time, and 40 min adsorption time. The current sampling method may not fully capture the profile of floral

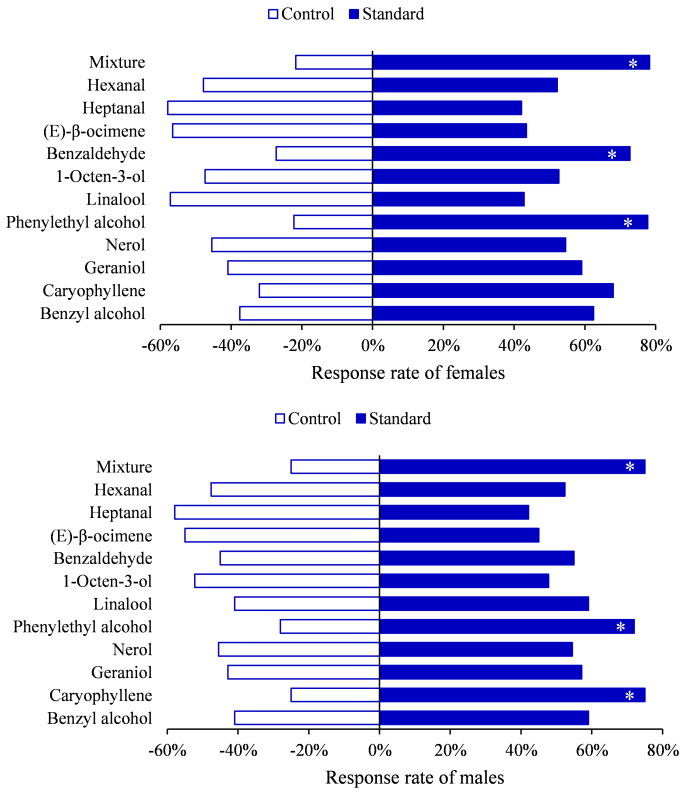

FIGURE 5
Behavioral responses of *Heortia vitessoides* to each compound tested in Y-tube olfactometer. (*: $0.01 \leq p < 0.05$).

volatile components as released by the actual flowers, future research will focus on sampling blooming flowers *in situ* to accurately compare and understand the differences in volatile profiles. The floral scent profile of the host (AS) and non-host (ED, and DO) plants were then determined by GC×GC-QTOF-MS, revealing those aldehydes and alcohols as the two most abundant groups. OPLS-DA analysis showed a good fit of the mode and predictive ability, with samples harvested at different time periods being highly distinct groups. HCA divided flowers from the three species into two groups. Eleven compounds elicited responses in the *H. vitessoides* antenna through GC-EAD recordings, and in the Y-tube experiment, phenylethyl alcohol and a mixture of EAD-activate compounds were found to be attractive to both males and females. These results might provide candidate attractants based on FVOCs to monitor and control the *H. vitessoides* populations.

Data availability statement

The original contributions presented in the study are included in the article/Supplementary Material. Further inquiries can be directed to the corresponding author.

Author contributions

CQ: Data curation, Formal analysis, Investigation, Methodology, Validation, Visualization, Writing – original draft. WX: Investigation, Methodology, Writing – review & editing. ZS: Investigation, Software, Writing – review & editing. XW: Conceptualization, Supervision, Validation, Writing – review & editing. TM: Conceptualization, Data curation, Funding acquisition, Resources, Supervision, Validation, Writing – review & editing.

Funding

The author(s) declare financial support was received for the research, authorship, and/or publication of this article. This work was funded by the Central Financial Forestry Science and Technology Extension Project (grant number: 2022GDTK-06).

Acknowledgments

We wholeheartedly appreciate the editors and the anonymous reviewers for the insightful suggestion and valuable comments that improved the quality of this manuscript.

Conflict of interest

The authors declare that the research was conducted in the absence of any commercial or financial relationships that could be construed as a potential conflict of interest.

Publisher's note

Supplementary material

The Supplementary Material for this article can be found online at: https://www.frontiersin.org/articles/10.3389/fpls.2024.1439087/full#supplementary-material

References

Andersson, S., Nilsson, L. A., Groth, I., and Bergström, G. (2002). Floral scents in butterfly-pollinated plants: possible convergence in chemical composition. *Bot. J. Linn. Soc.* 140, 129–153. doi: 10.1046/j.1095-8339.2002.00068.x

Balducci, M. G., van der Niet, T., and Johnson, S. D. (2020). Diel scent and nectar rhythms of an African orchid in relation to bimodal activity patterns of hawkmoth pollinators. *Ann. Bot.* 126, 1155–1164. doi: 10.1093/aob/mcaa132

Bopp, S., and Gottsberger, G. (2004). Importance of *Silene latifolia* ssp *alba* and *S. dioica* (Caryophyllaceae) as host plants of the parasitic pollinator *Hadena bicruris* (Lepidoptera, Noctuidae). *Oikos* 105, 221–228. doi: 10.1111/j.0030-1299.2004.12625.x

Borg-Karlson, A., Groth, I., Ågren, L., and Kullenberg, B. (1993). Form-specific fragances from *Ophrys insectifera* L. (Orchidaceae) attract species of different pollinator genera. Evidence of sympatric speciation? *Chemoecology* 4, 39–45. doi: 10.1007/BF01245895

Chen, G., Liu, C., and Sun, W. (2016). Pollination and seed dispersal of *Aquilaria sinensis* (Lour.) Gilg (Thymelaeaceae): an economic plant species with extremely small populations in China. *Plant Divers.* 38, 227–232. doi: 10.1016/j.pld.2016.09.006

Cheng, J., Wang, C. Y., Lyu, Z. H., Chen, J. X., Tang, L. P., and Lin, T. (2019). Candidate olfactory genes identified in *Heortia vitessoides* (Lepidoptera: Crambidae) by antennal transcriptome analysis. *Comp. Biochem. Phys. - Part D* 29, 117–130. doi: 10.1016/j.cbd.2018.11.006

Doetterl, S., Juergens, A., Wolfe, L., and Biere, A. (2009). Disease status and population origin effects on floral scent: potential consequences for oviposition and fruit predation in a complex interaction between a plant, fungus, and noctuid moth. *J. Chem. Ecol.* 35, 307–319. doi: 10.1007/s10886-009-9601-0

Domínguez, I., Arrebola, F. J., Romero-González, R., Nieto-García, A., Martínez Vidal, J. L., and Garrido Frenich, A. (2017). Solid phase microextraction and gas chromatography coupled to magnetic sector high resolution mass spectrometry for the ultra-trace determination of contaminants in surface water. *J. Chromatogr. A* 1518, 15–24. doi: 10.1016/j.chroma.2017.08.061

Dötterl, S., Jahreiß, K., Jhumur, U. S., and Jürgens, A. (2012). Temporal variation of flower scent in *Silene otites* (Caryophyllaceae): a species with a mixed pollination system. *Bot. J. Linn. Soc.* 169, 447–460. doi: 10.1111/j.1095-8339.2012.01239.x

Dudareva, N., and Negre, F. (2005). Practical applications of research into the regulation of plant volatile emission. *Curr. Opin. Plant Biol.* 8, 113–118. doi: 10.1016/j.pbi.2004.11.007

Eby, C., Gardiner, M. G. T., Gries, R., Judd, G. J. R., Khaskin, G., and Gries, G. (2013). Phenylacetaldehyde attracts male and female apple clearwing moths, *Synanthedon myopaeformis*, to inflorescences of showy milkweed, *Asclepias speciosa*. *Entomol. Exp. Appl.* 147, 82–92. doi: 10.1111/eea.12045

Ho, C. W., Aida, W. W., Maskat, M. Y., and Osman, H. (2006). Optimization of headspace solid phase microextraction (HS-SPME) for gas chromatography mass spectrometry (GC-MS) analysis of aroma compound in palm sugar (*Arenga pinnata*). *J. Food Compos. Anal.* 19, 822–830. doi: 10.1016/j.jfca.2006.05.003

Issa, M. Y., Mohsen, E., Younis, I. Y., Nofal, E. S., and Farag, M. A. (2020). Volatiles distribution in jasmine flowers taxa grown in Egypt and its commercial products as analyzed via solid-phase microextraction (SPME) coupled to chemometrics. *Ind. Crop Prod* 144, 112002. doi: 10.1016/j.indcrop.2019.112002

Kessler, D., Gase, K., and Baldwin, I.T. (2008). Field experiments with transformed plants reveal the sense of floral scents. *Science* 321, 1200–1202. doi: 10.1126/science.1160072

Klatt, B. K., Burmeister, C., Westphal, C., Tscharntke, T., and von Fragstein, M. (2013). Flower volatiles, crop varieties and bee responses. *PloS One* 8, e72724. doi: 10.1371/journal.pone.0072724

Knudsen, J.T., Eriksson, R., Gershenzon, J., and Stahl, B. (2006). Diversity and distribution of floral scent. *Bot. Rev.* 72, 1–120. doi: 10.1663/0006-81

Liang, M., Zhang, Z. M., Wu, Y. J., Wang, R., and Liu, Y. P. (2022). Comparison of *Amomum tsaoko* crevost et Lemaire from four regions via headspace solid-phase microextraction: Variable optimization and volatile characterization. *Ind. Crop Prod* 191, 115924. doi: 10.1016/j.indcrop.2022.115924

Ma, Q. L., Hamid, N., Bekhit, A. E. D., Robertson, J., and Law, T. F. (2013). Optimization of headspace solid phase microextraction (HS-SPME) for gas chromatography mass spectrometry (GC–MS) analysis of aroma compounds in cooked beef using response surface methodology. *Microchem. J.* 111, 16–24. doi: 10.1016/j.microc.2012.10.007

Ma, T., Liu, Z. T., Zhang, Y. Y., Sun, Z. H., Li, Y. Z., Wen, X. J., et al. (2015). Electrophysiological and behavioral responses of *Diaphania glauculalis* males to female sex pheromone. *Environ. Sci. pollut. Res.* 22, 15046–15054. doi: 10.1007/s11356-015-4711-4

Magsi, F., Zongxiu, L., Yingjie, Z., Li, Z., Cai, X., Lei, B., et al. (2021). Electrophysiological and behavioral responses of *Dasychira baibarana* (Lepidoptera: Lymantriidae) to tea plant volatiles. *Environ. Entomol* 50, 589–598. doi: 10.1093/ee/nvab016

Marinaki, M., Sampsonidis, I., Lioupi, A., Arapitsas, P., Thomaidis, N., Zinoviadou, K., et al. (2023). Development of two-level Design of Experiments for the optimization of a HS-SPME-GC-MS method to study Greek monovarietal PDO and PGI wines. *Talanta* 253, 123987. doi: 10.1016/j.talanta.2022.123987

Mu, X. Q., Lu, J., Gao, M. X., Li, C. W., and Chen, S. (2021). Optimization and validation of a headspace solid-phase microextraction with comprehensive two-dimensional gas chromatography time-of-flight mass spectrometric detection for quantification of trace aroma compounds in Chinese liquor (Baijiu). *Molecules* 26, 6910. doi: 10.3390/molecules26226910

Muñoz-Redondo, J. M., Ruiz-Moreno, M. J., Puertas, B., Cantos-Villar, E., and Moreno-Rojas, J. M. (2020). Multivariate optimization of headspace solid-phase microextraction coupled to gas chromatography-mass spectrometry for the analysis of terpenoids in sparkling wines. *Talanta* 208, 120483. doi: 10.1016/j.talanta.2019.120483

Muñoz-Redondo, J. M., Valcárcel-Muñoz, M. J., Rodríguez Solana, R., Puertas, B., Cantos-Villar, E., and Moreno-Rojas, J. M. (2022). Development of a methodology based on headspace solid-phase microextraction coupled to gas chromatography-mass spectrometry for the analysis of esters in brandies. *J. Food. Compost. Anal.* 108, 104458. doi: 10.1016/j.jfca.2022.104458

Oliveira, L. F. C., Tega, D. U., Duarte, G. H. B., Barbosa, L. D., Ribeiro, H. C., Castello, A. C. D., et al. (2022). Foodomics for agroecology: Differentiation of volatile profile in mint (*Mentha* × *gracilis* Sole) from permaculture, organic and conventional agricultural systems using HS-SPME/GC-MS. *Food Res. Int.* 155, 111107. doi: 10.1016/j.foodres.2022.111107

Pati, S., Tufariello, M., Crupi, P., Coletta, A., Grieco, F., and Losito, I. (2021). Quantification of volatile compounds in wines by HS-SPME-GC/MS: critical issues and use of multivariate statistics in method optimization. *Processes* 9, 622. doi: 10.3390/pr9040662

Pawliszyn, J., Risticevic, S., Lord, H., Gorecki, T., and Arthur, C. L. (2010). Protocol for solid-phase microextraction method development. *Nat. Protoc.* 5, 122–139. doi: 10.1038/nprot.2009.179

Pichersky, E., and Gershenzon, J. (2002). The formation and function of plant volatiles: perfumes for pollinator attraction and defense. *Curr. Opin. Plant Biol.* 5, 237–243. doi: 10.1016/S1369-5266(02)00251-0

Pico, J., Nozadi, K., Gerbrandt, E. M., Dossett, M., and Castellarin, S. D. (2022). Determination of bound volatiles in blueberries, raspberries, and grapes with an optimized protocol and a validated SPME-GC/MS method. *Food Chem.* 403, 134304. doi: 10.1016/j.foodchem.2022.134304

Piri-Moghadam, H., Alam, M. N., and Pawliszyn, J. (2017). Review of geometries and coating materials in solid phase microextraction: Opportunities, limitations, and future perspectives. *Anal. Chim. Acta* 984, 42–65. doi: 10.1016/j.aca.2017.05.035

Powers, J. M., Seco, R., Faiola, C. L., Sakai, A. K., Weller, S. G., Campbell, D. R., et al. (2020). Floral scent composition and fine-scale timing in two moth-pollinated *Hawaiian Schiedea* (Caryophyllaceae). *Front. Plant Sci.* 11. doi: 10.3389/fpls.2020.01116

Qiao, H. L., Lu, P. F., Chen, J., Ma, W. S., Qin, R. M., and Li, X. M. (2012). Antennal and behavioural responses of *Heortia vitessoides* females to host plant volatiles of *Aquilaria sinensis*. *Entomol. Exp. Appl.* 143, 269–279. doi: 10.1111/j.1570-7458.2012.01264.x

Raguso, R. A., and Pichersky, E. (1999). New perspectives in pollination biology: floral fragrances. A day in the life of a linalool molecule: Chemical communication in a plant-pollinator system. Part 1: Linalool biosynthesis in flowering plants. *Plant Spec. Biol.* 14, 95–120. doi: 10.1046/j.1442-1984.1999.00014.x

Rajhi, I., Baccouri, B., Rajhi, F., Hammami, J., Souibgui, M., Mhadhbi, H., et al. (2022). HS-SPME-GC-MS characterization of volatile chemicals released from microwaving and conventional processing methods of fenugreek seeds and flours. *Ind. Crops Prod* 182, 114824. doi: 10.1016/j.indcrop.2022.114824

Reisenman, C. E., Riffell, J. A., Bernays, E. A., and Hildebrand, J. G. (2010). Antagonistic effects of floral scent in an insect-plant interaction. *Proc. R. Soc B* 277, 2371–2379. doi: 10.1098/rspb.2010.0163

Schiestl, F. P., Huber, F. K., and Gomez, J. M. (2011). Phenotypic selection on floral scent: trade-off between attraction and deterrence? *Evol. Ecol.* 25, 237–248. doi: 10.1007/s10682-010-9409-y

Steen, R., Norli, H. R., and Thöming, G. (2019). Volatiles composition and timing of emissions in a moth-pollinated orchid in relation to hawkmoth (Lepidoptera: Sphingidae) activity. *Arthropod Plant Interact.* 13, 581–592. doi: 10.1007/s11829-019-09682-3

van der Niet, T., Jürgens, A., and Johnson, S. D. (2015). Is the timing of scent emission correlated with insect visitor activity and pollination in long-spurred Satyrium species? *Plant Biol.* 17, 226–237. doi: 10.1111/plb.12196

Waelti, M. O., Page, P. A., Widmer, A., and Schiestl, F. P. (2009). How to be an attractive male: floral dimorphism and attractiveness to pollinators in a dioecious plant. *BMC Evol. Biol.* 9, 190. doi: 10.1186/1471-2148-9-190

Wang, Y., Hussain, M., Jiang, Z., Wang, Z., Gao, J., Ye, F., et al. (2021). *Aquilaria* species (Thymelaeaceae) distribution, volatile and non-volatile phytochemcals, pharmacological uses, agarwood grading system, and induction methods. *Molecules* 26, 7708. doi: 10.3390/molecules26247708

Wei, S., Xiao, X., Wei, L., Li, L., Li, G., Liu, F., et al. (2020). Development and comprehensive HS-SPME/GC-MS analysis optimization, comparison, and evaluation of different cabbage cultivars (*Brassica oleracea* L. var. *capitata* L.) volatile components. *Food Chem.* 340, 128166. doi: 10.1016/j.foodchem.2020.128166

Yan, J., Wang, G., Sui, Y., Wang, M., and Zhang, L. (2016). Pollinator responses to floral colour change, nectar and scent promote reproductive fitness in *Quisqualis indica* (Combretaceae). *Sci. Rep.* 6, 24408. doi: 10.1038/srep24408

Zhang, C., Liu, H., Hu, S., Zong, Y., Xia, H., and Li, H. (2022). Transcriptomic profiling of the floral fragrance biosynthesis pathway of Liriodendron and functional characterization of the LtuDXR gene. *Plant Sci.* 314, 111124. doi: 10.1016/j.plantsci.2021.111124

Zhang, Z., and Pawliszyn, J. (1993). Headspace solid-phase microextraction. *Anal. Chem.* 65, 1843–1852. doi: 10.1021/ac00062a008

Zhou, W., Kuegler, A., McGale, E., Haverkamp, A., Knaden, M., Guo, H., et al. (2017). Tissue-specific emission of (*E*)-alpha-bergamotene helps resolve the dilemma when pollinators are also herbivores. *Curr. Biol.* 27, 1336–1341. doi: 10.1016/j.cub.2017.03.017

Zhou, L., Yu, C., Cheng, B., Wan, H., Luo, L., Pan, H., et al. (2020). Volatile compound analysis and aroma evaluation of tea-scented roses in China. *Ind. Crops Prod* 155, 112735. doi: 10.1016/j.indcrop.2020.112735

frontiers | Frontiers in Plant Science

TYPE Original Research
PUBLISHED 18 September 2024
DOI 10.3389/fpls.2024.1467957

OPEN ACCESS

EDITED BY
Bo Sun,
Sichuan Agricultural University, China

REVIEWED BY
Yanjie Zhang,
Zhengzhou University, China
Xiaoming Song,
North China University of Science and Technology, China

*CORRESPONDENCE
Guang-Long Wang
11160021@hyit.edu.cn
Ai-Sheng Xiong
xiongaisheng@njau.edu.cn

RECEIVED 21 July 2024
ACCEPTED 02 September 2024
PUBLISHED 18 September 2024

CITATION
Wang G-L, Wu J-Q, Chen Y-Y, Xu Y-J, An Y-H, Ren X-Q and Xiong A-S (2024) Integrated volatile metabolome and transcriptome analyses provide insights into the warm aroma formation elicited by methyl jasmonate in carrot root. *Front. Plant Sci.* 15:1467957. doi: 10.3389/fpls.2024.1467957

Integrated volatile metabolome and transcriptome analyses provide insights into the warm aroma formation elicited by methyl jasmonate in carrot root

Guang-Long Wang[1,2*], Jia-Qi Wu[1], Yang-Yang Chen[1], Yu-Jie Xu[1], Ya-Hong An[1], Xu-Qin Ren[1,2] and Ai-Sheng Xiong[3*]

[1]School of Life Science and Food Engineering, Huaiyin Institute of Technology, Huaian, China, [2]Jiangsu Provincial Agricultural Green and Low Carbon Production Technology Engineering Research Center, Huaiyin Institute of Technology, Huaian, China, [3]State Key Laboratory of Crop Genetics & Germplasm Enhancement and Utilization, College of Horticulture, Nanjing Agricultural University, Nanjing, China

Carrot is a highly significant vegetable cultivated worldwide and possesses a unique aroma with abundant edible and medicinal values. However, it remains largely unknown whether jasmonic acid could regulate aroma formation in carrot. Here, an integrated analysis of the volatile metabolome and transcriptome of carrot roots exposed to different concentrations of methyl jasmonate (MeJA) was performed. The results revealed 1,227 volatile organic compounds and 972 differential accumulated metabolites, with terpenes representing the largest portion. MeJA treatment evidently increased the relative odor activity values as well as the accumulation of most volatile compounds. In addition, 4,787 differentially expressed genes were identified and subjected to function enrichment analysis, indicating a role of terpene biosynthesis and metabolism in response to MeJA application. A network consisting of 4,680 transcription factor-structural pairs that showed highly significant positive correlations was constructed, which may be utilized as genetic targets for examining terpene accumulation and aroma formation elicited by methyl jasmonate. The results from the present work substantially improved our understanding of MeJA-mediated aroma formation in carrot.

KEYWORDS

volatile metabolome, transcriptome, MeJA, terpenes, transcription-structural genes, carrot

Introduction

Plant volatile organic compounds (VOCs) are a class of volatile products generated during metabolic processes, mainly consisting of terpenoids, alcohols, aldehydes, ketones, esters, phenols, and organic acids (Abbas et al., 2022; Brosset and Blande, 2022). The composition and proportion of these compounds contribute to a special aroma of each plant species. The types and contents of plant VOCs vary in response to different metabolic processes and enzyme catalysis, resulting in different VOC characteristics in different plants or the same plant at different physiological states or developmental stages (Bao et al., 2023; Dady et al., 2023). They play an important role in attracting pollinators and seed spreaders, resisting against biotic and abiotic attack, as well as in signal transduction between plants (Hu, 2022; Kessler et al., 2023; Ninkovic et al., 2021). Therefore, studying plant VOCs can not only help to understand plant physiology and metabolism characteristics, but also provide theoretical basis and practical guidance for biological control of plant diseases and pests, and promote innovation and development of plant germplasm resources with special aroma.

Unlike the aboveground parts, there is still a lack of research on the types and regulation of volatile metabolites in plant roots. However, for many root vegetables, volatile metabolites determine the quality of the product and affect people's preference and ways of consumption to some extent. In radish, sulfur and nitrogen-containing compounds were deemed to play an important role in flavor formation, with diallyl sulfide and dimethyl disulfide being the primary sulfides responsible for the unpleasant flavor in radish (Gamba et al., 2021; Cai et al., 2024). In fresh turnip, isothiocyanato-cyclopropane and (2-isothiocyanatoethyl)-benzene were identified as the predominant volatiles (Xue et al., 2020). These studies have increased our understanding of volatile compounds in root vegetables, but the accumulation patterns and regulatory mechanisms of these substances under specific conditions in root vegetables are still unclear.

Carrots are a nutritious root vegetable belonging to the family Apiaceae, which are annual or biennial herbaceous plants. It is abundant in various nutrients such as carotene, ascorbate, and dietary fibre, and has various health benefits such as protecting vision, enhancing immunity, and promoting digestion and absorption of human bodies (Deng et al., 2023; Duan et al., 2024; Loarca et al., 2024). Whether eaten raw, cooked, or juiced, carrots can bring health and deliciousness to people. Therefore, carrots play an important role in daily diet and are deeply loved by people. Carrots not only have high nutritional value, but also have a pleasant flavor (Muchlinski et al., 2020; Yahyaa et al., 2018). The aroma of carrots comes from the volatile compounds within carrot plants, which give them a unique aroma. This odor may vary slightly due to factors such as carrot variety, tissues, growth environment, and maturity (Fukuda et al., 2013). These compounds mainly consist of α-pinene, β-myrcene, limonene, (E)-β-caryophyllene, γ-terpinene, bornyl acetate, and cymene, most of which belong to the terpenoids (Quarrell et al., 2023; Tian et al., 2024). It is reported that terpenoids account for nearly 98% of the VOCs in carrot tissues.

Jasmonic acid (JA) is an endogenous growth regulator present in higher plants and is a derivative of fatty acids (Li et al., 2022). It is widely present in plant tissues and organs such as flowers, stems, leaves, and roots, and plays an important role during plant growth and development processes (Li et al., 2021; Nguyen et al., 2022). JA is involved in root elongation, flower development, leaf senescence, stomatal opening and closing, epidermal hair initiation (Chang et al., 2024; Furuta et al., 2024; Han et al., 2023b). In addition, JA can mediate plant resistance against insects and pathogens and regulate plant response to stress such as drought, high temperature, ozone, and ultraviolet radiation (Escobar-Bravo et al., 2019; Raza et al., 2021; Zhao et al., 2024). Further studies have shown that JA can also induce the accumulation of secondary metabolites, such as anthocyanins and flavonoids, which in turn contribute to the formation of crop quality (Fang et al., 2023; Wang et al., 2022).

Although the roles of JA in VOC accumulation have been discovered in some plant species, whether JA could induce enhanced aroma formation in carrot is still unclear. Here, we evaluated the dynamics of VOC accumulation in carrot plants exposed to exogenous methyl jasmonate (MeJA). In addition, we focused on the changes of terpenoids, the characteristic volatile substances of carrots, during this process, and analyzed the structural genes and regulatory factors that regulate the synthesis of terpenoids. We constructed a possible regulatory network of MeJA-mediated terpenoid accumulation in carrots. The results of the current study may lay foundation for the research on JA-regulated volatile accumulation and offer new genetic resources and targets for quality regulation in crops.

Materials and methods

Plant materials and experimental design

'Kurodagosun' is a carrot variety with high yield and quality, and is widely cultivated in Asia. It has an orange color on the root surface with a dense texture in the flesh. In this study, the seeds of carrot variety 'Kurodagosun' were sown in pots holding a mixture of vermiculite and organic matter, and were transferred to a greenhouse for seedling rearing. After 38 d, each pot was sprayed with 300 mL of 100 μM MeJA (MeJA100), 200 μM MeJA (MeJA200), and 10 mM sodium diethyldithiocarbamate trihydrate (DIECA, a JA biosynthesis inhibitor) weekly via root irrigation, with clean water (CK) as the control. Carrot plants were totally exposed to different concentration of MeJA five times, and the carrot fleshy root samples from different treatments were respectively collected at 70 days after sowing. The harvested samples were immediately frozen in liquid nitrogen and stored in an ultra-low temperature freezer for further analysis.

Sample preparation and GC-MS analysis of VOCs

The collected carrot root samples were ground into a fine powder in liquid nitrogen. Approximately 0.5 g of the powder was immediately transferred to a 20 mL head-space vial (Agilent, Palo Alto, CA, USA) harboring a saturated NaCl solution to inhibit enzyme reaction. The crimp-top caps equipped with TFE-silicone headspace septa (Agilent) were introduced to tightly seal the vials.

For SPME analysis, each vial was placed in a 60°C environment and vibrated for 5 min, followed by headspace extraction for 15 min at 60°C with insertion of an Agilent 120 μm DVB/CWR/PDMS fibre (CA, USA). Desorption of the VOCs from the fibre coating was implemented at 250°C for 5 min in the splitless mode.

The volatile metabolites were identified and determined by an Agilent Model 8890 GC and a 7000D mass spectrometer (Agilent), equipped with a 30 m × 0.25 mm × 0.25 μm DB-5MS (5% phenyl-polymethylsiloxane) capillary column. High-purity helium was utilized as the carrier gas at a linear velocity of 1.2 mL/min, with the temperature of the injector maintained at 250°C. The temperature gradient of the oven was set as described by a previous report (Wang et al., 2021). Mass spectra were noted in the electron impact ionization mode at 70 eV. The temperatures of quadrupole mass detector, ion source, and transfer line were adjusted to 150, 230, and 280°C, respectively. The selected ion monitoring (SIM) mode was applied for the precise identification and quantification of analytes. Volatile organic compounds were differentiated by comparing the mass spectra with the data system library (MWGC or NIST) and linear retention index. The average values of each metabolite in different treatment groups were generated from six biological samples (Supplementary Table 1). Compounds with a fold change ≥ 2 or ≤ 0.5 in contents and variable importance in project (VIP) > 1 were referred to differential metabolites (Supplementary Table 2). The principal component analysis (PCA) and K-Means clustering were carried out by R base package with data scaled by unit variance.

Transcriptome sequencing

Transcriptome sequencing data of each treatment group were produced from three biological replicates. Total RNA from carrot root samples was isolated by ethanol precipitation and CTAB-PBIOZOL and dissolved with 50 μL of DEPC-treated water. Subsequently, a Qubit fluorescence quantifier and a Qsep400 high-throughput biofragment analyzer were adopted to identify and quantify RNA concentration and integrity. To construct a cDNA library, mRNAs with polyA tails were enriched by Oligo(dT) magnetic beads, since most eukaryotic mRNAs harbor a polyA tail. Subsequently, a fragmentation buffer was added to break the RNA into short fragments, which was then used as a template to synthesize the first strand cDNA with random hexamer primers. Then, buffer solution, dNTPs, and DNA polymerase were added to yield the second strand cDNA. The purified second strand cDNA was subjected to end repair, dA-Tailing, and adapter ligation. Then, DNA magnetic bead purification, fragment selection, and ligated product PCR amplification were carried out to obtain the final cDNA library. After library inspection, different libraries were pooled according to the target output data volume and sequenced using the Illumina NovaSeq 6000 sequencing platform by Metware Biotechnology Co., Ltd. (Wuhan, China). The generated raw reads were uploaded in the NCBI Sequence Read Archive (SRA) database with a Bioproject accession number PRJNA1150744.

Differentially expressed genes identification

The raw data were filtered by removing reads below the quality cutoff. Then the generated clean data were mapped to the reference genome (https://ftp.ensemblgenomes.ebi.ac.uk/pub/plants/release-55/fasta/daucus_carota/dna) using HISAT2 software. The genes with an absolute value of log2 fold change ≥ 1 were recognized as differentially expressed genes (DEGs). The DEGs were then subjected to functional annotation and enrichment analysis, such as k-means, GO enrichment. The gene co-expression network ($P \leq 0.01$, $r \geq 0.9$) between transcription factors (TFs) and terpenoid synthase genes was visualized by using Cytoscape (v.3.9.1) software.

Quantitative real-time PCR validation

To determine the accuracy of the expression trends of candidate genes from RNA-seq, quantitative real-time PCR (qRT-PCR) was introduced. In brief, the synthesis of cDNA was strictly carried out according to the instructions of the HiScript II QRT SuperMix for qPCR (Nanjing Novozymes Biotechnology Co., Ltd.) reverse transcription kit. The primers designed for qRT-PCR were displayed in Supplementary Table 3. The reactions were performed on a CFX96 fluorescence quantitative PCR instrument (Bio Rad, USA) using carrot *DcACTIN* as an internal reference gene (Tian et al., 2015). The specific operation programmes strictly conformed to the Cham Q SYBR qPCR Master Mix kit and its instructions provided by Nanjing Novozymes Biotechnology Co., Ltd. The relative expression levels of the target genes in different samples were determined using the $2^{-\Delta\Delta CT}$ method (Livak and Schmittgen, 2001).

Results

Metabolite analysis in the MeJA-treated root samples

A total of 1227 VOCs were identified in 12 samples (four groups with three biological replicates). In terms of their chemical structures, these VOCs can be divided into 16 groups (Figure 1). Among them, terpenoids accounted for the largest group, followed by esters, heterocyclic compounds, alcohols, and ketones. It is convenient to gain a preliminary understanding of the overall metabolite differences across all groups and the variability magnitude among samples within the same group by conducting principal component analysis (PCA). The PCA results, showing the trend of metabolome separation among groups, indicated there were no evident differences detected in metabolome within the sample groups (Figure 2). Compared with the control group, the relative odor activity value (rOAV) was obviously higher in MeJA-treated carrots, whereas a slight a decrease was observed in root samples exposed to DIECA (Figure 3).

10.3389/fpls.2024.1467957

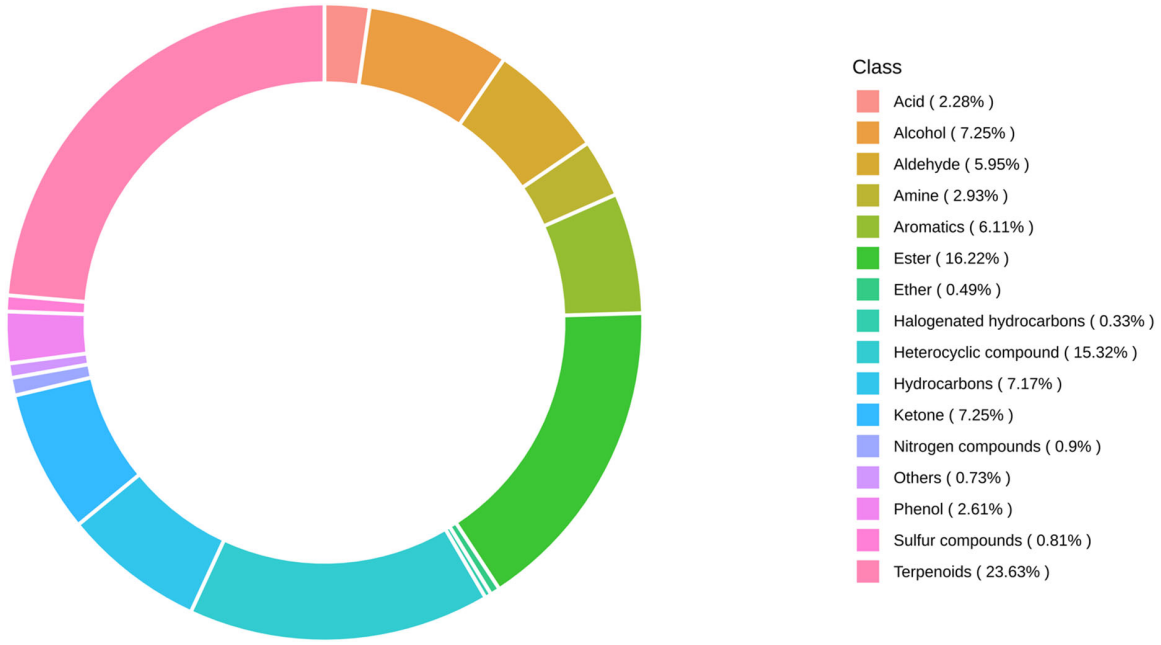

FIGURE 1
Distribution of volatile organic compounds in carrot root samples exposed to MeJA.

Characterization and function analysis of differential metabolites

To characterize the dynamic changes of metabolites in response to MeJA application, comparison of the volatile metabolites among the four samples (CK, MeJA100, MeJA200, and DIECA) was carried out (Figure 4). There were 530, 490, 26, 68, and 99 up-regulated and 63, 124, 330, 771, and 687 down-2regulated volatile compounds detected in "CK vs MeJA100", "CK vs MeJA200", "CK vs DIECA", "MeJA100 vs DIECA" and "MeJA200 vs DIECA" comparisons. Obviously, Exogenous MeJA application substantially increased the accumulation of volatile metabolites, whereas DIECA did the opposite. Totally, 972 differential metabolites were determined

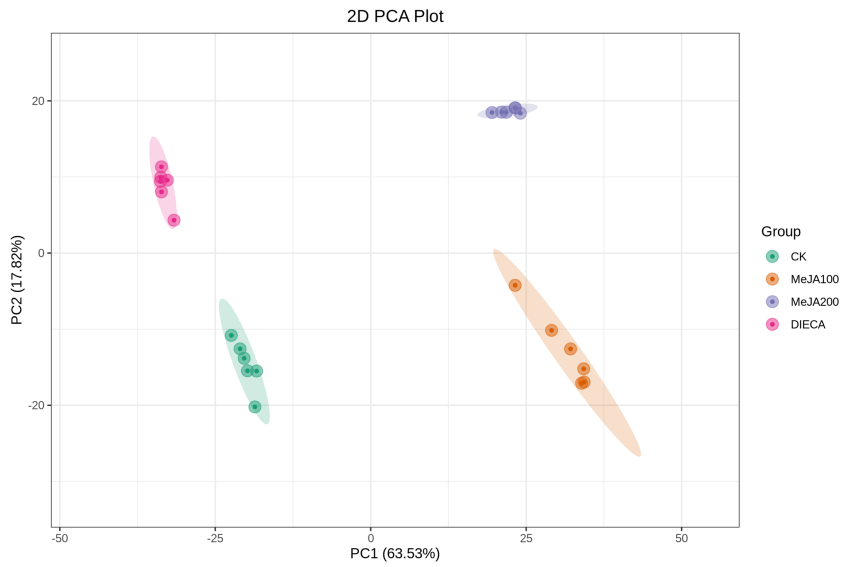

FIGURE 2
PCA analysis of the MeJA-treated samples. PC1 and PC2 represented the first and second principal component, respectively, whereas percentages indicated the explanatory power of these principal components on the dataset. Each point in the figure stood for a biological sample, and samples from the same group were represented by the same color.

10.3389/fpls.2024.1467957

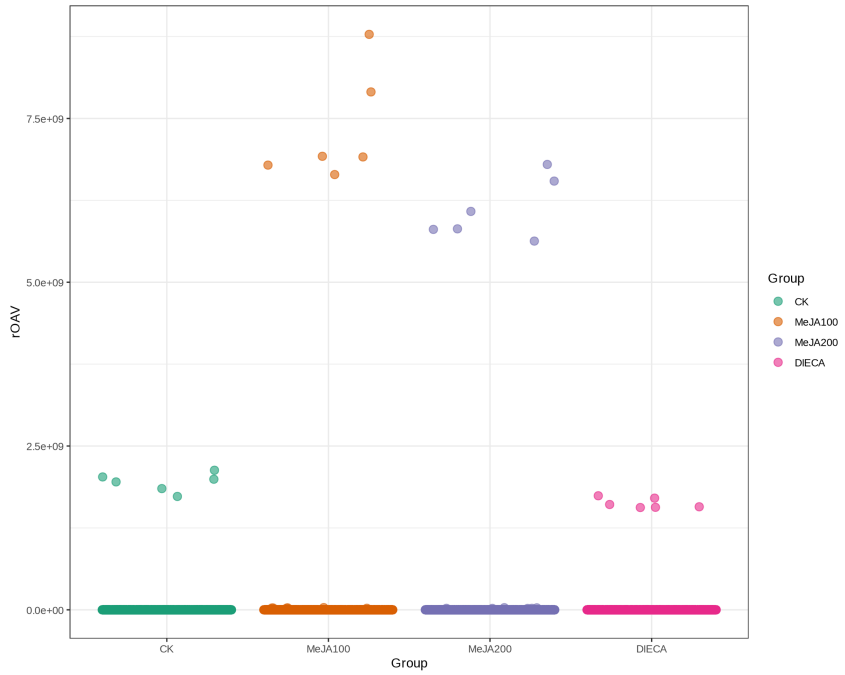

FIGURE 3
Scatter plot of relative odor activity values for MeJA-treated root samples. The horizontal axis represented different groups, whereas the vertical axis indicated the rOAVs of flavor compounds.

among the five comparisons, accounting for 79.22% of all the volatile compounds detected (Figure 5). Among them, 159 metabolites differed in concentrations across all the comparisons. Then, the differentially accumulated metabolites were then visualized by a heat map (Figure 6). The figure showed that the concentrations of most of the differential metabolites were the highest in MeJA-treated groups, whereas the lowest levels were detected in the plants exposed to DIECA, an inhibitor for JA biosynthesis. To further excavate the general accumulation trends of VOCs in response to MeJA treatment, the K-means clustering algorithm was introduced to classify the different characteristics of the accumulation profiles of differential metabolites. Overall, six different accumulation classes (Class 1 to Class 6) were identified, with 277, 309, 98, 56, 165, and 67 members, respectively (Figure 7).

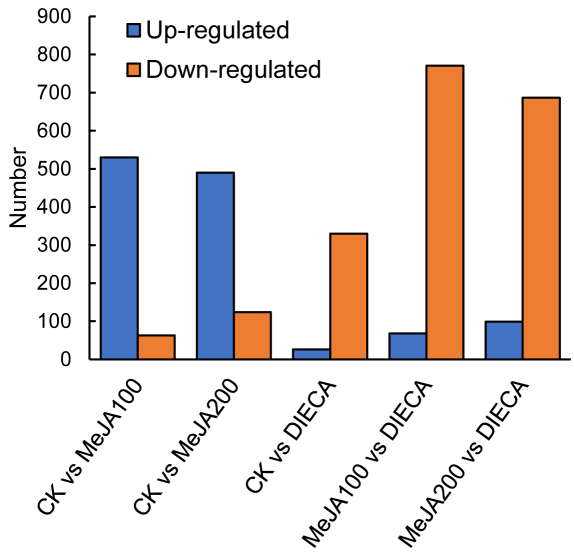

FIGURE 4
Comparison of differential accumulated metabolites between MeJA-treated groups.

10.3389/fpls.2024.1467957

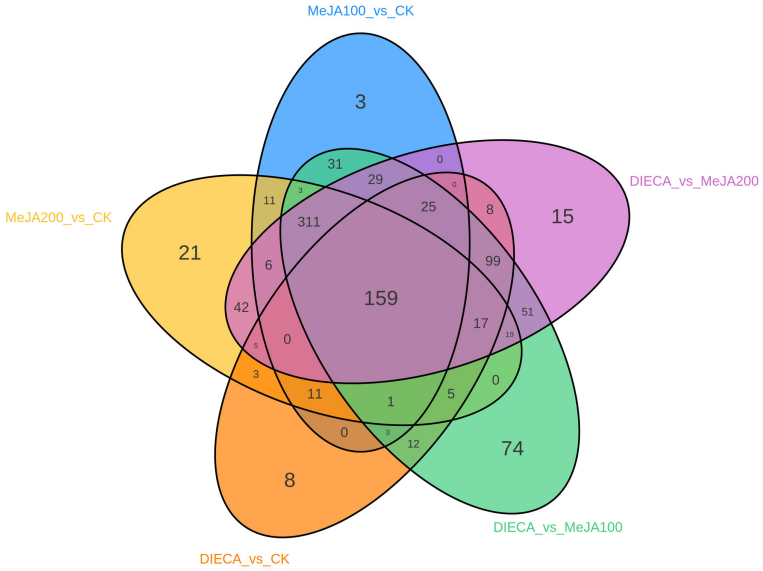

FIGURE 5
Venn diagram of distribution of differential metabolites in five comparisons.

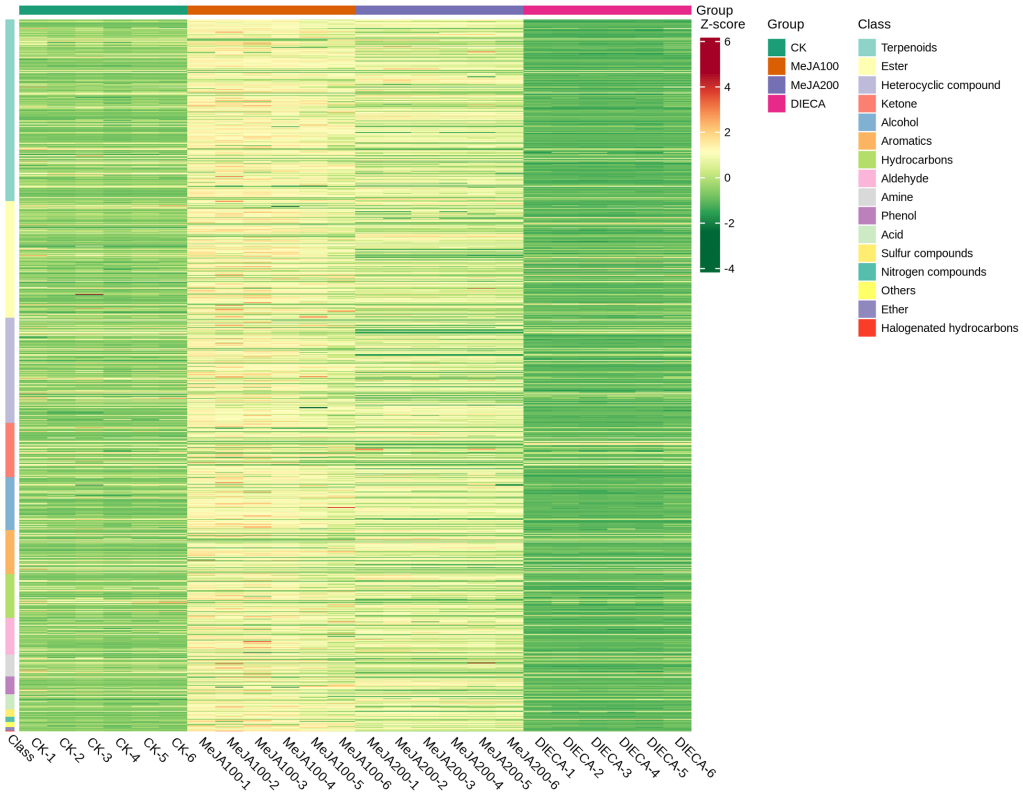

FIGURE 6
Heat map of the differential volatile metabolites in MeJA-treated carrot roots. The red and green represented high and low levels of metabolites, respectively.

Identification of the differentially expressed genes during MeJA treatment

The raw reads were filtered and mapped to the carrot reference genome (Supplementary Table 4). Approximately 90% of the clean reads of each sample were respectively mapped to the reference genome. Specifically, 2004, 1360, 943, 815, and 476 up-regulated and 664, 480, 678, 1829, and 1109 down-regulated genes were respectively determined in "CK vs MeJA100", "CK vs MeJA200", "CK vs DIECA", "MeJA100 vs DIECA" and "MeJA200 vs DIECA" comparisons. A total of 4,787 differentially expressed genes were identified in the various groups. The DEGs detected were then subjected to Gene Ontology (GO) enrichment analysis (Figure 8). In the biological process group, "isoprenoid metabolic process", "secondary metabolite biosynthetic process", and "isoprenoid biosynthetic process" were the most enriched terms, followed by "phenylpropanoid metabolic process", "regulation of defense response", "terpenoid metabolic process", and "terpenoid biosynthetic process". In the molecular function cluster, "monooxygenase activity" and "hexosyltransferase activity" were the most abundant terms. In order to further understand the expression profiles of DEGs among the MeJA treatments, k-means were utilized and the DEGs were apparently classified into 5 subcategories (Figure 9). Given the relative odor activity values and the metabolite accumulation patterns, the 2,386 DEGs from class 2 and 3 were further analyzed.

Analysis of the terpenoid accumulation and terpenoid synthase expression

It is reported that the specific aroma in carrot derived mainly from the terpenoids within carrot tissues. Under normal conditions, the most abundant terpenes determined were γ-E-bisabolene (WMW0052), caryophyllene (KMW0565), terpinolene (KMW0296), ocimene (KMW0252*154), bornyl acetate (WMW0016), β-pinene (KMW0193*119), m-cymene (XMW0126*016), and so on (Supplementary Table 1). It is obvious that the accumulation of most terpenoids examined was highest in MeJA-treated groups, which was similar to the change profiles observed in the relative odor activity value (Figure 7). Terpene synthases are capable of generating multiple terpenoid products with one substrate, thus largely resulting in numerous and different structures of plant terpenoids. Totally, 27 terpenoid synthase genes were found to be differentially expressed in response to MeJA application (Figure 10). Among them, 20 were distributed in clusters 2 and 3 during K-means analysis, corresponding to the change trends of most terpenoids.

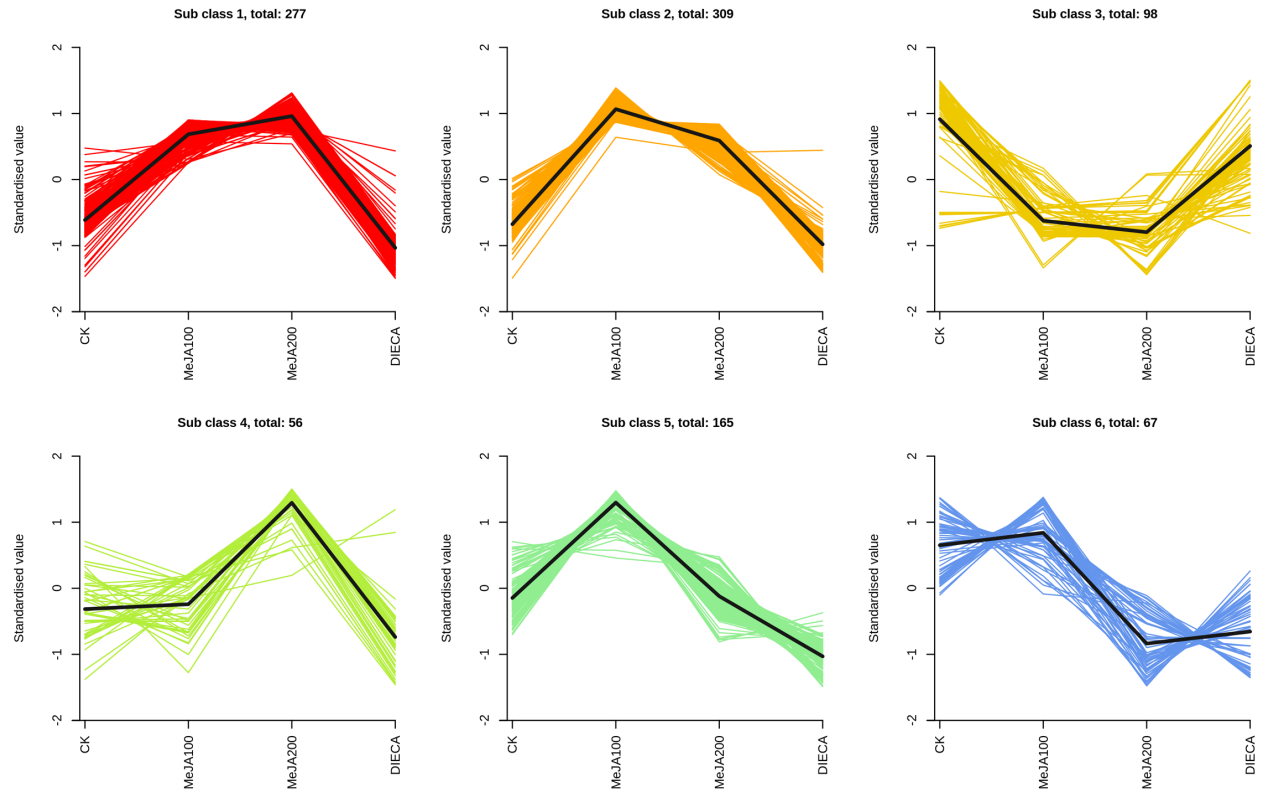

FIGURE 7
Six K-means clusters showed differential accumulated trends of volatile metabolites.

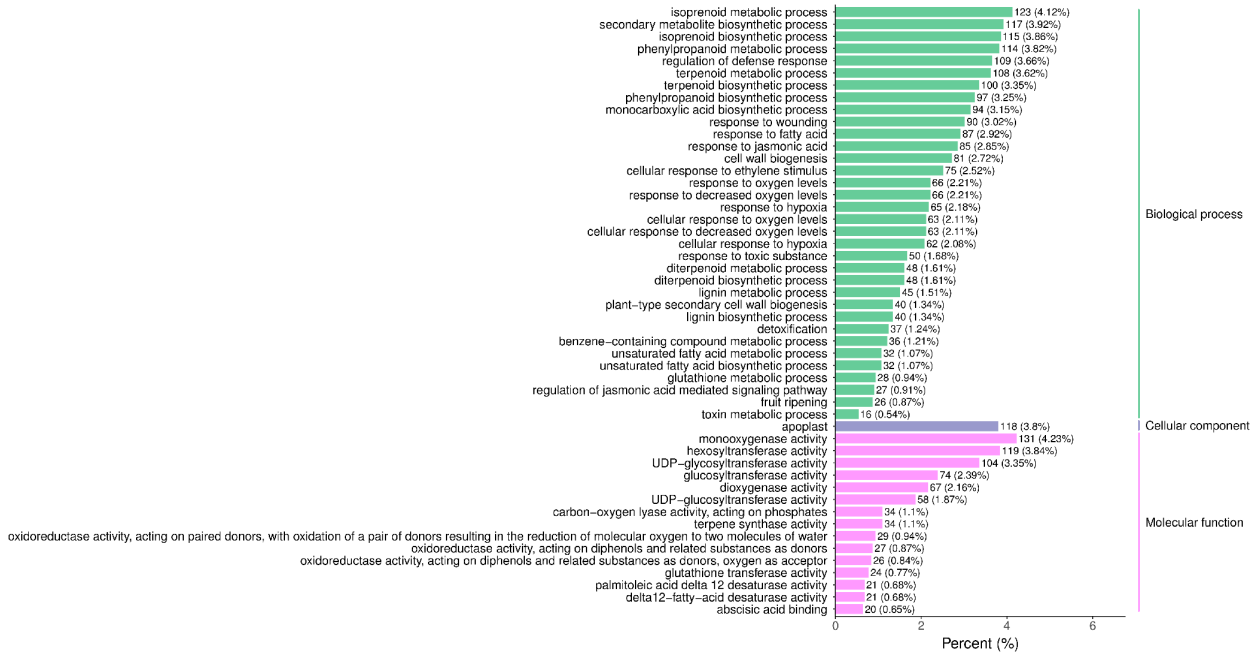

FIGURE 8
GO enrichment analysis of the differentially expressed genes. The top 50 GO terms with lowest p-value were displayed.

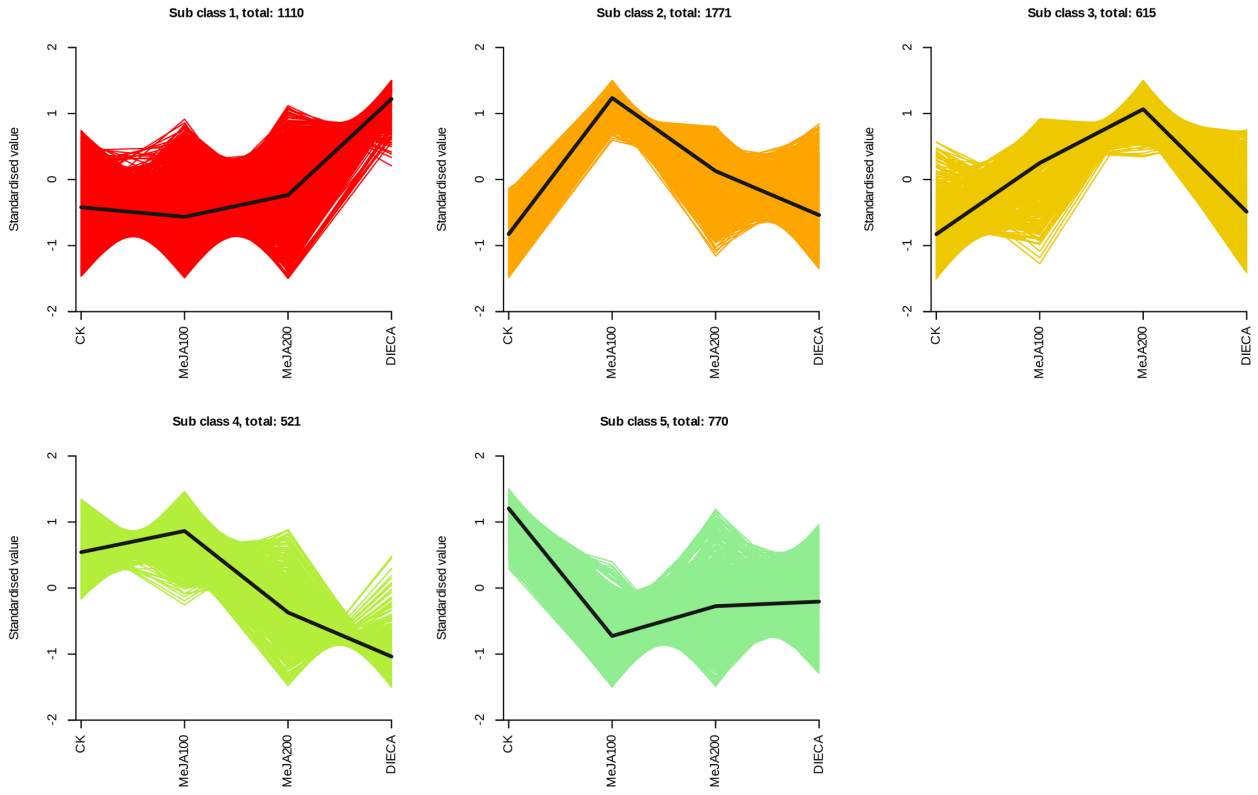

FIGURE 9
Different expression patterns of differentially expressed genes identified by K-means analysis.

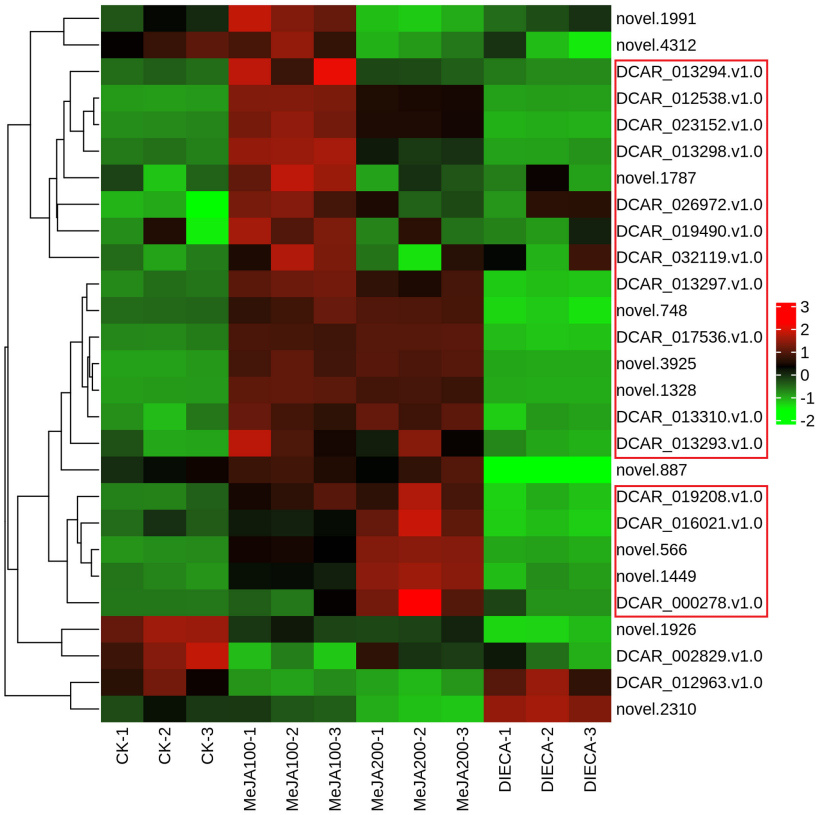

FIGURE 10
Heat map representing the expression of terpenoid synthase genes in different samples after MeJA application. The red and green indicated high and low expression, respectively.

Co-expression of candidate terpenoid synthase genes and related transcription factors

To further examine the possible roles of transcription factors (TFs) in regulating flavor formation during MeJA application, the correlation between 20 structural (terpenoid synthase) genes and TFs within the same clusters was investigated based on fragments per kilobase of transcript per million mapped reads (FPKM) values (Figure 11). The results generated a complex network consisting of 14 structural genes and 106 TFs with 4, 680 TF-structural pairs that showed highly significant positive correlations ($P \leq 0.01$, $r \geq 0.9$). The most enriched TFs are ERF, bHLH, and WRKY, followed by MYB, C2H2, and Tify, indicating that these TFs might be involved in JA-mediated terpenoid accumulation indirectly by manipulating the transcript levels of structural genes. To confirm the accuracy of the digital gene expression from RNA-seq, 9 genes (4 structural genes and 5 TF genes) within the network were randomly selected for qRT-PCR analysis (Figure 12). The relative gene expression of all genes determined was well correlated with the RNA-seq data, suggesting a high credibility of the transcriptome results.

Discussion

The aroma of horticultural products not only enriches people's sensory experience, but may also have health benefits, and is an important component of the quality of horticultural products (Abbas et al., 2023). Horticultural products possess a special odor because of various volatile compounds within the plants, which play important roles in plant growth and development, defense mechanisms, and attracting pollinators (Hu et al., 2021; Picazo-Aragonés et al., 2020; Sharifi et al., 2022). Different horticultural products emit their own unique aromas due to their cultivars, growth environments, maturity, and processing methods (Chen et al., 2023; Karabulut et al., 2018). These special odors not only make horticultural products more attractive, but also give them unique flavors and nutritional value. Understanding and utilizing these odor characteristics in horticultural planting and food processing can create a more diverse range of products and experiences. Carrots are an important vegetable crop widely grown worldwide and loved by consumers (Coe et al., 2023). The characteristic volatile compounds in carrots are one of their main features and have been hot issues in quality breeding and scientific

10.3389/fpls.2024.1467957

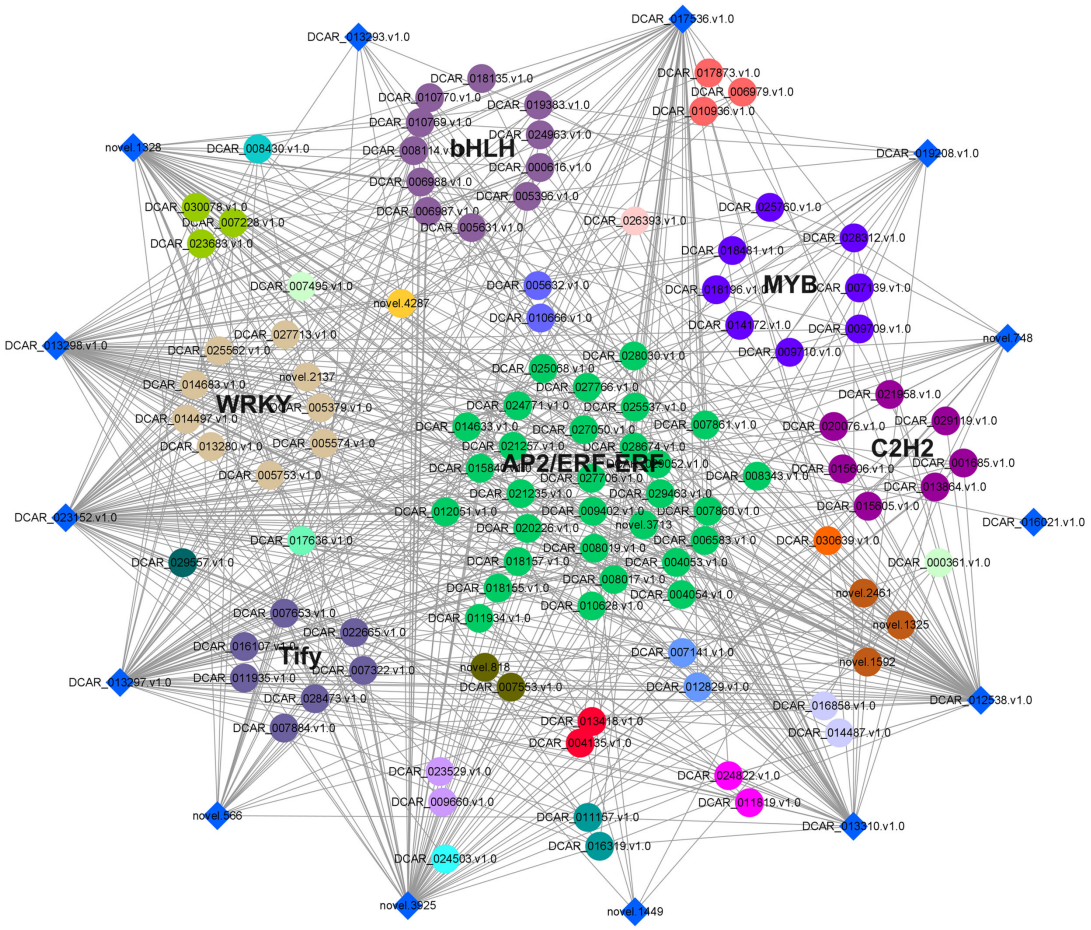

FIGURE 11
Co-expression network of TFs and terpenoid synthase genes in class 2 and 3 was constructed by Cytoscape (v.3.9.1) software. The diamonds around the periphery represented the structural genes, whereas different TF families were expressed as circles of different colors.

research in recent years. JA is an important regulatory factor in plant secondary metabolism, but can it regulate carrot flavor formation? What is its specific underlying mechanism? These issues have not yet been explained.

With the advancement and development of sequencing technology, people's opportunities to obtain information on volatile metabolites have further been increased. In recent years, integrated transcriptome and metabolic analyses had contributed to elucidating the molecular mechanisms controlling VOC accumulation. In grape, bZIPs, AP2/ERFs, MYBs, and NACs were found to be implicated in the regulation of stress-responsive volatile metabolites by integrated network analyses (Savoi et al., 2017). Similarly, an integrated analysis of the volatilomics and transcriptomics revealed that the MYB-related transcription factor LATE ELONGATED HYPOCOTYL (JsLHY) may be involved in regulating the aroma formation of jasmine flowers, which was further demonstrated to activate the gene promoter regions of six aroma-related structural genes (Zhou et al., 2023). These results indicated that integrated multi-omics analysis had been an effective way to identify candidate genes responsible for volatile formation and regulation.

It is reported that terpenes account for approximately most of the flavor attributes in carrot, and much effort was devoted to investigating terpenoid accumulation and regulation (Keilwagen et al., 2017; Reichardt et al., 2020). In this manuscript, many other volatile compounds including esters, heterocyclic compounds, alcohols, ketones, hydrocarbons, and aromatics, were identified, although terpenoids still occupied the first place. It should be pointed out that some terpenes may also be classified as aromatic hydrocarbons or heterocyclic compounds according to different classification criteria for compounds. The components and relative contents of terpenes may be different owing to various carrot varieties, thus contributing to distinct aroma formation (Yahyaa et al., 2015). For example, a previous work indicated that the volatiles in the Kuroda type were relatively lower compared with those of other carrot types (Fukuda et al., 2013). Here, the terpenes present in great quantity detected in the control group were ocimene, γ-E-bisabolene, and bornyl acetate, followed by terpinolene, caryophyllene, β-pinene, and m-cymene (Supplementary Table 1).

JA may increase the odor intensity of horticultural commodities by altering different volatile compounds. Spraying MeJA pre-harvest can improve the concentrations of phenolics, thus conferring reinforced tolerance to chilling and decay during storage (Serna-Escolano et al., 2019). MeJA treatment promoted volatile accumulation and increased the contents of monoterpenoids and

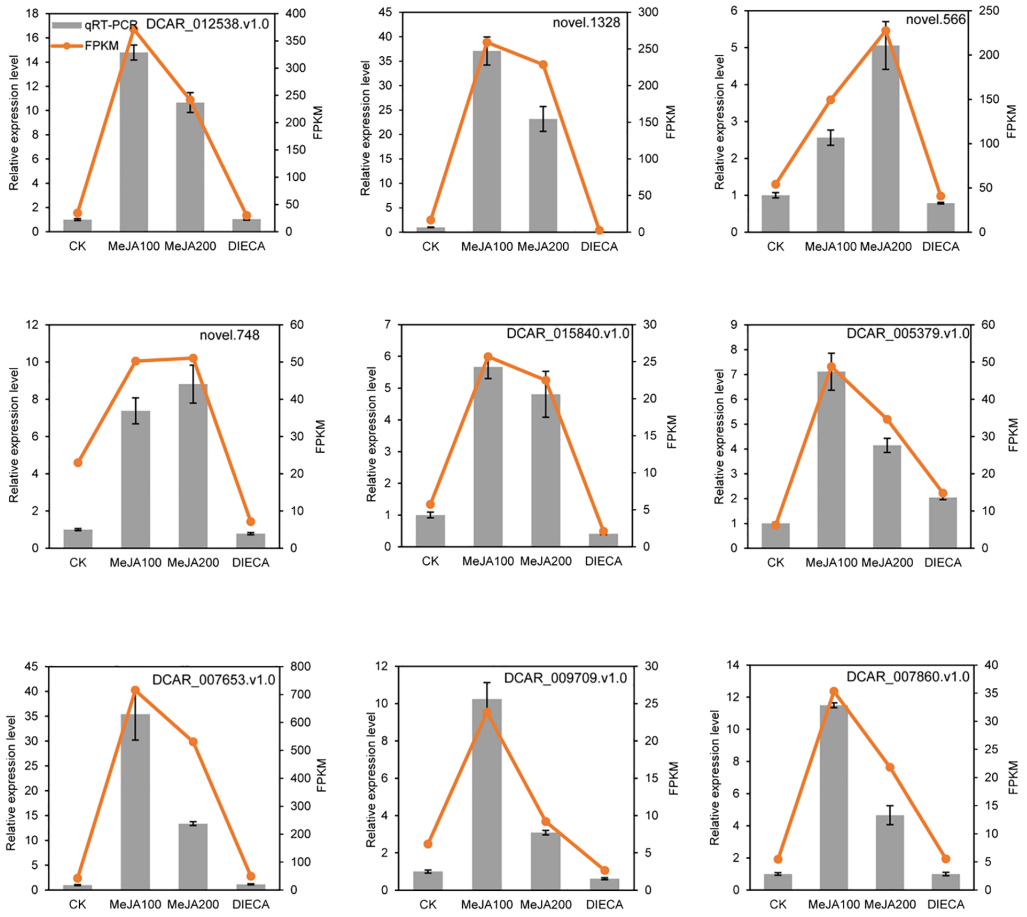

FIGURE 12
Quantitative real-time PCR validation of selected candidate genes. Error bars represent the standard deviation of three independent replicates.

sesquiterpenoids in a dose-dependent manner (Dong et al., 2022). Similarly, in the current work, the accumulation of most volatile compounds was substantially increased after MeJA application, whereas DIECA did the opposite, suggesting a vital role of MeJA in VOC formation (Figure 6). JAs themselves are a type of derivatives of fatty acid with a unique aroma. Here, JA regulated the accumulation of terpenoids and the expression of terpenoid synthase genes. Most of the terpenoids and terpenoid synthase genes increased in response to JA, whereas some of them were inhibited, creating different terpenoid compositions and odor characteristics.

Plant transcription factors are a class of proteins that play a crucial role in the regulation of gene expression in plants. They regulate the transcription of genes by recognizing specific DNA sequences, thereby affecting plant growth, development, metabolism, and response to environmental changes (Han et al., 2023a; Kidokoro et al., 2022; Wang et al., 2023). Currently, Numerous studies have revealed that transcription factors are involved in the process of JA-mediated volatile metabolites. *MdMYC2* and *MdMYB85* from apple were strongly induced upon MeJA treatment and mediated the JA signaling to regulate ester aroma emission by collectively binding to the promoter of *ALCOHOL ACYLTRANSFERASE 1*, a gene responsible for ester synthesis (Li et al., 2023). Also, some transcription factors responsive to MeJA were also found to be correlated with terpene synthesis. *DobHLH4*, a transcription factor responsive to MeJA in *Dendrobium officinale*, directly interacted with the *DoTPS10* promoter and increased its expression, thus contributing to linalool biosynthesis (Yu et al., 2021). Similarly, a MeJA-induced bHLH transcription factor *TaMYC2* from dandelion, could act as a positive regulator of triterpene accumulation by binding to the promoter of the *squalene synthase* (*TaSS*) gene (Liu et al., 2023). Although several terpenoid synthases that can manipulate terpenoid metabolism have been identified in carrot, there is limited research on its transcriptional regulation. So far, no transcription factor has been reported to regulate carrot terpenoid biosynthesis. Here, 4,680 TF-structural pairs were identified after MeJA spraying, which can serve as positive gene resources for in-depth research on the regulation of terpenoid accumulation, thus providing precise targets for enriching carrot flavor quality.

To our knowledge, this is the first work of global volatile metabolome analysis and characterization of differential accumulated metabolites in carrot upon MeJA treatment. The results generated 1,227 volatile organic compounds and 972 differential accumulated metabolites, with terpenes accounting for the largest group. MeJA

treatment strongly increased the relative odor activity values as well as the accumulation of most volatile compounds. In addition, 4,787 differentially expressed genes were further identified to understand the potential underlying mechanism. The expression profiles of terpenoid synthase genes and their correlations with transcription factors were extensively investigated. This study improved our understanding of the methyl jasmonate-mediated responses in carrot at the metabolic and molecular levels.

Data availability statement

The datasets presented in this study can be found in online repositories. The names of the repository/repositories and accession number(s) can be found in the article/supplementary material.

Ethics statement

The manuscript presents research on animals that do not require ethical approval for their study.

Author contributions

G-LW: Conceptualization, Funding acquisition, Writing – original draft, Writing – review & editing. J-QW: Data curation, Formal analysis, Writing – review & editing. Y-YC: Data curation, Writing – review & editing. Y-JX: Writing – review & editing. Y-HA: Data curation, Writing – review & editing. X-QR: Conceptualization, Writing – review & editing. A-SX: Funding acquisition, Resources, Writing – review & editing.

Funding

The author(s) declare financial support was received for the research, authorship, and/or publication of this article. This study was funded by the National Natural Science Foundation of China (32372681, 32102369), Natural Science Foundation of Jiangsu Province (BK20211366), New Century Excellent Talent of the Ministry of Education (NCET-11-0670) and Jiangsu Natural Science Foundation for Distinguished Young Scholars (BK20130027).

Conflict of interest

The authors declare that the research was conducted in the absence of any commercial or financial relationships that could be construed as a potential conflict of interest.

Publisher's note

Supplementary material

The Supplementary Material for this article can be found online at: https://www.frontiersin.org/articles/10.3389/fpls.2024.1467957/full#supplementary-material

References

Abbas, F., O'Neill Rothenberg, D., Zhou, Y., Ke, Y., and Wang, H. C. (2022). Volatile organic compounds as mediators of plant communication and adaptation to climate change. *Physiol. Plant* 174, e13840. doi: 10.1111/ppl.13840

Abbas, F., Zhou, Y., O'Neill Rothenberg, D., Alam, I., Ke, Y., and Wang, H. C. (2023). Aroma components in horticultural crops: Chemical diversity and usage of metabolic engineering for industrial applications. *Plants (Basel)* 12, 1748. doi: 10.3390/plants12091748

Bao, X., Zhou, W., Xu, L., and Zheng, Z. (2023). A meta-analysis on plant volatile organic compound emissions of different plant species and responses to environmental stress. *Environ. pollut.* 318, 120886. doi: 10.1016/j.envpol.2022.120886

Brosset, A., and Blande, J. D. (2022). Volatile-mediated plant–plant interactions: volatile organic compounds as modulators of receiver plant defence, growth, and reproduction. *J. Exp. Bot.* 73, 511–528. doi: 10.1093/jxb/erab487

Cai, X., Zhu, K., Li, W., Peng, Y., Yi, Y., Qiao, M., et al. (2024). Characterization of flavor and taste profile of different radish (*Raphanus Sativus* L.) varieties by headspace-gas chromatography-ion mobility spectrometry (GC/IMS) and *E*-nose/tongue. *Food Chem. X* 22, 101419. doi: 10.1016/j.fochx.2024.101419

Chang, W., Zhao, H., Chen, H., Jiao, G., Yu, J., Wang, B., et al. (2024). Transcription factor NtNAC56 regulates jasmonic acid-induced leaf senescence in tobacco. *Plant Physiol.* 195, 1925–1940. doi: 10.1093/plphys/kiae116

Chen, J., Zhang, Y., Liu, F., Chen, J., Wang, W., Wu, D., et al. (2023). The potential of different ripeness of blood oranges (*Citrus sinensis* L. Osbeck) for sale in advance after low-temperature storage: Anthocyanin enhancements, volatile compounds, and taste attributes. *Food Chem.* 417, 135934. doi: 10.1016/j.foodchem.2023.135934

Coe, K., Bostan, H., Rolling, W., Turner-Hissong, S., Macko-Podgórni, A., Senalik, D., et al. (2023). Population genomics identifies genetic signatures of carrot domestication and improvement and uncovers the origin of high-carotenoid orange carrots. *Nat. Plants* 9, 1643–1658. doi: 10.1038/s41477-023-01526-6

Dady, E. R., Kleczewski, N., Ugarte, C. M., and Ngumbi, E. (2023). Plant variety, mycorrhization, and herbivory influence induced volatile emissions and plant growth characteristics in tomato. *J. Chem. Ecol.* 49, 710–724. doi: 10.1007/s10886-023-01455-w

Deng, Y. J., Duan, A. Q., Liu, H., Wang, Y. H., Zhang, R. R., Xu, Z. S., et al. (2023). Generating colorful carrot germplasm through metabolic engineering of betalains pigments. *Hortic. Res.* 10, uhad024. doi: 10.1093/hr/uhad024

Dong, Y., Li, J., Zhang, W., Bai, H., Li, H., and Shi, L. (2022). Exogenous application of methyl jasmonate affects the emissions of volatile compounds in lavender (*Lavandula angustifolia*). *Plant Physiol. Biochem.* 185, 25–34. doi: 10.1016/j.plaphy.22022.05.022

Duan, A. Q., Deng, Y. J., Tan, S. S., Liu, S. S., Liu, H., Xu, Z. S., et al. (2024). DcGST1, encoding a glutathione S-transferase activated by DcMYB7, is the main contributor to anthocyanin pigmentation in purple carrot. *Plant J.* 117, 1069–1083. doi: 10.1111/tpj.16539

Escobar-Bravo, R., Chen, G., Kim, H. K., Grosser, K., van Dam, N. M., Leiss, K. A., et al. (2019). Ultraviolet radiation exposure time and intensity modulate tomato resistance to herbivory through activation of jasmonic acid signaling. *J. Exp. Bot.* 70, 315–327. doi: 10.1093/jxb/ery347

Fang, S., Zhang, C., Qiu, S., Xiao, Y., Chen, K., Lv, Z., et al. (2023). SbWRKY75- and SbWRKY41-mediated jasmonic acid signaling regulates baicalin biosynthesis. *Front. Plant Sci.* 14. doi: 10.3389/fpls.2023.1213662

Fukuda, T., Okazaki, K., and Shinano, T. (2013). Aroma characteristic and volatile profiling of carrot varieties and quantitative role of terpenoid compounds for carrot sensory attributes. *J. Food Sci.* 78, S1800–S1806. doi: 10.1111/1750-3841.12292

Furuta, Y., Yamamoto, H., Hirakawa, T., Uemura, A., Pelayo, M. A., Iimura, H., et al. (2024). Petal abscission is promoted by jasmonic acid-induced autophagy at Arabidopsis petal bases. *Nat. Commun.* 15, 1098. doi: 10.1038/s41467-024-45371-3

Gamba, M., Asllanaj, E., Raguindin, P. F., Glisic, M., Franco, O. H., Minder, B., et al. (2021). Nutritional and phytochemical characterization of radish (*Raphanus sativus*): A systematic review. *Trends Food Sci. Tech.* 113, 205–218. doi: 10.1016/j.tifs.2021.04.045

Han, X., Kui, M., He, K., Yang, M., Du, J., Jiang, Y., et al. (2023b). Jasmonate-regulated root growth inhibition and root hair elongation. *J. Exp. Bot.* 74, 1176–1185. doi: 10.1093/jxb/erac441

Han, H., Wang, C., Yang, X., Wang, L., Ye, J., Xu, F., et al. (2023a). Role of bZIP transcription factors in the regulation of plant secondary metabolism. *Planta* 258, 13. doi: 10.1007/s00425-023-04174-4

Hu, L. (2022). Integration of multiple volatile cues into plant defense responses. *New Phytol.* 233, 618–623. doi: 10.1111/nph.17724

Hu, L., Zhang, K., Wu, Z., Xu, J., and Erb, M. (2021). Plant volatiles as regulators of plant defense and herbivore immunity: molecular mechanisms and unanswered questions. *Curr. Opin. Insect Sci.* 44, 82–88. doi: 10.1016/j.cois.2021.03.010

Karabulut, I., Gokbulut, I., Bilenler, T., Sislioglu, K., Ozdemir, I. S., and Bahar, B. (2018). Effect of fruit maturity level on quality, sensory properties and volatile composition of two common apricot (*Prunus Armeniaca* L.) varieties. *J. Food Sci. Technol.* 55, 2671–2678. doi: 10.1007/s13197-018-3189-8

Keilwagen, J., Lehnert, H., Berner, T., Budahn, H., Nothnagel, T., Ulrich, D., et al. (20171930). The terpene synthase gene family of carrot (*Daucus carota* L.): Identification of QTLs and candidate genes associated with terpenoid volatile compounds. *Front. Plant Sci.* 8. doi: 10.3389/fpls.2017.01930

Kessler, A., Mueller, M. B., Kalske, A., and Chautá, A. (2023). Volatile-mediated plant–plant communication and higher-level ecological dynamics. *Curr. Biol.* 33, R519–R529. doi: 10.1016/j.cub.2023.04.025

Kidokoro, S., Shinozaki, K., and Yamaguchi-Shinozaki, K. (2022). Transcriptional regulatory network of plant cold-stress responses. *Trends Plant Sci.* 27, 922–935. doi: 10.1016/j.tplants.2022.01.008

Li, L. X., Fang, Y., Li, D., Zhu, Z. H., Zhang, Y., Tang, Z. Y., et al. (2023). Transcription factors MdMYC2 and MdMYB85 interact with ester aroma synthesis gene *MdAAT1* in apple. *Plant Physiol.* 193, 2442–2458. doi: 10.1093/plphys/kiad459

Li, C., Xu, M., Cai, X., Han, Z., Si, J., and Chen, D. (2022). Jasmonate signaling pathway modulates plant defense, growth, and their trade-offs. *Int. J. Mol. Sci.* 23, 3945. doi: 10.3390/ijms23073945

Li, M., Yu, G., Cao, C., and Liu, P. (2021). Metabolism, signaling, and transport of jasmonates. *Plant Commun.* 2, 100231. doi: 10.1016/j.xplc.2021.100231

Liu, T., Liao, J., Shi, M., Li, L., Liu, Q., Cui, X., et al. (2023). A jasmonate-responsive bHLH transcription factor TaMYC2 positively regulates triterpenes biosynthesis in *Taraxacum antungense* Kitag. *Plant Sci.* 326, 111506. doi: 10.1016/j.plantsci.2022.111506

Livak, K. J., and Schmittgen, T. D. (2001). Analysis of relative gene expression data using real-time quantitative PCR and the $2^{-\Delta\Delta CT}$ method. *Methods* 25, 402–408. doi: 10.1006/meth.2001.1262

Loarca, J., Liou, M., Dawson, J. C., and Simon, P. W. (2024). Evaluation of shoot-growth variation in diverse carrot (*Daucus carota* L.) germplasm for genetic improvement of stand establishment. *Front. Plant Sci.* 15. doi: 10.3389/fpls.2024.1342512

Muchlinski, A., Ibdah, M., Ellison, S., Yahyaa, M., Nawade, B., Laliberte, S., et al. (2020). Diversity and function of terpene synthases in the production of carrot aroma and flavor compounds. *Sci. Rep.* 10, 9989. doi: 10.1038/s41598-020-66866-1

Nguyen, T. H., Goossens, A., and Lacchini, E. (2022). Jasmonate: A hormone of primary importance for plant metabolism. *Curr. Opin. Plant Biol.* 67, 102197. doi: 10.1016/j.pbi.2022.102197

Ninkovic, V., Markovic, D., and Rensing, M. (2021). Plant volatiles as cues and signals in plant communication. *Plant Cell Environ.* 44, 1030–1043. doi: 10.1111/pce.13910

Picazo-Aragonés, J., Terrab, A., and Balao, F. (2020). Plant volatile organic compounds evolution: Transcriptional regulation, epigenetics and polyploidy. *Int. J. Mol. Sci.* 21, 8956. doi: 10.3390/ijms21238956

Quarrell, S. R., Weinstein, A. M., Hannah, L., Bonavia, N., del Borrello, O., and Flematti, G. R. (2023). Critical pollination chemistry: Specific sesquiterpene floral volatiles in carrot inhibit honey vee feeding. *J. Agric. Food Chem.* 71, 16079–16089. doi: 10.1021/acs.jafc.3c03392

Raza, A., Charagh, S., Zahid, Z., Mubarik, M. S., Javed, R., Siddiqui, M. H., et al. (2021). Jasmonic acid: a key frontier in conferring abiotic stress tolerance in plants. *Plant Cell Rep.* 40, 1513–1541. doi: 10.1007/s00299-020-02614-z

Reichardt, S., Budahn, H., Lamprecht, D., Riewe, D., Ulrich, D., Dunemann, F., et al. (2020). The carrot monoterpene synthase gene cluster on chromosome 4 harbours genes encoding flavour-associated sabinene synthases. *Hortic. Res.* 7, 190. doi: 10.1038/s41438-020-00412-y

Savoi, S., Wong., D. C. J., Degu, A., Herrera, J. C., Bucchetti, B., Peterlunger, E., et al. (2017). Multi-omics and integrated network analyses reveal new insights into the systems relationships between metabolites, structural genes, and transcriptional regulators in developing grape berries (*Vitis vinifera* L.) exposed to water deficit. *Front. Plant Sci.* 8. doi: 10.3389/fpls.2017.01124

Serna-Escolano, V., Valverde, J. M., García-Pastor, M. E., Valero, D., Castillo, S., Guillén, F., et al. (2019). Pre-harvest methyl jasmonate treatments increase antioxidant systems in lemon fruit without affecting yield or other fruit quality parameters. *J. Sci. Food Agric.* 99, 5035–5043. doi: 10.1002/jsfa.9746

Sharifi, R., Jeon, J. S., and Ryu, C. M. (2022). Belowground plant–microbe communications via volatile compounds. *J. Exp. Bot.* 73, 463–486. doi: 10.1093/jxb/erab465

Tian, Z., Dong, T., Wang, S., Sun, J., Chen, H., Zhang, N., et al. (2024). A comprehensive review on botany, chemical composition and the impacts of heat processing and dehydration on the aroma formation of fresh carrot. *Food Chem. X* 22, 101201. doi: 10.1016/j.fochx.2024.101201

Tian, C., Jiang, Q., Wang, F., Wang, G. L., Xu, Z. S., and Xiong, A. S. (2015). Selection of suitable reference genes for qPCR normalization under abiotic stresses and hormone stimuli in carrot leaves. *PloS One* 10, e0117569. doi: 10.1371/journal.pone.0117569

Wang, H., Chen, W., Xu, Z., Chen, M., and Yu, D. (2023). Functions of WRKYs in plant growth and development. *Trends Plant Sci.* 28, 630–645. doi: 10.1016/j.tplants.2022.12.012

Wang, S., Li, L. X., Fang, Y., Li, D., Mao, Z., Zhu, Z., et al. (2022). MdERF1B-MdMYC2 module integrates ethylene and jasmonic acid to regulate the biosynthesis of anthocyanin in apple. *Hortic. Res.* 9, uhac142. doi: 10.1093/hr/uhac142

Wang, P., Yu, J., Jin, S., Chen, S., Yue, C., Wang, W., et al. (2021). Genetic basis of high aroma and stress tolerance in the oolong tea cultivar genome. *Hortic. Res.* 8, 107. doi: 10.1038/s41438-021-00542-x

Xue, Y. L., Han, H. T., Liu, C. J., Gao, Q., Li, J. H., Zhang, J. H., et al. (2020). Multivariate analyses of the volatile components in fresh and dried turnip (*Brassica rapa* L.) chips via HS-SPME-GC-MS. *J. Food Sci. Technol.* 57, 3390–3399. doi: 10.1007/s13197-020-04372-y

Yahyaa, M., Ibdah, M., Marzouk, S., and Ibdah, M. (2018). Profiling of the terpene metabolome in carrot fruits of wild (*Daucus carota* L. ssp. *carota*) accessions and characterization of a geraniol synthase. *J. Agric. Food Chem.* 66, 2378–2386. doi: 10.1021/acs.jafc.6b03596

Yahyaa, M., Tholl, D., Cormier, G., Jensen, R., Simon, P. W., and Ibdah, M. (2015). Identification and characterization of terpene synthases potentially involved in the formation of volatile terpenes in carrot (*Daucus carota* L.) roots. *J. Agric. Food Chem.* 63, 4870–4878. doi: 10.1021/acs.jafc.5b00546

Yu, Z., Zhang, G., Teixeira da Silva, J. A., Zhao, C., and Duan, J. (2021). The methyl jasmonate-responsive transcription factor DobHLH4 promotes *DoTPS10*, which is involved in linalool biosynthesis in *Dendrobium officinale* during floral development. *Plant Sci.* 309, 110952. doi: 10.1016/j.plantsci.2021.110952

Zhao, Y., Zhu, X., Shi, C. M., Xu, G., Zuo, S., Shi, Y., et al. (2024). OsEIL2 balances rice immune responses against (hemi)biotrophic and necrotrophic pathogens via the salicylic acid and jasmonic acid synergism. *New Phytol.* 243, 362–380. doi: 10.1111/nph.19809

Zhou, C., Tian, C., Wen, S., Yang, N., Zhang, C., Zheng, A., et al. (2023). Multiomics analysis reveals the involvement of JsLHY in controlling aroma production in jasmine flowers. *J. Agric. Food Chem.* doi: 10.1021/acs.jafc.3c05768

frontiers | Frontiers in Plant Science

TYPE Original Research
PUBLISHED 28 February 2025
DOI 10.3389/fpls.2025.1548564

OPEN ACCESS

EDITED BY
Robin Joshi,
University of Pennsylvania, United States

REVIEWED BY
Antim Maurya,
University of Mississippi, United States
Shruti Sharma,
University of Alabama, United States

*CORRESPONDENCE
Islam El-Sharkawy
islam.elsharkawy@famu.edu

†These authors have contributed equally to this work

RECEIVED 19 December 2024
ACCEPTED 27 January 2025
PUBLISHED 28 February 2025

CITATION
Darwish AG, Das PR, Olaoye E, Gajjar P, Ismail A, Mohamed AG, Tsolova V, Hassan NA, El Kayal W, Walters KJ and El-Sharkawy I (2025) Untargeted flower volatilome profiling highlights differential pollinator attraction strategies in muscadine. *Front. Plant Sci.* 16:1548564. doi: 10.3389/fpls.2025.1548564

Untargeted flower volatilome profiling highlights differential pollinator attraction strategies in muscadine

Ahmed G. Darwish[1,2†], Protiva R. Das[3†], Eniola Olaoye[1†], Pranavkumar Gajjar[1], Ahmed Ismail[4,5], Ahmed G. Mohamed[1], Violeta Tsolova[1], Nasser A. Hassan[6], Walid El Kayal[7], Kellie J. Walters[3] and Islam El-Sharkawy[1*]

[1]Center for Viticulture and Small Fruit Research, College of Agriculture and Food Sciences, Florida A&M University, Tallahassee, FL, United States, [2]Department of Horticultural Sciences, Texas A&M University, College, Station, TX, United States, [3]Plant Sciences Department, University of Tennessee, Knoxville, TN, United States, [4]Department of Botany and Plant Sciences, University of California Riverside, Riverside, CA, United States, [5]Department of Horticulture, Faculty of Agriculture, Damanhour University, Damanhour, Egypt, [6]Synthetic Unit, Department of Photochemistry, Chemical Industries Research Institute, National Research Center, Cairo, Egypt, [7]Faculty of Agricultural and Food Sciences, American University of Beirut, Beirut, Lebanon

Floral aromas are a mixture of volatile organic compounds, essential attributes associated with the attraction of different pollinators. This investigation is the first in-depth exploration of the volatile profiles of sixteen muscadine grape genotypes, producing female and perfect flowers using the headspace solid-phase microextraction (HS-SPME)-GC-MS-based untargeted volatilomics approach. A total of one hundred fifty volatile metabolites were identified in the muscadine flower genotypes, including the functional groups of hydrocarbons, esters, alcohols, ketones, aldehydes, miscellaneous, and acids. Multivariate statistical analysis for volatile terpenes revealed eleven bio-marker terpene volatiles that primarily distinguish between female and perfect flowers. The β-elemene, β-bisabolene, and α-muurolene were the marker volatiles characterizing perfect flowers; however, α-selinene, (*Z*,*E*)-α-farnesene, and (*E*,*E*)-geranyl linalool were the typical marker terpene in the female flowers. Perfect flowers exhibited better pollinator attraction capacity associated with a higher number of flowers per inflorescence, enhanced pollinator rewards, and higher numbers and quantities of terpene volatiles than female flowers, resulting in superior pollinator attraction capacity and fruit set efficiency. The pollinator attraction mechanism of female flowers exhibited several morphological and biochemical floral defects, causing random pollinator visits and low fruit set efficiency. The controlled pollination assay could express female flowers' full fruit set capabilities by avoiding casual insect pollination. This comprehensive study suggests that these marker terpenes might contribute to pollinator attraction in muscadine flower genotypes and should be considered an excellent reference for agroecosystem ecologists and entomologists.

KEYWORDS

floral aromas, muscadine flowers, marker volatiles, pollination attraction, volatilomics

Introduction

Over the past few decades, muscadine grapes have been getting increasing attention from consumers, growers, and breeders due to accumulating numerous human health functional metabolites, having distinct musky aromas, and producing unique flavors that are essential for processed beverage production and fresh market consumption (Darwish et al., 2021; Deng et al., 2022). *Muscadinia* is closely related to *Vitis* species that grow in the southeastern United States (Olien, 1990; Wen et al., 2018). Over 100 muscadine cultivars have been released in the southeastern region of the United States and extended to Chile and southern China (Wei et al., 2017; Hickey et al., 2019). Successful natural pollination is vital in flowering plants to achieve fruit production and seed development, thus maintaining ecological balance (Kearns and Inouye, 1997). The high efficiency and specificity of pollinator attraction are likely mediated through olfactory and/or visual cues, and there is increasing evidence that olfactory cues are paramount in attraction (Barragán-Fonseca et al., 2019). Muscadine grape flowers offer pollen and nectar as a reward to insect pollinators; however, pollen may be thrust upon them as calyptras eject (McGregor, 1976). The ability of insect pollinators to fertilize muscadine flowers has been associated with pollinator abundance and particular pollen-collection behavior. However, our knowledge about plant pollination on a biochemical level is still poorly understood (Mayer et al., 2011). Muscadine flower types include staminate (male), pistillate (female), or hermaphrodite (perfect). Pistillate vines produce large berries that are usually used for fresh consumption, in contrast, hermaphrodite vines produce smaller berries that are typically used for processed beverages (Campbell et al., 2021). Hermaphrodite flower muscadine genotypes are self-compatible and may be wind-pollinated. Conversely, wind plays a minor role in pistillate vines, where the majority of fruit set is attributed to insect pollination. Natural pollination in pistillate flower muscadines plays a crucial role in defining the yield; thus, lower pollination could result in less production due to a diminished fruit set (Sampson et al., 2001).

Floral volatile compounds greatly influence the attraction of pollinators and have been suggested as the critical mediator of plant-pollination networking (Dötterl and Vereecken, 2010; Dötterl and Gershenzon, 2023). These volatiles are highly variable among species regarding the disparities in their functional groups or due to differences in the absolute or relative amounts of compounds (Burkle and Runyon, 2019). Other biological studies have illustrated that floral volatiles serve additional functions, such as defending reproductive tissue against pathogens and attracting predators of plant pests (Boachon et al., 2019; Li et al., 2020). Floral volatiles are classified into a few primary functional groups according to their chemical structure and biosynthetic origin, such as fatty acid derivatives, terpenoids, phenylpropanoids, and benzenoids. Among all groups, floral terpenoids are the most dominant volatiles reported in horticultural crops and economically important plants (Dötterl and Gershenzon, 2023). Central floral volatile terpenes, including hemiterpenes (C5), monoterpenes (C10), sesquiterpenes (C15), and a few diterpenes (C20) are emitted into the air due to their high vapor pressures (Knudsen et al., 2006; Raguso, 2016; Pichersky and Raguso, 2018). Monoterpenes and sesquiterpenes are among the most abundant terpene components of floral scents and play crucial roles in plant development, chemical ecology, and pollinator attraction (Qiao et al., 2021; Dötterl and Gershenzon, 2023). For instance, sesquiterpenes, including (*E*)-β-caryophyllene, contribute to flower defense against bacterial pathogens (Huang et al., 2012). (*E*)-β-farnesene and (*E*)-α-bergamotene protect plants from microbial pathogens by recruiting their pollinators and pests predators. Similarly, the monoterpene linalool and its enantiomers attract bees and moths, enhance pollination in several flowering plants, and protect plants from microbial pathogens (Qiao et al., 2021). Flowers that produce the monoterpene (*E*)-β-ocimene are primarily attractive to honeybees and bumblebees (Crowell et al., 2002; Farré-Armengol et al., 2017). Recently, the identification of floral volatile profiles in flowering plants has increased rapidly due to advanced high-throughput analytical methods (Dötterl and Gershenzon, 2023). However, the volatile profiling of Vitaceae grape family flowers has not been substantially investigated. To our knowledge, only two reports are available on volatile analysis from grape (*Vitis vinifera*) flowers. Barbagallo et al. (2014) identified more than fifty volatiles from the flowers of several grape varieties while Gil et al. (2014) identified twelve volatiles that have a protective role against ultraviolet-B solar radiation and constitutive of the grape reproductive tissues. However, no reports are available on the volatile profiling of muscadine flowers.

Gas chromatography-mass spectrometry (GC-MS)-based untargeted volatilomics is currently the most utilized method to profile plant volatilome that allows a wide range of volatile compounds identification in different plant organs based on large reference libraries (e.g., NIST mass spectral library) and assessed for their discriminative impact (Pontes et al., 2009; Bryant and McClung, 2011; Bojko et al., 2014; Tieman et al., 2017). A study of GC-MS-based untargeted volatilomics analysis in strawberry flowers (*Fragaria* × *ananassa*) unveiled that the bee species *Bombus terrestris* or *Apis mellifera* showed strong responses to the floral compounds ethyl benzoate, (*Z*)-3-hexenyl propionate, (*Z*)-3-hexenyl acetate, benzeneacetaldehyde, and melonal (Liu et al., 2023). Another untargeted volatilomics study of twenty representative cucumber lines from various geographical locations revealed that 2-hexenal, 2,4-nonadienal, and 2,6-nonadienal are the key volatile metabolites that are relatively low in Korean cucumber lines, resulting in lower flavor intensity (Jo et al., 2022). Similarly, untargeted volatilomics analysis of forty-two citrus cultivars identified thymol derivatives, particularly *cis*-sabinene hydrate, sabinene, thymol, and thymol methyl ether, as the distinguishing marker volatile metabolites between citrus cultivars (Deng et al., 2022). Moreover, they showed that (*Z*)-3-hexen-1-ol contributes to the "green" aroma and also plays a role in distinguishing between orange and mandarin citrus groups.

In this study, untargeted volatile profiles of sixteen muscadine flower genotypes, including eight perfect and eight female flower vines, were characterized using HS-SPME-GC-MS-based analysis. Multivariate statistical analysis methods were utilized to determine the pivotal floral terpenoid volatiles, including principal component

analysis (PCA), partial least-discriminate analysis (PLS-DA), and hierarchical heatmap analysis. Our results provide a foundation for further exploration of the functional characterization and evolution of marker volatile metabolites variation in muscadine flowers to understand their role in chemical ecology.

Materials and methods

Plant materials and experimental conditions

Sixteen muscadine grape genotypes (*Muscadinia rotundifolia* Michx.), including eight standard cultivars and eight breeding lines, were used in this study (Supplementary Table S1). All muscadine vines were grown at the Center for Viticulture, Tallahassee, Florida (30°28′45.63′′ N, 84°10′16.43′′ W). Vineyard management and practices followed the guidelines outlined in the Muscadine Production Guide for Florida written by the Center for Viticulture and Small Fruit Research (CVSFR), Florida Agricultural & Mechanical University (FAMU) (https://famu.edu/viticulture). The breeding lines were developed under the grape-breeding program of the CVSFR at FAMU (Tallahassee, FL, USA). The muscadine genotypes were selected according to the diversity in their flower type, perfect (hermaphrodite) and female (pistillate) that produce bronze and red berries (Figure 1A). Samples were collected from 15-year-old grapevines at the open flower stage. The flower buds were carefully separated from the flower cluster, and samples were randomly assembled in three biological replicates. All samples were immediately frozen in liquid nitrogen and stored at −80°C for further analysis.

Muscadine sample preparation for HS-SPME

The floral volatile compounds (VOCs) from muscadine flowers were assessed using HS-SPME. Frozen samples were lyophilized and ground into a fine powder using a Geno/Grinder 2010 (Metuchen, NJ, USA). A 200 mg powder was mixed with 20 µl of 2-octanol and transferred to a 25 ml glass vial (Thermo Scientific, Bellefonte, PA, USA). A 5 ml of saturated sodium chloride (NaCl) solution was added to inhibit enzyme degradation during extraction. All samples were incubated with a magnetic stirrer to facilitate VOC release before the glass vial was capped. The homogenized samples were incubated for 30 min in a 60°C water bath with continuous agitation (vortex every 5 min). Afterward, the VOCs were collected using a 2 cm DVB/CAR/PMDS SPME fiber (50/30µm, Supelco Inc., Bellefonte, PA, USA) by exposing the fiber to the headspace for another 30 min under the same conditions. The fibers were activated before sampling according to the manufacturer's instructions. After the incubation step, the SPME fiber was inserted directly into the injection port of the GC system for thermal desorption (4 min at 250°C) in a splitless mode.

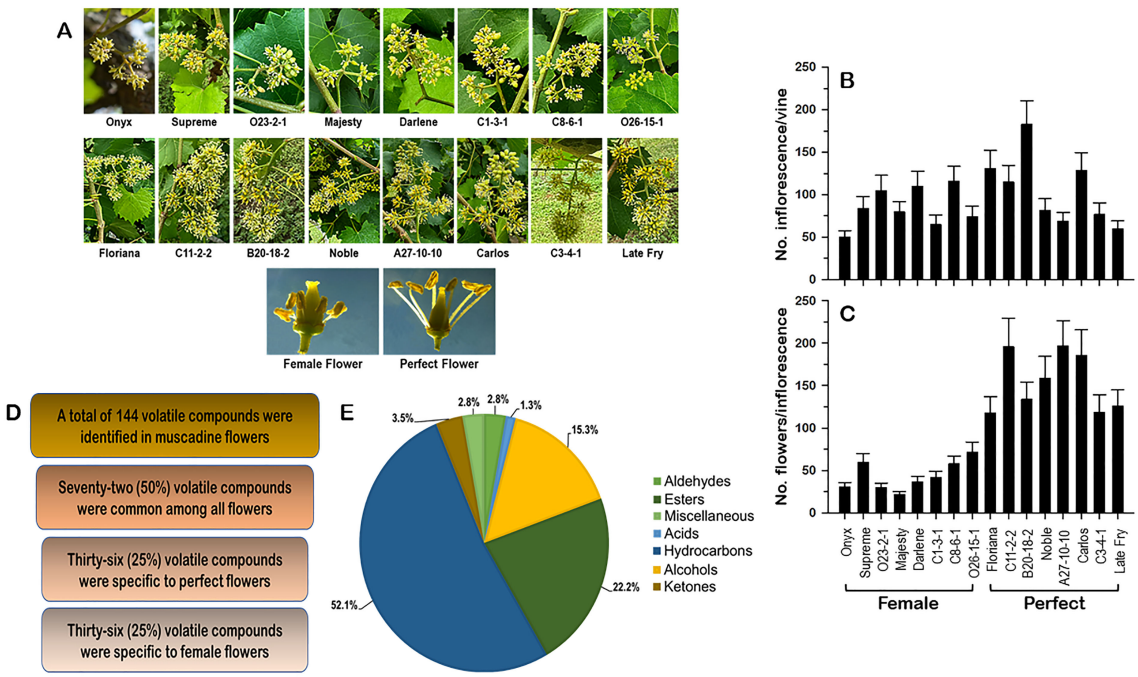

FIGURE 1
(A) Close-up views of the female and perfect muscadine flower genotypes used in this study, defining the differences in the inflorescence and flower structures. The characterization of the number of inflorescences/vine **(B)** and the number of flowers/inflorescence **(C)** of muscadine genotypes used in this study. **(D)** Number of identified volatile compounds in female and perfect muscadine flowers. **(E)** Pie chart of volatile functional groups identified in muscadine flowers.

Gas chromatography-mass spectrometer analysis

GC-MS analysis was performed using a Shimadzu-QP2010SE (Shimadzu Scientific Instruments, INC, Columbia, MD 21046, USA) coupled with an SH-Rxi-5Sil MS column (30 m x 0.25 mm i.d., film thickness 0.25 µm). The column oven temperature program was initiated at 40°C for 4 min, then ramped up to 245°C at a rate of 5°C min^{-1} and held for 5 min. The SPME fiber was inserted manually into the GC-MS apparatus operating in EI mode at 70 eV. The transfer line, ion source, and quadrupole mass detector temperature values were set to 250°C, 230°C, and 150°C, respectively. The carrier gas (Helium) flow rate was 0.8 ml/min using splitless mode. The relative percentage quantity of each component was calculated by comparing its average peak area to the total area. MS solution software provided by the supplier was used to control the system and to acquire the data.

Identification and quantification of floral volatiles

The peaks obtained from GC-MS (Supplementary Figure S1) were first processed using Shimadzu software (Shimadzu Scientific Instruments, INC, Columbia, MD 21046, USA). The parameters used for raw peak extraction, data baseline filtering and calibration of the baseline, peak alignment, deconvolution analysis, peak identification, integration, and spectrum match of the peak area were the same for all samples. VOCs were identified by matching their retention indices (RI) and mass spectra with those available from the National Institute Standard and Technology (NIST) database (Gaithersburg, MA, USA) and Wiley libraries. Relative amounts of the identified VOCs were calculated from the total ion chromatogram (TIC). Correspondingly, the peak area of each VOC was converted into a relative concentration value.

Pollination assay

Five female and perfect vines of muscadine cultivars 'Darlene' and 'Floriana', respectively, were selected for pollination assay. All vines were 15 years of age and planted in a 53-muscadine cultivar trial block. For each vine, 20 inflorescences at a similar developmental stage and size were randomly selected and separated into two groups of 10 inflorescences used for controlled and open pollination. The flowers designated for controlled pollination of the perfect genotype 'Floriana' were subjected to an emasculation procedure to prevent potential self-pollination. All controlled pollination inflorescences were bagged and checked daily for readiness for pollination. Pollination began when about 20% of the flowers opened and continued every morning until stigmas showed dryness typical of post-pollination, which usually lasted a week. Fresh flowers from ′Granny Val′ were directly applied to the female 'Darlene' and emasculated 'Floriana' flowers. Pollinated inflorescences remained in bags until the fruit set was completed. After harvest, all clusters were collected and separated based on vine, cultivar, and type of pollination assay (open or controlled). All clusters were evaluated for the traits of cluster weight, weight of berries per cluster without the rachis, number of berries per cluster, and individual berry weight. All records were the average of five values (± standard deviation).

Multivariate statistical analysis

All multivariate statistical analyses, including principal components analysis (PCA), partial least-squares–discriminant analysis (PLS-DA), and heatmap of Pearson correlation analysis, were performed using MetaboAnalyst 6.0 online software. The data were normalized into a logarithmic base for statistical analysis, and Autoscaling was performed. PCA was first used as an unsupervised method to determine whether there were fundamental differences among muscadine flower genotypes. Furthermore, supervised regression modeling was performed on the data set using PLS-DA to obtain the variable importance in the projection (VIP). The marker volatile metabolites were filtered and confirmed by combining the results of the VIP, |p|, and |p(corr)|, and the screened volatile compounds were analyzed by the heatmap of Pearson correlation with flower genotypes to characterize key volatile metabolites variation among genotypes. Figures were generated using Prism (GraphPad Prism 5.01Inc. La Jolla, CA, USA) statistical software.

Results and discussion

Muscadine flower characteristics

Grapevine flower traits, such as the number of inflorescences per vine and the number of flowers per inflorescence, provide crucial insights for assessing yield potential. From a quantitative standpoint, a higher number of inflorescences and flowers per vine enhances the floral signal display, increases the quantity of volatile organic compounds (VOCs), and improves floral rewards, which collectively optimize pollinator attraction and fruit set efficiency (de Ibarra et al., 2015). In this study, sixteen muscadine grape genotypes were analyzed, with eight producing female (pistillate) flowers and eight producing perfect (hermaphrodite) flowers (Figure 1A; Supplementary Table S1). Muscadine inflorescences are typically small and consist of tiny green flowers. To assess each vine genotype's ability to attract pollinators, the number of inflorescences per vine was counted (Figure 1B). The number of inflorescences varied widely depending on the genotype, independent of flower type (female or perfect). The average number of inflorescences across all genotypes was 95.6 ± 8.5. The female cultivar 'Onyx' had the lowest inflorescences number (50 ± 7.5), while the perfect-flowered genotype 'B20-18-2' exhibited the highest number (183 ± 27.5). Similarly, the number of flowers per inflorescence showed significant variation among genotypes, with a clear distinction based on flower type (Figure 1C). Female flower

genotypes had fewer flowers per inflorescence (44 ± 6.2), with 'Majesty' having the lowest count (22 ± 3.3) and 'O26-15-1' the highest (72 ± 9.6). In contrast, perfect-flower genotypes exhibited a higher average flower count per inflorescence (168.6 ± 10.5). Among these genotypes, 'Floriana' had the lowest average, with 118 ± 18.9 flowers per inflorescence, while 'A27-10-10' boasted the highest average, reaching 197 ± 29.6 flowers per inflorescence.

The number of inflorescences per vine and the number of flowers per inflorescence are valuable parameters for pre-evaluating the yield. The inflorescences of female muscadine vines displayed a weaker morphological phenotype. The floral signal is smaller than in perfect flower and the number of flowers in the inflorescence is lower, negatively affecting the efficiency of their interaction with pollinators. The attractiveness of muscadine flowers for pollinators is largely determined by VOCs and the quality of floral rewards in the form of nectar and pollen (Knauer and Schiestl, 2015; Cane, 2016; Delle-Vedove et al., 2017). This preliminary assessment suggested that perfect flowers are endowed with an absolute advantage in terms of all floral traits, affecting pollinators' attraction and the ability to set fruit.

Volatile profiles of muscadine flowers

Volatile organic compounds (VOCs) are essential in attracting pollinators, boosting yield and quality, and protecting flowers from pathogens (Bouwmeester et al., 2019). In this study, untargeted volatile profiling using HS-SPME-GC-MS, coupled with NIST mass spectral library identification, highlighted significant differences between female and perfect muscadine flowers. A total of 144 volatile metabolites were identified across muscadine flower genotypes (Supplementary Table S2). Among them, 25% were specific to female flowers, while another 25% were exclusive to perfect flowers. The remaining 50% were shared between both flower types (Figure 1D). The identified VOCs predominantly consisted of hydrocarbons (52.1%), followed by esters (22.2%) and alcohols (15.3%). Smaller proportions were contributed by ketones (3.5%), aldehydes (2.8%), miscellaneous compounds (2.8%), and acids (1.3%) (Figure 1E, Supplementary Table S2). These results are consistent with the known VOC profiles of other floral species (Dötterl and Gershenzon, 2023).

The total VOC emissions varied widely among muscadine genotypes, with perfect flowers producing nearly double the amount of VOCs compared to female flowers. Total VOC levels ranged from 417.4 ± 66.3 µg/100g in the female cultivar 'Darlene' to 8632.7 ± 1294.9 µg/100g in the perfect-flowered 'Late Fry' (Supplementary Table S2). Overall, female flowers emitted a significantly lower number of volatile compounds (35.3 ± 3.3) compared to perfect flowers (45.9 ± 3.1). Among examined muscadine genotypes, 'Darlene' produced the fewest volatile compounds, with only 21 identified, while 'Late Fry' yielded the highest number, with a total of 65 volatiles. The diversity, quantity, and functionality of these VOCs are critical factors in attracting pollinators (Burkle and Runyon, 2016). These findings suggest that perfect muscadine flowers, which emit higher levels and numbers of VOCs, may have an ecological advantage in reproductive success due to enhanced pollinator attraction.

Muscadines' floral alcohol volatiles

The diversity and level of alcohols in floral scents vary across species and even between genotypes within the same species, influencing pollinator preferences and specialization (Pichersky and Gershenzon, 2002). In the muscadine flowers, 22 alcohols were identified, with distinct differences in their distribution between female and perfect flowers. Of these alcohols, seven (31.8%) were specifically emitted by female flowers, and three (13.6%) were exclusively detected in perfect flowers, suggesting that these alcohol volatiles may serve specific roles depending on the flower type (Supplementary Table S2). However, twelve alcohols (54.6%) were present in both flower types, indicating commonalities in their function across female and perfect flowers, likely contributing to shared characteristics of muscadine flower fragrance. The average number of alcohols produced per genotype was 6.1 ± 0.5. The female 'O23-2-1' flowers had the highest number of alcohols (11), while the perfect 'Noble' flowers produced the lowest (3), illustrating significant variation in alcohol production across different flower types and genotypes.

The total alcohol production in muscadine flowers also varied widely across genotypes. The lowest alcohol content was observed in the female 'Darlene' flowers (40.7 µg/100g), while the highest was found in the perfect 'Late Fry' flowers (2115.6 µg/100g). Interestingly, these two genotypes also represented the extremes in total VOC content, underscoring the considerable contribution of alcohols to the overall volatile profile. The predominant alcohol detected in female flowers was (6*E*)3,7,11-trimethyl-1,6,10-dodecatrien-3-ol. In contrast, no specific alcohols were identified in perfect flowers. However, several alcohols, including 1-hexanol, 1-octanol, 1-decanol, (*E*)-2-octen-1-ol, and 2,3,6-trimethyl-7-octen-3-ol, were common to both flower types, highlighting some overlap in their volatile profiles (Supplementary Table S2).

Alcohols are vital components of floral VOCs, playing key roles in pollinator attraction, plant defense, and ecological communication. They contribute uniquely to the floral scent bouquet, influencing a plant's reproductive success by attracting specific pollinators. For instance, (6*E*)3,7,11-trimethyl-1,6,10-dodecatrien-3-ol, with its sweet, floral aroma, attracts moths and bees (Raguso and Pichersky, 1999). Other alcohols, like 2,3,6-trimethyl-7-octen-3-ol, add fruity notes, while 1-hexanol provides a fresh, green scent (Pichersky and Gershenzon, 2002; Dudareva et al., 2006; Knudsen et al., 2006). Complex floral fragrances result from synergistic interactions between alcohols and other VOCs, enhancing pollinator attraction through nuanced scent profiles (Dudareva et al., 2006; Knudsen et al., 2006). Beyond attracting pollinators, alcohols like 1-decanol and (*E*)-2-octen-1-ol play defensive roles, signaling beneficial insects and protecting plants from herbivores and pathogens. For example, 1-decanol has antimicrobial properties that support plant defense, while 1-octanol and (*E*)-2-octen-1-ol attract natural enemies of herbivores, contributing to plant fitness and survival (Kessler and Baldwin, 2001;

Pichersky and Dudareva, 2007; Park et al., 2008; Schiestl, 2010). In summary, alcohols are crucial in shaping floral scents, attracting pollinators, defending plants, and facilitating ecological interactions, highlighting their significance in plant ecology and evolution.

Muscadines' floral ester volatiles

In muscadine flowers, 32 volatile esters were identified, with five (15.6%) found only in female flowers and eight (25%) exclusively in perfect flowers. The remaining 19 esters (59.4%) were common to both flower types. In general, perfect flowers released a considerably higher number of volatile esters (11 ± 0.7) when compared to female flowers (8.4 ± 0.9). The female 'C8-6-1' genotype exhibited the lowest number of esters, producing only five, while the perfect 'Late Fry' flowers generated the most, with 15 esters. The total quantity of esters emitted by muscadine flowers varied significantly, ranging from 35.5 ± 5.3 μg/100g in the female genotype 'C8-6-1' to 2961.8 ± 473.9 μg/100g in the perfect cultivar 'Noble' (Supplementary Table S2). On average, perfect flowers emitted ~2.9 times more ester volatiles than female flowers. The dominant esters in perfect flowers included methyl stearidonate, *cis*-9-Tetradecenoic acid, propyl ester, and butyl myristate, while no unique esters were identified for female flowers. However, esters such as octyl formate, butyl dodecanoate, *Z*-5,17-octadecadien-1-ol acetate, methyl tetradecanoate, octyl octanoate, 2-*O*-(2-ethylhexyl) 1-*O*-tridecyl oxalate, and 2-ethylhexyl pentyl sulfite were detected in both flower types (Supplementary Table S2).

Volatile esters play essential roles in flower odors by contributing to pollinator attraction and enhancing scent complexity. These compounds are crucial in determining the floral fragrance profile via shaping specific scent signals. For example, esters like *Z*-5,17-octadecadien-1-ol acetate and 2-*O*-(2-ethylhexyl) 1-*O*-tridecyl oxalate may contribute to species-specific scent signatures. They are often detected in particular plant species and serve as critical components in distinguishing the scent profiles of those species, ensuring that pollinators can easily locate their preferred flowers (Verdonk et al., 2003). Other esters like octyl formate and methyl tetradecanoate enhance the complexity of floral scents and play a role in plant ecological communication (Pichersky and Gershenzon, 2002; Pichersky and Dudareva, 2007). They add fruity and floral notes to flowers, increasing their appeal to diverse pollinators (Knudsen et al., 2006; Dudareva et al., 2013). Finally, the unique and synergistic interaction of esters with other VOCs makes them essential in ensuring effective plant-pollinator interactions. Esters such as octyl octanoate and butyl dodecanoate interact synergistically with alcohols, terpenes, and aldehydes to refine and enhance floral odors. These interactions are crucial for developing complex floral scent profiles that can appeal to different types of pollinators (Dudareva et al., 2004, 2013).

Other minor volatile compounds

The volatilome profiling of muscadine flowers revealed the presence of several minor volatile compounds, including aldehydes, ketones, miscellaneous compounds, and acids.

Aldehydes

Four aldehyde volatiles were identified in muscadine flowers (Supplementary Table S2). The total aldehyde levels produced by muscadine flowers varied significantly among genotypes, with a range of 210.2 μg/100g, from a minimum of 4.8 ± 0.8 μg/100g in female flowers of the 'Supreme' cultivar to a maximum of 215 ± 32.3 μg/100g in female flowers of 'Majesty'. On average, perfect flowers emitted ~2.5 times more aldehydes than female flowers. Aldehydes are essential contributors to floral scents, playing key roles in pollinator attraction and plant defense (Surburg and Panten, 2005). They are also involved in the biosynthesis of aroma-volatile esters, interconverting them into alcohols and serving as substrates for ester formation (El-Sharkawy et al., 2005; Manríquez et al., 2006). In muscadine flowers, aldehydes contribute to unique odor profiles and ecological functions. For example, (*E*)-2-hexenal provides a sharp, green fragrance reminiscent of freshly cut grass and acts as a defense signal to attract pollinators or predators of herbivores (Schwery et al., 2023). Heptanal, with its sweet, fruity, and slightly oily scent, appeals to nocturnal pollinators like moths and may repel herbivores (Unsicker et al., 2009). The genotype-dependent accumulation of *n*-octanal in 'Carlos' and 'Late Fry' cultivars, known for its citrusy and sweet fragrance, suggests a role in attracting pollinators such as bees and butterflies while also contributing to plant defense (Schwab et al., 2008).

Ketones

Five ketones were identified in muscadine flowers; however, their accumulation seems to be genotype-dependent irrespective of flower type (Supplementary Table S2). Several muscadine flower genotypes exhibited undetectable ketones; however, the maximal total ketones production was identified in female flower genotype 'O26-15-1' with an average level of 1455 ± 247.4 μg/100g. The 6*Z*-pentadecen-2-one ketone was detected in perfect flower genotypes of 'C11-2-2'. In the female flowers, the pentadecan-2-one was identified in 'Onyx', 'O23-2-1', and 'Darlene'; however, 'O23-2-1' produces an extra ketone of 2-ethyl-5-methyl-1,3,2-dioxaborolan-4-one. The ketones of 2-pentadecanone and 2-nonadecanone were detected in both flower types (Supplementary Table S2). The ketones identified in muscadine flowers contribute in distinct ways to the complexity of floral scent and the ecological interactions that support pollination and defense. Their presence and concentration appear to be genotype-dependent, with certain flower types exhibiting unique ketone profiles.

The compounds of 6*Z*-pentadecen-2-one and pentadecan-2-one provide subtle, waxy, and fatty odors that add depth and persistence to floral scents to attract pollinators such as bees and nocturnal insects over long distances. These less volatile ketones linger, making the fragrance effective throughout the day and night (Schwab et al., 2008; Gibernau et al., 2021). Similarly, 2-pentadecanone and 2-nonadecanone contribute a persistent, waxy scent, enhancing the complexity and duration of the floral fragrance, which boosts pollinator attraction while potentially

signaling defense to herbivores (Unsicker et al., 2009). The boron-containing compound 2-ethyl-5-methyl-1,3,2-dioxaborolan-4-one, though less characterized, likely contributes to ecological interactions and plant defense (Gibernau et al., 2021).

Miscellaneous

Four miscellaneous volatiles, including givaudan, linoleoyl chloride, methyl (6*Z*,9*Z*,12*Z*,15*Z*)-octadeca-6,9,12,15-tetraenoate, and 6,7-dimethyl-5,6,7,8-tetrahydrotetrazolo[1,5-b][1,2,4]triazine were identified in muscadine flowers, with these compounds being more abundant in perfect flowers. Linoleoyl chloride, an acyl chloride derivative of linoleic acid, serves as a precursor in the biosynthesis of various volatile compounds, such as aldehydes, esters, and alcohols, which contribute significantly to floral fragrances. Though it does not directly produce scent, its derivatives play a crucial role in floral signals that mediate plant interactions with their environment, balancing attraction and defense against herbivores (Dudareva and Pichersky, 2006). Methyl (6*Z*,9*Z*,12*Z*,15*Z*)-octadeca-6,9,12,15-tetraenoate, a methyl ester of linolenic acid, adds sweet, fatty, and fruity undertones to the overall floral fragrance. These methyl esters are important for long-distance scent dispersion and contribute to the plant´s chemical signaling pathways, attracting pollinators like bees and butterflies while also aiding in defense responses (Pichersky and Gershenzon, 2002). The nitrogen-containing heterocyclic compound 6,7-dimethyl-5,6,7,8-tetrahydrotetrazolo[1,5-b][1,2,4]triazine adds earthy or spicy qualities to floral scents. These nitrogenous volatiles play a distinct role in plant-pollinator and plant-herbivore interactions, offering a unique scent signature that can influence ecological dynamics by attracting or repelling insects (David and Doro, 2023).

Acids

Only two acids were detected in muscadine flowers, where the female flowers genotype, 'O23-2-1', produced the 2,5-diamino-2-methyl pentanoic acid, while 3-decenoic acid was only identified in perfect flower cultivars 'Floriana' and 'Carlos' (Supplementary Table S2). The 2,5-diamino-2-methylpentanoic acid is not directly involved in scent production, but it could influence floral fragrance through its role in amino acid and nitrogen metabolism, indirectly contributing to the synthesis of volatile compounds (Dudareva et al., 2006). The 3-decenoic acid, on the other hand, may serve as a precursor to floral volatiles that contributes to the fruity, green, or waxy characteristics of flower scents, and it could also play a role in plant defense mechanisms (Pichersky and Gershenzon, 2002; Dötterl and Jürgens, 2005; Knudsen et al., 2006). Both compounds exemplify how primary metabolites are linked to the production of secondary metabolites, which are essential for ecological interactions and pollinator attraction.

Hydrocarbon dominates the volatile profiling in muscadine flowers

A total of seventy-seven (52.1%) hydrocarbons were detected in muscadine flowers (Supplementary Table S2). Among them, thirty-six (25%) volatiles were categorized under aliphatic compounds, and thirty-nine (27.1%) volatiles were classified under terpene volatiles based on their chemical properties (Figure 2A). Within the aliphatic groups, thirteen (36.1%) volatiles were exclusive to female flowers, seven (19.4%) volatiles were specific to perfect flowers, and sixteen (44.4%) were detected in both flower types. Overall, perfect flowers emitted a significantly higher number of aliphatic compounds (11.1 ± 1.1) compared to female flowers (7.8 ± 1.2). The female 'Darlene' flowers showed the lowest aliphatics number (3), while the perfect 'Late Fry' flowers emitted the highest (18), highlighting considerable variation in aliphatics production across different genotypes. The levels of total aliphatics produced by muscadine flowers considerably altered between genotypes and displayed a wide range with a minimum and maximum level of 122.5 ± 20.8 µg/100g (female flower 'Darlene') and 3110 ± 497.6 µg/100g (female flower 'Majesty'), respectively. The *n*-tetradecane and (*E*)-9-octadecene were dominant in perfect flowers. In contrast, no unique aliphatic compound was identified for female flowers. On

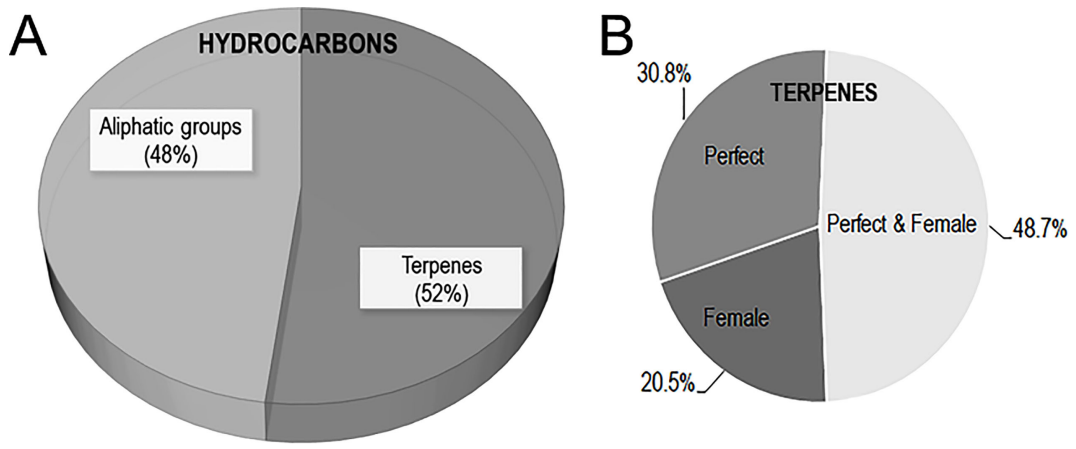

FIGURE 2
(A) Pie chart of hydrocarbon sub-class volatiles in muscadine flowers. **(B)** Pie chart of the distribution of terpenes volatiles in perfect and female muscadine flowers.

average, perfect flowers emitted ~1.4 times more aliphatic compounds than female flowers. The 5-methylundecane, 3-methylundecane, *n*-dodecane, *n*-nonadecane, *n*-heneicosane, *n*-docosane, and tricyclo[3.1.0.0(2,4)]hexane, 3,6-diethyl-3,6-dimethyl-, trans- were detected among different flower types (Supplementary Table S2). Aliphatic hydrocarbons are a diverse group of compounds that contribute to the overall floral scent profile, particularly in species like muscadine grapes. Although they tend to be less volatile than other VOCs, they play a critical role in the structure and persistence of floral aromas. These hydrocarbons provide subtle background notes, such as waxy, oily, or occasionally woody scents, which complement and enhance the more prominent floral fragrance compounds. The primary functional roles of these aliphatic hydrocarbons include contributing to the physical stability of the flower, helping to prevent water loss, and providing a barrier against herbivory and pathogens. By forming a protective layer, they help maintain the structural integrity of the flower, which is essential for its reproductive success (Kapoor et al., 2023). Beyond their protective functions, aliphatic hydrocarbons influence pollinator behavior by stabilizing the emission of more volatile, attractive compounds, thus extending the duration of floral scent in the air. This extended-release can increase the flower's attractiveness to pollinators, particularly those that rely on long-range scent detection, such as bees, moths, and butterflies. These insects are drawn to flowers that maintain a consistent olfactory signal over time, helping them to navigate toward the floral source (Paré and Tumlinson, 1999; Jürgens, 2004; Junker and Blüthgen, 2010). Thus, while aliphatic hydrocarbons may be less prominent in odor, their ecological and functional roles are crucial for both the plant's defense mechanisms and its interactions with pollinators.

Among 39 terpene volatiles identified in muscadine flowers, eight (20.5%) were found exclusively in female flowers, twelve (30.8%) were specific to perfect flowers, and nineteen (48.7%) were detected in both flower types (Figure 2B). Female flowers produced a significantly lower number of terpene volatiles (9.8 ± 1.2) than perfect flowers (13.5 ± 1.3). Among the evaluated flower types, the perfect 'Late Fry' flowers stood out with the highest terpene production, generating a total of 19 distinct terpenes. In contrast, the female 'Darlene' flowers exhibited the lowest terpene number, with only 4 terpenes identified. This variation in terpene production highlights the differences in volatile compound profiles between various flower types and genotypes, suggesting that the genetic background and flower structure may influence the biosynthesis of these important aromatic compounds. Understanding these differences can provide valuable insights into the factors that contribute to flower scent and, consequently, pollinator attraction. The total terpene levels in muscadine flowers varied widely, ranging from 51.4 ± 7.3 μg/100g in female 'C8-6-1' flowers to 4072.8 ± 576.6 μg/100g in perfect 'B20-18-2' flowers. Notably, the sesquiterpenes (*Z,E*)-α-farnesene and α-selinene, along with the diterpenoid alcohol (*E,E*)-geranyl linalool, were exclusively detected in female flowers (Supplementary Table S2). In contrast, four terpenes, including β-elemene, ϒ-elemene, α-muurolene, and β-bisabolene, were unique to perfect flowers. Several terpenes, though present in both flower types, exhibited significantly higher accumulation levels in perfect flowers. These included selina-4,11-diene (~19.8-fold), selina-4(15),7(11)-diene (~4.4-fold), valencene (~8.4-fold), (*E*)-β-farnesene (~2.6-fold), α-farnesene (~3.3-fold), germacrene D (~5.6-fold), junenol (~2.4-fold), and (–)-kaurene (~6.4-fold). Among these, valencene has been identified as an effective floral volatile in *Vitis* species, primarily localized in the anthers and pollen grains (Martin et al., 2009). This compound is also a key active terpene in orchid flowers, where it plays a crucial role in attracting Euglossine bees (Gerlach and Schill, 1991). Similarly, α-farnesene is a major terpene emitted by butterfly bush (*Buddleja davidii*) flowers, eliciting strong antennal responses in butterflies and moths (Andersson, 2003; Guédot et al., 2008). Likewise, (*Z,E*)-α-farnesene has been shown to stimulate antennal responses in honeybees (Dötterl and Vereecken, 2010).

Terpene volatiles are integral to floral scent profiles and serve vital ecological functions, including attracting pollinators and deterring herbivores. Muscadine floral terpenes, which include sesquiterpenes, diterpenoid alcohols, and monoterpenoid alcohols, contribute a range of aromas from fruity and floral to woody and earthy. These terpenes are particularly important for the short- and long-range attraction of pollinators. This diversity adds complexity to the floral bouquet, enabling individual flowers to stand out to pollinators. Most muscadine terpenes, significantly contribute to defining floral scent profiles and play dual roles in both attracting pollinators and defending against herbivores by making the plant less palatable, attracting predators of herbivores, or repelling herbivores or pathogens (Pichersky and Gershenzon, 2002; Dudareva et al., 2006; Knudsen et al., 2006; Junker and Blüthgen, 2010; Schiestl, 2010). The floral organs, petals, stamens, pistils, sepals, and nectaries, are the primary sources of floral volatiles in many plant species (Dobson et al., 1996). However, pollen plays a critical role in pollinator attraction, producing substantial quantities of volatiles distinct from those emitted by other floral organs (Dobson and Bergstroem, 2000). In *Vitis* species, sesquiterpene biosynthesis has been localized specifically within the anthers and developing pollen grains (Martin et al., 2009). This suggests that volatile emissions decrease after pollination, signaling the availability of pollen to pollinators. Since pollen is a major reward for pollinators, its quantity and viability significantly influence pollinator visits (Carr et al., 2015). Consequently, female flowers, which lack pollen, may suffer from reduced pollinator attraction due to lower terpene emissions and the absence of the pollen reward. Perfect muscadine flowers exhibited ~4.5-fold higher terpene production compared to female flowers. This enhanced production likely gives perfect flowers a competitive edge in attracting pollinators.

Cross-correlation analysis among muscadine variables

The relationships between the accumulation of different VOCs and the type of muscadine flowers were examined using the Pearson correlation coefficient. Results revealed a strong positive correlation between the number of flowers per inflorescence and terpene level ($r^2 = 0.75$, $P = 8.5 \times 10^{-4}$), suggesting that the higher terpene output in perfect flowers may enhance pollinator attraction compared to female flowers. This higher terpene production in perfect flowers is likely due to the presence of pollen, which has been shown to influence VOC levels (Carr et al., 2015).

Moreover, the accumulation of the aldehydes was positively correlated with esters ($r^2 = 0.84$, $P = 5.5 \times 10^{-5}$), terpenes ($r^2 = 0.73$, $P = 1.4 \times 10^{-3}$), aliphatic ($r^2 = 0.77$, $P = 5.1 \times 10^{-4}$), and miscellaneous levels ($r^2 = 0.87$, $P = 1.4 \times 10^{-5}$). Esters accumulation was also positively correlated with terpenes ($r^2 = 0.71$, $P = 1.9 \times 10^{-3}$), aliphatic ($r^2 = 0.76$, $P = 7.3 \times 10^{-4}$), and miscellaneous compounds ($r^2 = 0.75$, $P = 8.6 \times 10^{-4}$). These correlations can be due to the overlapping biosynthetic pathways, co-regulation by similar environmental factors, synergism effects due to the combination of VOCs, and/or their complementary contributions to the floral attractive and complex scents (Pichersky and Gershenzon, 2002; Dudareva et al., 2006; Knudsen et al., 2006; Pichersky et al., 2006; Tholl et al., 2006). Such coordinated production allows the maximum effect of the flower on the pollinators and plant protection from herbivores. Besides, a significant correlation was observed for terpenes and aliphatic hydrocarbons ($r^2 = 0.52$, $P = 3.8 \times 10^{-2}$). Both terpenes and aliphatic hydrocarbons originate from the common pool of primary metabolites. Aliphatic hydrocarbons are derived from the fatty acid metabolite while terpenes are produced via the mevalonate or methylerythritol phosphate pathways, starting from acetyl-CoA. The production of terpenes and aliphatic hydrocarbons can be associated with the plant's metabolic state. Increased flux of primary metabolites as acetyl-CoA can be beneficial for enhancing the production of both classes of compounds (Dudareva et al., 2013).

Multivariate statistical analysis of terpene volatiles in muscadine flowers

Multivariate statistical analysis was performed using the terpene volatiles detected in muscadine flowers to determine the potential differences between female and perfect flowers. Terpenes were chosen due to their key roles in pollinator attraction, floral scents, and biological relevance (Crowell et al., 2002; Farré-Armengol et al., 2017; Qiao et al., 2021). Principal component analysis (PCA) revealed that the first two components accounted for 39.9% and 17.3% of the variance, respectively (Figure 3A). Perfect and female flowers deviated from each other and clustered depending on their similarities in the terpene volatile context. However, certain genotypes, including the perfect 'Noble' and female 'Majesty' flowers, were located out of the two groups, suggesting that their terpene accumulation is more genotype-dependent than flower-type-dependent. PCA biplot analysis also displayed the separation of flowers' type and their close aggregation based on their similarities in composition (Figure 3B). The (*Z*,*E*)-α-farnesene and (*E*,*E*)-geranyl linalool were computed as dominant contributors to the cluster of female flowers. At the same time, the selina-4,11-diene, selina-4(15),7(11)-diene, and valencene were the primary volatile terpenes contributing to the perfect flower group.

To further assess the diversity in terpenes among muscadine flowers, a supervised partial least squares-discriminant analysis (PLS-DA) was performed. The analysis identified key terpenes based on variable importance in projection (VIP) scores. Eleven volatile terpenes with VIP scores above 1.0 were identified, including (*E*,*E*)-geranyl linalool, β-elemene, germacrene D, α-gurjunene, (*Z*,*E*)-α-farnesene, junenol, α-muurolene, α-farnesene, β-bisabolene, (*E*)-α-bergamotene, and α-selinene (Figure 4A).

Floral terpenes are volatile compounds that play pivotal roles in plant development, defense, and pollinator attraction (Degenhardt et al., 2009). These molecules serve a variety of ecological functions, from attracting pollinators to providing direct and indirect protection against insects, bacteria, and fungi (Gershenzon and Dudareva, 2007; Boncan et al., 2020). To examine the differences in terpene profiles between muscadine flowers, a heatmap was generated using Pearson correlation analysis, illustrating the relationships between the relative levels of key volatile terpenes and each flower genotype (Figure 4B). The analysis identified both positive and negative correlations, with the eleven volatile metabolites emerging as key marker terpenes. These markers effectively differentiate female and perfect flowers. Among them, five shared terpene markers were found to be significantly higher in perfect flowers (~4.7-fold), highlighting the distinct variation in terpene context between the two flower types. Of these, only two

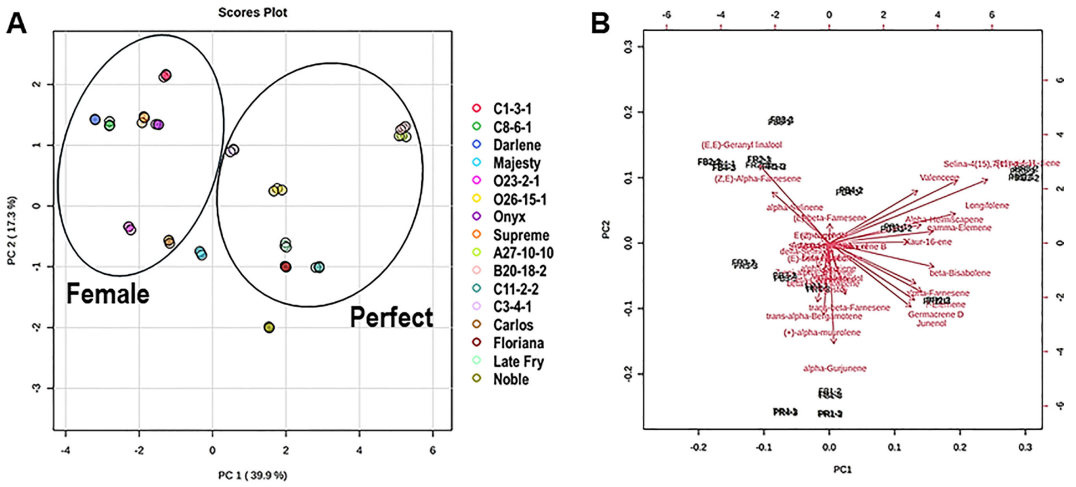

FIGURE 3
(A) Principal component analysis (PCA) 2D score plot and **(B)** Biplot of terpenes in different muscadine flowers. In the 2D score plot, the several colors and shapes represent muscadine flower genotypes. The scores of the observations (i.e., muscadine flower genotypes) are indicated. The vectors that point toward the same direction correspond to the variables (i.e., volatile metabolites) with similar response profiles.

terpenes, the sesquiterpenes α-farnesene ($r^2 = 0.71$, $P = 1.9 \times 10^{-3}$) and germacrene D ($r^2 = 0.73$, $P = 1.4 \times 10^{-3}$), showed a significant positive correlation with perfect flowers, suggesting their critical role in defining floral scent and ecological interactions. Both α-farnesene and germacrene D are integral components of floral scents, contributing to their complexity and appeal (Mostafa et al., 2022). Their unique aromatic profiles, along with their interactions with other volatile compounds, enhance the overall fragrance of flowers, making them attractive to pollinators and vital for plant reproduction. Understanding their roles in flower odor provides valuable insights into the ecological dynamics between plants and their pollinators.

The different flower organs generally contribute to the overall floral volatiles (Dobson et al., 1996). Female and perfect flowers display similar structures, excluding stamens and pollen. Pollens produce considerable amounts of floral volatiles that serve as master attractants for pollinators, and they can be easily distinguished from the scents of other floral organs due to their remarkable effectiveness (Dobson and Bergstroem, 2000; Martin et al., 2009). It is tempting to suggest that the difference in terpene quality between female and perfect flowers (i.e., type, number, and quantity) may be due to pollen presence. Three terpene markers, β-elemene, α-muurolene, and β-bisabolene, were exclusively accumulated in perfect flowers. The β-elemene sesquiterpene has been previously identified as a marker volatile for pollen odor in bay laurel (*Laurus nobilis*) flowers (Flamini et al., 2002). Known for its unique odor profile, β-elemene contributes spicy, woody, and citrusy notes to floral fragrances, enhancing the complexity and distinctiveness of flower aromas (Knudsen et al., 2006; Raguso, 2008). Variations in β-elemene content across species and within genotypes create distinct olfactory profiles that attract specific pollinators. Its presence in flowers like *Cymbidium* orchids and *Rosa* species further underscores its significance in shaping fragrance landscapes (Dobson, 2006; Farré-Armengol et al., 2017). Additionally, β-elemene facilitates ecological interactions by attracting pollinators and providing indirect defenses against herbivores (Dudareva et al., 2006; Zhang, 2018). Similarly, α-muurolene serves as a distinctive marker for perfect flower genotypes. This sesquiterpene, known for its woody, earthy, and slightly spicy scent, enhances the olfactory signatures of flowers. Identified in the volatile emissions of several flowers, including *Rosa* and *Lilium* species, α-muurolene adds depth to floral aromas and aids in differentiating flowers based on their scent profiles (Knudsen et al., 2006). It plays a crucial ecological role, acting as an attractant for pollinators while deterring herbivores and pathogens. By adding earthy undertones, α-muurolene can enhance the appeal of flowers to specific insect visitors (Dudareva et al., 2013). Its presence often complements other terpenes, contributing to the overall complexity of the floral bouquet and distinguishing species or varieties with pronounced earthy or resinous scents (Jürgens et al., 2003; Raguso, 2008). Finally, β-bisabolene is pivotal in distinguishing floral fragrances due to its characteristic woody, spicy, and mildly sweet scent. This compound enriches the olfactory profile of certain plant species and plays a dual role in attracting pollinators while providing defensive properties against herbivores and pathogens through its antimicrobial and insect-repellent activities (Gershenzon and Dudareva, 2007; Maffei et al., 2011). Its exclusive presence in perfect flowers emphasizes its role in differentiating floral types within the species, contributing to the richness of the terpene blend (Degenhardt et al., 2009).

Another set of three terpenes, (*Z*,*E*)-α-farnesene, (*E*,*E*)-geranyl linalool, and α-selinene, was found exclusively in female muscadine flowers. The (*Z*,*E*)-α-farnesene is particularly significant due to its contribution to the scent profiles of various flowers, including jasmine, where it imparts sweet, floral, and fruity characteristics (Zhang et al., 2021). This sesquiterpene interacts synergistically with other volatile compounds, such as linalool and geraniol, enhancing the overall fragrance profile (Murray et al., 2024). Additionally, its appealing fruity aroma attracts pollinators, thus playing a crucial role in plant reproduction (Wang and Erb, 2022). The (*E*,*E*)-geranyl linalool is a floral compound that possesses a unique structure that includes both geranyl and linalool moieties, allowing it to emit a complex sweet and slightly citrusy scent. It works synergistically with other volatile compounds to enhance the

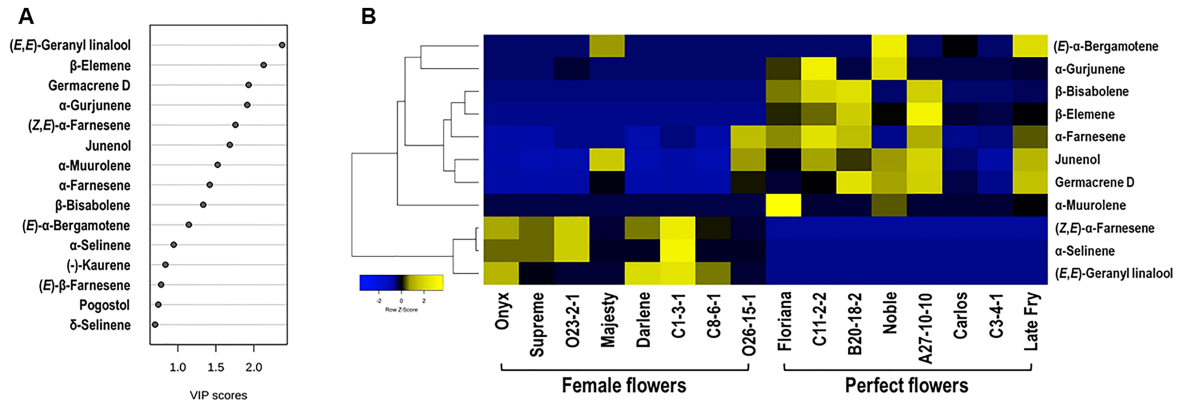

FIGURE 4
(A) Variable importance in projection (VIP ≥ 1.0) measure in PLS-DA analysis. **(B)** Hierarchical Clustering Heatmap of VIP (score ≥ 1.0) terpenes in muscadine flower genotypes. In Heatmap analysis, each column refers to the muscadine flower genotype, and each row indicates the marker volatile terpenes. The blue and yellow colors with values (ranging from −2 to +2) describe the lower and higher terpene intensities; the higher the yellow color intensity (> 0 to +2 values), the higher terpene levels. In contrast, the higher blue color intensity (< 0 to −2 values) represents the lower terpene levels.

overall fragrance, resulting in a more rounded and complex floral scent (Xu et al., 2021). Its presence in floral scents can signal the availability of nectar, thus attracting essential pollinators and promoting plant reproduction (Raguso, 2008). Studies have shown that specific floral fragrances, including those containing (*E*,*E*)-geranyl linalool, can influence pollinator behavior, leading to increased visitation rates and enhancing the success of fertilization (Knudsen et al., 2006). On the other side, the female flower-exclusive α-selinene, while enhancing floral aromas, has been reported as a repellent sesquiterpene that negatively affects bee attraction in other plant species (Quarrell et al., 2023). In muscadine, such emissions may compromise female flowers' ability to attract pollinators.

VOCs facilitate the interaction between plants and mutualists, pests, and pathogenic antagonists. Semiochemicals that function in these interactions can be produced constitutively or in response to outside interactions and stimuli that occur above and below ground (Massalha et al., 2017). Although semiochemicals can travel long distances, plant/plant and plant/microbe communication usually occurs at relatively short distances, while plant volatiles with a role in plant/insect interaction are perceived at long distances. The resulting extreme dilution and the significant variation in chemical structures and properties of the VOCs pose a challenge to the analysis of the volatiles and their precursors (Fu et al., 2017). Floral terpenes are widely classified based on the disparity in composition, amount, and emission (Muhlemann et al., 2014). They are further categorized based on their scent spread efficiency to long- and short-distance terpenes, targeting specific or broad pollinators (Guterman et al., 2002; Schiestl et al., 2003). These terpene volatiles can effectively attract different pollinators such as bees, lovebugs, ants, and wasps (Bouwmeester et al., 2019). The composition of muscadine floral volatiles is complex and diverse. It may be challenging for the pollination vectors to identify their flower hosts quickly and accurately in a complex environment if relying solely on the attractiveness of a specific floral volatile compound. Accordingly, it is tempting to speculate that the identified floral terpene volatile markers are potentially coordinated to attract long-range and short-range localized pollinators, ensuring appropriate fruit set efficiency.

Determination of fruit set efficiency in female and perfect flowers

Our results suggested that perfect flower muscadine genotypes potentially exhibit a greater pollinator attraction capacity than female flowers, likely due to the superior quality of terpenes produced. The interaction between flowers and insect pollinators can be assessed by evaluating the efficiency of flower-to-fruit set progression within the inflorescence. To explore this further, we assessed the fruit set capacity of both female and perfect flowers under two pollination conditions: open pollination (insect-dependent) and controlled pollination. The female cultivar 'Darlene' and the perfect flower cultivar 'Floriana' were selected for the study, with pollen from the perfect flower cultivar 'Granny Val' used in the controlled pollination experiments (Figure 5A).

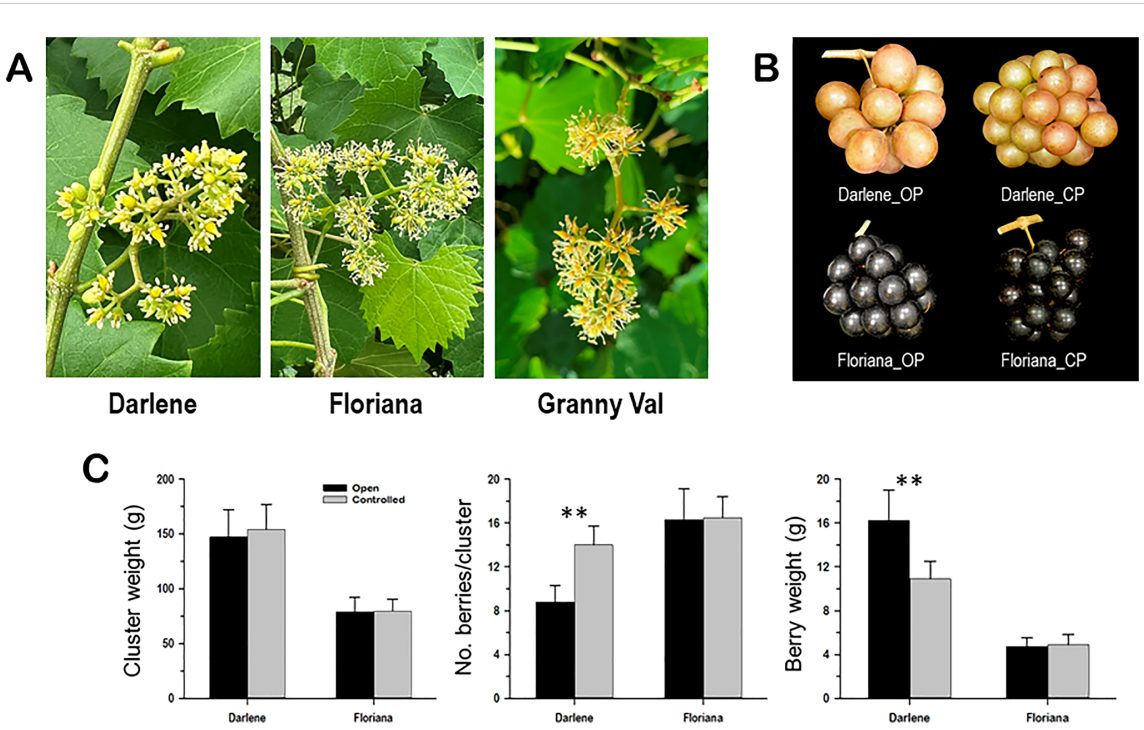

FIGURE 5
(A) Close-up views of the female 'Darlene' and perfect 'Floriana' muscadine flowers used for the fruit set efficiency assay; however, the perfect 'Granny Val' flowers were used as a source of pollens. **(B)** Close-up views of 'Darlene' and 'Floriana' ripe clusters resulted from open pollination (OP) and controlled pollination (CP). **(C)** Determination of the capacity of perfect and female flowers to set berries in response to open and controlled pollination. The characters of cluster weight (g), number of berries/cluster, and berry weight (g) were used for the assessment. Data represent the mean values ± SD (n = 5). ** Significant at $p \leq 0.01$.

Controlled pollination significantly altered fruit set efficiency and cluster characteristics in 'Darlene' but not in 'Floriana' (Figure 5B). In 'Darlene' controlled pollination resulted in very compact clusters, driven by a ~60% increase in the number of berries per cluster, coupled with a ~33% reduction in individual berry weight, leading to only minor changes in total cluster weight (Figure 5C). Interestingly, no significant changes in fruit set efficiency or cluster characteristics were observed in 'Floriana' under controlled pollination.

These results suggested that female muscadine flowers may not reach their full fruit set potential due to lower pollinator attraction efficiency, leading to sporadic pollinator visits. When this limitation was eliminated through hand pollination, fruit set accuracy improved significantly. In contrast, perfect flower muscadines do not perceive this challenge, as they are self-pollinated, and supported by a well-developed floral volatilome machinery that attracts pollinators.

Conclusions

The dynamic of plant/insect pollinator interaction is a bi-directional communication procedure. Consequently, many mechanisms have evolved to engage organisms in different types of interactions. Flower factors, including morphological parameters, reward potentials, and allelochemicals context coordinate the dialogue between flowers and pollinators. Allelochemicals, mainly volatile terpenes, can mediate these critical interactions. However, the interaction mechanism and the kind of vector pollinator depend on the context of terpenes and VOCs emitted in terms of style, number, intensity, function, and environmental circumstances. The self-pollinated perfect muscadine flowers are distinguished from the obligatory cross-pollinated female flowers by possessing several floral attributes, including visual (i.e., flower number), reward (i.e., pollen and nectar), and biochemical (i.e., VOCs and terpenes) parameters to ensure an accurate pollination procedure (Figure 6A). The prevalence of these floral parameters was, to some extent, compromised in female flowers, but even more, female flowers emit volatile terpenes that contradict pollinators rather than attract them (Figure 6B). The development of the knowledge on species-dependent floral parameters, particularly VOCs emitted by flowers is of great importance for plant ecology in the context of environmental and climate changes. The findings in this study show that floral scent plays an important role in structuring flower–insect relations in complex and challenging environmental circumstances. Understanding the effect of flower sex patterns in floral VOC profiles may have important implications for plant-pollinator interactions among communities differing in species composition.

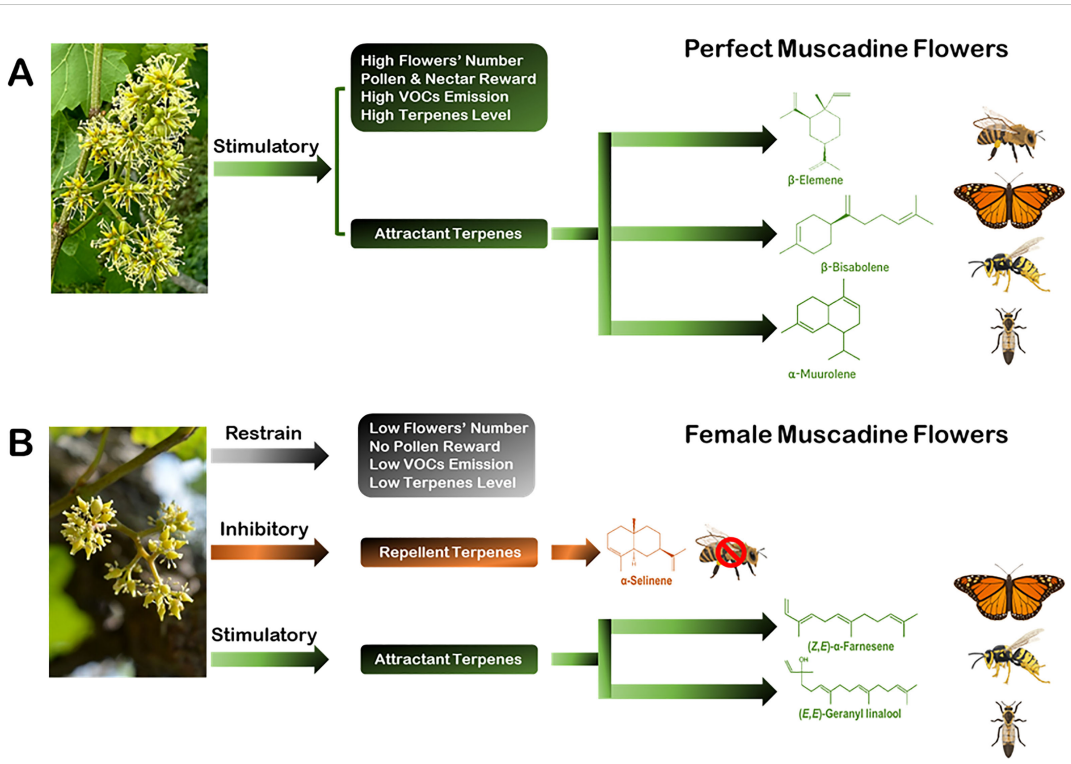

FIGURE 6
Descriptions of the characteristics of perfect and female muscadine flowers highlight several parameters influencing their ability to attract pollinators. These parameters encompass floral morphology, rewards, the emission of VOCs, and specific terpenoid profiles. Such traits play a vital role in drawing diverse pollinators, including butterflies, lovebugs, wasps, and bees. **(A)** Perfect muscadine flowers exhibit notable advantages for pollinator attraction through a combination of favorable attributes. They are characterized by a high number of flowers, abundant pollen, nectar availability, and elevated levels of effective VOCs and terpenes. These features work synergistically to support efficient and reliable pollination processes. **(B)** By contrast, female muscadine flowers show a reduced prevalence of these floral traits. They are defined by a lower flower count, the absence of pollen, and diminished levels of attractive VOCs and terpenes. Furthermore, female flowers emit volatile terpenes, such as α-selinene (indicated in orange), which may deter bees instead of attracting them. However, certain volatile compounds associated with pollinator stimulation, marked in green, still showcase their capacity to draw in other visitors, albeit to a lesser extent.

Data availability statement

The original contributions presented in the study are included in the article/Supplementary Material. Further inquiries can be directed to the corresponding author.

Author contributions

AD: Data curation, Formal analysis, Investigation, Methodology, Software, Validation, Visualization, Writing – original draft. PD: Formal analysis, Methodology, Software, Validation, Visualization, Writing – original draft. EO: Data curation, Formal analysis, Investigation, Methodology, Validation, Visualization, Writing – original draft. PG: Investigation, Methodology, Visualization, Writing – original draft. AI: Formal analysis, Writing – original draft. AM: Formal analysis, Writing – original draft. VT: Resources, Writing – review & editing. NH: Formal analysis, Writing – review & editing. WK: Investigation, Writing – review & editing. KW: Conceptualization, Writing – review & editing. IE-S: Conceptualization, Data curation, Formal analysis, Funding acquisition, Investigation, Methodology, Project administration, Resources, Software, Supervision, Validation, Visualization, Writing – original draft, Writing – review & editing.

Funding

The author(s) declare financial support was received for the research, authorship, and/or publication of this article. This work was supported by the Florida Department of Agriculture and Consumer Services (FDACS) – Viticulture Advisory Council (VAC) (Project # 008667) to Dr. Islam El-Sharkawy.

Conflict of interest

The authors declare that the research was conducted in the absence of any commercial or financial relationships that could be construed as a potential conflict of interest.

Generative AI statement

The author(s) declare that no Generative AI was used in the creation of this manuscript.

Publisher's note

Supplementary material

The Supplementary Material for this article can be found online at: https://www.frontiersin.org/articles/10.3389/fpls.2025.1548564/full#supplementary-material

References

Andersson, S. (2003). Antennal responses to floral scents in the butterflies *Inachis io*, *Aglais urticae* (Nymphalidae), and *Gonepteryx rhamni* (Pieridae). *Chemoecology* 13, 13–20. doi: 10.1007/s000490300001

Barbagallo, M., Antonino, P., and Filippo, S. (2014). Identification of aroma compounds of *Vitis vinifera* L. flowers by SPME GC-MS analysis. *Vitis* 53, 111–113. doi: 10.5073/vitis.2014.53.111-113

Barragán-Fonseca, K. Y., van Loon, J. J. A., Dicke, M., and Lucas-Barbosa, D. (2019). Use of visual and olfactory cues of flowers of two brassicaceous species by insect pollinators. *Ecol. Entomol.* 45, 45–55. doi: 10.1111/een.12775

Boachon, B., Burdloff, Y., Ruan, J. X., Rojo, R., Junker, R. R., Vincent, B., et al. (2019). A promiscuous *CYP706A3* reduces terpene volatile emission from *Arabidopsis* flowers, affecting florivores and the floral microbiome. *Plant Cell* 31, 2947–2972. doi: 10.1105/tpc.19.00320

Bojko, B., Reyes-Garcés, N., Bessonneau, V., Goryński, K., Mousavi, F., Souza Silva, E. A., et al. (2014). Solid-phase microextraction in metabolomics. *Trac. Trends Anal. Chem.* 61, 168–180. doi: 10.1016/j.trac.2014.07.005

Boncan, D. A. T., Tsang, S. S. K., Li, C., Lee, I. H. T., Lam, H. M., Chan, T. F., et al. (2020). Terpenes and terpenoids in plants: Interactions with environment and insects. *Int. J. Mol. Sci.* 21, 7382. doi: 10.3390/ijms21197382

Bouwmeester, H., Schuurink, R. C., Bleeker, P. M., and Schiestl, F. (2019). The role of volatiles in plant communication. *Plant J.* 100, 892–907. doi: 10.1111/tpj.14496

Bryant, R. J., and McClung, A. M. (2011). Volatile profiles of aromatic and non-aromatic rice cultivars using SPME/GC–MS. *Food Chem.* 124, 501–513. doi: 10.1016/j.foodchem.2010.06.061

Burkle, L. A., and Runyon, J. B. (2016). Drought and leaf herbivory influence floral volatiles and pollinator attraction. *Glob. Change Biol.* 22, 1644–1654. doi: 10.1111/gcb.13149

Burkle, L. A., and Runyon, J. B. (2019). Floral volatiles structure plant–pollinator interactions in a diverse community across the growing season. *Funct. Ecol.* 33, 2116–2129. doi: 10.1111/1365-2435.13424

Campbell, J., Sarkhosh, A., Habibi, F., Ismail, A., Gajjar, P., Zhongbo, R., et al. (2021). Biometrics assessment of cluster- and berry-related traits of muscadine grape population. *Plants* 10, 1067. doi: 10.3390/plants10061067

Cane, J. H. (2016). Adult pollen diet essential for egg maturation by a solitary *Osmia* bee. *J. Insect Physiol.* 95, 105–109. doi: 10.1016/j.jinsphys.2016.09.011

Carr, D. E., Haber, A. I., LeCroy, K. A., Lee, D. A. E., and Link, R. I. (2015). Variation in reward quality and pollinator attraction: The consumer does not always get it right. *AoB Plants* 7, plv034. doi: 10.1093/aobpla/plv034

Crowell, A. L., Williams, D. C., Davis, E. M., Wildung, M. R., and Croteau, R. (2002). Molecular cloning and characterization of a new linalool synthase. *Arch. Biochem. Biophys.* 405, 112–121. doi: 10.1016/s0003-9861(02)00348-x

Darwish, A. G., Das, P. R., Ismail, A., Gajjar, P., Balasubramani, S. P., Sheikh, M. B., et al. (2021). Untargeted metabolomics and antioxidant capacities of muscadine grape genotypes during berry development. *Antioxidants* 10, 914. doi: 10.3390/antiox10060914

David, O. R., and Doro, F. (2023). Industrial fragrance chemistry: A brief historical perspective. *Eur. J. Org. Chem.* 26, e202300900. doi: 10.1002/ejoc.202300900

Degenhardt, J., Köllner, T. G., and Gershenzon, J. (2009). Monoterpene and sesquiterpene synthases and the origin of terpene skeletal diversity in plants. *Phytochemistry* 70, 1621–1637. doi: 10.1016/j.phytochem.2009.07.030

de Ibarra, N. H., Langridge, K. V., and Vorobyev, M. (2015). More than colour attraction: Behavioural functions of flower patterns. *Curr. Opin. Insect. Sci.* 12, 64–70. doi: 10.1016/j.cois.2015.09.005

Delle-Vedove, R., Schatz, B., and Dufay, M. (2017). Understanding intraspecific variation of floral scent in light of evolutionary ecology. *Ann. Bot.* 120, 1–20. doi: 10.1093/aob/mcx055

Deng, H., He, R., Huang, R., Pang, C., Ma, Y., Xia, H., et al. (2022). Optimization of a static headspace GC-MS method and its application in metabolic fingerprinting of the leaf volatiles of 42 citrus cultivars. *Front. Plant Sci.* 13. doi: 10.3389/fpls.2022.1050289

Dobson, H. E. M. (2006). "Relationship between floral fragrance composition and type of pollinator," in *Biology of Floral Scent*. Eds. N. Dudareva and E. Pichersky (Taylor and Francis, Boca Raton), 147–198.

Dobson, H. E. M., and Bergstroem, G. (2000). The ecology and evolution of pollen odors. *Plant Syst. Evol.* 222, 63–87. doi: 10.1007/BF00984096

Dobson, H. E. M., Groth, I., and Bergström, G. (1996). Pollen advertisement: Chemical contrasts between whole-flower and pollen odors. *Am. J. Bot.* 83, 877–885. doi: 10.2307/2446264

Dötterl, S., and Gershenzon, J. (2023). Chemistry, biosynthesis, and biology of floral volatiles: Roles in pollination and other functions. *Nat. Prod. Rep.* 40, 1901. doi: 10.1039/D3NP00024A

Dötterl, S., and Jürgens, A. (2005). Spatial fragrance patterns in flowers of *Silene latifolia*: Lilac compounds as olfactory nectar guides? *Plant Syst. Evol.* 255, 99–109. doi: 10.1007/s00606-005-0344-2

Dötterl, S., and Vereecken, N. J. (2010). The chemical ecology and evolution of bee–flower interactions: A review and perspectives. *Can. J. Zool.* 88, 668–697. doi: 10.1139/Z10-031

Dudareva, N., Klempien, A., Muhlemann, J. K., and Kaplan, I. (2013). Biosynthesis, function and metabolic engineering of plant volatile organic compounds. *New Phytol.* 198, 16–32. doi: 10.1111/nph.12145

Dudareva, N., Negre, F., Nagegowda, D. A., and Orlova, I. (2006). Plant volatiles: Recent advances and future perspectives. *Crit. Rev. Plant Sci.* 25, 417–440. doi: 10.1080/07352680600899973

Dudareva, N., and Pichersky, E. (2006). *Biology of floral scent*. *1st ed* (Boca Raton: CRC Press). doi: 10.1201/9781420004007

Dudareva, N., Pichersky, E., and Gershenzon, J. (2004). Biochemistry of plant volatiles. *Plant Physiol.* 135, 1893–1902. doi: 10.1104/pp.104.049981

El-Sharkawy, I., Manríquez, D., Flores, F. B., Regad, F., Bouzayen, M., Latché, A., et al. (2005). Functional characterization of a melon alcohol acyl-transferase gene family involved in the biosynthesis of ester volatiles. Identification of the crucial role of a threonine residue for enzyme activity. *Plant Mol. Biol.* 59, 345–362. doi: 10.1007/s11103-005-8884-y

Farré-Armengol, G., Filella, I., Llusià, J., and Peñuelas, J. (2017). Floral volatile organic compounds: Between attraction and deterrence of visitors under global change. *Perspect. Plant Ecol. Evol. Syst.* 15, 56–67. doi: 10.1016/j.ppees.2012.12.002

Flamini, G., Cioni, P. L., and Morelli, I. (2002). Differences in the fragrances of pollen and different floral parts of male and female flowers of *Laurus nobilis*. *J. Agric. Food Chem.* 50, 4647–4652. doi: 10.1021/jf020269x

Fu, X., Zhou, Y., Zeng, L., Dong, F., Mei, X., Liao, Y., et al. (2017). Analytical method for metabolites involved in biosynthesis of plant volatile compounds. *RSC Adv.* 7, 19363–19372. doi: 10.1039/C7RA00766C

Gerlach, G., and Schill, R. (1991). Composition of orchid scents attracting Euglossine bees. *Bot. Acta* 104, 379–384. doi: 10.1111/j.1438-8677.1991.tb00245.x

Gershenzon, J., and Dudareva, N. (2007). The function of terpene natural products in the natural world. *Nat. Chem. Biol.* 3, 408–414. doi: 10.1038/nchembio.2007.5

Gibernau, M., Maia, A. C. D., and Amaral Navarro, D.M.d. (2021). Pollination ecology and floral scent chemistry of *Philodendron fragrantissimum* (Araceae). *Bot. Lett.* 168, 384–394. doi: 10.1080/23818107.2021.1909497

Gil, M., Bottini, R., Pontin, M., Berli, F. J., Salomon, M. V., and Piccoli, P. (2014). Solar UV-B radiation modifies the proportion of volatile organic compounds in flowers of field-grown grapevine (*Vitis vinifera* L.) cv. Malbec. *Plant Growth Regul.* 74, 193–197. doi: 10.1007/s10725-014-9911-2

Guédot, C., Landolt, P. J., and Smithhisler, C. L. (2008). Odorants of the flowers of butterfly bush, *Buddleja davidii*, as possible attractants of pest species of moths. *Fla. Entomol.* 91, 576–582. doi: 10.1653/0015-4040-91.4.576

Guterman, I., Shalit, M., Menda, N., Piestun, D., Dafny-Yelin, M., Shalev, G., et al. (2002). Rose scent: Genomics approach to discovering novel floral fragrance-related genes. *Plant Cell* 14, 2325–2338. doi: 10.1105/tpc.005207

Hickey, C. C., Smith, E. D., Cao, S., and Conner, P. (2019). Muscadine (*Vitis rotundifolia* Michx., syn. *Muscadinia rotundifolia* (Michx.) Small): The resilient, native grape of the southeastern US. *Agriculture* 9, 131. doi: 10.3390/agriculture9060131

Huang, M., Sanchez-Moreiras, A. M., Abel, C., Sohrabi, R., Lee, S., Gershenzon, J., et al. (2012). The major volatile organic compound emitted from *Arabidopsis thaliana* flowers, the sesquiterpene (*E*)-β-caryophyllene, is a defense against a bacterial pathogen. *New Phytol.* 193, 997–1008. doi: 10.1111/j.1469-8137.2011.04001.x

Jo, H. E., Song, K., Kim, J. G., and Lee, C. H. (2022). Non-targeted metabolomic analysis for the comparative evaluation of volatile organic compounds in 20 globally representative cucumber lines. *Front. Plant Sci.* 13. doi: 10.3389/fpls.2022.1028735

Junker, R. R., and Blüthgen, N. (2010). Floral scents repel facultative flower visitors but attract obligate ones. *Ann. Bot.* 105, 777–782. doi: 10.1093/aob/mcq045

Jürgens, A. (2004). Flower scent composition in diurnal *Silene* species (Caryophyllaceae): phylogenetic constraints or adaption to flower visitors? *Biochem. Syst. Ecol.* 32, 841–859. doi: 10.1016/j.bse.2004.03.009

Jürgens, A., Witt, T., and Gottsberger, G. (2003). Flower scent composition in *Dianthus* and *Saponaria* species (Caryophyllaceae) and its relevance for pollination biology and taxonomy. *Biochem. Syst. Ecol.* 31, 345–357. doi: 10.1016/S0305-1978(02)00173-4

Kapoor, D., Bhardwaj, S., and Sharma, N. R. (2023). Fragrance stimulation mechanisms of flowers and their regulation under environmental constraints. *J. Plant Growth. Regul.* 42, 60–82. doi: 10.1007/s00344-021-10555-4

Kearns, C. A., and Inouye, D. W. (1997). Pollinators, flowering plants, and conservation biology. *Biosci.* 47, 297–307. doi: 10.2307/1313191

Kessler, A., and Baldwin, I. T. (2001). Defensive function of herbivore-induced plant volatile emissions in nature. *Science* 291, 2141–2144. doi: 10.1126/science.291.5511.2141

Knauer, A. C., and Schiestl, F. P. (2015). Bees use honest floral signals as indicators of reward when visiting flowers. *Ecol. Lett.* 18, 135–143. doi: 10.1111/ele.12386

Knudsen, J. T., Eriksson, R., Gershenzon, J., and Ståhl, B. (2006). Diversity and distribution of floral scent. *Bot. Rev.* 72, 1–120. doi: 10.1663/0006-8101(2006)72[1:DADOFS]2.0.CO;2

Li, H. M., Liu, W. B., Yang, L. L., Cao, H. Q., Pelosi, P., Wang, G. R., et al. (2020). Aromatic volatiles and odorant receptor 25 mediate attraction of *Eupeodes corollae* to flowers. *J. Agric. Food Chem.* 68, 12212–12220. doi: 10.1021/acs.jafc.0c03854

Liu, J., Chen, M., Ma, W., Ralle, B., Tunström, K., Sigsgaard, L., et al. (2023). Composition of strawberry flower volatiles and their effects on behavior of strawberry pollinators, *Bombus terrestris* and *Apis mellifera*. *Agronomy* 13, 339. doi: 10.3390/agronomy13020339

Maffei, M. E., Gertsch, J., and Appendino, G. (2011). Plant volatiles: Production, function, and pharmacology. *Nat. Prod. Rep.* 28, 1359–1380. doi: 10.1039/c1np00021g

Manríquez, D., El-Sharkawy, I., Flores, F. B., El-Yahyaoui, F., Regad, F., Bouzayen, M., et al. (2006). Two highly divergent alcohol dehydrogenases of melon exhibit fruit ripening-specific expression and distinct biochemical characteristics. *Plant Mol. Biol.* 61, 675–685. doi: 10.1007/s11103-006-0040-9

Martin, D. M., Toub, O., Chiang, A., Lo, B. C., Ohse, S., Lund, S. T., et al. (2009). The bouquet of grapevine (*Vitis vinifera* L. cv. Cabernet Sauvignon) flowers arises from the biosynthesis of sesquiterpene volatiles in pollen grains. *Proc. Natl. Acad. Sci. U.S.A.* 106, 7245–7250. doi: 10.1073/pnas.0901387106

Massalha, H., Korenblum, E., Tholl, D., and Aharoni, A. (2017). Small molecules below-ground: The role of specialized metabolites in the rhizosphere. *Plant J.* 90, 788–807. doi: 10.1111/tpj.13543

Mayer, C., Adler, L., Armbruster, W. S., Dafni, A., Eardley, C., Huang, S. Q., et al. (2011). Pollination ecology in the 21st century: Key questions for future research. *J. Poll. Ecol.* 3, 8–23. doi: 10.26786/1920-7603(2011)1

McGregor, S. E. (1976). Insect pollination of cultivated crop plants. *USDA Agr. Res. Serv. Handbook. No.* 496, 1–411.

Mostafa, S., Wang, Y., Zeng, W., and Jin, B. (2022). Floral scents and fruit aromas: Functions, compositions, biosynthesis, and regulation. *Front. Plant Sci.* 13. doi: 10.3389/fpls.2022.860157

Muhlemann, J. K., Klempien, A., and Dudareva, N. (2014). Floral volatiles: From biosynthesis to function. *Plant Cell Environ.* 37, 1936–1949. doi: 10.1111/pce.12314

Murray, A. F., Chen, X., Chen, F., and Russo, L. (2024). Pollinator visitation patterns are influenced by floral volatile profiles. *Plant Ecol.* 225, 929–942. doi: 10.1007/s11258-024-01444-3

Olien, W. C. (1990). The muscadine grape: Botany, viticulture, history, and current industry. *HortScience* 25, 732–739. doi: 10.21273/HORTSCI.25.7.732

Paré, P. W., and Tumlinson, J. H. (1999). Plant volatiles as a defense against insect herbivores. *Plant Physiol.* 121, 325–332. doi: 10.1104/pp.121.2.325

Park, I. K., Kim, J. N., Lee, Y. S., Lee, S. G., Ahn, Y. J., and Shin, S. C. (2008). Toxicity of plant essential oils and their components against *Lycoriella ingenua* (Diptera: Sciaridae). *J. Econ. Entomol.* 101, 139–144. doi: 10.1093/jee/101.1.139

Pichersky, E., and Dudareva, N. (2007). Scent engineering: Toward the goal of controlling how plants smell. *Trends Plant Sci.* 12, 69–75. doi: 10.1016/j.tibtech.2007.01.002

Pichersky, E., and Gershenzon, J. (2002). The formation and function of plant volatiles: Perfumes for pollinator attraction and defense. *Curr. Opin. Plant Biol.* 5, 237–243. doi: 10.1016/S1369-5266(02)00251-0

Pichersky, E., Noel, J. P., and Dudareva, N. (2006). Biosynthesis of plant volatiles: Nature's diversity and ingenuity. *Science* 311, 808–811. doi: 10.1126/science.1118510

Pichersky, E., and Raguso, R. A. (2018). Why do plants produce so many terpenoid compounds? *New Phytol.* 220, 692–702. doi: 10.1111/nph.14178

Pontes, M., Marques, J. C., and Câmara, J. S. (2009). Headspace solid-phase microextraction-gas chromatography-quadrupole mass spectrometric methodology for the establishment of the volatile composition of *Passiflora* fruit species. *Microchem. J.* 93, 1–11. doi: 10.1016/j.microc.2009.03.010

Qiao, Z., Hu, H., Shi, S., Yuan, X., Yan, B., and Chen, L. (2021). An update on the function, biosynthesis, and regulation of floral volatile terpenoids. *Horticulturae* 7, 451. doi: 10.3390/horticulturae7110451

Quarrell, S. R., Weinstein, A. M., Hannah, L., Bonavia, N., Del Borrello, O., Flematti, G. R., et al. (2023). Critical pollination chemistry: Specific sesquiterpene floral volatiles in carrots inhibit honey bee feeding. *J. Agric. Food Chem.* 71, 16079–16089. doi: 10.1021/acs.jafc.3c03392

Raguso, R. A. (2008). Wake up and smell the roses: The ecology and evolution of floral scent. *Ann. Rev. Ecol. Evol. Syst.* 39, 549–569. doi: 10.1146/annurev.ecolsys.38.091206.095601

Raguso, R. A. (2016). More lessons from Linalool: Insights gained from a ubiquitous floral volatile. *Curr. Opin. Plant Biol.* 32, 31–36. doi: 10.1016/j.pbi.2016.05.007

Raguso, R. A., and Pichersky, E. (1999). New perspectives in pollination biology: Floral fragrances. A day in the life of a linalool molecule: Chemical communication in a plant-pollinator system. Part 1: Linalool biosynthesis in flowering plants. *Plant Species Biol.* 14, 95–120. doi: 10.1046/j.1442-1984.1999.00014.x

Sampson, B. J., Noffsinger, S. L., Gupton, C. L., and Magee, J. B. (2001). Pollination biology of the muscadine grape, *Vitis rotundifolia* Michx. *HortScience* 36, 120–124. doi: 10.21273/HORTSCI.36.1.120

Schiestl, F. P. (2010). The evolution of floral scent and insect chemical communication. *Ecol. Lett.* 13, 643–656. doi: 10.1111/j.1461-0248.2010.01451.x

Schiestl, F. P., Peakall, R., Mant, J. G., Ibarra, F., Schulz, C., Franke, S., et al. (2003). The chemistry of sexual deception in an orchid-wasp pollination system. *Science* 302, 437–438. doi: 10.1126/science.1087835

Schwab, W., Davidovich-Rikanati, R., and Lewinsohn, E. (2008). Biosynthesis of plant-derived flavor compounds. *Plant J.* 54, 712–732. doi: 10.1111/j.1365-313X.2008.03446.x

Schwery, O., Sipley, B. N., Braga, M. P., Yang, Y., Rebollo, R., and Zu, P. (2023). Plant scent and plant-insect interactions—Review and outlook from a macroevolutionary perspective. *J. Syst. Evol.* 61, 465–486. doi: 10.1111/jse.12933

Surburg, H., and Panten, J. (2005). *Common fragrance and flavor materials: Preparation, properties and uses. 5th ed* (Weinheim, Germany: Wiley-VCH). doi: 10.1002/3527608214

Tholl, D., Boland, W., Hansel, A., Loreto, F., Röse, U. S., and Schnitzler, J. P. (2006). Practical approaches to plant volatile analysis. *Plant J.* 45, 540–560. doi: 10.1111/j.1365-313X.2005.02612.x

Tieman, D., Zhu, G., Resende, M. F. Jr., Lin, T., Nguyen, C., Bies, D., et al. (2017). A chemical genetic roadmap to improved tomato flavor. *Science* 355, 391. doi: 10.1126/science.aal1556

Unsicker, S. B., Kunert, G., and Gershenzon, J. (2009). Protective perfumes: The role of vegetative volatiles in plant defense against herbivores. *Curr. Opin. Plant Biol.* 12, 479–485. doi: 10.1016/j.pbi.2009.04.001

Verdonk, J. C., De Vos, C. R., Verhoeven, H. A., Haring, M. A., Van Tunen, A. J., and Schuurink, R. C. (2003). Regulation of floral scent production in petunia revealed by targeted metabolomics. *Phytochemistry* 62, 997–1008. doi: 10.1016/S0031-9422(02)00707-0

Wang, L., and Erb, M. (2022). Volatile uptake, transport, perception, and signaling shape a plant's nose. *Essays Biochem.* 66, 695–702. doi: 10.1042/EBC20210092

Wei, Z., Luo, J., Huang, Y., Guo, W., Zhang, Y., Guan, H., et al. (2017). Profile of polyphenol compounds of five muscadine grapes cultivated in the United States and in newly adapted locations in China. *Int. J. Mol. Sci.* 18, 1–18. doi: 10.3390/ijms18030631

Wen, J., Lu, L. M., Nie, Z. L., Liu, X. Q., Zhang, N., Ickert-Bond, S., et al. (2018). A new phylogenetic tribal classification of the grape family (Vitaceae). *J. Syst. Evol.* 56, 262–272. doi: 10.1111/jse.12427

Xu, J. B., Li, Y. Z., Huang, S., Chen, L., Luo, Y. Y., Gao, F., et al. (2021). Diterpenoid alkaloids from the whole herb of *Delphinium grandiflorum* L. *Phytochemistry* 190, 112866. doi: 10.1016/j.phytochem.2021.112866

Zhang, X. M. (2018). Floral volatile sesquiterpenes of *Elsholtzia rugulosa* (Lamiaceae) selectively attract Asian honey bees. *J. Appl. Entomol.* 142, 359–362. doi: 10.1111/jen.12481

Zhang, J., Li, J., Wang, J., Sun, B., Liu, Y., and Huang, M. (2021). Characterization of aroma-active compounds in *Jasminum sambac* concrete by aroma extract dilution analysis and odour activity value. *Flavour Fragr. J.* 36, 197–206. doi: 10.1002/ffj.3631

frontiers | Frontiers in Plant Science

TYPE Original Research
PUBLISHED 02 April 2025
DOI 10.3389/fpls.2025.1559012

OPEN ACCESS

EDITED BY
Mariam Gaid,
Independent Researcher,
Braunschweig, Germany

REVIEWED BY
Lourin Malak,
Assiut University, Egypt
Junjun Fan,
Jinling Institute of Technology, China

*CORRESPONDENCE
Dongsheng Wang
wdse66@126.com

†These authors have contributed equally to this work

RECEIVED 11 January 2025
ACCEPTED 12 March 2025
PUBLISHED 02 April 2025

CITATION
Wang J, Guo X, Wu Z, Wang D, Guo P, Han Y, Jiang H and Lü Z (2025) Integration of volatile and non-volatile metabolites and the transcriptome reveals the formation mechanisms of differential aroma compounds between *Pyrus communis* and *Pyrus pyrifolia* cultivars. *Front. Plant Sci.* 16:1559012. doi: 10.3389/fpls.2025.1559012

Integration of volatile and non-volatile metabolites and the transcriptome reveals the formation mechanisms of differential aroma compounds between *Pyrus communis* and *Pyrus pyrifolia* cultivars

Jiao Wang[1,2†], Xianping Guo[1,2†], Zhongying Wu[1,2], Dongsheng Wang[1,2*], Peng Guo[1], Yongping Han[1], Hui Jiang[1] and Zhenzhen Lü[1]

[1]Institute of Horticulture, Henan Academy of Agricultural Sciences, Zhengzhou, China, [2]Henan Horticulture and Floriculture Engineering Research Center, Zhengzhou, China

Introduction: Aroma compounds are important flavor components in pear fruit. Among cultivated pears, fruits from *Pyrus communis* (hereafter referred to as *P. communis*) cultivars are famous for their abundant aroma, while the fruits of most *Pyrus pyrifolia* (hereafter referred to as *P. pyrifolia*) cultivars lack aroma compounds. A comparative study on the formation of differential aroma compounds between the two species could provide a theoretical foundation for improving the aroma quality of *P. pyrifolia* cultivars. However, there is a lack of systematic research on this subject.

Methods: An analysis of volatile and non-volatile metabolites was combined with transcriptome analysis to explore the formation mechanism of differential aroma compounds between three *P. communis* and three *P. pyrifolia* cultivars.

Results: In this study, a total of 510 volatile compounds were identified in the six cultivars. Of these, sixteen ester and alcohol compounds, including butyl acetate, hexyl acetate, ethyl-2-methylbutyrate, ethanol, butanol, propanol, and 2-methylbutanol, with higher contents in the *P. communis* cultivars than in the *P. pyrifolia* cultivars were identified as the primary differential aroma compounds. Among the possible synthesis pathways for these 16 aroma compounds, certain amino acid degradation processes, including isoleucine, valine, and alanine oxidation and threonine dehydration, were found to provide important intermediate substances for synthesis. Within the key enzyme genes in the synthesis pathway, several critical enzyme genes, including monoacylglycerol lipase (PcMAGL, pycom08g09340), threonine dehydrase (PcTD, pycom12g10020), and acyl CoA dehydrogenase (PcACD, pycom16g13880), might be important factors contributing to the disparity in aromatic compounds between *P. communis* and *P. pyrifolia* cultivars.

Discussion: The aforementioned results provide valuable information into the formation mechanisms of differential aroma compounds and offer novel target sites for enhancing pear aroma quality through gene editing.

KEYWORDS

aroma compounds, volatile metabolite, transcriptome, pear fruit, synthesis pathways

Introduction

Aroma compounds are small molecular compounds generated during metabolic processes in plant roots, stems, leaves, flowers, fruits, and other organs. They typically exhibit lipophilic properties and can be released from plants via cell membranes (Pichersky et al., 2006). Aroma compounds in fruit are crucial constituents of fruit flavor and significantly contribute to the assessment of fruit quality (Arimura et al., 2001). They are typically involved in multiple metabolic pathways, which can be categorized into the following three categories based on variations in precursor substances: fatty acid oxidation pathways, amino acid oxidation pathways, and terpenoid synthesis pathways.

Fatty acid oxidation pathways encompass the lipoxygenase (LOX) and β-oxidation pathways. The former uses unsaturated fatty acids as substrates, undergoing a series of enzymatic reactions to produce C6 aldehydes, alcohols, and C9 aldehydes, alcohols, and their corresponding esters (Schwab et al., 2008; Matsui, 2006). For example, aroma compounds such as hexal, hexyl alcohol, hexenal, hexenol, and hexenyl ester, which are found in fruits such as peach, melon, strawberry, and banana, are synthesized through this metabolic pathway. Key enzymes involved in this process include LOX, hydroperoxide lyase (HPL), ethanol dehydrogenase (ADH), and alcohol acyltransferase (AAT) (Beekwilder et al., 2004; Zhang et al., 2010; Chen et al., 2016).

β-oxidation pathways use saturated fatty acids as substrates, which undergo a series of catalytic reactions, including oxidation, hydration, dehydrogenation, and thiolysis, to yield acetyl CoA and fatty acyl CoA. These compounds serve as essential precursors for straight-chain ester synthesis (Napora-Wijata et al., 2014). Furthermore, this pathway provides the primary source for the biosynthesis of volatile substances, such as γ-decalactone, δ-valerolactone, and γ-caprolactone (Xi et al., 2012; Zhang et al., 2017).

A significant portion of volatile aroma compounds, such as alcohols, aldehydes, and esters with a low carbon atomic number, are synthesized via amino acid oxidation pathways (Knudsen et al., 2006). These pathways are responsible for the synthesis of aroma compounds such as 3-methyl-1-butanol, 3-methylbutyl ester, 3-methylbutyric acid, and eugenol methyl ether in banana (Jordán et al., 2001), eugenol methyl ether in strawberry (Aragüez et al., 2013), and eugenol and cinnamate in melon (Gonda et al., 2010). The key enzymes involved in these pathways primarily include aminotransferase (ATF), pyruvate decarboxylase (PDC), alcohol acyltransferase (AAT), and aromatic amino acid aminotransferase (ArAT).

Terpenoids are compounds characterized by an isoprene unit (C5H8) as their fundamental skeleton and serve as crucial constituents of plant aroma substances (Zeng et al., 2020). Grape and citrus fruits exhibit high levels of terpenoids, including s-linalool, which is primarily synthesized through this pathway (Asikin et al., 2012; Yue et al., 2021). The key enzymes involved in this process include 3-hydroxy-3-methylglutarate monoacyl CoA reductase (HMGR), 1-deoxy-D-xylulose-5-phosphate synthetase (DXS), and terpene synthetase (TPS).

Pear (*Pyrus*), which belong to the Pomoideae in the family Rosaceae, originated in the western or southwestern mountains of China during the Tertiary period (Wu et al., 2018). Throughout their dispersal, over thirty recognized species have emerged, with five being most extensively cultivated: *Pyrus pyrifolia*, *Pyrus bretschneideri*, *Pyrus sinkiangensis*, *Pyrus communis*, and *Pyrus ussuriensis* (Li and Zhang, 2020). Most *P. pyrifolia* and *P. bretschneideri* cultivars exhibit either no aroma or a weak aroma (Li and Zhang, 2020; Taiti et al., 2017). However, the *Pyrus sinkiangensis* cultivar 'Korla' has a distinct aroma (Tian et al., 2014), while *P. communis* and *P. ussuriensis* develop a pronounced aroma after ripening and softening (Chen et al., 2018; Qin et al., 2012).

Research on fruit aroma in *Pyrus ussuriensis* is primarily focused on 'Nanguo' pear. The predominant fruit aroma compounds consist of esters, aldehydes, alcohols, and ketones, with esters being the most abundant (Wei et al., 2016). Ethyl hexanoate, hexyl acetate, and ethyl butanoate are representative aroma compounds found in 'Nanguo' pear, and they are predominantly synthesized in the fatty acid oxidation pathway (Li et al., 2022; Shi et al., 2019). In this biosynthesis pathway, the high expression levels of *PuFAD2*, *PuLOX2*, *PuLOX5*, and *PuAAT* are significantly associated with elevated ester concentrations in 'Nanguo' pear fruit (Wei et al., 2016; Li et al., 2022). Following treatment with ethylene, low temperature, and methyl jasmonate, significant changes have been observed in aroma compounds and key genes involved in the fatty acid oxidation pathway (Yao et al., 2022; Wu et al., 2023; Shi et al., 2019).

Volatile compounds, including methyl acetate, ethyl acetate, propyl acetate, ethyl dimethylbutyrate, hexanol, and ethanol, are found in high concentrations in *P. communis* pears and are the major contributors to their fruity aroma (Wang M, et al., 2019;

Kahle et al., 2005). The contents of these compounds can be reduced through long-term low-temperature storage and melatonin and 1-methylcyclopropene treatment, which may be directly correlated with the decreased activities of LOX, HPL, and AAT in fatty acid oxidation pathways (Makkumrai et al., 2014; Liu et al., 2019; Rizzolo et al., 2005). Ethyl acetate, ethyl butyrate, ethyl acetate butyrate, and hexal have been detected at a significant level in many 'Korla' pears, suggesting that these compounds contribute to the characteristic aroma of these pears (Tian et al., 2014).

'Nanguo', *P. communis*, and 'Korla' pears have been well studied for their aroma characteristics, providing a foundation for further research on pear fruity aroma. However, there is a lack of systematic research on the characteristics and metabolic pathways of differential aroma between aromatic and non-aromatic pear cultivars. In this study, three *P. communis* and three *P. pyrifolia* cultivars were used as materials, and an analysis of their volatile and non-volatile metabolites was combined with transcriptome analysis to investigate the formation mechanisms of differential aroma compounds in the two species. This will establish a theoretical foundation for enhancing the aroma quality of *P. pyrifolia* cultivars and enable further research on the mechanism of aroma formation in *P. communis* cultivars.

Materials and methods

Plant materials

A total of six varieties, comprising three *P. communis* cultivars ('Radana', 'Red Clapp's Favorite', and 'Qiu Yang') and three *P. pyrifolia* cultivars ('Akizuki', 'Wonhwang', and 'Sucui No.1'), were used to determine volatile compounds (Figure 1). A total of 10 varieties, comprising five *P. communis* cultivars ('Abate Fetel', 'Red Clapp's Favorite', 'Qiu Yang', 'Radana', and 'Packham's Triumph') and five *P. pyrifolia* cultivars ('Akizuki', 'Wonhwang', 'Whasan', 'Mansoo', and 'Sucui No.1'), were utilized to investigate the expression levels of key genes in the biosynthesis pathway. For simplification, 'Radana', 'Red Clapp's Favorite', 'Qiu Yang', 'Abate Fetel', 'Packham's Triumph', 'Akizuki', 'Wonhwang', and 'Sucui No.1', 'Whasan', and 'Mansoo' were abbreviated as 'Rad', 'RCF', 'QY', 'AF', 'PT', 'Aki', 'Won', 'SC1', 'Wha', and 'Man', respectively. 'Rad', 'RCF', and 'QY' fruits were harvested at 120, 110, and 160 days after pollination, respectively. They were then left at room temperature for 2 weeks. Once the flesh began to soften, the fruit was cut into small cubes and transferred to an ultra-low temperature refrigerator. The 'Aki', 'Won', and 'SC1' fruits were

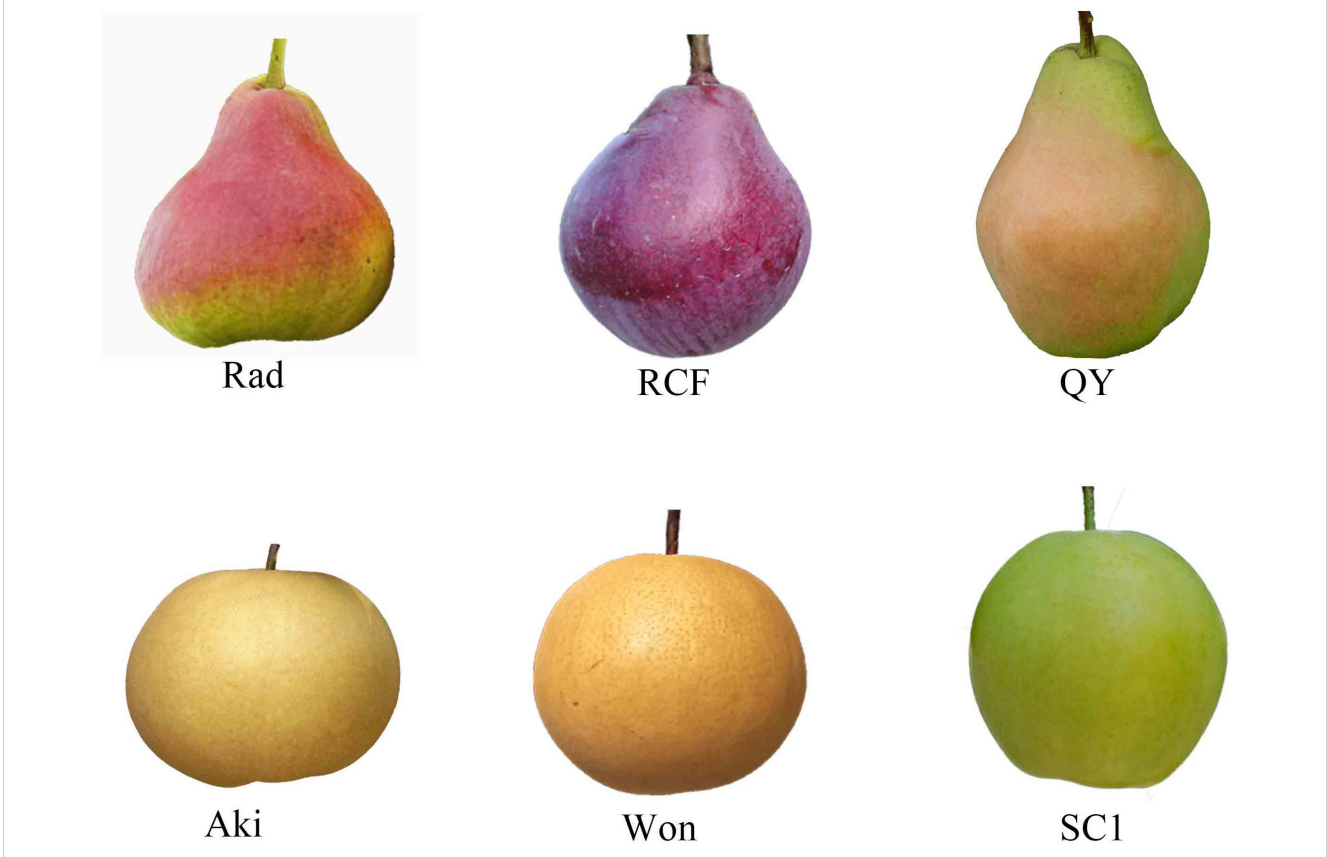

FIGURE 1
Fruit photographs of 6 pear cultivars for volatile compound determination. The top three belong to the *P. communis* cultivars, while the bottom three are *P. pyrifolia* cultivars.

harvested at 160, 130, and 100 days after pollination, respectively. These fruits were also stored at room temperature for 2 weeks before the flesh was collected. Days after pollination were determined using conventional indices, such as seed color, amylum content, peel color and fruit size (Chen et al., 2018). At fruit maturity, ten fruits were collected from each cultivar. The fruits were peeled, cored, and sliced, after which the sliced flesh from the ten fruits was mixed for volatile compound analysis and transcriptome sequencing.These cultivars were planted at the Yuanyang Test Base of the Henan Academy of Agricultural Sciences, Henan Province, China.

Volatile compound analysis

The headspace solid-phase microextraction (HS-SPME) technique was employed for the collection of volatile compounds from the fruit of the six cultivars analyzed. Specifically, 2 g of fruit flesh was weighed and placed in a clean vial, which was then sealed with a lid. The sample was agitated at 250 rpm and maintained at 50°C for 15 min and then extracted at 55°C for 30 min. A 50/30 μm DVB/CAR/PDMS fiber (Supelco, Sigma, USA) was utilized for volatile substance extraction from the fruit sample, followed by desorption at 25°C for 5 min to facilitate subsequent gas chromatography–mass spectrometry analysis (Man et al., 2023).

A 7890B gas chromatography system, 5977B mass spectrometry system, and DB-Wax column (30 m × 0.25 mm × 0.25 μm, Agilent Technologies, CA, USA) were employed to detect desorbed volatile compounds. The volatile compounds of the fruit were separated using a constant flow of helium gas at a rate of 1 mL/min, and these separated compounds were then directed to the column. The inlet temperature was set to 260°C. The heating procedure commenced with an initial temperature of 40°C for 5 min, followed by a gradual increase to 220°C at a rate of 5°C/min and further elevation to 250°C at a rate of 20°C/min for 2.5 min. The mass spectra was recorded at 70 eV in electron impact ionization (EI) mode. The ion source temperature was set to 230°C, and the quadrupole mass detector temperature was maintained at 150°C. A comprehensive scanning method was employed to fully analyze the mass spectra of volatile compounds within a scanning range of 20–400 m/z. The chromatogram of each flavor compound was acquired using the LECO Pegasus BT GC-TOF-MS system. The NIST 2017 database was employed to annotate the raw data to obtain the relevant information including the name, retention time, CAS number, and peak area for each compound. A total of 2uL of internal standard (2-octanol) solution were injected into the vial using a syringe.

The content of the volatile compound was determined using the following formula (Wang C, et al., 2019).

$$\text{Content (ug/g)} = \frac{\frac{S1}{S2} \times C2 \times V2 \times 10^{-3}}{m}$$

S1: Peak area of the volatile compound.

S2: Peak area of the internal standard (2-octanol)

C2: Concentration of the internal standard (40ug/mL)

V2: Volume of the internal standard (2uL)

m: Quality of the fruit flesh (g)

OAV were calculated according to the following formula (Nuzzi et al., 2008):

$$OAV_i = \frac{C_i}{OT_i}$$

Ci: Concentration of the volatile compound i in the fruit flesh.

OTi: Odor threshold concentration of the volatile Compound i.

Non-volatile compound analysis

Thermo Vanquish (Thermo Fisher Scientific, MA, USA) was employed for liquid chromatography analysis. An ACQUITY UPLC® HSS T3 (2.1 × 100 mm, 1.8 μm) column (Waters, Milford, MA, USA) was utilized with a flow rate of 0.3 mL/min at a column temperature of 40°C and a sample size of 2 μL. In the LC-ESI (+)-MS mode, the mobile phase consisted of 0.1% formic acid in acetonitrile (v/v) (B2) and 0.1% formic acid in water (v/v) (A2). The elution procedure was as follows: 0–1 min, 8% B2; 1–8 min, 8–98% B2; 8–10 min, 98% B2; 10–10.1 min, 98–8% B2; 10.1–12 min, 8% B2. In LC-ESI (-)-MS mode, the mobile phase consisted of acetonitrile (B3) and ammonium formate (5 mM) (A3). The elution procedure was as follows: 0–1 min, 8% B3; 1–8 min, 8–98% B3; 8–10 min, 98% B3; 10–10.1 min, 98–8% B3; 10.1–12 min, 8% B3.

A Thermo Orbitrap Exploris 120 (Thermo Fisher Scientific, USA) with an electrospray ionization (ESI) ion source was utilized for mass spectrometric detection. Simultaneous MS1 and MS/MS (Full MS-ddMS2 mode, data-dependent MS/MS) acquisition were employed. The spray voltages ESI(+) and ESI(−) were set at 3.50 kV and −2.50 kV, respectively. The sheath gas pressure was maintained at 40 arb, and the aux gas flow remained steady at 10 arb. The capillary temperature was set at 325°C. The HCD technique was employed for secondary fragmentation, with a normalized collision energy of 30% and MS2 resolving power of 15,000 FWHM. The initial four ions within the signal were subjected to fragmentation, while superfluous MS/MS data were eliminated through automatic dynamic exclusion (Zelena et al., 2009; Want et al., 2013).

RNA extraction and sequencing analysis

Approximately 0.2 g fruit flesh was used for RNA extraction. Total RNA was extracted using a kit (Waryong, Beijing, China), treated with RNase-free DNAase (Takara, Dalian, China). NanoDrop 2000 (Thermo, Waltham, MA, USA) was used to measure the oligonucleotide concentration. Purity could be given from the A260/A280 and A260/A230 values and the Agilent Bioanalyzer 2100 Bioanalyzer (Agilent Technologies, Santa Clara, CA, USA).

Magnetic beads with Oligo (dT)s were used to enrich mRNA from 5 mg of total RNA. The mRNA was randomly fragmented with fragmentation buffer, and first-strand cDNA was synthesized with random hexamers (TIANGEN, Beijing, China). Double-stranded cDNA was then synthesized with dNTPs, RNase H, and DNA

polymerase I. The double-stranded cDNA was enriched by adding poly-(A)s and PCR amplification. The enriched cDNA was linked to a vector, which was used to construct a sequencing library and analyzed using the Agilent Bioanalyzer 2100 system (Agilent Technologies, CA, USA). cDNA library sequencing was performed in a HiSeq 2500 system (Illumina, San Diego, CA, USA). All of the pear fruit flesh sequencing was performed with three biological replicates. The low-quality reads were removed, and the high-quality data were aligned to the peach reference genome (Bartlett DH Genome v2.0) with TopHat2 using its default parameters. The gene expression levels were calculated as fragments per kilobase per million reads (FPKM). Differentially expressed genes were selected according to FPKM > 1 and fold change (Rad vs/SC1) > 1.5 or< 0.5 (Wang et al., 2022).

RT-qPCR analysis

RNA was extracted from fruit flesh using a rapid extraction kit (Aidlab, Beijing, China). Approximately 1.5 μg of the RNA was reverse-transcribed into cDNA using the FastKing RT Kit (with gDNASE) (TIANGEN, Beijing, China). The 20-μL PCR reaction system contained 2.0 μL cDNA diluted 10 times by adding ddH_2O, 0.5 μL forward primer, 0.5 μL reverse primer, 7 μL ddH_2O and 10 μL SYBR premix (Vazyme, Nanjing, China). Details of the amplification program were listed in Supplementary Table S12. The amplification program was run in the LightCycler® 480 II real-time fluorescent quantitative PCR instrument (Roche, BSL, CH). A pear tubulin gene was selected as a control (Wei et al., 2016). The primers used in this study were shown in Supplementary Table S13. We utilized the Primer-BLAST tool from the NCBI (National Center for Biotechnology Information) (https://www.ncbi.nlm.nih.gov/) database to design the primers. The amplification efficiency was obtained by referring to the formula $E=-1 + 10^{-1/S}$, with minor modification in the calculation (Pfaffl, 2001). E denoted the efficiency of qPCR, while S indicated the slope derived from the standard curve. cDNA mixture from ten cultivars (as detailed in the Plant materials section) was utilized as templates to evaluate primer amplification efficiency. The relative expression levels of genes were quantified using the 2^ –ΔΔCt method as described by Livak and Schmittgen (2001). Specifically, the mean ΔCt value for a certain gene was first determined. The ΔΔCt value was then calculated by subtracting ΔCt of other gene from the mean ΔCt of the certain gene. Finally, the relative gene expression levels were derived using the formula Power (2, –ΔΔCt).

Statistical analysis

The pheatmap package in R (v3.3.2) was used to conduct hierarchical cluster analysis (HCA) of volatile compounds. Principal component analysis (PCA) and Kyoto Encyclopedia of Genes and Genomes (KEGG) enrichment analysis of nonvolatile compounds and transcription products were performed using the Omicshare online tool (https://www.omicshare.com/tools/). Analysis of variance (ANOVA) was employed to assess the differences in gene expression across various cultivars, utilizing SPSS statistical software (SPSS 19.0, IBM) for the statistical analysis. Differences were denoted by lowercase letters (e.g., a, b, c, d) (Gai, 2000). P-values for volatile and non-volatile metabolites and transcriptome analysis, as well as the relative expression levels of genes, were calculated utilizing Microsoft Excel 2007.

Results

Analysis of volatile compounds in the flesh of *P. communis* and *P. pyrifolia* cultivars

The volatile compounds in the flesh of three *P. communis* and three *P. pyrifolia* cultivars were analyzed using HS-SPME and gas chromatography. A total of 510 volatile compounds were detected in 6 cultivars (Supplementary Table S1), with the following constituting the predominant constituents: esters (Rad (21%), RCF (23%), QY (28%), Aki (32%), Won (28%), and SC1 (19%)), alcohols (Rad (23%), RCF (18%), QY (16%), Aki (12%), Won (13%), and SC1 (14%)), and aldehydes (Rad (17%), RCF (15%), QY (13%), Aki (14%), Won (13%), and SC1 (22%)) (Figure 2C). The highest proportion in the three *P. communis* cultivars was comprised of esters and alcohols, consistent with the detection results in the flesh of 'Conference' and 'Packham' (two *P. communis* cultivars) (Torregrosa et al., 2019; Wang et al., 2019). However, a notable difference was observed in three *P. pyrifolia* cultivars, where esters and aldehydes constituted the predominant components, consistent with the detection results in 'Atago', 'Niitaka', 'Banndainiitaka', and 'Jinqiu' (Zhong et al., 2008). These findings suggest that the difference in alcohol and aldehyde levels between *P. communis* and *P. pyrifolia* cultivars contributes to the divergence in their aroma profiles. Subsequently, we conducted HCA on the shared volatile compounds among the six cultivars (Figure 2A), revealing distinct components unique to each cultivar. PCA of the volatile compounds also differentiated the three *P. communis* cultivars from the *P. pyrifolia* cultivars (Figure 2B). This suggests that volatile compounds among the three *P. communis* and three *P. pyrifolia* cultivars were significantly different and suitable for the subsequent identification of distinct aromatic compounds.

Identification of the key differentiating aroma compounds in the flesh of *P. communis* and *P. pyrifolia* cultivars

Comprehensive analysis was conducted on the volatile profiles of the six cultivars to further elucidate the key volatile compounds contributing to the aroma variations between *P. communis* and *P. pyrifolia* cultivars. As shown in Figure 3A, among the volatile compounds found in the three *P. communis* cultivars, 71 were shared by all three cultivars, while 116, 45, and 83 compounds were unique to 'Rad', 'RCF', and 'QY', respectively. Of these shared compounds, 19 exhibited significantly higher levels in the three *P. communis* cultivars than in the three *P. pyrifolia* cultivars, with esters

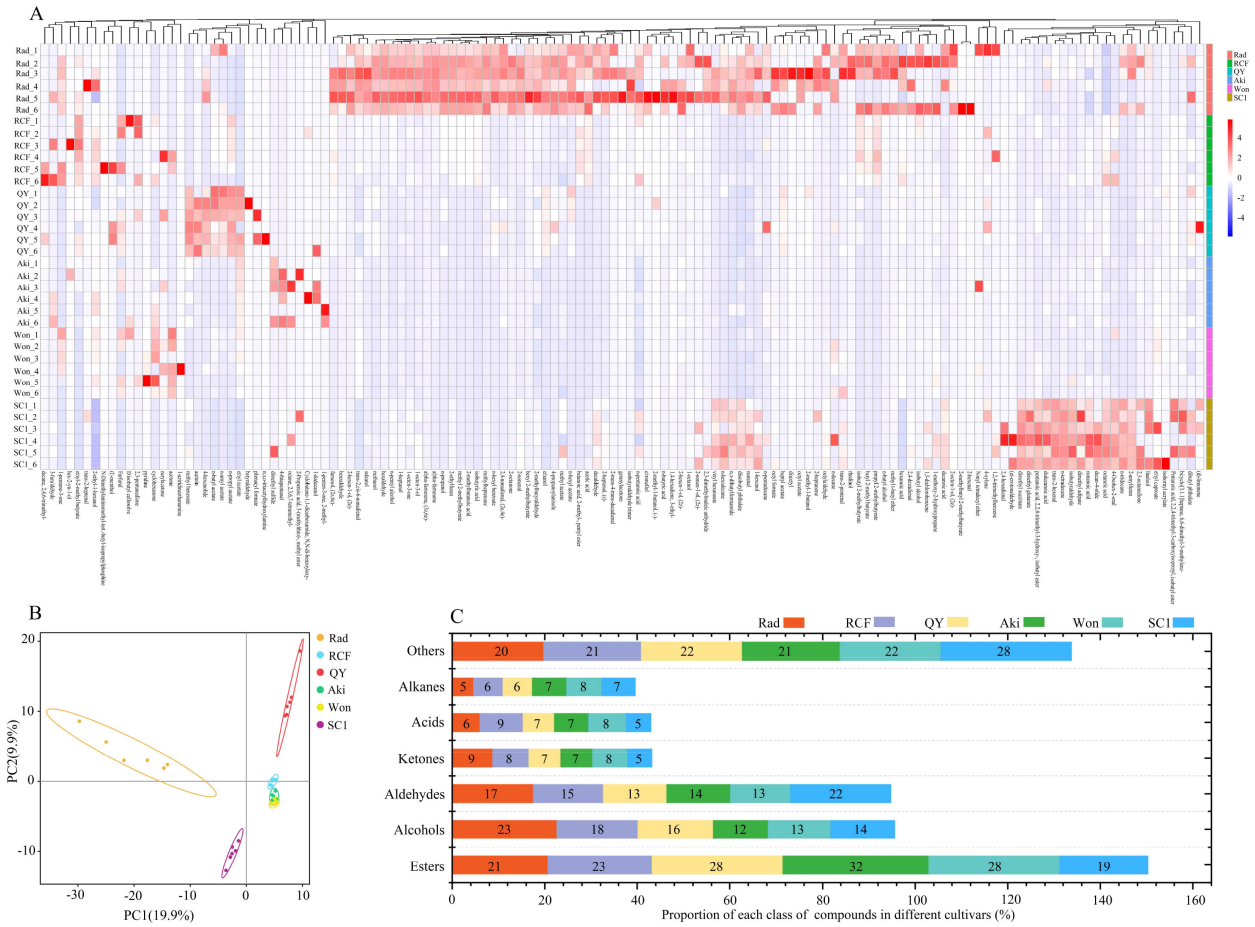

FIGURE 2
Analysis of volatile compounds in the flesh of six pear cultivars. **(A)** Hierarchical cluster analysis (HCA), **(B)** principal component analysis (PCA), and **(C)** chemical classification of volatile compounds in six pear cultivars.

and alcohols being the predominant compounds, accounting for 84% (Figures 3A, C; Supplementary Table S4). Among the esters and alcohols mentioned above, butyl acetate, hexyl acetate, amyl acetate, ethyl-2-methylbutyrate, butanol, propanol, and 2-methylbutanol have also been found in high concentrations in 'Conference', 'Comice', and 'Bartlett' cultivars, and all have floral and fruity flavors and high OAV values (Makkumrai et al., 2014; Zlatić et al., 2016; Torregrosa et al., 2019), indicating that they play an important role in enhancing the fruit flavor of *P. communis* pear. Among the 116, 45, and 83 unique volatile compounds identified in the 'Rad', 'RCF', and 'QY' cultivars, 33, 13, and 28, respectively, exhibited significantly higher levels compared to the other 5 cultivars (Figure 3A; Supplementary Tables S5–S7). Esters and alcohols accounted for the highest proportion of these compounds, at approximately 61, 54, and 64% in each cultivar (Figure 3C; Supplementary Tables S5–S7). Among these esters and alcohols, 1-nonanol, hexenyl acetate, (2z)-, and methyl propionate in 'Rad', Hydroxymethyl 2-hydroxy-2-methylpropionate and nerol in 'RCF', and 5-hexenyl acetate, isoamyl benzoate, and methyl benzoate in 'QY', these volatile compounds not only exhibit high concentrations but also possess floral and fruity flavors, (Supplementary Tables S5–S7), indicating they also play a key role in enhancing the aroma of these fruits.

Among the volatile compounds detected in the three *P. pyrifolia* cultivars, 47 compounds were shared by the three varieties, while 50, 35, and 88 compounds were unique to 'Aki', 'Won', and 'SC1', respectively (Figure 3B). Of the 47 volatile compounds, only ethyl caproate exhibited a significantly higher concentration in the three *P. pyrifolia* cultivars compared to the three *P. communis* samples (Figure 3B; Supplementary Table S11). This compound is characterized by its floral and fruity aroma, but the concentration remains relatively low when compared to the high levels of volatile compounds found in the three *P. communis* cultivars. Among the 50, 35, and 88 unique volatile compounds identified in 'Aki', 'Won', and 'SC1' cultivars, 7, 4, and 8, respectively, exhibited significantly higher levels compared to the other 5 cultivars (Figure 3B; Supplementary Tables S8–S10). Esters and aldehydes constituted the largest proportion. However, their quantities were limited, and most of them were present at low concentrations, consistent with findings in cultivar 'Hosui' (Taiti et al., 2017). The limited content and quantity of these compounds was likely the primary factor contributing to the faint fruit aroma of most *P. pyrifolia* cultivars.

As shown above, the quantity of volatile compounds with high contents shared by the three *P. communis* cultivars was greater than that of these present in the three *P. pyrifolia* cultivars. Similarly, the

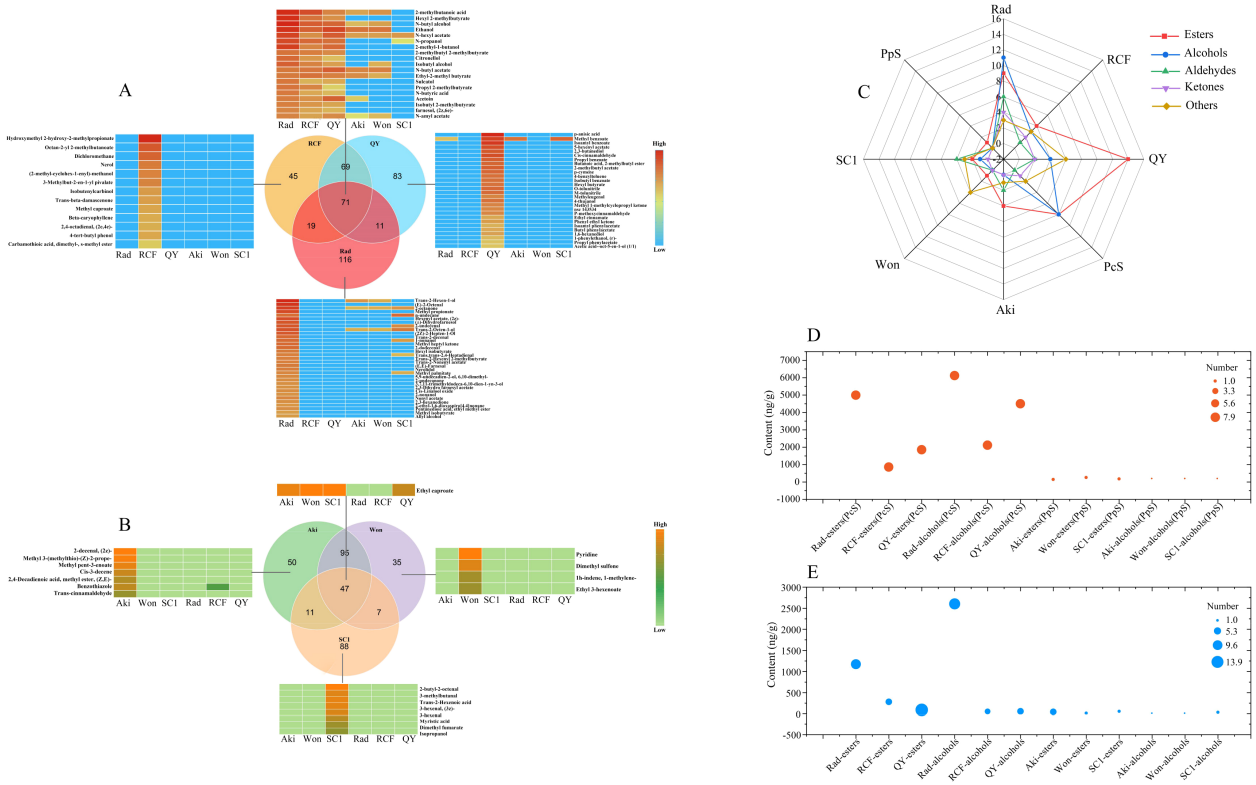

FIGURE 3
Determination of volatile compounds differing between three *P. communis* and three *P. pyrifolia* cultivars. **(A)** Venn and heat diagrams of common and unique volatile compounds in three *P. communis* and **(B)** three *P. pyrifolia* cultivars. **(C)** Radar map illustrating the distribution characteristics of esters, alcohols, aldehydes, ketones, and other constituents of common and unique volatile compounds found in three *P. communis* and three *P. pyrifolia* cultivars. The 'common volatile compounds' herein refer to the constituents that are present in three *P. communis* or three *P. pyrifolia* cultivars, with their concentrations markedly exceeding those found in three *P. pyrifolia* or three *P. communis* cultivars. The 'unique volatile compounds' are only expressed in one of three *P. communis* or three *P. pyrifolia* cultivars and constitute the predominant components in six cultivars. 'Rad', 'RCF', 'QY', 'Aki', 'Won', and 'SC1' denote the unique volatile compounds of the corresponding cultivars. 'PcS' and 'PpS' indicate the common volatile compounds present in three *P. communis* and three *P. pyrifolia* cultivars. The coordinate unit on the radar map is the quantity of each class of volatile compound **(D, E)** indicate bubble diagrams of esters and alcohols in the 'common volatile compounds' and 'unique volatile compounds'.

amount of volatile compounds specific to one *P. communis* cultivar at the highest concentration among the six cultivars was significantly higher than that of those unique to one *P. pyrifolia* cultivar. Among the common and unique volatile compounds in the three *P. communis* cultivars, esters and alcohols constituted the largest proportion, and most of them were present at high concentrations (Figures 3D, E). Considering that the majority of these alcohols and esters exhibit floral and fruity fragrances (Supplementary Tables S4–S7), they were identified as the primary aromatic compounds responsible for the differences between *P. pyrifolia* and *P. pyrifolia* cultivars.

Synthesis pathways of differential aroma compounds initially elucidated through transcriptomic and non-volatile metabolomic analyses

As previously mentioned, the primary reason for the intense aroma of *P. communis* cultivars was likely attributed to the substantial quantity and high concentration of common and unique esters and alcohols. We selected 16 esters and alcohols from the 19 volatile compounds common to the three *P. communis* cultivars and conducted a preliminary analysis on their biosynthesis pathways (Table 1). Our initial objective was to target the synthesis pathways of these 16 esters and alcohols using KEGG pathway enrichment. However, the limited number of volatile compounds included in the KEGG database restricted the effectiveness of pathway enrichment. Considering that volatile compounds are catalyzed by non-volatile substances through enzyme genes, we measured the non-volatile and transcriptomic profiles of 'Rad' and 'SC1' and compared these data ('Rad' vs 'SC1') to facilitate enrichment analysis. A total of 31,030 expressed genes and 331 non-volatile compounds were detected in the two varieties (Supplementary Tables S2, S3). PCA was conducted on the identified genes and non-volatile compounds (Figures 4A, F). The results revealed a distinct separation between the two cultivars, suggesting significant differences in their gene expression profiles and non-volatile compound contents. Further, the biological replicates of each cultivar exhibited consistent clustering (Figures 4A, F), indicating the good repeatability of the data. This ensured data quality and satisfied the requirements for subsequent analysis.

Among the detected genes, 2913 were up-regulated and assigned KEGG Orthology (referred to as KO), and 1717 were down-regulated and assigned KO. The total number of genes with KO was 9746 (Figures 4B, C). Of the detected non-volatile compounds, 103 were up-regulated and had a compound number (referred to as C number), and 50 were down-regulated and had a C number. A total of 331 were non-volatile substances with a C number (Figures 4G, H). KEGG enrichment analysis was performed on genes and non-volatile compounds with KO and C numbers. These differentially expressed genes and non-volatile compounds were primarily enriched in pathways related to carbohydrate, amino acid, lipid, energy metabolism, and secondary metabolite biosynthesis. Their sub-pathways included glycine, serine, and threonine metabolism, valine, leucine, and isoleucine degradation, linoleic acid and alpha-linolenic acid metabolism, and fatty acid degradation (Figures 4D, E, I, J). Due to their role in providing intermediate compounds for aromatic compound synthesis, these sub-pathways were selected as the primary sources for the production of 16 esters and alcohols.

Further identification of the synthesis pathways for differential aroma compounds

Ester compounds are synthesized through the reaction of acyl-CoA with alcohol, which is catalyzed by alcohol acyltransferase (AAT) (Liu et al., 2023). Among the 16 esters and alcohols, acyl-

TABLE 1 Contents and odor descriptions of 16 volatile esters and alcohols that are common at significantly higher levels in three *P. communis* cultivars than in three *P. pyrifolia* cultivars.

Name	RT[a]	CAS[b]	Contents (ng/g)						Odor[c]	Odor threshold[d]
			Rad	RCF	QY	Aki	Won	SC1		
Hexyl 2-methylbutyrate	17.9805	10032-15-2	14651.25	1608.00	284.10	----	----	----	Apple, Fruit, Green Apple, Strawberry	0.022ug/g (e)
2-Methylbutyl 2-Methylbutyrate	13.7919	2445-78-5	1081.04	858.21	414.03	----	----	----	Apple, Berry, Rum	/
Ethyl-2-methyl butyrate	6.53076	7452-79-1	729.32	1811.83	750.96	347.22	54.08	----	Apple, Ester, Green Apple, Kiwi, Strawberry	0.011ug/g (e)
Propyl 2-methylbutyrate	9.28241	37064-20-3	1042.49	564.09	5.68	----	----	----	Fruit	0.019ug/g (e)
Isobutyl 2-Methylbutyrate	10.5272	2445-67-2	514.79	204.39	84.92	----	----	----	/	/
N-amyl acetate	10.3782	628-63-7	378.85	91.80	407.29	2.43	23.94	----	Apple, Banana, Pear	0.043ug/g (e)
N-hexyl acetate	13.5093	142-92-7	20373.86	310.77	7192.09	124.17	118.88	122.11	Apple, Banana, Grass, Herb, Pear	0.002ug/g (e)
N-butyl acetate	7.09138	123-86-4	1197.35	1399.40	5698.55	511.30	746.71	----	Apple, Banana	0.066ug/g (e)
Ethanol	3.67776	64-17-5	8721.25	5596.28	27140.96	1605.09	1504.02	----	alcohol	950ug/g (g)
N-propanol	6.227075	71-23-8	13468.83	3017.64	1945.79	----	----	----	Alcohol, Candy, Pungent	9ug/g (e)
N-butyl alcohol	9.59839	71-36-3	11588.30	6793.57	3609.03	22.30	108.37	----	Fruit	0.5ug/g (e)
Isobutyl alcohol	7.980455	78-83-1	3711.05	652.88	111.36	----	41.61	----	Apple, Bitter, Cocoa, Wine	0.033-500 mg/m^3 (f)
2-Methyl-1-butanol	11.5418	137-32-6	8425.43	575.53	3695.70	----	----	----	Green, Malt, Onion, Wine	0.25ug/g (e)
Citronellol	26.041	106-22-9	3814.20	192.78	16.91	----	----	----	Citrus, Green, Rose	/
Sulcatol	18.8719	1569-60-4	786.13	36.73	59.08	----	----	----	Floral, fruity, vegetable	/
Farnesol, (2z,6e)-	37.3818	3790-71-4	355.93	78.79	32.16	----	----	----	Oil	/

[a]Retention time by DB-Wax column. [b]CAS number. [c]Odor descriptor were obtained via the website 'https://www.femaflavor.org/flavor-library'. [d]Odor threshold were obtained through: (e) Li, 2012; (f) Van Gemert, 2011; (g) 'https://mffi.sjtu.edu.cn/database'. '----'indicates that the volatile compounds were not detected by GC–TOFMS. '/' indicates an absence of aroma information associated with the volatile compound.

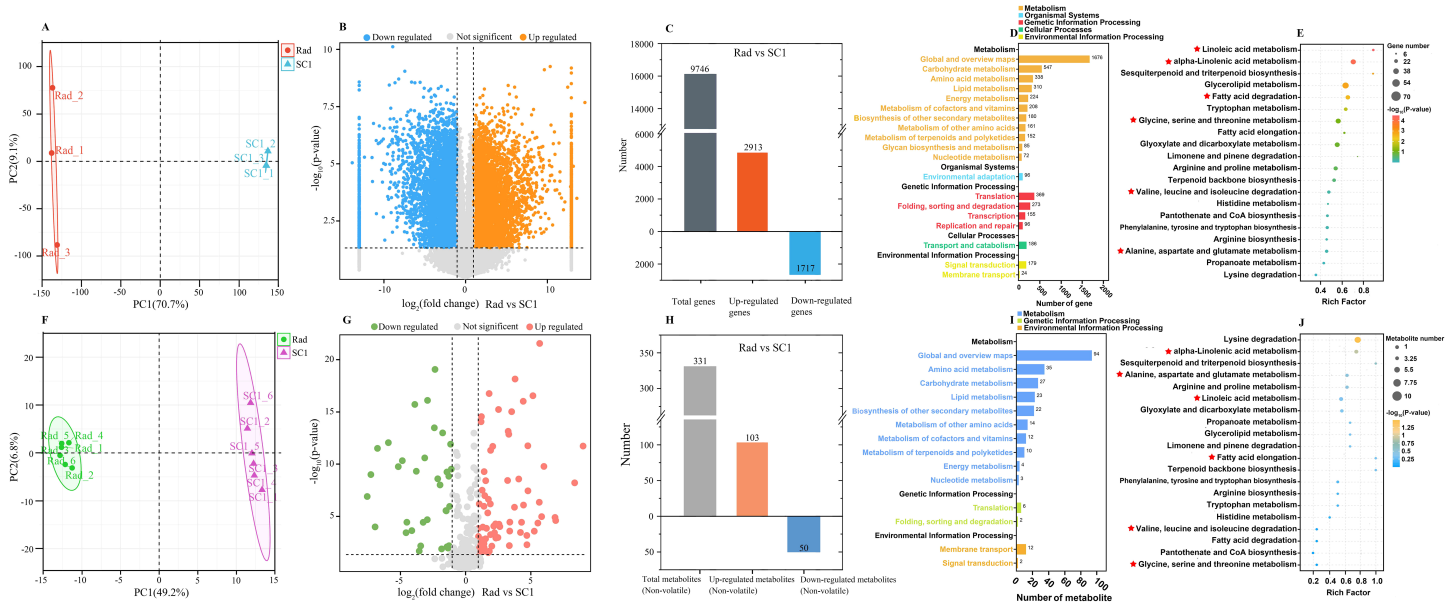

FIGURE 4
Analysis of the transcriptome and non-volatile compounds of 'Rad' and 'SC1'. **(A)** Principal component analysis (PCA) of genes expressed in 'Rad' and 'SC1'. **(B)** Volcano plot of up- and down-regulated genes ('Rad' vs 'SC1'). **(C)** Histogram of up- and down-regulated genes with KO ('Rad' vs 'SC1'). **(D, E)** KEGG enrichment analysis of up- and down-regulated genes with KO. **(F)** Principal component analysis (PCA) of non-volatile compounds detected in 'Rad' and 'SC1'. **(G)** Volcano plot of up- and down-regulated non-volatile compounds ('Rad' vs 'SC1'). **(H)** Histogram of up- and down-regulated non-volatile compounds with C numbers ('Rad' vs 'SC1'). **(I, J)** KEGG enrichment analysis of up- and down-regulated non-volatile compounds with C numbers.

10.3389/fpls.2025.1559012

10.3389/fpls.2025.1559012

CoA can be categorized into two groups: 2-methylbutyryl-CoA and acetyl-CoA. According to the KEGG enrichment results (Figures 4E, J), 2-methylbutyryl CoA was likely derived from isoleucine degradation, while acetyl CoA was probably produced by the degradation of saturated fatty acids. In these two approaches, the enzyme genes responsible for catalyzing each step in the reaction exhibited higher expression levels. In particular, the genes for fatty acyl CoA synthetase (pycom09g05270), acyl CoA dehydrogenase (pycom16g13880), enoyl CoA hydratase (pycom16g12990), acyl CoA thiolase (pycom05g16560), and branched amino acid tranminase (pycom15g26550) showed significantly higher expression levels in 'Rad' than in 'SC1' (Figure 5). Alcohols that undergo reactions with two types of fatty acyl CoA and those that were detected independently were categorized into two groups. The first group consisted of straight-chain alcohols, including ethanol, propanol, butanol, pentanol, and hexanol. The second category comprised branched-chain alcohols, such as 2-methylbutanol, 2-methylpropanol, and citronellol. Based on the KEGG enrichment analysis (Figures 4E, J) and the existing literature, ethanol might originate from alanine degradation, while propanol might primarily result from threonine dehydration (Wang et al., 2002). The expression levels of key enzyme genes involved in these two degradation processes, including branched amino acid tranminase (pycom15g26550), threonine dehydratase (pycom12g10020), and pyruvate decarboxylase (pycom12g16360, pycom10g23650), were markedly elevated in 'Rad' compared to 'SC1' (Figure 5). Hexanol has been proposed to be synthesized via the LOX pathway of linoleic acid (Scala et al., 2013). Key enzymes in this pathway included lipases (encoded by pycom08g09340 and pycom11g06350), pyruvate decarboxylases (encoded by pycom12g16360, pycom10g23650), and alcohol dehydrogenases (encoded by pycom10g00870 and pycom10g00890). The expression levels of these genes were higher in 'Rad' than in 'SC1' (Figure 5).

Currently, the fatty acid pathway, particularly the LOX pathway, is a focal point in pear fruit aroma research (Shi et al., 2019; Li et al., 2022). This study revealed that, in addition to the fatty acid pathway, some amino acid degradation processes, especially threonine dehydration, which has been rarely documented, also played a significant role in aroma synthesis in

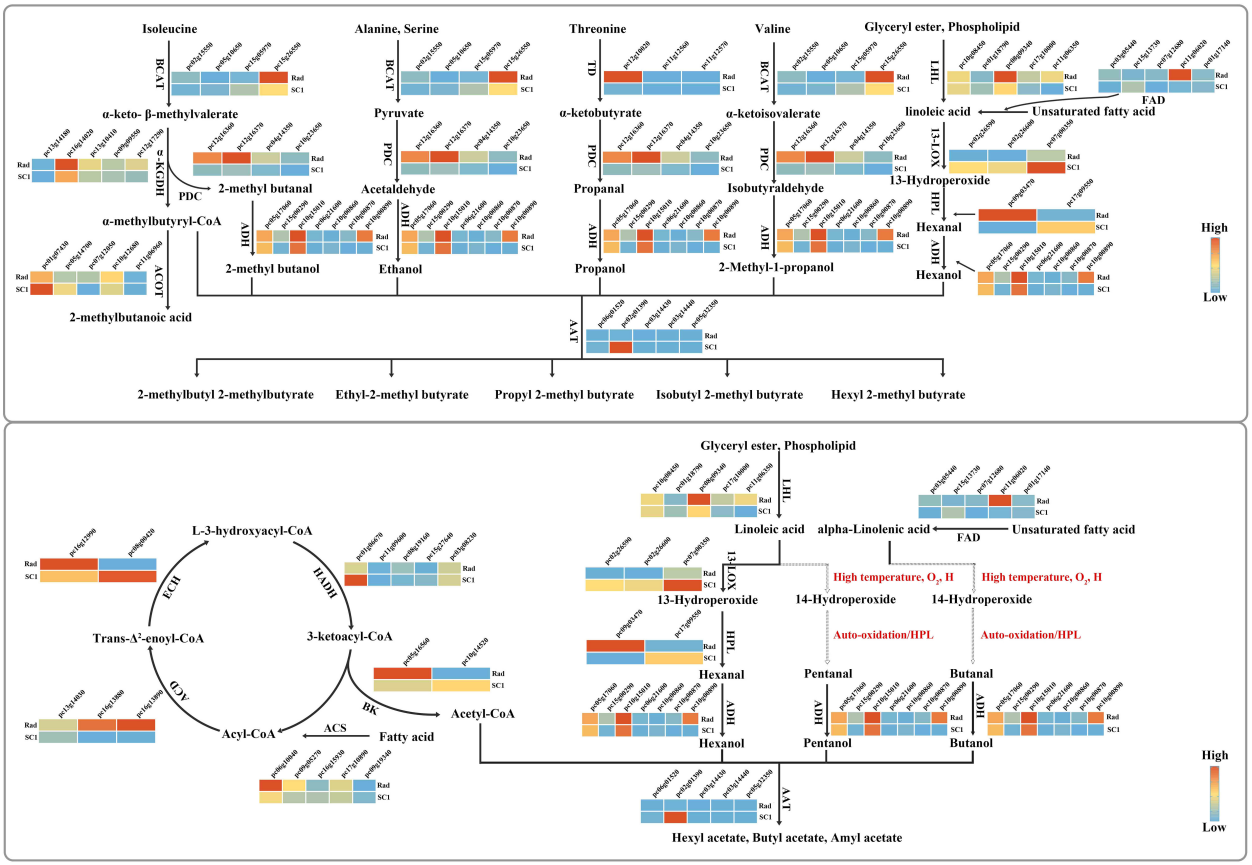

FIGURE 5
Potential synthesis pathways of 16 esters and alcohols. For simplification, 'pycom' in gene nomenclature is abbreviated as 'pc'. The solid arrows indicate that each step of the reaction has been documented. The dashed arrows suggest that the reaction steps are not explicitly recorded and are inferred based on the existing literature.The following are the full names of the key enzymes. BCAT, Branched-chain amino acid aminotransferase; α-KGDH, α-Ketoglutarate dehydrogenase; ACOT, Acyl-CoA thioeaterase; PDC, Pyruvate decarboxylase; ADH, Alcohol dehydrogenase; AAT, Alcohol acetyltransferase; TD, Threonine dehydratase; LHL, Lipid hydrolase; FAD, Fatty acid desaturase; 13-LOX, 13-Lipoxygenase; HPL, Hydroperoxide lyase; ACS, Acyl-CoA Synthetase; ACD, acyl-CoA dehydrogenase; ECH, Enoyl-CoA hydratase; HADH, Hydroxyacyl-CoA dehydrogenase; BK, Beta-ketothiolase.

10.3389/fpls.2025.1559012

P. communis cultivars. These results offer valuable information into the synthesis pathways of other aromatic compounds in pear fruit.

Identification of key enzyme genes in synthesis pathways

To identify the key enzyme genes involved in the synthesis pathways of 16 esters and alcohols, we selected 20 enzyme genes from the synthesis pathway shown in Figure 5, which showed significantly higher expression in 'Rad' than in 'SC1', and analyzed their expression levels in five *P. communis* and five *P. pyrifolia* cultivars. Subsequently, we performed RT-qPCR analysis on these 20 genes. The results demonstrated that the amplification efficiency of each primer pair ranged from 90% to 109% (Supplementary Table S14), which was consistent with the findings of Dai et al. (2023) and Yao (2023). This indicated that the PCR conditions, including the quality and concentration of the cDNA, were well optimized and satisfied the requirements for subsequent gene quantification analysis. The relative expression levels of genes were quantified using the 2^ −ΔΔCt method as described by Livak and Schmittgen (2001). As shown in Figure 6, the expression levels of nine genes, namely, *PcTD* (*pycom12g10020*), *PcACD* (*pycom16g13880*), *PcPDC* (*pycom10g23650*), *PcADH* (*pycom10g00890*), *PcLHL*

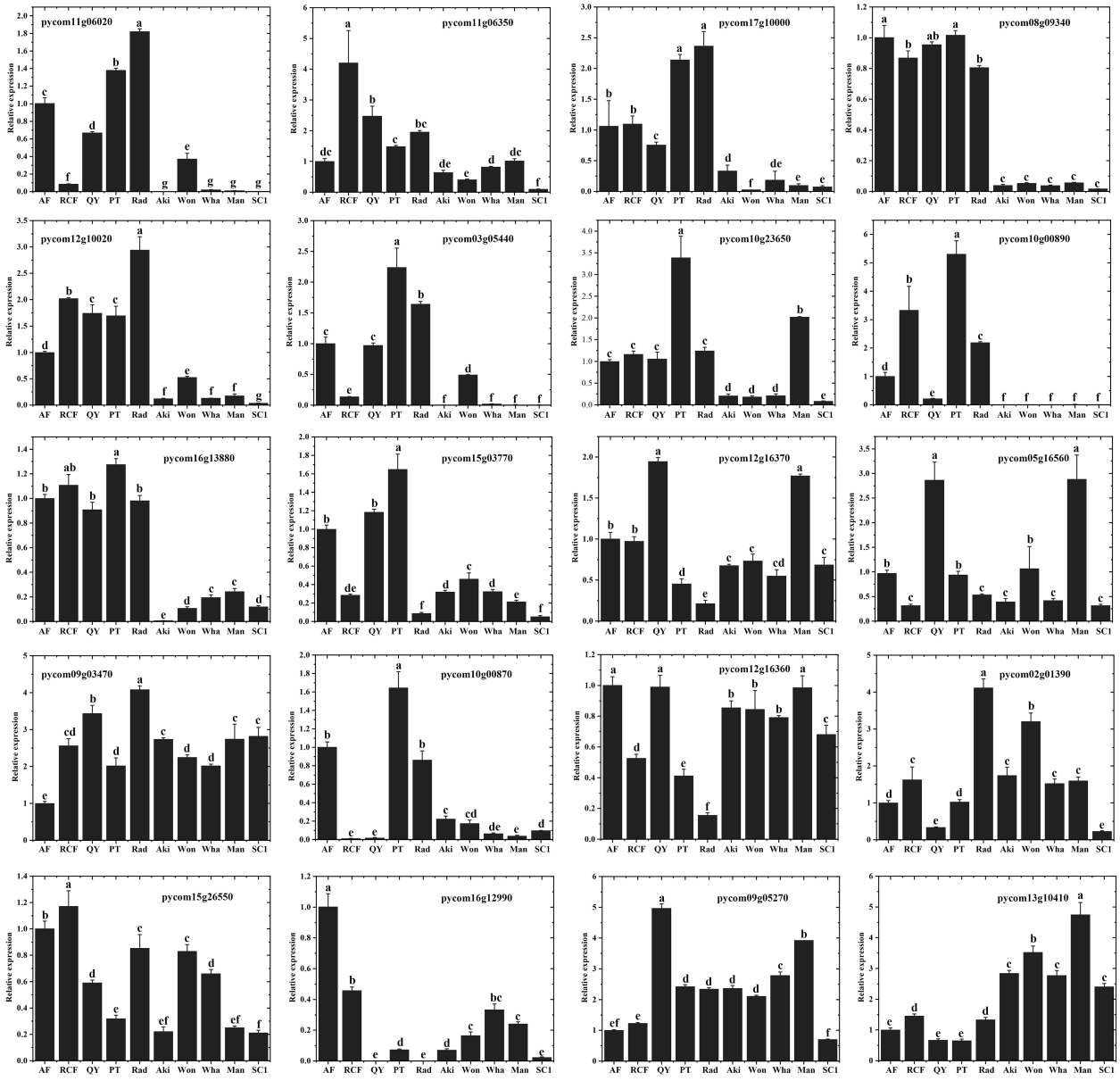

FIGURE 6
Expression of 20 key enzyme genes in the synthesis pathway across five *P. communis* and five *P. pyrifolia* cultivars. The error bars were calculated based on standard deviation. Different letters indicate significant differences at level p value = 0.05.

(*pycom08g09340*, *pycom11g06350*, *pycom17g10000*), and *PcFAD* (*pycom11g06020*, *pycom03g05440*), were significantly higher in the five *P. communis* cultivars than in the five *P. pyrifolia* cultivars. There were no significant differences in the expression levels of the remaining eleven genes between the five *P. communis* and five *P. pyrifolia* cultivars (Figure 6). This suggests that the nine genes play a crucial role in the synthesis of 16 esters and alcohols in *P. communis* cultivars, and their high expression might constitute a primary factor leading to the disparity in aromatic compounds between the *P. communis* and *P. pyrifolia* cultivars.

Discussion

Speculation on the synthesis of butanol and pentanol in volatile compounds

Based on the current literature, the synthesis pathways for butanol and pentanol remain undetermined and can only be hypothesized through existing analysis and research. There are three primary methods for alcohol synthesis in plants. First, amino acids are catalyzed to form alcohols via pyruvate decarboxylase (PDC) (Song et al., 2015). Second, fatty acyl CoA is catalyzed by acyl CoA reductase to produce alcohols (Napora-Wijata et al., 2014). Lastly, unsaturated fatty acids generate alcohols through the LOX pathway (Scala et al., 2013). Amino acids containing a greater number of carbon atoms typically undergo decarboxylation to form alcohols with functional groups, which deviate from straight-chain alcohols, such as butanol and pentanol. The expression of annotated acyl-CoA reductase genes was not detected in 'Rad' or 'SC1', suggesting that butanol and pentanol synthesis via acyl-CoA reductase was highly improbable (genes encoding acyl-CoA reductase were detected in the pear genome annotation file, https://www.rosaceae.org). Unsaturated fatty acids, including linoleic acid and alpha-linolenic acid, are catalyzed by 9-LOX or 13-LOX to form 9-hydroperoxides (9-ROOH) or 13-hydroperoxides (13-ROOH) after the loss of hydrogen atoms at C11. These hydroperoxides subsequently undergo cleavage to produce C6 alcohols or C9 enols (Buescher and Buescher, 2001; Scala et al., 2013).

Prior studies have indicated that hydrogen atoms adjacent to the C=C double bond are more prone to abstraction compared to those directly on the C=C double bond (Porter et al., 1995), and hydrogen atoms adjacent to either side of the C=C double bond are likely to be abstracted (Cao et al., 2020). Therefore, in linoleic acid and α-linolenic acid, in addition to hydrogen atoms at C11, hydrogen atoms at C14 are prone to loss. This phenomenon has been documented by Feussner and Kühn (2000). However, there are limited reports of enzymes that catalyze the formation of 12-ROOH or 16-ROOH following the loss of hydrogen atoms at C14. There is also a lack of information regarding this in the pear genome annotation file (https://www.rosaceae.org). Recent studies have indicated that under high-temperature conditions, the hydrogen atoms at positions C8 and C11, which are bonded to the C=C double bond in oleic acid, can undergo dehydrogenation (Cao et al., 2020). These molecules undergo rearrangement and react with oxygen to form 8-ROOH, 10-ROOH, 11-ROOH, and 9-ROOH. This process leads to the formation of octanol, nonyl alcohol, and decanol through cleavage reactions (Cao et al., 2020). Therefore, we further hypothesize that the hydrogen atoms at the C14 position of linoleic acid are lost during the high-temperature extraction phase of HS-SPME. C14-ROOH and C12-ROOH were generated following rearrangement and subsequent oxygenation, with the former potentially decomposing to form pentanol. Similarly, following the loss of hydrogen atoms at the C14 position of α-linolenic acid, a series of rearrangements and oxygenations led to the formation of C14-ROOH, C12-ROOH, and C16-ROOH. C14-ROOH might decompose to yield butanol (Figure 5).

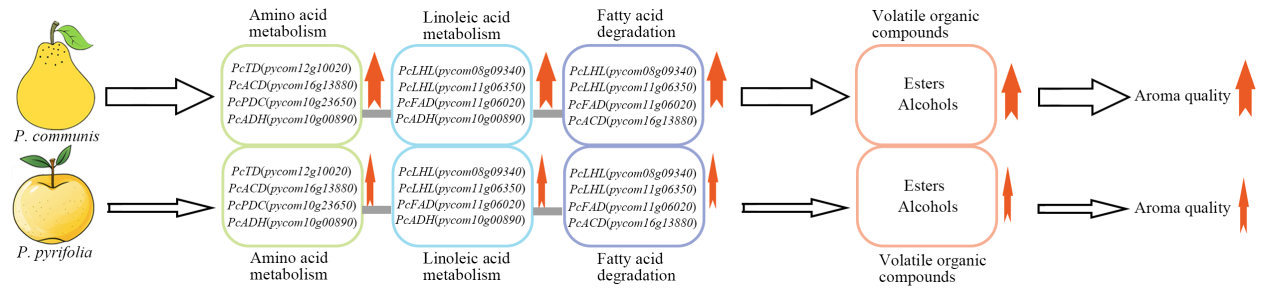

FIGURE 7
Potential formation model of differential aroma compounds between *P. communis* and *P. pyrifolia* cultivars. Bold red arrows adjacent to the green, blue, and purple oval frames represent a high level of expression of key genes that are crucial for the synthesis of differential aroma compounds. The thick red arrow next to the orange oval frame indicates a potential increase in the ester and alcohol concentrations. The bold red arrow situated at the base of the upper row indicates an enhancement in the aromatic quality of *P. communis* cultivar fruit. The hollow thick arrows denote the significant roles of elevated expression levels of key genes and increased ester and alcohol concentrations in enhancing fruit aroma. Thin red arrows indicate low expression levels and concentrations of genes and metabolites within the oval frame. The hollow and thin arrows indicate low expression of key genes, and reduced levels of esters and alcohols have a minimal influence on the development of fruit aroma. The thin red arrow at the base of the row indicates a diminished aromatic quality in *P. pyrifolia* cultivar fruit.

The role of highly expressed key genes in enhancing the aroma content of *P. communis* cultivar fruit

PcACD (*pycom16g13880*) encodes acyl-CoA dehydrogenase, a crucial enzyme involved in isoleucine degradation and fatty acid β-oxidation (Maggio-Hall et al., 2008). In this study, the elevated expression of this gene in *P. communis* cultivars compared to *P. pyrifolia* cultivars might result in increased 2-methylbutanoyl-CoA and acetyl-CoA production, leading to 2-methylbutyryl and acetyl ester formation. *PcTD* (*pycom12g10020*) encodes threonine dehydratase, which catalyzes the conversion of threonine to α-ketobutyric acid. This intermediate is subsequently decarboxylated and dehydrogenated to form propanol (Wang et al., 2002). The high expression of this gene in the *P. communis* cultivars could account for the higher levels of propanol and 2-methylbutyrate propanol compared to those in the *P. pyrifolia* cultivars. *PcLHL* (*pycom08g09340*, *pycom11g06350*, *pycom17g10000*) encodes lipid hydrolases, of which *pycom08g09340* encodes monoacylglycerol lipase, *pycom17g10000* encodes triacylglycerol lipase, and *pycom11g06350* encodes phospholipase. All three enzymes catalyze the release of fatty acids via hydrolysis reactions (Zimmermann et al., 2004; Scala et al., 2013; Grabner et al., 2017). The high expression levels of the three genes in the *P. communis* cultivars might contribute to increased fatty acid production, thereby providing essential precursors for the synthesis of numerous alcohols and esters. *PcFAD* (*pycom11g06020*, *pycom03g05440*) encodes fatty acid desaturases and catalyzes unsaturated fatty acid production (Somerville and Browse, 1996). The elevated expression of these genes in the *P. communis* cultivars might result in an increased content of unsaturated fatty acids, which can indirectly influence the formation of alcohols through the LOX pathway. *PcPDC* (*pycom10g23650*) and *PcADH* (*pycom10g00890*) encode pyruvate decarboxylase and alcohol dehydrogenase, respectively. These genes are positioned at the terminal position of the aroma synthesis pathway (Wang et al., 2019; Manríquez et al., 2006). The high expression levels in *P. communis* cultivars might have a direct impact on the final alcohol compound concentration.

In prior research on the aroma of pear fruits, *LOX*, *HPL*, *PDC*, *ADH*, and *AAT* were determined to be the primary structural genes in elucidating the aroma synthesis mechanism in pear fruit (Scala et al., 2013; Manríquez et al., 2006). This study found that, in addition to the aforementioned genes, threonine dehydratase *PcTD* (*pycom12g10020*), monoacylglycerol lipase (*pycom08g09340*), and triacylglycerol lipase (*pycom17g10000*) might also play crucial roles in aroma synthesis in *P. communis* cultivars. These findings not only expand the repertoire of significant structural genes involved in pear aroma synthesis pathways, but also provide novel target sites for enhancing the pear aroma content through gene editing. Furthermore, while ketones, acids, and other compounds constitute only a minor fraction of volatile compounds, certain high-concentration components such as 2-octanone, heptyl ketone, n-butyric acid, and n-undecane are noteworthy. Many of these compounds possess fruity aromatic properties (Supplementary Tables S5–S10). Therefore, future aroma research should also focus on these components.

Conclusion

Through the analysis and discussion of the aforementioned results, it was concluded that 2-methylbutyrate (2-methylhexyl butyrate and 3-methylbutyl 2-methylbutyrate), acetate (butyl acetate, hexyl acetate, and amyl acetate), and straight-chain alcohols (ethanol, butanol, propanol, and 2-methylbutanol) are likely the primary volatile compounds responsible for the differences in fruit aroma between *P. communis* and *P. pyrifolia* cultivars. These compounds might enhance their content primarily through the up-regulation of key enzyme genes in fatty acid and amino acid metabolism pathways, such as the enzyme genes identified in this research, including monoacylglycerol lipase, threonine deaminase, and long-chain acyl-CoA dehydrogenase. The elevated levels of these volatile compounds and the up-regulated expression of key genes might result in high aroma quality in *P. communis* cultivars compared to *P. pyrifolia* cultivars (Figure 7).

Data availability statement

The datasets presented in this study can be found in online repositories. The names of the repository/repositories and accession number(s) can be found in the article/Supplementary Material.

Author contributions

JW: Conceptualization, Writing – original draft, Writing – review & editing. XG: Data curation, Supervision, Writing – original draft. ZW: Methodology, Writing – review & editing. DW: Funding acquisition, Validation, Writing – review & editing. PG: Visualization, Writing – review & editing. YH: Methodology, Writing – review & editing. HJ: Formal Analysis, Writing – review & editing. ZL: Data curation, Writing – review & editing.

Funding

The author(s) declare that financial support was received for the research and/or publication of this article. This work was financially supported by the Major Science and Technology Projects of Henan Province (221100110400), the Science and Technology Innovation Team of the Henan Academy of Agricultural Sciences (2024TD41), and the earmarked fund for CARS (CARS-28). We thank LetPub (www.letpub.com.cn) for its linguistic assistance during the preparation of this manuscript.

Conflict of interest

The authors declare that the research was conducted in the absence of any commercial or financial relationships that could be construed as a potential conflict of interest.

Generative AI statement

The author(s) declare that no Generative AI was used in the creation of this manuscript.

Publisher's note

Supplementary material

The Supplementary Material for this article can be found online at: https://www.frontiersin.org/articles/10.3389/fpls.2025.1559012/full#supplementary-material

References

Aragüez, I., Osorio, S., Hoffmann, T., Rambla, J., Medina-Escobar, N., Granell, A., et al. (2013). Eugenol production in achenes and receptacles of strawberry fruits is catalyzed by synthases exhibiting distinct kinetics. *Plant Physiol.* 163, 946–958. doi: 10.1104/pp.113.224352

Arimura, G., Ozawa, R., Horiuchi, J., Nishioka, T., and Takabayashi, J. (2001). Plant–plant interactions mediated by volatiles emitted from plants infested by spider mites. *Biochem. Systematics Ecol.* 29, 1049–1061. doi: 10.1016/S0305-1978(01)00049-7

Asikin, Y., Taira, I., Inafuku, S., Sumi, H., Sawamura, M., Takara, K., et al. (2012). Volatile aroma components and antioxidant activities of the flavedo peel extract of unripe Shiikuwasha (Citrus depressa Hayata). *J. Food Sci.* 77, C469–C475. doi: 10.1111/j.1750-3841.2011.02604.x

Beekwilder, J., Alvarez-Huerta, M., Neef, E., Verstappen, F., Bouwmeester, H., and Aharoni, A. (2004). Functional characterization of enzymes forming volatile esters from strawberry and banana. *Plant Physiol.* 135, 1865–1878. doi: 10.1104/pp.104.042580

Buescher, R., and Buescher, R. (2001). Production and stability of (E,Z)-2,6-Nonadienal, the major flavor volatile of cucumbers. *J. Food Sci.* 66, 357–361. doi: 10.1111/j.1365-2621.2001.tb11346.x

Cao, J., Jiang, X., Chen, Q., Zhang, H., Sun, H., Zhang, W., et al. (2020). Oxidative stabilities of olive and camellia oils: Possible mechanism of aldehydes formation in oleic acid triglyceride at high temperature. *Food Sci. Technol.* 118, 108858. doi: 10.1016/j.lwt.2019.108858

Chen, H., Cao, S., Jin, Y., Tang, Y., and Qi, H. (2016). The relationship between CmADHs and the diversity of volatile organic compounds of three aroma types of melon (Cucumis melo). *Front. Physiol.* 7, 254. doi: 10.3389/fphys.2016.00254

Chen, Y., Yin, H., Wu, X., Shi, X., Qi, K., and Zhang, S. (2018). Comparative analysis of the volatile organic compounds in mature fruits of 12 Occidental pear (*Pyrus communis* L.) cultivars. *Scientia Hortic.* 240, 239–248. doi: 10.1016/j.scienta.2018.06.014

Dai, Y., Liu, X., Gan, L., Lan, C., Teng, Z., and Yang, X. (2023). Selection and application of reference genes for quantitative real-time PCR in exserohilum turcicum. *J. Agric. Biotechnol.* 31, 867–882. doi: 10.3969/j.issn.1674-7968.2023.04.019

Feussner, I., and Kühn, H. (2000). "Application of lipoxygenases and related enzymes for the preparation of oxygenated lipids," in *Enzymes in lipid modification*. Ed. U. T. Bornscheuer (Wiley-VCH, Weinheim, Germany), 309–336.

Gai, J. (2000). *Experimental Statistical Methodology* (Beijing: China Agriculture Press).

Gonda, I., Bar, E., Portnoy, V., Lev, S., Burger, J., Schaffer, A., et al. (2010). Branched-chain and aromatic amino acid catabolism into aroma volatiles in Cucumis melo L. fruit. *J. Exp. Bot.* 61, 1111–1123. doi: 10.1093/jxb/erp390

Grabner, G., Zimmermann, R., Schicho, R., and Taschler, U. (2017). Monoglyceride lipase as a drug target: At the crossroads of arachidonic acid metabolism and endocannabinoid signaling. *Pharmacol. Ther.* 175, 35–46. doi: 10.1016/j.pharmthera.2017.02.033

Jordán, M., Tandon, K., Shaw, P., and Goodner, K. (2001). Aromatic profile of aqueous banana essence and banana fruit by gas chromatography-mass spectrometry (GC-MS) and gas chromatography-olfactometry (GC-O). *J. Agric. Food Chem.* 49, 4813–4817. doi: 10.1021/jf010471k

Kahle, K., Preston, C., Richling, E., Heckel, F., and Schreier, P. (2005). On-line gas chromatography combustion/pyrolysis isotope ratio mass spectrometry (HRGC-C/P-IRMS) of major volatiles from pear fruit (Pyrus communis) and pear products. *Food Chem.* 91, 449–455. doi: 10.1016/j.foodchem.2004.06.026

Knudsen, J., Eriksson, R., Gershenzon, J., and Ståhl, B. (2006). Diversity and distribution of floral scent. *Botanical Rev.* 72, 1–120. doi: 10.1663/0006-8101(2006)72[1:DADOFS]2.0.CO;2

Li, G. (2012). *Studys on volatiles in fruit of Chinese pear cultivars and expression of biosynthesis related genes* (Zhejiang University), 3–4.

Li, X., Qi, L., Zang, N., Zhao, L., Sun, Y., Huang, X., et al. (2022). Integrated metabolome and transcriptome analysis of the regulatory network of volatile ester formation during fruit ripening in pear. *Plant Physiol. Biochem.* 185, 80–90. doi: 10.1016/j.plaphy.2022.04.030

Li, X., and Zhang, S. (2020). *Pear Tree of China* (Beijing: China Agriculture Press). (Chapter 3).

Liu, G., Huang, L., and Lian, J. (2023). Alcohol acyltransferases for the biosynthesis of esters. *Biotechnol. Biofuels Bioprod* 16, 93. doi: 10.1186/s13068-023-02343-x

Liu, J., Liu, H., Wu, T., Zhai, R., Yang, C., Wang, Z., et al. (2019). Effects of melatonin treatment of postharvest pear fruit on aromatic volatile biosynthesis. *Molecules* 24, 4233. doi: 10.3390/molecules24234233

Livak, K., and Schmittgen, T. (2001). Analysis of relative gene expression data using real-time quantitative PCR and the 2 −ΔΔCt method. *Methods* 25, 402–408. doi: 10.1006/meth.2001.1262

Maggio-Hall, L., Lyne, P., Wolff, J., and Keller, N. (2008). A single acyl-CoA dehydrogenase is required for catabolism of isoleucine, valine and short-chain fatty acids in Aspergillus nidulans. *Fungal Genet. Biol.* 45, 180–189. doi: 10.1016/j.fgb.2007.06.004

Makkumrai, W., Sivertsen, H., Sugar, D., Ebeler, S., Negre-Zakharov, F., and Mitcham, E. J. (2014). Effect of ethylene and temperature conditioning on sensory attributes and chemical composition of 'Comice' pears. *J. Agric. Food Chem.* 62, 4988–5004. doi: 10.1021/jf405047v

Man, L., Ren, W., Qin, H., Sun, M., Yuan, S., Zhu, M., et al. (2023). Characterization of the relationship between lipids and volatile compounds in donkey, bovine, and sheep meat by UHPLC–ESI–MS and SPME–GC–MS. *Food Sci. Technol.* 175, 114426. doi: 10.1016/j.lwt.2023.114426

Manríquez, D., El-Sharkawy, I., Flores, F., El-Yahyaoui, F., Regad, F., Bouzayen, M., et al. (2006). Two highly divergent alcohol dehydrogenases of melon exhibit fruit ripening-specific expression and distinct biochemical characteristics. *Plant Mol. Biol.* 61, 675–685. doi: 10.1007/s11103-006-0040-9

Matsui, K. (2006). Green leaf volatiles: hydroperoxide lyase pathway of oxylipin metabolism. *Curr. Opin. Plant Biol.* 9, 274–280. doi: 10.1016/j.pbi.2006.03.002

Napora-Wijata, K., Strohmeier, G., and Winkler, M. (2014). Biocatalytic reduction of carboxylic acids. *Biotechnol. J.* 9, 822–843. doi: 10.1002/biot.201400012

Nuzzi, M., Scalzo, R., Testoni, A., and Rizzolo, A. (2008). Evaluation of Fruit Aroma Quality: Comparison between gas chromatography–olfactometry (GC–O) and odour activity value (OAV) aroma patterns of strawberries. *Food Analytical Methods* 1, 270–282. doi: 10.1007/s12161-008-9039-y

Pfaffl, M. (2001). A new mathematical model for relative quantification in real-time RT-PCR. *Nucleic Acids Res.* 29, e45. doi: 10.1093/nar/29.9.e45

Pichersky, E., Noel, J., and Dudareva, N. (2006). Biosynthesis of plant volatiles: nature's diversity and ingenuity. *Science* 311, 808–811. doi: 10.1126/science.1118510

Porter, N., Caldwell, S., and Mills, K. (1995). Mechanisms of free radical oxidation of unsaturated lipids. *Lipids* 30, 277–290. doi: 10.1007/BF02536034

Qin, G., Tao, S., Cao, Y., Wu, J., Zhang, H., Huang, W., et al. (2012). Evaluation of the volatile profile of 33 Pyrus ussuriensis cultivars by HS-SPME with GC-MS. *Food Chem.* 134, 2367–2382. doi: 10.1016/j.foodchem.2012.04.053

Rizzolo, A., Cambiaghi, P., Grassi, M., and Zerbini, P. E. (2005). Influence of 1-methylcyclopropene and storage atmosphere on changes in volatile compounds and fruit quality of conference pears. *J. Agric. Food Chem.* 53, 9781–9789. doi: 10.1021/jf051339d

Scala, A., Mirabella, R., Mugo, C., Matsui, K., Haring, M., and Schuurink, R. (2013). E-2-hexenal promotes susceptibility to Pseudomonas syringae by activating jasmonic acid pathways in Arabidopsis. *Front. Plant Sci.* 4, 74. doi: 10.3389/fpls.2013.00074

Schwab, W., Davidovich-Rikanati, R., and Lewinsohn, E. (2008). Biosynthesis of plant-derived flavor compounds. *Plant J.* 54, 712–732. doi: 10.1111/j.1365-313X.2008.03446.x

Shi, F., Zhou, X., Yao, M., Zhou, Q., Ji, S., and Wang, Y. (2019). Low-temperature stress-induced aroma loss by regulating fatty acid metabolism pathway in 'Nanguo' pear. *Food Chem.* 297, 124927. doi: 10.1016/j.foodchem.2019.05.201

Somerville, C., and Browse, J. (1996). Dissecting desaturation: plants prove advantageous. *Trends Cell Biol.* 6, 148–153. doi: 10.1016/0962-8924(96)10002-7

Song, J., Du, L., Li, L., Palmer, L., Forney, C., Fillmore, S., et al. (2015). Targeted quantitative proteomic investigation employing multiple reaction monitoring on quantitative changes in proteins that regulate volatile biosynthesis of strawberry fruit at different ripening stages. *J. Proteomics* 126, 288–295. doi: 10.1016/j.jprot.2015.06.004

Taiti, C., Marone, E., Lanza, M., and Azzarello, E. (2017). Nashi or Williams pear fruits? Use of volatile organic compounds, physicochemical parameters, and sensory evaluation to understand the consumer's preference. *Eur. Food Res. Technol.* 243, 1917–1931. doi: 10.1007/s00217-017-2898-y

Tian, H., Zhan, P., Deng, Z., Yan, H., and Zhu, X. (2014). Development of a flavour fingerprint by GC-MS and GC-O combined with chemometric methods for the quality control of Korla pear (Pyrus serotina Reld). *Int. J. Food Sci. Technol.* 49, 2546–2552. doi: 10.1111/ijfs.2014.49.issue-12

Torregrosa, L., Echeverria, G., Illa, J., and Giné-Bordonaba, J. (2019). Ripening behaviour and consumer acceptance of 'Conference' pears during shelf life after long term DCA-storage. *Postharvest Biol. Technol.* 155, 94–101. doi: 10.1016/j.postharvbio.2019.05.014

Van Gemert, L. (2011). *Odour thresholds: compilations of odour threshold values in air, water and other media (second enlarged and revised edition)* (The Netherlands: Oliemans Punter & Partners BV). (Part1 and Part 2).

Wang, J., Cao, K., Wang., L., Dong, W., Zhang, X., and Liu, W. (2022). Two MYB and three bHLH family genes participate in anthocyanin accumulation in the flesh of peach fruit treated with glucose, sucrose, sorbitol, and fructose *in vitro*. *Plants (Basel)* 11, 507. doi: 10.3390/plants11040507

Wang, M., Zhang, L., Boo, K., Park, E., Drakakaki, G., and Zakharov, F. (2019). PDC1, a pyruvate/α-ketoacid decarboxylase, is involved in acetaldehyde, propanal and pentanal biosynthesis in melon (Cucumis melo L.) fruit. *Plant J.* 98, 112–125. doi: 10.1111/tpj.2019.98.issue-1

Wang, C., Zhang, W., Li, H., Mao, J., Guo, C., Ding, R., et al. (2019). Analysis of volatile compounds in pears by HS-SPME-GC×GC-TOFMS. *Molecules* 24, 1795. doi: 10.3390/molecules24091795

Wang, J., Zhu, S., and Xu, C. (2002). *Biochemistry. 3th ed* (Beijing: Higher Education Press). (Chapter 30).

Want, E., Masson, P., Michopoulos, F., Wilson, I. D., Theodoridis, G., Plumb, R. S., et al. (2013). Global metabolic profiling of animal and human tissues via UPLC-MS. *Nat. Protoc.* 8, 17–32. doi: 10.1038/nprot.2012.135

Wei, S., Tao, S., Qin, G., Wang, S., Tao, J., Wu, J., et al. (2016). Transcriptome profiling reveals the candidate genes associated with aroma metabolites and emission of pear (*Pyrus ussuriensis* cv.). *Scientia Hortic.* 206, 33–42. doi: 10.1016/j.scienta.2016.04.019

Wu, X., Chen, Y., Wang, Y., Qi, K., Qiao, X., Li, Q., et al. (2023). New insights into aroma regulation in pear peel and flesh under methyl jasmonate treatment obtained by metabolite and whole-transcriptome RNA sequencing analyses. *Postharvest Biol. Technol.* 201, 112347. doi: 10.1016/j.postharvbio.2023.112347

Wu, J., Wang, Y., Xu, J., Korban, S., Fei, Z., Tao, S., et al. (2018). Diversification and independent domestication of Asian and European pears. *Genome Biol.* 19, 77. doi: 10.1186/s13059-018-1452-y

Xi, W., Zhang, B., Liang, L., Shen, J., Wei, W., Xu, C., et al. (2012). Postharvest temperature influences volatile lactone production via regulation of acyl-CoA oxidases in peach fruit. *Plant Cell Environ.* 35, 534–545. doi: 10.1111/j.1365-3040.2011.02433.x

Yao, J. (2023). *The highly effective approach of copy number detection with quantitative real-time PCR for transgenic cotton* (Huazhong Agricultural University), 21–58.

Yao, M., Zhou, X., Ji, Y., Luo, M., Sun, Y., Zhou, Q., et al. (2022). Potential of ethylene in alleviating cold-induced volatile esters loss of'Nanguo' Pears by regulating the lipoxygenase pathway. *Environ. Exp. Bot.* 194, 104723. doi: 10.1016/j.envexpbot.2021.104723

Yue, X., Shi, P., Tang, Y., Zhang, H., Ma, X., Ju, Y., et al. (2021). Effects of methyl jasmonate on the monoterpenes of Muscat Hamburg grapes and wine. *J. Sci. Food Agric.* 101, 3665–3675. doi: 10.1002/jsfa.v101.9

Zelena, E., Dunn, W., Broadhurst, D., Francis-McIntyre, S., Carroll, K., Begley, P., et al. (2009). Development of a robust and repeatable UPLC-MS method for the long-term metabolomic study of human serum. *Analytical Chem.* 81, 1357–1364. doi: 10.1021/ac8019366

Zeng, Y., Wang, M., Hunter, D., Matich, A., McAtee, P., Knäbel, M., et al. (2020). Sensory-directed genetic and biochemical characterization of volatile terpene production in kiwifruit. *Plant Physiol.* 183, 51–66. doi: 10.1104/pp.20.00186

Zhang, L., Li, H., Gao, L., Qi, Y., Fu, W., Li, X., et al. (2017). Acyl-CoA oxidase 1 is involved in γ-decalactone release from peach (Prunus persica) fruit. *Plant Cell Rep.* 36, 829–842. doi: 10.1007/s00299-017-2113-4

Zhang, B., Shen, J., Wei, W., Xi, W., Xu, C., Ferguson, I., et al. (2010). Expression of genes associated with aroma formation derived from the fatty acid pathway during peach fruit ripening. *J. Agric. Food Chem.* 58, 6157–6165. doi: 10.1021/jf100172e

Zhong, H., Zhang, S., Sun, H., Li, Z., Yuan, H., and Xie, D. (2008). The volatile profile of selected juices of pyrus pyrifolia cultivars. *Acta Hortic.* 11, uhad265. doi: 10.17660/ActaHortic.2008.769.25

Zimmermann, R., Strauss, J., Haemmerle, G., Schoiswohl, G., Birner-Gruenberger, R., Riederer, M., et al. (2004). Fat mobilization in adipose tissue is promoted by adipose triglyceride lipase. *Science* 306, 1383–1386. doi: 10.1126/science.1100747

Zlatić, E., Zadnik, V., Fellman, J., Demšar, L., Hribar, J., Čejić, Ž., et al. (2016). Comparative analysis of aroma compounds in 'Bartlett' pear in relation to harvest date, storage conditions, and shelf-life. *Postharvest Biol. Technol.* 117, 71–80. doi: 10.1016/j.postharvbio.2016.02.004

frontiers | Frontiers in Plant Science

TYPE Original Research
PUBLISHED 28 April 2025
DOI 10.3389/fpls.2025.1544593

OPEN ACCESS

EDITED BY
Robin Joshi,
University of Pennsylvania, United States

REVIEWED BY
Nan Lu,
University of North Texas, United States
Prithvi Pal,
University of Georgia, United States

*CORRESPONDENCE
Sha Xie
xiesha@nwafu.edu.cn
Maosheng Ge
gmsnongshui@nwafu.edu.cn

RECEIVED 16 December 2024
ACCEPTED 01 April 2025
PUBLISHED 28 April 2025

CITATION
Wu G, Xin Y, Ren R, Chen H, Yang B, Ge M and Xie S (2025) Comprehensive aroma profiles and the underlying molecular mechanisms in six grape varieties with different flavors. *Front. Plant Sci.* 16:1544593. doi: 10.3389/fpls.2025.1544593

Comprehensive aroma profiles and the underlying molecular mechanisms in six grape varieties with different flavors

Guang Wu[1], Yuchen Xin[1], Ruihua Ren[1], Huawei Chen[1], Bowei Yang[1], Maosheng Ge[2*] and Sha Xie[1*]

[1]College of Enology, Northwest A & F University, Yangling, China, [2]College of Water Resources and Architectural Engineering, Northwest A & F University, Yangling, China

Aroma is a critical factor in determining grape quality, develops through complex interactions among various volatile compounds. This study revealed the differences of the six grape varieties with three different aroma types though the HS-SPME/GC-MS and RNA-sequencing technologies. Muscat-type grapes ('Shine 13' and 'Shine Muscat') exhibited the highest monoterpene and C13-norisoprenoid level, correlating with elevated expression of *DXS, TPS, and CCD4b* genes in the MEP/MVA pathways. Strawberry-type cultivars (particularly 'Hutai 8') accumulated abundant esters linked to high *AAT* expression, while neutral aromatic varieties showed enriched C6/C9 compounds associated with upregulated *LOXA* and *ADH2*. Muscat-type grapes dominated monoterpenes with OAVs >1, which explained the abundant Muscat flavors, while neutral aromatic aroma cultivars had the most abundant C6/C9 compounds OAVs associated with leaf-like scents. Strawberry-type cultivars exhibited the highest esters OAVs with strawberry aroma profiles. WGCNA analysis revealed four specific modules correlated with aroma compound biosynthesis correlated with alcohols (88genes), carbonyl compounds (451genes), fatty acids (110 genes), and monoterpenes (790genes) accumulation in these grapes, respectively. These findings were expected to advance our understanding of the metabolic pathways responsible for grape aroma and could provide valuable recommendations for the enhancement of grape aromatic quality.

KEYWORDS

grape, aroma, volatiles, HS-SPME/GC-MS, RNA-seq

1 Introduction

Grapes are one of the most famous fruits, typically consumed either as table grapes or processed into juice and wine (Dong et al., 2023). Grape aroma, a critical aspect of grape quality, arises from intricate chemical processes involving multiple compound classes, which shape the distinct sensory traits of various grape cultivars (Ghaste et al., 2015).

Previous studies have confirmed that monoterpenes, C6/C9 compounds, C13-norisoprenoids, and esters are the dominant substances contributing to grape aromas (Wu et al., 2020; Feng et al., 2022; Wang W.-N. et al., 2023). Grapes are categorized into Muscat, strawberry, and neutral aromatic cultivars based on the level of monoterpenes. Among these compounds, monoterpenes are the primary aroma compounds to Muscat cultivars (Mateo and Jiménez, 2000), C6/C9 compounds are regarded as the fundamental, underlying scents in grapes (Wu et al., 2016); Yao et al. (2021) found that esters were the key volatile compounds in 'Hutai 8' (Wu et al., 2016). In grape berries, aroma compounds occur in free and glycosidically bound forms. Glycosidically bound aromas predominantly exist in glycosylated molecules that are hydrophilic, non-volatile, and flavorless. Free volatile aroma can be converted into glycosylated precursor by UDP-glycosyltransferases (UGTs) (Ghaste et al., 2015), which can directly provide grapes with floral, fruity, rose-like, and green flavors (Wang et al., 2021; Liu et al., 2022). However, until now little information about comprehensive and detailed free and bound aroma profiles of different aroma types of grape varieties has been reported.

In grape berry, the synthesis of aromatic substances included terpene metabolism (Supplementary Figure S1A), amino acid metabolism (Supplementary Figure S1B), and fatty acid metabolism (Supplementary Figure S1C). Monoterpenes, including α-terpineol, linalool, and geraniol, are considered the primary fragrant substances in Muscat grape cultivars (Luan et al., 2006). Variation in Muscat flavor among grape cultivars is attributed to the diverse monoterpene profiles (Liu et al., 2022). Monoterpenes and norisoprenoids are primarily synthesized through the methyl-erythritol phosphate (MEP) and mevalonate (MVA) pathways (Li et al., 2025). The MEP pathway takes place in plastids, whereas the MVA pathway occurs in the cytosol (Vranová et al., 2013). Terpene biosynthesis begins with the generation of isopentenyl pyrophosphate (IPP), followed by the isomerization to form dimethylallyl pyrophosphate (DMAPP) (Leng et al., 2023). The genesis of grape aroma compounds also stems from the metabolism of fatty acids, whether saturated or unsaturated, which are channeled through β-oxidation and the LOX-HPL metabolic pathway, yielding alcohols, aldehydes, ketones, acids, and esters (Kiralan et al., 2019). Moreover, these volatiles act as signaling molecules for pollination and defense against pathogen invasion (D'Auria et al., 2007). It has been indicated that alcohol acyltransferase (AAT) plays a key role in catalyzing the formation of volatile esters in fruits by linking alcohols with acyl-CoA (Beekwilder et al., 2004). Two principal types of amino acids exist, classified by their structure: aliphatic and aromatic amino acids. Leucine, isoleucine, valine, alanine, and cysteine are among the amino acids that can serve as precursors for volatile compounds in fruits, which can metabolize into alcohols, aldehydes, ketones, and esters in plants (Pan et al., 2012). However, at present, the pathway and molecular regulation mechanism of grape aroma synthesis have not been fully clear.

In this research, the neutral grape cultivars 'Red Globe' (*V. vinifera*) and 'Moldova' (a hybrid of *V. labrusca* and *V. vinifera*), alongside the Muscat-scented 'Shine Muscat' and 'Shine 13' (both hybrid of *V. labrusca* and *V. vinifera*), as well as the strawberry-aroma varieties 'Summer Black' and 'Hutai 8' (both hybrids of *V. labrusca* and *V. vinifera*) were selected to analyze distinct aroma compounds and identify candidate genes impart to these aroma differences in the different aroma-type grapes. The volatile compounds of grape berries were identified by GC–MS. Weighted gene co-expression network analysis (WGCNA) was conducted to explore the candidate genes related to the target traits. RNA sequencing and qRT-PCR methods were employed to examine transcriptomic signatures. By integrating transcriptome and metabolome, we identified the differences in the aroma profiles of different aroma types and elucidate the genetic basis of cultivar-specific aroma formation. The findings from this research offer valuable understanding regarding the differences among aroma-type grape cultivars, the fundamental biological processes involved, and the core molecular dynamics within grape berries. This not only enhances our understanding of the chemical basis of grape aroma diversity but also offers practical guidance for vineyard management and breeding strategy. Moreover, our findings open up several avenues for future research. The correlations we found between certain molecular markers and aroma traits can be further explored through genetic studies, potentially leading to the development of new grape cultivars with desired flavor characteristics.

2 Materials and methods

2.1 Grape cultivars

This research used six grape cultivars with different aroma types as experimental materials. These grape cultivars were collected at maturity from Weinan-based vineyards (34°50′N,109°48′E), Shanxi, China. The grape cultivars in this study were all grown on their own roots and protected by rain shelters, ensuring uniformity in vineyard management across all varieties. Three biological replicates were gathered for each type of grape, with each replicate consisting of 200 berries. These berries were chosen at random from a pool of at least 50 vines, sampled from both the North-South sides of the vineyard canopy to ensure representation. The collected samples were then flash-frozen using liquid nitrogen and preserved at a temperature of -80 degrees Celsius for subsequent analysis of the metabolome and transcriptome.

2.2 Extraction of free and glycosidically bound aroma compounds

Forty frozen grape berries were de-seeded, and the pulp and skin were mashed into a powder with 2.0g of polyvinylpyrrolidone (PVPP) and 0.5g of *D*-gluconolactone, using liquid nitrogen. The pulp was processed by crushing, blending, and a 4-hour soak at 4°C. Following this, it was processed by centrifugation at 8000g for 15 minutes to yield purified grape juice. At last, clear grape juice was

used to detect the free volatile compounds. For each respective sample, three independent extractions were conducted.

The methods of extracting the glycosidically bound aroma compounds were consistent with (Wen et al., 2015). This process was repeated three times for each sample to create independent extracts.

2.3 HS-SPME/GC-MS analysis of aroma compounds

An automated HS-SPME system using a 2-cm DVB/CAR/PDMS fiber measuring 50/30 μm (Supelco, Bellefonte, PA, USA) and a CTC Combi PAL autosampler (CTC Analytics, Zwingen, Switzerland) was employed for extraction aromatic compounds from clear juice or mixtures. The SPME fiber underwent an activation step was consistent with (Lan et al., 2016).

Volatile compound analysis of six different grape cultivars was performed operating with an Agilent 6890 gas chromatograph integrated with an Agilent 5975 detector (GC-MS, Agilent Technologies, Santa Clara, CA). The conditions of GC-MS were consistent with (Sun et al., 2020).

The aroma compounds were pinpointed by correlating their mass spectral fingerprints with entries in the NIST14 mass spectrometry database and by aligning retention indices of the compounds against known reference values. This process was streamlined through the Automated Mass Spectral Deconvolution and Identification System (AMDIS), which seamlessly computed the retention indices and mass spectral data.

2.4 Odor activity values

OAVs were determined applying the formula OAV = c/t, with c representing the concentration of free volatiles and t referring to the odor threshold, derived from literature data.

2.5 RNA- sequencing and quantitative real-time PCR analyses

The Vazyme FastPure Universal Plant Total RNA Isolation Kit (RC411) was utilized to isolate total RNA from the pulp and skin of six grape varieties. RNA samples were used to build sequencing libraries, and subsequently examined using the BGISEQ-500 platform (Beijing Genomic Institution, www.genomics.org.cn) to produce 150-base end-sequences. Subsequently, a thorough transcriptomic analysis was conducted using the filtered initial reads sequencing data to the *Vitis vinifera* template genome accessible at Ensembl Plants. Gene expression was quantified using the FPKM approach. The 'limma' package in R (v. 4. 2. 3) was utilized to analyze expression Expression differences. A threshold of absolute log (2Fold change) ≥1 and $P < 0.05$ was applied for identifying differentially expressed genes (DEGs). The DEGs were employed in functional category enrichment within the KEGG pathway framework.

The primers for qRT-PCR were detailed in Supplementary Table S2.

2.6 Statistical analysis

Monoterpene concentrations of compound were compared using one-way ANOVA to evaluate differences. Subsequently, a Tukey's HSD test was conducted with a significance level of $P < 0.05$, utilizing the SPSS 20.0 software (IBM, Armonk, NY). Histograms were generated using OriginPro 2021 (OriginLab Corporation, Northampton, MA). 'pheatmap' package in R (v. 4. 2. 3) was used to plot the heatmaps. The KEGG analysis was performed using KOBAS, a freely accessible online data analysis service (Bu et al., 2021). The 'ggplot2' package in R (v. 4.2.3) was used to plot the KEGG analysis enrichment pathway and KOG function classification histograms. Co-expression analysis was conducted utilizing gene expression data across the six grape cultivars.

3 Results and discussion

3.1 Free aroma compounds in six grape varieties

Aromatic substances reside in the grape exocarp and pulp in free and bound glycosides. The free volatiles directly impart the characteristic flavors to the grapes (Wu et al., 2019). In this research, a total of 61, 61, 57, 56, 41, and 48 free aroma compounds were found in 'Shine Muscat', 'Shine 13', 'Hutai 8', 'Summer Black', 'Red Globe' and 'Moldova', individually (Supplementary Table S2; Figure 1A). The free aroma volatiles concentration was highest for 'Moldova' (11814.15μg/L) and 'Red Globe' (8935.6μg/L), followed by 'Shine Muscat' (8912.43μg/L) and 'Shine 13' (8829.95μg/L), while it was lowest concentration for 'Hutai 8' (8626μg/L) and 'Summer Black' (6056.3μg/L) (Supplementary Table S2; Figure 1A). Of the grape cultivars included in this study, 'Shine Muscat' and 'Shine 13' among the six table grapes as Muscat varieties (Wang et al., 2021). 'Hutai 8' and 'Summer Black' were classified as strawberry-type cultivars (Wu et al., 2019)."Red Globe" and "Moldova" were categorized as neutral aromatic cultivars (Xiang et al., 2022). 'Shine Muscat' and 'Shine 13' exhibited the highest levels of free monoterpenes, with 996.23μg/L and 994.03μg/L, respectively (Supplementary Table S2; Figure 1A). Monoterpenes are considered to be the dominant compound of the Muscat cultivars (Mateo and Jiménez, 2000). In this study, linalool, *trans*-*β*-ocimene, *cis*-*β*-ocimene, *β*-myrcene, and geraniol were the main monoterpenes in Muscat-type cultivars. Among them, linalool was the richest monoterpene in Muscat-type cultivars. Fenoll et al. (2009) investigated composition, concentration, and aromatic impact of monoterpenes during the development of muscat

humburg grape, identifying linalool as the most significant contributor to the aroma profiles. In line with our results, earlier research has indicated that linalool, geraniol, and β-myrcene were the dominant monoterpene in Muscat-type cultivars (Wang H. et al., 2023; Wang W.-N. et al., 2023; Yue et al., 2022). The concentration of free C13-norisoprenoids was highest in 'Shine Muscat'(109.38μg/L) and 'Shine 13'(28.09μg/L), followed by 'Summer Black'(20.85μg/L) and 'Hutai 8'(13.78μg/L), while in neutral aromatic cultivars were not detected. 6-Methyl-5-hepten-2-ol was the most abundant C13-norisoprenoids in Muscat-type cultivars (Supplementary Table S2; Figure 1A). Volatiles esters have been identified as the predominant volatile compounds in some hybrid cultivars derived from *V. vinifera and V. labrusca*, significantly contributing to the overall aromatic profile of these hybrids (Yang et al., 2011; Wu et al., 2016). In this study, the concentration of free esters was highest in 'Hutai 8'(838.16μg/L) and 'Summer Black'(275.55μg/L). Furthermore, ethyl 3-hydroxybutyrate was the most abundant ester in 'Hutai 8' and 'Summer Black', followed by ethyl butanoate and ethyl hexanoate (Supplementary Table S2; Figure 1A). Similarly, Yao et al. (2021) reported that the aldehydes and esters were the predominant aroma compounds in 'Hutai 8' grape. In accordance with our findings, previous studies reported ethyl butanoate and ethyl hexanoate were rich in strawberry-type grape cultivars (Qian et al., 2019; Yang et al., 2009). The highest levels of free C6/C9 compounds were found in 'Moldova' (8821.79μg/L) and 'Red Globe' (6828.49μg/L). Moreover, (E)-2-hexenal were the most abundant C6/C9 compounds in 'Moldova' and 'Red Globe', followed by hexanal, (E)-2-hexenol, and hexanoic acid (Supplementary Table S2; Figure 1A). Consistent with our results, previous investigations reported the neutral aromatic cultivars had the highest (E)-2-hexenal, followed by hexanal (Aubert and Chalot, 2018; Wang W.-N. et al., 2023). Terpenes and esters are present in low concentration in neutral cultivars, Koyama et al. (2022) observed that C6 compounds account for the main aroma compounds, though the concentration of terpenes and esters tends to be low in neutral grapes. It should be recognized that the concentration of C6/C9 compounds was the highest aroma compound in six grape cultivars. Wu et al. (2016) have indicated that the C6 compounds are the basic background volatile aromas, which is consistent with our findings. However, the aroma characteristics of grape berries mainly depend on the contents of monoterpenes and esters. Additionally, the neutral aromatic cultivars also had the most abundant carbonyl compounds. Among them, the concentration of benzaldehyde was the highest compound in neutral aromatic grapes.

3.2 Glycosidically-bound aroma compounds in six grape varieties

The bound aroma is mainly present in hydrophilic, non-volatile, and flavorless glycosylated molecules and the bound aroma compounds can be converted into their free form through hydrolysis (Wu et al., 2020). In grapes, the concentration of glycosylated aroma acting as a key indicator of the aromatic potential (Hernandez-Orte et al., 2015). In this research, a total of 59, 59, 55, 53, 48, and 46 bound aroma compounds were identified in 'Shine Muscat', 'Shine 13', 'Hutai 8', 'Summer Black', 'Red Globe', 'Moldova', respectively (Supplementary Table S2; Figure 1B). The bound monoterpene concentration was highest in 'Shine 13' (3613.85μg/L) and 'Shine Muscat'(2512.65μg/L), succeeded by 'Summer Black' (1462.62μg/L) and 'Hutai 8' (996.78μg/L), while the neutral aromatic cultivars 'Red Globe' (359.66μg/L) and 'Moldova' (290.28μg/L) had the lowest bound monoterpene concentration. This result was consistent with the concentration of free monoterpene. This study revealed that nerol was the highest concentration bound monoterpene identified in 'Shine 13' and 'Shine Muscat', followed by linalool and geraniol. Corresponding to our results, previous studies reported that bound nerol, linalool, and geraniol were the major glycosidically monoterpenes in Muscat-type cultivars (Ruiz-García et al., 2014). Linalool and nerol can be synthesized by geraniol, are characterized by their distinctive floral, sweet, and fruit aroma, and serve as the primary compounds responsible for the aromatic profile of Muscat grapes (Fenoll et al., 2009). The abundant linalool, nerol, and geraniol may suggest the related biosynthesis pathways in Muscat grapes. Matsumoto and Ikoma (2016) found that linalool, nerol, and geraniol are the most primary aromatic compounds and responsible for the aroma in Muscat cultivars. The bound C13-norisoprenoids concentration was highest in 'Shine 13' (267.64μg/L) and 'Shine Muscat' (158.99μg/L), followed by 'Hutai 8' (52.63μg/L) and 'Summer Black' (42.97μg/L), however, 'Red Globe' (40.9μg/L) and 'Moldova' (41.07μg/L) had the lowest C13-norisoprenoids. This result was in line with the free C13-norisoprenoids, and the bound C13-norisoprenoids were higher than the free form. 6-Methyl-5-hepten-2-ol was the most abundant bound C13-norisoprenoid in Muscat-type cultivars, while strawberry and neutral cultivars were not identified. The concentration of bound esters was highest for strawberry-type cultivars, specifically rich in 'Hutai 8' (5190.29μg/L). Ethyl 3-hydroxybutyrate was the predominant ester in 'Hutai 8', which is consistent with its high concentration among the free esters. Fatty acids undergo metabolic processes within fruits to yield volatile esters (Qin et al., 2014). Therefore, alcohols, as metabolic precursors, may play important roles in influencing the compounds and distribution of volatile esters within grape berries (Qian et al., 2019). The concentration of bound alcohols was found to be the highest in 'Hutai 8' (6674.97μg/L) and 'Summer Black' (5877.63μg/L). Phenylethyl alcohol emerged as the most abundant alcohol, followed by benzyl alcohol, which in agreement with an earlier study on strawberry-type cultivars (Qian et al., 2019).

3.3 Principal component analysis of free and glycosidically-bound aroma compounds in six grape cultivars

PCA was conducted on the six grape cultivars using the free and bound aroma compounds as the variables to evaluate their cultivar characteristics. The first and second principal components (PC1 and PC2) accounted for 33.42% and 27.06% of the total variance in

10.3389/fpls.2025.1544593

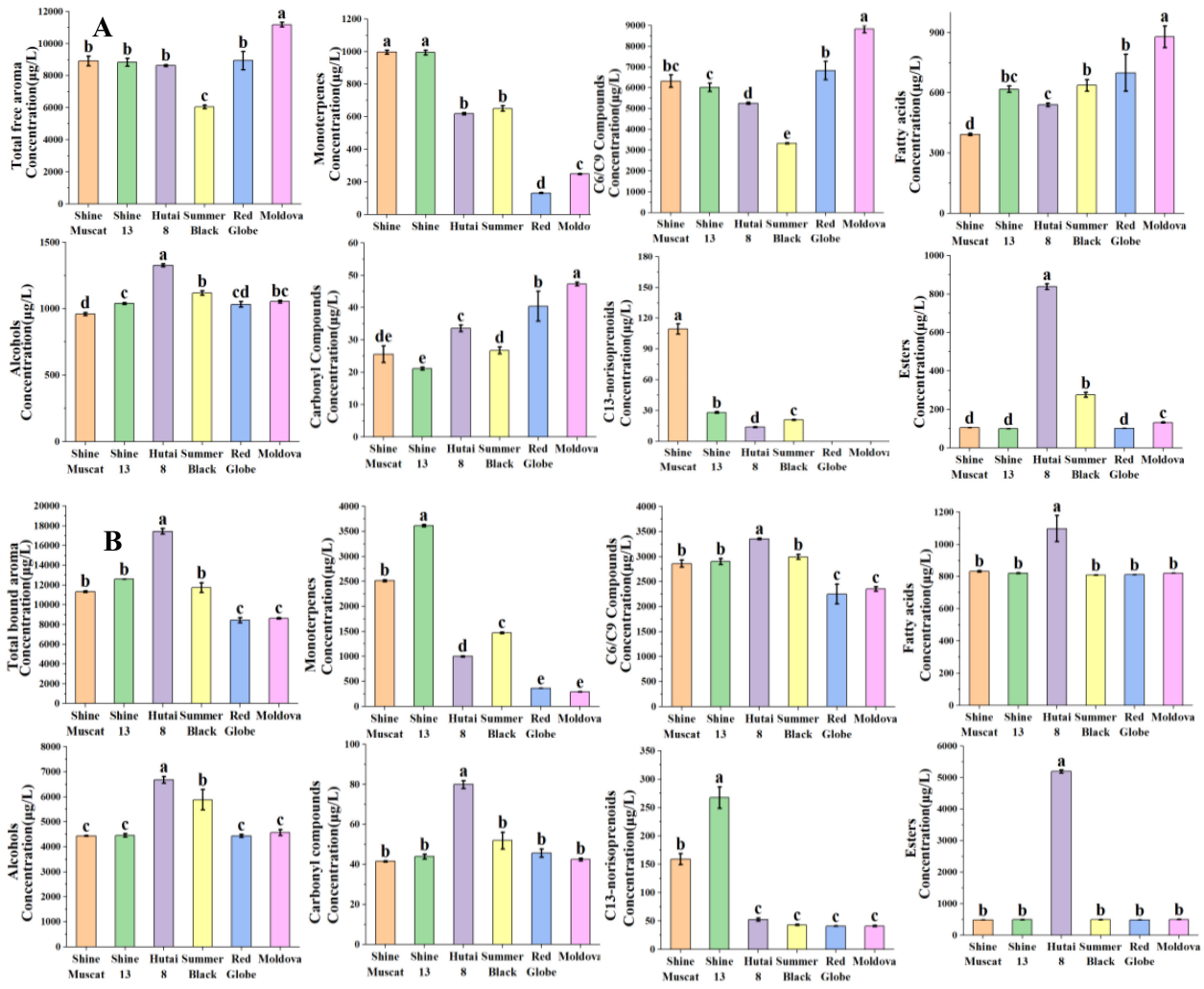

FIGURE 1
Concentrations of free **(A)** and **(B)** aroma compounds in six grape cultivars. Different letters in each graph indicated significant differences at $P < 0.05$.

the free aroma compounds of the six grape cultivars (Figure 2A), as well as 42.25% and 22.69% of the total variance in the bound aroma compounds of the six grape cultivars (Figure 2B), respectively. It was observed that both the free and glycosidically-bound aromas in the six grape cultivars were divided into three parts: 'Shine Muscat' and 'Shine 13', 'Hutai 8' and 'Summer Black', as well as 'Moldova' and 'Red Globe' were in the same group, respectively. Accordingly, all grapes in the same cultivar type had similar aroma profiles.

3.4 Heatmap analysis of free aroma compounds

To further explore the variations of the free and bound aroma profiles of six grape cultivars, a heatmap analysis was performed. The results revealed significant inter-cultivar differences in both the abundance and diversity of aroma compounds (Figure 2C), corroborating previous findings that even cultivars sharing the same aroma classification exhibit distinct compound profiles (Wu et al., 2019). Hierarchical clustering grouped the cultivars into three distinct clusters: Muscat-flavored cultivars ('Shine Muscat' and 'Shine 13'); strawberry-aroma cultivars ('Hutai 8' and 'Summer Black'); neutral-aroma cultivars ('Red Globe' and 'Moldova'). This observation was in alignment with the findings presented in Section 3.3, suggesting that grape cultivars of the same aroma type share similar aroma profiles and genetic backgrounds. In this study, a total of 27 monoterpenes, 12 C6/C9 compounds, 5 alcohols, 1 fatty acid, 3 carbonyl compounds, C13-norisoprenoids, and 10 esters were detected. Muscat-flavored clusters exhibited strong positive correlations with monoterpenes and C13-norisoprenoids. Strawberry-aroma clusters were predominantly associated with alcohol and esters. Neutral-aroma clusters showed higher affinity for C6/C9 compound. The distinct clustering further may support the utility of volatile compound profiling as a tool for cultivar classification and quality prediction.

10.3389/fpls.2025.1544593

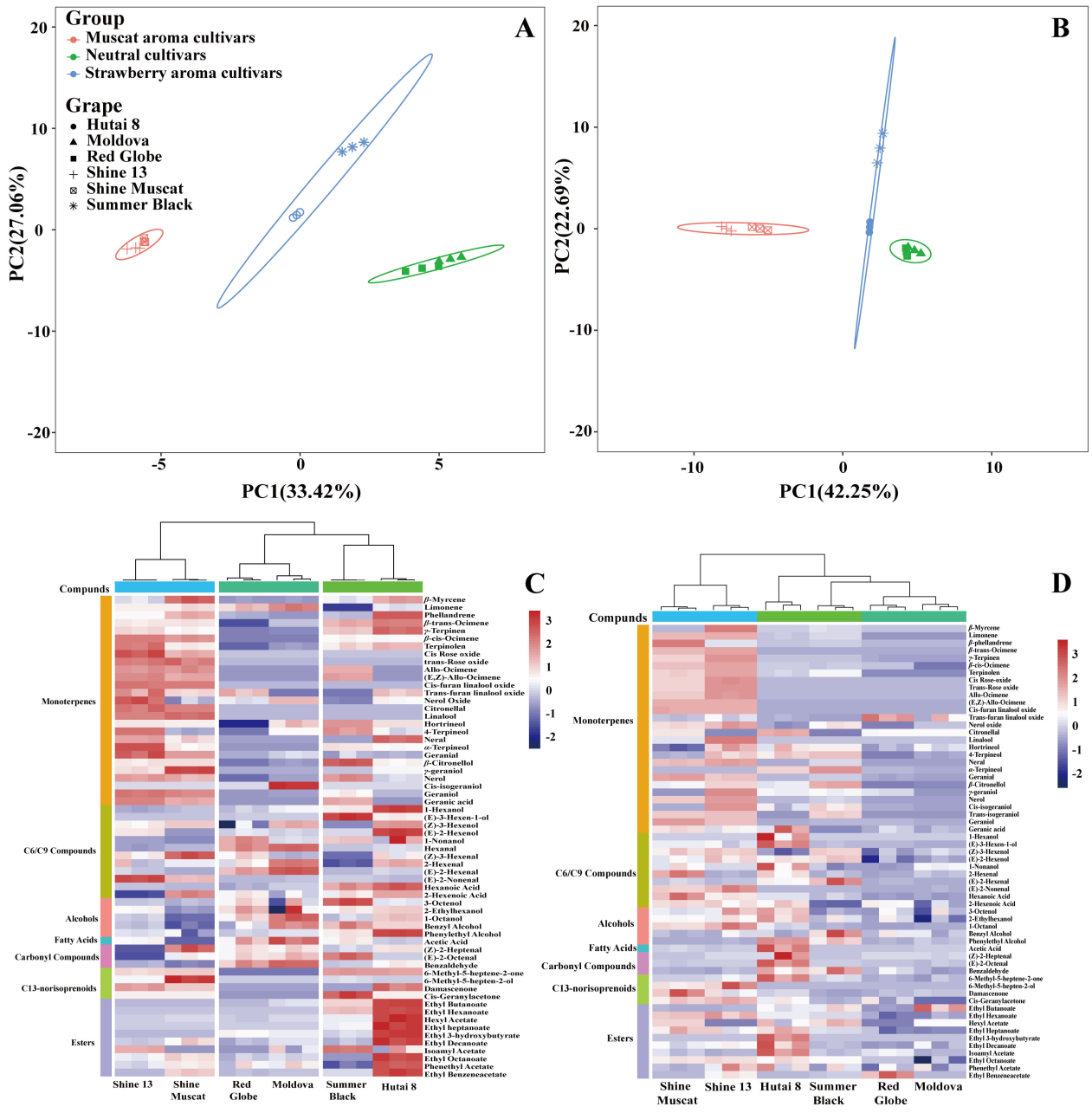

FIGURE 2
Principal component analysis (PCA) of free **(A)** and bound **(B)** volatile compounds of six grape cultivars. Heatmap analysis of free **(C)** and bound **(D)** aroma compounds.

3.5 Heatmap analysis of glycosidically-bound aroma compounds

Figure 2D illustrated the variability of bound aroma compounds across six grape cultivars. A total of 58 bound volatiles were identified, comprising 28 monoterpenes, 10 C6/C9 compounds, 5 alcohols, 1 fatty acid, 3 carbonyl compounds, 2 C13-norisoprenoids, and 10 esters. Hierarchical clustering revealed two distinct groups: Muscat-flavored cultivars ('Shine Muscat' and 'Shine 13'); neutral-aroma cultivars ('Red Globe' and 'Moldova'). This clustering aligns with their free aroma profiles, suggesting conserved biosynthetic regulation of both free and bound forms within cultivars. However, 'Hutai 8' and 'Summer Black' (strawberry-aroma cultivars) were not clustered, suggesting the lower concentration of bound aroma compounds in 'Summer Black'. Notably, Muscat-type cultivars ('Shine 13' and 'Shine Muscat') exhibited strong positive correlations with bound monoterpene and C13-norisoprenoids, mirroring their free volatile associations. In contrast, strawberry-

aroma cultivars ('Hutai 8' and 'Summer Black') showed higher affinity for fatty acid, carbonyl compounds, and ester, potentially contributing to their characteristic ripe-fruit aroma. These findings highlight the parallel between bound and free volatile profiles.

3.6 OAVs of volatile aroma compounds in six grape varieties

This study described the results of the OAVs in six grape cultivars, which were employed to evaluate the impact of each component on grape aromas (Table 1). The OAV, derived from the concentration of the aroma compound over its odor detection threshold, serves as a crucial metric for assessing the quality of grape aromas (Yang et al., 2019). However, only the OAV > 1 of volatile compounds was regarded as contributing to the aroma (Genovese et al., 2013b).

A total of 9, 9, 5, 4, 2, and 2 monoterpenes in 'Shine Muscat', 'Shine 13', 'Hutai 8', 'Summer Black', 'Red Globe', and 'Moldova' had OAVs >1, respectively. The Muscat-type cultivars exhibited the highest OAVs among the six grapes, with especially high proportions for linalool and rose oxide, which impart the floral, rose, and sweet taste characteristics (Wu et al., 2019). Corresponding to our results, previous results discovered linalool and α-terpineol with OAVs>1 as being linked to the Muscat aroma (Yang et al., 2024). It was observed that 6, 6, 7, 6, 7, and 6 free C6/C9 compounds in 'Shine Muscat', 'Shine 13', 'Hutai 8', 'Summer Black', 'Red Globe' and 'Moldova' had OAVs >1, respectively. The OAVs of C6/C9 compounds, which are known to primarily possess green leaf or floral and fruity odor (Kalua and Boss, 2009; Yue et al., 2023), were relatively high, thus may significantly influence the formation of the volatile profiles of six grape cultivars. Wu et al. (2016) reported that the C6 compounds are the basic background volatile aromas, while the aroma characteristics of grape pulp and peel mainly depend on the contents of monoterpenes and esters. Among the C6/C9 compounds, the OAV of hexanal, (Z)-3-hexenal, and (E)-2-hexenal were present in relatively high in six grape varieties. Yang et al. (2009) documented that hexanal and (E)-2-hexenal were the dominant C6 volatile compounds and they were detected in nearly all the grape samples, which were consistent with our results. A total of 3, 2, 2, 1, 0, and 0 free C13-norisoprenoids in 'Shine Muscat', 'Shine 13', 'Hutai 8', 'Summer Black', 'Red Globe' and 'Moldova' had OAVs >1, respectively. Damascenone and cis-geranylacetone were the main factors influencing the aroma profiles of both Muscat-type and strawberry-type cultivars, due to their relatively high OAVs and low thresholds. These compounds can contribute to the development of apple, rose, honey, and floral notes in these grape berries (Mayr et al., 2015; Guo et al., 2021). A total of 3, 3, 3, 3, 3, and 3 free esters in 'Shine Muscat', 'Shine 13', 'Hutai 8', 'Summer Black', 'Red Globe', and 'Moldova' had OAVs >1, respectively. However, 'Hutai 8' and 'Summer Black' exhibited the highest OAVs in esters, with ethyl butanoate as the primary compound with an OAV >1, thereby contributing to the fruity aroma profile of these grape varieties.

3.7 Characterization and functional profiling of genes showing differential expression in three grape varieties

In this research, DEGs were calculated based on the FPKM value using R (v 4.2.3) with limma package, DEG analysis revealed upregulated and downregulated genes in three grape varieties of different aroma types (adj. *P*. Val < 0.05, $|\log_2^{FC}| \geq 1$) (Figure 3). A total of 2328 DEGs were identified in 'RG' ('Red Globe') and 'S13' ('Shine 13'), of which 1157 and 1171 DEGs showed upregulated and downregulated expression levels, respectively (Figure 3A); A total of 2796 DEGs were found in 'RG' and 'SB' ('Summer Black'), of which 1358 and 1438 DEGs exhibited upregulated and downregulated expression levels, respectively (Figure 3B); A total of 2523 DEGs were selected in 'S13' and 'SB', of which 1232 and 1291 DEGs showed upregulated and downregulated expression levels, respectively (Figure 3C).

To further investigate the functions of these DEGs concerning the biosynthesis of aromatic compounds, we performed KEGG pathway enrichment analysis. It was noticed that 7, 7, and 2 pathways that were significantly enriched (P <0.01) in 'RG-S13', 'RG-SB', and 'SB-S13', respectively; KEGG enrichment showed significant enrichment in limonene and pinene degradation, glycine, serine and threonine metabolism, galactose metabolism, glyoxylate and dicarboxylate metabolism, protein processing in endoplasmic reticulum and biosynthesis of secondary metabolites and metabolic pathways at 'RG-S13' (Figure 3D); The significantly enriched KEGG pathways included diterpenoid biosynthesis, alanine, aspartate and glutamate metabolism, phenylalanine, tyrosine and tryptophan biosynthesis, glycine, serine and threonine metabolism, cysteine and methionine metabolism, arginine and proline metabolism and biosynthesis of secondary metabolites at 'RG-SB' (Figure 3E). KEGG pathway enrichment analysis of the 'SB-S13' revealed enrichment in protein processing in endoplasmic reticulum and plant-pathogen interaction (Figure 3F). These significantly KEGG enrichment pathways mostly relate to the anabolism of amino acids, which were implicated in the anabolic and catabolic processes related to volatile compounds, including aldehydes, alcohols, esters, and methoxypyrazines.

3.8 Gene coexpression network analyses

With the acquisition of RNA expression data, and the aroma data of 'RG', 'S13', and 'SB' in the three different aroma types of grape berries, the gene co-expression network with weights was established using the optimal soft threshold, and 23,445 genes were selected for WGCNA analysis (Figure 4B). The genes were categorized into 8 distinct expression clusters, and a dendrogram of the gene clusters was constructed (Figure 4A). Based on the correlation results between modules and the concentration of aromas (Figure 4C), the MEpink (790 genes) and MEgreenyellow (110 genes) showed a significant correlation with monoterpenes, the MEblack (88 genes), MEsalmon (451 genes) and MEpink (790 genes) modules showed a significant correlation with C6/C9 compounds, MEblack (88 genes), MEsalmon (451 genes) modules

10.3389/fpls.2025.1544593

TABLE 1 OAVs of free volatile aroma compounds from six grape varieties.

Aroma compunds (μg/L)	'Shine Muscat'	'Shine 13'	'Hutai 8'	'Summer Black'	'Red Globe'	'Moldova'	odour threshold (μg/L)	Odour descriptor
Monoterpenes								
Numbers	9	9	5	4	2	2		
Sub total	98.86 ± 0.34b	110.95 ± 3.95a	9.87 ± 0.06c	7.28 ± 0.06c	6.72 ± 0.38c	7.93 ± 0.31c		Rose, Flora
C6/C9 Compounds								
1-Hexanol	<1	<1	<1	<1	<1	<1	8000[1]	Resin, Flower, Green[1]
(E)-3-Hexen-1-ol	<1	<1	<1	<1	<1	<1	1000[2]	Moss, Fresh[2]
(Z)-3-Hexenol	3.69 ± 0.17ab	3.13 ± 0.11b	4.26 ± 0.07a	1.79 ± 0.01c	1.52 ± 0.14c	3.97 ± 0.11ab	40[1]	Grass[1]
(E)-2-Hexenol	2.99 ± 0.17d	15.92 ± 0.54b	35.89 ± 0.83a	9.46 ± 0c	9.83 ± 0.24c	8.7 ± 0.53c	40[3]	Green, Leaf, Walnut[3]
1-Nonanol	<1	<1	<1	<1	<1	<1	50[4]	Rose-Orange[4]
Hexanal	240.8 ± 7.25bc	218.43 ± 7.59c	102.78 ± 5.37d	80.1 ± 2.71d	257.2 ± 2.93b	310.2 ± 4.69a	10[5]	Green, Grassy[5]
(Z)-3-Hexenal	133.93 ± 9.11a	66.19 ± 4.04b	65.27 ± 14.77b	ND	74.87 ± 10.88b	32.62 ± 3.05c	0.25[4]	Grass[4]
2-Hexenal	<1	<1	<1	<1	<1	<1	400[6]	Herbaceous, Green[6]
(E)-2-Hexenal	180.83 ± 11.9b	150.06 ± 5.14c	87.41 ± 3.9d	69.84 ± 2.54d	190.66 ± 22.16b	267.92 ± 5.29a	17[3]	Green, Apple-Like[3] Bitter Almond-Like
(E)-2-Nonenal	33.1 ± 0.78b	59.75 ± 1.95a	5.05 ± 0.28d	8 ± 0.53c	4.61 ± 0.24d	5.1 ± 0.15d	0.69[5]	Fatty, Green[5]
Hexanoic acid	<1	<1	1.34 ± 0.03a	1.16 ± 0.07b	<1	<1	420[1]	Sweat[1]
2-Hexenoic acid	<1	<1	<1	<1	<1	<1	1000[4]	Fatty, Rancid[4]
Numbers	6	6	7	6	7	6		
Subtotal	595.55 ± 28ab	513.65 ± 19.38c	302.32 ± 12.63d	170.44 ± 0.79e	538.91 ± 36.34bc	628.88 ± 7.74a		
Alcohols								
3-Octenol	3.22 ± 0.23b	3.46 ± 0.11b	4.1 ± 0.08b	9.00 ± 0.6a	5.29 ± 0.7b	3.81 ± 0.01b	1[7]	Cucumber, Earth, Fat, Floral, Mushroom[7]
2-Ethylhexanol	<1	<1	<1	<1	<1	<1	270[8]	Rose, Green[8]
1-Octanol	<1	<1	<1	<1	<1	<1	10000[9]	Chemical, Metal, Burnt[9]
Benzyl alcohol	<1	<1	<1	<1	<1	<1	10000[10]	Sweet, Flower[10]
Phenylethyl Alcohol	<1	<1	<1	<1	<1	<1	14000[11]	Rose[11]
Numbers	1	1	1	1	1	1		
Subtotal	3.22 ± 0.23b	3.46 ± 0.11b	4.10 ± 0.08b	9.00 ± 0.6a	5.29 ± 0.7b	3.81 ± 0.01b		
Fatty acids								
Acetic acid	<1	<1	<1	<1	<1	<1	180000[5]	Vinegar-like[5]
Numbers	0	0	0	0	0	0		
Subtotal	<1	<1	<1	<1	<1	<1		

(Continued)

10.3389/fpls.2025.1544593

TABLE 1 Continued

Aroma compunds (μg/L)	'Shine Muscat'	'Shine 13'	'Hutai 8'	'Summer Black'	'Red Globe'	'Moldova'	odour threshold (μg/L)	Odour descriptor
Carbonyl Compounds								
(Z)-2-Heptenal	<1	<1	<1	<1	<1	<1	13[12]	Green[12]
(E)-2-Octenal	1.08 ± 0.03c	<1	1.03 ± 0d	1.22 ± 0.02a	1.09 ± 0.03bc	1.13 ± 0.02b	3[10]	Green Leaf, Walnut[10]
Benzaldehyde	<1	<1	<1	<1	<1	<1	350[10]	Almond[10]
Numbers	1	1	1	1	1	1		
Subtotal	1.08 ± 0.03c	<1	1.03 ± 0d	1.22 ± 0.02a	1.09 ± 0.03bc	1.13 ± 0.02b		Grass
C_{13}-norisoprenoids								
6-Methyl-5-heptene-2-one	<1	<1	<1	<1	ND	ND	50[10]	Green, Citrus-Like[10]
6-Methyl-5-hepten-2-ol	1.97 ± 0.1a	<1	ND	<1	ND	ND	50[10]	Pepper, mushroom, rubber[5]
Damascenone	51.16 ± 0.13c	66.42 ± 4.01b	78.83 ± 6.46a	ND	ND	ND	0.05[12]	Apple, Rose, Honey[12]
Cis-Geranylacetone	36.33 ± 0.22b	36.29 ± 0.24b	35.71 ± 0.39b	81.74 ± 6.67a	ND	ND	0.06[13]	Floral[13]
Numbers	3	2	2	1	0	0		
Sub total	89.46 ± 0.25c	103.04 ± 4.26b	114.54 ± 6.85a	81.90 ± 6.67c	ND	ND		Floral, Fruity
Esters								
Ethyl butanoate	1.38 ± 0.05d	1.56 ± 0.02d	114.26 ± 1.51a	46.55 ± 0.1b	1.44 ± 0.05d	15.02 ± 1.04c	2.4[5]	Fruity[5]
Ethyl hexanoate	<1	<1	<1	<1	<1	<1	580[12]	Fruit, Fat[12]
Hexyl acetate	<1	<1	<1	<1	<1	<1	10[14]	Fruit, Herb[14]
Ethyl heptanoate	4.78 ± 0c	4.78 ± 0c	5.05 ± 0.02a	4.82 ± 0.01b	4.78 ± 0c	4.78 ± 0c	2[4]	Wine-like, Brandy, Fruity[4]
Ethyl 3-hydroxybutyrate	<1	<1	<1	<1	<1	<1	20000[2]	Grape-like[2]
Ethyl decanoate	<1	<1	<1	<1	<1	<1	200[1]	Grape[1]
Isoamyl acetate	<1	<1	<1	<1	<1	<1	30[15]	Banana, Fruity, Pear[15]
Ethyl octanoate	1.12 ± 0b	1.12 ± 0b	1.13 ± 0a	1.12 ± 0b	1.12 ± 0b	1.12 ± 0b	14[1]	Apple, Peel, Fruit[1]
Phenethyl acetate	<1	<1	<1	<1	<1	<1	250[12]	Rose, Honey, Tobacco[12]
Numbers	3	3	3	3	3	3		
Subtotal	7.29 ± 0.05d	7.46 ± 0.02d	120.44 ± 1.49a	52.49 ± 0.1b	7.35 ± 0.06d	20.92 ± 1.04c		Fruity
Total	795.46 ± 28.9a	738.56 ± 27.72b	552.3 ± 21.11c	322.33 ± 8.24d	559.36 ± 37.51c	662.67 ± 9.12ab		

Data are presented as the mean ± standard deviation of three biological replicates; Different letters indicate significant differences at $P < 0.05$; ND, not detected; Reference, 1: (Ferreira et al., 2000); 2: (Noguerol-Pato et al., 2014); 3: (Genovese et al., 2013a); 4: (Kaya et al., 2022); 5: (Czerny et al., 2008); 6: (Genovese et al., 2013a); 7: (Yang et al., 2010); 8: (Pino and Mesa, 2006); 9: (Moyano et al., 2009); 10: (Buttery et al., 1988); 11: (Vilanova et al., 2013); 12: (Mayr et al., 2015); 13: (Guo et al., 2021); 14: (Xiao et al., 2023); 15: (Chang et al., 2014).

10.3389/fpls.2025.1544593

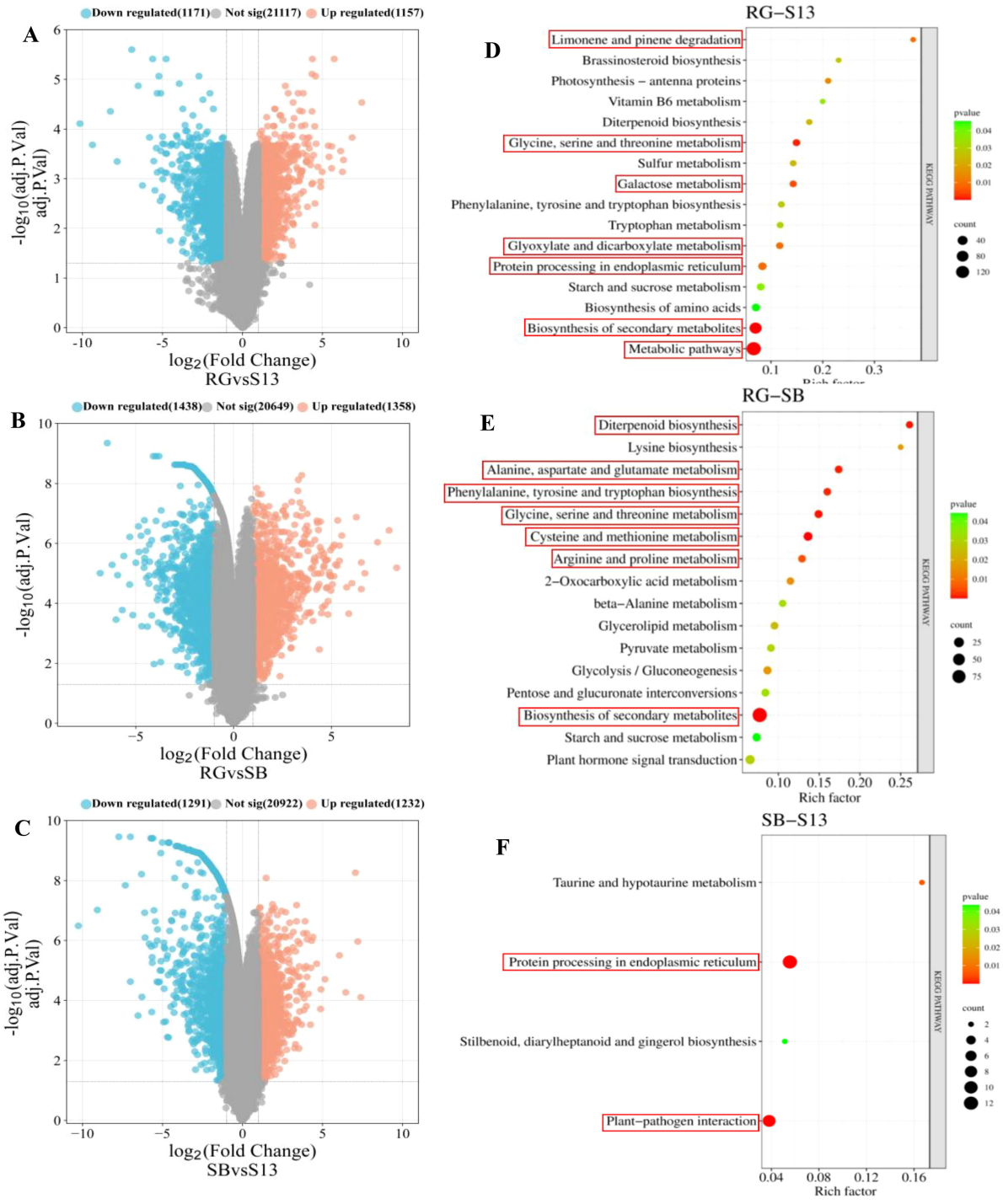

FIGURE 3
DEGs in three aroma types of grape varieties **(A–C)**. RG ('Red Globe'), S13 ('Shine 13'), SB ('Summer Black'), and KEGG pathway analysis of DEGs. **(D)** RG ('Red Globe') vs S13 ('Shine 13'); **(E)** RG vs SB ('Summer Black'); **(F)** S13 vs SB; Count represents the DEG number. Gene ratios are calculated as the ratio of DEGs in each KEGG pathway compared with the total number of DEGs.

were positively correlated with alcohols, MEgreenyellow (110 genes), MEpink (790 genes) modules were positively correlated with fatty acids, MEsalmon(451 genes), MEgreenyellow (110 genes) and MEpink (790 genes) modules were positively correlated with C13-norisoprenoids. MEblack (88 genes), MEsalmon (451 genes), and MEpink (790 genes) were positively correlated with esters.

The KOG function classification was performed on the RNA expression data (Figure 4D). There were 1373 and 1270 genes associated with lipid transport and metabolism and amino acid transport and metabolism, respectively. In addition, 1643 genes were related to secondary metabolites biosynthesis, transport and catabolism. These genes may regulate compounds related to aroma metabolism and catabolism.

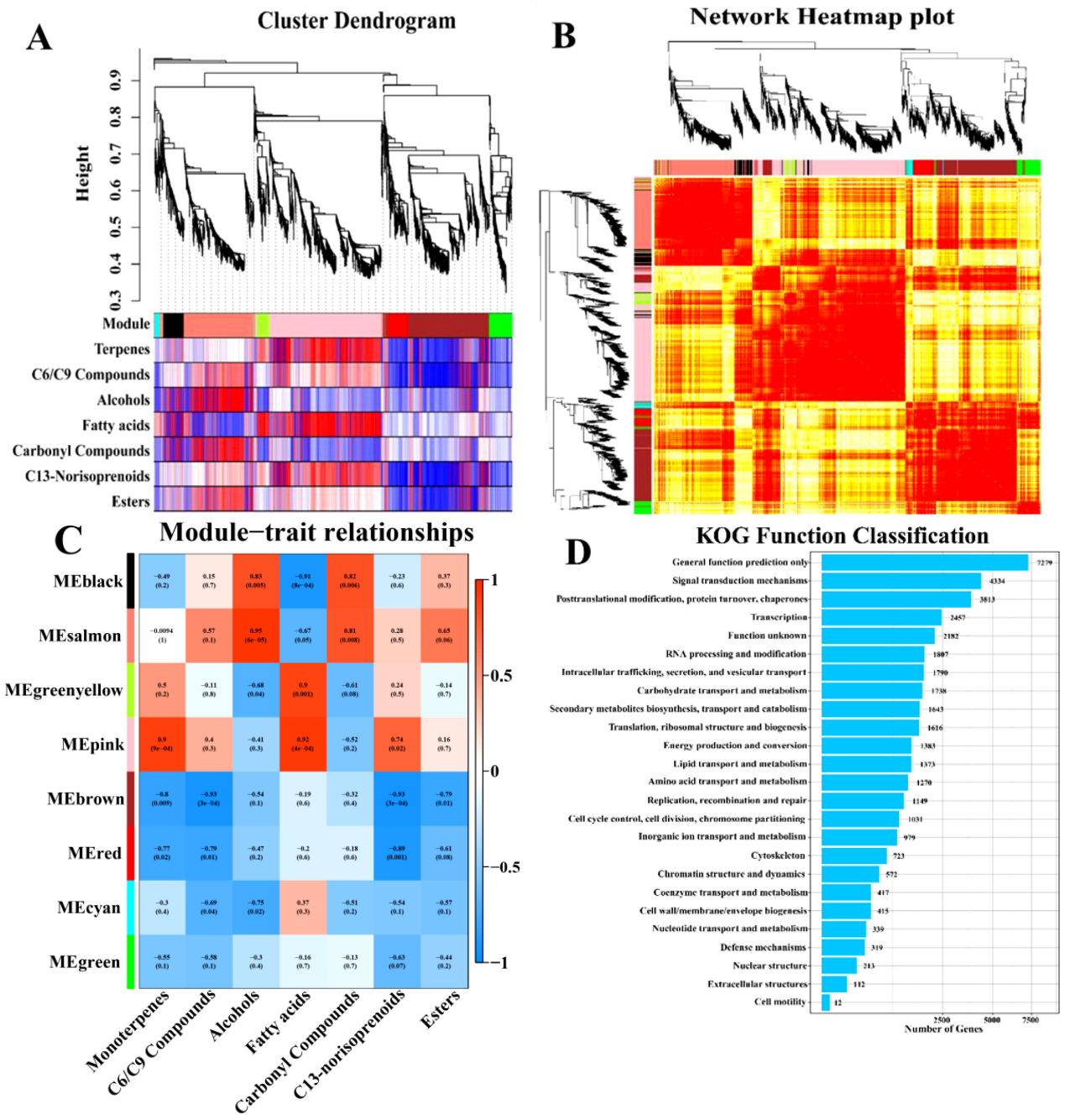

FIGURE 4
WGCNA and KOG function classification analysis in three aroma types of grape varieties. **(A)** Phylogenetic tree heatmap associated with volatile aroma compounds. **(B)** Gene co-expression network heatmap plot. **(C)** Heatmap of correlation between co-expressed gene modules and volatile aroma compounds traits. **(D)** KOG function classification in three aroma types of grape varieties.

3.9 Expression analysis of genes related to aroma biosynthesis in six types of grape cultivars

Monoterpenes and C13-norisoprenoids are predominantly produced through MEP and MVA pathways which occur in grapes plastids and cytosol, respectively (Wen et al., 2015). C6/C9 compounds, alcohols, carbonyl compounds, and esters are primarily biosynthesized in β-oxidation and lipoxygenase-hydroperoxide lyase (LOX-HPL) pathways (Lin et al., 2019; Schwab et al., 2008; Wang et al., 2001).

The elevated expression of key terpenoid biosynthetic genes (*DXS, CMK, HDS, HDR, TPS, HMGR, CCD4a CCD4b, PNlinNer2, CSLinNer2* and *LIS*) in muscat-flavored cultivars ('Shine Muscat' and 'Shine 13') (Figure 5) strongly supports their role in monoterpene accumulation. Estévez et al. (2001) reported that

10.3389/fpls.2025.1544593

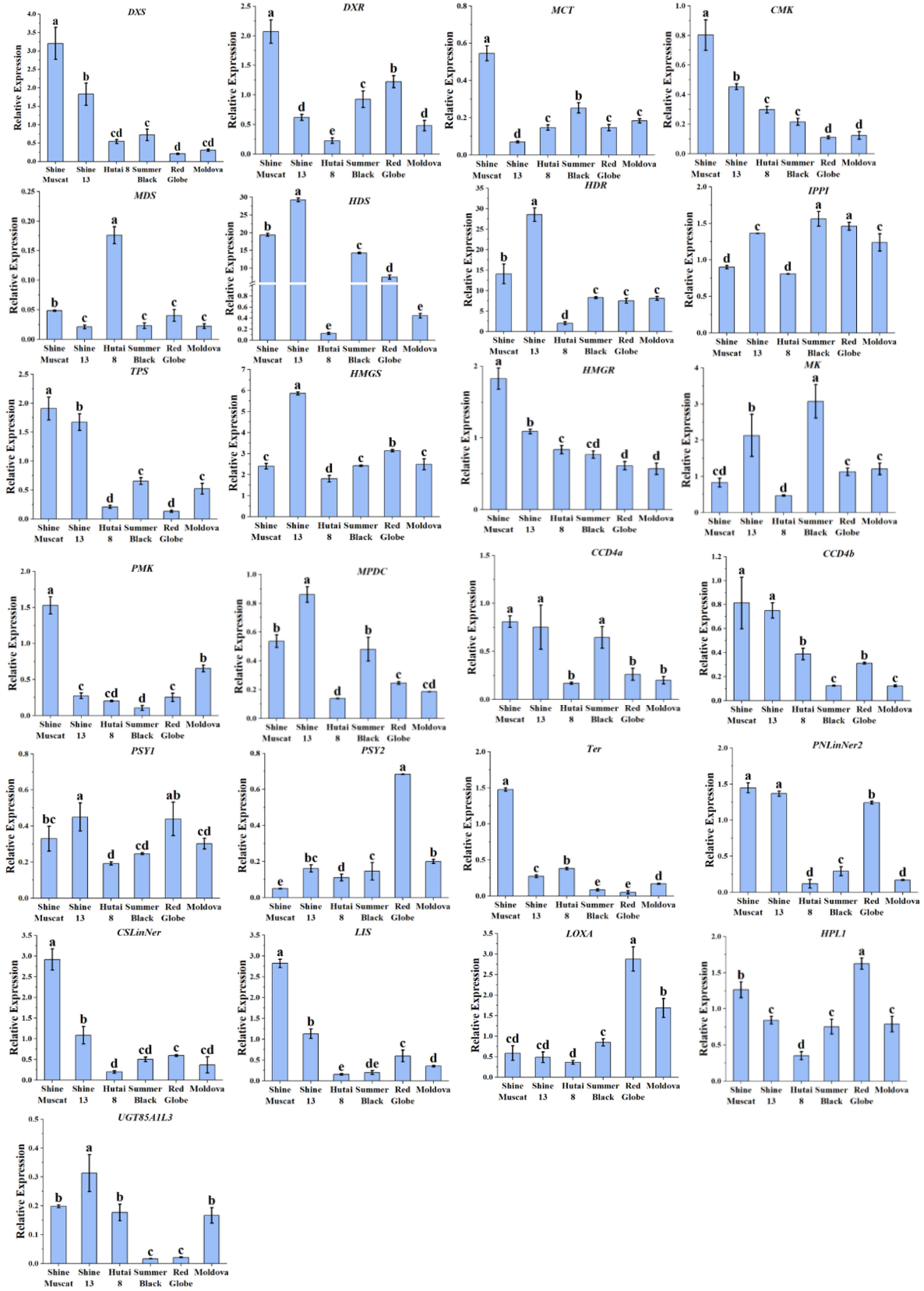

FIGURE 5
qRT-PCR analysis of the aroma related biosynthesis genes in six grape cultivars. Different letters in each graph indicated significant differences at $P < 0.05$.

DXS acts as the pivotal enzyme that initiates the first step in the MEP pathway. Furthermore, previous quantitative trait loci (QTL) analyses have indicated that *DXS* exhibited a strong correlation with the flavor profile of Muscat grape berries (Emanuelli et al., 2010), suggesting that genetic selection for *DXS* activity may drive cultivar-specific flavor differentiation. Overexpression of the *DXS1* gene in Nicotiana benthamiana leaves was demonstrated to enhance monoterpene biosynthesis, as reported by Wang et al. (2021). Notably, Yang et al. (2024) reported that relative expression levels of *CMK* and *HDR* were higher in muscat-type cultivars compared to neutral cultivars, which is consistent with our results. As a key rate-limiting enzyme in the MEP pathway, *HDR* regulates the synthesis of isoprenoids in plants (Banerjee and Sharkey, 2014). A previous study reported that *HDR* is the most expressed gene of the MEP pathway in 'Sangiovese' grape (D'Onofrio et al., 2018). Similarly, in this study, *HDR* also exhibited high expression levels in six grape cultivars. *TPSs* accelerate the concluding stage of free monoterpenes in the MEP pathway (Tholl, 2006). Until now, a total of 43 TPSs (terpene synthases) have been biochemically identified and characterized in grape berries (Lücker et al., 2004; Martin et al., 2010; Martin and Bohlmann, 2004). *TPS*, *PNlinNer2, CSLinNer*, and *LIS* belonged to *TPSs* gene family. *HMGR* is the key enzymes that catalyze the third step of the MVA pathway. A previous study indicated that the expression of *HMGR* genes was considerably elevated in Muscat grape varieties compared to strawberry-type cultivars (Zheng et al., 2021). Consistent with our results, the expression levels of *HMGR* in Muscat-type cultivars were significantly higher than in strawberry-type cultivars and neutral aromatic cultivars. The *CCD4* contributes to the creation of norisoprenoid aroma compounds and produces a range of water-soluble, low-threshold volatile compounds through the targeted cleavage of oxidized carotenoids (Zhong et al., 2020). The levels of *CCD4a*/*4b* expression were considerably high in Muscat-type cultivars. Additionally, the high abundance of *CCD4a*/*4b* suggests potential crosstalk between carotenoid cleavage and monoterpene modification pathways, which may diversify volatile profiles through secondary transformations. In line with our results, an earlier investigation found that the abundance of *CCD4* was more abundant in Muscat-type grape cultivars in comparison with those with a neutral aroma (Yang et al., 2024). These gene expression patterns correlated with the levels of terpene compounds, implying that these genes may play a predominant role in the variation of Muscat aroma among the six grape cultivars.

Among the five genes in β-oxidation and LOX-HPL pathways, *LOXA* and *HPL1* had the highest expression levels in 'Red Globe' (Figure 5). Our findings were in agreement with previous studies, which also reported that *LOXA* and *HPL1* exhibited high expression levels in neutral aromatic cultivars (Qian et al., 2016). Significantly, 'Hutai 8' had the highest expression levels of *AAT*, followed by the 'Summer Black' and 'Shine 13'. Additionally, 'Hutai 8' exhibited the highest concentration of free and bound esters, which was consistent with the expression levels of *AAT*. It was proposed that *AAT* genes could substantially impact the enzyme activity of *AATs* in fruits, thereby influencing ester production (Balbontín et al., 2010; El-Sharkawy et al., 2005; Souleyre et al., 2005).

3.10 Correlations between the expression levels of genes involved in aroma biosynthesis pathways and the composition of aroma compounds across six grape cultivar types

To explore the link between aroma concentrations and gene expression across six grape cultivars, Pearson correlation analysis was performed, and visualized with a correlation heatmap (Figure 6A). It was observed that the concentrations of linalool, γ-geraniol, and trans-rose oxide were significantly positively correlated with the expression levels of *DXS*. The concentrations of linalool, geranial, and cis-rose oxide were markedly related to the expression levels of *HDR*. The concentration of geraniol and geranic acid was substantially correlated to the expression levels of *DXS*. Previous studies found the expression level of VvDXS shows a positive correlation with the accumulation of monoterpenes in grape berries (Costantini et al., 2017; Wang et al., 2021). The concentration of γ-geraniol was considerably correlated with the expression levels of *HMGR*, *LIS*, and *Ter*. Furthermore, *HMGR* is a rate-limiting enzyme in the MVA pathway, controlling the monoterpene synthesis, and facilitates the enzymatic conversion of HMG-CoA to MVA (Leng et al., 2023). Additionally, previous studies have demonstrated that overexpression of *HMGR* (*PtHMGR*) in Populus trichocarpa modulates the expression of genes associated with the MVA and MEP pathways and markedly enhances the synthesis of terpenoid compounds (Wei et al., 2019). The concentration of trans-furan linalool oxide, citronellal, linalool, geranial, geraniol, and trans-rose oxide showed a marked positive association with the expression levels of *TPS*. Similarly, several studies reported that *HDS, MVK, PNLinNer1*, and *DXS* showed strong correlations with monoterpenes accumulation (Yang et al., 2024; Ji et al., 2021; Zhou et al., 2022).

The expression levels of *ADH1* and *AAT* showed a marked positive association with the concentrations of alcohols and esters. (Figure 6C). Qian et al. (2019) observed that the genes (*LOXA* and *LOXO*) in the LOX pathway were positively related with their corresponding volatile esters. However, in this research, the expression levels of *HPL1* were negatively correlated with the concentrations of esters and alcohols, it may be due to the differences of varieties, environment and cultivation conditions. The expression levels of *CCD4a* and *CCD4b* were positively correlated with the concentration of C13-norisoprenoids, whereas the expression levels of *PSY1* and *PSY2* were negatively correlated with the concentration of C13-norisoprenoids (Figure 6B). *UGT85AIL3* expression correlated positively with bound C13-norisoprenoid and monoterpene concentrations, while GT7 expression showed a negative correlation with bound C6/C9 compound and monoterpene concentrations (Figure 6D). These discoveries align with the findings referred to in section 3.9 above.

10.3389/fpls.2025.1544593

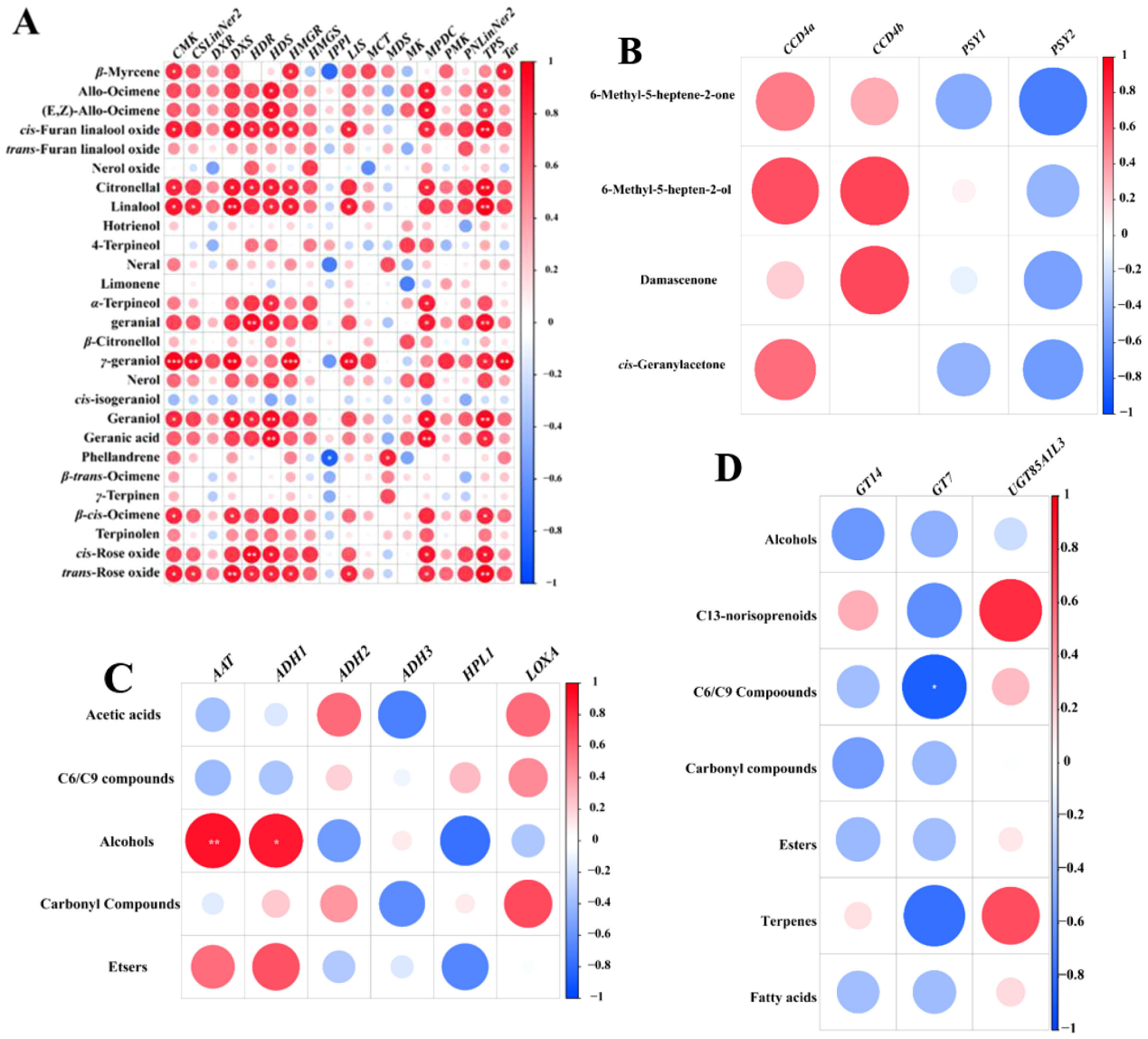

FIGURE 6
Correlations between the expression of aroma biosynthesis related genes and aroma compounds in six grape cultivars. **(A)** Correlation analysis of gene expression and monoterpene contents in MEP and MVA pathway; **(B)** Correlation analysis of gene expression and C13-norisoprenoids in MEP pathway; **(C)** Correlation analysis of gene expression and metabolite contents in LOX-HPL and *β*-oxidation pathway; **(D)** Correlation analysis of gene expression and bound aroma compounds. * indicates $0.01 < P < 0.05$, ** indicates $0.001 < P < 0.01$, *** indicates $P \leq 0.001$.

4 Conclusions

This study provided comprehensive insights into the molecular and biochemical mechanisms underlying aroma diversity across six grape cultivars. There were 61, 61, 57, 56, 41, and 48 free aroma compounds as well as 59, 59, 55, 53, 48, and 46 bound aroma compounds were identified in 'Shine Muscat', 'Shine 13', 'Hutai 8', 'Summer Black', 'Red Globe' and 'Moldova', respectively. This reserach revealed distinct volatile profiles among the three aroma types, Muscat-type cultivars exhibited the highest levels of monoterpenes and C13-norisoprenoids, strawberry-type 'Hutai 8' was characterized by elevated ester content, while neutral aromatic cultivars showed dominance in C6/C9 and carbonyl compounds. PCA analysis further confirmed significant differences in aroma profiles, clustering the six cultivars into three distinct groups, aligning with their sensory classifications. Notably, there were 14, 13, 14, 12 12, and 11 volatiles with OAVs > 1 in six grape cultivars, respectively. Linalool, rose oxide, damascenone, and *cis*-geranylacetone were the main aroma compounds with OAVs >1 in Muscat-type grapes; ethyl butanoate was the main aroma compound with OAVs > 1 in strawberry-type grapes. RNA-sequencing and WGCNA analyses showed that 88 genes, 451 genes, 110 genes, and 790 genes had significantly positively correlated with alcohols, carbonyl compounds, fatty acids, and monoterpenes in three aroma types of grapes, respectively. Specifically, genes in the MEP pathway (*DXS*, *CMK*, *HDS*, *HDR*, *TPS*) and MVA pathway (*HMGR*) were highly expressed

in Muscat-type cultivars, correlating strongly with monoterpenes accumulation. *LOXA* and *ADH2* expression peaked in 'Red Globe', while *AAT* dominated in 'Hutai 8', consistent with their respective volatile signatures. Crucially, correlation analyses highlighted functional linkages between gene expression and aroma compound synthesis. For instance, *CCD4a*/*b* expression positively correlated with C13-norisoprenoid levels, while *UGT85AIL3* was associated with bound monoterpenes and C13-norisoprenoids. Additionally, *AAT* and *ADH1* expression aligned with ester and alcohol biosynthesis, respectively.

An understanding of the aroma profiles metabolism and genetic mechanism of volatile compounds is particularly important for breeding new grape cultivars. These findings not only elucidate the genetic basis of cultivar-specific aroma formation but also offer a framework for targeted breeding strategies to enhance flavor complexity in grape berries.

Data availability statement

The datasets presented in this study can be found in online repositories. The names of the repository/repositories and accession number(s) can be found in the article/Supplementary Material.

Author contributions

GW: Formal Analysis, Investigation, Methodology, Software, Writing – original draft. YX: Investigation, Writing – review & editing. RR: Writing – review & editing. HC: Investigation, Software, Writing – review & editing. BY: Conceptualization, Investigation, Writing – review & editing. MG: Methodology, Project administration, Supervision, Writing – review & editing. SX: Conceptualization, Funding acquisition, Resources, Supervision, Writing – review & editing.

Funding

The author(s) declare that financial support was received for the research and/or publication of this article. This work was supported by National Natural Science Foundation of China (Grant No. 32302477), Postdoctoral Research Foundation of China (2023M732897) and Postdoctoral Research Foundation of Shaanxi Province (2023BSHEDZZ122).

Acknowledgments

We express our appreciation to Institute of Forestry and Pomology at the Beijing Academy of Agricultural and Forestry Sciences for providing access to their HS-SPME/GC-MS facilities.

Conflict of interest

The authors declare that the research was conducted in the absence of any commercial or financial relationships that could be construed as a potential conflict of interest.

Generative AI statement

The author(s) declare that no Generative AI was used in the creation of this manuscript.

Publisher's note

All claims expressed in this article are solely those of the authors and do not necessarily represent those of their affiliated organizations, or those of the publisher, the editors and the reviewers. Any product that may be evaluated in this article, or claim that may be made by its manufacturer, is not guaranteed or endorsed by the publisher.

Supplementary material

The Supplementary Material for this article can be found online at: https://www.frontiersin.org/articles/10.3389/fpls.2025.1544593/full#supplementary-material

References

Aubert, C., and Chalot, G. (2018). Chemical composition, bioactive compounds, and volatiles of six table grape varieties (*Vitis vinifera L.*). *Food Chem.* 240, 524–533. doi: 10.1016/j.foodchem.2017.07.152

Balbontín, C., Gaete-Eastman, C., Fuentes, L., Figueroa, C. R., Herrera, R., Manriquez, D., et al. (2010). *VpAAT1*, a gene encoding an alcohol acyltransferase, is involved in ester biosynthesis during ripening of mountain papaya fruit. *J. Agric. Food Chem.* 58, 5114–5121. doi: 10.1021/jf904296c

Banerjee, A., and Sharkey, T. D. (2014). Methylerythritol 4-phosphate (MEP) pathway metabolic regulation. *Nat. Prod. Rep.* 31, 1043–1055. doi: 10.1039/C3NP70124G

Beekwilder, J., Alvarez-Huerta, M., Neef, E., Verstappen, F. W. A., Bouwmeester, H. J., and Aharoni, A. (2004). Functional characterization of enzymes forming volatile esters from strawberry and banana. *Plant Physiol.* 135, 1865–1878. doi: 10.1104/pp.104.042580

Bu, D., Luo, H., Huo, P., Wang, Z., Zhang, S., He, Z., et al. (2021). KOBAS-i: Intelligent prioritization and exploratory visualization of biological functions for gene enrichment analysis. *Nucleic Acids Res.* 49, W317–W325. doi: 10.1093/nar/gkab447

Buttery, R. G., Turnbaugh, J. G., and Ling, L. C. (1988). Contribution of volatiles to rice aroma. *J. Agric. Food Chem.* 36, 1006–1009. doi: 10.1021/jf00083a025

Chang, E.-H., Jung, S.-M., and Hur, Y.-Y. (2014). Changes in the aromatic composition of grape cv. Cheongsoo wine depending on the degree of grape ripening. *Food Sci. Biotechnol.* 23, 1761–1771. doi: 10.1007/s10068-014-0241-y

Costantini, L., Kappel, C. D., Trenti, M., Battilana, J., Emanuelli, F., Sordo, M., et al. (2017). Drawing links from transcriptome to metabolites: The evolution of aroma in

the ripening berry of Moscato Bianco (*Vitis vinifera* L.). *Front. Plant Sci.* 8. doi: 10.3389/fpls.2017.00780

Czerny, M., Christlbauer, M., Christlbauer, M., Fischer, A., Granvogl, M., Hammer, M., et al. (2008). Re-investigation on odour thresholds of key food aroma compounds and development of an aroma language based on odour qualities of defined aqueous odorant solutions. *Eur. Food Res. Technol.* 228, 265–273. doi: 10.1007/s00217-008-0931-x

D'Auria, J. C., Pichersky, E., Schaub, A., Hansel, A., and Gershenzon, J. (2007). Characterization of a BAHD acyltransferase responsible for producing the green leaf volatile (*Z*)-3-hexen-1-yl acetate in *Arabidopsis thaliana*. *Plant J.* 49, 194–207. doi: 10.1111/j.1365-313X.2006.02946.x

D'Onofrio, C., Matarese, F., and Cuzzola, A. (2018). Effect of methyl jasmonate on the aroma of Sangiovese grapes and wines. *Food Chem.* 242, 352–361. doi: 10.1016/j.foodchem.2017.09.084

Dong, Y., Duan, S., Xia, Q., Liang, Z., Dong, X., Margaryan, K., et al. (2023). Dual domestications and origin of traits in grapevine evolution. *Science* 379, 892–901. doi: 10.1126/science.add8655

El-Sharkawy, I., Manríquez, D., Flores, F. B., Regad, F., Bouzayen, M., Latché, A., et al. (2005). Functional characterization of a melon alcohol acyl-transferase gene family involved in the biosynthesis of ester volatiles. Identification of the crucial role of a threonine residue for enzyme activity. *Plant Mol. Biol.* 59, 345–362. doi: 10.1007/s11103-005-8884-y

Emanuelli, F., Battilana, J., Costantini, L., Cunff, L. L., Boursiquot, J., This, P., et al. (2010). A candidate gene association study on muscat flavor in grapevine (*Vitis vinifera L.*). *BMC Plant Biol.* 10, 241. doi: 10.1186/1471-2229-10-241

Estévez, J. M., Cantero, A., Reindl, A., Reichler, S., and León, P. (2001). 1-Deoxy-D-xylulose-5-phosphate synthase, a limiting enzyme for plastidic isoprenoid biosynthesis in plants. *J. Biol. Chem.* 276, 22901–22909. doi: 10.1074/jbc.m100854200

Feng, M., Jin, X., Yao, H., Zhu, T., Guo, S., Li, S., et al. (2022). Evolution of volatile profile and aroma potential of 'Gold Finger' table grapes during berry ripening. *J. Sci. Food Agric.* 102, 291–298. doi: 10.1002/jsfa.11357

Fenoll, J., Manso, A., Hellin, P., Ruiz, L., and Flores, P. (2009). Changes in the aromatic composition of the Vitis vinifera grape Muscat Hamburg during ripening. *Food Chem.* 114, 420–428. doi: 10.1016/j.foodchem.2008.09.060

Ferreira, V., LóPez, R., and Cacho, J. F. (2000). Quantitative determination of the odorants of young red wines from different grape varieties. *J. Sci. Food Agriculture/Journal Sci. Food Agric.* 80, 1659–1667. doi: 10.1002/1097-0010(20000901)80:11

Genovese, A., Gambuti, A., Lamorte, S. A., and Moio, L. (2013a). An extract procedure for studying the free and glycosilated aroma compounds in grapes. *Food Chem.* 136 (2), 822–834. doi: 10.1016/j.foodchem.2012.08.061

Genovese, A., Lamorte, S. A., Gambuti, A., and Moio, L. (2013b). Aroma of Aglianico and Uva di Troia grapes by aromatic series. *Food Res. Int.* 53 (1), 15–23. doi: 10.1016/j.foodres.2013.03.051

Ghaste, M., Narduzzi, L., Carlin, S., Vrhovsek, U., Shulaev, V., and Mattivi, F. (2015). Chemical composition of volatile aroma metabolites and their glycosylated precursors that can uniquely differentiate individual grape cultivars. *Food Chem.* 188, 309–319. doi: 10.1016/j.foodchem.2015.04.056

Guo, X., Ho, C., Schwab, W., and Wan, X. (2021). Aroma profiles of green tea made with fresh tea leaves plucked in summer. *Food Chem.* 363, 130328. doi: 10.1016/j.foodchem.2021.130328

Hernandez-Orte, P., Concejero, B., Astrain, J., Lacau, B., Cacho, J., and Ferreira, V. (2015). Influence of viticulture practices on grape aroma precursors and their relation with wine aroma. *J. Sci. Food Agric.* 95, 688–701. doi: 10.1002/jsfa.6748

Ji, X., Wang, B., Wang, X., Wang, X., Liu, F., and Wang, H. (2021). Differences of aroma development and metabolic pathway gene expression between Kyoho and 87-1 grapes. *J. Integr. Agric.* 20, 1525–1539. doi: 10.1016/s2095-3119(20)63481-5

Kalua, C. M., and Boss, P. K. (2009). Evolution of Volatile Compounds during the Development of Cabernet Sauvignon Grapes (*Vitis vinifera* L.). *J. Agric. Food Chem.* 57, 3818–3830. doi: 10.1021/jf803471n

Kaya, O., Incesu, M., Ates, F., Keskin, N., Verdugo-Vásquez, N., and Gutiérrez-Gamboa, G. (2022). Study of volatile organic compounds of two table grapes (cv. Italia and bronx seedless) along ripening in vines established in the aegean region (Turkey). *Plants* 11, 1935. doi: 10.3390/plants11151935

Kiralan, M., Çalik, G., Kiralan, S., Özaydin, A., Özkan, G., and Ramadan, M. F. (2019). Stability and volatile oxidation compounds of grape seed, flax seed and black cumin seed cold-pressed oils as affected by thermal oxidation. *Grasas y Aceites* 70, 295. doi: 10.3989/gya.0570181

Koyama, K., Kono, A., Ban, Y., Bahena-Garrido, S. M., Ohama, T., Iwashita, K., et al. (2022). Genetic architecture of berry aroma compounds in a QTL (quantitative trait loci) mapping population of interspecific hybrid grapes (*Vitis labruscana*× *Vitis vinifera*). *BMC Plant Biology* 22 (1), 458.

Lan, Y., Qian, X., Yang, Z., Xiang, X., Yang, W., Liu, T., et al. (2016). Striking changes in volatile profiles at sub-zero temperatures during over-ripening of 'Beibinghong' grapes in Northeastern China. *Food Chem.* 212, 172–182. doi: 10.1016/j.foodchem.2016.05.143

Leng, X., Cong, J., Cheng, L., Wan, H., Liu, Y., Yuan, Y., et al. (2023). Identification of key gene networks controlling monoterpene biosynthesis during grape ripening by integrating transcriptome and metabolite profiling. *Hortic. Plant J.* 9, 931–946. doi: 10.1016/j.hpj.2023.03.005

Li, W., Zheng, T., Zhang, J., Li, W., Chen, K., Zhang, K., et al. (2025). Supplementary light with different wavelengths improved the monoterpenes aroma and quality traits of 'Shine Muscat'grape berries under facility cultivation. *Food Chem.* 474. doi: 10.1016/j.foodchem.2025.143255

Lin, J., Massonnet, M., and Cantu, D. (2019). The genetic basis of grape and wine aroma. *Hortic. Res.* 6, 81. doi: 10.1038/s41438-019-0163-1

Liu, S., Shan, B., Zhou, X., Gao, W., Liu, Y., Zhu, B., et al. (2022). Transcriptome and metabolomics integrated analysis reveals terpene synthesis genes controlling linalool synthesis in grape berries. *J. Agric. Food Chem.* 70, 9084–9094. doi: 10.1021/acs.jafc.2c00368

Luan, F., Mosandl, A., Gubesch, M., and Wüst, M. (2006). Enantioselective analysis of monoterpenes in different grape varieties during berry ripening using stir bar sorptive extraction- and solid phase extraction-enantioselective-multidimensional gas chromatography-mass spectrometry. *J. Chromatogr. A* 1112, 369–374. doi: 10.1016/j.chroma.2005.12.056

Lücker, J., Bowen, P., and Bohlmann, J. (2004). *Vitis vinifera* terpenoid cyclases: Functional identification of two sesquiterpene synthase cDNAs encoding (+)-valencene synthase and (−)-germacrene D synthase and expression of mono- and sesquiterpene synthases in grapevine flowers and berries. *Phytochemistry* 65, 2649–2659. doi: 10.1016/j.phytochem.2004.08.017

Martin, D. M., Aubourg, S., Schouwey, M. B., Daviet, L., Schalk, M., Toub, O., et al. (2010). Functional annotation, genome organization and phylogeny of the grapevine (*Vitis vinifera*) terpene synthase gene family based on genome assembly, FLcDNA cloning, and enzyme assays. *BMC Plant Biol.* 10, 226. doi: 10.1186/1471-2229-10-226

Martin, D. M., and Bohlmann, J. (2004). Identification of Vitis vinifera (−)-α-terpineol synthase by in silico screening of full-length cDNA ESTs and functional characterization of recombinant terpene synthase. *Phytochemistry* 65, 1223–1229. doi: 10.1016/j.phytochem.2004.03.018

Mateo, J. J., and Jiménez, M. (2000). Monoterpenes in grape juice and wines. *J. Chromatogr. A* 881, 557–567. doi: 10.1016/S0021-9673(99)01342-4

Matsumoto, H., and Ikoma, Y. (2016). Effect of postharvest temperature on the muscat flavor and aroma volatile content in the berries of 'Shine Muscat' (*Vitis labruscana* Baily×*V. vinifera* L.). *Posth. Biol. Technol.* 112, 256–265. doi: 10.1016/j.postharvbio.2015.09.004

Mayr, C. M., Capone, D. L., Pardon, K. H., Black, C. A., Pomeroy, D., and Francis, I. L. (2015). Quantitative analysis by GC-MS/MS of 18 aroma compounds related to oxidative off-flavor in wines. *J. Agric. Food Chem.* 63, 3394–3401. doi: 10.1021/jf505803u

Moyano, L., Zea, L., Villafuerte, L., and Medina, M. (2009). Comparison of odor-active compounds in sherry wines processed from ecologically and conventionally grown pedro ximenez grapes. *J. Agric. Food Chem.* 57, 968–973. doi: 10.1021/jf802252u

Noguerol-Pato, R., Sieiro-Sampredro, T., González-Barreiro, C., Cancho-Grande, B., and Simal-Gándara, J. (2014). Effect on the aroma profile of graciano and tempranillo red wines of the application of two antifungal treatments onto vines. *Molecules* 19, 12173–12193. doi: 10.3390/molecules190812173

Pan, Q.-H., Chen, F., Zhu, B.-Q., Ma, L.-Y., Li, L., and Li, J.-M. (2012). Molecular cloning and expression of gene encoding aromatic amino acid decarboxylase in 'Vidal blanc' grape berries. *Mol. Biol. Rep.* 39, 4319–4325. doi: 10.1007/s11033-011-1219-y

Pino, J. A., and Mesa, J. (2006). Contribution of volatile compounds to mango (*Mangifera indica* L.) aroma. *Flavour Fragrance J.* 21, 207–213. doi: 10.1002/ffj.1703

Qian, X., Liu, Y., Zhang, G., Yan, A., Wang, H., Wang, X., et al. (2019). Alcohol acyltransferase gene and ester precursors differentiate composition of volatile esters in three interspecific hybrids of *Vitis labrusca* x *V. Vinifera* during berry development period. *Food Chem.* 295, 234–246. doi: 10.1016/j.foodchem.2019.05.104

Qian, X., Xu, X., Yu, K., Zhu, B., Lan, Y., Duan, C., et al. (2016). Varietal dependence of GLVs accumulation and LOX-HPL pathway gene expression in four *vitis vinifera* wine grapes. *Int. J. Mol. Sci.* 17, 1924. doi: 10.3390/ijms17111924

Qin, G., Tao, S., Zhang, H., Huang, W., Wu, J., Xu, Y., et al. (2014). Evolution of the aroma volatiles of pear fruits supplemented with fatty acid metabolic precursors. *Molecules* 19, 20183–20196. doi: 10.3390/molecules191220183

Ruiz-García, L., Hellín, P., Flores, P., and Fenoll, J. (2014). Prediction of Muscat aroma in table grape by analysis of rose oxide. *Food Chem.* 154, 151–157. doi: 10.1016/j.foodchem.2014.01.005

Schwab, W., Davidovich-Rikanati, R., and Lewinsohn, E. (2008). Biosynthesis of plant-derived flavor compounds. *Plant J.* 54, 712–732. doi: 10.1111/j.1365-313X.2008.03446.x

Souleyre, E. J. F., Greenwood, D. R., Friel, E. N., Karunairetnam, S., and Newcomb, R. D. (2005). An alcohol acyl transferase from apple (cv. Royal Gala), MpAAT1, produces esters involved in apple fruit flavor. *FEBS J.* 272, 3132–3144. doi: 10.1111/j.1742-4658.2005.04732.x

Sun, L., Zhu, B., Zhang, X., Wang, H., Yan, A., Zhang, G., et al. (2020). The accumulation profiles of terpene metabolites in three Muscat table grape cultivars through HS-SPME-GCMS. *Sci. Data* 7, 5. doi: 10.1038/s41597-019-0321-1

Tholl, D. (2006). Terpene synthases and the regulation, diversity and biological roles of terpene metabolism. *Curr. Opin. Plant Biol.* 9, 297–304. doi: 10.1016/j.pbi.2006.03.014

Vilanova, M., Escudero, A., Graña, M., and Cacho, J. (2013). Volatile composition and sensory properties of North West Spain white wines. *Food Res. Int.* 54, 562–568. doi: 10.1016/j.foodres.2013.07.036

Vranová, E., Coman, D., and Gruissem, W. (2013). Network analysis of the MVA and MEP pathways for isoprenoid synthesis. *Annu. Rev. Plant Biol.* 64, 665–700. doi: 10.1146/annurev-arplant-050312-120116

Wang, W., Feng, J., Wei, L., Khalil-Ur-Rehman, M., Nieuwenhuizen, N. J., Yang, L., et al. (2021). Transcriptomics Integrated with Free and Bound Terpenoid Aroma Profiling during "Shine Muscat" (*Vitis labrusca* × *V. vinifera*) Grape Berry Development Reveals Coordinate Regulation of MEP Pathway and Terpene Synthase Gene Expression. *J. Agric. Food Chem.* 69, 1413–1429. doi: 10.1021/acs.jafc.0c06591

Wang, W.-N., Qian, Y.-H., Liu, R.-H., Liang, T., Ding, Y.-T., Xu, X.-L., et al. (2023). Effects of table grape cultivars on fruit quality and aroma components. *Foods* 12, 3371. doi: 10.3390/foods12183371

Wang, H., Wang, X., Yan, A., Liu, Z., Ren, J., Xu, H., et al. (2023). Metabolomic and transcriptomic integrated analysis revealed the decrease of monoterpenes accumulation in table grapes during long time low temperature storage. *Food Res. Int.* 174, 113601. doi: 10.1016/j.foodres.2023.113601

Wang, C., Xing, J., Chin, C.-K., Ho, C.-T., and Martin, C. E. (2001). Modification of fatty acids changes the flavor volatiles in tomato leaves. *Phytochemistry* 58, 227–232. doi: 10.1016/S0031-9422(01)00233-3

Wei, H., Xu, C., Movahedi, A., Sun, W., Li, D., and Zhuge, Q. (2019). Characterization and function of 3-hydroxy-3-methylglutaryl-CoA reductase in *Populus trichocarpa*: Overexpression of *PtHMGR* enhances terpenoids in transgenic poplar. *Front. Plant Sci.* 10. doi: 10.3389/fpls.2019.01476

Wen, Y.-Q., Zhong, G.-Y., Gao, Y., Lan, Y.-B., Duan, C.-Q., and Pan, Q.-H. (2015). Using the combined analysis of transcripts and metabolites to propose key genes for differential terpene accumulation across two regions. *BMC Plant Biol.* 15, 240. doi: 10.1186/s12870-015-0631-1

Wu, Y., Duan, S., Zhao, L., Gao, Z., Luo, M., Song, S., et al. (2016). Aroma characterization based on aromatic series analysis in table grapes. *Sci. Rep.* 6, 31116. doi: 10.1038/srep31116

Wu, Y., Zhang, W., Song, S., Xu, W., Zhang, C., Ma, C., et al. (2020). Evolution of volatile compounds during the development of Muscat grape 'Shine Muscat' (*Vitis labrusca* × *V. vinifera*). *Food Chem.* 309, 125778. doi: 10.1016/j.foodchem.2019.125778

Wu, Y., Zhang, W., Yu, W., Zhao, L., Song, S., Xu, W., et al. (2019). Study on the volatile composition of table grapes of three aroma types. *LWT* 115, 108450. doi: 10.1016/j.lwt.2019.108450

Xiang, N., Xie, H., Qin, L., Wang, M., Guo, X., and Zhang, W. (2022). Effect of Climate on Volatile Metabolism in 'Red Globe' Grapes (*Vitis vinifera* L.) during Fruit Development. *Foods* 11, 1435. doi: 10.3390/foods11101435

Xiao, Z., Li, B., Niu, Y., Xiong, J., and Zhang, J. (2023). Characterization of key aroma-active compounds in yellow peach (*Prunus persica* L. 'Jinxiu') based on GC–MS–O, OAV, aroma recombination and omission experiment. *J. Food Measure. Charact.* 17, 4448–4461. doi: 10.1007/s11694-023-01970-0

Yang, C., Wang, Y., Wu, B., Fang, J., and Li, S. (2011). Volatile compounds evolution of three table grapes with different flavour during and after maturation. *Food Chemistry* 128 (4), 823–830.

Yang, C., Li, Y., He, L., Song, Y., Zhang, P., and Liu, S. (2024). Metabolomic and transcriptomic analyses of monoterpene biosynthesis in Muscat and Neutral grape hybrids. *Scientia. Hortic.* 336, 113434. doi: 10.1016/j.scienta.2024.113434

Yang, C., Luo, L., Zhang, H., Yang, X., Lv, Y., and Song, H. (2010). Common aroma-active components of propolis from 23 regions of China. *J. Sci. Food Agric.* 90, 1268–1282. doi: 10.1002/jsfa.3969

Yang, C., Wang, Y., Liang, Z., Fan, P., Wu, B., Yang, L., et al. (2009). Volatiles of grape berries evaluated at the germplasm level by headspace-SPME with GC–MS. *Food Chem.* 114, 1106–1114. doi: 10.1016/j.foodchem.2008.10.061

Yang, Y., Zheng, F., Yu, A., and Sun, B. (2019). Changes of the free and bound volatile compounds in Rubus corchorifolius L. f. fruit during ripening. *Food Chem.* 287, 232–240. doi: 10.1016/j.foodchem.2019.02.080

Yao, H., Jin, X., Feng, M., Xu, G., Zhang, P., Fang, Y., et al. (2021). Evolution of volatile profile and aroma potential of table grape Hutai-8 during berry ripening. *Food Res. Int.* 143, 110330. doi: 10.1016/j.foodres.2021.110330

Yue, X., Ju, Y., Cui, Y., Wei, S., Xu, H., and Zhang, Z. (2023). Evolution of green leaf volatile profile and aroma potential during the berry development in five *Vitis vinifera* L. Cultivars. *Food Chem.: X* 18, 100676. doi: 10.1016/j.fochx.2023.100676

Yue, X., Ju, Y., Zhang, H., Wang, Z., Xu, H., and Zhang, Z. (2022). Integrated transcriptomic and metabolomic analysis reveals the changes in monoterpene compounds during the development of Muscat Hamburg (*Vitis vinifera L.*) grape berries. *Food Res. Int.* 162, 112065. doi: 10.1016/j.foodres.2022.112065

Zheng, T., Guan, L., Yu, K., Haider, M. S., Nasim, M., Liu, Z., et al. (2021). Expressional diversity of grapevine 3-Hydroxy-3-methylglutaryl-CoA reductase (*VvHMGR*) in different grapes genotypes. *BMC Plant Biol.* 21, 279. doi: 10.1186/s12870-021-03073-8

Zhong, Y., Pan, X., Wang, R., Xu, J., Guo, J., Yang, T., et al. (2020). ZMCCD10A encodes a distinct type of carotenoid cleavage dioxygenase and enhances plant tolerance to low phosphate. *Plant Physiol.* 184, 374–392. doi: 10.1104/pp.20.00378

Zhou, X., Liu, S., Gao, W., Hu, B., Zhu, B., and Sun, L. (2022). Monoterpenoids evolution and MEP pathway gene expression profiles in seven table grape varieties. *Plants* 11 (16), 2143.

frontiers | Frontiers in Plant Science

TYPE Original Research
PUBLISHED 03 June 2025
DOI 10.3389/fpls.2025.1588888

OPEN ACCESS

EDITED BY
Vikas Dadwal,
Texas A and M University, United States

REVIEWED BY
Anukool Vaishnav,
GLA University, India
Aditya Kulshreshtha,
Texas A&M AgriLife Research and Extension Center at Weslaco, United States
Yog Raj,
Academy of Scientific and Innovative Research (AcSIR), India

*CORRESPONDENCE
Ruifang Li
lrf@haut.edu.cn
Yanling Zhang
zhangyanling@ztri.com.cn

†These authors have contributed equally to this work

RECEIVED 06 March 2025
ACCEPTED 01 May 2025
PUBLISHED 03 June 2025

CITATION
Jia Y, Wang J, Lin X, Liang T, Dai H, Wu B, Yang M, Zhang Y and Li R (2025) Integrated metabolomics and metagenomics reveal plant-microbe interactions driving aroma differentiation in flue-cured tobacco leaves. *Front. Plant Sci.* 16:1588888. doi: 10.3389/fpls.2025.1588888

Integrated metabolomics and metagenomics reveal plant-microbe interactions driving aroma differentiation in flue-cured tobacco leaves

Yifan Jia[1,2†], Jianwei Wang[3†], Xiaojie Lin[1,2], Taibo Liang[3], Huaxin Dai[3], Baojian Wu[3], Mengmeng Yang[3], Yanling Zhang[3*] and Ruifang Li[1,2*]

[1]Zhengzhou Key Laboratory of Functional Molecules for Biomedical Research, Henan University of Technology, Zhengzhou, Henan, China, [2]College of Biological Engineering, Henan University of Technology, Zhengzhou Henan, China, [3]Key Laboratory of Eco-environment and Tobacco Leaf Quality, Zhengzhou Tobacco Research Institute of China National Tobacco Corporation (CNTC), Zhengzhou, Henan, China

Current research on tobacco aroma predominantly focuses on single-omics approaches. In this study, we conducted a comprehensive investigation of the relationships between tobacco metabolite profiles, microbial communities, and aroma characteristics. Untargeted metabolomics and metagenomic analyses were performed on flue-cured upper tobacco leaves to compare light aromatic tobacco (LAT) and strong aromatic tobacco (SAT). The results showed that sugar metabolite levels in LAT were significantly higher than those in SAT, whereas levels of specific acids and amino acid metabolites in SAT exceeded those in LAT. Redundancy analysis (RDA) and metabolomic correlation analyses indicated that the genera *Methylorubrum* and *Pseudomonas* may promote sugar metabolite accumulation, while *Pseudokineococcus* potentially regulates both sugar and acid metabolites. In contrast, *Methylobacterium* and *Sphingomonas* were associated with acid and amino acid metabolism, with *Methylobacterium* additionally exhibiting inhibitory effects on sugar metabolism. Metagenomic analysis revealed that *Methylorubrum*, *Pseudomonas*, and *Pseudokineococcus* were abundant in LAT, whereas *Methylobacterium* and *Sphingomonas* dominated in SAT. Notably, the bidirectional regulation of aromatic metabolites by microbial genera such as *Pseudokineococcus* highlights the universality of plant-microbe interactions in shaping metabolic networks—a mechanism potentially applicable to other crop systems. These findings reveal conserved microbial functional traits (e.g., metabolic pathway modulation) that may drive plant phenotypic differentiation beyond tobacco, offering insights into microbiome-mediated crop quality improvement. The results provide theoretical guidance for tobacco aging and aroma regulation and underscore the broader significance of microbial community engineering in agriculture for manipulating plant metabolic outputs.

KEYWORDS

flue-cured tobacco, aroma, untargeted metabolomics, metagenomics, plant-microbe interaction

Introduction

Plant-microbe interactions play a fundamental role in shaping plant metabolism, secondary metabolite biosynthesis, and overall phenotypic quality across diverse species (Wang et al., 2022). These interactions are driven by complex microbial communities, which participate in biochemical transformations of plant-derived substrates, modulate host metabolic pathways, and influence organoleptic properties (Wang et al., 2022; Shi et al., 2024; Vorholt, 2012). Such mechanisms are pivotal for ecological adaptation and critical for determining the crops' economic value, as exemplified by tobacco (*Nicotiana tabacum* L.), one of the most studied systems in this context.

Globally, the microbiome contributes to plant fitness through nutrient metabolism (Vorholt, 2012), degradation of complex polymers (e.g., cellulose, starch), and synthesis of volatile organic compounds (VOCs) that define aroma profiles (Lindow and Brandl, 2003; Gong and Xin, 2021). For instance, microbial genera such as *Bacillus*, *Pseudomonas*, and *Aspergillus* are ubiquitous across plant species, where they catalyze the conversion of primary metabolites (e.g., carbohydrates, amino acids) into aromatic precursors via enzymatic activity and metabolic cross-talk with host tissues (Durán et al., 2017). This process is central to the formation of secondary metabolites in many crops, including tea (Li et al., 2018), grapes (Bokulich et al., 2014), coffee (Zhang et al., 2019), aloe vera (Chandel et al., 2025) and tobacco (Huang et al., 2022), where microbial-driven Maillard reactions, protein degradation, and carbohydrate metabolism directly impact sensory attributes (Berg et al., 2014; Banožić et al., 2020).

In tobacco, the interplay between leaf surface microbiota and host biochemistry is particularly evident (Shi et al., 2024). The aroma characteristics of flue-cured tobacco are classified as light, intermediate, or strong aromatic types shaped by microbial-mediated degradation of macromolecules (e.g., proteins, polysaccharides) and subsequent synthesis of flavor-enhancing compounds such as pyrazines and phenolic derivatives. Carbohydrates, phenols, amino acids, organic acids, alcohols, and alkaloids, which are the precursors of tobacco aroma, are the main metabolic compounds (Liu et al., 2022), and carbohydrates are also one of the most important precursors of the tobacco aroma. Study have shown that sugars act as aroma enhancers in the smoke during combustion, producing acids that neutralize the harsh aromas in the smoke, reduce the astringent taste during inhalation, and enhance the overall aromas (Yin et al., 2019). Similar mechanisms have been observed in other aromatic plant, like coffee (Zhao et al., 2024; Wang et al., 2019), where microbial communities regulate the balance of key metabolites (e.g., sugars, organic acids) (Vandenkoornhuyse et al., 2015), ultimately determining product quality. However, the universal principles governing these plant-microbe interactions remain poorly characterized, particularly regarding how the taxonomic and functional diversity of microbiota coordinates with host metabolic networks to drive species-specific phenotypes.

Advancements in multi-omics technologies, including untargeted metabolomics and metagenomics, now empower systematic dissection of these interactions (Diwan et al., 2022). For example, gas chromatography-mass spectrometry (GC-MS)-based metabolomics can reveal conserved metabolic pathways (e.g., carbohydrate degradation, phenylpropanoid biosynthesis) influenced by microbial activity, while microbiome profiling tools (e.g., MetaPhlAn4) elucidate taxonomic shifts linked to functional outcomes. By integrating these approaches, researchers can identify cross-species microbial markers (e.g., *Bacillus subtilis*) that enhance aromatic compound synthesis or mitigate the accumulation of irritants (e.g., ammonia) through nitrogen metabolism regulation (Huang et al., 2022). Such insights transcend individual crops and offer a framework for optimizing microbial consortia in agriculture, fermentation, and post-harvest processing.

This study employs tobacco as a model system to investigate the mechanisms underlying plant-microbe interactions. Using untargeted metabolomics (GC-MS) (Patti et al., 2012), microbiome annotation (MetaPhlAn4) (Segata et al., 2012; Blanco-Míguez et al., 2023), and multivariate analyses, we explore how microbial communities modulate metabolic profiles across different aroma types of flue-cured tobacco, by linking microbial diversity to differential metabolic pathways (Hou et al., 2024).

In this study, we postulate that tobacco aroma is caused by tobacco metabolism and microbial regulation, driving distinct tobacco aroma types. We aim to uncover the conserved principles applicable to broader plant systems, thereby advancing strategies for microbial-driven quality enhancement in crops.

Materials and methods

Materials

After collecting from the production area, the fresh upper tobacco leaves were immediately sent to the tobacco curing barn. The flue-cured tobacco leaf samples were collected from the cured tobaccos using aseptic fresh-keeping bags, and sent to laboratory for further research. The four strong aromatic tobacco (SAT) samples were collected from the production areas in Henan province and Hunan province, China. An equal amount of light aromatic tobacco (LAT) samples was collected from the production areas in Sichuan province and Yunnan province, China. Two production areas in each province. One sample from one production area. The detailed information of the samples is described in Table 1. The samples were stored at -20°C and returned to room temperature 24 hours before metabolomics and metagenomics experiments. For metabolomics analysis, three replicates for each sample. For metagenomics analysis, one library was performed without replicates.

Abbreviations: ACE, abundance-based coverage estimator; ANOSIM, analysis of similarities; BSTFA, bis(trimethylsilyl)trifluoroacetamide; GC-MS, gas chromatography-mass spectrometry; KEGG, kyoto encyclopedia of genes and genomes; LAT, light aromatic tobacco; LDA, linear discriminant analysis; LEfSe, linear discriminant analysis effect size; PCs, principal components; PLS-DA, partial least squares discriminant analysis; RDA, redundancy analysis; SAT, strong aromatic tobacco; TCA, tricarboxylic acid cycle; VIP, variable importance in projection.

TABLE 1 Samples' given names and their detailed information.

Sample names	Cultivar	Aromatic type	Tobacco production area	Province
YNCY	Yun87	light aroma	Yao'an County, Chuxiong City	Yunnan
YNCZ	Yun87	light aroma	Ziwu Town, Yao'an County, Chuxiong City	Yunnan
SCLX	Yun87	light aroma	Xinyun Town, Liangshan Yi Autonomous Prefecture	Sichuan
SCLH	Yun87	light aroma	Huidong County Liangshan Yi Autonomous Prefecture	Sichuan
HeNLL	Zhongyan100	strong aroma	Lingying County, Luohe City	Henan
HeNXY	Zhongyan100	strong aroma	Yulin Town, Xuchang City	Henan
HuNYN	Yun87	strong aroma	Ningyuan County, Yongzhou City,	Hunan
HuNYD	Yun87	strong aroma	Daoxian County, Yongzhou City	Hunan

Metabolite extraction and derivatization

Referring to the reported method (Liu et al., 2020), the tobacco leaf samples were ground into powder after removing the stems. 20 mg of the tobacco leaf powder was added into 1.5 mL of isopropanol-acetonitrile-water (3:3:2, v/v/v), and sonicated in an ice bath for one hour. After centrifugation at 14,000 rpm for 10 min, 500 μL of the supernatant was transferred into a 1.5 mL injection bottle for vacuum drying. Then 100 μL of 20 mg/mL methoxamine pyridine solution was added and incubated at 37°C, 200 rpm for 90 min. then, 100 μL of N,O-Bis(trimethylsilyl)trifluoroacetamide (BSTFA) was added and incubated at 60°C, 200 rpm for 60 min. The metabolite analysis was performed after the samples were cooled to room temperature.

GC-MS untargeted metabolomics and metabolic data preprocessing

Metabolomic analysis was performed on an Agilent 5975C instrument (Agilent, USA). Metabolite was separated on a DB-5 MS capillary column (0.25 μm, 0.25 mm × 30 m). The temperature of the injection port was maintained at 300°C. The helium carrier gas flow rate was kept constant at 1.2 mL/min, the injection volume was 1 μL, and the split ratio was 30:1. The mass spectrometer operated in electron impact (EI) mode, and the energy was 70 eV. The detector voltage was kept at 1.2 kV.

The MATLAB high-resolution mass spectrometry data analysis toolkit was used to perform baseline correction, peak extraction, annotation, and alignment of the collected metabolic data. Relative quantification of metabolites was performed using area normalization.

Statistical analysis of metabolomics data

Metabolites were characterized and identified referring to the MS spectral database library (NIST v2.3, https://chemdata.nist.gov/dokuwiki/doku.php?id=chemdata:nist17). Data processing and graphing were performed using Prism. Partial least squares discriminant analysis (PLS-DA) was performed on the data using R language (v4.4, https://cloud.r-project.org/) (Xia and Sun, 2022). PLS-DA reduces the dimensionality of the data and performs discriminant analysis on regression results with specific discriminative thresholds by combining a regression model.

The R^2 coefficient quantifies the proportion of variance in the data that the model explains. A higher R^2 value indicates a better fit between the model and the data. Q^2 is an indicator of the predictive ability of a model. A higher Q^2 value indicates better predictive performance, and R^2 should be greater than Q^2 (Blaise et al., 2021). Metabolites were ranked according to the contribution of each component (Variable Importance in Projection, VIP) to the PLS-DA model. VIP>1 was used as the threshold. Metabolites that reached the threshold were considered differential metabolites. MetaboAnalyst 5.0 (https://www.metaboanalyst.ca/) analyzed the kyoto encyclopedia of genes and genomes (KEGG) pathway enrichment of differentially expressed metabolites. A significance threshold of $P \leq 0.05$ was used to obtain the results of significantly enriched metabolic pathways, and final illustrations were refined using Adobe Illustrator (Pang et al., 2024).

Genomic library construction, sequence and data preprocessing

Shotgun metagenomics sequencing method was performed by Novogene Co. Ltd (Beijing, China). The total genomic DNA from tobacco leaf samples was extracted using the Magnetic Plant Genomic DNA Kit (Tiangen, China) following the manufacturer's instructions. All operations of DNA extraction were carried out in a sterile environment. The genomic DNA purity and integrity were checked by 1% agarose gel electrophoresis. The genomic DNA was randomly sheared into short fragments of approximately 350 bp. The DNA fragments were subjected to end-repaired, A-tail and further ligated with Illumina adapters. The quantitative real-time polymerase chain reaction method was then used to quantify the effective concentration of the library (>3 nM) to ensure its quality. The quantified library was pooled and sequenced on Illumina Novaseq6000 (Illumina, USA), producing 2 × 150 bp paired-end reads. Metagenomic data were quality-controlled and trimmed for adaptors using fastp (https://github.com/OpenGene/fastp).

Considering the possibility of host contamination in samples, Bowtie2 software (http://bowtie-bio.sourceforge.net/bowtie2/index.shtml) filter out reads that may come from host origin. Taxonomic profiling of the filtered sequence data was performed using MetaPhlAn4 (Blanco-Míguez et al., 2023).

Statistical analysis of metagenomic

The alpha diversity indices, including ACE, Chao1, Shannon, and Simpson, were calculated by Mothur (https://mothur.org/wiki/calculators/). Alpha diversity is mainly used to study the diversity of microbial communities in a sample and is evaluated using a series of alpha diversity indices to obtain microbial information such as microbial species richness and diversity. R was used for ANOSIM (Analysis of similarities), beta diversity, and RDA analysis. ANOSIM is a non-parametric test method based on permutation and rank sum tests. The obtained R-value represents the relationship of the intergroup and intragroup differences. In this study, the ANOSIM on the genus level was performed. Beta diversity is used to describe the inter habitats variation in biological communities. RDA analysis (Redundancy analysis) is an environmental factor-constrained PCA analysis mainly used to explore the relationship between community species composition and environmental variables. This study used genus-level microorganisms as environmental factors to explore the relationship between metabolites and microbial communities. Galaxy 2.0 (http://galaxy.biobakery.org/) was used for LEfSe analysis to screen biomarkers with significant differences between groups, detecting the different species of the subgroups using the rank sum test and downscaling and evaluating the effect size of the different species or functions using LDA (Linear Discriminant Analysis). The SPSS (v29.0, https://www.ibm.com/spss) software for correlation analysis was used to calculate coefficients and significance, with the R for visualization. Correlation analysis is the process of analyzing two or more correlated variables to measure the closeness of the correlation between two variables.

Results

Metabolite composition in flue-cured tobacco leaves

A total of 74 small metabolites were identified (with a matching score >700 in the NIST database). Based on their structural and chemical characteristics, these metabolites were classified into four categories: 28 sugars, 7 alcohols, 7 amino acids, and 28 acids (Figure 1A). The relative contents of tobacco metabolites in the flue-cured upper tobacco leaves are shown in Table 2. A bar chart of the relative contents of the different aromatic types is shown in Figure 1B. The relative contents of sugars in all samples were the highest, while the relative contents of acids were much lower than those of sugars. The relative contents of sugar compounds in SAT samples were significantly lower than those in LAT samples. The relative contents of amino acids and acids in SAT samples were higher than those in LAT but not significant. The relative contents of alcohols showed no significant differences between SAT and LAT samples. The results demonstrated that sugars, acids, and amino acids may be the main effectors on the aromas of the flue-cured tobacco. Sugars are positively correlated with light aromas of tobacco. They are negatively correlated with strong tobacco aromas, while the effects of acids and amino acids on tobacco aromas were inversely related to sugars.

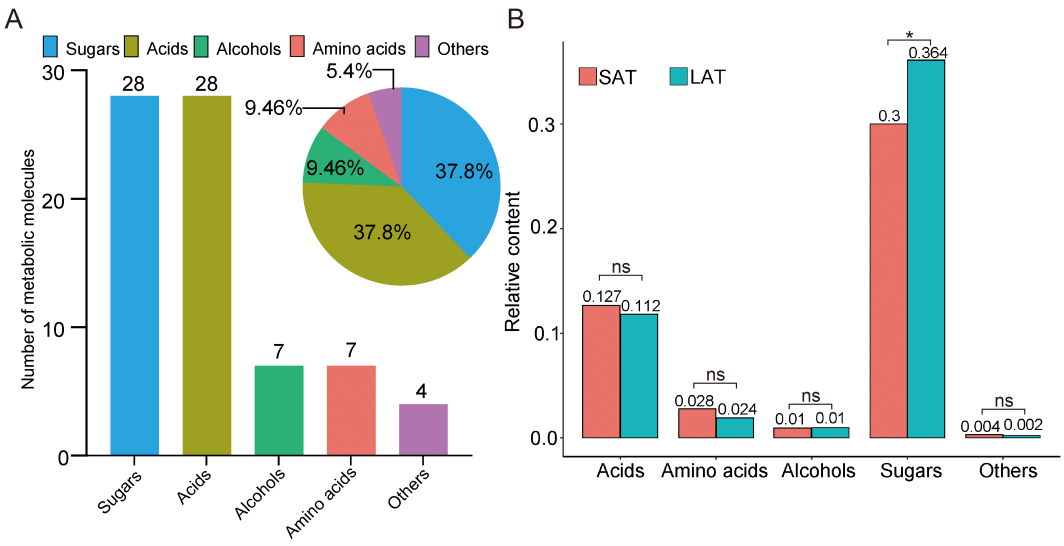

FIGURE 1
Untargeted metabolomics data of tobacco from GC-MS. **(A)** Metabolic molecule (Bar plot) and their proportion (Pie plot). **(B)** The relative contents of metabolites in different aromatic flue-cured tobacco. *P<0.05, ns, no significance. SAT, strong aromatic tobacco; LAT, light aromatic tobacco.

10.3389/fpls.2025.1588888

TABLE 2 Relative content of metabolites in different tobacco samples.

Metabolite type	HeNLL	HeNXY	HuNYD	HuNYN	SCLX	SCLH	YNCZ	YNCY
Amino acids	0.035	0.038	0.017	0.02	0.02	0.02	0.028	0.022
Acids	0.099	0.101	0.132	0.174	0.140	0.123	0.127	0.059
Alcohols	0.008	0.01	0.01	0.01	0.009	0.011	0.008	0.009
Sugars	0.328	0.34	0.261	0.27	0.349	0.354	0.356	0.4
Others	0.004	0.003	0.004	0.004	0.004	0.002	0.002	0.002

Bioinformatics characteristics of metabolites in different aroma types of flue-cured tobacco leaves

Multivariate analysis of metabolic profiles was conducted through PLS-DA to characterize aromatic differentiation in flue-cured tobacco leaves (Figure 2A). In the PLS-DA analysis, the first two principal components (PCs) explained 40.8% of the total variance, with PC1 and PC2 explaining 21.3% and 19.5%, respectively. The samples were clearly separated in the score plot. The R^2 and Q^2 values in PLS-DA were 0.99 and 0.96, respectively, indicating the model has a high stability and predictive ability. The results of the score plot exhibited a good separation between LAT and SAT.

The metabolites' relative importance value (VIP) with the projection variable greater than 1 as the threshold for differential metabolites, a total of 26 characteristic biomarkers were found (Figure 2B). After classifying, sugar metabolites were still the most numerous, indicating that sugar, as the main differential metabolites, play an important role in the metabolic regulation of the tobacco aromatic type (Figure 2C). Subsequently, the heat map of the characteristic metabolites is shown in Figure 3D. All the differential metabolites abundance can be divided into two categories (Figure 2D), group I and group II, according to their different types. In group I, the relative contents of most sugar metabolites, such as Sucrose, Fructose, Maltose, were higher in the LAT samples. In comparison, the relative contents of most acids and amino acids metabolites, such as L-Phenylalanine, L-5-Oxoproline, Hydracrylic acid, and Xylonic acid, in group II were higher in the SAT samples. Among them, the contents of sugar metabolites, such as 3α-Mannobiose and Maltose, in the LAT subgroup were higher than those in the SAT subgroup, indicating that sugar metabolites are important LAT biomarkers. In contrast, amino acids, such as L-5-Oxoproline and L-Phenylalanine, as well as acids metabolites, such as Hydracrylic acid and Xylonic acid, have high contents in the SAT subgroup, indicating that amino acids and acids metabolites may be SAT biomarkers. Notably, the total amino acid content in SAT samples from HuNYD and HuNYN was notably lower than that from HeNLL and HeNXY. Despite this regional variation, L-phenylalanine, a key aromatic precursor, showed elevated levels in three out of four SAT samples compared to their LAT counterparts. The exception was HuNYD, where L-phenylalanine content was marginally lower in SAT, possibly due to site-specific environmental stressors. These findings suggest that L-phenylalanine accumulation in SAT is not universally consistent across regions but may still contribute to aroma profiles when upregulated.

Metabolic pathway of flue-cured tobacco leaves

In order to gain an in-depth understanding of the differences in the metabolic networks between the SAT and LAT samples, the metabolic pathways of all differential metabolites were analyzed using MetaboAnalyst 5.0, and 12 differential metabolites were involved in 17 metabolic pathways (Table 3). The metabolic pathways with a p-value less than 0.05 were selected as differential ones; 10 differential metabolites were enriched in 4 differential metabolic pathways. The metabolic pathways in Figure 3 showed the overall situation of the differential metabolites in the tobacco leaf samples. Four metabolic pathways (glycolysis, sugar metabolism, acid metabolism, amino acid metabolism, and tricarboxylic acid cycle (TCA) were extracted and connected according to the KEGG pathway database. Most of the differential metabolites were concentrated in the pathways related to sugar metabolism. In the SAT samples, the relative contents of differential metabolite related to amino acid metabolism were significantly higher than those in the LAT. In comparison, the relative contents of most sugar metabolites, such as sucrose, fructose, and maltose in the LAT samples were significantly higher than those in the SAT.

Microbial community alpha diversity of flue-cured tobacco leaves

After cleaning the reads of the tobacco leaf sample, species annotation was performed using MetaPhlAn; 68 microbial species were detected in the LAT and SAT samples. The ACE, Chao1, Shannon, and Simpson indices reflect the number of communities, species abundance, species diversity, and species evenness in the sample (Zhang et al., 2022). The α diversity index is shown in Supplementary Table S1. The ACE index, Chao1, Shannon, and Simpson indices of SAT were higher than those of LAT, indicating that the SAT leaves contain more microbial species than those of LAT, and the microbial composition was even.

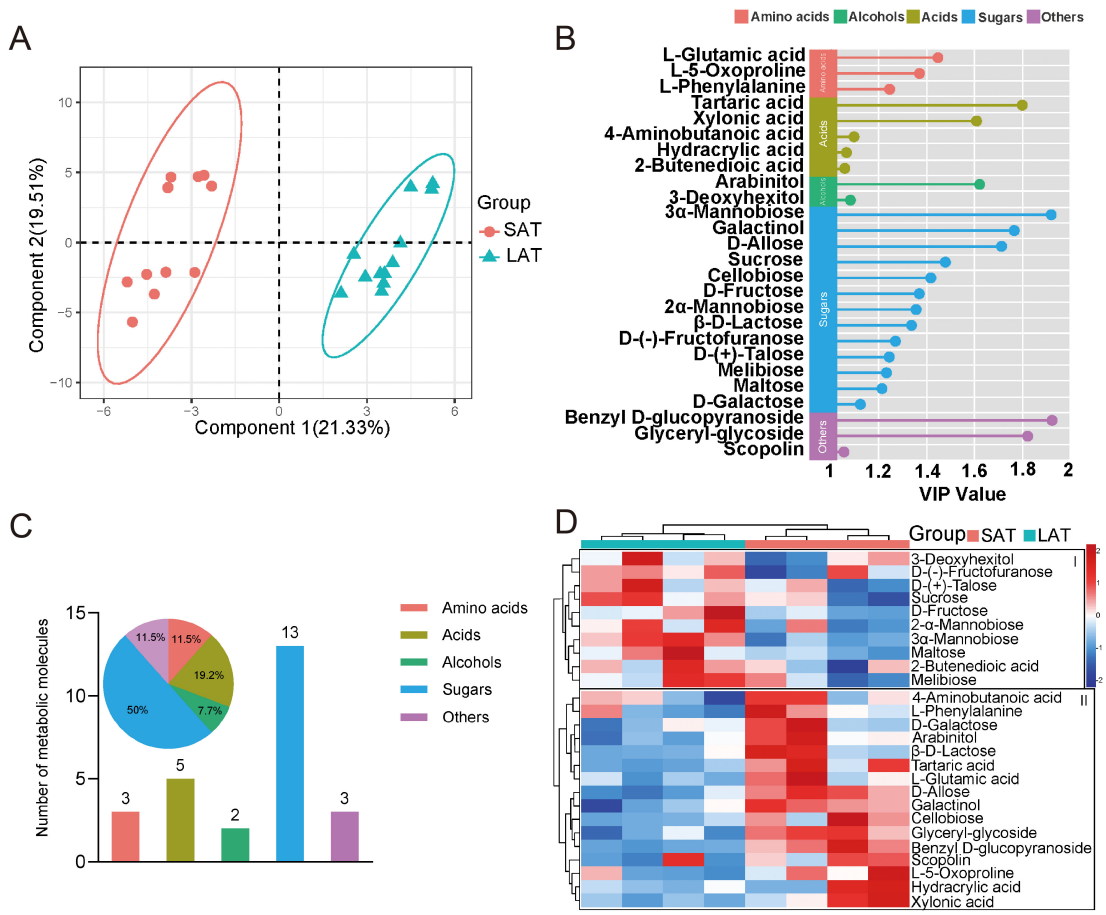

FIGURE 2
Multivariate analysis of the aromatic flue-cured tobacco leaf metabolites. **(A)** PLS-DA score plot, ellipses represent 95% confidence intervals for each group. **(B)** Dot plot of metabolites with variable importance in projection (VIP) scores >1.0 in the PLS-DA model. **(C)** Metabolite composition, bar plot showing the number of the metabolite molecules, pie plot displaying the proportion of metabolites. **(D)** Heat map of differential metabolites relative content in tobacco leaves with different flavors (Euclidean distance). SAT, strong aromatic tobacco; LAT, light aromatic tobacco.

Microbial community beta diversity of flue-cured tobacco leaves

Beta diversity is used as a measure of the variation in species diversity. The principal coordinates analysis (PCoA) of the Bray-Curtis distance on the species level is shown in Supplementary Figure S1A. The SAT and LAT samples were significantly separated, and the two principal coordinate axes, PCo1 and PCo2, explain 63.08% of the total variance. The differences in microbial communities between SAT and LAT samples were apparent. Hierarchical clustering divided the flue-cured tobacco leaves from different production areas into two branches (Supplementary Figure S1B). One branch contained all tobacco leaf samples from Henan and Hunan provinces, which are SAT leaf samples. The other branch contained tobacco leaf samples from Sichuan and Yunnan which are LAT leaf samples. It is worth noting that only one species, *Aspergillus_flavus*, was found in the species annotation of the SCLH, an LAT leaf sample in MetaPhlAn, indicating that *Aspergillus_flavus* may be the abundant species among the microorganisms on the surface of the tobacco leaves from Liangshan Yi Autonomous Prefecture in Huidong County, Sichuan Province.

Characteristics of microbial communities of flue-cured tobacco leaves

The Anosim result at the genus level is shown in Supplementary Figure S2A, where R>0 and p<0.05, demonstrating significantly greater inter-group variation compared to intra-group differences. Significant differences existed in the aromatic types and relative abundances of microbial genera between SAT and LAT.

The distribution of the microbial composition at the phylum level of SAT and LAT samples was shown in Supplementary Figure S2B. Five bacterial phyla and one fungal phylum were detected at the phylum level. Five bacterial phyla were *Proteobacteria*, *Actinobacteria*, *Bacteroidetes*, *Firmicutes*, and *Deinococcus_thermus*; one fungal phylum was *Ascomycota*. Among them, *Proteobacteria*, *Actinobacteria*, and *Bacteroidetes* were the main abundant taxa in the SAT samples (relative abundance > 1%), while in the LAT samples, *Proteobacteria* was the abundant bacterial phylum and *Ascomycota* was the abundant fungal phylum. *Proteobacteria* was the abundant t bacterial phylum in both types of aromatic tobacco leaves, with a relative abundance of 95% and 72% of the total microbial community in the SAT and LAT samples, respectively. In contrast, the relative

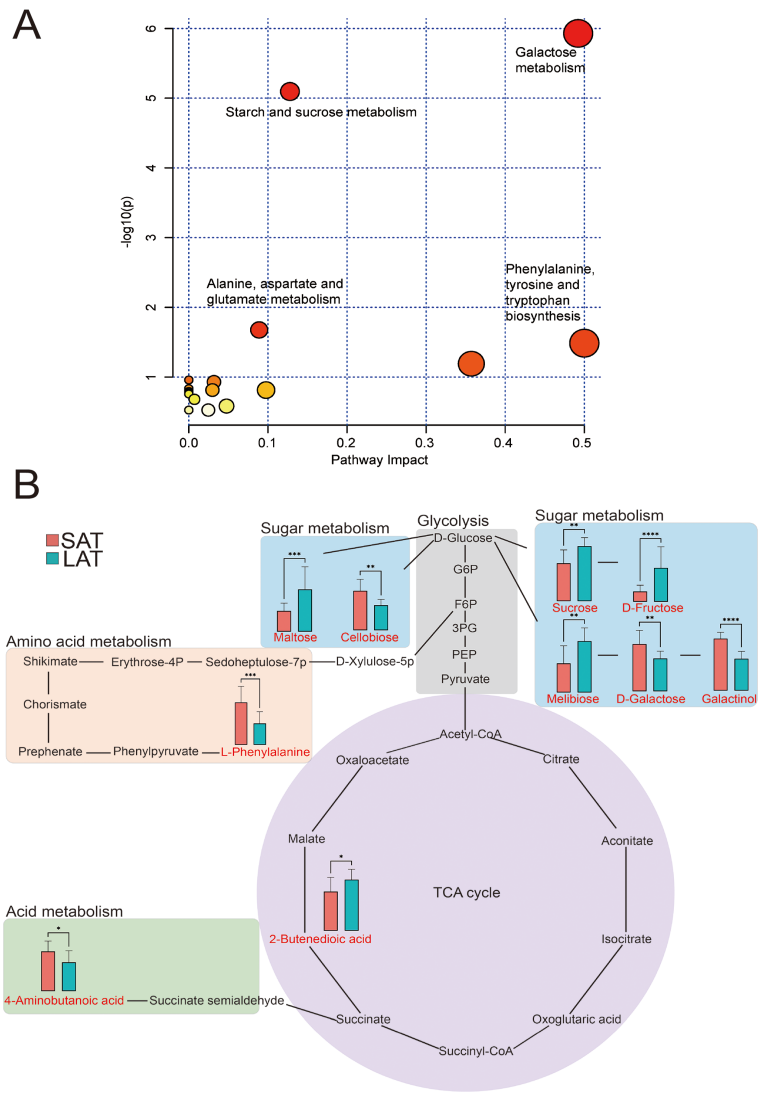

FIGURE 3
Metabolome analysis of differential metabolites in light and strong aromatic tobacco leaves. **(A)** Overview of metabolic pathways. **(B)** Metabolic pathway map of the differential metabolites. *P<0.05, **P<0.01, ***P<0.001, ****P<0.0001. In **(A)**, the bubbles represent the metabolic pathways, and the color of the bubbles (from yellow to red) indicates the significant level of the metabolites in the data.

abundance of the fungal phylum *Ascomycota* in the LAT leaves (27.37%) was higher than that in the SAT samples (0.29%). The relative abundance of the bacterial phylum *Actinobacteria* in the SAT samples (2.7%) was higher than that in the LAT samples (0.005%).

At the genus level (Supplementary Figure S2C), ten bacterial genera and one fungal genus (relative abundance >1%) were identified. Among them, *Pseudomonas*, *Sphingomonas*, *Methylobacterium*, *Methylorubrum*, *Aureimonas*, *Enterobacter*, *Pseudokineococcus*, *Spirosoma*, *Pantoea*, and *Afipia* were the main abundant bacterial genera. *Aspergillus* was the main abundant fungal genus. The composition and relative abundance of the main bacterial and fungal genera differed. The relative abundance of *Sphingomonas* (57.5%) in the SAT group was significantly higher than that in the LAT group (23%), the relative abundance of *Aspergillus* (27.4%), *Pseudomonas* (36.1%), and *Methylorubrum* (9.7%) in the LAT group was higher than that in the SAT group (0.3%, 9.2%, and 2.5%). *Methylobacterium* (23.5%), *Aureimonas* (1.2%), *Spirosoma* (1.2%), and *Pseudokineococcus* (1.9%) were only found in the SAT group. In comparison, the genus *Pantoea* (1.1%) was only found in the LAT group.

Supplementary Figure S2D shows the LEfSE analysis of the LAT samples and SAT samples at the genus level. Three bacterial genera were identified as differential abundant species between the two tobacco groups based on the threshold of greater than 4 in LDA score and less than 0.05 in P value.

Overall, the two types of aromatic samples showed species differences and microbial communities' abundance at the phylum and genus levels. Combined with the results of the LEfSe analysis, the differences in microbial communities between the two types of aromatic samples were mainly reflected in the differences in the abundance of *Methylobacterium*, *Pseudokineococcus*, and *Quadrisphaera*, which may potentially influence tobacco aroma development.

10.3389/fpls.2025.1588888

TABLE 3 Metabolic pathways of differential metabolites in tobacco leaves.

Pathway Name	Total	Expected	Hits	Raw p	Impact	Hit Metabolites
Galactose metabolism	27	0.22286	5	1.18E-06	0.49222	Sucrose
						Melibiose
						D-Galactose
						D-Fructose
						Galactinol
Starch and sucrose metabolism	18	0.14857	4	8.03E-06	0.12786	Sucrose
						Maltose
						Cellobiose
						D-Fructose
Alanine, aspartate and glutamate metabolism	28	0.23111	2	0.021069	0.08894	4-Aminobutanoic acid
						2-Butenedioic acid
Phenylalanine, tyrosine and tryptophan biosynthesis	4	0.033016	1	0.03264	0.5	L-Phenylalanine
Phenylalanine metabolism	8	0.066032	1	0.064294	0.35714	L-Phenylalanine
Arginine biosynthesis	14	0.11556	1	0.10999	0	2-Butenedioic acid
Butanoate metabolism	15	0.12381	1	0.1174	0.03175	4-Aminobutanoic acid
Pentose and glucuronate interconversions	19	0.15683	1	0.14648	0	Arabinitol
Tricarboxylic acid cycle (TCA)	20	0.16508	1	0.15361	0.02981	2-Butenedioic acid
Fructose and mannose metabolism	20	0.16508	1	0.15361	0.09765	D-Fructose
beta-Alanine metabolism	21	0.17333	1	0.16069	0	Hydracrylic acid
Propanoate metabolism	22	0.18159	1	0.16771	0	Hydracrylic acid
Pyruvate metabolism	23	0.18984	1	0.17468	0	Hydracrylic acid
Glutathione metabolism	28	0.23111	1	0.20871	0.00709	Hydracrylic acid
Arginine and proline metabolism	36	0.29714	1	0.26048	0.04767	Hydracrylic acid
Amino sugar and nucleotide sugar metabolism	42	0.34667	1	0.29724	0	Hydracrylic acid
Tyrosine metabolism	42	0.34667	1	0.29724	0.02463	Hydracrylic acid

Association of abundant microorganisms and metabolites of flue-cured tobacco leaves

Redundancy analysis (RDA) of the influence of the abundant microbial genera on metabolites showed that the first two axes RDA1 and RDA2 collectively explained 98.51% of the variation in the relationship between metabolites and microorganisms of the samples, with RDA1 contributing 86.14% and RDA2 12.37% (Figure 4A), indicating that RDA1 is the main dimension that distinguishes the relationship between metabolites and microbial communities in LAT and SAT samples. In the statistical validation identified, the effects of the microbial genera *Methylobacterium* and *Methylorubrum* on metabolites were significant, with p-values of 0.003 and 0.035, respectively, indicating that they are key genera in the microbial community that regulate the metabolites distribution and cause differences in the aromas of tobacco. Sugar metabolites associated with light aromas showed positive correlations with Methylorubrum (RDA1=-0.691) and Pseudomonas (RDA1=-0.375) but negative correlations with Methylobacterium (RDA1 = 0.733). Conversely, acid metabolites associated with strong aromas, were positively correlated with the genera *Methylobacterium* and *Aureimonas* (RDA1 = 0.733 and 0.619) and negatively correlated with the genera *Methylorubrum* and *Pseudomonas* (RDA1 = -0.691 and -0.375). In addition, amino acids, which are also important for tobacco to form strong aromas, were positively correlated with the genus *Sphingomonas* (RDA2 = -0.736) and negatively correlated with the genera *Aureimonas* (RDA2 = 0.228).

The distribution of the metabolites and the superior microbial genus (relative abundance >1%) showed that the genus *Methylobacterium* was closely related to strong aromas, indicating that acids and amino acids dominate its metabolic characteristics; the genus *Methylorubrum* and *Pseudomonas* were closely related to light aromas, indicating that sugars dominated its metabolic

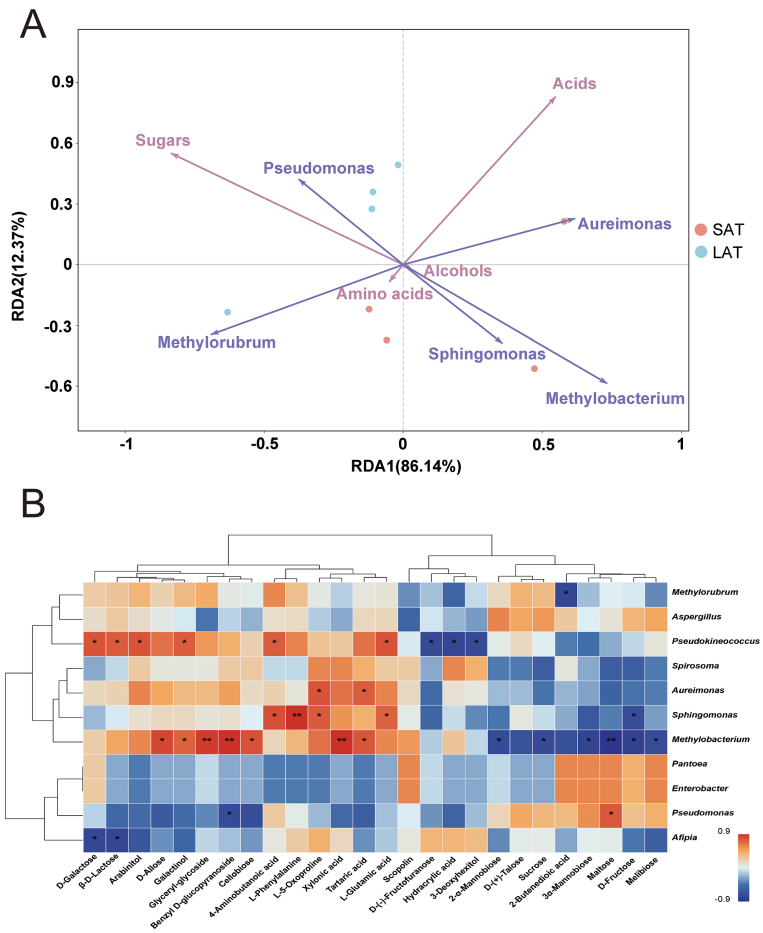

FIGURE 4
Metabolites and microorganisms of the flue-cured tobacco leaves. **(A)** RDA analysis, the angle between two variables less than 90° indicates a positive correlation, otherwise a negative correlation. **(B)** Correlation analysis between microorganisms at the genus level and metabolites. *P<0.05, **P<0.001.

characteristics. This result suggested that the selective regulation of metabolites by different abundant genera in the microbial community may influence the aromatic types.

From the analysis results, the genus *Methylobacterium* and *Methylorubrum* are the core genus in regulating the LAT and SAT metabolites, and their contribution to the metabolism of acids, amino acids, and sugars are particularly significant. The association analysis between abundant microorganisms and metabolites is shown in Figure 4B. Combined with the RDA analysis results, the microbial genus *Methylobacterium* was significantly positively correlated with the acid metabolites Xylonic acid and Tartaric acid and also significantly negatively correlated with most of the sugar metabolites, such as Sucrose, Maltose, and D-Fructose. The results indicated that *Methylobacterium* may play an important role in the overall metabolic regulation of the sample by promoting acid metabolism and inhibiting the accumulation of sugar metabolites, resulting in a strong aroma of tobacco.

The genus *Sphingomonas* is significantly positively correlated with the acid metabolite 4-Aminobutanoic acid, as well as the amino acid metabolites L-Phenylalanine, L-Glutamic acid, and L-5-Oxoproline, negatively correlated with the sugar metabolite D-Fructose. The results indicated that the genus *Sphingomonas* plays a facilitating role in amino acid and acid metabolism while inhibiting some sugar metabolism and resulting in a strong tobacco aroma.

The genus *Pseudokineococcus* was significantly positively correlated with the sugar and acid metabolites D-Galactose, β-D-Lactose and 4-Aminobutanoic acid, also significantly negatively correlated with D-(-)-Fructofuranose and Hydracrylic acid, indicating that the genus *Pseudokineococcus* plays an important role in the formation of the metabolites related to tobacco aroma. From the results of species abundance at the genus level (Supplementary Figure S2C), *Pseudokineococcus* existed more in LAT than in SAT, illustrating that it may play an important role in sugar metabolism and results in a light aroma of tobacco.

In summary, the complex regulation between abundant microbial genera and metabolites was clarified through redundancy analysis (RDA) and correlation analysis. The genus *Methylobacterium* played a key role in promoting acid metabolism and inhibiting sugar metabolism, highlighting its central position in distinguishing the metabolic characteristics of tobacco. The genera *Methylorubrum* and *Pseudomonas* were mainly involved in the sugar metabolic pathway, promoting the accumulation of sugar

metabolites in the LAT sample, while the main function of the genus *Sphingomonas* was promoting the amino acid and some acid metabolic pathways, which benefit strong aromas formation. In addition, the bidirectional regulation of sugars and acid metabolites by the genus *Pseudokineococcus* further reflects its important role in the metabolic network. These results revealed that different abundant microbial genera jointly drive the metabolic differences between the two types of aromatic tobacco samples by selectively regulating the distribution of metabolites.

Discussion

This study revealed significant differences and the association of the metabolite composition and microbial communities of the flue-cured tobacco leaves of the light aroma and strong aroma by combining analysis of untargeted metabolomics and metagenomics results. The results showed that tobacco leaves with different aromas exhibited significant differences in metabolites distribution and were regulated by specific abundant microbial genera. Importantly, the findings align with broader principles of plant-microbe interactions observed across plant species, offering insights into evolutionary conserved mechanisms and functional modularity in microbial communities (de Vries et al., 2020; Frantzeskakis et al., 2020; Mesny et al., 2023).

The composition and content of the metabolites in tobacco are highly consistent with the sensory characteristics of tobacco aroma (Zhang et al., 2024). The high content of sugar metabolites gives the tobacco a soft aroma by flavoring and reducing the pungent taste. In contrast, the rich acids and amino acids enhance the depth and complexity of the tobacco aromas by participating in the Maillard reaction and other chemical reactions (Geng et al., 2023). In the present study, the metabolite analysis showed that sugar and acid metabolites were the main contributors to tobacco aromas, manifesting the metabolic differences between LAT and SAT samples. The LAT sample significantly contained higher levels of sugar metabolites (e.g., sucrose, maltose) than the SAT sample, consistent with the findings of Jing et al (Jing et al., 2024). Conversely, the SAT samples contained higher acid metabolites (e.g., xylonic acid, tartaric acid) and amino acid metabolites (e.g., L-5-Oxoproline, L-Glutamic acid). However, in the study by Tie et al (Tie et al., 2024), LAT tobacco leaves had a higher content of amino acids, which contradicts our conclusion. This discrepancy may arise from differences in tobacco varieties or cultivation practices. Notably, such context-dependent metabolic variations are also observed in Arabidopsis-microbiome studies, where host genotype and environmental factors significantly reshaped microbial functional outputs (Beck et al., 2022; Gonçalves et al., 2023). However, unlike the simplified model system of Arabidopsis, tobacco's complex secondary metabolism and agricultural management introduce additional layers of microbial community regulation.

Microorganisms indirectly affect tobacco leaves' aroma by modulating metabolites' types and contents. *Sphingomonas* degrades dimeric lignin compounds into flavor precursors, while *Methylobacterium* utilizes methanol to drive one-carbon metabolism. *Pseudomonas* participates in nicotine degradation, redirecting intermediates into the TCA cycle. These functional roles reflect the "core-accessory" framework of microbial metabolic networks, where core functions (e.g., carbon/nitrogen cycling) are conserved across plant species, while accessory functions (e.g., specialized aroma synthesis) are niche-specific (Mazurie et al., 2010; Roume et al., 2015; Ramon and Stelling, 2023). For instance, *Methylobacterium*'s methanol metabolism is a core trait in both tobacco and Arabidopsis phyllosphere communities, but its contribution to aroma formation is uniquely amplified in tobacco due to host-specific secondary metabolism (Zhang et al., 2020; Zheng et al., 2024). Evolutionarily, such conservation suggests that plant-microbe co-adaptation in agricultural systems builds upon ancient symbiotic mechanisms repurposed for crop-specific traits (de Vries et al., 2020).

The identification of *Quadrisphaera* as a differentially abundant taxon in the LEfSe analysis despite its low relative abundance (0.12%) highlights the interplay between statistical significance and biological relevance in microbiome studies. The possible explanations are listed as below: (1) LEfSe identifies taxa with significant differences in relative abundance between groups by combining non-parametric tests with effect size estimation (LDA score). In this study, *Quadrisphaera* was exclusively detected in SAT group but absent in LAT group, leading to statistically significant differences ($P < 0.05$) even at low abundance. LEfSe's non-parametric approach is sensitive to such categorical differences, especially when taxa are uniquely associated with a group. (2) Microbial communities often include rare taxa that contribute disproportionately to functional processes. Although *Quadrisphaera*'s abundance was low, its metabolic activity (e.g., niche-specific enzymatic functions) or interactions with other microbes could amplify its ecological impact. For instance, *Quadrisphaera* might participate in pathways influencing secondary metabolite synthesis or niche competition, indirectly shaping aroma differentiation. Anyway, the biological significance of Quadrisphaera in this context requires further validation (e.g., strain isolation, functional assays). However, its identification aligns with emerging evidence that rare taxa can serve as biomarkers in plant-microbe systems. Future studies with larger sample sizes and metatranscriptomics could clarify its role.

Cross-species comparisons further highlight conserved metabolic pathways shaped by microbial activity. For example, phenylpropanoid biosynthesis-a pathway critical for aroma in tobacco, tea, and grapes—is similarly modulated by microbial hydroxylation and methylation enzymes in diverse plants (Zhao et al., 2020, 2023; Wang et al., 2023). In our study, the enrichment of sugar degradation pathways in LAT tobacco mirrors microbial-driven carbohydrate metabolism in maize rhizosphere communities, underscoring a universal strategy for balancing carbon allocation and secondary metabolite synthesis (Thoenen et al., 2023). These parallels emphasize and also support our hypothesis that microbial functional redundancy and metabolic flexibility are key drivers of plant phenotypic diversity.

Although amplicon sequencing (e.g., 16S/ITS rRNA gene sequencing) is widely recognized as a cost-effective and standardized approach for taxonomic profiling, in this research, shotgun

metagenomic sequencing was selected over amplicon sequencing to (i) avoid PCR amplification biases, and (ii) integrate taxonomic data with metabolomic profiles for holistic plant-microbe interaction modeling.

Conclusion and prospects

On the flue-cured tobacco leaves with a light aromatic smell, the abundant genera *Methylorubrum* and *Pseudomonas* promote sugar metabolism, while the genus *Pseudokineococcus* exhibits a bidirectional regulation of aromatic metabolites. While on the flue-cured tobacco leaves with a strong aromatic smell, the abundant genera *Methylobacterium* and *Sphingomonas* promote the metabolism of acids and amino acids. Meanwhile, the genus *Methylobacterium* inhibits sugar metabolism. This study provides a theoretical basis for improving tobacco leaf quality through metabolomic and metagenomic analysis. However, a limitation of this study is the absence of direct functional annotation of microbial genes (e.g., KEGG pathways). Future work combining metatranscriptomics or MAG-based approaches with controlled experiments (e.g., gnotobiotic systems) will validate the hypothesized roles of taxa like *Methylobacterium* in sugar/acid metabolism. Meanwhile, evolutionary perspectives (e.g., phylogenetic conservation of microbial traits) and multi-omics modeling should also be integrated in the future research to dissect how core-accessory microbial functions coevolve with host metabolic networks. Additionally, exploring the molecular mechanisms of microbial-metabolite interactions in tobacco could inform microbiome engineering strategies applicable to other crops, such as enhancing stress tolerance or flavor profiles through targeted microbial consortia.

Data availability statement

The raw data supporting the conclusions of this article will be made available by the authors, without undue reservation.

Author contributions

YJ: Writing – original draft, Formal Analysis, Investigation, Methodology, Software, Visualization. JW: Investigation, Methodology, Conceptualization, Resources, Writing – review & editing. XL: Methodology, Formal Analysis, Investigation, Writing – original draft. TL: Methodology, Data curation, Writing – review & editing. HD: Methodology, Formal Analysis, Writing – review & editing. BW: Methodology, Validation, Writing – review & editing. MY: Investigation, Writing – review & editing. YZ: Conceptualization, Funding acquisition, Resources, Writing – review & editing. RL: Conceptualization, Funding acquisition, Project administration, Supervision, Writing – original draft, Writing – review & editing.

Funding

The author(s) declare that financial support was received for the research and/or publication of this article. This work was supported by Key Research and Development Program of CNTC (110202102035) and Natural Science Foundation of Henan Province (232300421165).

Acknowledgments

The authors thank Dr. Xiaoge Hou for her expert guidance in analyzing the metabolomics and genomics data of flue-cured upper tobacco leaves.

Conflict of interest

The authors declare that the research was conducted in the absence of any commercial or financial relationships that could be construed as a potential conflict of interest.

Generative AI statement

The author(s) declare that no Generative AI was used in the creation of this manuscript.

Publisher's note

Supplementary material

The Supplementary Material for this article can be found online at: https://www.frontiersin.org/articles/10.3389/fpls.2025.1588888/full#supplementary-material

References

Banožić, M., Jokić, S., Ačkar, Đ., Blažić, M., and Šubarić, D. (2020). Carbohydrates-key players in tobacco aroma formation and quality determination. *Molecules* 25, 1734. doi: 10.3390/molecules25071734

Beck, A. E., Kleiner, M., and Garrell, A.-K. (2022). Elucidating plant-microbe-environment interactions through omics-enabled metabolic modelling using synthetic communities. *Front. Plant Sci.* 13. doi: 10.3389/fpls.2022.910377

Berg, G., Köber, M., Rybakova, D., Müller, H., Grosch, R., and Smalla, K. (2014). Plant microbial diversity is suggested as the key to future biocontrol and health trends. *FEMS Microbiol. Ecol.* 90, 609–621. doi: 10.1093/femsec/fix050

Blaise, B. J., Correia, G. D., Haggart, G. A., Surowiec, I., Sands, C., Lewis, M. R., et al. (2021). Statistical analysis in metabolic phenotyping. *Nat. Protoc.* 16, 4299–4326. doi: 10.1038/s41596-021-00579-1

Blanco-Míguez, A., Beghini, F., Cumbo, F., McIver, L. J., Thompson, K. N., Zolfo, M., et al. (2023). Extending and improving metagenomic taxonomic profiling with uncharacterized species using MetaPhlAn 4. *Nat. Biotechnol.* 41, 1633–1644. doi: 10.1038/s41587-023-01688-w

Bokulich, N. A., Thorngate, J. H., Richardson, P. M., and Mills, D. A. (2014). (2014). Microbial biogeography of wine grapes is conditioned by cultivar, vintage, and climate. *Proc. Natl. Acad. Sci. United States America* 111, E139–E148. doi: 10.1073/pnas.1317377110

Chandel, N., Singh, H., and Vaishnav, A. (2025). Mechanistic understanding of metabolic cross-talk between Aloe vera and native soil bacteria for growth promotion and secondary metabolites accumulation. *Front. Plant Sci.* 16. doi: 10.3389/fpls.2025.1577521

de Vries, S., Stukenbrock, E. H., and Rose, L. E. (2020). Rapid evolution in plant–microbe interactions–an evolutionary genomics perspective. *New Phytol.* 226, 1256–1262. doi: 10.1111/nph.16458

Diwan, D., Rashid, M. M., and Vaishnav, A. (2022). Current understanding of plant-microbe interaction through the lenses of multi-omics approaches and their benefits in sustainable agriculture. *Microbiological Res.* 265, 127180. doi: 10.1016/j.micres.2022.127180

Durán, P., Thiergart, T., Garrido-Oter, R., Agler, M., Kemen, E., Schulze-Lefert, P., et al. (2017). Microbial interkingdom interactions in roots promote Arabidopsis survival. *Cell* 175, 973–983. doi: 10.1016/j.cell.2018.10.020

Frantzeskakis, L., Di Pietro, A., Rep, M., Schirawski, J., Wu, C. H., and Panstruga, R. (2020). Rapid evolution in plant–microbe interactions–a molecular genomics perspective. *New Phytol.* 225, 1134–1142. doi: 10.1111/nph.15966

Geng, Z., He, P., Gao, H., Liu, J., Qiu, J., and Cai, B. (2023). Aroma precursors of cigars from different tobacco parts and origins, and their correlations with sensory characteristics. *Front. Plant Sci.* 14. doi: 10.3389/fpls.2023.1264739

Gonçalves, O. S., Creevey, C. J., and Santana, M. F. (2023). Designing a synthetic microbial community through genome metabolic modeling to enhance plant–microbe interaction. *Environ. microbiome* 18, 81. doi: 10.1186/s40793-023-00536-3

Gong, T., and Xin, X. F. (2021). Phyllosphere microbiota: Community dynamics and its interaction with plant hosts. *J. Integr. Plant Biol.* 63, 297–304. doi: 10.1111/jipb.13060

Hou, X., Hui, M., Gu, X., Shi, X., Fan, C., Wang, J., et al. (2024). Differential characteristics of the metabolic profiles and microbial community between superior and normal grades of *Nongxiangxing-daqu*. *Foods* 13, 914. doi: 10.3390/foods13060914

Huang, S., Liu, D., Chen, M., Xi, G., Yang, P., Jia, C., et al. (2022). Effects of *Bacillus subtilis* subsp. on the microbial community and aroma components of flue-cured tobacco leaves based on metagenome analysis. *Arch. Microbiol* 204, 726. doi: 10.1007/s00203-022-03347-1

Jing, Y., Chen, W., Qiu, X., Qin, S., Gao, W., Li, C., et al. (2024). Exploring metabolic characteristics in different geographical locations and yields of nicotiana tabacum L. Using gas chromatography–mass spectrometry pseudotargeted metabolomics combined with chemometrics. *Metabolites* 14, 176. doi: 10.3390/metabo14040176

Li, Q., Chai, S., Li, Y., Huang, J., Luo, Y., Xiao, L., et al. (2018). Biochemical components associated with microbial community shift during the pile-fermentation of Primary Dark Tea. *Front. Microbiol.* 9. doi: 10.3389/fmicb.2018.01509

Lindow, S. E., and Brandl, M. T. (2003). Microbiology of the phyllosphere. *Appl. Environ. Microb.* 69, 1875–1883. doi: 10.1128/AEM.69.4.1875–1883.2003

Liu, P., Luo, J., Zheng, Q., Chen, Q., Zhai, N., Xu, S., et al. (2020). Integrating transcriptome and metabolome reveals molecular networks involved in genetic and environmental variation in tobacco. *DNA Res.* 27, dsaa006. doi: 10.1093/dnares/dsaa006/5824296

Liu, A., Yuan, K., Xu, H., Zhang, Y., Tian, J., Li, Q., et al. (2022). Proteomic and metabolomic revealed differences in the distribution and synthesis mechanism of aroma precursors in Yunyan 87 tobacco leaf, stem, and root at the seedling stage. *ACS Omega* 7, 33295–33306. doi: 10.1021/acsomega.2c03877

Mazurie, A., Bonchev, D., Schwikowski, B., and Buck, G. A. (2010). Evolution of metabolic network organization. *BMC Syst. Biol.* 4, 1–10. doi: 10.1186/1752-0509-4-59

Mesny, F., Hacquard, S., and Thomma, B. P. (2023). Co-evolution within the plant holobiont drives host performance. *EMBO Rep.* 24, e57455. doi: 10.15252/embr.202357455

Pang, Z., Lu, Y., Zhou, G., Hui, F., Xu, L., Viau, C., et al. (2024). MetaboAnalyst 6.0: towards a unified platform for metabolomics data processing, analysis and interpretation. *Nucleic Acids Res.* 52, W398–W406. doi: 10.1093/nar/gkae253

Patti, G. J., Yanes, O., and Siuzdak, G. (2012). Metabolomics: the apogee of the omics trilogy. *Nat. Rev. Mol. Cell Biol.* 13, 263–269. doi: 10.1038/nrm3314

Ramon, C., and Stelling, J. (2023). Functional comparison of metabolic networks across species. *Nat. Commun.* 14, 1699. doi: 10.1038/s41467-023-37429-5

Roume, H., Heintz-Buschart, A., Muller, E. E., May, P., Satagopam, V. P., Laczny, C. C., et al. (2015). Comparative integrated omics: identification of key functionalities in microbial community-wide metabolic networks. *Biofilms Microbiomes* 1, 1–11. doi: 10.1038/npjbiofilms.2015.7

Segata, N., Waldron, L., Ballarini, A., Narasimhan, V., Jousson, O., and Huttenhower, C. (2012). Metagenomic microbial community profiling using unique clade-specific marker genes. *Nat. Methods* 9, 811–814. doi: 10.1038/nmeth.2066

Shi, Y., He, Y., Zheng, Y., Liu, X., Wang, S., Xiong, T., et al. (2024). Characteristics of the phyllosphere microbial community and its relationship with major aroma precursors during the tobacco maturation process. *Front. Plant Sci.* 15. doi: 10.3389/fpls.2024.1346154

Thoenen, L., Giroud, C., Kreuzer, M., Waelchli, J., Gfeller, V., Deslandes-Hérold, G., et al. (2023). Bacterial tolerance to host-exuded specialized metabolites structures the maize root microbiome. *Proc. Natl. Acad. Sci.* 120, e2310134120. doi: 10.1073/pnas.2310134120

Tie, J., Li, S., He, W., Li, Y., Liao, F., Xue, J., et al. (2024). Study of metabolite differences of flue-cured tobacco from Canada (CT157) and Yunnan (Yunyan 87). *Heliyon* 10, e32417. doi: 10.1016/j.heliyon.2024.e32417

Vandenkoornhuyse, P., Quaiser, A., Duhamel, M., Le Van, A., and Dufresne, A. (2015). The importance of the microbiome of the plant holobiont. *New Phytol.* 206, 1196–1206. doi: 10.1111/nph.13312

Vorholt, J. A. (2012). Microbial life in the phyllosphere. *Nat. Rev. Microbiol.* 10, 828–840. doi: 10.1038/nrmicro2910

Wang, J. Q., Dai, Z. S., Gao, Y., Wang, F., Chen, J. X., Feng, Z. H., et al. (2023). Untargeted metabolomics coupled with chemometrics for flavor analysis of Dahongpao oolong tea beverages under different storage conditions. *Lwt* 185, 115128. doi: 10.1016/j.lwt.2023.115128

Wang, C., Sun, J., Lassabliere, B., Yu, B., Zhao, F., Zhao, F., et al. (2019). Potential of lactic acid bacteria to modulate coffee volatiles and effect of glucose supplementation: fermentation of green coffee beans and impact of coffee roasting. *J. Sci. Food Agr.* 99, 409–420. doi: 10.1002/jsfa.9202

Wang, Y., Wu, J., Sun, P., Chen, C., and Shen, J. (2022). Community structure of phyllosphere bacteria in different cultivars of fingered citron (Citrus medica 'Fingered') and their correlations with fragrance. *Front. Plant Sci.* 13. doi: 10.3389/fpls.2022.936252

Xia, Y., and Sun, J. (2022). *Statistical data analysis of microbiomes and metabolomics (Vol. 13)* (Washington, USA: American Chemical Society).

Yin, F., Karangwa, E., Song, S., Duhoranimana, E., Lin, S., Cui, H., et al. (2019). Contribution of tobacco composition compounds to characteristic aroma of Chinese faint-scent cigarettes through chromatography analysis and partial least squares regression. *J. Chromatogr. B* 1105, 217–227. doi: 10.1016/j.jchromb.2018.12.001

Zhang, S. J., De Bruyn, F., Pothakos, V., Torres, J., Falconi, C., Moccand, C., et al. (2019). Following coffee production from cherries to cup: microbiological and metabolomic analysis of wet processing of Coffea arabica. *Appl. Environ. Microbiol.* 85, e02635–e02618. doi: 10.1128/AEM.02635-18

Zhang, Y., Ding, F., Shen, Y., Cheng, W., Xue, Y., Han, B. Z., et al. (2022). Characteristics of the microbiota and metabolic profile of high-temperature Daqu with different grades. *World J. Microbiol. Biotechnol.* 38, 137. doi: 10.1007/s11274-022-03303-7

Zhang, Q., Geng, Z., Li, D., and Ding, Z. (2020). Characterization and discrimination of microbial community and co-occurrence patterns in fresh and strong flavor style flue-cured tobacco leaves. *MicrobiologyOpen* 9, e965. doi: 10.1002/mbo3.965

Zhang, M., Guo, D., Wu, G., Han, P., Shi, Y., Zheng, T., et al. (2024). Analysis of volatile compound metabolic profiles during the fermentation of filler tobacco leaves through integrated E-nose, GC–MS, GC-IMS, and sensory evaluation. *J. Chromatogr. A* 1737, 465472. doi: 10.1016/j.chroma.2024.465472

Zhao, S., Cheng, H., Xu, P., and Wang, Y. (2023). Regulation of biosynthesis of the main flavor-contributing metabolites in tea plant (*Camellia sinensis*): A review. *Crit. Rev. Food Sci.* 63, 10520–10535. doi: 10.1080/10408398.2022.2078787

Zhao, N., Kokawa, M., Suzuki, T., Khan, A. R., Dong, W., Nguyen, M. Q., et al. (2024). Refermentation with yeast and lactic acid bacteria isolates: a strategy to improve the flavor of green coffee beans. *J. Sci. Food Agr.* 104, 9137–9150. doi: 10.1002/jsfa.13735

Zhao, J., Li, P., Xia, T., and Wan, X. (2020). Exploring plant metabolic genomics: chemical diversity, metabolic complexity in the biosynthesis and transport of specialized metabolites with the tea plant as a model. *Crit. Rev. Biotechnol.* 40, 667–688. doi: 10.1080/07388551.2020.1752617

Zheng, L., Tian, Q., Yu, X., Le, Z., Luo, W., Kai, D., et al. (2024). Similarity in the microbial community structure of tobacco from geographically similar regions. *Sci. Rep.* 14, 30933. doi: 10.1038/s41598-024-81565-x

frontiers | Frontiers in Plant Science

TYPE Original Research
PUBLISHED 18 July 2025
DOI 10.3389/fpls.2025.1603963

OPEN ACCESS

EDITED BY
Robin Joshi,
University of Pennsylvania, United States

REVIEWED BY
Ashok Gehlot,
Institute of Himalayan Bioresource Technology (CSIR), India
Tahir Ali,
University of Mississippi, United States

*CORRESPONDENCE
Zhihang Zhuo
zhuozhihang@foxmail.com

†These authors have contributed equally to this work and share first authorship

RECEIVED 01 April 2025
ACCEPTED 27 June 2025
PUBLISHED 18 July 2025

CITATION
Peng Y, Xu D, Liao W, Qian Q, Wu J, Gan T and Zhuo Z (2025) Dynamic analysis of composition, insecticidal, and antifungal activities of *Zanthoxylum armatum* DC. at different harvesting periods. *Front. Plant Sci.* 16:1603963. doi: 10.3389/fpls.2025.1603963

Dynamic analysis of composition, insecticidal, and antifungal activities of *Zanthoxylum armatum* DC. at different harvesting periods

Yaqin Peng[1†], Danping Xu[1†], Wenkai Liao[1], Qianqian Qian[1], Junhao Wu[1], Tingjiang Gan[2] and Zhihang Zhuo[1*]

[1]College of Life Science, China West Normal University, Nanchong, China, [2]Engineering Research Center of Chuanxibei Rural Human Settlement Construction, Mianyang Teachers' College, Mianyang, China

Introduction: Essential oils from plants contain various volatile compounds with antifungal and antioxidant properties. The synthesis and accumulation of these volatile compounds are closely related to factors such as the plant's geographical origin and harvest period. Investigating the insect-repellent and antimicrobial effects of *Zanthoxylum armatum* DC. essential oils (EOs) at different harvest stages can optimize its harvest and utilization while also promoting the development of eco-friendly agents.

Methods: This study analyzed the changes in the composition and content of volatile compounds in *Z. armatum* EOs at different growth stages in Nanchong City using GC-MS.

Results: The results indicate that the accumulation period of volatile compounds occurs before the t5 stage (August 4). Linalool, D-Limonene, and Sabinene were the three most abundant volatile components in the essential oil of *Z. armatum* pericarp. Many monoterpenes, such as α-Pinene, Sabinene, and β-Myrcene, were found in higher concentrations during the early stages of fruit maturation. Principal component analysis (PCA) revealed a significant difference in volatile composition between the t3, t4, and t5 (t3: July 3, t4: July 18, t5: August 4) stages and the t1, t2, t6, (t1: May 26, t2: June 16, t6: September 9) and t7 (September 28) stages of *Z. armatum*. Volatile compounds were relatively higher in samples collected in July and August, making these months the optimal harvest period for processing and manufacturing related products. As the fruit of *Z. armatum* matures, the content of structurally more complex compounds, such as alcohols and esters, increases. The insect-repellent and antifungal experiments demonstrated that *Z. armatum* EOs exhibited a strong repellent effect against *T.*

10.3389/fpls.2025.1603963

castaneum, although the EO's toxicity was not lethal. The antifungal effect was most pronounced in the EO collected during the t4 stage, where the relative content of various antifungal compounds was higher.

Discussion: This suggests that the antifungal activity of the EOs may result from synergistic or antagonistic interactions among its compounds. By exploring the composition, content, and bioactivities (insect-repellent and antifungal) of *Z. armatum* EOs at different harvest periods, this study provides theoretical support for developing market-oriented commercial products.

KEYWORDS

Z. armatum* DC., GC-MS, essential oil, *T. castaneum*, *C. cassiicola

1 Introduction

Essential oils (EOs) are typically extracted from various parts of plant materials, such as flowers, buds, seeds, leaves, branches, bark, herbs, wood, fruits, and roots. They are aromatic, oil-like liquids that are volatile in nature (Burt, 2004). EOs contain a variety of low molecular weight volatile components, such as terpenes and terpenoid compounds, phenolic-derived aromatic components, and fatty components (Bakkali et al., 2008). At different maturity stages, the components of EOs change with the plant's physiological metabolism. Research by Wu et al. demonstrated that the contents of 3-carene, α-pinene, and β-pinene in *Citrus medic*a EO vary significantly across different stages (Zhen et al., 2013). EOs contain a variety of bioactive plant secondary metabolites that can inhibit or slow the growth of harmful microorganisms (Shenglan et al., 2022). They play a crucial role in plant defense against pathogens and insects. Plant essential oils, as a natural product, are commonly used as natural antimicrobial agents. The essential oils of certain aromatic plants are widely used as food preservatives, helping to extend shelf life and improve the quality of stored foods (Gutierrez et al., 2009). Bhanu et al (Prakash et al., 2012). investigated the antifungal, anti-aflatoxin, and antioxidant properties of *Zanthoxylum alatum* Roxb. essential oil. They found that the main component of the essential oil, methyl cinnamate, exhibited antifungal and anti-aflatoxin effects at low concentrations (0.6 μl/ml), with fungicidal toxicity. Additionally, the essential oil showed strong antioxidant activity.

Zanthoxylum armatum DC. is a common shrub or small tree in the Rutaceae family, with approximately 250 species of Zanthoxylum plants found worldwide. These aromatic plants are native to subtropical and temperate regions globally and are particularly cultivated extensively in China, Korea, and Japan (Di et al., 2021). Its fruit is green in color and features slightly raised oil gland dots. Due to its enticing aromatic properties, the fruits and extracts of *Z. armatum* are among the key flavoring agents in the food industry (Hong et al., 2017; Shun et al., 2019). Additionally, as a traditional medicinal plant, *Z. armatum* is commonly used to treat wounds, toothaches, stomachaches, nausea, diarrhea, and ascariasis. Studies have indicated that Zanthoxylum plants contain various bioactive compounds, such as essential oils, alkaloids, lignans, coumarins, flavonoids, amides, polyphenols, and sterols. In the pericarp of *Z. armatum*, EOs are abundant and exhibit antioxidant, antibacterial, and anti-inflammatory effects (Gao and Hanbin, 2014). Currently, there is extensive research on the antimicrobial and insecticidal properties of *Z. armatum* EO, but studies focusing on its specific application in agricultural production are relatively scarce. This may be partly due to the inherent lag in practical agricultural activities and partly due to cost-related challenges associated with the research and application of such green agents.

Tribolium castaneum (Coleoptera: Tenebrionidae) (Campbell et al., 2022) is a significant cosmopolitan storage pest with a wide range of hosts. Due to its high reproductive rate and long reproductive lifespan, it exhibits one of the highest population growth rates among all stored-product beetles. Consequently, it is distributed in nearly 156 countries worldwide (Campbell et al., 2022). The eggs of this pest are scattered on the surface of grain kernels, within grain crevices, or among debris and fine particles. The eggs are often coated with a sticky substance, causing powder and debris to adhere to them, making them difficult to detect. This insect secretes odorous fluids from its scent glands, imparting a musty odor to its host. Furthermore, its secretions contain the carcinogenic compound benzoquinone (J. D. and Roth, 1953). In the search for pest control agents with limited adverse effects on the environment and non-target organisms, researchers have continually explored plant resources in the hope of discovering new plant-based insecticides with high insecticidal activity to address pesticide challenges. The EOs of *Cymbopogon* spp., *Ocimum* spp., and *Eucalyptus* spp. show great promise as repellents against insects and arthropods (Ravi Kant and Gayatri, 2007). *Corynespora cassiicola* is one of the pathogens causing target spot disease in mulberry trees. This fungal disease significantly impacts the yield and quality of mulberry trees, posing serious threats to the economy and ecological environment (Xinqi, 2023). While chemical control is relatively effective against this pathogen, it still presents certain challenges. Consequently, the

development of environmentally friendly agents is expected to become a key focus of future research.

The composition and content of essential oils are influenced by various factors, including the variety, origin, harvest time, and storage year (Qianqian et al., 2024). Therefore, the composition and content of EOs extracted from *Z. armatum* in different regions may vary, and their inhibitory effects on different pests and fungi may also differ. In this study, samples collected from Nanchong City, Sichuan Province, were analyzed using GC-MS to determine the composition and content of volatile oils, and the insect repellent and antimicrobial activities of the essential oil were subsequently validated. The insecticidal and antimicrobial activities of the EOs were then investigated. This study provides the first systematic time-course analysis of volatile compound profiles in *Z. armatum* EOs across seven distinct growth stages (from May to September), revealing previously unreported temporal accumulation patterns. By integrating GC-MS metabolomics, PCA-based chemometrics, and bioactivity assays, we developed an innovative framework that correlates harvest timing with optimal functional properties, thereby overcoming the limitations of traditional compositional studies. This research will provide data support for the development of natural plant-based insecticidal/antimicrobial agents.

2 Materials and methods

2.1 Plant materials

The sample collection site is located in the *Z. armatum* plantation in Ca'er Town, Gaoping District, Nanchong City, Sichuan Province (N 30.91438, E 106.28455, Altitude 426 m) (Figure 1). *Z. armatum* samples were collected through local forestry bureaus or zanthoxylum planting companies. In the plantation, 20 healthy *Z. armatum* trees aged 2–3 years were randomly selected, and fruit was collected from each tree seven times between May and September. The collection dates were as follows: (t1: May 26, t2: June 16, t3: July 3, t4: July 18, t5: August 4, t6: September 9, t7: September 28). The fresh *Z. armatum* fruit collected during each sampling was dehydrated in an oven at 60 °C for 48 hours. After dehydration, the seeds and pericarps of the *Z. armatum* were separated, placed into sealed bags, and stored at -20 °C for later use. All the specimens were authenticated by Professor Danping Xu of China West Normal University and stored in the School of Life Sciences (NC 20230526), China West Normal University.

2.2 Biological materials

T. castaneum samples were sourced from the Forest Protection Research Group at the School of Life Sciences, China West Normal University. Healthy adult beetles, 4–7 days post-emergence, were selected for the experiment. The *C. cassiicola* strain, which is responsible for the target spot disease, was obtained from the Sichuan Academy of Agricultural Sciences. The mycelium was inoculated onto PDA agar medium with an inoculation needle and incubated at a constant temperature in an incubator for 3 days before use. All the specimens were authenticated by Professor Zhihang Zhuo of China West Normal University.

2.3 Chemical reagents and equipment

Reagents: Purified water, anhydrous ethanol (purity >99.8%, Sigma-Aldrich, Germany); sodium carbonate, aluminum nitrate, sodium nitrite, sodium hydroxide, Folin-Ciocalteu reagent (analytical grade, Shanghai Yuanye Biotechnology Co., Ltd.), n-hexane, n-tridecane (HPLC grade, Sigma-Aldrich, Germany), C7-C40 n-alkane series (HJ894-2017, Anpel-Trace, China), anhydrous sodium sulfate (purity >98%, Shanghai Yisheng Biotechnology Co., Ltd.), dimethyl sulfoxide (analytical grade, Arabidopsis Biotechnology Co., Ltd., Chongqing), agar (Xiqiong Biotechnology, Beijing), glucose (purity >98%, Sichuan Baiochurui Biotechnology Co., Ltd., Chengdu), potatoes.

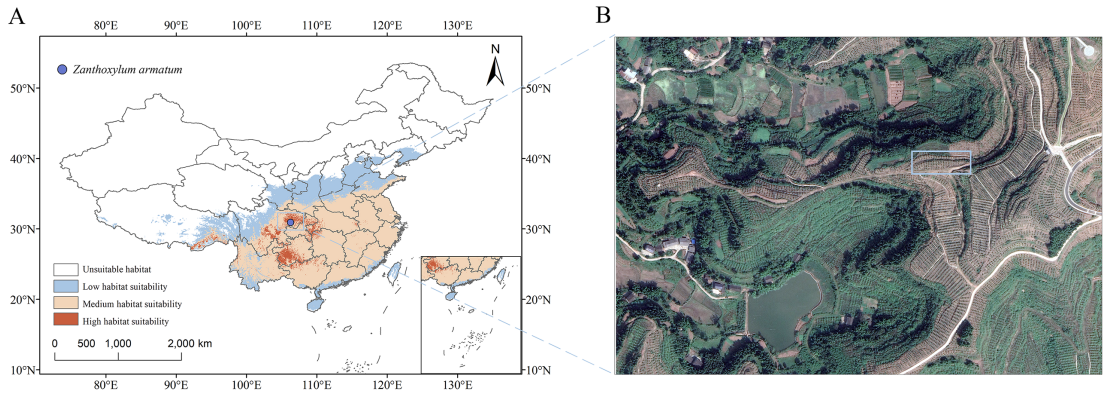

FIGURE 1
Geographic location map of the sampling points.

Instruments and Equipment: Balance (Suzhou Science Instrument Co., Ltd.); essential oil extractor, moisture analyzer (Sichuan Shubo Group Co., Ltd.), stereomicroscope (Leica Microsystems), grinder (XICHU Equipment Co., Ltd.), C18 preparative chromatography column [Agilent HC-C18 (4.6×250 mm, 10 μm)], gas chromatography-mass spectrometry (GC-MS) system (Agilent GC-MS 7890A-5975C), HP-5MS chromatography column (30 m×0.25 mm, 0.25 μm), laminar flow cabinet, constant temperature incubator, autoclave, induction cooker, microwave.

2.4 Extraction of essential oil

The oil content of fresh *Z. armatum* was determined according to the national standard GB/T 17527-2009, with the experiment repeated three times (ACFSMC, 2009). The oil content of dried *Z. armatum*: A certain amount of dried *Z. armatum* was ground using a grinder (XICHU Equipment Co., Ltd.) and passed through a 40-mesh sieve. Subsequently, 40 g of the resulting powder and 400 mL of pure water (1:10, v/v) were placed into a round-bottom flask of a volatile oil determination apparatus. The sample was heated with an electric heating mantle for distillation, which lasted for 3 hours at a rate of approximately 5 drops per minute. The distillate was collected in a graduated receiver tube, and anhydrous Na^2SO^4 was added to achieve water-oil separation. The volume of the oil was recorded, and the oil yield was calculated. The experiment was repeated three times (Qianqian et al., 2024). The extracted volatile oil was stored in amber glass bottles at -20°C, protected from light. The formula for calculating the essential oil extraction yield is as follows:

$$\text{Extractionrate of volatile oil}\,(\,\%\,) = \frac{V}{m} \times 100\,\%$$

V (mL) represents the volume of essential oil measured through hydrodistillation during the experiment, and m (g) represents the dry or wet weight of the sample used for extraction in the experiment.

2.5 Analysis of volatile components

GC-MS Analysis: Gas chromatography-mass spectrometry (GC-MS, Agilent GC-MS 7890A-5975C) was used to identify the components of the essential oil. The obtained *Z. armatum* essential oil was first dried with anhydrous sodium sulfate, then filtered through a 0.22 μm filter membrane and diluted 40 times with n-hexane before being injected. The internal standard used was n-tridecane (HPLC grade, Sigma-Aldrich, Germany). The GC-MS conditions were as follows: 1 mL of the sample solution was placed in an automatic injection vial, with an injection volume set to 10 μL. The chromatography column used was an HP-5MS (30 m×0.25 mm, 0.25 μm) elastic quartz capillary column (30 m×0.25 mm, 0.25 μm). The temperature program was as follows: column temperature set to 50°C (hold for 1 min), then ramped at 1°C/min to 75°C, held for 1 min, ramped at 6°C/min to 120°C, hold for 1 min, ramped at 1°C/min to 135°C, held for 1 min, then ramped at 15°C/min to 200°C and held for 5 min. Helium was used as the carrier gas, with a flow rate of 1.0 mL/min, and a split flow rate of 3 mL/min. The pressure was set to 7.6522 psi, and the injection port temperature was 250°C. The ion source used was electron impact (EI), with an ion source temperature of 230°C and a quadrupole temperature of 150°C (maximum 200°C), electron energy set at 70 eV, interface temperature at 280°C, and the mass scan range was 50–550 amu (Jingxuan et al., 2018). In this study, three methods were employed for the qualitative analysis of the components, including the calculation of retention index (RI) values, comparison with RI values reported in the literature, and the retrieval and matching of collected mass spectra against the NIST library to identify volatile components in the samples. Additionally, the content of each component was analyzed using the internal standard method.

$$RI = 100 \times n + \frac{\log t_R(x) - \log t_R(n)}{\log t_R(n+1) - \log t_R(n)}$$

tR(x) represents the retention time of the analyte, tR(n) is the retention time of the n-alkane with n carbon atoms, and tR(n+m) is the retention time of the n-alkane with (n+1) carbon atoms.

2.6 Establishment of fingerprint map

Fingerprint map technology refers to the chromatographic or spectroscopic maps obtained through appropriate processing of complex substances, followed by analysis using certain techniques (chromatography, spectroscopy). These maps reflect the chemical characteristics of the substances and are primarily used to evaluate the authenticity, quality, and stability of samples. Establishing a fingerprint map for the volatile components of *Z. armatum* is of significant importance for quality control, authenticity identification, and other aspects. The GC-MS mass spectra were analyzed using Agilent OpenLab CDS software. A fingerprint map was established for seven batches of *Z. armatum* samples using the "Traditional Chinese Medicine Chromatographic Fingerprint Similarity Evaluation System (2012 edition)." A reference map was generated using the median method, with a time window width of 0.1. After multi-point calibration and automatic matching, the volatile component fingerprint map of *Z. armatum* was obtained.

2.7 The attraction-avoidance experiment of *Z. armatum* essential oil on *T. castaneum*

The attraction-avoidance experiment on *T. castaneum* (male and female) was conducted using the *Z. armatum* essential oil obtained from previous experiments. The experiment followed the method described by Jilani et al (Jilani and Saxena, 1990), with some modifications. The specific procedure is as follows: First, preliminary experiments were conducted using four solvents: DMSO, acetone, methanol, and ethanol, to determine ethanol as the solvent for the essential oil. Then, several 4–7 day-old adult

beetles were selected and kept in a wheat flour incubator for 24 hours. Filter paper (9 cm in diameter) was placed at the bottom of a 9 cm diameter petri dish, and the paper was divided into two halves, completely covering the bottom of the dish with a clear cutting line in the middle.

The *Z. armatum* essential oil was diluted with 75% ethanol to prepare solutions with volume fractions of 1%, 3%, and 5%. Using a pipette, 300 μL of the *Z. armatum* essential oil solution was evenly spread on the filter paper on the right side of the petri dish, and left to stand for thirty minutes to allow the solvent to evaporate. Ten healthy male and ten healthy female *T. castaneum* adults (7 days post-eclosion) were selected and placed in a petri dish. The chosen beetles displayed robust body condition, high mobility, and quick responses to stimuli (e.g., light and vibration). The petri dish was then placed in an incubator at room temperature and away from light. Every 12 hours, the number of *T. castaneum* beetles on the left and right sides of the petri dish was recorded, and the avoidance rate was calculated. The negative control was an ethanol solution with the same volume. All experiments were repeated three times. The avoidance rate was calculated using the following formula:

$$\text{Avoidance rate } (\%) = \frac{n1 - n2}{n1} \times 100\,\%$$

Where n1 is the number of insects placed in the petri dish, and n2 is the number of insects observed on the filter paper coated with the essential oil solution.

2.8 The antifungal experiment of *Z. armatum* essential oil against *C. cassiicola*

The growth inhibition experiment on *C. cassiicola* was conducted using the *Z. armatum* essential oil obtained in previous experiments. The *Z. armatum* essential oil was diluted with a 2.5% dimethyl sulfoxide (DMSO, analytical grade, Arabidopsis Biotechnology Co., Ltd., Chongqing) solution to concentrations of 0.5%, 0.1%, and 0.05%. Using a pipette, 5 mL of the solution was added to 25 mL of PDA medium, thoroughly mixed to ensure uniformity. The 30 mL mixture was evenly poured into three Petri dishes. After the medium solidified, the *C. cassiicola* strain, obtained through isolation and purification, was inoculated. The colony diameter was observed and recorded every 24 hours (Na et al., 2017). The negative control was a 2.5% DMSO solution, and the blank control was distilled water.

2.9 Data processing

The data were analyzed using one-way ANOVA in SPSS 22 software. The volatile component fingerprint of *Z. armatum* was established using the "Traditional Chinese Medicine Chromatographic Fingerprint Similarity Evaluation System (2012 version)". Principal component analysis (PCA) was performed based on the content of each component in the essential oil. Correlation heatmaps were generated using the OmicShare tool (https://www.omicshare.com/), and all other figures were created with Origin Pro 2022.

3 Results and analysis

3.1 Morphological changes in the fruits of *Z. armatum* at different harvesting periods

Photographs of *Z. armatum* fruits at different harvesting periods were taken under a stereomicroscope, clearly revealing the morphological changes in the fruits (as shown in Figure 2). In the early stages, the fruits exhibit a bright green exterior with

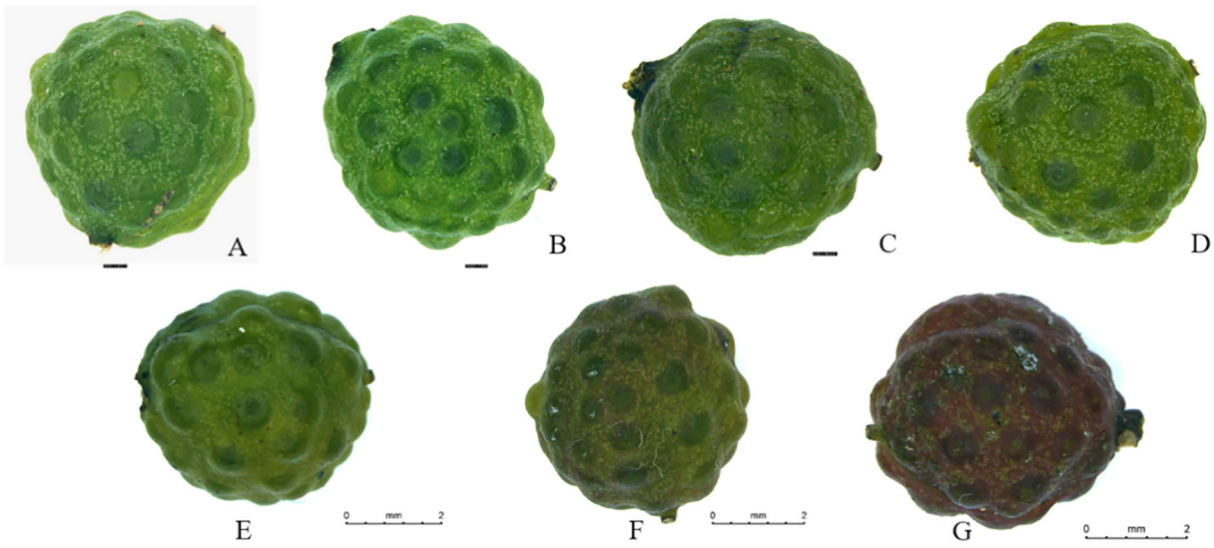

FIGURE 2
Morphology of *Z. armatum* fruits at different harvest periods [**(A-G)**, t1-t7 periods respectively].

slightly raised oil glands. As the growth and development process progresses, the color gradually deepens, and the peel turns yellowish-green with more prominent oil glands. By the t7 period, the fruits have transitioned from yellowish-green to red, displaying a more oily sheen on the surface, indicating that the fruits are fully mature at this stage.

3.2 Analysis of volatile components

The volatile components in *Z. armatum* essential oil were analyzed by GC-MS. For statistical analysis, we selected volatile compounds meeting the following criteria: (1) concentration ≥2 mg/mL and (2) match confidence >95% against the NIST database. Through this approach, we initially identified 26 volatile constituents. The compounds are arranged in order of their elution sequence. As shown in Table 1, the relative content of various components varied across different growth stages. Linalool (399.92–529.48 mg/mL), D-Limonene (126.94–200.14 mg/mL), and Sabinene (71.26–140.64 mg/mL) were the three most abundant volatile components in the essential oil of *Z. armatum* pericarp, followed by β-Myrcene (16.42–29.67 mg/mL), Nerolidol (3.18–15.07 mg/mL), and Terpinen-4-ol (6.59–13.24 mg/mL). These volatile compounds are the primary components of *Z. armatum* essential oil and contribute to its rich herbal, piney, and fresh aroma (Xiya et al., 2022). Among the three main volatile components, the relative content variations of Sabinene and D-Limonene closely mirrored the overall changes in the essential oil yield. Sabinene reached its minimum relative content of 71.26 mg/mL at the t5 stage and its maximum of 140.64 mg/mL at the t7 (September 28) stage. Similarly, D-Limonene showed a minimum relative content of 126.94 mg/mL at the t5 stage and a maximum of 200.14 mg/mL at the t7 stage, though there was no significant difference compared to the t2 stage. In contrast, Linalool had the lowest relative content of 399.92 mg/mL at the t1 stage and the highest of 529.48 mg/mL at the t5 stage.

Other volatile components with lower concentrations generally show a pattern similar to D-Limonene and Sabinene, decreasing and then increasing as the developmental stages progress, exhibiting a "concave" shape. These include α-Pinene, β-Myrcene, Terpinen-4-ol, Linalyl acetate, etc. Some volatile components, such as α-Phellandrene, β-Ocimene, and γ-Terpinene, show little variation throughout the entire growth period. Overall, the content of volatile oil and the main aromatic compounds in the fruit peel of *Z. armatum* accumulate most abundantly in August, making it the optimal time for harvesting for further processing and utilization.

3.3 Establishment of the volatile component fingerprint

The "Chinese Medicine Chromatographic Fingerprint Characteristic Map Similarity Evaluation System (2012 version)" was used to establish fingerprint maps for *Z. armatum* at seven different maturity stages. The shared fingerprint map for the seven stages was matched, and the relative peak areas of the shared fingerprint map were analyzed.

The similarity between the samples from different periods is relatively low between t5 and t2, and between t5 and t7, with similarities of 0.966 and 0.964, respectively (sample similarity comparisons are shown in Table 2). This indicates that the volatile components of t5 differ slightly from those of the other two periods. Overall, the similarity between the seven samples is above 0.96, suggesting that the volatile components of *Z. armatum* from different periods exhibit good consistency.

The fingerprint spectrum is shown in Figure 3. The relative peak area of the fingerprint spectrum represents the variation of target substances from t1 to t7. By comparing with the mass spectrum, 15 common mass spectrum peaks with relative peak areas were identified. As shown in Figure 4, the relative peak area of Linalool is 11.79%, indicating that its variation is the smallest during the fruit's growth and development process. D-Limonene and β-Ocimene also show relatively small changes. In contrast, the relative peak area of Nerolidol is 81.97%, showing the largest variation during the fruit's growth and development. Following Nerolidol is Terpinolene. The significant changes in these two components, which have strong citrus aromas, may be one of the reasons for the large flavor differences observed in *Z. armatum* at different maturity stages.

3.4 Principal component analysis

To preliminarily understand the differences and similarities of volatile compounds in *Z. armatum* at different harvest stages, the PCA analysis of the volatile components is shown in Figure 5. The first principal component (PC1) explains 74.2% of the variance, while the second principal component (PC2) explains 11.6%. In the Figures 5, samples t1, t2, t6, and t7 cluster together and are distributed on the negative half of PC1, while samples t3, t4, and t5 cluster on the positive half of PC1. This suggests that the volatile oil components of *Z. armatum* during t1 (May 26), t2 (June 16), t6 (September 9), and t7 (September 28) are similar, with significant differences compared to those at t3 (July 3), t4 (July 18), and t5 (August 4). This indicates that the volatile components of the pepper peel continuously change in the early stages of maturity and significantly differ from other growth stages. As the fruit matures, the accumulation of volatile components gradually slows down and tends to stabilize.

3.5 Analysis of insect repellent experiment results

The results of the repellent experiment with *Z. armatum* EO against *T. castaneum* are presented in Figure 6 and Table 3. As the treatment time increased, the repellent rate of the essential oil at different concentrations significantly decreased. The highest repellent rate of 100% at 12 hours post-treatment dropped to a maximum of 88% at 36 hours post-treatment, with a significant

10.3389/fpls.2025.1603963

TABLE 1 Volatile content at different harvest times.

Compound	RI[a]	CAS	Compound content (mg/ml)							Significance level
			t1	t2	t3	t4	t5	t6	t7	P-value
α-Pinene	917	80-56-8	8.56636288	9.68013504	5.08812672	6.45506632	4.09436612	8.06151152	10.72558572	*P<0.01*
Sabinene	970	3387-41-5	119.563481	125.9186286	77.48707836	92.6637054	71.2609966	117.2219146	140.6438818	*P<0.01*
β-Myrcene	994	123-35-3	26.31376088	28.77508788	18.47107412	21.18433656	16.41665564	26.36525388	29.67266176	*0.22*
α-Phellandrene	1004	99-83-2	4.72410976	4.57629132	3.47297924	3.27007232	2.37972444	4.628221	4.61221724	*P<0.01*
D-Limonene	1020	5989-27-5	185.8556566	198.325901	147.9515164	159.6444335	126.9446598	188.1898186	200.1371184	*P<0.01*
β-Ocimene	1034	13877-91-3	9.11552192	9.24845536	6.75645952	7.055808	5.5082226	9.67103252	9.68026292	*P<0.01*
γ-Terpinene	1040	99-85-4	9.227553	9.32074512	6.48201852	7.12339924	6.34593132	9.52492348	10.25516676	*P<0.01*
Terpinolene	1064	586-62-9	4.09290364	4.74538744	2.13091712	2.79945372	2.54815428	3.78787432	4.67278668	*0.106*
Linalool	1087	78-70-6	399.9164031	401.1676404	451.2484544	471.042912	529.4837364	409.1016716	414.3012924	*P<0.01*
Terpinen-4-ol	1170	562-74-3	12.47652984	8.72399972	6.5909376	7.10201308	10.91187824	12.69601744	13.243583	*P<0.01*
α-Terpineol	1187	98-55-5	4.94793692	-	-	-	3.87853496	8.31836416	-	*P<0.01*
2-Penten-4-yn-1-ol	824	5557-88-0	0.12338144	-	-	-	-	-	-	*P<0.01*
Linalyl acetate	1290	115-95-7	8.853537	7.71461584	5.12503416	4.950635	6.58939408	8.74490676	10.2155162	*0.022*
Isobornyl acetate	1280	125-12-2	0.29128196	-	-	-	-	0.5852336	-	*P<0.01*
Nerylacetate	1361	141-12-8	0.15263684	-	-	-	-	-	0.40700808	*P<0.01*
β-elemene	1390	515-13-9	2.30736004	1.51454716	2.62379924	2.12108488	2.25563448	2.258364	1.947868	*0.05*
Caryophyllene	1411	17627-40-6	4.71252376	3.72933348	6.96463416	5.82680692	6.144992	5.2360978	4.61680972	*P<0.01*
Humulene	1434	6753-98-6	2.86468724	2.88202008	4.18502872	3.49848908	3.88182936	3.39041792	2.76497592	*P<0.01*
Germacrene D	1472	23986-74-5	7.37283916	4.70815148	11.9498594	9.1824182	10.28684032	8.48448824	6.78569596	*P<0.01*
germacrene B	1417	15423-57-1	3.38432372	-	-	-	-	-	3.10289604	*P<0.01*
Nerolidol	1557	7212-44-4	3.4929832	4.22766696	15.0714184	3.95416096	11.15071252	8.43784564	3.1782044	*P<0.01*
Geranyl phenylacetate	1432	102-22-7	0.0381592	-	-	-	-	-	0.37216232	*P<0.01*
α-thujene	940	2867-05-2	2.22437176	4.55050472	-	3.4911792	2.290896	-	-	*P<0.01*
α-Terpinene	1012	99-86-5	3.55909864	3.65208396	2.91572732	3.28140164	2.90115724	3.4890124	4.13389516	*P<0.01*
2-Carene	1031	554-61-0	4.12228368	1.83899256	-	-	-	5.0391162	-	*P<0.01*
bicyclogermacrene	1482	24703-35-3	-	-	5.43166316	4.22497996	4.58936464	-	-	*P<0.01*

difference compared to the control group. At 36 hours post-treatment, the 5% concentration of *Z. armatum* EO still maintained a repellent rate of nearly 80% against *T. castaneum*. The 3% concentration of *Z. armatum* EO showed relatively high repellent activity (65%-100%) at 12 hours and 24 hours post-treatment, but the activity was lost after 36 hours. The 1% concentration of *Z. armatum* EO showed significant repellent effects against *T. castaneum* only within the first 12 hours post-treatment.

The EO repellent experiment data were normalized and a clustering heatmap was generated, as shown in Figure 6. The *Z. armatum* EOs from different maturation stages were grouped into three categories: t1 (May 26), t2 (June 16), t6 (September 9) and t7 (September 28)were clustered into one group; t3 (July 3) and t5 (August 4), into another group; and t4 (July 18) was grouped separately. The clustering results are consistent with the previous analysis of volatile components. This indicates that the primary repellent mechanism of the essential oil relies on fumigant toxicity

10.3389/fpls.2025.1603963

TABLE 2 Comparison of similarity of *Z. armatum* fingerprints at different maturity stages.

Similarity	t1	t2	t3	t4	t5	t6	t7	Reference fingerprint map
t1	1	0.999	0.99	0.993	0.975	1	0.999	0.998
t2	0.999	1	0.984	0.988	0.966	0.999	1	0.995
t3	0.99	0.984	1	1	0.996	0.989	0.982	0.997
t4	0.993	0.988	1	1	0.994	0.992	0.987	0.998
t5	0.975	0.966	0.996	0.994	1	0.973	0.964	0.987
t6	1	0.999	0.989	0.992	0.973	1	0.999	0.998
t7	0.999	1	0.982	0.987	0.964	0.999	1	0.994
Reference fingerprint map	0.998	0.995	0.997	0.998	0.987	0.998	0.994	1

rather than contact toxicity, providing a reference for the development of insect repellent formulations based on *Z. armatum* essential oil (Table 4).

3.6 Analysis of antifungal experiment results

The essential oil of *Z. armatum* from different maturity stages exhibited significant inhibitory effects on *C. cassiicola*, with the inhibitory effect varying significantly at different concentrations of the essential oil solution. The 0.5% concentration showed the strongest antifungal effect. After 3 days of culture, the colony diameter in the negative control group was 64.1%-70.51% larger compared to the 0.5% group, 55.13%-62.82% larger compared to the 0.1% group, and 8.97%-19.23% larger compared to the 0.05% group (Figure 7). The increase in essential oil concentration significantly enhanced the antifungal effect against *C. cassiicola*. At 0.5% and 0.1% concentrations, only the essential oil from the t4 stage showed significant differences in antifungal effect compared to the other stages.

After normalizing the antifungal data of the EOs, a cluster analysis was performed, and the results are shown in Figure 8. The samples from t1 (May 26), t2 (June 16), t3 (July 3), and t5 (August 4) were grouped together, while t4 (July 18) was grouped separately, and t6 (September 9) and t7 (September 28) were grouped together. These results differ from the previous clustering analysis, further indicating that the antifungal properties of the essential oil

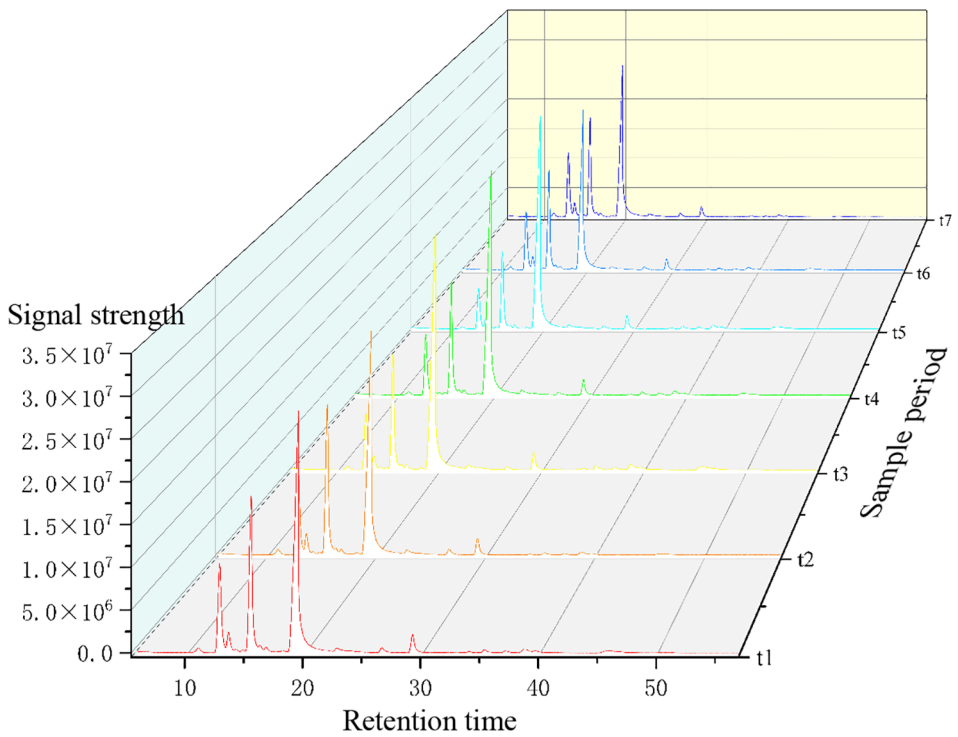

FIGURE 3
Fingerprint of *Z. armatum* volatile components.

10.3389/fpls.2025.1603963

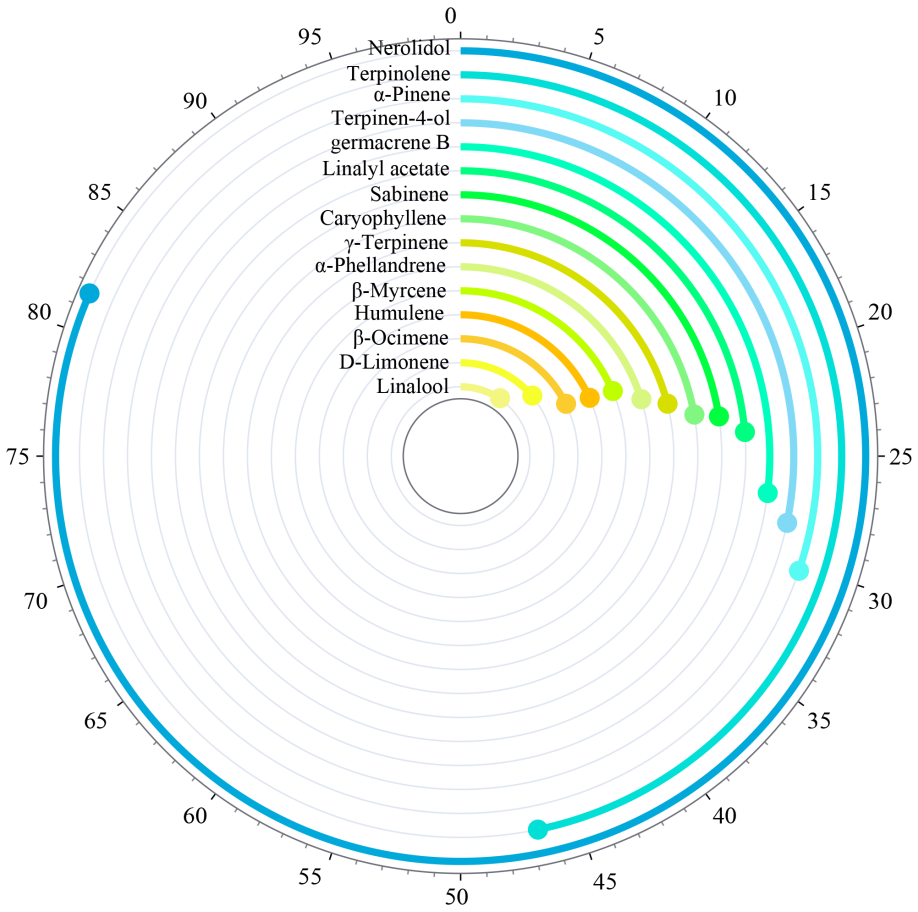

FIGURE 4
Relative peak area of fingerprint of volatile components.

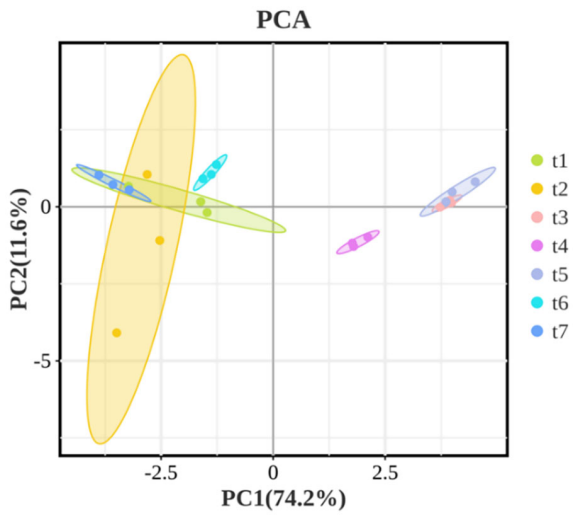

FIGURE 5
PCA based on volatile components.

are not solely influenced by the volatile components or any single component, but rather by the combined effect of multiple components.

4 Discussion

The production, composition, and content of secondary metabolites in plants are influenced by various conditions. Based on market data of volatile oil compounds from Chinese *Z. armatum*, the projected demand for 2025–2030 is estimated at 40,000-47,500 thousand metric tons, with China's market share accounting for 15%-18% of the global market. The primary growth drivers stem from expanding applications in: Food and Flavoring Industry, Cosmetics and Personal Care, Pharmaceuticals and Traditional Chinese Medicine, Green Pesticides and so on (Research Report on Monitoring and Analysis of Chinese Zanthoxylum Essential Oil Market (2025 -2030), 2025). For economically important plants with commercial value, optimizing planting time and harvest periods can help obtain commercial

10.3389/fpls.2025.1603963

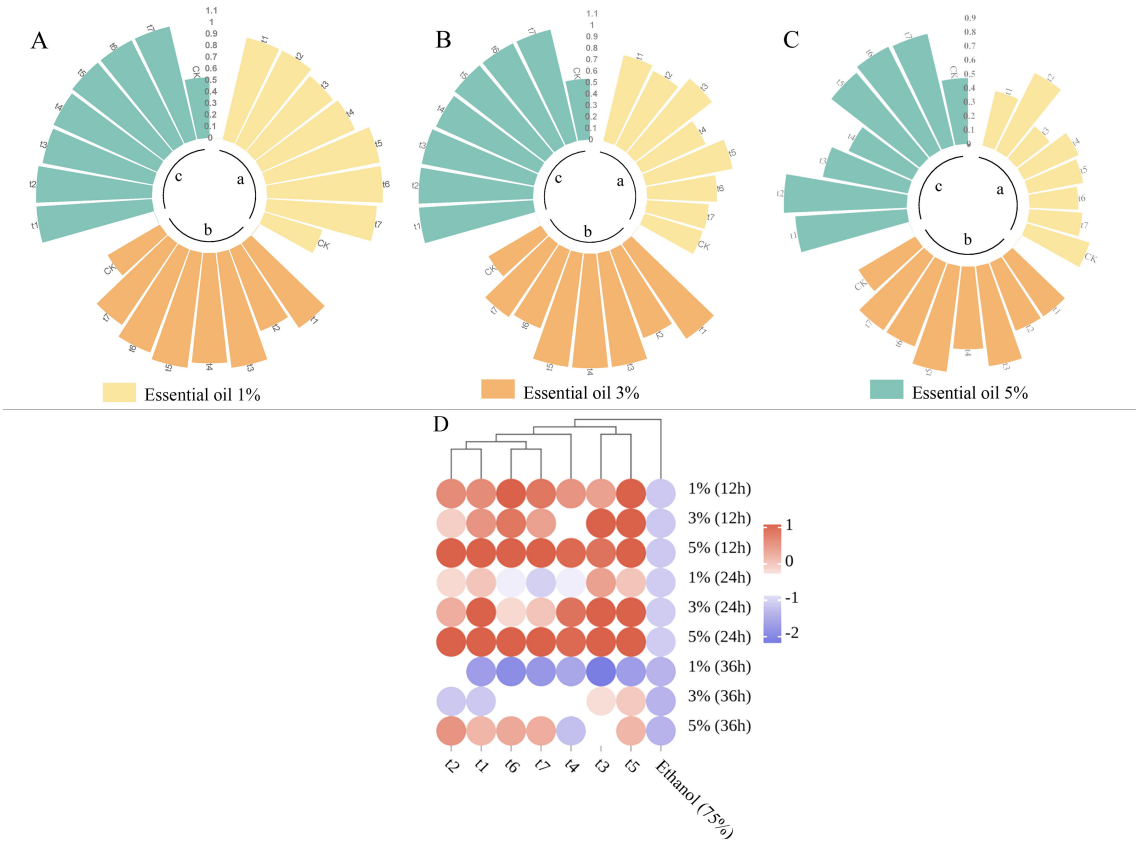

FIGURE 6
Repellent rates and clustering heatmap of *Z. armatum* essential oil at different concentrations against *T. castaneum* after 12, 24, and 36 hours of application. [**(A)** Repellent rates at 12 hours; **(B)** Repellent rates at 24 hours; **(C)** Repellent rates at 36 hours; **(D)** Clustering heatmap].

TABLE 3 The repellent rate of different concentrations of *Z. armatum* essential oil to Tribolium castaneum after 12, 24 and 36 hours of application.

Time	Pharmaceuticals	Concentration	Sample sampling period						
			t1	t2	t3	t4	t5	t6	t7
12h	Essential oil	1%	0.9	0.9	0.85	0.88	1	1	0.95
		3%	0.88	0.75	1	0.95	1	0.95	0.85
		5%	1	1	0.97	0.98	1	1	1
	Ethanol (CK)	60%	0.52						
24h	Essential oil	1%	0.77	0.73	0.85	0.61	0.77	0.61	0.54
		3%	1	0.82	1	1	1	0.73	0.77
		5%	1	1	1	0.98	1	1	1
	Ethanol (CK)	60%	0.53						
36h	Essential oil	1%	0.40	0.62	0.30	0.43	0.40	0.35	0.38
		3%	0.52	0.52	0.72	0.59	0.76	0.64	0.64
		5%	0.80	0.88	0.62	0.50	0.80	0.83	0.82
	Ethanol (CK)	60%	0.47						

(The data is the average of three experiments).

10.3389/fpls.2025.1603963

TABLE 4 Main effects and interaction effects results.

Factors	F-value	p-value	Significant effect (α=0.05)	Effect Size (η^2)
Time	45.72	<0.001	Significant	0.38
Concentration	28.15	<0.001	Significant	0.25
Period	5.64	<0.001	Significant	0.12
Time × Concentration	4.33	0.002	Significant	0.09
Time × Period	1.98	0.061	Not significant	-
Concentration × Period	1.12	0.341	Not significant	-
The third-order interaction	0.87	0.512	Not significant	-

products that better meet market demands (A. Cristina et al., 2008). The volatile components of *Z. armatum* are primarily stored in the fruit peel, with its linalool and d-limonene content being influenced by precipitation-related climatic factors (Qianqian et al., 2024). Therefore, we analyzed the volatile oil components and their content in the fruit peel of *Z. armatum* from different periods in Nanchong, Sichuan Province. This study aimed to explore the accumulation pattern of volatile oil substances in *Z. armatum* at different stages of growth and development by measuring the volatile components and their content. We conducted GC-MS analysis of the volatile components in *Z. armatum* essential oil using an internal standard method, preliminarily identifying and quantifying 28 volatile constituents in relative content. However, since reference standards were not employed for verification, the experimental results have certain limitations. The results show that the accumulation of volatile components occurs before the t5 stage. Studies have shown that in the early developmental stages, the stimulating and aromatic substances produced by *Zanthoxylum bungeanum* are mainly stored in the leaves and gradually transfer to the fruit peel in the later developmental stages (Lei et al., 2019). Therefore, the volatile components in the fruit may accumulate in the later stages of development. *Z. armatum* harvested in July and August has a higher content of volatile components compared to other periods, making it the preferred choice for processing and

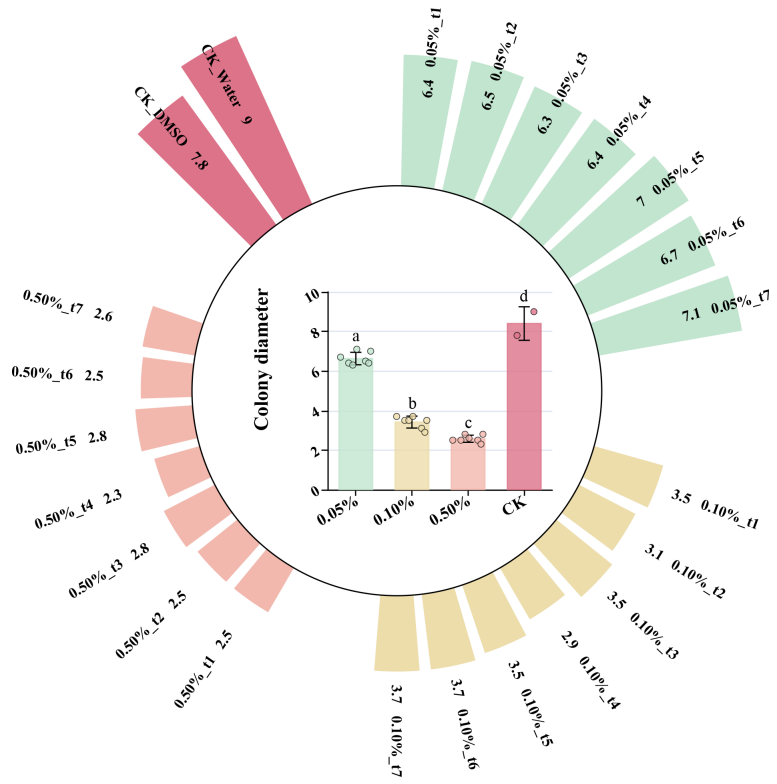

FIGURE 7
After three days of culture, the colony diameter of *C. cassiicola* was affected by different concentrations of *Z. armatum* essential oil solution.

10.3389/fpls.2025.1603963

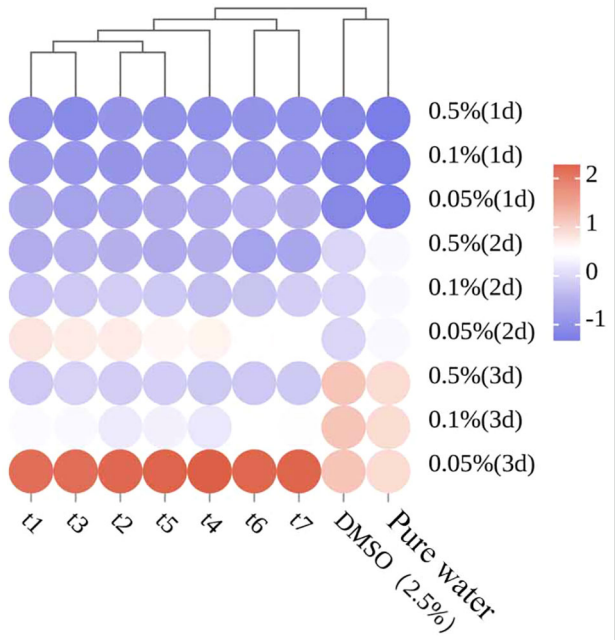

FIGURE 8
Cluster thermogram analysis of bacteriostatic experiment.

making other products. The principal component analysis results show that there are significant differences in the volatile components of the pepper fruits between the t3 (July 3), t4 (July 18), t5 (August 4) stages and the t1 (May 26), t2 (June 16), t6 (September 9), t7 (September 28) stages. In the early stages of fruit maturation, plants exhibit vigorous metabolic activity, producing a significant amount of monoterpenes (Telci et al., 2009) such as α-Pinene, Sabinene, β-Myrcene, α-Phellandrene, and D-Limonene. As the fruits of *Z. armatum* mature, the content of more structurally complex compounds, such as alcohols (Kamel et al., 2007) and esters (Moghaddam et al., 2015), increases. For instance, compounds like Linalyl acetate, Terpinen-4-ol, and α-Terpineol are relatively abundant during the fruit's maturation period. The significantly lower oil yield from dried *Z. armatum* pericarps during the mid-maturity stage may also be related to the physiological metabolism of the plant. In the early stage, low-molecular-weight volatile compounds accumulate rapidly. During the mid-stage, high-molecular-weight lipid compounds are generated. By the fully mature stage, the content of volatile alcohols and esters in the fruits increases.

Z. armatum EO has a strong repellent effect on *T. castaneum*, and the effect changes in a gradient with concentration, indicating that the repellent effect is positively correlated with the essential oil content to some extent. Low concentrations of *Z. armatum* EO solution can also produce a strong repellent effect on *T. castaneum* at the early stage of application. The volatile compounds in the EO, such as monoterpenes, usually have a strong odor, which may stimulate *T. castaneum*, causing it to exhibit avoidance behavior. Furthermore, because the odor threshold of various volatile components is relatively low, even at low concentrations, these compounds can induce a repellent response in *T. castaneum* (Daokui, 2023). Studies have shown that substances like α-pinene and laurene can induce a strong repellent effect on *T. castaneum* (Kim et al., 2010; Maurya et al., 2018). This all demonstrates that the volatile components of *Z. armatum* EO have a good repellent effect on *T. castaneum*. However, the effect decreases as the active ingredients volatilize. Preventing the evaporation of the essential oil could significantly extend its repellent effectiveness. Unlike previous studies, no mortality of *T. castaneum* adults was observed in this experiment. In previous experiments, *Z. armatum* essential oil solutions applied to the abdomen of *T. castaneum* also did not result in insect death within 48 hours. This suggests that the low content of Terpinen-4-ol and the absence of decanal, a compound with strong insecticidal activity, may be the reasons for the lack of mortality in the tested insects (Yang et al., 2019). Another possible reason is that *T. castaneum* perceives chemical signals in the surrounding environment through sensory organs such as its antennae (Feng et al., 2014). The volatile chemicals in the EO may only interact with the receptors on the insect's sensory organs (Thomas S. et al., 2012), triggering a repellent response, but not enough to cause death. The specific activity and mechanism need to be determined through more detailed experiments and studies.

In the antimicrobial experiment, the baseline antifungal activity of *Z. armatum* EOs was determined by comparing the antifungal activities of EOs extracted at different sampling periods and against the negative control. However, since no positive control was included, the practical application value of the EOs could not be fully validated. The results showed that *Z. armatum* EOs from different maturity stages exhibited significant inhibitory effects on *C. cassiicola*, and the antimicrobial activity increased with higher EO concentrations. A study by Nirmala et al. showed that methanol extracts of the peel, seeds, and bark of *Z. armatum* also exhibited antifungal activity against microorganisms such as *Bacillus subtilis*, *Enterococcus faecalis*, *Staphylococcus aureus*, and *Staphylococcus epidermidis* (Phuyal et al., 2020). Since the best antifungal effect was observed during the t4 period, the EO extracted from *Z. armatum* harvested in mid-July showed more prominent antifungal activity. Previous studies have shown that the antifungal effect is positively correlated with the content of linalool (Wei et al., 2023). In this study, the t4 period, which exhibited the best antifungal effect, was not the period with the highest linalool content. However, by comparing samples from other periods, it was found that although the relative contents of various compounds in the t4 period were not the highest, they still ranked among the top. Examples include Linalool, Germacrene D, Nerolidol, (+)-Citronellal, and Bicyclogermacrene. These compounds exhibit varying degrees of antibacterial and antifungal activity (M J. et al., 2009; Ricardo et al., 2011; Xiuming et al., 2023). We hypothesize that the specific compositional ratio of components at t4 may lead to synergistic enhancement (e.g., through multi-target disruption of cell membranes), whereas the isolated increase in linalool at t5, accompanied by a decline in other constituents, could result in reduced overall bioactivity. However, this conclusion requires further experimental validation. Studies on the essential oil of *Tetraclinis articulata* have shown that the combination of antibiotics with extracts from this species is more effective, exhibiting 100% synergistic or partial synergistic effects against the tested bacteria (Djouahri et al., 2014). Therefore, the antifungal effects

of different chemical components are inconsistent. Investigating the synergistic and antagonistic interactions between different chemical components in terms of antifungal activity can serve as a new direction for future research.

In the insect repellent and antifungal experiments, different concentrations of *Z. armatum* essential oil exhibited insecticidal/antifungal activity against *T. castaneum* and *C. cassiicola*, with a gradient relationship as the concentration increased. *Z. armatum* essential oil is characterized by high levels of oxygenated monoterpenes and monoterpene hydrocarbons. These monoterpenes are common components of essential oils and are used as fragrances and flavorings in cosmetics, perfumes, pharmaceuticals, and food products (Domenico et al., 2005). The EO used in the *in vitro* antifungal tests contains a significant number of monoterpenes. The main components in *Z. armatum* EO, such as Linalool, D-Limonene, and Sabinene, have been proven to exhibit strong insecticidal/antifungal properties (Djenane, 2015; Xue et al., 2020). This may be the basis for the strong insecticidal and antifungal activities of *Z. armatum* EO. Regarding the mechanism of action of the EO, it may involve interactions between enzymes and membrane proteins. In some cases, the active compounds in the EO can penetrate the lipid bilayer of the cell membrane, increasing the cell's permeability and leading to the leakage of important cellular contents (Alvarez-Martinez et al., 2021; Maurya et al., 2022). The antimicrobial activity data herein provide a foundation for future mechanistic studies, though specific targets (e.g., membrane disruption/enzyme inhibition) require validation via component-specific assays. *Z. armatum* EO, rich in these components, can become a key part of natural plant-based insecticidal and antifungal agents. Additionally, the *Z. armatum* EO from the t4 period shows superior antifungal effects. For the development of antifungal drugs based on *Z. armatum* EO, it is recommended to harvest the fruits in mid-July.

5 Conclusion

The different growth and development stages are important factors influencing the accumulation of secondary metabolites in *Z. armatum* fruits. This study performed GC-MS analysis on the *Z. armatum* EOs from Nanchong City, Sichuan Province, and conducted insect-repellent and antifungal experiments using EOs from different stages. The GC-MS results showed that the accumulation of volatile compounds occurred before the t5 stage, as low-molecular-weight monoterpenes were rapidly generated in the early fruit ripening stages, while alcohols and esters accumulated in later stages. The EO content and its major fragrance components accumulated richly in July and August. Both insect-repellent and antimicrobial experimental results indicated that the EO from the t4 stage had higher insect-repellent and antifungal activity. Therefore, the insect-repellent and antimicrobial effects of the EOs may result from the synergistic or antagonistic interactions among various compounds. This study provides a reference for utilizing *Z. armatum*'s different commercial values based on harvest periods and offers a research direction for using plant EOs as natural insect-repellent/antimicrobial agents. Future research can delve into analyzing the interaction mechanisms between different compounds in the essential oil and the underlying mechanisms of its insect-repellent and antifungal activities.

Data availability statement

The datasets presented in this study can be found in online repositories. The names of the repository/repositories and accession number(s) can be found in the article/supplementary material.

Author contributions

YP: Data curation, Formal Analysis, Investigation, Methodology, Project administration, Resources, Writing – original draft. DX: Conceptualization, Methodology, Supervision, Writing – review & editing. WL: Data curation, Formal Analysis, Investigation, Methodology, Software, Writing – original draft. QQ: Data curation, Investigation, Software, Writing – review & editing. JW: Investigation, Software, Writing – review & editing. TG: Investigation, Resources, Writing – review & editing. ZZ: Conceptualization, Supervision, Writing – review & editing.

Funding

The author(s) declare that financial support was received for the research and/or publication of this article. This research was supported by the Fundamental Research Funds of China West Normal University (20A007, 20E051, 21E040 and 22kA011).

Conflict of interest

The authors declare that the research was conducted in the absence of any commercial or financial relationships that could be construed as a potential conflict of interest.

Generative AI statement

The author(s) declare that no Generative AI was used in the creation of this manuscript.

Publisher's note

References

ACFSMC (2009). ""Determination of pepper essential oils content"," in *GB/T 17527-2009* (China Standards Press, Beijing).

A. Cristina, F., Jose, B., Luis, P., and Johannes, J. C. (2008). Factors affecting secondary metabolite production in plants: volatile components and essential oils. *Flavour Frag. J.* 23, 213–226. doi: 10.1002/ffj.1875

Alvarez-Martinez, F. J., Barrajon-Catalan, E., Herranz-Lopez, M., and Micol, V. (2021). Antibacterial plant compounds, extracts and essential oils: an updated review on their effects and putative mechanisms of action. *Phytomedicine* 90, 153626. doi: 10.1016/j.phymed.2021.153626

Bakkali, F., Averbeck, S., Averbeck, D., and Idaomar, M. (2008). Biological effects of essential oils – a review. *Food. Chem. Toxicol.* 46, 446–475. doi: 10.1016/j.fct.2007.09.106

Burt, S. (2004). Essential oils: their antibacterial properties and potential applications in foods—a review. *Int. J. Food Microbiol.* 94, 223–253. doi: 10.1016/j.ijfoodmicro.2004.03.022

Campbell, J. F., Athanassiou, C. G., Hagstrum, D. W., and Zhu, K. Y. (2022). Tribolium castaneum: a model insect for fundamental and applied research. *Annu. Rev. Entomol.* 67, 347–365. doi: 10.1146/annurev-ento-080921-075157

Daokui, W. (2023). *Study on the insecticidal activity of two kinds of plant essential oils against tribolium castaneum herbst.* [Master's thesis] (Anhui Province: Anhui Agricultural University).

Di, Z., Xiaoxia, S., Maurizio, B., Xiaoou, W., Jiyong, S., Lei, Z., et al. (2021). A comparative overview on chili pepper (capsicum genus) and sichuan pepper (zanthoxylum genus): from pungent spices to pharma-foods. *Trends Food Sci. Technol.* 117, 148–162. doi: 10.1016/j.tifs.2021.03.004

Djenane, D. (2015). Chemical profile, antibacterial and antioxidant activity of *Algerian citrus* essential oils and their application in sardina pilchardus. *Foods* 4, 208–228. doi: 10.3390/foods4020208

Djouahri, A., Saka, B., Boudarene, L., Benseradj, F., Aberrane, S., Aitmoussa, S., et al. (2014). *In vitro* synergistic/antagonistic antibacterial and anti-inflammatory effect of various extracts/essential oil from cones of *tetraclinis articulata* (vahl) masters with antibiotic and anti-inflammatory agents. *Ind. Crop Prod.* 56, 60–66. doi: 10.1016/j.indcrop.2014.02.035

Domenico, T., Francesco, C., Maria, G. S., Vincenza, V., Mariateresa, C., et al. (2005). Mechanisms of antibacterial action of three monoterpenes. *Antimicrob. Agents. Chemother.* 49, 2474–2478. doi: 10.1128/AAC.49.6.2474

Feng, L., Kenneth F., H., Arthur G., A., and Nannan, L. (2014). Antennal olfactory sensilla responses to insect chemical repellents in the common bed bug. *J. Chem. Ecol.* 40, 522–533. doi: 10.1007/s10886-014-0435-z

Gao, W., and Hanbin, W. (2014). Analgesia synergism of essential oil from pericarp of *zanthoxylum schinifolium* and verapamil. *Evid.-Based Complement Altern. Med.* 2014, 505876. doi: 10.1155/2014/505876

Gutierrez, J., Barry-Ryan, C., and Bourke, P. (2009). Antimicrobial activity of plant essential oils using food model media: efficacy, synergistic potential and interactions with food components. *Food Microbiol.* 26, 142–150. doi: 10.1016/j.fm.2008.10.008

Hong, L., Jing, W., Qing, W., Anxiang, S., Mei, X., Qin, L., et al. (2017). Inhibitory effect of *zanthoxylum bungeanum* essential oil (zbeo) on escherichia coli and intestinal dysfunction. *Food Funct.* 8, 1569–1576. doi: 10.1039/c6fo01739h

J. D., L., and Roth, L. (1953). Composition of the odorous secretion of tribolium castaneum. *Biology* 46, 282–288. doi: 10.1093/AESA/46.2.281

Jilani, G., and Saxena, R. C. (1990). Repellent and feeding deterrent effects of turmeric oil, sweetflag oil, neem oil, and a neem-based insecticide against lesser grain borer (coleoptera: bostrychidae. *J. Economic Entomology* 83, 629–634. doi: 10.1093/jee/83.2.629

Jingxuan, K., Yuan, Q., Shanshan, L., Guanghui, S., Qingying, L., Hejun, W., et al. (2018). Establishment of gc-ms fingerprint based on essential oil components in zanthoxylum and application on hanyuan *zanthoxylum bungeanum*. *J. Chin. Cereals Oils Assoc.* 33, 116–126. doi: 10.3969/j.issn.1003-0174.2018.11.020

Kamel, M., Karim, H., Mouna Ben, T., Thouraya, C., Mohamed Elyes, K., and Brahim, M. (2007). Changes on essential oil composition of coriander (*coriandrum sativum* l.) Fruits during three stages of maturity. *Food Chem.* 102, 1131–1134. doi: 10.1016/j.foodchem.2006.06.046

Kim, S., Yoon, J., Jung, J., Ki-Bae, H., Young-Joon, A., and Hyung Wook, K. (2010). Toxicity and repellency of origanum essential oil and its components against *tribolium castaneum* (coleoptera: tenebrionidae) adults. *J. Asia-Pac. Entomol.* 13, 369–373. doi: 10.1016/j.aspen.2010.06.011

Lei, Z., Li, W., Xi, C., Wei, P., Yujie, L., Linying, Y., et al. (2019). Comparative studies on flavor substances of leaves and pericarps of *zanthoxylum bungeanum* maxim. At different harvest periods. *Trop. J. Pharm. Res.* 18, 279–286. doi: 10.4314/tjpr.v18i2.9

Maurya, A. K., Devi, R., Kumar, A., Koundal, R., Thakur, S., Sharma, A., et al. (2018). Chemical composition, cytotoxic and antibacterial activities of essential oils of cultivated clones ofjuniperus communis and wildjuniperus species. *Chem. Biodivers.* 15, e1800183. doi: 10.1002/cbdv.201800183

Maurya, A. K., Sharma, A., Mukhia, S., Rani, D., Kumar, A., Kumar, D., et al. (2022). Essential oil composition, *in vitro* biological activities and safety evaluation of cultivated hedychium spicatum seeds. *Indian J. Pharm. Sci.* 84, 783–790. doi: 10.36468/pharmaceutical-sciences.973

Moghaddam, M., Miran, S. N. K., Pirbalouti, A. G., Mehdizadeh, L., and Ghaderi, Y. (2015). Variation in essential oil composition and antioxidant activity of cumin (*cuminum cyminum* l.) Fruits during stages of maturity. *Ind. Crop Prod.* 70, 163–169. doi: 10.1016/j.indcrop.2015.03.031

Na, G., Yuping, Z., Qi, C., Qingyan, G., Jiao, J., Wei, W., et al. (2017). The preservative potential of *amomum tsaoko* essential oil against e. Coil, its antibaterial property and mode of action. *Food Control* 75, 236–245. doi: 10.1016/j.foodcont.2016.12.013

Phuyal, N., Jha, P. K., Raturi, P. P., and Rajbhandary, S. (2020). *In vitro* antibacterial activities of methanolic extracts of fruits, seeds, and bark of*zanthoxylum armatum* dc. *J. Trop. Med.* 2020, 1–7. doi: 10.1155/2020/2803063

Prakash, B., Singh, P., Mishra, P. K., and Dubey, N. K. (2012). Safety assessment of *zanthoxylum alatum* roxb. Essential oil, its antifungal, antiaflatoxin, antioxidant activity and efficacy as antimicrobial in preservation of piper nigrum l. Fruits. *Int. J. Food Microbiol.* 153, 183–191. doi: 10.1016/j.ijfoodmicro.2011.11.007

Qianqian, Q., Zhihang, Z., Yaqin, P., and Danping, X. (2024). Chemical composition variation in essential oil and their correlation with climate factors in chinese prickly ash peels (*zanthoxylum armatum* dc.) From different habitats. *Molecules* 29, 1343. doi: 10.3390/molecules29061343

Ravi Kant, U., and Gayatri, J. (2007). Evaluation of biological activities of piper nigrumoil against tribolium castaneum. *Bull. Insectol.* 60, 57–61.

Research report on monitoring and analysis of chinese zanthoxylum essential oil market, (2025-2030) (2025). *Research report on monitoring and analysis of chinese zanthoxylum essential oil market, (2025-2030)*. Available online at: https://max.book118.com/html/2025/0404/8002034041007050.shtm.

Ricardo, M. M., Luiz, C. A. B., Antonio, J. D., Cleber, J. S., Larissa, S. C., Nélio, J. A., et al. (2011). Chemical composition and antibacterial activity of essential oils from verbenaceae species: alternative sources of (e)-caryophyllene and germacrene-d. *Química Nova* 34, 1550–1555. doi: 10.1590/S0100-40422011000900013

Shenglan, L., Gang, Y., Shan, H., Bin, L., Aijun, L., and Jianquan, K. (2022). Chemical composition of *zanthoxylum schinifolium* siebold & zucc. Essential oil and evaluation of its antifungal activity and potential modes of action on malassezia restricta. *Ind. Crop Prod.* 180, 114698. doi: 10.1016/j.indcrop.2022.114698

Shun, D., Haibo, R., He, T., Bingxin, Z., Xiaoyuan, M., Liyang, Z., et al. (2019). Molecular basis of neurophysiological and antioxidant roles of sichuan pepper. *Biomed. Pharmacother.* 112, 108696. doi: 10.1016/j.biopha.2019.108696

Telci, I., Demirtas, I., and Sahin, A. (2009). Variation in plant properties and essential oil composition of sweet fennel (*foeniculum vulgare* mill.) Fruits during stages of maturity. *Ind. Crop Prod.* 30, 126–130. doi: 10.1016/j.indcrop.2009.02.010

Thomas S., M., Alban, M., Erika, P., Yves Le, C., and Wolfgang, R. (2012). Sensory reception of the primer pheromone ethyl oleate. *Naturwissenschaften.* 99, 421–425. doi: 10.1007/s00114-012-0909-1

Wei, L., Kongfa, Z., Fenglun, Z., Shikun, G., Yinjiang, H., Wei, N., et al. (2023). Chemical composition analysis and *in vitro* inhibition of helicobacter pylori in essential oil of zanthoxylum schinifolium from different producing areas. *Chin. Wild Plant Resour.* 42, 68–74. doi: 10.3969/j.issn.1006-9690.2023.10.012

Xinqi, D. (2023). *Integrated transcriptomic and un-targetedmetabolomics analysis the defenseresponse of mulberry against thepathogen fungi of mulberry ring rotdisease.* [Master's thesis] (Sichuan Province: West Normal University).

Xiuming, L., Qifang, W., Haosen, L., Xiaoyun, W., Ruimin, Z., Xiaoyu, Y., et al. (2023). Revealing the mechanisms for linalool antifungal activity against fusarium oxysporum and its efficient control of fusarium wilt in tomato plants. *Int. J. Mol. Sci.* 24, 458. doi: 10.3390/ijms24010458

Xiya, F., Hongwei, W., Zhirong, W., Pimiao, H., and Jianquan, K. (2022). Discrimination and characterization of the volatile organic compounds in eight kinds of huajiao with geographical indication of China using electronic nose, hs-gc-ims and hs-spme-gc–ms. *Food Chem.* 375, 131671. doi: 10.1016/j.foodchem.2021.131671

Xue, L., Jiaxin, C., Haiming, C., Qiuping, Z., Yaqi, H., Weijun, C., et al. (2020). Antibacterial activity and mechanism of linalool against *pseudomonas aeruginosa*. *Microb. Pathog.* 141, 103980. doi: 10.1016/j.micpath.2020.103980

Yang, W., Liting, Z., Yixi, F., Shanshan, G., Xue, P., Di, Z., et al. (2019). Insecticidal and repellent efficacy against stored-product insects of oxygenated monoterpenes and 2-dodecanone of the essential oil from *zanthoxylum planispinum* var. Dintanensis. *Environ. Sci. pollut. Res.* 26, 24988–24997. doi: 10.1007/s11356-019-05765-z

Zhen, W., Hong, L., Yong, Y., Yong, Z., and Dawei, T. (2013). Variation in the components and antioxidant activity of *citrus medica* l. Var. Sarcodactylis essential oils at different stages of maturity. *Ind. Crop Prod.* 46, 311–316. doi: 10.1016/j.indcrop.2013.02.015

frontiers | Frontiers in Plant Science

TYPE Original Research
PUBLISHED 14 August 2025
DOI 10.3389/fpls.2025.1642854

OPEN ACCESS

EDITED BY
Robin Joshi,
University of Pennsylvania, United States

REVIEWED BY
Rituraj Khound,
University of Nebraska-Lincoln, United States
Shruti Sharma,
University of Alabama, United States

*CORRESPONDENCE
Jianguo Li
jianli@scau.edu.cn
Jisen Zhang;
zjisen@126.com
Shaoquan Zheng
zsq333555@163.com

†These authors have contributed equally to this work

RECEIVED 07 June 2025
ACCEPTED 24 July 2025
PUBLISHED 14 August 2025

CITATION
Hu W, Zhang Q, Deng C, Xu Q, Jiang J, Chen X, Li J, Zhang J and Zheng S (2025) Construction of high-density bin genetic map and QTL mapping of fruit aroma in longan (*Dimocarpus longan* Lour.). *Front. Plant Sci.* 16:1642854. doi: 10.3389/fpls.2025.1642854

Construction of high-density bin genetic map and QTL mapping of fruit aroma in longan (*Dimocarpus longan* Lour.)

Wenshun Hu[1†], Qing Zhang[2†], Chaojun Deng[1], Qizhi Xu[1], Jimou Jiang[1], Xiuping Chen[1], Jianguo Li[3*], Jisen Zhang[2*] and Shaoquan Zheng[1*]

[1]Fruit Research Institute, Fujian Academy of Agricultural Sciences, Fujian Breeding Engineering Technology Research Center for Longan and Loquat, Fuzhou, China, [2]State Key Lab for Conservation and Utilization of Subtropical Agro-Biological Resources, College of Agriculture, Guangxi University, Nanning, China, [3]College of Horticulture, South China Agricultural University, Guangzhou, China

Aroma is a crucial factor influencing the flavor quality and economic value of longan fruits. This study employed a mapping population consisting of 98 F_1 progeny of 'Shixia × Xiangcui' (exhibiting broad segregation in fruit aroma trait) and their parents. We performed the SNP genotyping through whole-genome resequencing to construct a high-density linkage map, followed by QTL mapping and candidate gene screening for aroma trait. We obtained a total of 554.9 Gbp of sequencing data, with an average depth of approximately 15× for the parents and 12× for the progeny. Three types of SNP markers (lm×ll, nn×np, and hk×hk) were developed, totaling 317 877. After merging with a 100 kb sliding window, 6 134 Bin markers were generated. A first high-density Bin map was constructed, comprising 15 linkage groups with 3 517 Bin markers (containing 264 385 SNPs), covering a total map length of 1 666.79 cM. The average marker interval was 0.48 cM, with 99.18% of gaps being less than 5 cM. Collinearity analysis confirmed the high quality of the map. Fifty-six QTLs were mapped for 9 aroma-related traits, including (E)-2-hexenal, ethyl acetate, ethyl butyrate, ethyl crotonate, (E)-2-hexenoate, ethanol, linalool, ocimene, and total ester content. These QTLs explained 19.8%–51.0% of the phenotypic variation rates and were distributed across 11 linkage groups, with two QTL-rich regions on LG7 and LG8. Seven pleiotropic QTLs were detected. By analyzing the expression patterns of 1 535 annotated genes within the mapped intervals, six candidate genes potentially regulating the synthesis of ester characteristic aroma compounds were identified: aldo-keto reductase AKRs, acetolactate synthase small subunit ALS2, ACC oxidase ACO1-1, and transcription factors bHLH122, AGL103, and bZip1. This work provides novel insights into the fruit aroma formation, and facilitates breeding efforts to improve quality in longan and potentially other fruit crops.

KEYWORDS

longan, high-density bin map, characteristic aroma components, QTL mapping, candidate gene

1 Introduction

Longan (*Dimocarpus longan* Lour.) is a renowned specialty fruit in tropical and subtropical regions of China and Southeast Asia, occupies approximately ~5.7 million hectares globally with annual production reaching ~4.2 million tons. China is the origin and the leading producer of longan (Zheng et al., 2019), but cultivation is dominated by two varieties, 'Shixia' and 'Chuliang', which account for about 80% of the national acreage, and the fruit also lacks fragrance. In contrast, the 'Chompoo', 'Biew Kiew', and 'E-Daw' cultivated in Thailand, as well as the 'Kohala' grown commercially in the United States and Australia, are all well-known strong fragrant longan varieties in the international fruit market. Therefore, deepening the understanding of the molecular mechanisms underlying longan fruit aroma formation and related breeding research has important significance.

Genetic mapping, also known as linkage mapping, is an effective method for locating genes associated with important economic traits. The construction of genetic maps and QTL mapping for economic traits in longan (2n=2x=30) started relatively late and has evolved through two stages: reference-free and reference-based mapping. Guo et al. (Guo et al., 2009) used 94 F_1 progenies of 'Fengliduo × Dawuyuan' as mapping population, and constructed the first molecular genetic map of longan by RAPD, ISSR, SRAP, and AFLP markers. The maternal and paternal maps contained 21 and 22 linkage groups, with 183 and 251 marker loci, respectively, and average intervals of 5.84 cM and 4.65 cM. Subsequent studies based on this map identified QTLs for traits such as single fruit weight, soluble solid content, seed weight, peel weight, and edible rate (Guo et al., 2011), as well as trunk circumference (Guo et al., 2012). After the release of the first longan reference genome (at the contig level) (Lin et al., 2017), high-throughput SNP detection methods were applied to linkage mapping. Jue et al. (Jue et al., 2021) expanded the 'Fengliduo × Dawuyuan' population to 200 F_1 progeny and used RAD-Seq to construct a high-density SNP genetic map with 15 linkage groups (first consistent with chromosome count), 8014 SNPs, and an average interval of 0.36 cM. This map enabled the identification of 17 stable QTLs for single fruit weight and edible rate across years, along with 3 candidate genes. However, the above studies have limitations such as the use of a single hybrid combination, low density of traditional markers like RAPD, or the absence of a chromosome-level reference genome, which hinder the accurate localization of the map.

Currently, high-throughput sequencing can easily generate millions of SNP markers, but this volume exceeds the computational capacity of commonly used mapping software. The recombination breakpoint strategy addresses this by fusing identical genotypes within the sliding window into Bin markers, reducing marker redundancy while retaining complete genetic information. Compared to RFLP, SSR, InDel, or single SNP markers, Bin markers offer greater informativeness for a given population, and the sliding window approach helps eliminate false positives caused by sequencing errors. In recent years, high-density Bin genetic map construction and QTL mapping have been applied to various annual crops such as rice (Zhao et al., 2022), soybean (Ma et al., 2023), maize (Zhou et al., 2016), rapa (Li F. M. et al., 2023), and melon (Pereira et al., 2018), as well as a few woody fruit crops like apple (Di Pierro et al., 2016) and pear (Qin et al., 2022).

Aroma is a typical quantitative trait controlled by multiple genes. High-density genetic maps have proven effective for QTL mapping of aroma trait in annual crops like rice (Amarawathi et al., 2008), wheat (Kiszonas et al., 2017), tomato (Tikunov et al., 2020), cucumber (Sun et al., 2022), and strawberry (Rey-Serra et al., 2022). Perennial fruit trees face challenges such as long breeding cycles, large space requirements, and the complexity of aroma compound identification and quantification. However, with the increasing attention to fruit quality, progress has been made in aroma-related QTL mapping for kiwifruit (Zeng et al., 2020; Souleyre et al., 2022), grape (Koyama et al., 2022), apple (Yang et al., 2023), peach (Eduardo et al., 2013; Sánchez et al., 2014), and citrus (Yu et al., 2017). To date, no studies have reported Bin map construction and aroma-related QTL mapping in longan. Based on the chromosome-level reference genome of the 'Shixia' cultivar, this study constructed a high-density Bin-marker linkage map through whole-genome resequencing of an F_1 population derived from a 'Shixia × Xiangcui' cross. This map was then leveraged to identify aroma-related QTLs/candidate genes, ultimately aiming to elucidate the molecular mechanisms of aroma formation in longan fruit and support marker-assisted breeding.

2 Materials and methods

2.1 Plant material

With high yield, premium quality and rich aroma as the breeding objectives, in 2009, the non-aromatic early-maturing cultivar 'Shixia' (a major domestic cultivar) and the aromatic late-maturing large-fruit cultivar 'Xiangcui' (a bud sport of Thailand's major cultivar 'Biew Kiew') were cross-pollinated to obtain the F_1 progeny. The fruit aroma of the offsping exhibits a wide variation, including none, weak and strong (Hu et al., 2015). For this study, the parental lines and 98 F_1 offspring grafted on trees were selected as the mapping population (Figure 1).

2.2 Experimental methods

2.2.1 Extraction and detection of genome DNA

Young leaves were collected, and genomic DNA was extracted by modified CTAB method. DNA integrity was assessed via 1% agarose gel electrophoresis, and the concentration was measured using a Nanodrop spectrophotometer. Qualified DNA samples were used for high-throughput sequencing.

2.2.2 Resequencing library construction and sequencing

The NEBNext Ultra DNA Library Prep Kit was used to construct whole-genome resequencing libraries of 100 samples

FIGURE 1
Ear trait of parental lines and partial F_1 hybrids progeny. Progeny with light fruit aroma: 09-1-70, and 09-1-107; Progeny with strong fruit aroma: 09-1-37; Progeny without fruit aroma: 09-1-110.

from the parents 'Shixia', 'Xiangcui' and their 98 F_1 offspring. The Qualified libraries were sequenced on the Illumina HiSeq 2500 platform at the Fujian Agriculture and Forestry University Genomics and Biotechnology Research Center. The sequencing modes for the hybrid progeny and parents were High-throughput 1×100 nt and High-throughput 2×100 nt, respectively, with a sequencing depth of >10×.

2.2.3 SNP detection

Raw reads from the 100 resequenced samples were quality-controlled using Trimmomatic (Bolger et al., 2014) to remove low-quality reads and adapter sequences. Clean reads were aligned to the 'Shixia' reference genome (https://www.ncbi.nlm.nih.gov/bioproject/PRJNA741049/) using BWA (Jo and Koh, 2015) with default parameters. PCR duplicates were marked and removed using Picard (http://sourceforge.net/projects/picard/). SNP calling and filtering were performed using GATK (https://github.com/broadinstitute/gatk/releases) and VCFtools (Danecek et al., 2011) to obtain a SNP dataset.

2.2.4 SNP genotyping and genetic map construction

The SNP dataset was filtered to remove markers located on non-chromosomal contigs. Markers were classified into three types based on parental genotypes: lm×ll, nn×np, and hk×hk. Chi-square tests ($P < 0.05$) were applied to retain markers with segregation ratios of 1:1, 1:1, and 1:2:1, respectively.

To reduce redundancy while retaining sufficient genetic information, Bin markers were created using the Slide window method in Binmarker-v2.3 (). Methods such as recombination breakpoints determination, genotyping error correction, and window merging of the same genotype were referred to Qin et al. (Qin et al., 2022).

According to the principle of 'double false testcross', the CP (Cross Pollinator) model in JoinMap 4.1 was used for genetic map construction through a systematic workflow. First, the three types of Bin markers were combined and loaded into the software, and the population was created after checking the data format. Second, parameters included regression mapping, Kosambi mapping

function, a single iteration, and a minimum LOD score of 10.0 for linkage group clustering. Third, markers with severe segregation distortion (χ^2 test, $P < 0.05$), missing rates ≥10%, and similarity = 1.0 were removed. Fourth, nodes of linkage group were determined, and the map was drawn after three iterations. MapChart 2.2 was used for visualization (Voorrips, 2002), and ALLMAPs assessed the consistency between the Hi-C-based chromosome-level genome and the genetic map (Tang et al., 2015).

2.2.5 Data acquisition of fruit aroma trait in hybrid population

Prior research by our group identified 22 characteristic aroma compounds through volatile profiling of parental fruits across developmental stages. Comprehensive phenotypic datasets were obtained, including: five-year aroma sensory evaluations (2012–2015 and 2018, 83 progeny) and volatile compound GC-MS detection (2018, 48 progeny), which will be published separately. For the present QTL mapping study, we selected ten key traits: (E)-2-hexenal (A6), ethyl acetate (E1), ethyl butyrate (E3), ethyl crotonate (E4), ethyl (E)-2-hexenoate (E7), ethanol (AO1), ocimene (M1), linalool (M5), total ester content (TE), and 5-year comprehensive value of aroma sensory evaluation (FS). The content of E1, E3, E4, E7, AO1, and TE were significantly correlated with aroma intensity, and A6, M1, and M5 were the main characteristic aroma components.

2.2.6 QTL mapping for aroma traits

QTL analysis was performed using MapQTL 6.0 (Van Ooijen, 2009). Normally distributed traits were analyzed using Interval Mapping, while others used the Kruskal-Wallis (KW) test (Qin et al., 2022). Missing phenotypic data for individual plants were treated as null values. Significance thresholds were established through 10 000 permutation tests (PT), with LOD scores determined as follows: primary threshold calculation considered genome-wide confidence levels (0.95 or 0.90), adopting the more stringent value; if no significant interval was detected, linkage group-specific thresholds (0.95 or 0.90 confidence) were applied, again selecting the higher value. The minimum initial LOD threshold was set at ≥3.0. Bin markers meeting these criteria were designated as putative QTLs. The '1 LOD-drop' method (Lander and Botstein, 1989) defined QTL confidence intervals, and phenotypic variance explained (PVE) was calculated for each QTL. QTLs were named as 'trait code + peak Bin marker' (e.g., M1-hk0303 denotes an ocimene-related QTL with peak signal at marker hk0303).

2.2.7 Candidate gene identification

QTL intervals from the genetic map were anchored to physical genomic of 'Shixia' genome for gene retrieval and functional annotation. The expression level of gene was derived from prior RNA-seq data (a total of 17 developmental stages of 'Shixia', 'Xiangcui', and 'Lidongben' cultivars), and the mean FPKM < 0.5 genes were filtered out. Subsequent KEGG enrichment analysis was performed using ClusterProfiler in R package (Yu et al., 2012). The goodSamplesGenes function of the WGCNA package was used to detect and remove genes with low-variance (standard deviation ≤ 0.5). Gene correlations were calculated via biweight mid-correlation, with soft-thresholding power (β) determined by pickSoftThreshold (Peter and Steve, 2008). Modules were detected (minModuleSize = 20) and merged (mergeCutHeight = 0.25), followed by co-expression network visualization in Cytoscape v3.7.1 (Shannon et al., 2003). Pearson correlations between gene expression and characteristic aroma compounds were analyzed using SPSS 25. Key candidate genes were screened by referring to metabolic pathway, gene function, and literature report etc.

3 Results

3.1 Resequencing of the hybrid population and SNP detection

Whole-genome resequencing of the two longan parents and 98 F_1 progeny generated a total of 554.9 Gb of raw data (Table 1). The parental cultivars 'Shixia' and 'Xiangcui' yielded 7.1 Gb and 6.9 Gb of data, respectively, and the sequencing amount of the F_1 population was 3.9-7.1 Gb. The Q30 values of all samples exceeded 90%, indicating high base accuracy. After filtering, the clean reads were aligned to the 'Shixia' reference genome (about 483 Mb). The sequencing depth reached 15.47× for the maternal parent 'Shixia' and 15.03× for the paternal parent 'Xiangcui', and the average sequencing depth of hybrid offspring was 12.25×.

Through GATK SNP calling and VCFtools filtering, 4 261 436 high-confidence SNP loci were obtained from 11 521 588 raw SNPs. Genotyping and subsequent screening (excluding markers with chi-square test p-values < 0.05 and missing rates ≥ 10%) yielded a total of 317 877 markers suitable for CP model mapping These comprised three types: 59,744 lm×ll (maternal heterozygous, paternal homozygous), 5,704 nn×np (maternal homozygous, paternal heterozygous), and 252,429 hk×hk (both parents heterozygous). The total number of these SNPs far exceeds the computational limits of general mapping

TABLE 1 The sequences data of parents and progenies.

Sample	Total reads	Total bases (Gbp)	Q30 percentage (%)	Ave-depth (x)
Shixia	70 013 962	7.1	92.81	15.47
Xiangcui	67 986 648	6.9	94.11	15.03
Progenies	37 268 146-70 436 894	3.9-7.1	91.76-95.10	12.25
Total	5 493 228 903	554.9	/	/

Q30 Percentage refers to the percentage of bases with sequencing quality values greater than or equal to 30.

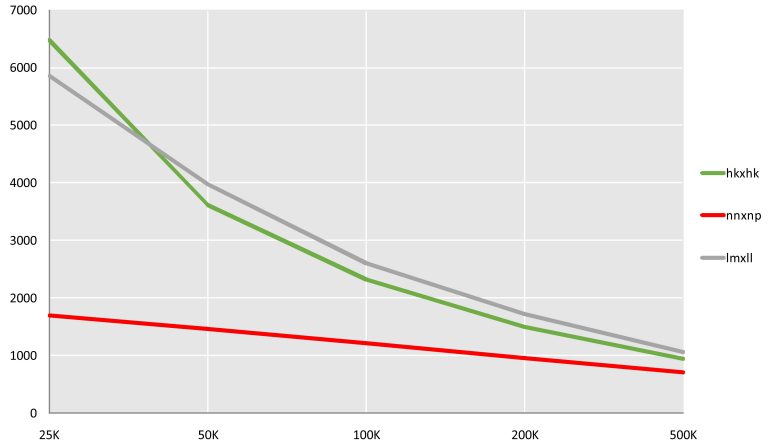

FIGURE 2
Quantity statistics of Bin markers in slide windows of different length. The X-axis represents the length of the slide window, and the Y-axis represents the number of markers.

software. Five sliding windows with different scales of 25, 50, 100, 200 and 500 kb were used to compare the fusion of three types of markers. and the 100 kb sliding window, which produced 6 134 Bin markers, was determined to be optimal (Figure 2). These Bin markers ranged in length from 1 bp to 874 474 bp (average 58.4 kb) and contained 1 to 1 791 internal SNPs (average 52 SNPs). Joinmap was then used to re-eliminate markers with severe segregation distortion (chi-square test $P < 0.01$) and missing rate ≥ 10% for three types of markers, and 5 626 Bin markers were obtained for final mapping, of which lm × ll, nn × np, hk × hk were 2 414, 1 189, and 2 023, respectively.

3.2 Construction and evaluation of the high-density genetic map

The three types of final markers obtained above were loaded together into Joinmap 4.1 software for grouping, and 15 strong linkage groups (LGs) were selected for map construction. A total of 3 517 Bin markers were ultimately mapped, comprising 1 407 lm×ll, 394 nn×np, and 1 716 hk×hk markers, which collectively contained 264,385 SNPs (Figure 3; Table 2; Supplementary Figure S1). The lengths of the 15 linkage groups ranged from 74.12 cM (LG12) to 181.74 cM (LG8). The number of Bin markers per LG varied from 193 (LG15) to 276 (LG3), and the number of SNP markers ranged from 7 666 (LG5) to 29 368 (LG12). The proportion of gaps <5 cM per linkage group ranged from 98.09% (LG10) to 100% (LG3, LG7, LG12). Overall, the map spanned a total length of 1 666.79 cM, with an average marker interval of 0.48 cM. The proportions of gaps <5 cM and <1 cM reached 99.18% and 90.89%, respectively, indicating uniform marker distribution and small intervals.

Visualization and evaluation using ALLMAPs software showed that the Spearman's correlation coefficient (ρ) between the marker order on the genetic map and their corresponding positions on the physical map ranged from 0.578 to 0.994, with an average value of 0.870. Except for LG5, all linkage groups had ρ value greater than 0.8. Seven linkage groups (LG1, LG3, LG6, LG9, LG10, LG11, LG12) exhibited high collinearity with the genomic map in terms of marker order (Table 2; Supplementary Figures S2, S3), all exceeding ρ > 0.9. These results indicate that this linkage map is of high quality and suitable for subsequent QTL analysis.

3.3 Phenotypic data analysis of aroma traits

Genetic variation in progeny of nine aroma-related traits including (E)-2-hexenal (A6), ethyl acetate (E1), ethyl butyrate (E3), ethyl crotonate (E4), ethyl (E)-2-hexenoate (E7), ethanol (AO1), ocimene (M1), linalool (M5), and total ester content (TE) was analyzed. Results showed that all nine traits exhibited quantitative genetic characteristics with continuous and extensive variation (Table 3). Due to the large difference in content between different volatiles and the moderately positive skewness distribution (Z-score > 3), the log2 value was converted and then subjected to normality testing (Table 3). E1, E7, AO1, M1, and TE conformed to normal distributions.

3.4 QTL mapping of characteristic aroma compounds

Using the high-density Bin map, 56 QTLs associated with nine aroma traits were identified. These QTLs were unevenly distributed across 11 linkage groups such as LG2, LG4, LG5, with significant enrichment observed on LG7 and LG8 (Table 4; Figure 4).

Two QTLs for (E)-2-hexenal (A6) content were mapped on LG12, both exhibiting LOD scores >5.0 and explaining 38.9%-42.4% of phenotypic variation. One QTLs for ethanol (AO1) content was also detected on LG12 (30.4% PVE). Five QTLs for ethyl acetate (E1) content were localized to LG10, LG12, and LG15 (28.5%-31.3% PVE).

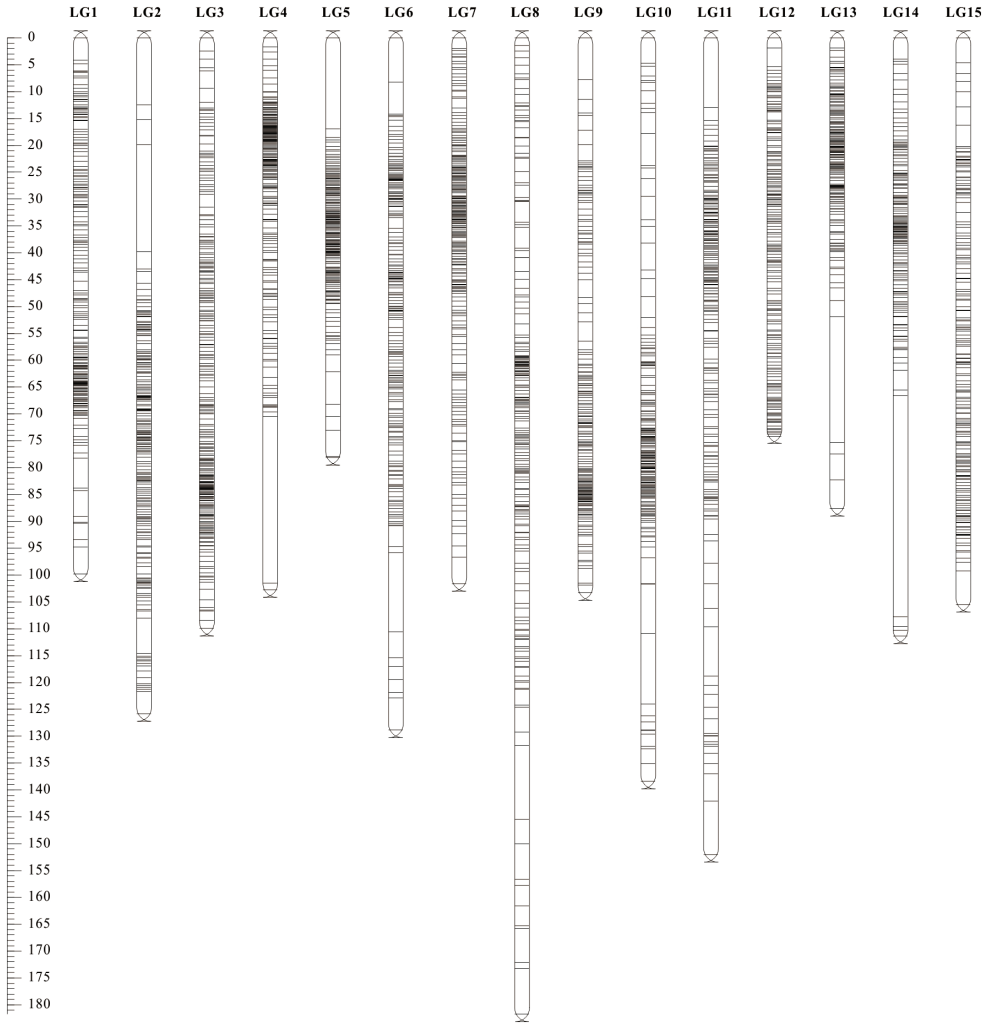

FIGURE 3
High-density SNP genetic map of longan.

Sixteen QTLs for ethyl butyrate (E3) and four for ethyl crotonate (E4) were all mapped on LG7, and most of them were clustered within the LG7:19.961-55.629 cM region (blue zone, LOD=3.75-7.29, 30.8%-51.0% PVE). Eighteen QTLs for ethyl (E)-2-hexenoate (E7) were mapped on LG6, LG8, and LG11 (33.0%-43.7% PVE), with 16 concentrated in the LG8:51.262-71.286 cM segment (magenta zone). Three QTLs for ocimene (M1) on LG2, LG5, and LG12 explained 27.3%-29.2% PVE. Two adjacent QTLs for linalool (M5) on LG4 explained 27.0%-29.1% PVE. For total ester content (TE), four QTLs on LG7 and one on LG9, explaining 29.5%-37.2% PVE.

Additionally, six of eight QTLs for the 5-year comprehensive value of aroma sensory evaluation were located in the enrichment regions on LG7 and LG8 (Table 4). In summary, seven pleiotropic QTLs were identified across traits, including A6/AO1-lm1799 on LG12, FSP/FS-lm0687 on LG1, and E3/TE-hk0743, E3/FSP/FS-hk0913, E3/TE-lm2174, E3/E4-lm0748, and E3/TE-lm0158 on LG7.

3.5 Pathway enrichment and WGCNA analysis

Within the physical map intervals corresponding to the 56 QTL loci (after deduplication), a total of 1 535 genes were retrieved, with 747 genes retained based on an FPKM value ≥ 0.5. KEGG analysis revealed that 319 genes were assigned to 134 pathways based on their functions (Supplementary Table S3). Among the 14 significantly enriched pathways, four pathways—Butanoate metabolism, Carotenoid biosynthesis, Amino sugar and nucleotide sugar metabolism, Valine, leucine and isoleucine biosynthesis, and Glycine, serine and threonine metabolism—were potentially related to volatile metabolite synthesis in longan fruit (Figure 5A). After filtering the 747 genes for variance in expression levels, WGCNA was performed on the 319 genes. When β=22, the average connectivity approached 0, so this β value was selected to construct the scale-free network (Supplementary Figure S4). The TOM algorithm was used to

TABLE 2 SNP genetic map information of longan constructed based on resequencing.

Link group	Length (cM)	Anchored Bin	Anchored SNP	Average distance (cM)	ρ value	Max Gap (cM)	Gap<5 cM (%)
LG1	99.82	251	19 341	0.40	0.921	5.65	99.20
LG2	125.76	224	21 850	0.56	0.865	19.92	98.66
LG3	109.92	276	18 509	0.40	0.904	3.25	100.00
LG4	102.68	268	20 942	0.38	0.820	30.99	99.63
LG5	78.09	238	7 666	0.33	0.578	16.88	99.16
LG6	128.77	248	18 593	0.52	0.923	14.77	98.39
LG7	101.65	247	10 567	0.41	0.869	4.98	100.00
LG8	181.74	233	19 622	0.78	0.861	13.72	98.28
LG9	103.33	231	17 269	0.45	0.915	7.71	99.57
LG10	138.39	209	11 728	0.66	0.932	13.15	98.09
LG11	152.02	240	15 725	0.63	0.921	12.88	98.33
LG12	74.12	219	29 368	0.34	0.994	3.54	100.00
LG13	87.56	235	17 242	0.37	0.862	23.37	99.15
LG14	111.25	205	20 307	0.54	0.807	41.07	99.51
LG15	105.54	193	15 656	0.55	0.879	6.31	99.48
Total	1 666.79	3 517	264 385	0.48	0.870	41.07	99.18

TABLE 3 Phenotypic statistics of fruit aroma related traits.

Compounds	Parents			F_1 population					
	Shixia	Xiangcui	Mid-parent value	Average	Range	CV (%)	Kurtosis	Skewness	*P*-value
A6	1248.4 ± 191.9	1155.8 ± 281.1	1202.1	413.6	31.8 - 2800.0	134.09	4.47	-1.81	0.003
E1	927.7 ± 284.8	4360.0 ± 1017.3	2643.8	229.0	26.3 - 792.0	73.61	-0.52	-0.21	0.639
E3	65.3 ± 15.2	345.2 ± 91.9	205.2	65.6	2.5 - 238.5	104.00	-0.71	-0.85	0
E4	252.5 ± 55.8	527.0 ± 108.7	389.7	132.9	11.5 - 841.5	120.56	1.26	-1.22	0
E7	6.8 ± 1.8	71.3 ± 33.5	39.1	11.4	1.6 - 70.1	117.47	0.49	-0.42	0.320
AO1	958.9 ± 210.0	1345.8 ± 271.4	1152.4	642.3	285.6 - 2030.7	43.14	1.81	0.56	0.148
M1	28750.4 ± 5375.8	19526.5 ± 5482.1	24138.4	13376.7	486.3 - 55309.7	97.66	-0.52	-0.36	0.310
M5	12.1 ± 11.9	38.2 ± 14.4	25.1	22.1	2.6 - 56.1	65.98	1.47	-1.06	0.004
TE	1629.0	7539.3	4584.2	778.9	225.6 - 1712.8	44.77	0.28	-0.50	0.134

The unit of volatile compound content was ng·g^{-1} FW. The Shapiro-Wilk method of SPSS 25 was used, a *P*-value > 0.05 indicates a normal distribution.

generate a gene hierarchical clustering tree. Gene modules were partitioned using the dynamic tree cut algorithm, and similar modules were subsequently merged, resulting in 10 final co-expression modules (Figure 5B). The gene count within modules ranged from a maximum of 71 in the purple module to a minimum of 12 in the salmon module.

An association analysis was conducted between the mapping traits in Table 4 and gene modules (Figure 5C). The results revealed

10.3389/fpls.2025.1642854

TABLE 4 QTL mapping results of key aroma compounds on the 'Shixia×Xiangcui' linkage map.

Trait	QTL	Confidence interval (cM)	Physical location (Mb)	LOD	Expl.%
A6	A6-lm1799	LG12: 15.639	Chr14: 2.159-2.248	5.02	38.9
	A6-lm0922	LG12: 16.935	Chr14: 5.554-5.644	5.64	42.4
AO1	AO1-lm1799	LG12: 15.639	Chr14: 2.159-2.248	3.70	30.4
E1	E1-np0963	LG10: 126.233	Chr11: 12.066-12.094	3.43	28.5
	E1-lm0725	LG10: 127.271	Chr11: 4.101-4.174	3.59	29.7
	E1-hk1000	LG12: 45.355	Chr14: 10.587-10.686	3.84	31.3
	E1-np1059	LG15: 44.663	Chr15: 5.002-5.202	3.73	30.6
	E1-lm1917	LG15: 44.743	Chr15: 8.713-8.789	3.72	30.5
E3	E3-hk0743	LG7: 19.961	Chr01: 27.407-27.610	4.19	33.7
	E3-hk0913	LG7: 20.136	Chr01: 28.772-29.772	4.52	35.8
	E3-lm2177	LG7: 29.404	Chr01: 21.179-21.266	4.45	35.4
	E3-lm2174	LG7: 32.137-32.179	Chr01: 19.981-21.849	3.91	31.8
	E3-np0163	LG7: 36.570-36.813	Chr01: 26.639-28.697	4.73	37.1
	E3-hk0642	LG7: 38.064-38.202	Chr01: 28.502-30.569	4.98	38.6
	E3-lm2265	LG7: 38.556-39.562	Chr01: 29.725-31.043	7.29	51.0
	E3-lm0749	LG7: 40.112	Chr01: 32.249-32.348	4.26	34.1
	E3-hk0614	LG7: 40.724-42.156	Chr01: 30.413-31.393	4.97	38.6
	E3-lm0748	LG7: 42.287-43.929	Chr01: 32.127-33.633	5.54	41.9
	E3-hk0613	LG7: 44.951-46.037	Chr01: 33.416-34.025	4.57	36.1
	E3-lm0888	LG7: 48.225-51.648	Chr01: 35.161-35.890	5.43	41.2
	E3-lm0694	LG7: 52.749-53.890	Chr01: 36.262-36.512	4.57	36.1
	E3-lm0696	LG7: 55.629	Chr01: 35.986-36.031	4.30	34.4
	E3-hk0912	LG7: 75.238	Chr01: 29.552-29.613	5.02	38.8
	E3-lm0158	LG7: 77.512-78.803	Chr01: 40.484-42.168	4.41	35.1
E4	E4-lm2221	LG7: 38.172-38.365	Chr01: 29.827-30.569	3.81	31.2
	E4-lm0748	LG7: 43.690-44.383	Chr01: 33.360-33.734	3.87	31.5
	E4-hk0615	LG7: 44.951-45.336	Chr01: 33.529-34.025	3.85	31.5
	E4-hk0619	LG7: 45.473-46.427	Chr01: 33.416-34.135	3.75	30.8
E7	E7-lm2160	LG6: 82.093	Chr12: 2.190-2.207	4.26	34.1
	E7-hk0851	LG8: 51.262	Chr13: 21.015-21.105	4.15	33.4
	E7-np1029	LG8: 57.475	Chr13: 18.748-18.766	5.87	43.7
	E7-np0896	LG8: 58.440	Chr13: 25.310-25.376	5.08	39.2
	E7-hk1766	LG8: 59.093	Chr13: 19.150-19.153	4.09	33.0
	E7-np0100	LG8: 59.298	Chr13: 17.213-17.307	4.32	34.5
	E7-hk1539	LG8: 61.840	Chr13: 22.236-22.328	4.48	35.5
	E7-hk1485	LG8: 61.840	Chr13: 24.263-25.207	4.48	35.5
	E7-hk0584	LG8: 62.610	Chr13: 13.993-14.193	4.53	35.8
	E7-hk1349	LG8: 62.779	Chr13: 16.487-16.584	4.53	35.8

(Continued)

10.3389/fpls.2025.1642854

TABLE 4 Continued

Trait	QTL	Confidence interval (cM)	Physical location (Mb)	LOD	Expl.%
	E7-hk1347	LG8: 62.779-62.947	Chr13: 15.219-15.538	4.53	35.8
	E7-np0323	LG8: 63.694	Chr13: 13.791-13.791	4.82	37.6
	E7-hk0063	LG8: 66.881-67.309	Chr13: 13.853-14.097	5.19	39.9
	E7-hk1551	LG8: 67.901-68.131	Chr13: 13.435-13.651	4.57	36.1
	E7-hk0059	LG8: 69.492	Chr13: 14.198-14.298	4.82	37.7
	E7-np0842	LG8: 69.442-70.795	Chr13: 11.707-12.459	5.52	41.8
	E7-hk0585	LG8: 71.286	Chr13: 16.596-16.690	4.54	35.9
	E7-lm2298	LG11: 31.329	Chr03: 38.249-39.182	4.17	33.6
M1	M1-hk0303	LG2: 81.568-81.957	Chr09: 10.737-11.04	3.53	29.2
	M1-lm1240	LG5: 35.553	Chr05: 17.836-18.038	3.25	27.3
	M1-hk0761	LG12: 23.789	Chr14: 4.922-5.020	3.26	27.4
M5	M5-np0889	LG4: 13.690	Chr02: 8.563-8.625	3.21	27.0
	M5-lm2110	LG4: 13.743	Chr02: 4.025-4.084	3.52	29.1
TE	TE- hk0743	LG7: 19.961	Chr01: 27.407-27.610	4.01	32.5
	TE-lm2174	LG7: 32.137-32.179	Chr01: 19.981-21.849	3.57	29.5
	TE-lm0158	LG7: 78.803	Chr01: 42.036-42.268	3.65	30.0
	TE-lm0148	LG7: 80.028	Chr01: 44.890-45.172	3.80	31.1
	TE-hk1131	LG9: 68.832-69.602	Chr10: 14.920-17.224	4.75	37.2
FSP	FSP-lm0687	LG1: 54.359-54.518	Chr07: 17.568-18.568	3.45	28.7
	FSP-hk0913	LG7: 20.136	Chr01: 28.772-29.772	6.56	47.4
FS	FS-lm0687	LG1: 54.359-54.518	Chr07: 17.568-18.568	3.95	21.8
	FS-hk0913	LG7: 20.136	Chr01: 28.772-29.772	3.58	20.0
	FS-lm0813	LG7: 20.947	Chr01: 12.301-12.401	3.80	21.1
	FS-lm1141	LG7: 25.539-26.398	Chr01: 14.619-15.236	3.82	21.2
	FS-np0865	LG8: 56.619	Chr07: 4.386-4.586	3.55	19.8
	FS-lm1760	LG8: 56.861-58.131	Chr07: 6.080-6.353	3.67	20.4

Expl.%-The percentage of the variance explained for by the QTL. TE-Total content of ester substances, FSP-Comprehensive value of five-year aroma sensory evaluation for partial plants (48 plants tested in 2018), FS- Comprehensive value of five-year aroma sensory evaluation (83 offspring plants).

that both the pink and purple modules exhibited a highly significant negative correlation with monoterpene M1 ($p<0.01$), while the black module showed a significant negative correlation with monoterpene M5 ($p<0.05$). The green and yellow modules demonstrated highly significant correlations (generally $|r|>0.75$ and $p<0.001$) with four straight-chain acetate esters (E1, E3, E4, E7), total ester content (TE), the five-year aroma sensory evaluation value (FS), and ethanol (AO1)—the precursor substrate for acetate ester synthesis. This suggests that these two modules may both harbor common candidate genes regulating the synthesis of multiple aroma compounds. Gene co-expression networks were constructed for each module (Supplementary Figure S5; Supplementary Table S4), identifying genes with high connectivity such as AGL103 (*Dil.03g026050.1*) and bZip1 (*Dil.01g036450.1*) in the green module (Figure 5D) and bHLH122 (*Dil.13g013320.1*) in the yellow module.

3.6 Candidate gene screening and expression pattern validation

Further analysis of correlations between gene expression and characteristic aroma compound contents across 17 developmental stages of 3 longan cultivars, combined with functional relevance assessment, revealed 13 candidate genes significantly or highly significantly associated with aroma synthesis (Table 5; Figure 6; Supplementary Tables S2, S3). These included an S-acyltransferase gene (*Dil.*15g011360.1) associated with ethyl acetate (E1); six genes

10.3389/fpls.2025.1642854

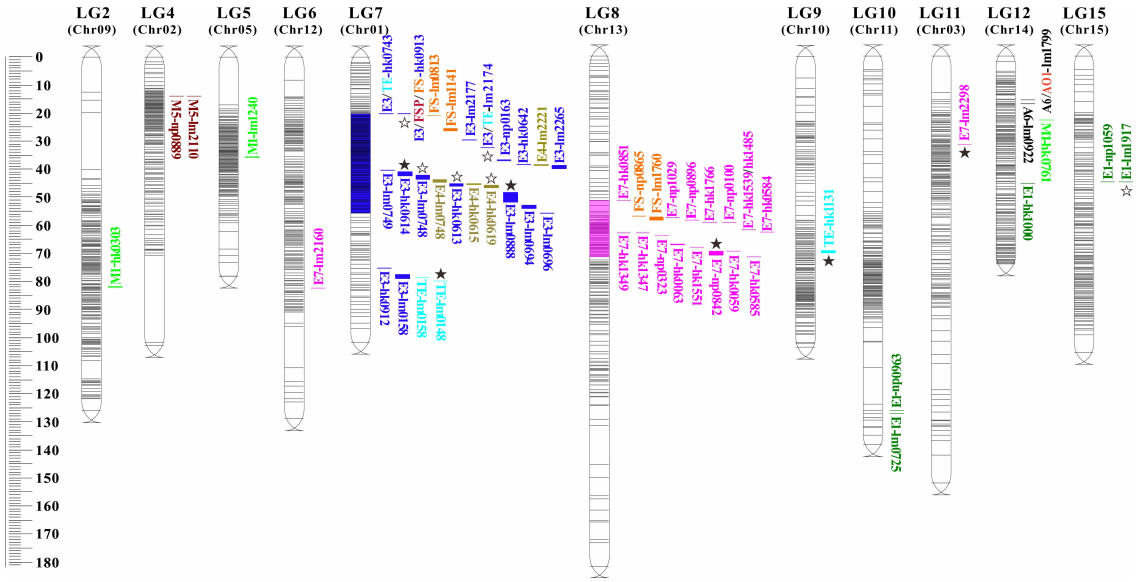

FIGURE 4
Distribution of QTLs related to characteristic aroma compounds in longan. The QTL loci for traits are named according to Table 3-3. Different colored markers represent different aroma compounds, and the blue and purple red segments labeled on linkage groups (LG) are the loci enrichment regions. The ☆ and ★ represent identified preliminary candidate genes and key candidate genes, respectively.

linked to ethyl butyrate (E3): RING-H2 zinc finger protein (*Dil*.01g017920.1), acetolactate synthase (*Dil*.01g022650.1), endochitinases (*Dil*.01g024580.1, *Dil*.01g025280.1), and ACC oxidases (*Dil*.01g026660.1, *Dil*.01g026750.1), with endochitinase *Dil*.01g025280.1 also showing a significant positive correlation with ethyl crotonate (E4); three transcription factors associated with ethyl (E)-2-hexenoate (E7): bHLH122 (*Dil*.13g013320.1), FAR1 (*Dil*.13g013360.1), and AGL103 (*Dil*.03g026050.1); and three genes related to total ester content (TE): RING-H2 zinc finger protein (*Dil*.01g017920.1), bZip1 (*Dil*.01g036450.1), and aldo-keto reductase AKRs (*Dil*.10g007540.1).

During the critical S1-S3 stages of aroma formation in longan fruit (aroma profile begins to emerge at S2 stage in the strong-aroma cultivar, and the interval between adjacent stages was 10d), differential accumulation of characteristic aroma compounds (E1, E3, E4, E7) occurred alongside corresponding expression changes in candidate genes (Figure 6). At stage S3, endochitinase Chi-2 (*Dil*.01g025280.1) expression in the strong-aroma cultivar 'Xiangcui' (XC) was approximately triple that of non-aromatic cultivars SX and LDB, and E1 content in XC was 35-40 times higher. Expression of the ALS2 (*Dil*.01g022650.1) and bHLH122 (*Dil*.13g013320.1) decreased progressively during fruit development, with their expression in XC was approximately half and one-third of that in SX and LDB at S3, respectively. Concurrently, ethyl butyrate (E3) and ethyl (E)-2-hexenoate (E7) levels were significantly higher in XC.

Further combined with LOD value, Expl. % value, locus overlap stability, and direct correlation degree of gene function, the above 13 candidates genes related to the five aroma compound was re-evaluated. Six genes were ultimately identified as key candidate genes, including AKRs, ALS2, ACO1-1, transcription factors bHLH122, AGL103, and bZip1. These exhibited LOD scores of 3.80–5.52 and Expl.% values of 31.1%–41.8%.

4 Discussion

4.1 Obtaining and evaluating high-quality genetic maps

High-quality genetic linkage maps are fundamental for precise QTL mapping, and its evaluation indicators mainly include marker density, saturation, and ordering accuracy. Traditional genetic maps constructed using first- and second-generation markers (RFLP, AFLP, RAPD, SSR) typically contain only several hundred markers. These are labor-intensive to develop and suffer from low marker density, large intervals, and limited chromosomal position matching, resulting in poor candidate gene localization.

High-throughput SNP detection methods based on reduced-representation genome sequencing, whole-genome resequencing, or SNP arrays have become mainstream for building high-density genetic maps. Such SNP maps contain thousands or tens of thousands of markers, significantly improving density and saturation (Li P. et al., 2023). However, intervals ≥5 cM or 10 cM may persist, and generally ≤1 cM is considered suitable for gene mapping. Strategies to reduce intervals include combining second- and third-generation markers, expanding population size to increase recombination events, and constructing secondary populations for fine-mapping. Of course, if the marker intervals reside in genomic regions with identical parental backgrounds (preventing segregation in progeny) or assembly gaps, alternative approaches are required. Additionally, while marker order should

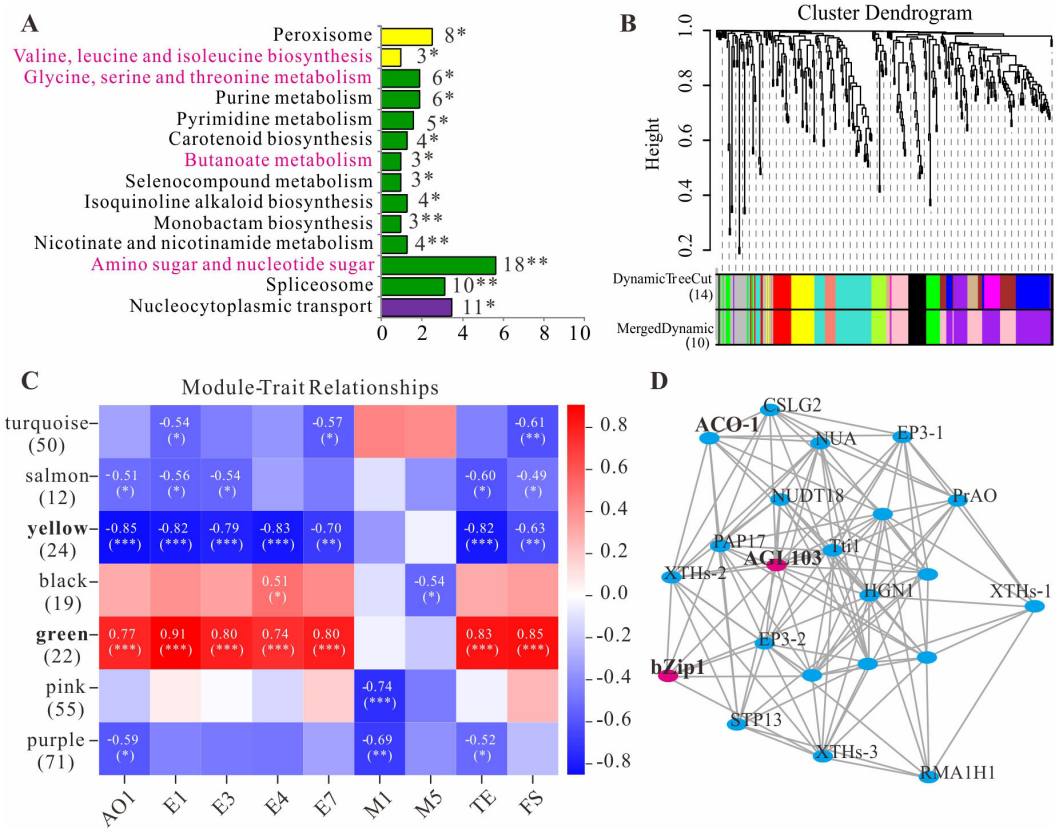

FIGURE 5
Pathway enrichment and WGCNA analysis of QTL mapping genes. **(A)**, KEGG enrichment pathways. **(B)**, Clustering dendrogram of genes and module division. **(C)**, Heat map of the relationship between modules and aroma traits. **(D)**, Gene co-expression networks within green module. The symbols *, ** and *** indicate statistical significance at $P < 0.05$, $P < 0.01$ and $P < 0.001$, respectively.

theoretically align with physical positions, several factors can disrupt collinearity: different methods for dividing the marker into linkage group (according to LOD thresholds of linkage relationship or chromosomal origins), insufficient SNPs/Bin markers within contigs for orientation determination, chromosomal inversions, and regional variation in recombination rates (Chen Y. Y. et al., 2022).

This study constructed the first high-density Bin genetic map of longan using whole-genome resequencing of a 'Shixia × Xiangcui' population. The map comprises 15 linkage groups anchored by 3 517 Bin markers (representing 264 385 SNPs), spanning 1 666.79 cM at an average marker interval of 0.48 cM, demonstrating high density and uniform distribution. The numbers of mapped markers in this study far exceeded those in previous studies. For example, the framework map developed by Guo et al. (Guo et al., 2011) contained only 243 and 184 markers for the paternal and maternal parents, respectively, while exhibiting inconsistent linkage group numbers (19 and 20) relative to the haploid chromosome number (n=15). Although the map constructed by Jue et al. (Jue et al., 2021) using RAD-seq featured linkage groups matching the haploid chromosome count and with an average marker interval of 0.36 cM, it contained only 8 014 SNPs. The limited occurrence of gaps >5 cM (0.82%) in our map may stem from insufficient population size or localization within non-recombinant regions of the genome (Chen Y. Y. et al., 2022). Collinearity analysis revealed an average Spearman's ρ of 0.870 between genetic and physical maps (Table 2), with ρ > 0.9 for LG1, 3, 6, 9-12 confirming consistent marker order. However, LG5 showed lower collinearity (ρ = 0.578), potentially due to its fewer SNPs (7 666 markers) reducing recombination events—which may compromise ordering accuracy. Alternative explanations include misassembled contigs or chromosomal translocations/inversions arising from divergent genetic backgrounds of the parental cultivars (Huang et al., 2020). Future efforts could employ F_2 populations to increase recombination frequency and further improve map resolution.

4.2 Genome-wide distribution of QTLs for longan fruit aroma

This study represents the first quantitative trait locus (QTL) analysis of fruit aroma compounds in longan. Leveraging the high-density Bin map, 56 QTLs related to 9 compounds such as (E)-2-hexenal (A6), ethyl acetate (E1), ethanol (AO1) were identified in the whole genome of longan (Table 4). These QTLs exhibited LOD scores of 3.21–7.29 and explained phenotypic variation of 19.8%–

TABLE 5 13 candidate gene information related to the synthesis of longan aroma compounds.

Trait	QTL	Gene ID	Gene function	Related coefficient	Module
E1	E1-lm1917	*Dil*.15g011360.1	Probable protein S-acyltransferase 14 (*PAT14*)	0.644**	/
E3	E3-hk0913	*Dil*.01g021540.1	F-box/kelch-repeat protein At3g06240 (F-box)	0.501*	pink
	E3-lm2174	*Dil*.01g017920.1[a]	RING-H2 finger protein ATL56 (*RING-H2*)	0.814**	/
	E3-hk0614	*Dil*.01g022650.1[b]	Acetolactate synthase small subunit 2 (*ALS2*)	-0.616**	/
	E3-lm0748	*Dil*.01g024580.1[c]	Endochitinase EP3 (*Chi-1*)	0.583*	greenyellow
	E3-hk0613	*Dil*.01g025280.1[a,c]	Endochitinase EP3 (*Chi-2*)	0.824**	/
	E3-lm0888	*Dil*.01g026660.1[b,d]	1-aminocyclopropane-1-carboxylate oxidase homolog 1 (*ACO1-1)*	0.699**	green
	E3-lm0888	*Dil*.01g026750.1	1-aminocyclopropane -1-carboxylate oxidase homolog 1 (*ACO1-2)*	-0.681**	purple
E4	E4-hk0619	*Dil*.01g025280.1[a]	Endochitinase EP3 (*Chi-2*)	0.681**	/
E7	E7-np0842	*Dil*.13g013320.1[b]	Transcription factor bHLH122 (bHLH122)	-0.558*	yellow
	E7-np0842	*Dil*.13g013360.1	Protein FAR1-RELATED SEQUENCE 4 (FAR1)	0.611**	/
	E7-lm2298	*Dil*.03g026050.1[b]	Agamous-like MADS-box protein AGL103 (AGL103)	0.642**	green
TE	TE-lm2174	*Dil*.01g017920.1	RING-H2 finger protein ATL56 (RING-H2)	0.824**	/
	TE-lm0148	*Dil*.01g036450.1[b]	Basic leucine zipper 1 (bZip1)	0.791**	green
	TE-hk1131	*Dil*.10g007540.1[b]	Aldo-keto reductase family 4 member C10 (*AKRs*)	-0.609*	/

E1, E3, E4, E7 represent Ethyl Acetate, Ethyl butyrate, Ethyl crotonate and Ethyl 2-hexenoate; [a]Genes were repeatedly located between different traits. [b]Key candidate genes. [c]Amino sugar and nucleotide sugar metabolism pathway. [d]Butanoate metabolism pathway. The * and ** indicate that the correlation between gene expression and compound content reached significant ($P < 0.05$) and extremely significant ($P < 0.01$) levels in all 17 developmental stages of the three longan varieties, respectively.

10.3389/fpls.2025.1642854

10.3389/fpls.2025.1642854

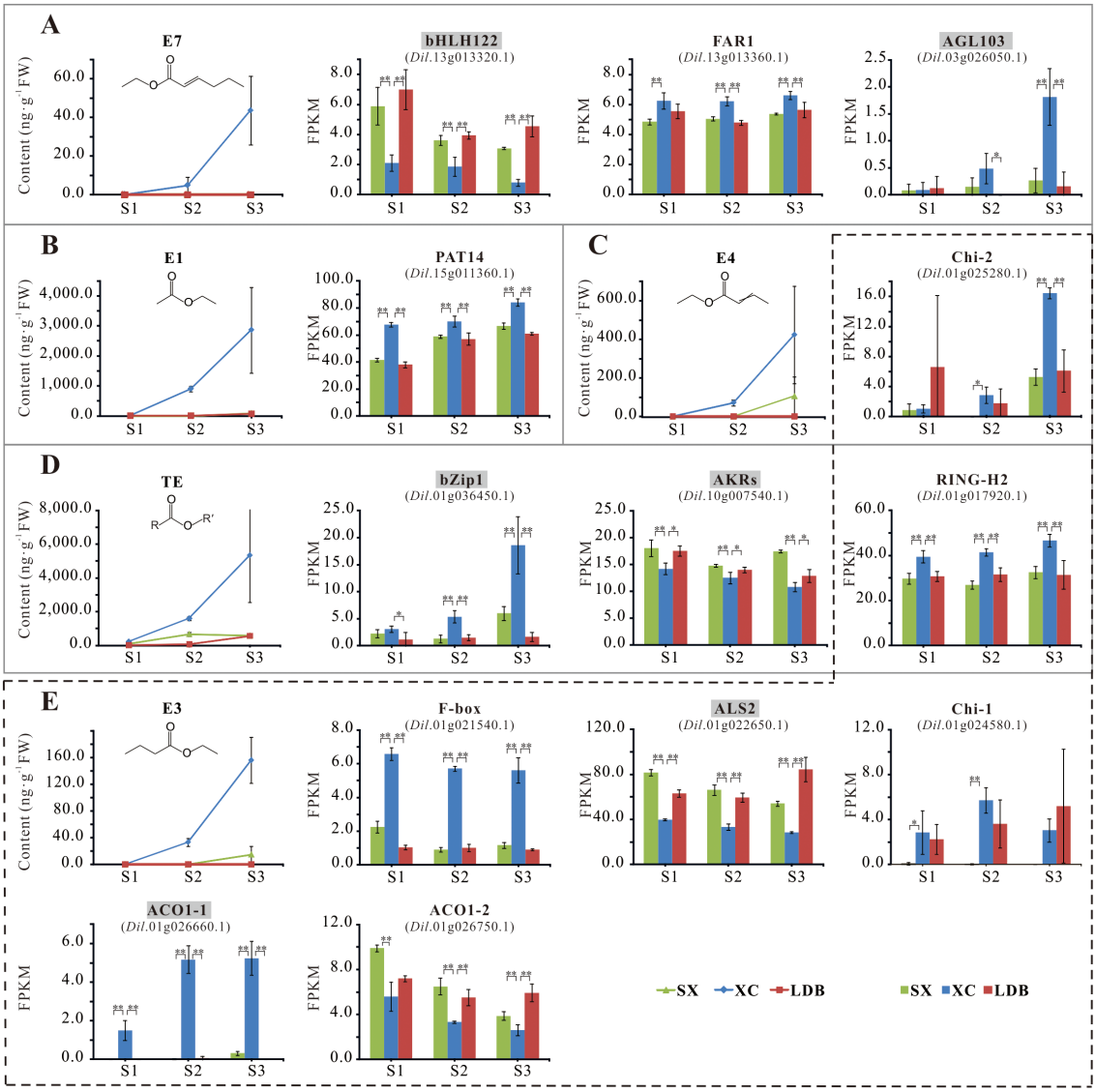

FIGURE 6
Accumulation of representative aroma compounds and differential expression of 13 candidate genes. **(A-E)** represents the content of E7, E1, E4, TE, E3, and the expression of candidate genes related to their synthesis, respectively. SX, XC, and LDB represent Shixia, Xiangcui, and Lidongben, respectively, while S1-S3 represent different stages of fruit development. FPKM values are calculated based on RNA-seq data from three biological replicates at each developmental stage. The names of key candidate genes are filled in gray. The * and ** represent significant ($P < 0.05$) and extremely significant ($P < 0.01$) differences, respectively.

51.0%. These QTLs were unevenly distributed across 11 linkage groups. Notably, two enriched regions—LG7: hk0743-lm0696 and LG8: hk0851-hk0585—harbored 36 QTLs, which were QTL hotspots controlling the synthesis of ethyl butanoate (E3), ethyl crotonate (E4), and ethyl (E)-2-hexenoate (E7). This phenomenon of QTLs clustering for structurally similarity or same biosynthetic pathway of volatile compounds has been reported in other fruit trees. For instance, Koyama et al. (Koyama et al., 2022) detected a QTL-rich region associated with 14 monoterpene contents in grape, which was located at the top of LG5 on the paternal and consensus maps and the QTLs were closely overlapped. Yang et al. (2023) detected 87 QTLs related to 15 volatiles on 14 linkage groups of apple. Among them, seven QTLs associated with four ester compounds were identified and confirmed on the same region of LG6.

The fruit aroma profile is complex and susceptible to maturity, light, temperature, soil and other factors (Sánchez et al., 2014); thus, multi-year assessment is essential. We conducted longitudinal evaluations of aroma traits in the 'Shixia × Xiangcui' population, collecting sensory evaluation data from 83 individuals across five years (2012–2015, 2018) and volatile compound detection from 48 individuals in 2018. These datasets were integrated to cross-validate QTL positions for enhanced accuracy. From the results, six of the eight QTLs for the five-year integrated sensory traits (FSP/FS) fell in two enrichment regions of the characteristic aroma compound traits. In addition, seven pleiotropic QTLs were identified, which

did not include some partially overlapping QTLs. This co-localization suggests shared genetic regulation of closely related aroma compounds, such as ethyl butyrate (E3), ethyl crotonate (E4), and total esters content (TE). Collectively, these findings demonstrate robust reliability and stability of the mapped QTLs.

4.3 Key genes regulating ester aroma biosynthesis in longan

Ketoreductase (KRED), a member of the oxidoreductase family, catalyzes the reversible conversion between aldehydes/ketones and alcohols using coenzyme NAD(H) or NADP(H). KREDs is mainly divided into three groups: short-chain dehydrogenases/reductases (SDRs), medium-chain dehydrogenases/reductases (MDRs), and aldo-keto reductases (AKRs). While sharing similar catalytic functions, they exhibit structural and functional distinctions. Notably, the MDR family contains alcohol dehydrogenases (ADHs) (Persson et al., 2008). In this study, an AKRs gene (SwissProt-annotated) showing significant negative correlation with total ester content was identified at the LG9 TE-hk1131 locus, but it was annotated as an ADH enzyme (EC 1.1.1.2) that performs the same function in the KEGG database. We thus hypothesize it primarily catalyzes the conversion of ethanol (an important substrate for ethyl ester synthesis) to acetaldehyde in longan fruit: Ethanol + $NADP^+$ ⇌ Acetaldehyde + NADPH + H^+. Both AKRs and ADHs exhibit substrate specificity. For example, the enzyme kinetic analysis of grape *VvAdh2* and *VvAdh3* revealed differential binding affinities for ethanol versus acetaldehyde (Tesniere and Verries, 2000).

Acetolactate synthase (ALS, EC 2.2.1.6), also termed acetohydroxyacid synthase, comprises distinct large and small subunits (Liu et al., 2017). Here, the ALS small subunit ALS2 demonstrated a highly significant negative correlation with ethyl butyrate at the LG7 E3-hk0614 locus. Within plant butanoate metabolism (map00650), ALS catalyzes the first committed step in branched-chain amino acid synthesis, efficiently converting pyruvate to (S)-2-acetolactate. Alternatively, pyruvate undergoes oxidative decarboxylation to acetyl-CoA, which can be further converted to butanoyl-CoA—a precursor for ethyl butyrate synthesis via alcohol acyltransferase (AAT). We propose that ALS2 activity redirects pyruvate flux toward amino acid biosynthesis, thereby reducing ethyl butyrate accumulation.

ACC oxidase (ACO) and ACC synthase (ACS) are pivotal enzymes in ethylene biosynthesis. Ethylene-mediated aroma synthesis has received considerable attention. In 'Fuji' apple, ethylene release was positively correlated with total aroma content during cold storage, in which the ethyl butyrate and ethyl caproate were main volatile components (Qi et al., 2020). Defilippi et al. (Defilippi et al., 2004) reported that the esters biosynthesis in apple ACS/ACO gene-suppressed lines and fruits treated with 1-methylcyclopropene (1-MCP) was significantly reduced, and speculated that AAT enzyme gene was regulated by ethylene. Similarly, ethylene release could not be detected in the fruit of ACO-antisense apple plant, yet exogenous ethylene significantly promoted the production of volatile compounds such as esters and terpenes (Schaffer et al., 2007). Although non-climacteric fruits generate minimal ethylene, emerging evidence implicates ethylene in their ripening (Jiang et al., 2011). We identified ACO1-1 at LG7 E3-lm0888 locus, exhibiting strong positive correlation with ethyl butyrate and cultivar-specific expression in aromatic varieties. Notably, this locus harbors a tandem cluster of 16 ACO genes—mostly negatively correlated with ethyl butyrate—suggesting specialized roles in aroma development of non-climacteric longan. Furthermore, we discovered a tandem cluster of 16 ACO genes at this locus, most negatively correlated with ethyl butyrate content. Their specific roles in aroma formation in non-climacteric longan fruits are worthy of attention.

Transcriptional regulation of fruit ester biosynthesis, primarily through LOX pathway, involves MADS-box, bHLH, bZip, NAC and so on. Tomato MADS-box RIN directly regulates TomloxC, ADH2, and HPL, and rin mutants show reduced hexanal and (E)-2-hexenal during ripening (Qin et al., 2012). Apple *MdMADS24* activates *MdLOX1a*, enhancing ester accumulation in calli (Yue, 2020). Pear *PubHLH61*, *PuMYB91*, and *PuNAC100*-like synergistically positively regulate *PuLOX3* and *PuAAT*, thereby mediating the aroma of 'Nanguo' pear during cold storage (Luo, 2022). Banana *MabZip4/5* directly activates *BaAAT* promoters, with reduced expression diminishing aroma under refrigeration (Guo et al., 2018). In this study, bHLH122 and MADS-box AGL103 were identified at LG8:E7-np0842 and LG11:E7-lm2298 sites, which were significantly negatively correlated and positively correlated with ethyl (E)-2-hexenoate, respectively; And bZip1 at LG7:TE-lm0148 demonstrated significant positive correlation with the total content of esters. In our previous transcriptome analysis results, AGL103 and bZip1 were also identified as core transcription factors, which were significantly positively correlated 12 straight-chain esters including ethyl (E)-2-hexenoate (to be published separately).

Additional candidate genes were identified (Table 5), including S-acyltransferase PAT14 (protein palmitoylation) (Liu et al., 2024), RING-H2 zinc finger protein [ubiquitin-mediated degradation (Chen et al., 2022)], endochitinases Chi-1/-2 (β-1,4-glycosidic bond hydrolysis) (Gong et al., 2019), F-box protein (transcription factor specificity modulation) (Rieu et al., 2023), and FAR1 transcription factor (fruit development regulation) (Chen et al., 2021). These genes may indirectly influence aroma accumulation.

5 Conclusions

A first high-density Bin genetic map for longan was constructed using whole-genome resequencing, comprising 15 linkage groups with 3 517 Bin markers (264 385 SNPs). Spanning a total length of 1 666.79 cM, the map features an average marker interval of 0.48 cM, exceptional continuity (99.18% gaps <5 cM) and high collinearity (mean ρ=0.870). We mapped 56 QTLs associated with aroma trait and identified six key candidate genes regulating characteristic ester biosynthesis: aldo-keto reductase AKRs, acetolactate synthase small subunit ALS2, ACC oxidase ACO1-1, and transcription factors bHLH122, AGL103, and bZip1. These results are helpful to further

understand the fruit aroma formation and provide valuable guidance for directed breeding of longan.

Data availability statement

The datasets presented in this study can be found in online repositories. The names of the repository/repositories and accession number(s) can be found in the article/Supplementary Material.

Author contributions

WH: Conceptualization, Writing – review & editing, Methodology, Funding acquisition, Writing – original draft. QZ: Data curation, Writing – review & editing. CD: Data curation, Writing – review & editing. QX: Writing – review & editing, Investigation. JJ: Methodology, Writing – review & editing. XC: Writing – review & editing, Investigation. JL: Conceptualization, Writing – review & editing. JZ: Writing – review & editing, Conceptualization, Methodology. SZ: Writing – review & editing, Conceptualization, Funding acquisition.

Funding

The author(s) declare that financial support was received for the research and/or publication of this article. This research was funded by Basic Research Project of Provincial Public Welfare Research Institutes (2021R1028009), Natural Science Foundation of Fujian Province (2023J01370), Research Project of Fujian Academy of Agricultural Sciences (2023, YCZX202504), China Agriculture Research System of MOF and MARA (CARS-32-06) and Fujian Science and Technology Major Project (2024NZ029029).

Acknowledgments

The authors would like to acknowledge Mengfan Qin for assisting in data processing and map construction.

Conflict of interest

The authors declare that the research was conducted in the absence of any commercial or financial relationships that could be construed as a potential conflict of interest.

Generative AI statement

The author(s) declare that no Generative AI was used in the creation of this manuscript.

Publisher's note

Supplementary material

The Supplementary Material for this article can be found online at: https://www.frontiersin.org/articles/10.3389/fpls.2025.1642854/full#supplementary-material

References

Amarawathi, Y., Singh, R., Singh, A. K., and Singh, V. P. (2008). Mapping of quantitative trait loci for basmati quality traits in rice (*Oryza sativa* L.). *Mol. Breed.* 21, 49–65. doi: 10.1007/s11032-007-9108-8

Bolger, A. M., Lohse, M., and Usadel, B. (2014). Trimmomatic: a flexible trimmer for Illumina sequence data. *Bioinformatics* 30, 2114–2120. doi: 10.1093/bioinformatics/btu170

Chen, Y., Deng, J., Chen, J. Y., Zeng, T., Yu, T. T., Huang, Q. H., et al. (2021). Genome-wide identification and expression analysis of FAR1/FHY3 transcription factor family in tomato. *Plant Physiol. J.* 57, 1983–1995. doi: 10.13592/j.cnki.ppj.2021.0061

Chen, Y. Y., Schreiber, M., Bayer, M. M., Dawson, I. K., Hedley, P. E., Lei, L., et al. (2022). The evolutionary patterns of barley pericentromeric chromosome regions. as shaped by linkage disequilibrium and domestication. *Plant J.* 111, 1580–1594. doi: 10.1111/tpj.15908

Chen, S. J., Xu, K., Kong, D. Y., Wu, L. Y., Chen, Q., Ma, X. S., et al. (2022). Ubiquitin ligase OsRINGzf1 regulates drought resistance by controlling the turnover of OsPIP2;1. *Plant Biotechnol. J.* 20, 1743–1755. doi: 10.1111/pbi.13857

Danecek, P., Auton, A., Abecasis, G., Albers, C. A., Banks, E., DePristo, M. A., et al. (2011). The variant call format and VCFtools. *Bioinformatics* 27, 2156–2158. doi: 10.1093/bioinformatics/btr330

Defilippi, B. G., Kader, A. A., and Dandekar, A. M. (2004). Apple aroma: alcohol acyltransferase.; a rate limiting step for ester biosynthesis, is regulated by ethylene. *Plant Sci.* 168, 1199–1210. doi: 10.1016/j.plantsci.2004.12.018

Di Pierro, E. A., GianFranceschi, L., Di Guardo, M., Koehorst-van Putten, H. J., Kruisselbrink, J. W., Longhi, S., et al. (2016). A high-density.; multi-parental SNP genetic map on apple validates a new mapping approach for outcrossing species. *Horticult. Res.* 3, 16057. doi: 10.1038/hortres.2016.57

Eduardo, I., Chietera, G., Pirona, R., Pacheco, I., Troggio, M., Banchi, E., et al. (2013). Genetic dissection of aroma volatile compounds from the essential oil of peach fruit: QTL analysis and identification of candidate genes using dense SNP maps. *Tree Genet. Genomes* 9, 189–204. doi: 10.1007/s11295-012-0546-z

Gong, K. L., Chen, S. H., Ji, X. C., Lin, Y. R., and Zhang, Q. (2019). The research progress of plant chitinases. *Mol. Plant Breed.* 17, 6840–6849. doi: 10.13271/j.mpb.017.006840

Guo, Y. F., Zhang, Y. L., Shan, W., Cai, Y. J., Liang, S. M., Chen, J. Y., et al. (2018). Identification of two transcriptional activators MabZIP4/5 in controlling aroma biosynthetic genes during banana ripening. *J. Agric. Food Chem.* 66, 6142–6150. doi: 10.1021/acs.jafc.8b01435

Guo, Y. S., Zhao, Y. H., Fu, J. X., Huang, S. S., Wang, Y., Lu, B. B., et al. (2012). Identification of stable QTLs related to trunk girth in Longan. *Sci. Horticult.* 134, 248–252. doi: 10.1016/j.scienta.2011.11.007

Guo, Y. S., Zhao, Y. H., and Liu, C. M. (2011). QTLs analysis of several traits in Longan. *Biotechnol. Biotechnol. Equip.* 25, 2203–2209. doi: 10.5504/bbeq.2011.0014

Guo, Y. S., Zhao, Y. H., Liu, C. J., Reng, P. F., Huang, T. L., Fu, J. X., et al. (2009). Construction of a molecular genetic map for Longan based on RAPD, ISSR, SRAP and

AFLP markers. *Acta Hortic. Sin.* 36, 655–662. doi: 10.16420/j.issn.0513-353x.2009.05.006

Hu, W. S., Huang, A. P., Jiang, F., Jiang, J. M., Chen, X. P., and Zheng, S. Q. (2015). Identification and genetic diversity of reciprocal hybrids in longan (*Dimocarpus longan*) by SSR. *Acta Hortic. Sin.* 42, 1899–1908. doi: 10.16420/j.issn.0513-353x.2015-0131

Huang, G., Wu, Z., Percy, R. G., Bai, M. Z., Li, Y., Frelichowski, J. E., et al. (2020). Genome sequence of Gossypium herbaceum and genome updates of Gossypium arboreum and Gossypium hirsutum provide insights into cotton A-genome evolution. *Nat. Genet.* 52, 516–524. doi: 10.1038/s41588-020-0607-4

Jiang, T. M., Yin, X. R., Wang, P., Sun, C. D., Xu, C. J., Li, X., et al. (2011). Research advance in regulation of ethylene during ripening and senescence of non-climacteric fruit. *Acta Hortic. Sin.* 38, 371–378. doi: 10.16420/j.issn.0513-353x.2011.02.023

Jo, H., and Koh, G. (2015). Faster single-end alignment generation utilizing multi-thread for BWA. *Bio-med. Mater. Eng.* 26, S1791–S1796. doi: 10.3233/BME-151480

Jue, D. W., Liu, L. Q., Sang, X. L., Shu, B., Wang, J. H., Wang, Y. C., et al. (2021). SNP-based high-density genetic map construction and candidate gene identification for fruit quality traits of Dimocarpus longan Lour. *Sci. Hortic.* 284, 110086. doi: 10.1016/j.scienta.2021.110086

Kiszonas, A. M., Boehm Jeffrey, D., See, D., and Morris, C. F. (2017). Identification of SNPs, QTLs and dominant markers associated with wheat grain flavor using genotyping-by-sequencing. *J. Cereal Sci.* 76, 140–147. doi: 10.1016/j.jcs.2017.06.006

Koyama, K., Kono, A., Ban, Y., Bahena-Garrido, S. M., Ohama, T., Iwashita, K., et al. (2022). Genetic architecture of berry aroma compounds in a QTL (quantitative trait loci) mapping population of interspecific hybrid grapes (*Vitis labruscana* × *Vitis vinifera*). *BMC Plant Biol.* 22, 458. doi: 10.1186/s12870-022-03842-z

Lander, E. S., and Botstein, D. (1989). Mapping Mendelian factors underlying quantitative traits using RFLP markers. *Genetics* 121, 185–199. doi: 10.1093/genetics/121.1.185

Li, F. M., Liu, Z. Y., Chen, H. X., Wu, J., Cai, X., Wang, H., et al. (2023). QTL mapping of leaf-related traits using a high-density bin map in Brassica rapa. *Horticulturae* 9, 433. doi: 10.3390/horticulturae9040433

Li, P., Liu, R. T., Tan, X. B., Zhang, Y., and Liu, C. H. (2023). Research progress in genetic map construction and QTL mapping for disease resistance in grapevine. *J. Fruit Sci.* 40, 1245–1254. doi: 10.13925/j.cnki.gsxb.20220031

Lin, Y. L., Min, J. M., Lai, R. L., Wu, Z. Y., Chen, Y. K., Yu, L. L., et al. (2017). Genome-wide sequencing of longan (Dimocarpus longan Lour.) provides insights into molecular basis of its polyphenol-rich characteristics. *Gigascience* 5, 1–14. doi: 10.1093/gigascience/gix023

Liu, Y. D., Li, Y. Y., and Wang, X. Y. (2017). Molecular evolution of acetohydroxyacid synthase in bacteria. *Microbiologyopen* 6, 524. doi: 10.1002/mbo3.524

Liu, F., Qu, P. Y., Li, J. P., Yang, L. N., Geng, Y. J., Lu, J. Y., et al. (2024). Arabidopsis protein S-acyl transferases positively mediates BR signaling through S-acylation of BSK1. *Proc. Natl. Acad. Sci. United States America* 121, e2322375121. doi: 10.1073/pnas.2322375121

Luo, M. L. (2022). *Molecular mechanism of different transcription factors synergistically regulating key genes of ester biosynthesis to mediate aroma loss in cold-stored 'Nanguo' pears. Ph.D. Thesis* (Shenyang, China: Shenyang Agricultural University). doi: 10.27327/d.cnki.gshnu.2022.000003

Ma, X., Fan, L., Zhang, Z. F., Yang, X., Liu, Y. C., Ma, Y. M., et al. (2023). Global dissection of the recombination landscape in soybean using a high-density 600K SoySNP array. *Plant Biotechnol. J.* 21, 606–620. doi: 10.1111/pbi.13975

Pereira, L., Ruggieri, V., Pérez, S., Alexiou, K. G., Fernández, M., Jahrmann, T., et al. (2018). QTL mapping of melon fruit quality traits using a high-density GBS-based genetic map. *Plant Biol.* 18, 324. doi: 10.1186/s12870-018-1537-5

Persson, B., Hedlund, J., and Jornvall, H. (2008). The MDR superfamily. *Cell. Mol. Life Sci.* 65, 3879–3894. doi: 10.1007/s00018-008-8587-z

Peter, L., and Steve, H. (2008). WGCNA: an R package for weighted correlation network analysis. *BMC Bioinf.* 9, 1–32. doi: 10.1186/1471-2105-9-559

Qi, W. Y., Wang, H. J., Zhou, Z., Yang, P., Wu, W. B., Li, Z. M., et al. (2020). Ethylene emission as a potential indicator of Fuji apple flavor quality evaluation under low temperature. *Hortic. Plant J.* 6, 231–239. doi: 10.1016/j.hpj.2020.03.007

Qin, M. F., Li, L. T., Singh, J., Sun, M. Y., Bai, B., Li, S. W., et al. (2022). Construction of a high-density bin-map and identification of fruit quality-related quantitative trait loci and functional genes in pear. *Horticult. Res.* 9, uhac141. doi: 10.1093/hr/uhac141

Qin, G. Z., Wang, Y. Y., Cao, B. H., Wang, W. H., and Tian, S. P. (2012). Unraveling the regulatory network of the MADS box transcription factor RIN in fruit ripening. *Plant J.* 70, 243–255. doi: 10.1111/j.1365-313X.2011.04861.x

Rey-Serra, P., Mnejja, M., and Monfort, A. (2022). Inheritance of esters and other volatile compounds responsible for the fruity aroma in strawberry. *Front. Plant Sci.* 13. doi: 10.3389/fpls.2022.959155

Rieu, P., Turchi, L., Thévenon, E., Zarkadas, E., Nanao, M., Chahtane, H., et al. (2023). The F-box protein UFO controls flower development by redirecting the master transcription factor LEAFY to new cis-elements. *Nat. Plants* 9, 315–329. doi: 10.1038/s41477-022-01336-2

Sánchez, G., Martínez, J., Romeu, J., García, J., Monforte, A. J., Badenes, M. L., et al. (2014). The peach volatilome modularity is reflected at the genetic and environmental response levels in a QTL mapping population. *BMC Plant Biol.* 14, 137. doi: 10.1186/1471-2229-14-137

Schaffer, R. J., Friel, E. N., Souleyre, E. J. F., Bolitho, K., Thodey, K., Ledger, S., et al. (2007). A genomics approach reveals that aroma production in apple is controlled by ethylene predominantly at the final step in each biosynthetic pathway. *Plant Physiol.* 144, 1899–1912. doi: 10.1104/pp.106.093765

Shannon, P., Markiel, A., Ozier, O., Baliga, N. S., Wang, J. T., Ramage, D., et al. (2003). Cytoscape: a software environment for integrated models of biomolecular interaction networks. *Genome Res.* 13, 2498–2504. doi: 10.1101/gr.1239303

Souleyre, E. J. F., Nieuwenhuize, N. J., Wang, M. Y., Winz, R. A., Matich, A. J., Ileperuma, N. R., et al. (2022). Alcohol acyl transferase genes at a high-flavor intensity locus contribute to ester biosynthesis in kiwifruit. *Plant Physiol.* 190, 1100–1116. doi: 10.1093/plphys/kiac316

Sun, Y. H., Li, X. Z., Ma, Z. Y., and Chen, S. X. (2022). Quantitative trait locus mapping of fruit aroma compounds in cucumber (*Cucumber sativus* L.) based on a recombinant inbred line population. *Horticult. Res.* 9, 2960–2973. doi: 10.1093/hr/uhac151

Tang, H. B., Zhang, X. T., Miao, C. Y., Zhang, J. S., Ming, R., Schnable, J. C., et al. (2015). ALLMAPS: robust scaffold ordering based on multiple maps. *Genome Biol.* 16, 3. doi: 10.1186/s13059-014-0573-1

Tesniere, C., and Verries, C. (2000). Molecular cloning and expression of cDNAs encoding alcohol dehydrogenases from *vitis vnifera* L. during berry development. *Plant Sci.* 157, 77–88. doi: 10.1016/s0168-9452(00)00274-0

Tikunov, Y., Roohanitaziani, R., Meijer-Dekens, F., Molthoff, J., Paulo, J., Finkers, R., et al. (2020). The genetic and functional analysis of flavor in commercial tomato: the FLORAL4 gene underlies a QTL for floral aroma volatiles in tomato fruit. *Plant J.* 103, 1185–1204. doi: 10.1111/tpj.14795

Van Ooijen, J. W. (2009). *MapQTL 6.0, software for the mapping of quantitative trait loci in experimental populations of diploid species [Z]* (Wageningen, Netherlands: Kyazma B.V).

Voorrips, R. E. (2002). MapChart: software for the graphical presentation of linkage maps and QTLs. *J. Heredity* 93, 77–78. doi: 10.1093/jhered/93.1.77

Yang, S. B., Yu, J., Yang, H. J., and Zhao, Z. Y. (2023). Genetic analysis and QTL mapping of aroma volatile compounds in the apple progeny 'Fuji'×'Cripps Pink'. *Front. Plant Sci.* 14. doi: 10.3389/fpls.2023.1048846

Yu, Y., Bai, J. H., Chen, C. X., Plotto, A., Yu, Q. B., Baldwin, E. A., et al. (2017). Identification of QTLs controlling aroma volatiles using a 'Fortune'×'Murcott' (*Citrus reticulata*) population. *BMC Genomics* 18, 646. doi: 10.1186/s12864-017-4043-5

Yu, G. C., Wang, L. G., Han, Y. Y., and Yu, Q. (2012). clusterProfiler: an R package for comparing biological themes among gene clusters. *Omics* 16, 284–287. doi: 10.1089/omi.2011.0118

Yue, S. S. (2020). *Study on apple ethylene response factor* ERF1B *regulating aroma biosynthesis in LOX pathway. Ph.D. Thesis* (Taian, China: Shandong Agricultural University). doi: 10.27277/d.cnki.gsdnu.2020.000588

Zeng, Y., Wang, M. Y., Hunter, D. C., Matich, A. J., McAtee, P. A., Knäbel, M., et al. (2020). Sensory-directed genetic and biochemical characterization of flavor-related volatile terpene production in ripe kiwifruit. *Plant Physiol.* 183, 51–66. doi: 10.1104/pp.20.00186

Zhao, L., Zhang, Y., Wei, X. D., Liang, W. H., Zhao, C. F., Zhou, L. H., et al. (2022). Mapping of QTLs for chlorophyll content in flag leaves of rice on high-density bin map. *Sci. Agricult. Sin.* 55, 825–836. doi: 10.3864/j.issn.0578-1752.2022.05.001

Zheng, S. Q., Zeng, L. H., Zhang, J. S., Lin, H. T., Deng, C. J., and Zhuang, Y. M. (2019). Fruit scientific research in New China in the past 70 years: Longan. *J. Fruit Sci.* 36, 1414–1420. doi: 10.13925/j.cnki.gsxb.Z15

Zhou, Z. Q., Zhang, C. S., Zhou, Y., Hao, Z. F., Wang, Z. H., Zeng, X., et al. (2016). Genetic dissection of maize plant architecture with an ultra-high density bin map based on recombinant inbred lines. *Genomics* 17, 178. doi: 10.1186/s12864-016-2555-z

frontiers | Frontiers in Plant Science

TYPE Original Research
PUBLISHED 05 September 2025
DOI 10.3389/fpls.2025.1640218

OPEN ACCESS

EDITED BY
Robin Joshi,
University of Pennsylvania, United States

REVIEWED BY
Md. Abu Sayed,
Hajee Mohammad Danesh Science and Technology University, Bangladesh
Antim Maurya,
University of Mississippi, United States

*CORRESPONDENCE
Hongmei Huang
hhm7418@hunau.edu.cn

RECEIVED 03 June 2025
ACCEPTED 11 August 2025
PUBLISHED 05 September 2025

CITATION
Li M, Yi Z, Shang H, Zhu C and Huang H (2025) Biochemical mechanisms underlying the differences in fruit characteristics among three kumquat varieties. *Front. Plant Sci.* 16:1640218. doi: 10.3389/fpls.2025.1640218

Biochemical mechanisms underlying the differences in fruit characteristics among three kumquat varieties

Manti Li[1,2], Zili Yi[1,2], Haole Shang[1,2], Changwei Zhu[1,2] and Hongmei Huang[1,2]*

[1]College of Bioscience and Biotechnology, Hunan Agricultural University, Changsha, China, [2]Hunan Engineering Laboratory of Miscanthus Ecological Applications, Hunan Agricultural University, Changsha, China

To elucidate different fruit trait mechanisms among Changshou (FOT) (*Fortunella obovata* Tanaka), Liuyang (FCSLY) (*Fortunella crassifolia* Swingle), and Huapi (FCSHP) (*Fortunella crassifolia* Swingle) kumquats, fruit traits, and their metabolite compositions were comprehensively analyzed. The main factors affecting fruit sweetness and bitterness are the sucrose and limonin contents. Differential metabolite analysis showed that FOT peels had the highest redness and more up-regulated anthocyanin and carotenoid compounds. Therefore, anthocyanin and carotenoid metabolites were related to the kumquat peel color. FOT peels had the highest flavonoid content. A total of 1719 metabolites were identified using non-targeted metabolomics, Flavonoid metabolites are more abundant in kumquat peels than in seeds, so the peel's medicinal value is higher. The total limonin content in seeds is higher than in peels, so the seeds are used as raw materials for extracting limonin compounds. This study analyzed the biochemical mechanisms of fruit trait differences in three kumquat (*Fortunella* Swingle) varieties and provided a reference for targeted kumquat development and utilization.

KEYWORDS

traits, non-targeted metabolomics, flavor, sucrose, limonin, flavonoids, active ingredients

1 Introduction

Kumquat originates from China and boasts a long history of cultivation. It can be classified into six species: *Fortunella hindsii* Swingle, *Fortunella polyandra* Tanaka, *Fortunella margarita* Swingle, *Fortunella japonica* Swingle, *Fortunella crassifolia* Swingle, and *Fortunella obovata* Tanaka (Palma and D'Aquino, 2018). Kumquat is closely related to citrus, and both belong to the citrus plants of Rutaceae. However, they exhibit distinct differences in their phytochemical compositions (Li et al., 2023; Ogawa et al., 2001) the peel, offering rich nutrients such as flavonoids, phenolic acids, carotenoids, vitamins, and

polysaccharides (Liu et al., 2019). Due to its phytochemical profile, it has been traditionally used in Chinese herbal medicine (Liu et al., 2019). Its peel also contains abundant essential oils and lipids (Liu et al., 2019). Modern medical experiments have demonstrated kumquat's efficacy in preventing vascular rupture, reducing capillary fragility, improving vascular permeability, and delaying vascular sclerosis. It also exhibits a two-way regulatory effect on blood pressure and enhances the body's cold resistance, thus helping prevent colds (Abirami et al., 2014; Tan et al., 2016).

Current metabolomic studies on kumquat remain limited compared with Citrus fruits, particularly regarding flavonoids, coumarins, phenolic acids and essential oils. (Min-Hung et al., 2017) revealed that traditional small citrus fruits in Taiwan (kumquats and calamondins) predominantly contain bioactive metabolites including terpenes in essential oils, flavonoids, phytosterols and limonoids, all of which contribute to their antioxidant properties. The juice of kumquat contains flavonoids as its primary metabolites (Barreca et al., 2011). Phloretin 3'5'-di-C-glucoside represents the most abundant flavonoid. Several other flavonoid components were identified including avicularin 3,6-di-C-glucoside which was reported for the first time in kumquat juice. Metabolic profiling and gene expression analysis revealed cultivar-specific differences between 'Huapi' kumquat (*F.crassifolia* Swingle) and its wild type. The peel of 'Huapi' kumquat contained higher levels of hexosylated flavonoids compared to the wild type. In contrast, its pulp showed lower flavonoid content. The differentially accumulated lipids were mainly lysophosphatidylcholines and lysophosphatidylethanolamines. These lipids were less abundant in both peel and pulp of 'Huapi' kumquat (Ma et al., 2021). Sadek et al (Sadek et al., 2009) investigated the peels of two Fortunella margarita specimens from Greece and Egypt. They identified major metabolites including phenolic acids and derivatives. Flavanones were detected in both C-glycosyl and O-glycosylated forms, along with flavonols and chalcones. The ethyl acetate fractions showed high polyphenol content and strong antioxidant activity. However, these studies primarily focused on the metabolite composition, content variations and bioactivities of kumquat. No comparative metabolomic analysis was conducted between kumquats and citrus fruits, and the metabolomics of kumquat seeds remains completely unexplored. Furthermore, the metabolome of 'Changshou' kumquat is still lacking.

'Changshou' kumquat is a hybrid between kumquat and Citrus species. Kiichi Yasuda's CMA analysis revealed E-type Citrus chromosomes in Changshou kumquat (Yasuda et al., 2016). This confirms its hybrid origin from both genera. 'Changshou' kumquat exhibits distinct phenotypic differences from traditional Fortunella crassifolia. Its peel shows easier detachment characteristics. This feature facilitates peel processing and component extraction. Both 'Liuyang' kumquat and 'Changshou' kumquat possess prominent oil glands. In contrast, 'Huapi' kumquat exhibits smooth peel with pale coloration, sparse oil gland density, and reduced pungency. Current knowledge gaps remain in Fortunella metabolomics, particularly for 'Changshou' kumquat. This study presents the first comparative metabolomic analysis of peel and seed tissues from 'Changshou' kumquat, 'Liuyang' kumquat, and 'Huapi' kumquat, while also incorporating the fruit traits of these three kumquat varieties. The results reveal metabolic bases underlying their phenotypic differences. These findings facilitate understanding metabolite variations between kumquat and Citrus. This work provides fundamental data for identifying unique metabolites and elucidating functional differences between these medicinal-edible plants.

2 Materials and methods

2.1 Plant materials

The study investigated two kumquat species. *F. obovata* Tanaka (commonly called 'Changshou' kumquat, voucher numbers: IMC0088085, deposited at the Chinese Virtual Herbarium) is a small spineless tree (Zhang, 2019). It bears dark green, broad-ovate leaves (4.5 cm long × 2-3.5 cm wide). The petals are approximately 1.48 cm long × 0.15 cm wide. The mature fruits are pyriform and lemon-yellow (2.5–4 cm longitudinal × 2.5-3.5 cm transverse diameter), averaging 23.0 g in weight. *F. crassifolia* Swingle (voucher numbers: PE 01470066, deposited at the Chinese Virtual Herbarium) is a shrub-like small tree with nearly spineless branches (Zhang, 2019). It features winged leaves that are ovate, slightly thick, and acuminate at the apex (4.4-7.5 cm long × 2.2-3.4 cm wide). The flowers are relatively large, with a spreading diameter of 1.9-2.0 cm. Petals measure 0.7-0.9 cm long × 0.3-0.4 cm wide. As the primary commercial cultivar in kumquat, its fruits are oblong-ovate (2.3-3.1 cm transverse diameter × 2.3-3.3 cm longitudinal diameter), averaging 12.7-20.6 g in weight. The edible fruits contain almost no oil glands and produce polyembryonic seeds. The study focused on two horticultural cultivars derived from *F. crassifolia* Swingle: 'Liuyang' kumquat and 'Huapi' kumquat. "Liuyang" kumquat is the main variety and has a long cultivation history in Liuyang City, Hunan Province, China. The 'Huapi' kumquat, identified through screening efforts in the 1980s, represents a naturally occurring seedling mutant derived from 'Rongan' kumqua (*F. crassifolia* Swingle).

The experimental materials included peel and seed samples from three kumquat cultivars:(1) 'Changshou' kumquat (*F. obovata* Tanaka; full name: FOT, peel: FOTP, seed: FOTS), (2) 'Liuyang' kumquat (*F. crassifolia* Swingle; full name: FCSLY, peel: FCSLYP, seed: FCSLYS), and (3) 'Huapi' kumquat (*F. crassifolia* Swingle; full name: FCSHP, peel: FCSHPP, seed: FCSHPS). The materials are currently cultivated at the experimental base of Hunan Agricultural University, located in Guandu Town, Liuyang City (28°347622 N; 113.886829 E). The region experiences a subtropical monsoon humid climate, with an average temperature of 17.4°C, an annual average of 1650 hours of sunshine, and an average annual precipitation of 1640 millimeters. The soils are typical Quaternary red clay (Ultisols) developed from plate shale weathering, characteristic of subtropical citrus-growing regions in Central China. Soil analysis showed acidic conditions (pH 5.2 ± 0.4) with moderate fertility (organic matter 2.8 ± 0.5%, total N 1.3 ± 0.2 g/kg, available P 15.3 ± 3.2 mg/kg, exchangeable K 125 ± 18 mg/kg).

Under identical management conditions, fruits from three kumquat cultivars were collected from the same orchard, with mature fruits harvested from five randomly selected trees per

cultivar. Five fruits of the same size were selected from different locations on each tree. The peels and seeds were separated, and the peels of the same variety were mixed. Similarly, the seeds of the same variety were mixed. The samples were immediately frozen in liquid nitrogen for approximately 15 minutes and divided into seven parts, which were labeled accordingly. Three parts were utilized to determine the total flavonoid content(TFC), total phenolic content(TPC), total limonoid content(TLC), and total fat content(TFAC) in kumquat. The remaining four parts were used for LC-MS metabolomics analysis.

2.2 Determination of color, flavor, and oil gland density in ripe fruit

Fruit color was measured using a colorimeter (Konica Minolta CR-400, Japan). Five fruits were selected for each variety, and the color difference values (L*, a*, b* values) were measured in three directions along the equator.

According to the sensory analysis method, the selection of tasters, sample selection and preparation, and error control during sensory evaluation were conducted. In accordance with the sensory analysis method (China National Institute Of Standardization, 2020), specifically the 'A-non-A' test method, 5–10 tasters were invited to taste the fruits of each variety, with each taster sampling five fruits from each variety.

The oil gland density was assessed following the citrus germplasm resource description specification and data standard (Dongjiang and Gong, 2006). During the fruit maturity stage, ten representative fruits of uniform size from the middle of the canopy were selected as observation samples. The number of oil glands along the equator of the peel was observed under a magnifying glass. Based on the oil gland count per unit area, the oil gland density level was determined for each variety. Oil gland densities below 45/cm^2 were classified as sparse, densities between 45~65/cm^2 were categorized as medium, and densities exceeding 65/cm^2 were considered dense.

2.3 Determination of sugar and acid content in mature fruits of three kumquat varieties

The 20 kumquat fruits from each variety were sliced into pieces, freeze–dried, and ground into powder (Dongjiang and Gong, 2006). A total of 0.75 g of powder was mixed with ultra-pure water to create a suspension. Three samples were prepared for each variety. The suspension was then subjected to a 70°C water bath for 30 minutes, followed by supernatant collection. The supernatant was further diluted in a 25mL volumetric flask to obtain the loading solution for the quantification of sugar and acid content. The sugar analysis included sucrose(SC), glucose(GC), and fructose(FC), while the acid analysis comprised citric acid(CA) and malic acid(MA).

The sugar and acid contents were analyzed using high-performance liquid chromatography (HPLC)(LC-40, SHIMADZU Co., Ltd., Kyoto, Japan). For sugar determination, the chromatographic column employed was a Shodex SUGAR SP0810(8.0 mm × 300 mm, 7.0μm), operated at a temperature of 80°C. The mobile phase consisted of ultrapure water at a flow rate of 0.5 mL/min. The analysis was performed using a refractive index detector (RID 20A, SHIMADZU Co., Ltd., Kyoto, Japan), and the injection volume was set at 5 μL. As for acid determination, the chromatographic column utilized was an Inertsil ODS-2 C18 column (4.6 mm × 250 mm, 5 μm; GL Sciences, Inc., Japan). The solvent used was 50 mM KH_2PO_4 at a flow rate of 0.6 mL/min. The eluted peaks were detected using an ultraviolet detector (Shimadzu, Japan) operated at 210 nm, and each acid was quantified using the area under the peak relative to that of known standards. Triplicate tissue samples were also analyzed.

2.4 Determination of total flavonoids, total phenols, limonoids, and total lipids in peels and seeds from three kumquat varieties

The TFC was determined using the $NaNO_2$-$AlCl_3$-NaOH method from a biochemical kit (NMKD0120, Norminkoda Biotechnology Co., Ltd., Wuhan, China) (Hu et al., 2023). In each experiment, about 0.1 g of the flesh tissue was extracted using 2 mL of extraction solution in 60°C water in an ultrasonic bath for 30 min. The solution was centrifuged at 10,000g at 25°C for 10 min, and the supernatant was collected. The supernatant was combined and standardized to a final volume of 10 mL with extraction solution. The spectrophotometer microplate reader was preheated for 30 min, and the absorbance was measured at the wavelength of 510 nm. The concentration of total flavonoids was expressed as mg of rutin equivalent (RE) per gram fresh weight (FW). A rutin standard was used as the positive control. These analyses were performed in triplicate.

The TPC was extracted and quantified using a total phenol biochemicals kit (NMKD0120, Norminkoda Biotechnology Co., Ltd., Wuhan, China) (Sun et al., 2023). Under alkaline conditions, phenols reduce tungsten molybdate to form a slightly blueish compound with a characteristic absorption peak at 760 nm. About 0.1 g of tissue and 2.0 mL of the extract was added, and the TPC was extracted using an ultrasonic extraction. The ultrasonic power was 300 W, and the mixture was crushed for 5 s, intermittently for 8 s, before being extracted for 30 min at 60°C. The mixture was centrifuged for 10 min at 12,000 rpm, at 25°C, and the supernatant was taken and diluted to 2.5 mL with extract solution. After the extraction, the absorbance at 760 nm was determined using a spectrophotometer to obtain the TPC in each sample. A total of 1 mg of tannic acid was added to 1 ml of extractive solution and then diluted to different concentrations to plot the standard curve, and the results were expressed as mg of tannic acid equivalent (TAE) per gram fresh weight (FW). Tannic acid standard was used as the positive control. The analyses were performed in triplicate.

The total content of limonoids is determined by colorimetric method (Qingguo Tian, 1999) using the biochemical reagent kit (NM-W-0739, Norminkoda Biotechnology Co., Ltd. Wuhan, China). The experiment used petroleum ether for degreasing, followed by extraction with acetone and detection of absorbance at 470nm. Using limonin as a standard(y = 0.1095x - 0.0046, R2 = 0.9914), calculate the content in the sample. The results were expressed as mg of imonin equivalent per g fresh weight (mg/g FW). The analyses were performed in triplicate.

The TFAC was extracted using the Soxhlet extraction method (Aravind et al., 2021). Briefly, about 1g of tissue was dried and put into a Soxhlet extractor to extract TFAC with petroleum ether as the solvent and turned back 60 times at 65°C using a kit from Norminkoda Biotechnology Co., Ltd. Wuhan, China.

2.5 Extraction process for metabolite analysis

A total of 25 mg of the sample was weighed into an EP tube after grinding with liquid nitrogen, and 500 µL extract solution (methanol: water = 3:1, with an isotopically labeled internal standard mixture) was added. Then, the samples were homogenized at 35 Hz for 4 min and sonicated for 5 min in an ice–water bath. The homogenization and sonication cycle was repeated three times. Then, the samples were incubated for 1 h at −40°C and centrifuged at 12000 rpm (RCF=13800(×g), R= 8.6cm) for 15 min at 4°C. The resulting supernatant was transferred to a fresh glass vial for analysis.Besides, the quality control (QC) sample was formed by mixing an equal aliquot of the supernatants from all samples (Wu et al., 2018).

2.6 LC-MS/MS analysis

LC-MS/MS analyses were performed using a UHPLC system (Vanquish, Thermo Fisher Scientific) with a UPLC HSS T3 column (2.1 mm × 100 mm, 1.8µm) coupled to an Orbitrap Exploris 120 mass spectrometer (Orbitrap MS, Thermo). The mobile phase consisted of 5 mmol/L ammonium acetate and 5 mmol/L acetic acid in water (A) and acetonitrile (B). The gradient profile was as follows: gradient program, 0–0.7 min, 1% B, 0.35 ml/min; 0.7–11.8 min, 99% B, 0.35 ml/min; 11.8–14.6 min, 1% B, 0.50 ml/min; 14.6–15 min, 1% B, 0.35ml/min. The auto-sampler temperature was 4°C, and the injection volume was 2µL.

The QE HFX mass spectrometer was used for its ability to acquire MS/MS spectra on Information-Dependent Acquisition mode in the control of the acquisition software (Xcalibur, Thermo). In both positive and negative ion modes, the acquisition software continuously evaluates the full scan MS spectrum. The Electron Spray Ionization source conditions were set as follows: a sheath gas flow rate of 30 Arb, Aux gas flow rate of 25 Arb, a capillary temperature of 350°C, full MS resolution as 60000, MS/MS resolution as 7500, collision energy as 10/30/60 in Normalized Collision Energy mode, a spray voltage of 3.6 kV (positive) or −3.2 kV (negative), respectively. Comparative analysis of differential metabolites was conducted by integrating detection data from both positive and negative ion modes.

After the original data were converted intomzXML format using the software ProteoWizard (https://proteowizard.sourceforge.io/),the Rpackage XCMS (version 3.2) was used for the peak recognition, extraction, alignment, and integration. The preprocesses of the original data included the following: (1) Data filtering: The filtering standard was to remove the data with no definite substance name or no spectrum comparison similarity. (2) Missing values processing: Substances of more than 50% missing in comparisons were filtered directly, and substances of less than 50% missing were performed the imputation of missing values using the k-nearest neighbor algorithm. (3) Normalization: The IS or total ion current of each sample was used for the normalization. A total of 1,426 and 293 peaks of the original data were retained for positive and negative ion modes, respectively. The excel sheets, including the name of peak and sample, and the standard data of normalized peak area were obtained for further data analysis.

The peak area of each metabolite was normalized to the area of the internal standard (IS), and subsequent analyses were conducted based on these normalized values. Identified metabolites were annotated using the KEGG COMPOUND database "https://www.kegg.jp/kegg/compound (accessed on 10 February 2022)", PubChem database, and Human Metabolome Database (HMDB) V4.0. SIMCA (V14.1) software was used for the principal component analysis (PCA) and orthogonal partial-least-squares discriminant analysis (OPLS-DA), and the variable importance projection (VIP) values of metabolites were calculated. All metabolites with VIP values greater than 1.0 and p-values of the Student's t-test that were less than 0.05 were identified as differential metabolites (DMs) in each paired comparison.

2.7 Data preprocessing and annotation

The contents of total sucrose (SC), glucose (GC), fructose (FC), citric acid (CA), and malic acid (MA) in the fruit, as well as the TFC, TPC, TLC, and TFAC in the peel and seed of all samples, were analyzed using ANOVA. All data analyses were performed using SPSS Statistics (Chicago, IL, United States) and expressed as the mean ± standard error of triplicates. Data visualization was conducted using multiple platforms: column charts were generated with GraphPad Prism 9 (v9.5.1, GraphPad Software, San Diego, CA, USA), while Venn diagrams, correlation heatmaps, and butterfly plots were created using OriginPro 2021 (v9.8, OriginLab Corporation, Northampton, MA, USA).

Raw data were converted to the mzXML format using ProteoWizard and processed with an in-house program, which was developed using R and based on XCMS for peak detection, extraction, alignment, and integration. Then, the MS2 database was applied to metabolite annotation. The cutoff for annotation was set at 0.3.

TABLE 1 Kumquat fruit flavor and oil gland density.

Variety name	Variety name code	Mature fruit		
		Fruit flavor	Bitterness	Oil gland density
'Changshou' kumquat	FOT	1	1	7
'Liuyang' kumquat	FCSLY	7	1	5
'Huapi' kumquat	FCSHP	9	0	3

Flesh flavor (1: acid; 7:slightly sweet; 9: sweet); bitterness (0: no; 1: yes); oil gland (3: sparse; 5: medium; 7: dense).

3 Results

3.1 Comparison of fruit traits of different kumquat varieties

The mature fruits of the three kumquat varieties exhibited significant differences in flavor, oil gland density (Table 1), and peel color (Table 2). FCSHP was characterized by the sweetest flavor, followed by FCSLY with a slightly sweet taste, while FOT presented an acidic flavor. Both FCSLY and FOT displayed bitterness, whereas FCSHP did not. FOTP exhibited the highest oil gland density, followed by FCSLY and FCSHP (Table 1). In terms of fruit color, FCSLY demonstrated the highest gloss brightness value and yellow–blue value, indicating the most pronounced glossiness and deepest yellow hue, respectively. FOT had the highest red–green value, reflecting the most intense red coloration, while FCSHP exhibited the lowest gloss brightness, red–green value, and yellow–blue value (Figure 1).

3.2 Comparison of metabolite contents in fruits of different kumquat cultivars

3.2.1 Comparison of sugar and acid content in fruit

The determination of SC, GC, FC, CA, and MA contents in three mature kumquat varieties revealed significant variations among the groups (Figure 2). Regarding SC, the three varieties exhibited distinct differences. FCSHP had the highest SC content, measuring 233.37 ± 11.40 mg/g, followed by FCSLY with 185.57 ± 3.60 mg/g. On the other hand, FOT displayed the lowest SC concentration of 108.46 ± 11.71 mg/g. In terms of GC and FC content, FOT and FCSLY did not differ significantly from each other. Both had higher values compared with FCSHP. Specifically, FOT exhibited the highest GC content of 177.82 ± 9.03 mg/g, followed by FCSLY with 169.77 ± 3.67 mg/g and FCSHP with 138.52 ± 2.41mg/g. Similarly, FOT had the highest FC content of 186.09 ± 14.92 mg/g, followed by FCSLY with 168.77 ± 3.43 mg/g. Furthermore, the CA and MA contents of the three kumquat varieties also displayed significant variations. FOT had the highest CA content of 68.61 ± 4.14 mg/g, followed by FCSHP with 9.42 ± 2.19 mg/g, and FCSLY with 6.49 ± 2.46 mg/g. In terms of MA content, FCSLY had the highest value of 6.73 ± 1.97 mg/g, followed by FCSHP with 6.32 ± 1.99 mg/g, and FOT with 2.31 ± 0.78 mg/g.

3.2.2 Comparison of secondary metabolite content in fruit peel and seeds

The peels and seeds of three kumquat varieties were analyzed to determine the TFC, TPC, TLC, and TFAC (Figure 3). These examined parameters showed significant variations among the peels of the three kumquat varieties. FOTP exhibited a higher TFC (0.60 ± 0.03 mg/g) compared with FCSLYP (0.52 ± 0.03 mg/g) and FCSHPP (0.53 ± 0.01 mg/g). FCSHPP had the highest TPC (2.24 ± 0.03 mg/g), followed by FOTP (1.91 ± 0.03 mg/g) and FCSLYP (1.35 ± 0.06 mg/g). FCSLYP had the highest TLC (8.43 ± 0.38 mg/g), followed by FOTP (5.66 ± 0.63 mg/g) and FCSHPP (2.24 ± 0.04 mg/g). There was no significant difference in TFAC among the three varieties, ranging from 1.77 ± 0.04 to 2.48 ± 0.08 g/100 g. In the comparison of seed groups, all four secondary metabolite content indices showed significant differences. FCSLYS had significantly higher TFC (1.16 ± 0.03 mg/g), TPC (1.58 ± 0.04 mg/g), and TFAC (21.58 ± 1.09 g/100 g) compared with FOTS and FCSHPS. FOTS (93.99 ± 5.38 mg/g) exhibited significantly higher TLC compared with the other two comparison groups. When comparing kumquat peels with seeds, the TFC, TLC, and TFAC were all significantly higher in kumquat seeds, while the TPC was higher in kumquat peels. To gain further insights into the major metabolite compositions of these varieties, we investigated the metabolomic profiles of the three kumquat peels and seeds.

TABLE 2 Kumquat fruit color.

Variety name	Variety name code	L*	a*	b*	CCI
'Changshou' kumquat	FOT	66.81 ± 0.52	19.74 ± 0.70	69.05 ± 0.84	4.28 ± 0.15
'Liuyang' kumquat	FCSLY	68.11 ± 1.90	16.15 ± 1.75	71.19 ± 2.87	3.35 ± 0.53
'Huapi' kumquat	FCSHP	67.96 ± 0.51	15.57 ± 0.90	70.84 ± 1.13	3.23 ± 0.13

The L* value represents gloss brightness, with higher values indicating greater brightness. The a* value represents the red–green value, where larger positive values indicate deeper red tones and smaller negative values indicate deeper green tones. The b* value represents the yellow–blue value, where larger positive values indicate deeper yellow tones and smaller negative values indicate deeper blue tones.

10.3389/fpls.2025.1640218

FIGURE 1
Morphological characteristics of mature kumquat fruit. **(A)** FOT. **(B)** FCSLY. **(C)** FCSHP.

3.3 Comparative metabolomic analysis of kumquat varieties: peel and seed comparison

3.3.1 Multivariate statistical analysis

The identification of primary and secondary metabolites in the samples was carried out using the UPLC-MS platform, employing non-targeted metabolomics technology. A comprehensive analysis led to the detection of a total of 1719 metabolites (Supplementary Tables S1, S2). These metabolites can be categorized into 15 compound classes, encompassing 161 flavonoids, 32 coumarins, 28 cinnamic acids, 25 lignans, 32 nucleotides, 175 organic acids, 511 lipids, 115 amino acids and their derivatives, 114 terpenes, 4 tannins, 38 alkaloids, 49 phenols, 44 phenolic acids, 151 carbohydrates, and 253 other compounds. The sum of all compounds within each class differed among the kumquat variety and its corresponding parts (Figure 4A), such that FCSHPP was rich in flavonoids, FCSLYP in lipids and carbohydrates, FOTS in limonin and organic acids, FCSLYS in carotenoids, and FCSHPS in anthocyanins and phenolic acids. These results indicate that each sample has unique nutritional and medicinal values.

The principal component analysis (PCA) results indicated that the four replicates of each sample clustered closely together (Figure 4B). Additionally, there was a clear separation between different samples, suggesting strong data repeatability and stability. Moreover, the metabolites in different parts of the various kumquat varieties exhibited significant differences, consistent with their observed phenotypic variations. The first principal component (PC1) accounted for 34% of the variability in the original dataset. Analysis of the PC1 revealed a distinct separation of peel and seed data points, while variations between different varieties were observed on the second principal component, explaining 14% of the dataset's variance. All samples were classified into two categories, with FCSHPS, FCSLYS, and FOTS clustering together, similar to FCSHPP, FCSLYP, and FOTP. This clustering pattern aligned with the PCA plot results, suggesting that disparities in metabolites may contribute to the observed differences in fruit phenotypes among the kumquat varieties. The Venn diagram (Figure 4C) illustrated that the peel and seed comparison groups of the three varieties contained 1650 and 1610 metabolites, respectively, with relatively few differing metabolites between the groups. This indicates a high degree of similarity in metabolite composition across the three kumquat varieties.

3.3.2 Analysis of differential metabolites

We conducted a differential metabolite analysis of pairwise comparisons among the peel and seed of three different varieties of kumquats, as well as the peel and seed within the same variety, resulting in a total of nine comparison groups. The differential metabolites were screened using Student's t-test *p*-values and the variable importance in projection (VIP) values from the OPLS-DA model. Metabolites with a *p*-value less than 0.01 were considered

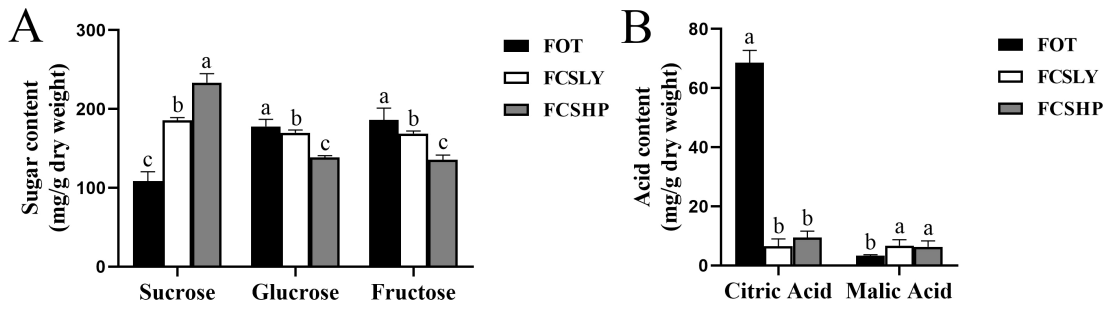

FIGURE 2
Sugar and acid content of mature kumquat fruit. **(A)** Sugar content in mature kumquat fruits. **(B)** Acid content in mature kumquat fruits. The line represents the average (n = 3), and the error line represents the standard error of the average (SD). Multiple comparisons using the Duncan method revealed significant differences ($p < 0.05$). No significant difference was observed for labels with the same letters, while histograms with different letters showed significant variations ($p < 0.05$).

10.3389/fpls.2025.1640218

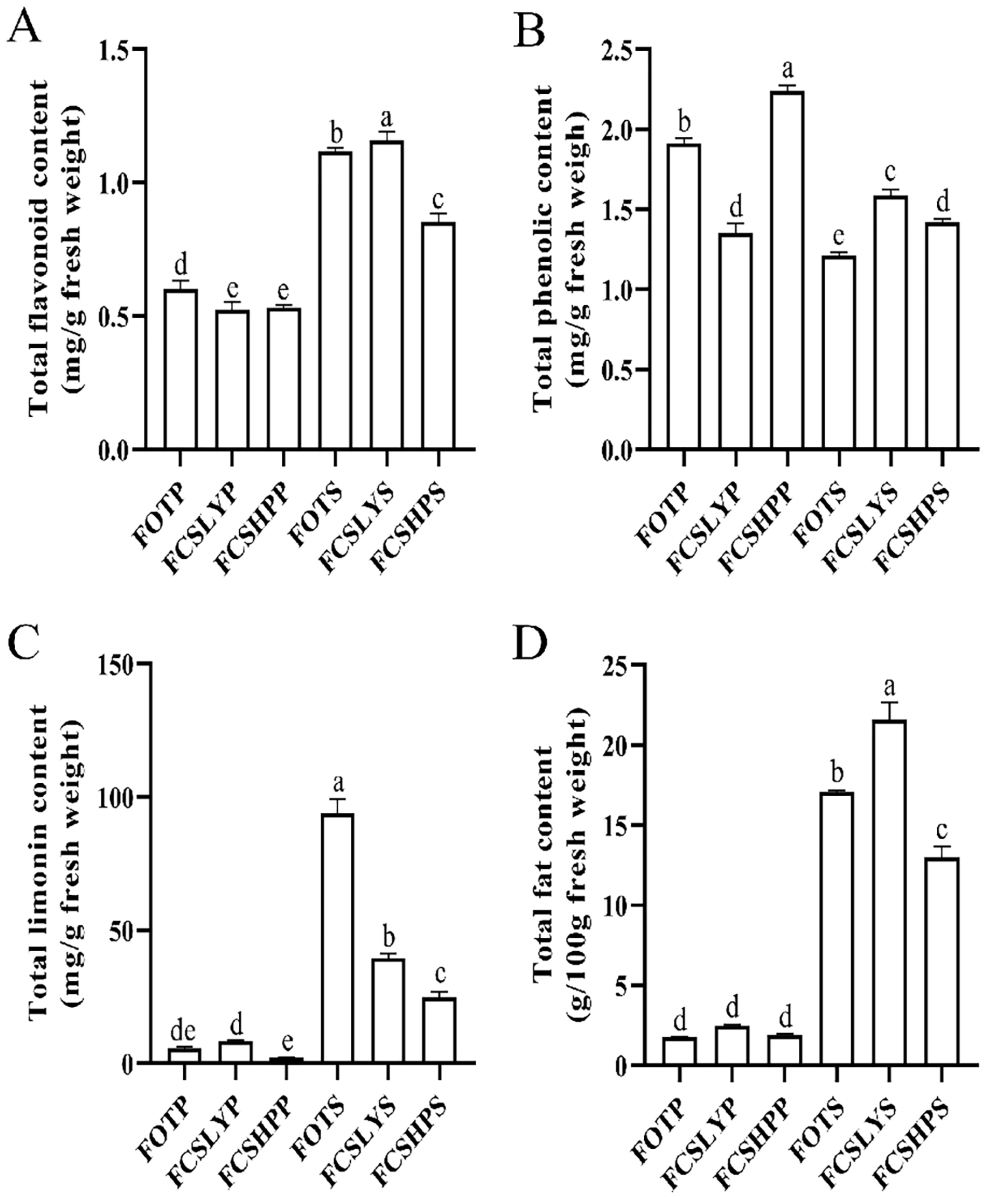

FIGURE 3
Secondary Metabolite Content in Three Kumquat Varieties. The figure illustrates the content of secondary metabolites in three kumquat varieties, namely FOTP, FCSLYP, and FCSHPP. The metabolites analyzed include TFC **(A)**, TPC **(B)**, TLC **(C)**, and TFAC **(D)**. Each data point represents the average value from three replicates, and the error bars indicate the SD. To assess the significance of differences, multiple comparisons were performed using the Duncan method, with a significance level of $p < 0.05$. Labels with the same letters indicate no significant difference, while different letters on the histograms indicate significant differences ($p < 0.05$).

statistically significant, and the results of this screening process are presented as a histogram (Figure 5).

In the comparison between the FCSHPP and FCSHPS groups, a total of 791 differential metabolites were identified, among which 291 were up-regulated and 504 were down-regulated. The comparative analyses for other groups are presented in Figure 5. Specifically, in the peel comparison group, FCSLYP exhibited the highest number of up-regulated metabolites, with 159 identified as such. Conversely, in the seed comparison group, FCSHPS displayed the highest count of up-regulated metabolites. In the comparison of peels and seeds, all three varieties demonstrated a greater number of up-regulated metabolites in the peel. These findings indicate that FCSLYP and FCSHPS possess a higher metabolite abundance and greater medicinal value, with the peel exhibiting a higher medicinal value than the seeds.

3.3.3 Differential accumulation of flavonoids and phenolic acids metabolites

This study conducted a comprehensive analysis of flavonoid and phenolic acid metabolites in the peels and seeds of three kumquat varieties. For flavonoid metabolites, most compounds were found in glycosylated forms, primarily classified as O-glycosides and C-

10.3389/fpls.2025.1640218

A

Compound Class	FOTP	FCSLYP	FCSHPP	FOTS	FCSLYS	FCSHPS
Flavonoids	247.98	324.97	346.58	60.90	41.94	41.09
Lipids	891.95	1379.42	721.53	775.58	606.02	878.38
Phenolic acids	7.05	6.44	5.96	2.18	3.86	9.97
limonin	0.16	0.12	0.06	1.04	0.28	0.16
Organic acids	719.74	1207.22	546.47	1272.05	1038.10	395.09
Carbohydrates	296.62	498.51	273.28	138.71	133.50	136.98
Carotenoid	0.02	0.05	0.14	0.30	0.38	0.19
Anthocyanidin	0.52	0.32	0.49	0.64	0.38	0.79

B

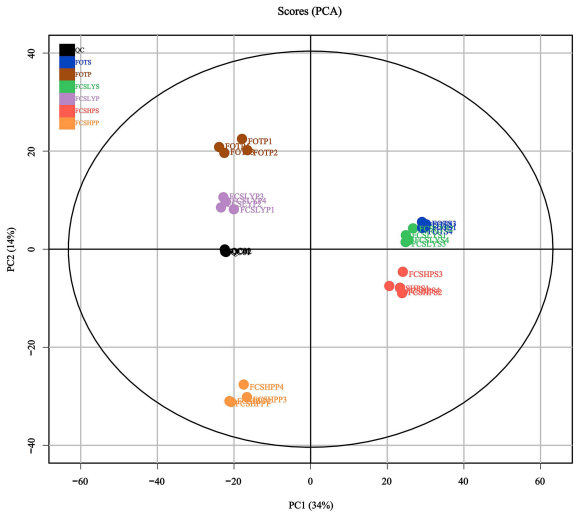

C

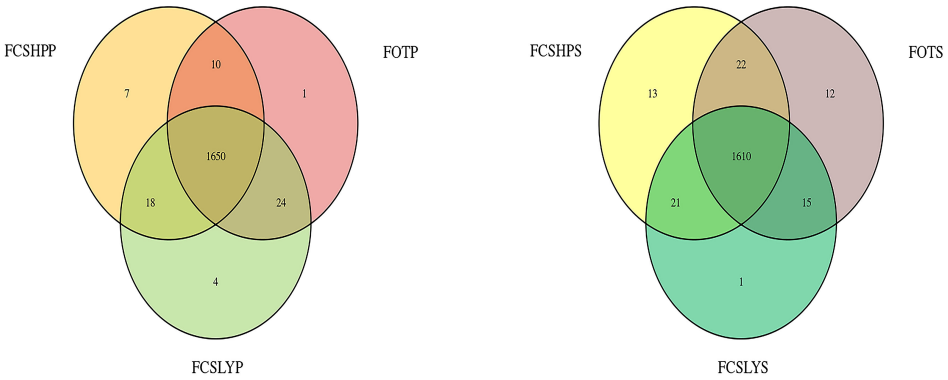

FIGURE 4
Overview of metabolic analysis detected in the peels and seeds of three kumquats. **(A)** The strength of each compound type. The color intensity in Figure **(A)** represents the relative content of each compound. **(B)** Principal component analysis of peel and seed metabolites of three kumquat varieties. **(C)** The Venn diagram of the distribution of seed metabolites in three kumquat varieties.

glycosides. The major glycosylation sites were at 3-O, 5-O, 7-O (O-glycosides) and 6-C, 8-C (C-glycosides), while O-glycosides at 6-OH or 8-OH positions were less common. The glycosyl groups included glucose, rhamnose, rutinose, and neohesperidose. In peel comparisons, FOTP showed higher accumulation of diverse flavonoids (Figures 6B, C). Examples include O-glycosylated flavonoids such as Vitexin 4'-O-α-L-rhamnopyranoside and Quercetin 3-O-glucosyl-rutinoside, flavanones like 2-(3,4-dihydroxyphenyl)-5-hydroxy-3,6,7-trimethoxy-4H-chromen-4-one, and flavanols such as Epicatechin. FCSLYP showed increased accumulation of both methylated flavonoids (e.g., 4',5-dihydroxy-3',5',7,8-tetramethoxyflavone) and upregulated isoflavones (e.g., 5,7-dihydroxy-4'-methoxy-8-methylisoflavanone and dihydrodaidzein) (Figures 6A, C). FCSHPP exhibited significant accumulation of polymethoxyflavones (PMFs) including Nobiletin, Diosmetin, Poncirin, and Hesperetin 7-glucoside, as well as upregulated C-glycosylated flavonoids and their derivatives like Orientin and Quercetin 8-C-(2''-rhamnosylglucoside) (Figures 6A, B). In seed comparisons, FOTS primarily upregulated C-glycosylated flavonoids (Vicenin 2, Vitexin 4'-O-α-L-Rhamnopyranoside, Orientin 2''-

10.3389/fpls.2025.1640218

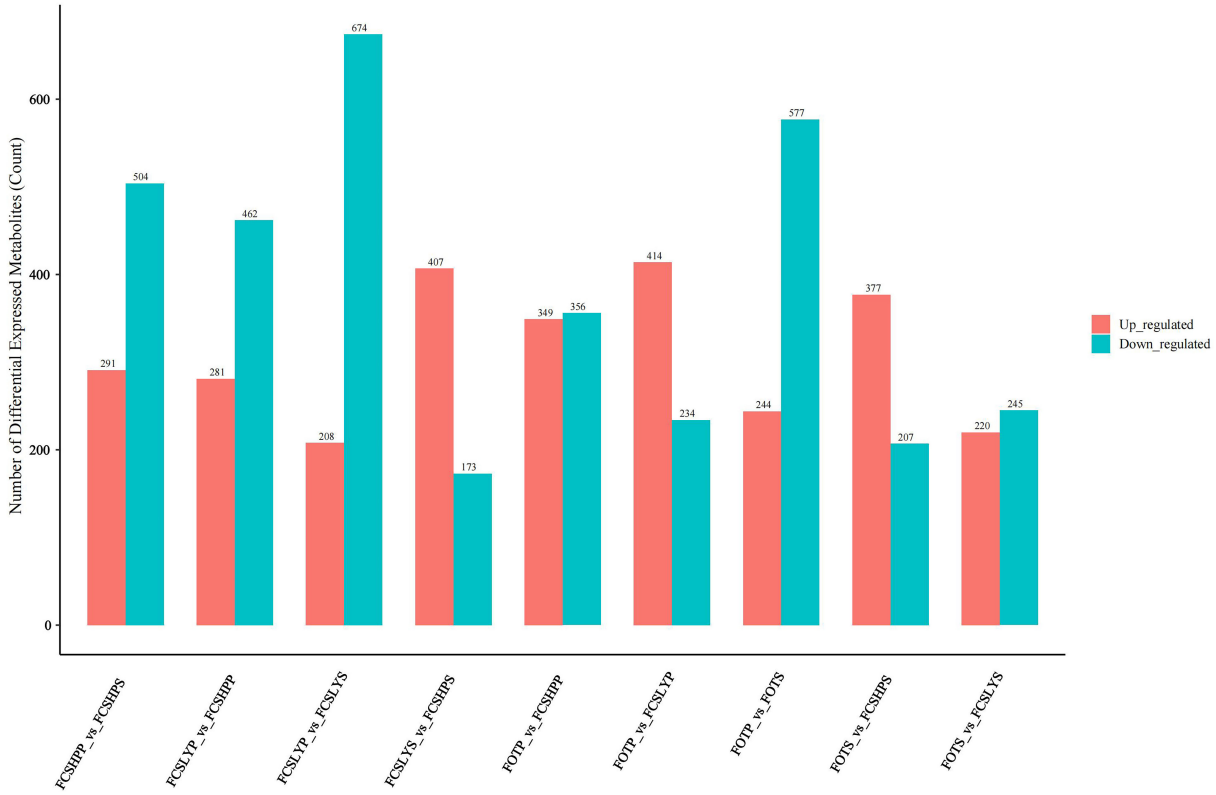

FIGURE 5
Statistical histogram of differential metabolites.

rhamnoside) and O-glycosylated flavonoids (Naringin, Diosmetin 7-neohesperidoside, Diosmetin 8-C-(2"-rhamnosylglucoside)), along with the prenylated flavonoid Xanthohumol (Figures 6E, F). FCSLYS was characterized by methylated flavonoids (Isorhamnetin) and flavanol derivatives (4'-O-Methyl-epicatechin 3'-O-glucuronide), and contained isoflavones such as 3',4',5,7-Tetrahydroxyisoflavanone (Figures 6D, F). FCSHPS displayed a unique accumulation pattern of PMFs, including 3-Methoxynobiletin and Zapotin (Figures 6D, E).

Higher levels of phenolic acids were accumulated in both FCSHPP and FCSHPS (Figure 7). FOTP predominantly accumulated 4-Demethylsimmondsin 2'-(E)-ferulate, Simmondsin 2'-ferulate, and Isoacteoside (Figures 7B, C). In FCSLYP, Phenethyl 6-galloylglucoside showed significant upregulation (Figures 7A, C). FCSHPP accumulated various phenolic acid metabolites including Gallic acid, 4-Coumaroylputrescine, Caffeoyl glucuronide, Avenanthramide C, and Mesalazine (Figures 7A, B). In seed samples, Benzoic acid was highly accumulated in FOTS (Figures 7E, F). The upregulated metabolites in FCSLYS included Caffeoyl C1-glucuronide, 2-O-Acetyl-trans-coutaric acid, and Salicylic acid beta-D-glucoside (Figures 7D, F). FCSHPS exhibited the most complex phenolic acid profile (Figures 7D, E), with multiple compounds detected including Vanillic acid, Mesalazine, Mono-trans-p-coumaroylmesotartaric acid, 1-O-Feruloylglucose, 2-O-Feruloyltartronic acid, 1-O-Sinapoylglucose, cis-Coutaric acid, 3,4,5-Trimethoxycinnamic acid, and Benzoyl glucuronide.

3.4 Association analysis between secondary metabolites and fruit traits in kumquat fruit

The correlation between phenotypic traits (fruit flavor, bitterness, and oil gland density) and fruit sugar and acid content (SC, GC, FC, CA, and MA contents) and peel secondary metabolite contents (total flavonoids, total phenols, total limonin, and total lipids) was investigated (Figure 8). The findings revealed that fruit flavor exhibited a positive correlation with SC content (r = 0.98) and a negative correlation with oil gland density and CA content (r = −0.96). Fruit bitterness demonstrated a strong positive correlation with oil gland density (r = 0.87) and TLC (r = 0.89) in the peel.

3.4.1 Correlation analysis between secondary metabolites and fruit flavor

FCSHP exhibited a sweet flavor without bitterness. FCSLY had a sweet and bitter flavor, while FOT had a sour and bitter taste (Table 1). We conducted measurements on the sugar and acid

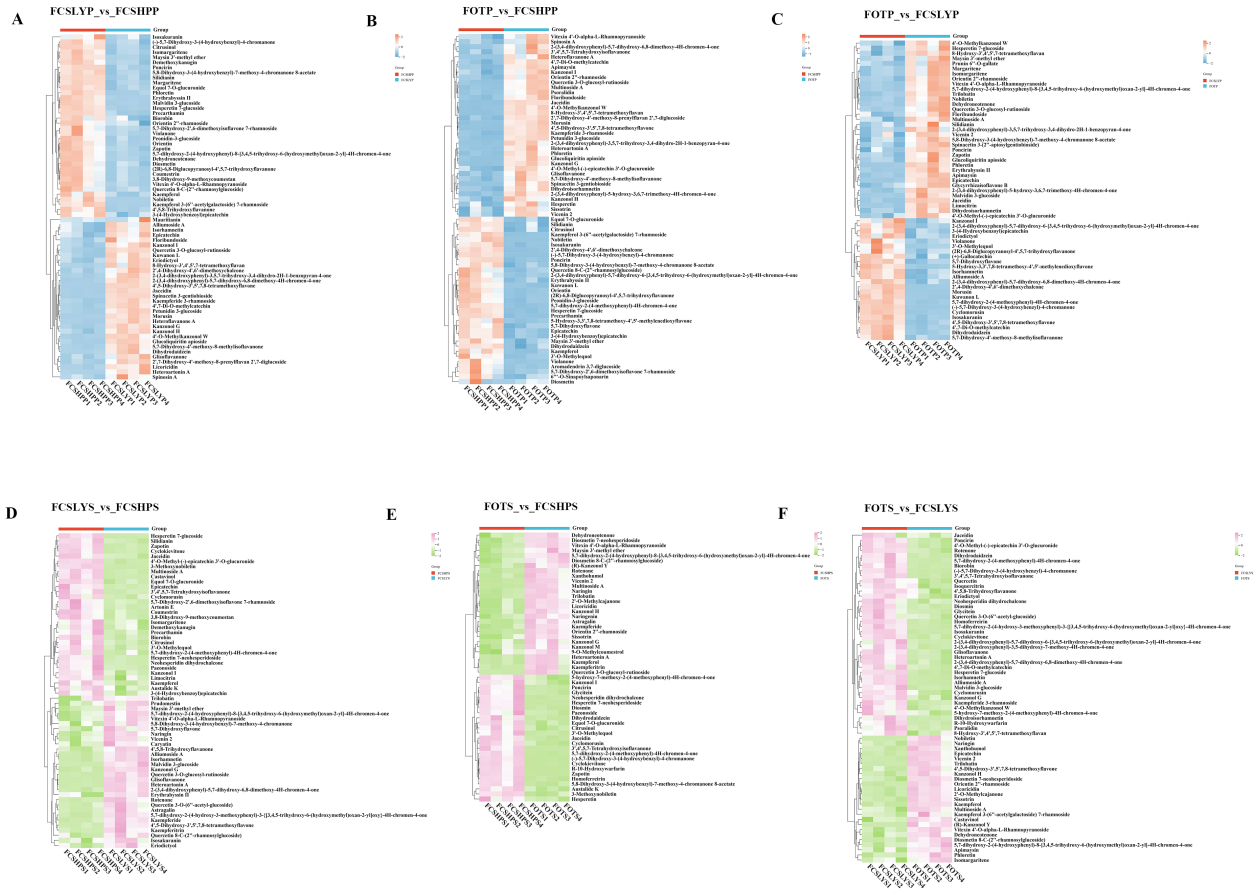

FIGURE 6
Heat map visualization of the relative content of differential flavonoid metabolites in the peel and seed comparison groups: **(A)** FCSLYP_vs_FCSHPP; **(B)** FOTP_vs_FCSHPP; **(C)** FOTP_vs_FCSLYP; **(D)** FCSLYS_vs_FCSHPS; **(E)** FOTS_vs_FCSHPS; **(F)** FOTS_vs_FCSLYS; Each column represents one sample. Each column represents one sample, and each row represents one metabolite. In the peel comparison groups, the color change from orange to blue indicates abundance changes from high to low; in the seed comparison groups, the color change from pink to green indicates abundance changes from high to low.

content of the entire fruit, and the SC content in the sweet FCSHP was significantly higher than in the other two varieties, reaching 233.37 ± 11.40 mg/g. The next highest SC content was found in the sweet FCSLY, whereas FOT had the lowest SC concentration (Figure 2A). A significant correlation was identified between fruit flavor and SC content (r = 0.98) (Figure 8), indicating that SC content is a crucial chemical indicator for determining the sweetness of kumquat. Regarding the flavor of FOT, it is characterized as acidic and it has the highest MA content. The MA content makes the fruit have sour taste characteristics. In terms of bitterness, FCSLYP exhibited the highest limonin content, followed by FOTP, with FCSHPP displaying the lowest content (Figure 3C). This result is consistent with the relative content of limonin in the three varieties and corroborates the phenotypic characteristic that FOT and FCSLY fruits exhibit bitterness, whereas FCSHP does not. Furthermore, a negative correlation was observed between fruit bitterness and SC content (correlation coefficient = −0.72) (Figure 8). The limonin content in the peel emerged as a crucial chemical indicator affecting fruit bitterness. Consequently, FCSHP is deemed more suitable for consumption as whole fruit fresh food.

3.4.2 Correlation analysis of secondary metabolites and pericarp oil gland

The oil gland density in the peel of the three kumquat varieties followed the order: FCSHPP < FCSLYP < FOTP. However, there was no significant difference in TFAC among the three varieties (Figure 3D). Analysis of non-targeted metabolomics data revealed that FCSHPP exhibited a greater number of down-regulated lipid compounds compared with FOTP and FCSLYP (Figure 9). Additionally, the relative content of lipid compounds was also lower in FCSHPP, which corresponded to the observed oil gland density (Figure 4A). Terpenes and sesquiterpenes are the main constituents of citrus essential oils found in lipids. It is plausible that these down-regulated lipids are key metabolites highly correlated with oil gland density (Table 3).

3.4.3 Secondary metabolites and peel color

The non-targeted metabolomics results revealed that FCSHPP, with a lighter fruit peel color, exhibited up-regulated expression of the 3-(4-Hydroxybenzoyl) epicatechin metabolite only compared with FCSLYP (Table 4). Additionally, FCSHPP demonstrated the highest carotenoid abundance (Figure 4A). Conversely, FOTP,

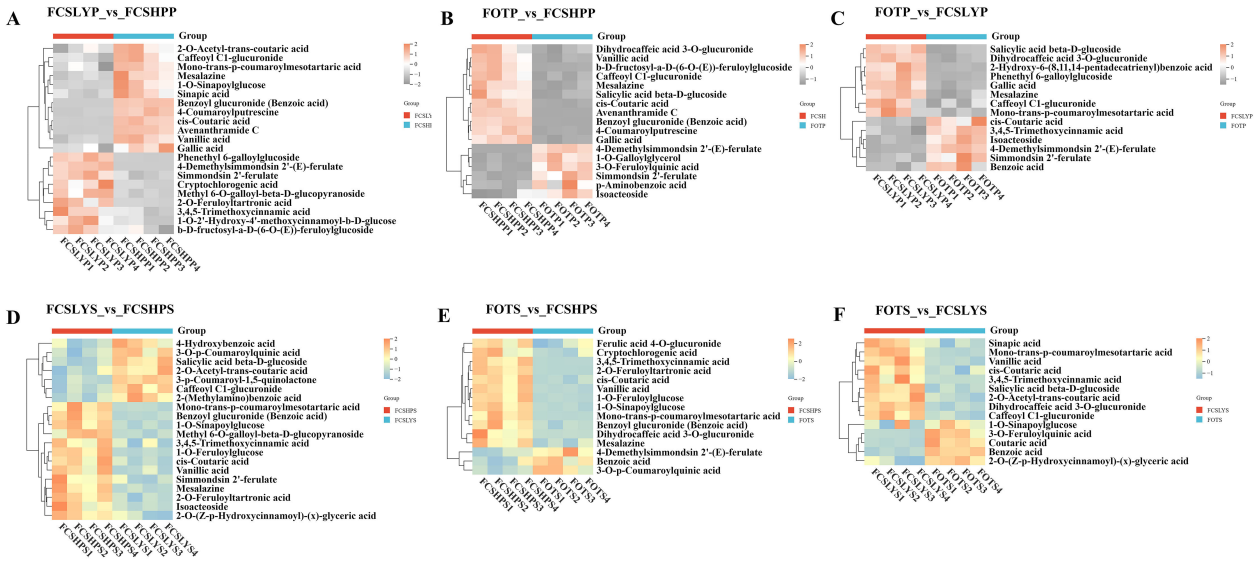

FIGURE 7
Differential phenolic acid metabolites in the peel and seed comparison groups **(A)** FCSLYP_*vs*_FCSHPP; **(B)** FOTP_*vs*_FCSHPP; **(C)** FOTP_*vs*_FCSLYP; **(D)** FCSLYS_*vs*_FCSHPS; **(E)** FOTS_*vs*_FCSHPS; **(F)** FOTS_*vs*_FCSLYS; Each column represents one sample, and each single row represents one metabolite. In the peel comparison groups, orange to gray indicates abundance changes from high to low; in the seed comparison groups, orange-yellow to blue indicates abundance changes from high to low.

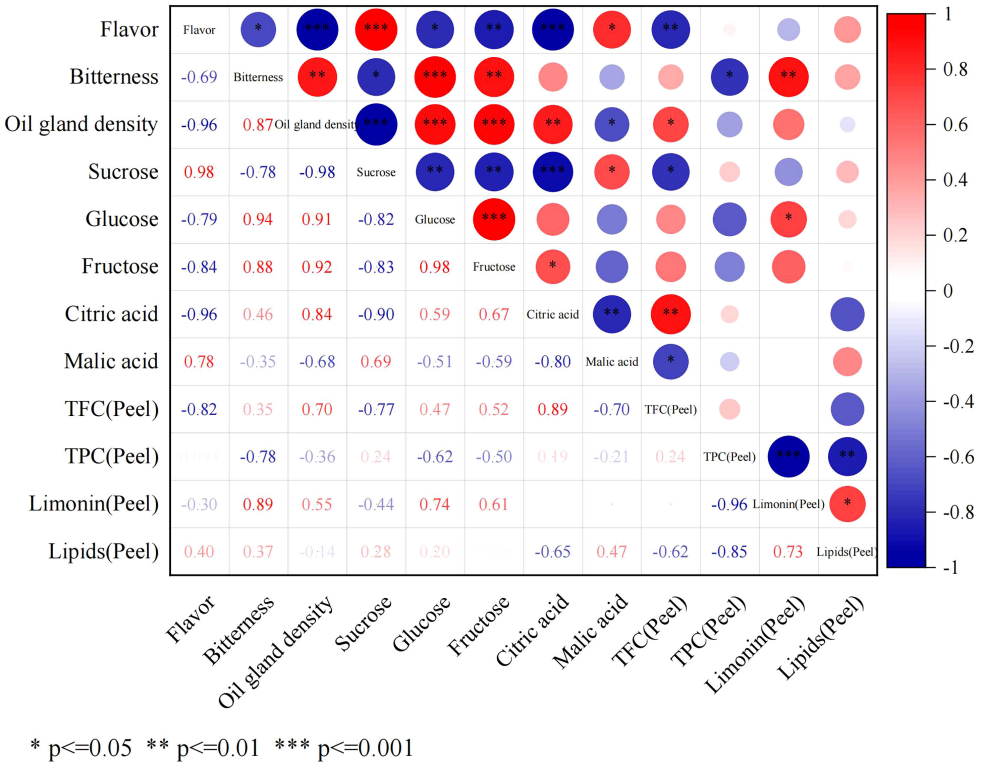

FIGURE 8
Correlation matrix between fruit flavor and all chemical indexes.

10.3389/fpls.2025.1640218

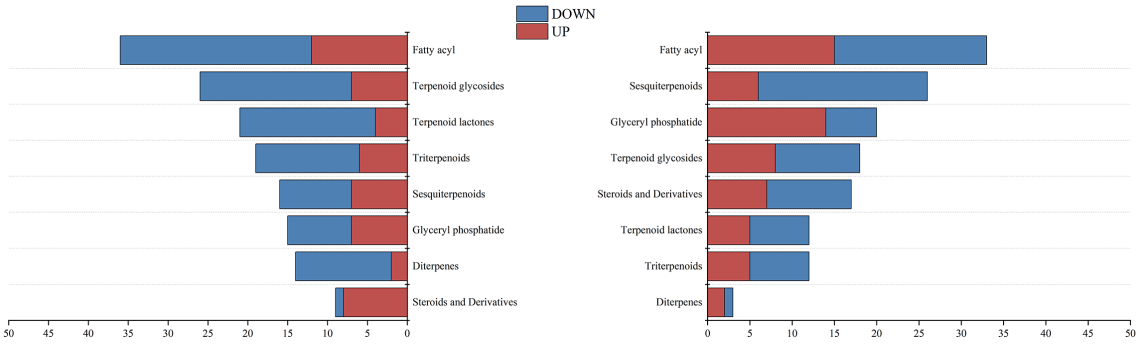

FIGURE 9
Differential expression of lipid metabolites between kumquat peel comparison groups.

characterized by the strongest redness, demonstrated a greater up-regulated expression of anthocyanin and carotene metabolites in comparison with the other two groups (Table 4), with the highest anthocyanin content (Figure 4A). Furthermore, compared with FCSHPP, FCSLYP exhibited a higher up-regulation of anthocyanin metabolites (Table 4). Consequently, it can be inferred that anthocyanin and carotene metabolites are associated with the color of kumquat peel. Notably, the metabolomic results aligned with the fruit color phenotype, with FOTP displaying the strongest redness, FCSLYP showcasing the brightest color brightness and strongest yellowness, and FCSHPP displaying the lowest brightness, redness, and yellowness (Table 2).

3.5 Differences of functional components of flavonoids and limonin between peels and seeds

In addition to the TPC, the TFC, TLC, and TFAC were found to be significantly higher in the seeds of the three kumquat varieties compared with the peels (Figure 3). Conversely, the peel exhibited a higher abundance of flavonoid metabolites. Analysis of these three varieties revealed that 35 flavonoid metabolites were up-regulated in the peel, while 18 flavonoid metabolites were up-regulated in the seeds (Table 5). Hence, it can be inferred that the peel possesses a greater medicinal value.

TABLE 3 Terpene and sesquiterpene metabolites down-regulated by FCSHPP.

Compound	Class	Compound	Class
10-Hydroxy-3-methoxy-1,3,5,7-cadinatetraen-9-one	Sesquiterpenoids	Isohumbertiol	Sesquiterpenoids
Diacetoxyscirpenol	Sesquiterpenoids	(1alpha,6alpha,7alphaH)-2,4-(15)-Copadiene	Sesquiterpenoids
Armillarin	Sesquiterpenoids	8beta-Angeloyloxy-15-hydroxy-1alpha,10R-dimethoxy-3-oxo-11-(13)-germacren-12,6alpha-olide	Terpene lactones
Lacinilene C	Sesquiterpenoids	Anhydrocinnzeylanol	Terpene lactones
3,7-Bisaboladiene-2,8-dione	Sesquiterpenoids	Eremopetasitenin C3	Terpene lactones
8-Oxodiacetoxyscirpenol	Sesquiterpenoids	Cadabicilone	Terpene lactones
Dehydrovomifoliol	Sesquiterpenoids	Veranisatin C	Terpene lactones
beta-Vatirenene	Sesquiterpenoids	(-)-trans-Carveol glucoside	Terpene glycosides
(1R,3R,4R,5S,6S,8x)-1-Acetoxy-8-angeloyloxy-3,4-epoxy-5-hydroxy-7 (14),10-bisaboladien-2-one	Sesquiterpenoids	Nepetaside	Terpene glycosides
Santalyl phenylacetate	Sesquiterpenoids	Perilloside A	Terpene glycosides
(+)-4,11-Eudesmadien-3-one	Sesquiterpenoids	Deoxyloganic acid	Terpene glycosides
Epioxylubimin	Sesquiterpenoids	(4R,5S,7R,11S)-11,12-Dihydroxy-1(10)-spirovetiven-2-one 11-glucoside	Terpene glycosides
Furoeremophilone 1	Sesquiterpenoids	(1S,4R)-10-Hydroxyfenchone glucoside	Terpene glycosides

TABLE 4 Comparison of anthocyanin and carotenoid metabolites in three peel comparison groups.

Compound	FCSLYP*vs*FCSHPP	FOTP*vs*FCSHPP	FOTP*vs*FCSLYP
anthocyanin			
(+)-Gallocatechin	ns	ns	0.026
3-(4-Hydroxybenzoyl)epicatechin	1.251	0.003	0.014
4',7-Di-O-methylcatechin	0.003	0.002	0.014
4'-O-Methyl-(-)-epicatechin 3'-O-glucuronide	NS	0.009	0.023
Epicatechin	0.026	0.008	0.012
Malvidin 3-glucoside	0.003	NS	0.036
Petunidin 3-glucoside	0.007	0.001	0.036
carotenoid			
Lutein	ns	0.081	ns
(9Z,7'Z,9'Z)-7,8-Dihydrolycopene	ns	ns	ns
Phytofluene	ns	ns	ns

The values presented in the table represent the FOLD CHANGE (FC) values. The fold change is calculated based on the ratio of the peak areas of each metabolite in the comparative group samples. For instance, in the comparison a versus b, the FC is determined by the formula Fc = b/a, where 'a' and 'b' correspond to the average peak areas of the metabolite from four replicates of the left and right samples in the comparative group, respectively. The value of FC>1 indicates that the expression of metabolites on the right side of the control group is up-regulated; The abbreviation "ns" denotes that the metabolite in question is not identified as a differential metabolite within the control group.

The kumquat seeds were found to contain higher levels of limonin compounds compared with peels, particularly with the TLC reaching 93.99 ± 5.38 mg/g in FOTS. Non-targeted metabolomics analysis detected four limonin compounds, namely deacetylnomilin, limonin, Obacunone, and nomilin. In the peel samples, Deacetylnomilin, Obacunone, and Limonin were detected in all three varieties (FCSHPP, FCSLYP, and FOTP) (Figure 10A), with FOTP showing the highest accumulation and FCSHPP the lowest. In seeds, in addition to these three limonoids, Nomilin was also detected (Figure 10B). All four limonoid metabolites accumulated most abundantly in FOTS. This suggests that kumquat seeds can be utilized as a raw material for extracting limonin.

4 Discussions

Various factors influence the flavor of kumquat fruit, and the SC content plays a crucial role in determining its sweetness. Limonoids contribute to the bitter taste in kumquats. Additionally, flavonoid metabolites, such as poncirin, naringin, and nobiletin, also contribute to the bitterness of citrus fruits. In our study, the aforementioned three metabolites were found to be up-regulated in FCSHPP. Furthermore, the accumulation of limonoid compounds was lowest in FCSHPP, which is consistent with the findings reported by Qiaoli Ma et al (Ma et al., 2021), indicating that limonoids are the main factors affecting bitterness. Naringin can be hydrolyzed to L-rhamnose and chernoside, with the bitterness reduced through further hydrolysis of 33% of the chernoside of naringin to non-bitter naringenin and D-glucose. However, naringenin is a unique FCSHPP flavonoid metabolite. We also observed the up-regulation of neohesperidin dihydrochalcone, an important sweetening compound, in addition to the highest SC concentration in FCSHP. These differences in metabolite underscore the reason why FCSHP imparts a pleasant taste, making it more suitable for fresh consumption of whole fruit.

The pigmentation of the peel is a crucial aspect of fruit appearance, as consumers make their selection based on factors such as red and yellow intensity, luminosity, and peel pigmentation (Ze et al., 2012). In citrus fruits, the peel color is primarily determined by water-soluble anthocyanins and fat-soluble carotenes (Xu and Deng, 2002). The peel color of the three kumquat varieties exhibited distinct differences. FOTP displayed the highest levels of redness and color index, with a greater abundance of up-regulated anthocyanin and carotene metabolites. FCSLYP exhibited superior color brightness and increased yellowness. In contrast, FCSHPP demonstrated the lowest color index, indicating that the anthocyanin and carotene metabolites impacted the kumquat peel coloration.

Lipids serve as key components or precursors of essential oils, primarily synthesized and stored in the oil glands of citrus fruits (Siau Sie et al., 2012). Sesquiterpenes and terpenes are the primary constituents of essential oils (Flamini et al., 2007). The oil gland density on the surface of FCSHP is the lowest, while the surface of FCSLY and FOT has a higher oil gland density. However, there was no significant difference in the TFAC among the three kumquat varieties. Nevertheless, the metabolomic analysis revealed that FOTP and FCSLYP exhibited a greater abundance of up-regulated differential metabolites in steroids, sesquiterpenes, triterpenoids, terpene lactones, terpenoid glycosides, and fatty acyl subclasses, compared with FCSHPP. These metabolites may be associated with the characteristic of oil gland density. Consequently, the oil gland density in kumquats appears unrelated to the total lipid content in the peel but influenced by specific lipid metabolites.

TABLE 5 Comparison of up-regulated flavonoid metabolites in the peels and seeds of three kumquat cultivars.

Compound	Class	Compound	Class
peel			
Phloretin	Chalcones and dihydrochalcones	Diosmetin 8-C-(2”-rhamnosylglucoside)	Flavonoid glycosides
epsilon-Viniferin	2-arylbenzofuran flavonoids	Margaritene	Flavonoid glycosides
(-)-5,7-Dihydroxy-3-(4-hydroxybenzyl)-4-chromanone	Homoisoflavonoids	Isoquercitrin	Flavonoid glycosides
5,8-Dihydroxy-3-(4-hydroxybenzyl)-7-methoxy-4-chromanone 8-acetate	Homoisoflavonoids	Isomargaritene	Flavonoid glycosides
5,7-dihydroxy-2-(4-methoxyphenyl)-4H-chromen-4-one	Flavonoids	Spinacetin 3-gentiobioside	Flavonoid glycosides
Cyclomorusin	Flavonoids	(2R)-6,8-Diglucopyranosyl-4’,5,7-trihydroxyflavanone	Flavonoid glycosides
Dihydroisorhamnetin	Flavonoids	Quercetin	Flavonoids
8-Hydroxy-3’,4’,5’,7-tetramethoxyflavan	Flavonoids	Isorhamnetin	Flavonoids
Heteroflavanone A	Flavonoids	5,7-Dihydroxyflavone	Flavonoids
Citrusinol	Flavonoids	Silidianin	Flavans
Vitexin 4’-O-alpha-L-Rhamnopyranoside	Flavonoid glycosides	Kanzonol I	Isoflavonoids
Kaempferide 3-rhamnoside	Flavonoid glycosides	4’-O-Methylkanzonol W	Isoflavonoids
Hesperetin 7-glucoside	Flavonoid glycosides	Dehydroneotenone	Isoflavonoids
Isosakuranin	Flavonoid glycosides	Violanone	Isoflavonoids
5,7-dihydroxy-2-(4-hydroxyphenyl)-8-[3,4,5-trihydroxy-6-(hydroxymethyl) oxan-2-yl]-4H-chromen-4-one	Flavonoid glycosides	Equol 7-O-glucuronide	Isoflavonoids
Alliumoside A	Flavonoid glycosides	Dihydrodaidzein	Isoflavans
Apimaysin	Flavonoid glycosides	3,8-Dihydroxy-9-methoxycoumestan	Isoflavonoids
2-(3,4-dihydroxyphenyl)-5,7-dihydroxy-6-[3,4,5-trihydroxy-6-(hydroxymethyl)oxan-2-yl]-4H-chromen-4-one	Flavonoid glycosides		
Seed			
R-10-Hydroxywarfarin	Homoisoflavonoids	Castavinol	Flavans
4’,5-Dihydroxy-3’,5’,7,8-tetramethoxyflavone	Flavonoids	Epicatechin	Flavans
Zapotin	Flavonoids	Licoricidin	Isoflavonoids
Poncirin	Flavonoid glycosides	Kanzonol H	Isoflavonoids
Maysin 3’-methyl ether	Flavonoid glycosides	3’-O-Methylequol	Isoflavonoids
Biorobin	Flavonoid glycosides	2’-O-Methylcajanone	Isoflavans
Heteroartonin A	Flavonoids	Psoralidin	Isoflavonoids
Kaempferol	Flavonoids	(R)-Kanzonol Y	Chalcones and dihydrochalcones
KB 2	Flavonoids	Viniferal	2-arylbenzofuran flavonoids

Limonoids, which are tetracyclic triterpenoids, represent a major source of bitterness in citrus plants. They exhibit a wide range of biological activities, including anticancer, antibacterial, antiviral, antioxidant, and insecticidal properties (Shunming et al., 2019). Bently et al. demonstrated that limonoids derived from citrus plants possess certain anti-feeding effects on Lepidoptera, Coleoptera, and Heteroptera (Bentley et al., 1990). Additionally, other studies have reported their inhibitory effects on insect growth (Essoung et al., 2018; Jimenez et al., 1997). The content of limonoids in FCSLYP and FOTP is higher compared with FCSHPP, which enhances their resistance to insects and diseases. Liu et al. (Can et al., 2012) reported the extraction yield of limonin from citrus

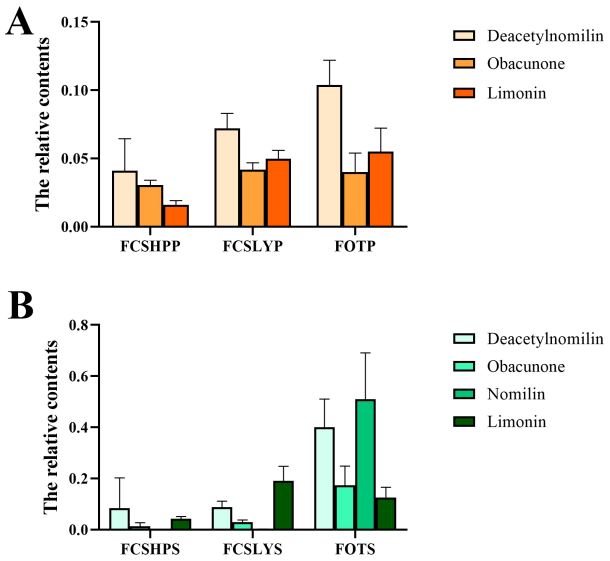

FIGURE 10
Relative abundance of metabolites in peels and seeds of three kumquats, analyzed using LC-MS/MS and HPLC. **(A)** Relative content of limonoid metabolites in the peel. **(B)** Relative content of limonoid metabolites in the seeds.

seeds to be 7.5 mg/g under optimal conditions. Vaniya Chinapongtitiwat et al. reported limonin contents in the peels of pomelo and lime to be 86 ± 10 ppm and 194 ± 34 ppm (DW), respectively. (Montoya et al., 2019) reported the TLC in the seeds of citrus, lemon, sweet orange, and sour orange, which were 7497 ± 870 mg/kg, 5349 ± 112 mg/kg, 4899 ± 385 mg/kg, and 1035 ± 140 mg/kg, respectively. Ma detected the TLC in Nanfeng mandarin peel within the range of 3.08 ± 0.07 to 5.51 ± 0.11 mg/g DW (Ma, 2019). The findings of this study revealed that the TLC in kumquat seeds was higher than in the peels, ranging from 24.85 ± 2.19 to 93.99 ± 5.38 mg/g and 2.24 ± 0.04 to 8.43 ± 0.38 mg/g, respectively. Notably, FOTS exhibited a remarkably higher limonin content of 93.99 ± 5.38 mg/g, surpassing the TLC found in the peels and seeds of other citrus fruits. FOTS contained four limonoids: deacetylnomilin, limonin, obacunone, and nomilin. However, (Kim, 2021) detected only limonin in the pulp of Changshou kumquat. This suggests limonoids mainly accumulate in kumquat seeds. Consequently, kumquat seeds represent an excellent source of limonoids.

In this study, a total of 161 flavonoid metabolites were identified in the peels and seeds of three kumquat varieties. The findings revealed that 35 flavonoid metabolites were up-regulated in the peels, while 18 flavonoids showed higher expression in the seeds. Notably, flavan 3-(4-Hydroxybenzoyl)epicatechin and flavonoid glycoside 6"'-O-Sinapoylsaponarin were exclusively detected in the peel. Among these compounds, neohesperidin dihydrochalcone, a chalcone derivative, is known for its high sweetness, caries-free properties, and low energy value, making it a viable sugar substitute (Tomás-Barberán and Clifford, 2000). This study also detected six chalcones and dihydrochalcones in the peels and seeds of the three kumquat cultivars, namely neohesperidin dihydrochalcone, (R)-Kanzonol Y, 2',4-Dihydroxy-4',6'-dimethoxychalcone, phloretin, xanthohumol D, and xanthohumol. Moreover the peels of long-lived kumquats are easier to peel, facilitating the extraction and application of chalcone compounds found in the peels. Consequently, the long-lived kumquat exhibits promising medicinal value.

The Citrus primarily contains O-glycosylated flavonoids and flavanones (Wang et al., 2017, Wang et al., 2021), while the kumquat is characterized by C-glycosylated flavonoids (Lou and Ho, 2017). The hybrid FOT showed distinct flavonoid accumulation patterns: O-glycosylated flavonoids were upregulated in the peel, while both O- and C-glycosylated flavonoids were enriched in the seeds. These metabolic features reflect contributions from both parental genera, enhancing flavonoid diversity. Both FCSLY and FCSHP exhibited significant accumulation of methylated flavonoids and polymethoxyflavones (PMFs) in their peel and seed tissues. Our analysis identified 49 O-glycosylated flavonoids and 5 C-glycosylated flavonoids across three kumquat varieties (Supplementary Table S3). Only three flavanones were detected: Eriodictyol, 4',5,8-Trihydroxyflavanone, and Naringenin, confirming relatively scarce flavanone distribution in kumquat. Notably, previous studies reported that isoflavones mainly exist in legumes or Chinese medicinal materials (e.g., soybeans) (Huang et al., 2022)and play important roles in plant defense. Fu Wang et al. identified 8 isoflavones in orange peels (Wang et al., 2019). In our study, 32 isoflavones were identified in kumquat peels and seeds, such as Coumestrin, Psoralidin, Cyclokievitone, Dihydrodaidzein, Glisoflavanone, and Rotenone (Supplementary Table S3). Furthermore, apart from previously reported flavonoids in kumquat (e.g., Phloretin, Diosmin, Isorhamnetin, Kaempferol, Quercetin, Luteolin, and Poncirin) (Lou et al., 2015; Lou and Ho, 2017), we detected additional flavonoids in kumquat, including Naringin (previously found in pomelos) (Xi et al., 2014), Nobiletin (in Citrus) (Cheng et al., 2024), and Diosmetin (in oranges, bergamots, and lemons) (Mandalari et al., 2006; Lin and Harnly, 2007). Notably, flavonoids rarely reported in kumquat, such as Limocitrin, Isosakuranin, Orientin, Kaempferitrin, and Hesperetin, were also identified, along with their glycosylated forms (e.g., Diosmetin 7-neohesperidoside, Hesperetin 7-neohesperidoside, Luteolin 7-glucoside, Quercetin 3-O-glucosyl-rutinoside, and Orientin 2"-rhamnoside). Our findings expand the diversity of flavonoid components in kumquat.

Phenolic acids significantly influence the flavor profile of citrus fruits and serve as important antioxidants in the peel (Bian et al., 2022; Peng et al., 2025). Both FCSHPP and FCSHPS exhibited upregulated expression of numerous phenolic acid metabolites, which may contribute substantially to their distinct flavor characteristics. In this study, we identified 44 phenolic acids in kumquat peel and seeds (Supplementary Table S4), including free phenolic acids (sinapic acid, gallic acid, vanillic acid, coumaroyl tartaric acid, cryptochlorogenic acid, syringic acid, benzoic acid, and salicylic acid) along with various derivatives (1-O-Feruloylglucose, 2-O-p-Coumaroyltartronic acid, Caffeoyl C1-glucuronide, and 1-O-Galloylglycerol). Previous studies reported different phenolic acid profiles in citrus species. Chen et al, detected 7 phenolic acids (gallic acid, chlorogenic acid, protocatechuic acid,

caffeic acid, p-coumaric acid, ferulic acid, and benzoic acid) in the peels of citrus, pomelo, and kumquat (Chen et al., 2021). Peng et al, identified 77 phenolic acids across five citrus varieties in both pulp and peel tissues (Peng et al., 2025). The distribution patterns of phenolic acids varied significantly depending on both cultivar types and tissue parts, which may also be attributed to growth conditions and fruit ripening stages.

Secondary metabolites play a pivotal role in influencing the quality, flavor, and medicinal properties of fruits. Currently, research on kumquat fruit secondary metabolites predominantly focuses on phenols, flavonoids, limonoids, and other compounds. High-throughput detection of secondary metabolites through non-targeted metabolomics can greatly facilitate the comprehensive development and utilization of kumquat plants.

5 Conclusion

In this study, a total of 1719 metabolites were identified, encompassing 15 compound categories and 27 subcategories. Specifically, FCSHP exhibited high SC content levels, and abundant peel flavonoids, rendering it nutritionally valuable and well-suited for whole fruit consumption. FCSLY possesses both edible and medicinal value. The peel of FOTS is rich in flavonoids and easy to peel, making it suitable for medicinal purposes, while the seeds of FOTS serve as a favorable source of limonoids. Therefore, this study delved into the correlation mechanisms between fruit flavor, oil gland, color variation, and the secondary metabolites of three kumquat varieties, providing valuable insights for the practical application of kumquats.

Data availability statement

The original contributions presented in the study are included in the article/Supplementary Material. Further inquiries can be directed to the corresponding author.

Author contributions

ML: Conceptualization, Data curation, Formal Analysis, Investigation, Methodology, Software, Visualization, Writing – original draft, Writing – review & editing. ZY: Investigation, Software, Writing – original draft. HS: Writing – review & editing. CZ: Resources, Writing – original draft. HH: Conceptualization, Funding acquisition, Project administration, Resources, Supervision, Writing – original draft, Writing – review & editing.

Funding

The author(s) declare financial support was received for the research and/or publication of this article. This work was financially supported by the Changsha Science and Technology Plan Project (kq2004033).

Acknowledgments

This is a short text to acknowledge the contributions of specific colleagues, institutions, or agencies that aided the efforts of the authors.

Conflict of interest

The authors declare that the research was conducted in the absence of any commercial or financial relationships that could be construed as a potential conflict of interest.

Generative AI statement

The author(s) declare that no Generative AI was used in the creation of this manuscript.

Any alternative text (alt text) provided alongside figures in this article has been generated by Frontiers with the support of artificial intelligence and reasonable efforts have been made to ensure accuracy, including review by the authors wherever possible. If you identify any issues, please contact us.

Publisher's note

Supplementary material

The Supplementary Material for this article can be found online at: https://www.frontiersin.org/articles/10.3389/fpls.2025.1640218/full#supplementary-material

References

Abirami, A., Nagarani, G., and Siddhuraju, P. (2014). *In vitro* antioxidant, anti-diabetic, cholinesterase and tyrosinase inhibitory potential of fresh juice from Citrus hystrix and C. maxima fruits. *Food Sci. Hum. Wellness.* 3 (1), 16-25. doi: 10.1016/j.fshw.2014.02.001

Aravind, S., Barik, D., Ragupathi, P., and Vignesh, G. (2021). Investigation on algae oil extraction from algae Spirogyra by Soxhlet extraction method. *Materials Today: Proc.* 43, 308-313. doi: 10.1016/j.matpr.2020.11.668

Barreca, D., Bellocco, E., Caristi, C., Leuzzi, U., and Gattuso, G. (2011). Kumquat (Fortunella japonica Swingle) juice: Flavonoid distribution and antioxidant properties. *Food Res. Int.* 44, 2190–2197. doi: 10.1016/j.foodres.2010.11.031

Bentley, M. D., Rajab, M. S., Mendel, M. J., and Alford, A. R. (1990). Limonoid model insect antifeedants. *J. Agric. Food Chem.* 38, 1403–1406. doi: 10.1021/jf00096a022

Bian, X., Xie, X., Cai, J., Zhao, Y., Miao, W., Chen, X., et al. (2022). Dynamic changes of phenolic acids and antioxidant activity of Citri Reticulatae Pericarpium during aging processes. *Food Chem.* 373, 131399. doi: 10.1016/j.foodchem.2021.131399

Can, L., Jing, L., Yonghai, R., Nvyong, L., and Long, R. (2012). Aqueous extraction of limonin from Citrus reticulate Blanco. *Czech J. Food Sci.* 30, 364–368. doi: 10.17221/108/2011-CJFS

Chen, Y., Pan, H., Hao, S., Pan, D., and Yu, W. (2021). Evaluation of phenolic composition and antioxidant properties of different varieties of Chinese citrus. *Food Chem.* 1), 130413. doi: 10.1016/j.foodchem.2021.130413

Cheng, Y., Feng, S., Sheng, C., Yang, C., and Li, Y. (2024). Nobiletin from citrus peel: a promising therapeutic agent for liver disease-pharmacological characteristics, mechanisms, and potential applications. *Front. Pharmacol.* 15. doi: 10.3389/fphar.2024.1354809

China National Institute Of Standardization (2020). "GB/T 39558–2020 Sensory analysis—Methodology—"A"-"not A" test," (Beijing: State Administration for Market Regulation and the Standardization Administration of China).

Dongjiang,, and Gong, G. (2006). Descriptors and Data Standard for Citrus (Citrus *spp.*). (Beijing: China Agriculture Press).

Essoung, F. R. E., Chhabra, S. C., Mba'ning, B. M., Mohamed, S. A., Lwande, W., Lenta, B. N., et al. (2018). Larvicidal activities of limonoids from Turraea abyssinica (Meliaceae) on Tuta absoluta (Meyrick). *J. Appl. Entomology* 142, 397–405. doi: 10.1111/jen.12485

Flamini, G., Tebano, M., and Cioni, P. L. (2007). Volatiles emission patterns of different plant organs and pollen of Citrus limon. *Analytica Chimica Acta* 589, 120–124. doi: 10.1016/j.aca.2007.02.053

Hu, F. G., Bi, X. F., Fu, X. F., Li, Y. A., Li, G. P., Li, Y. Q., et al. (2023). Comparative metabolome profiles and antioxidant potential of four coffea arabica L. Varieties differing in fruit color. *Diversity-Basel* 15, 724. doi: 10.3390/d15060724

Huang, L., Zheng, T., Hui, H., and Xie, G. (2022). Soybean isoflavones modulate gut microbiota to benefit the health weight and metabolism. *Front. Cell. Infection Microbiol.* 12. doi: 10.3389/fcimb.2022.1004765

Jimenez, A., Mata, R., Pereda-Miranda, R., Calderon, J., Isman, M. B., Nicol, R., et al. (1997). Insecticidal Limonoids from Swietenia humilis and Cedrela salvadorensis. *J. Chem. Ecol.* 23, 1225–1234. doi: 10.1023/B:JOEC.0000006460.25281.9d

Kim, H. J. (2021). Comparative metabolomics analysis of citrus varieties. *Foods* 10, 2826. doi: 10.3390/foods10112826

Li, X., Meenu, M., and Xu, B. (2023). Recent development in bioactive compounds and health benefits of kumquat fruits. *Food Rev. Int.* 39 (7), 4312-4332. doi: 10.1080/87559129.2021.2023818

Lin, L. Z., and Harnly, J. M. (2007). A screening method for the identification of glycosylated flavonoids and other phenolic compounds using a standard analytical approach for all plant materials. *J. Agric. Food Chem.* 55, 1084. doi: 10.1021/jf062431s

Liu, X., Liu, B., Jiang, D., Zhu, S., Shen, W., Yu, X., et al. (2019). The accumulation and composition of essential oil in kumquat peel. *Scientia Hortic.* 252, 121–129. doi: 10.1016/j.scienta.2019.03.042

Lou, S. N., and Ho, C. T. (2017). Phenolic compounds and biological activities of small-size citrus: Kumquat and calamondin. *J. Food Drug Anal.* 25, 162–175. doi: 10.1016/j.jfda.2016.10.024

Lou, S. N., Lai, Y. C., Huang, J. D., Ho, C. T., Ferng, L. H. A., and Chang, Y. C. (2015). Drying effect on flavonoid composition and antioxidant activity of immature kumquat. *Food Chem.* 171, 356–363. doi: 10.1016/j.foodchem.2014.08.119

Ma, Q. (2019). *Study on the change of nutrition and functional components in Nanfeng tangerine during ripening*. (master's thesis). (Nanchang (Jiangxi): Jiangxi Science and Technology Normal University). doi: 10.27751/d.cnki.gjxkj.2019.000161

Ma, Q. L., Hu, Y. W., Dong, X. H., Zhou, G. F., Liu, X., Gu, Q. Q., et al. (2021). Metabolic profiling and gene expression analysis unveil differences in flavonoid and lipid metabolisms between 'Huapi' Kumquat (Fortunella crassifolia swingle) and its wild type. *Front. Plant Sci.* 12. doi: 10.3389/fpls.2021.759968

Mandalari, G., Bennett, R. N., Bisignano, G., Saija, A., Dugo, G., Lo Curto, R. B., et al. (2006). Characterization of flavonoids and pectins from bergamot (Citrus bergamia Risso) peel, a major byproduct of essential oil extraction. *J. Agric. Food Chem.* 54, 197–203. doi: 10.1021/jf051847n

Min-Hung, C., Kai-Min, Y., Tzou-Chi, H., and Mei-Li, W. (2017). Traditional small-size citrus from Taiwan: essential oils, bioactive compounds and antioxidant capacity. *Medicines* 4, 28. doi: 10.3390/medicines4020028

Montoya, C., González, L., Pulido, S., Atehortúa, L., and Robledo, S. M. (2019). Identification and quantification of limonoid aglycones content of Citrus seeds. *Rev. Bras. Farmacognosia-Brazilian J. Pharmacognosy* 29, 710–714. doi: 10.1016/j.bjp.2019.07.006

Ogawa, K., Kawasaki, A., Omura, M., Yoshida, T., Ikoma, Y., and Yano, M. (2001). 3',5'-Di-C-beta-glucopyranosylphloretin, a flavonoid characteristic of the genus Fortunella. *Phytochemistry* 57, 737–742. doi: 10.1016/s0031-9422(01)00132-7

Palma, A., and D'Aquino, S. (2018). "Kumquat— Fortunella japonica," in *Exotic Fruits*. (San Diego, CA: Academic Press), 271–278.

Peng, Y., Cui, X., Sun, M., Huang, X., Tang, K., Hu, B., et al. (2025). Liquid chromatographyTandem mass spectrometry analysis of primary metabolites and phenolic acids across five citrus species. *Curr. Issues Mol. Biol.* 47, 223. doi: 10.3390/cimb47040223

Qingguo Tian, L. D. (1999). A rapid and simple spectrophotometric method for the determination of limonoids in citrus seeds. *J. Instrumental Chem.* 18, 456–460. doi: 10.3969/j.issn.1004-4957.1999.05.015

Sadek, E. S., Makris, D. P., and Kefalas, P. (2009). Polyphenolic composition and antioxidant characteristics of kumquat (Fortunella margarita) peel fractions. *Plant Foods Hum. Nutr.* 64, 297–302. doi: 10.1007/s11130-009-0140-1

Shunming, F., Chunling, Z., Ting, L., Jiaqi, W., Yu, T., Zhimin, C., et al. (2019). Limonin: a review of its pharmacology, toxicity, and pharmacokinetics. *Molecules* 24, 3679. doi: 10.3390/molecules24203679

Siau Sie, V., Grimes, H. D., and Lange, B. M. (2012). Assessing the biosynthetic capabilities of secretory glands in Citrus peel. *Plant Physiol.* 159, 81–94. doi: 10.1104/pp.112.194233

Sun, X. S., Wang, Z., Li, X., Du, S. H., Lin, D. M., and Shao, Y. X. (2023). Effects of Yucca schidigera extract on serum biochemical parameters, humoral immune response, and intestinal health in young pigeons. *Front. Veterinary Sci.* 9. doi: 10.3389/fvets.2022.1077555

Tan, S., Zhao, X., Yang, Y., Ke, Z., and Zhou, Z. (2016). Chemical profiling using uplc Q-tof/ms and antioxidant activities of fortunella fruits. *J. Food Sci.* 81, C1646–C1653. doi: 10.1111/1750-3841.13352

Tomás-Barberán, F. A., and Clifford, M. N. (2000). Flavanones, chalcones and dihydrochalcones – nature, occurrence and dietary burden. *J. Sci. Food Agric.* 80, 1073–1080. doi: 10.1002/(SICI)1097-0010(20000515)80:73.0.CO;2-B

Wang, F., Chen, L., Chen, H., Chen, S., and Liu, Y. (2019). Analysis of flavonoid metabolites in citrus peels (Citrus reticulata "Dahongpao") using UPLC-ESI-MS/MS. *Molecules* 24, 2680. doi: 10.3390/molecules24152680

Wang, S., Yang, C., Tu, H., Zhou, J., Liu, X., Cheng, Y., et al. (2017). Characterization and metabolic diversity of flavonoids in citrus species. *Sci. Rep.* 7, 10549. doi: 10.1038/s41598-017-10970-2

Wang, Y., Liu, X. J., Chen, J. B., Cao, J. P., and Sun, C. D. (2021). Citrus flavonoids and their antioxidant evaluation. *Crit. Rev. Food Sci. Nutr.* 2), 1–22. doi: 10.1080/10408398.2020.1870035

Wu, W., Jiao, C., Li, H., Ma, Y., and Liu, S. (2018). LC-MS based metabolic and metabonomic studies of Panax ginseng. *Phytochem. Anal.* 29, 331–340. doi: 10.1002/pca.2752

Xi, W., Fang, B., Zhao, Q., Jiao, B., and Zhou, Z. (2014). Flavonoid composition and antioxidant activities of Chinese local pummelo (Citrus grandis Osbeck.) varieties - ScienceDirect. *Food Chem.* 161, 230–238. doi: 10.1016/j.foodchem.2014.04.001

Xu, J., and Deng, X. X. (2002). Red juice sac of citrus and its main pigments. *Int. J. Fruit Sci.* 5, 30-36. doi: 10.3969/j.issn.1009-9980.2002.05.006

Yasuda, K., Yahata, M., and Kunitake, H. (2016). Phylogeny and classification of kumquats (Fortunella spp.) inferred from CMA karyotype composition. *Hort J.* 85, 115-121. doi: 10.2503/hortj.MI-078

Ze, Y., Shuai, J., Yuduan, D., Zhuang, W., Huijun, G., Zhiyong, P., et al. (2012). Comparative transcriptomics and proteomics analysis of citrus fruit, to improve understanding of the effect of low temperature on maintaining fruit quality during lengthy post-harvest storage. *J. Exp. Bot.* 63, 2873–2893. doi: 10.1093/jxb/err390

Zhang, Y. (2019). *Analysis of the distribution status and climate suitable distribution areas of Fortunella in China*. (dissertation/master's thesis). (Hunan Agricultural University). doi: 10.27136/d.cnki.ghunu.2019.000525

frontiers | Frontiers in Plant Science

TYPE Original Research
PUBLISHED 12 September 2025
DOI 10.3389/fpls.2025.1660363

OPEN ACCESS

EDITED BY
Robin Joshi,
University of Pennsylvania, United States

REVIEWED BY
Ashok Gehlot,
Institute of Himalayan Bioresource Technology (CSIR), India
Shruti Sharma,
University of Alabama, United States
Eliza De Jesus Barros Dos Santos,
Museu Paraense Emílio Goeldi, Brazil

*CORRESPONDENCE
Mukesh Meena
mukeshmeenamlsu@gmail.com;
drmukeshmeena321@mlsu.ac.in

RECEIVED 05 July 2025
ACCEPTED 11 August 2025
PUBLISHED 12 September 2025

CITATION
Sonigra P and Meena M (2025) Influence of growth stage on the chemical composition, antimicrobial, and antioxidant potential of *Cymbopogon martinii* (Roxb.) Wats. essential oil. *Front. Plant Sci.* 16:1660363. doi: 10.3389/fpls.2025.1660363

Influence of growth stage on the chemical composition, antimicrobial, and antioxidant potential of *Cymbopogon martinii* (Roxb.) Wats. essential oil

Priyankaraj Sonigra and Mukesh Meena*

Laboratory of Phytopathology and Microbial Biotechnology, Department of Botany, Mohanlal Sukhadia University, Udaipur, Rajasthan, India

Introduction: *Cymbopogon martinii* (Roxb.) Wats. essential oil (CMEO) exhibits significant variation in composition and bioactivity across different growth stages. Understanding these changes is crucial for optimizing its therapeutic and industrial applications.

Methods: CMEO was extracted at the vegetative, reproductive, and post-reproductive stages using hydro-distillation. Chemical composition was analyzed by GC-MS. Antimicrobial activity was assessed using disc diffusion and direct contact assays, while antioxidant potential was evaluated through DPPH, ABTS, and β-carotene bleaching assays. Correlation analysis was performed to link major bioactive compounds with biological activities.

Results: A total of 59 compounds were identified, with the reproductive stage showing the highest diversity (49 compounds, 97.86%) and oil yield. Major compounds varied across stages: carveol (20.87%), trans-p-mentha-1(7),8-dien-2-ol (12.9%), and D-limonene (6.2%) dominated the vegetative phase; cis-piperitol (15.27%), cis-p-mentha-1(7),8-dien-2-ol (15.52%), and carvone (3.31%) were abundant in the reproductive phase; while the post-reproductive phase was rich in trans-p-mentha-1(7),8-dien-2-ol (19.58%) and carveol (11.32%). Antibacterial and antifungal activities were highest during the reproductive stage, particularly against *Staphylococcus aureus* and *Alternaria alstroemeriae*. Antioxidant potential peaked during the post-reproductive phase, with the lowest IC_{50} values.

Discussion: Correlation analysis revealed negative associations between key bioactive compounds (e.g., carvone, D-limonene, α-methylcinnamaldehyde, and (S)-perillyl alcohol) and microbial/oxidative inhibition thresholds, confirming their contribution to CMEO bioactivity. These findings highlight the critical role of harvest timing in maximizing the chemical richness, antimicrobial efficacy, and antioxidant potential of CMEO.

KEYWORDS

***Cymbopogon martinii*, growth stages, essential oils, post-harvest pathogen, antimicrobial activity, antioxidant activity**

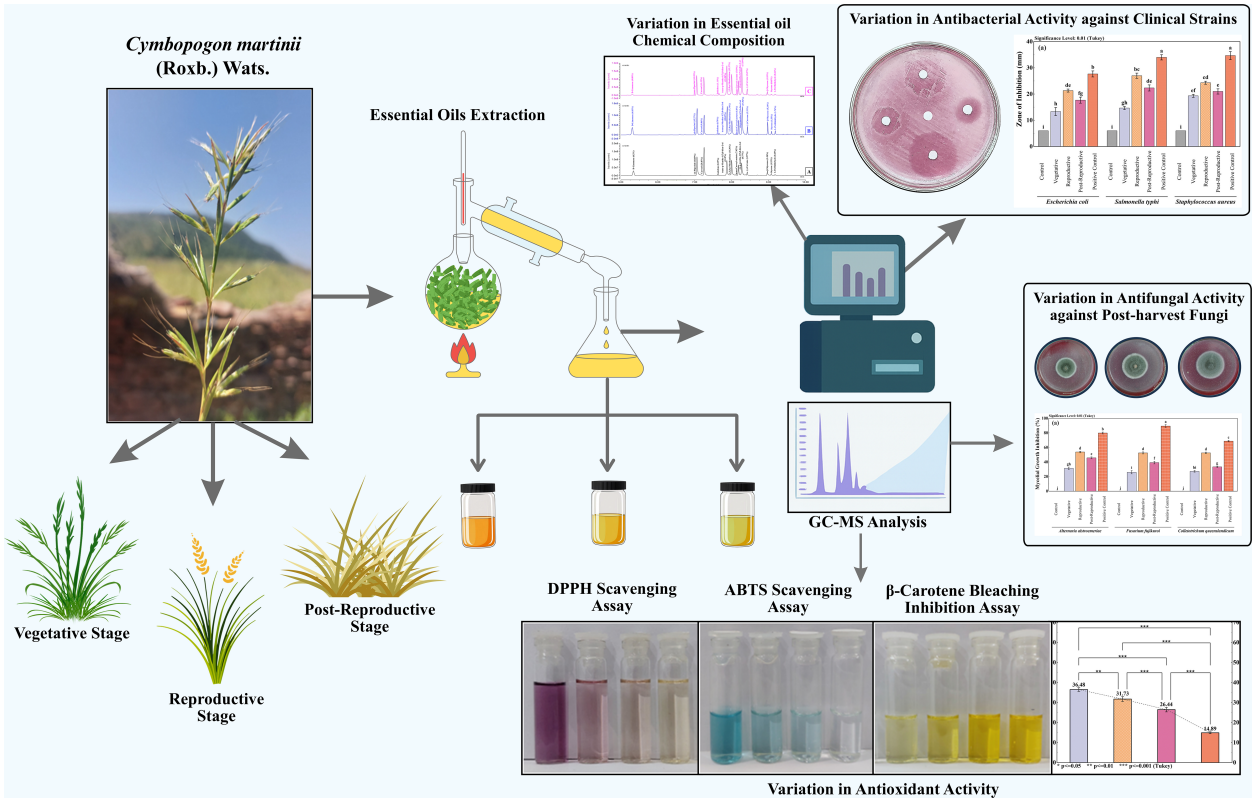

GRAPHICAL ABSTRACT

1 Introduction

Cymbopogon martinii (Roxb.) Wats., commonly known as palmarosa, is a perennial aromatic grass of the Poaceae family, cultivated primarily for its essential oil (EO), which holds high economic and industrial value in the pharmaceutical, cosmetic, and food sectors. It has gained significant economic importance due to its essential oil, which is rich in geraniol and other oxygenated monoterpenes. Globally, the palmarosa oil market was valued at approximately USD 120 million in 2023 and is projected to reach around USD 220 million by 2032, growing at a compound annual growth rate (CAGR) of ~6.5% (Dataintelo, 2023). India is the leading producer, accounting for nearly 80% of the global output, with an estimated production volume of approximately 2,000 metric tons per year (Market Report Analytics, 2023). Export analysis of Indian palmarosa oil between 2000 and 2020 revealed a CAGR of 22.3% in volume and 39.2% in export value, reflecting robust international demand in aromatherapy, perfumery, cosmetics, and natural preservatives (Choudhri et al., 2022). These trends underline the industrial and therapeutic relevance of optimizing harvest timing and essential oil composition, as investigated in the present study. Native to the Indian subcontinent and parts of Southeast Asia, *C. martinii* is one of approximately 140 species within the *Cymbopogon* genus, many of which are renowned for their rich essential oil content and broad biogeographical distribution across Africa, Asia, Australia, and the Americas (Jagadish Chandra, 1975; Prashara et al., 2003; Rao et al., 2005). Essential oils are volatile, aromatic plant metabolites stored in specialized secretory tissues and are widely recognized for their functional roles in plant defense and communication. Their bioactive properties, particularly antimicrobial and antioxidant activities, are increasingly valued as natural alternatives to synthetic preservatives in food systems and other applications (Rastogi et al., 2001; Mkaddem Mounira, 2024). These properties are largely attributed to diverse classes of phytochemicals, including monoterpenes, sesquiterpenes, aldehydes, and phenolic compounds.

The essential oil of *C. martinii* (CMEO) is rich in biologically active constituents such as geraniol, geranyl acetate, linalool, farnesol, caryophyllene, and nerolidol, which have demonstrated antimicrobial, antioxidant, insecticidal, and anti-inflammatory properties (Mallavarapu et al., 1998; Raina et al., 2003; Kakaraparthi et al., 2015; Liu et al., 2017; Chellappandian et al., 2018; Sharma et al., 2023; Tit and Bungau, 2023). Prior research has established that, the chemical composition and efficacy of EOs can vary considerably based on several factors, including geographic location, climate, soil conditions, and notably, the plant's developmental stage at the time of harvest (Moghaddam and Mehdizadeh, 2017; Chrysargyris et al., 2021; Jangi et al., 2022). Growth stage–related variation in EO composition is especially critical, as it can directly affect the biological activity and commercial value of the oil (Saeb and Gholamrezaee, 2012).

Although the essential oil (EO) of *Cymbopogon martinii* has been previously studied for its phytochemical composition and

biological activities, most existing research has focused on a single growth stage, with limited exploration of compositional variation throughout the plant's phenological development. Earlier studies often emphasized dominant compounds such as geraniol, without examining how the full metabolite profile and associated bioactivities shift over time. Moreover, few reports have integrated metabolomics-based tools to statistically associate specific volatile constituents with biofunctional outcomes. In contrast, the current study applies a stage-wise comparative approach combining GC-MS profiling with multivariate and correlation analysis to systematically assess how key metabolites correlate with antimicrobial and antioxidant activities. This integrated analysis framework offers a novel contribution to *C. martinii* metabolomics by uncovering stage-specific bioactive markers and *v*sorting evidence-based harvest strategies to maximize essential oil efficacy. To the best of our knowledge, such a comprehensive phytochemical–bioactivity correlation across growth stages has not yet been reported for this species.

2 Experimental methodology

2.1 Plant sample collection

The aerial parts of *C. martinii* were gathered at three distinct growth stages: (i) July (Vegetative stage), (ii) October (Reproductive stage), and (iii) January (Post-reproductive stage) from Kailashpuri, a hilly area in Udaipur, Rajasthan, India, across the years 2021 and 2022. The plant sample was submitted to the University of Rajasthan, Jaipur, India, for proper identification (Voucher number: RUBL21430). The collection site is located at 24° 44' 46" N and 73° 43' 20" E, with recorded environmental conditions: relative humidity between 33–72%, temperature ranging from 24–37°C, and precipitation varying from 76.8–235.6 mm.

2.2 Chemicals and reagents

All chemicals and reagents utilized in this study were of analytical grade, ensuring high purity for accurate and reliable results. Methanol (Merck, 34860, ≥99.9%) was employed as the solvent for gas chromatography-mass spectrometry (GC-MS) analysis. For the assessment of antioxidant activity, the following reagents were used: 2,2-diphenyl-1-picrylhydrazyl (DPPH) (Merck, 102839, ≥95%), ascorbic acid (Merck, A92902, ≥99%), ABTS (2,2'-azino-bis(3-ethylbenzothiazoline-6-sulfonic acid) diammonium salt) (Merck, A1888, ≥98%), potassium persulfate (Merck, 379824, ≥99%), β-Carotene (Merck, 22040, ≥97%), linoleic acid (Merck, L1376, ≥99%), and Tween 40 (Polysorbate 40) (Merck, P1504, ≥99%). These high-purity reagents were selected to ensure the reliability and consistency of the experimental results.

2.3 Volatile oil extraction and yield

The CMEOs was extracted following the method outlined by Rathore et al. (2022). Aerial parts of *C. martinii*, including leaves, stems, and flowers were collected at different intervals across the three growth stages: vegetative, reproductive, and post-reproductive. For each extraction, 500 g of fresh plant material was placed in a round-bottom flask (3 L capacity) with 1 L of water and subjected to hydro distillation for 4 hours using a Clevenger-type apparatus, suitable for extracting EOs lighter than water. The extracted oils were then dried over anhydrous sodium sulfate and stored in amber glass vials at 4°C until analysis. The essential oil yield at each growth stage was determined as a percentage of the fresh plant material weight, using the Equation (1).

$$\text{Yield}\,(\%) = \frac{\text{Weight of Essential oil (g)}}{\text{Weight of Fresh Plant Material (g)}} \times 100 \quad (1)$$

2.4 GC-MS analysis

The chemical profiling of the CMEOs was conducted with a Thermo Fisher Scientific gas chromatograph (TRACE™ 1300), coupled to a Thermo Fisher Scientific triple quadrupole mass spectrometer (TSQ 9000). The separation process utilized two columns: a TG-SQC front column (0.25 µm thickness, 0.25 mm ID, 15 m length) with 5% phenyl methyl polysiloxane and a TG-1MS back column (0.25 µm film thickness, 0.25 mm ID, 30 m length) made of 100% dimethyl polysiloxane. The oven temperature started at 60°C for an initial hold of 10 minutes. For analysis, 1 µL of diluted samples (1/100 in GC-MS grade methanol, v/v) was injected in split mode (split ratio 1/50) via an autosampler (AI 1310). Injection and ion source temperatures were set to 250°C and 300°C, respectively, with helium as the carrier gas at a flow rate of 1.0 mL/min. The column temperature was maintained at 60°C for 5 minutes, then increased to 250°C and held there for 15 minutes. Ionization was set at 70 eV with a 0.7 kV ionization current. The essential oil components were identified based on MS response, retention time, peak area, and relative peak percentage, with mass spectra matched to the Wiley 7 library. Retention indices of n-alkanes (C9-C40) were also compared with NIST database entries and relevant literature (de Alencar Filho et al., 2017). Component percentages were averaged from GC and GC-MS peak areas, with data processed using the Thermo Scientific™ Dionex™ Chromeleon™ 7 software, version 7.3.

2.5 Microbial strains and growth conditions

The antimicrobial activity of CMEOs was evaluated against a range of clinical bacterial pathogens, including *Escherichia coli*

(ATCC 25922), *Salmonella typhi* (MTCC 3216), and *Staphylococcus aureus* (ATCC 25923). Post-harvested fungal pathogens isolated from decayed fruits included *Alternaria alstroemeriae* (BG3; PP594937, Source: Black grapes), *Fusarium fujikuroi* (BN1; PP594939, Source: Banana), and *Colletotrichum queenslandicum* (PY1; PP594922, Source: Papaya). Bacterial and fungal cultures were maintained at 4°C and sub-cultured monthly to ensure viability. Prior to exposure to the essential oils, bacterial strains were incubated on Mueller-Hinton agar (MHA) at 37°C for 12–18 hours, while fungal strains were cultivated on Potato Dextrose Agar (PDA) at 26°C.

2.6 Antibacterial activity

2.6.1 Screening with disc diffusion assay

The antimicrobial efficacy of CMEOs was evaluated using a modified disc diffusion method, adapted from previously documented protocols (Ambrosio et al., 2019). Essential oil solutions were prepared at a 90% (v/v) concentration, with acetone used as an emulsifying agent. For comparison, ampicillin (20 µg/disc) and streptomycin (20 µg/disc) were included as positive controls for Gram-positive (*Staphylococcus aureus*) and Gram-negative (*Escherichia coli* and *Salmonella typhi*) bacteria, respectively. Bacterial suspensions were prepared by diluting colonies in sterile saline (0.85%), adjusting the optical density to 0.08–0.1 at 625 nm to match the 0.5 McFarland standard, which approximates a cell concentration of 1–2 × 10^8 CFU/mL. This suspension was then used to inoculate MHA plates. EO solutions, along with positive and negative controls (acetone), were added to sterile 6-mm paper discs (10 µL/disc, Whatman No. 3), which were then placed on the agar. After a 24-hour incubation at 37°C, zones of inhibition (ZI) around each disc were measured to assess antibacterial activity. Each test was conducted in triplicate to ensure accuracy.

2.6.2 Evaluation of minimum inhibitory concentration and minimum bactericidal concentration

The MIC and MBC of CMEOs was assessed using a modified macro-broth dilution method as described by Ahn and Jun (2007) and Sakkas et al. (2016). Inocula were prepared from overnight bacterial cultures, adjusting the turbidity of the bacterial suspension to match the 0.5 McFarland standard in sterile saline, resulting in a concentration of approximately 1.5 × 10^8 CFU/mL (Eliason, 1940). An initial EO stock solution (2 mg/mL) was prepared by dispersing essential oil in Mueller-Hinton broth (MHB) and thoroughly vortexing at room temperature. Serial dilutions of the EO stock were then made in Mueller-Hinton broth with 0.5% Tween 20, resulting in final EO concentrations of 2, 1, 0.5, 0.25, 0.125, and 0.05 mg/mL. A 10 µL portion of the bacterial suspension was added to each dilution, yielding a final bacterial concentration of 5 × 10^5 CFU/mL in each tube. Following incubation at 37°C for 36–48 hours, the lowest concentration at which no visible bacterial growth occurred was noted as the MIC. For MBC determination, 10 µL samples from tubes showing no visible growth were plated on Mueller-Hinton agar and incubated at 37°C for an additional 24–48 hours. The MIC was recorded as the lowest EO concentration that reduced bacterial growth by 90%, while the MBC was defined as the lowest concentration that either showed a 99.9% reduction in bacterial viability or displayed no visible bacterial growth on the agar plates (Eliason, 1940).

2.7 Antifungal activity

2.7.1 Screening with direct contact assay

The antifungal activity of CMEOs at various growth stages was assessed through a direct contact assay, following the protocol by Yexiao et al. (2020). A stock solution of EOs was prepared with 0.5% acetone to achieve final concentrations ranging from 0.25 to 2 mg/mL. Sterilized petri dishes (100 × 15 mm) were filled with PDA heated to 45°C, to which EO stock solutions were added. Negative controls were prepared using 0.5% acetone without EOs, while positive controls included 0.25 mg/mL of the fungicide Bavistin. A 6-mm mycelial plug from the active edge of a three-day-old fungal culture was positioned in the center of each petri dish. Plates were sealed with parafilm and incubated in the dark at 26 ± 2°C for 4–7 days. Each EO concentration was tested in triplicate to ensure accuracy. Mycelial growth inhibition (%) was calculated using the Equation (2).

$$\text{Mycelial Growth Inhibition (\%)} = \left(1 - \frac{\text{Radial Growth of Treatment (mm)}}{\text{Radial Growth of Control (mm)}}\right) \times 100 \quad (2)$$

2.7.2 Evaluation of minimum inhibitory concentration and minimum fungicidal concentration

The fungistatic and fungicidal activities of CMEOs was evaluated using the macro-dilution method as described by Balouiri et al. (2016). Serial dilutions of the oils were prepared in 0.5% acetone, with concentrations ranging from 0.25 to 2 mg/mL, in sterile tubes containing 5 mL of Potato Dextrose Broth (PDB). A spore suspension was added to each tube, with a final concentration of 0.4–5 × 10^5 CFU/mL. Positive controls (Bavistin at 0.1–0.5 mg/mL) and negative controls (0.5% acetone) were included. Tubes were incubated at 26±2°C in darkness for 4–7 days, depending on the fungal species. The MIC was defined as the lowest concentration with no visible fungal growth following incubation. For the MFC, 100 µL of broth from tubes with no visible growth was plated onto fresh PDA and incubated for an additional 24–48 hours at 26 ± 2°C. The MFC was identified as the lowest concentration that eliminated ≥99.9% of the initial fungal population, indicated by no fungal growth on the plates. All tests were carried out in triplicate to ensure precision and reliability (Enayatifard et al., 2021).

2.8 Antioxidant activity

2.8.1 DPPH free-radical scavenging assay

The antioxidant potential of CMEO was evaluated through the DPPH (2,2-diphenyl-1-picrylhydrazyl) assay, following the method

outlined by Braca et al. (2001). To perform this, varying concentrations of EOs (0–50 mg/mL) and ascorbic acid (used as a standard reference) were mixed with a 0.004% DPPH solution. The mixtures were incubated for 30 minutes at 25°C, after which their absorbance was measured at 517 nm using a UV-Vis spectrophotometer. Ascorbic acid at concentrations of 0–30 µg/mL was used as the positive control, while the 0.004% DPPH solution in methanol served as the control, and methanol was used as the blank. The percentage of radical scavenging activity was determined using the Equation (3).

$$\text{Radical Scavenging Activity (\%)} = \left(\frac{A_{\text{Control}} - A_{\text{Sample}}}{A_{\text{Control}}}\right) \times 100 \quad (3)$$

In this formula, $A_{control}$ represents the absorbance of the DPPH solution without any sample, while A_{sample} corresponds to the absorbance of the sample mixed with the DPPH solution. The antioxidant capacity of the essential oil samples was further expressed as the IC_{50} value, which indicates the concentration of the EO necessary to achieve a 50% decrease in absorbance relative to the control.

2.8.2 ABTS free-radical scavenging assay

The antioxidant activity of CMEO against ABTS radicals was assessed using the method described by Insawang et al. (2019). The ABTS radical cation was generated by combining a 7 mM ABTS solution with 2.45 mM potassium persulfate and allowing the mixture to react in the dark at room temperature for 6–8 hours. The EOs were dissolved in absolute methanol to prepare concentrations ranging from 0 to 50 mg/mL. For the assay, 50 µL of either the EO sample or Trolox (used as a standard) was combined with 1950 µL of the ABTS reagent, mixed thoroughly, and incubated in the dark at room temperature for 30 minutes. Absorbance readings were taken at 734 nm using a Shimadzu UV-1900i spectrophotometer, with methanol serving as the blank. The percentage scavenging activity was calculated using the previously mentioned formula (3), and the antioxidant capacity was expressed as IC_{50} values for both the CMEOs and Trolox. Each test was conducted in triplicate to ensure result reliability.

2.8.3 β-Carotene/linoleic acid bleaching assay

The β-carotene bleaching assay for assessing the antioxidant activity of CMEO was conducted following the procedure by Wettasinghe and Shahidi (1999). To begin, 2 mL of a β-carotene solution (0.2 mg/mL in chloroform) was added to a round-bottom flask along with 20 µL of linoleic acid and 200 µL of Tween 20. The mixture was then evaporated at 40°C for 10 minutes to remove the chloroform, and the residue was dissolved in 100 mL of distilled water to create an emulsion. The EOs were diluted in methanol to obtain final concentrations ranging from 0 to 50 mg/mL. For the assay, 150 µL of each EO dilution was added to 1.5 mL of the prepared emulsion in test tubes. The absorbance at 470 nm was recorded against an emulsion without β-carotene as the blank. The test tubes were incubated at 50°C, and absorbance readings at 470 nm were taken at intervals over a 60-minute period using a spectrophotometer. The same procedure was followed for the positive control, ascorbic acid, in concentrations of 10–100 µg/mL. The percentage inhibition of β-carotene bleaching was calculated using the Equation (4).

$$\%\ \beta\text{-Carotene Bleaching Inhibition} = \left(\frac{\text{Initial Absorbance} - \text{Sample Absorbance}}{\text{Initial Absorbance} - \text{Control Absorbance}}\right) \times 100 \quad (4)$$

In formula, initial absorbance (abs) is the absorbance of freshly preparing the emulsion at 0 minutes (t=0 min) min at 470 nm. The control absorbance is abs of emulsion without β-carotene. The sample absorbance is absorbance measured after 60 minutes (t=60 min) of adding EO or standard antioxidant.

The IC_{50} value (the concentration of EO that provides 50% inhibition) is calculated by plotting the inhibition percentages against different concentrations of the essential oils. The IC_{50} represents the concentration at which the antioxidants exhibit 50% reduction of oxidation in the system.

2.9 Statistical analysis

OriginPro software was utilized for statistical analysis. Descriptive statistics, including the calculation of means (n=3) and standard deviations (SD), were reported as mean ± SD for each treatment group. To evaluate statistical significance among groups, both one-way and two-way ANOVA were applied. One-way ANOVA was used to compare the means among the different essential oil treatments, while two-way ANOVA examined interaction effects between growth stages and variations in bioactivity. Following ANOVA, the Tukey test was performed to pinpoint significant differences between group means. Principal Component Analysis (PCA) was conducted to demonstrate how various growth stages of the plant influenced the bioactivity of the essential oils. All experimental procedures were conducted in triplicate to enhance reliability and reproducibility. The normal distribution of the data was checked before analysis, and statistical significance was defined at a p-value of less than 0.05 for all tests. IC_{50} values were determined using non-linear regression analysis with a sigmoidal dose-response model.

3 Result

3.1 Volatile oil yield and GC-MS analysis

As shown in Table 1 and Figure 1, the essential oils (EOs) isolated from *C. martinii* at different growth stages, vegetative, reproductive, and post-reproductive, exhibited significant variations in yield, composition, and appearance. CMEOs color transitioned from olive (vegetative) to pale yellow (reproductive) and dark (post-reproductive) as seen in Supplementary Figure S1. Oil yield was highest during the reproductive stage (0.73%), compared to the vegetative (0.35%) and post-reproductive (0.53%) stages. GC-MS analysis identified a total of 59 compounds across all stages. The reproductive phase had the highest number of constituents (49; 97.86%), followed by the post-

TABLE 1 The chemical profile of the essential oils of *Cymbopogon martinii* at different growth stages.

S. No.	Name of Compounds	CAS NO.	Molecular Weight	Molecular Formula	RI[a]	RI[b]	Vegetative		Reproductive		Post-Reproductive	
							RT	Area (%)	RT	Area (%)	RT	Area (%)
1	Styrene	100-42-5	104.15	C_8H_8	898	897	9.07	1.22 ± 0.11	9.08	1.55 ± 0.16	9.07	0.65 ± 0.05
2	Camphene	78-81-4	136.23	$C_{10}H_{16}$	928	931	3.11	0.31 ± 0.14	3.08	0.21 ± 0.10	-	-
3	trans-Decalin	87-46-4	148.25	$C_{10}H_{18}$	973	972	8.06	0.74 ± 0.09	8.06	0.24 ± 0.03	8.05	0.55 ± 0.04
4	β-Myrcene	123-35-3	136.22	$C_{10}H_{16}$	990	992	8.96	3.38 ± 0.37	8.97	5.24 ± 0.35	8.96	1.93 ± 0.29
5	p-Cymene	99-87-7	134.22	C_9H_{12}	1015	1017	6.61	0.28 ± 0.05	6.59	0.20 ± 0.11	6.59	0.24 ± 0.15
6	o-Cymene	95-63-6	134.22	C_9H_{12}	1021	1023	5.22	0.26 ± 0.05	5.19	0.17 ± 0.13	-	-
7	D-Limonene	138-86-3	136.24	$C_{10}H_{16}$	1024	1025	5.34	6.20 ± 0.35	5.31	6.83 ± 0.55	5.31	0.88 ± 0.13
8	1,3,8-p-Menthatriene	634-67-4	136.22	$C_{10}H_{14}$	1078	1079	8	11.36 ± 1.55	8	7.74 ± 1.08	8	13.37 ± 1.43
9	cis-Linalool oxide	120-81-0	152.25	$C_{10}H_{16}O$	1102	1103	-	-	9.7	0.18 ± 0.12	-	-
10	Limonene oxide	75-64-7	136.22	$C_{10}H_{16}O$	1123	1123	7.45	0.08 ± 0.10	7.44	0.19 ± 0.05	7.44	0.28 ± 0.10
11	2,6-Dimethyl-1,3,5,7-octatetraene, E,E-	537-70-6	152.24	$C_{10}H_{14}$	1130	1128	-	-	7.13	0.34 ± 0.10	-	-
12	Cosmene	20242-35-9	204.36	$C_{15}H_{24}$	1130	1129	-	-	-	-	5.18	0.23 ± 0.04
13	cis-p-Mentha-2,8-dien-1-ol	13224-60-6	152.25	$C_{10}H_{16}O$	1138	1136	-	-	8.54	0.12 ± 0.07	8.55	0.10 ± 0.13
14	4-Pentenylbenzene	25363-82-4	114.19	$C_{10}H_{12}$	1140	1141	-	-	11.22	0.08 ± 0.05	-	-
15	Isopinocarveol	139-10-3	152.25	$C_{10}H_{14}O$	1150	1149	-	-	8.46	0.15 ± 0.12	8.46	0.15 ± 0.06
16	β-Cyclocitral	93-83-6	136.21	$C_{10}H_{14}O$	1152	1153	-	-	14.44	0.25 ± 0.15	14.44	0.16 ± 0.15
17	Ethanone, 1-(3-methylphenyl)-	123-91-1	136.21	$C_9H_{10}O$	1157	1156	-	-	7.83	0.20 ± 0.06	-	-
18	4-Isopropenylcyclohexanone	587-46-7	152.25	$C_{10}H_{14}O$	1161	1163	-	-	7.5	0.19 ± 0.04	-	-
19	trans-Verbenol	15596-27-9	152.25	$C_{10}H_{16}O$	1166	1169	6.98	0.05 ± 0.11	6.96	0.06 ± 0.10	6.96	0.07 ± 0.10
20	Myrtenal	86-02-8	136.22	$C_{10}H_{14}O$	1170	1172	6.74	0.07 ± 0.03	6.73	0.10 ± 0.12	-	-
21	trans-p-mentha-1(7),8-dien-2-ol	20822-58-8	136.22	$C_{10}H_{16}O$	1185	1187	7.87	12.90 ± 1.90	7.88	15.02 ± 1.17	7.87	19.58 ± 1.84
22	Myrtenol	86-02-8	136.22	$C_{10}H_{14}O$	1192	1194	-	-	8.69	0.32 ± 0.11	8.69	0.47 ± 0.04
23	cis-Piperitol	3729-82-3	152.25	$C_{10}H_{16}O$	1197	1199	-	-	7.06	18.69 ± 1.90	7.06	15.27 ± 1.43
24	Pulegone	89-82-8	152.25	$C_{10}H_{16}O$	1201	1202	-	-	-	-	7.5	0.23 ± 0.13
25	Carveol	97-63-3	152.25	$C_{10}H_{16}O$	1203	1204	7.25	20.87 ± 2.78	7.25	9.86 ± 0.54	7.25	11.32 ± 1.03

(Continued)

10.3389/fpls.2025.1660363

TABLE 1 Continued

S. No.	Name of Compounds	CAS NO.	Molecular Weight	Molecular Formula	RI[a]	RI[b]	Vegetative		Reproductive		Post-Reproductive	
							RT	Area (%)	RT	Area (%)	RT	Area (%)
26	1,6-Dihydrocarveol	10428-17-5	152.25	$C_{10}H_{16}O$	1204	1203	-	-	7.94	0.40 ± 0.05	7.94	0.47 ± 0.12
27	trans-Piperitol	3729-83-4	152.25	$C_{10}H_{16}O$	1205	1207	-	-	-	-	7.05	13.29 ± 0.95
28	trans-Isopiperitenol	13248-42-5	152.25	$C_{10}H_{16}O$	1210	1212	-	-	7.29	0.57 ± 0.04	7.29	0.32 ± 0.13
29	cis-Verbenone	88-86-5	152.25	$C_{10}H_{14}O$	1218	1218	-	-	8.88	0.10 ± 0.15	8.87	0.08 ± 0.10
30	cis-Dihydrocarvone	15058-73-5	152.25	$C_{10}H_{14}O$	1220	1223	7.96	0.65 ± 0.05	7.96	0.36 ± 0.09	7.96	0.69 ± 0.05
31	3-Cyclohexene-1-acetaldehyde, α,4-dimethyl-	642-73-0	136.21	$C_{10}H_{14}O$	1222	1223	-	-	8.11	0.37 ± 0.10	-	-
32	Cyclohexene, 4-isopropenyl-1-methoxymethoxymethyl-	51115-67-4	196.29	$C_{12}H_{20}O_2$	1227	1228	8.79	0.15 ± 0.05	8.79	0.27 ± 0.12	8.79	0.25 ± 0.08
33	2-Cyclohexen-1-ol, 2-methyl-5-(1-methylethenyl)-, cis-	762-80-5	154.25	$C_{10}H_{16}O$	1229	1230	-	-	9.4	0.40 ± 0.10	-	-
34	cis-p-Mentha-1(7),8-dien-2-ol	14055-33-0	202.31	$C_{14}H_{22}O_2$	1231	1232	8.27	8.77 ± 0.60	8.29	15.52 ± 2.19	8.27	17.59 ± 2.21
35	Carvomenthenal	1195-33-8	152.25	$C_{10}H_{14}O$	1232	1233	-	-	-	-	8.11	0.51 ± 0.05
36	Piperitone	88-73-1	152.25	$C_{10}H_{16}O$	1233	1235	9.39	0.16 ± 0.07	-	-	9.39	0.05 ± 0.06
37	L-Perillaldehyde	495-75-8	136.22	$C_{10}H_{16}O$	1237	1236	9.17	0.65 ± 0.07	9.18	1.76 ± 0.23	9.17	0.66 ± 0.09
38	trans-Carveyl acetate	67435-59-4	176.27	$C_{13}H_{20}$	1238	1239	8.18	7.42 ± 0.69	8.19	6.60 ± 0.60	8.18	7.93 ± 0.67
39	Carvone	60-33-3	218.34	$C_{18}H_{32}O_2$	1243	1245	8.42	1.97 ± 0.16	8.43	3.31 ± 0.28	8.42	3.41 ± 0.48
40	5,7-Dodecadiyn-1,12-diol	21341-31-4	184.28	$C_{12}H_{16}O_2$	1282	1284	-	-	9.66	0.11 ± 0.14	-	-
41	(S)-Perillyl alcohol	1408-95-3	136.22	$C_{10}H_{16}O$	1297	1299	8.9	0.06 ± 0.10	8.9	0.06 ± 0.07	-	-
42	Oxycymol	499-75-2	150.22	$C_{10}H_{14}O$	1298	1297	-	-	-	-	9	0.16 ± 0.13
43	α-Methylcinnamaldehyde	118-73-1	136.21	$C_{10}H_{10}O$	1330	1332	8.69	0.31 ± 0.05	-	-	-	-
44	Bicyclo[3.1.1]hept-3-ene-spiro-2,4'-(1',3'-dioxane), 7,7-dimethyl-	101-40-6	194.27	$C_{12}H_{18}O_2$	1351	1350	-	-	9.54	0.16 ± 0.13	-	-
45	Eugenol	102-99-4	136.22	$C_{10}H_{16}O$	1362	1364	8.3	1.95 ± 0.15	8.33	0.90 ± 0.12	8.32	0.76 ± 0.07
46	Isoledene	593-84-0	204.36	$C_{15}H_{24}$	1377	1377	7.66	0.19 ± 0.07	7.66	0.79 ± 0.08	7.65	1.11 ± 0.07
47	Ageratriol	15401-90-2	228.35	$C_{15}H_{24}O$	1513	1514	-	-	14.76	0.23 ± 0.14	14.75	0.16 ± 0.05
48	Isoelemicin	487-11-6	194.26	$C_{12}H_{18}O_2$	1581	1585	7.58	0.08 ± 0.08	-	-	7.57	0.13 ± 0.03

(Continued)

10.3389/fpls.2025.1660363

TABLE 1 Continued

S. No.	Name of Compounds	CAS NO.	Molecular Weight	Molecular Formula	RI[a]	RI[b]	Vegetative		Reproductive		Post-Reproductive	
							RT	Area (%)	RT	Area (%)	RT	Area (%)
49	Humulenol-II	1084-35-1	220.35	$C_{15}H_{24}O$	1584	1585	-	-	-	-	8.73	0.06 ± 0.03
50	Methyl 3,5-tetradecadiynoate	2184-32-5	270.34	$C_{16}H_{18}O_2$	1653	1652	-	-	-	-	9.54	0.06 ± 0.07
51	Bergamotol, Z-a-trans-	88034-74-6	220.35	$C_{15}H_{24}O$	1693	1694	-	-	7.41	0.08 ± 0.04	7.4	0.08 ± 0.04
52	Methyl 7,9-octadecadiynoate	2184-36-9	296.42	$C_{20}H_{26}O_2$	1837	1838	9.49	0.11 ± 0.12	-	-	-	-
53	Methyl 8,10-octadecadiynoate	2184-39-2	296.42	$C_{20}H_{26}O_2$	1967	1969	9.22	0.05 ± 0.05	9.22	0.38 ± 0.04	9.22	0.12 ± 0.09
54	Methyl 4,6-tetradecadiynoate	2184-33-6	270.34	$C_{16}H_{18}O_2$	1987	1988	-	-	9.57	0.17 ± 0.11	9.56	0.06 ± 0.08
55	2,5-Octadecadiynoic acid, methyl ester	20822-59-9	136.22	$C_{10}H_{16}O$	2078	2076	-	-	8.62	0.05 ± 0.14	8.61	0.05 ± 0.04
56	10,13-Octadecadiynoic acid, methyl ester	2184-43-5	296.42	$C_{20}H_{26}O_2$	2085	2086	-	-	14.01	0.06 ± 0.05	-	-
57	Methyl linoleate	97-53-0	164.2	$C_{10}H_{12}O_2$	2086	2087	8.38	0.40 ± 0.09	8.38	0.36 ± 0.06	8.38	0.29 ± 0.09
58	Eicosapentaenoic acid (EPA)	104963-17-2	302.45	$C_{20}H_{30}O_2$	2138	2139	-	-	9.5	0.36 ± 0.11	9.5	0.06 ± 0.11
59	6,9,12,15-Docosatetraenoic acid, methyl ester	108-55-5	342.52	$C_{22}H_{34}O_2$	2234	2235	-	-	15.76	0.05 ± 0.05	-	-
Total identified (%)							99.77%		97.86%		98.70%	
Yield (mL/kg)							3.5 ± 0.4 (0.35%)		7.33 ± 0.40 (0.73%)		5.33 ± 0.25 (0.53%)	
Monoterpene hydrocarbons (%)							21.49		20.19		16.65	
Oxygenated monoterpenes (%)							75.16		75.88		78.74	
Sesquiterpene hydrocarbons (%)							1.01		1.37		0.68	
Oxygenated sesquiterpenes (%)							0		0.08		0.14	
Miscellaneous Compounds (%)							2.25		2.39		2.49	

[a]Literature Retention index (Adams, 2007); [b]calculated retention indices (DB-5 column).

10.3389/fpls.2025.1660363

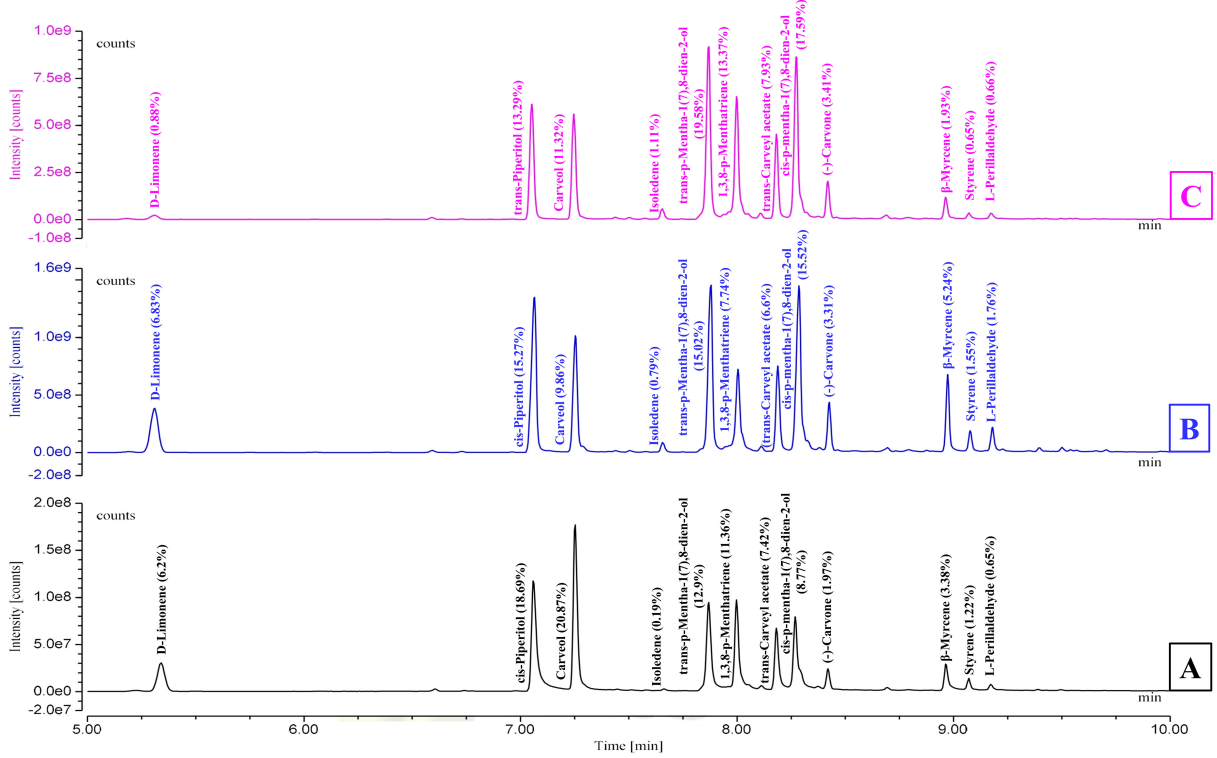

FIGURE 1
GC-MS chromatograms illustrating the chemical profile of *Cymbopogon martinii* essential oils across growth stages. **(A)** Vegetative stage, **(B)** Reproductive stage, and **(C)** Post-Reproductive stage. Chromatograms highlight the variation in compound composition as the plant matures.

reproductive (42; 98.70%) and vegetative (30; 99.77%) stages. In the vegetative stage, major compounds included carveol (20.87%), trans-p-mentha-1(7),8-dien-2-ol (12.9%), cis-p-mentha-1(7),8-dien-2-ol (8.77%), trans-carveyl acetate (7.42%), D-limonene (6.2%), and β-myrcene (3.38%). During the reproductive stage, the dominant constituents shifted to cis-piperitol (15.27%), cis-p-mentha-1(7),8-dien-2-ol (15.52%), carveol (9.86%), D-limonene (6.83%), trans-carveyl acetate (6.6%), and carvone (3.31%). In the post-reproductive stage, trans-p-mentha-1(7),8-dien-2-ol (19.58%), cis-p-mentha-1(7),8-dien-2-ol (17.59%), cis-piperitol (13.29%), carveol (11.32%), trans-carveyl acetate (7.93%), and carvone (3.41%) predominated. Across all stages, oxygenated monoterpenes constituted the majority (75–80%), followed by monoterpene hydrocarbons (15–20%), and a minor fraction (1–2%) of non-terpenoid compounds, including aromatic compounds, ethers, esters, alkane derivatives, and chalcones. Stage-specific variation in compound abundance and distribution was effectively visualized using a heat map (Supplementary Figure S2), clearly illustrating the dynamic changes in EO composition during plant development.

3.2 Antibacterial activity

The antibacterial activity of CMEOs from vegetative, reproductive, and post-reproductive stages was evaluated against *S. aureus*, *E. coli*, and *S. typhi*. Significant differences ($P < 0.0001$) were observed across growth stages and bacterial strains (Supplementary Figure S3), reflecting the variation in CMEOs chemical profiles. Reproductive-stage CMEO exhibited the highest antibacterial efficacy, with the largest ZI and lowest MIC and MBC values (Table 2). Post-reproductive CMEO showed moderate activity, while vegetative-stage CMEO was least effective. For *E. coli*, ZI was 27.7 mm in the reproductive stage, compared to 17.7 mm and 15.3 mm in post-reproductive and vegetative stages, respectively. *S. typhi* showed ZIs of 35.7 mm, 24.3 mm, and 19.3 mm across the respective stages. *S. aureus* followed the same trend: 33.7 mm (reproductive), 22.3 mm (post-reproductive), and 14.7 mm (vegetative) (Figure 2a). MIC and MBC values supported these findings (Figures 2b, c). *S. aureus* was the most sensitive strain across all stages, with an MIC of 383.3 µg/mL and MBC of 638.3 µg/mL during the reproductive stage. *S. typhi* and *E. coli* exhibited higher MICs (483.3 and 533.3 µg/mL) and MBCs (875.0 and 891.7 µg/mL, respectively). This pattern persisted in the other two growth stages, with *E. coli* consistently showing the lowest susceptibility. Although the positive control exhibited stronger antibacterial effects, CMEOs demonstrated considerable efficacy. Correlation analysis (Supplementary Figure S4) revealed a negative relationship between MIC values and key compounds such as trans-p-mentha-2,8-dien-1-ol, carvone, and D-limonene, suggesting their contribution to antibacterial activity.

TABLE 2 Antibacterial activity: minimum inhibitory concentration (MIC), minimum bactericidal concentration (MBC), and zone of inhibition for essential oils from different growth stages of *Cymbopogon martini*.

Bacterial Strain		Treatment Groups	Zone of Inhibition (mm)	MIC (µg/mL)	MBC (µg/mL)
Gram – negative	*Escherichia coli* (ATCC 25922)	Control	6.00 ± 0.00^{i}	–	–
		Vegetative	13.33 ± 1.53^{h}	658.3 ± 14.43^{f}	1170.0 ± 34.64^{a}
		Reproductive	21.33 ± 0.58^{de}	533.3 ± 5.77^{bc}	891.7 ± 14.43^{d}
		Post-Reproductive	17.67 ± 1.15^{fg}	583.3 ± 14.43^{b}	1025.0 ± 43.30^{bc}
		Positive Control (streptomycin)	27.67 ± 1.15^{b}	13.66 ± 1.52^{f}	57.33 ± 2.51g
	Salmonella typhi (MTCC 3216)	Control	6.00 ± 0.00^{i}	–	–
		Vegetative	14.67 ± 0.58^{gh}	641.7 ± 14.43^{a}	1083.3 ± 57.74^{ab}
		Reproductive	27.00 ± 1.00^{bc}	483.3 ± 28.87^{d}	875.0 ± 43.30^{d}
		Post-Reproductive	22.33 ± 1.15^{de}	560.0 ± 13.23^{bc}	938.3 ± 20.21^{cd}
		Positive Control (streptomycin)	34.00 ± 1.00^{a}	12.66 ± 2.08^{f}	55.66 ± 4.16g
Gram – Positive	*Staphylococcus aureus* (ATCC 25923)	Control	6.00 ± 0.00^{i}	–	–
		Vegetative	19.33 ± 0.58^{ef}	516.7 ± 14.43^{cd}	886.7 ± 23.09^{d}
		Reproductive	24.33 ± 0.58^{cd}	383.3 ± 14.43^{e}	638.3 ± 20.21^{f}
		Post-Reproductive	21.00 ± 1.00^{e}	475.0 ± 25^{d}	766.7 ± 28.87^{e}
		Positive Control (streptomycin)	34.67 ± 1.53^{a}	1.66 ± 0.28^{f}	3.5 ± 0.25^{g}

Mean values ± SD (n=3) for MIC, MBC, and zone of inhibition, with significant differences ($p<0.01$).
The superscript letters indicate significant differences among mean values as determined by Tukey's test ($p < 0.01$). Values sharing the same letter are not significantly different, while those with different letters differ significantly.

3.3 Antifungal activity

The antifungal activity of CMEOs from vegetative, reproductive, and post-reproductive stages was evaluated against *C. queenslandicum*, *F. fujikuroi*, and *A. alstroemeriae* (Supplementary Figure S5). As shown in Table 3 and Figure 3, variations in CMEO composition significantly influenced fungal growth inhibition, MIC, and MFC ($P < 0.0001$). Among the tested strains, *A. alstroemeriae* was the most sensitive. Inhibition increased from 31.36% (vegetative) to 53.70% (reproductive), before declining to 45.72% (post-reproductive). MIC values followed the same trend: 850 µg/mL (vegetative), 660 µg/mL (reproductive), and 810 µg/mL (post-reproductive). Corresponding MFC values were 1270, 930, and 1200 µg/mL, respectively. *F. fujikuroi* showed moderate sensitivity. The lowest inhibition (25.91%) and highest MIC (600 µg/mL) and MFC (1010 µg/mL) were recorded in the vegetative stage. The reproductive-stage CMEO exhibited the highest efficacy (52.50% inhibition, 500 µg/mL MIC, and 960 µg/mL MFC), while post-reproductive EO showed moderate improvements over the vegetative stage (39.21% inhibition, 500 µg/mL MIC, and 960 µg/mL MFC). *C. queenslandicum* was the least sensitive. Inhibition was 27.26% in the vegetative stage, peaking at 52.52% in the reproductive stage, then dropping to 33.32% in the post-reproductive stage. MIC and MFC values showed a similar pattern: highest in the vegetative stage (950 and 1270 µg/mL), lowest in the reproductive stage (800 and 1170 µg/mL), and intermediate in the post-reproductive stage (850 and 1250 µg/mL). Although the positive control showed substantially higher antifungal activity (Figure 3), CMEOs demonstrated meaningful inhibitory effects. Correlation analysis (Supplementary Figure S4) indicated strong negative correlations between MFC values and compounds such as (S)-perillyl alcohol, α-methylcinnamaldehyde, and isoeugenol, suggesting their potential contribution to antifungal activity against *A. alstroemeriae*, *F. fujikuroi*, and *C. queenslandicum*.

3.4 Antioxidant activity

The antioxidant activity of CMEOs from vegetative, reproductive, and post-reproductive stages was evaluated using DPPH, ABTS, and β-carotene bleaching assays, with significant variation observed across stages ($P < 0.0001$) (Figures 4–6). In the DPPH assay (Figure 4), post-reproductive EO exhibited the highest

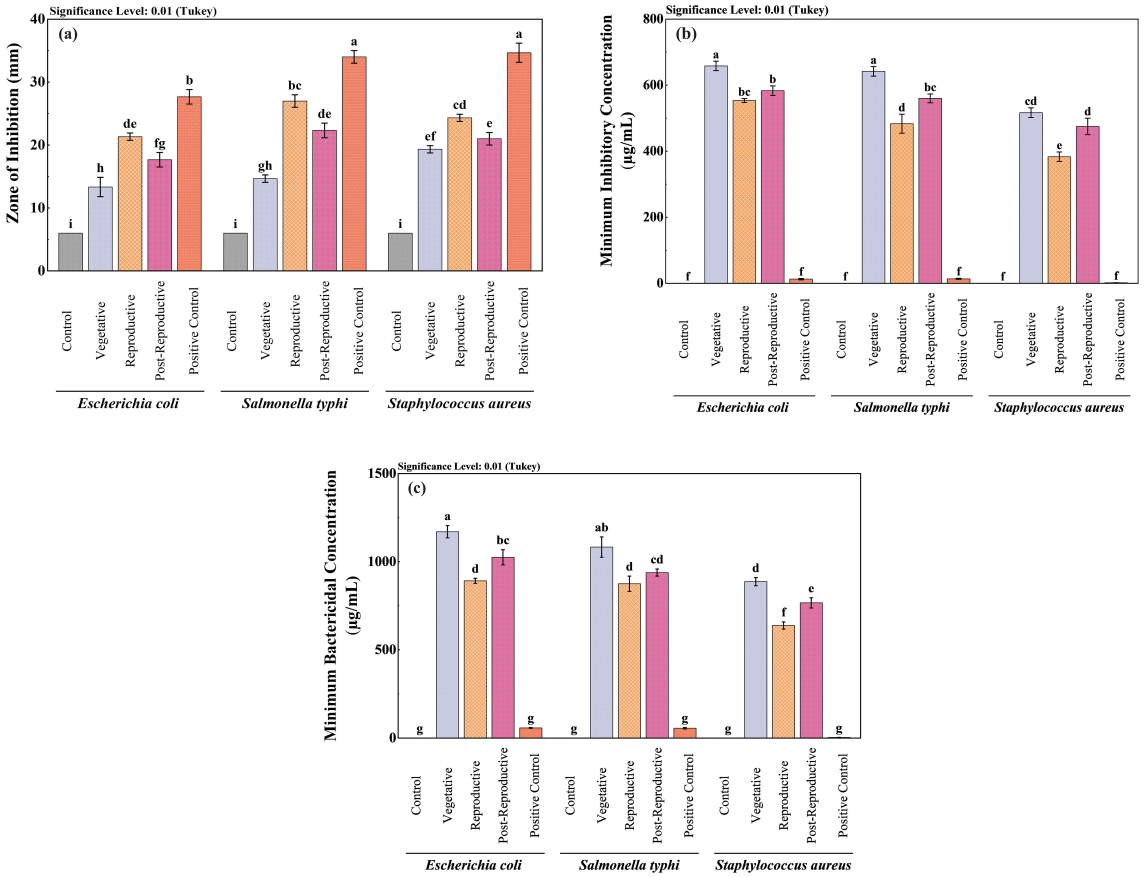

FIGURE 2
Comparative antibacterial efficacy of *Cymbopogon martinii* essential oils across growth stages. Bar graphs show **(a)** Zone of inhibition (ZI), **(b)** Minimum Inhibitory Concentration (MIC), and **(c)** Minimum Bactericidal Concentration (MBC). Positive control (ampicillin, streptomycin) was included for all assays to benchmark the efficacy of the essential oils. Significant differences across stages are denoted ($p < 0.01$), reflecting potency shifts in antibacterial properties at each growth stage. The lowercase letters indicate significant differences among the mean values as determined by Tukey's test ($p < 0.01$). Means sharing the same letter are not significantly different, whereas means with different letters differ significantly.

scavenging activity (92.29% at 50 mg/mL), followed by reproductive (84.29%) and vegetative (79.77%) stages. IC_{50} values followed the same trend: post-reproductive (26.44 mg/mL), reproductive (31.73 mg/mL), and vegetative (36.48 mg/mL). Ascorbic acid (standard) achieved 98.87% inhibition at 30 µg/mL with an IC_{50} of 14.89 µg/mL (Table 4). The ABTS assay (Figure 5) also showed stage-dependent activity. Post-reproductive EO demonstrated the strongest inhibition (92.90% at 50 mg/mL, IC_{50}= 13.81 mg/mL), followed by reproductive (87.49%, IC_{50} = 16.05 mg/mL) and vegetative (81.87%, IC_{50} = 20.64 mg/mL). Trolox (standard) reached 92.90% inhibition at 20 µg/mL with an IC_{50} of 4.01 µg/mL (Table 5). In the β-carotene bleaching assay (Figure 6), inhibition ranged from 76.6% to 87.26%. The post-reproductive EO showed the highest activity (87.26%), followed by reproductive (79.64%) and vegetative (76.6%) stages. IC_{50} values were lowest in the post-reproductive EO (18.15 mg/mL), followed by reproductive (22.24 mg/mL) and vegetative (28.16 mg/mL) (Table 6). Ascorbic acid again showed strong activity (IC_{50} = 15.81 µg/mL). Kinetic monitoring of β-carotene degradation (Figure 6c) confirmed sustained inhibition over time, strongest in post-reproductive EO, followed by reproductive and vegetative stages. Overall, the antioxidant potential of CMEO increased progressively from vegetative to post-reproductive stages across all assays. Correlation analysis (Supplementary Figure S4) revealed strong negative correlations between IC_{50} values and compounds such as α-methylcinnamaldehyde, (S)-perillyl alcohol, and eugenol, indicating their key contribution to antioxidant activity.

3.5 Principal component analysis

Principal component analysis (PCA) was performed to assess the chemical variation and bioactivity profile of CMEO across different growth stages. The analysis included the relative abundance (% area) of identified chemical constituents along with corresponding biological parameters (MIC, MBC, MFC, IC_{50}). The PCA model demonstrated high statistical validity, accounting for 100% of the total variance. The first two principal components (PC1 and PC2) captured the full variability in the dataset, with PC1 explaining 56.07% and PC2 accounting for 43.93% of the total variance (Supplementary Table S1). The 2D biplot (Figure 7a) effectively visualizes the grouping of CMEO samples across different stages and their relationship with both

TABLE 3 Antifungal activity: percent growth inhibition, minimum inhibitory concentration (MIC), and minimum fungicidal concentration (MFC), of essential oils from different growth stages of *Cymbopogon martini*.

Fungal Stains	Treatment Groups	Growth Inhibition (%)	MIC (µg/mL)	MFC (µg/mL)
Alternaria alstroemeriae (BG3; PP594937)	Control	0.00 ± 0.00 ^{j}	–	–
	Vegetative	31.36 ± 1.69^{gh}	850.0 ± 32.0^{b}	1270.0 ± 76.0^{c}
	Reproductive	53.70 ± 1.14^{d}	660.0 ± 18.0^{c}	930.0 ± 76.0^{e}
	Post-Reproductive	45.72 ± 1.33^{e}	810.0 ± 26.0^{b}	1200.0 ± 86.0^{cd}
	Positive Control (Bavistin)	79.77 ± 1.33^{b}	200.0 ± 23.0^{g}	310.0 ± 18.0^{g}
Fusarium fujikuroi (BN1; PP594939)	Control	0.00 ± 0.00 ^{j}	–	–
	Vegetative	25.91 ± 2.17^{i}	600.0 ± 25.0^{c}	1010.0 ± 36.0^{de}
	Reproductive	52.50 ± 1.39^{d}	460.0 ± 21.0^{de}	840.0 ± 81.0^{ef}
	Post-Reproductive	39.21 ± 1.78^{f}	500.0 ± 30.0^{d}	960.0 ± 32.0^{e}
	Positive Control (Bavistin)	89.27 ± 1.94^{a}	310.0 ± 23.0^{f}	490.0 ± 34.0^{g}
Colletotrichum queenslandicum (PY1; PP594922)	Control	0.00 ± 0.00 ^{j}	–	–
	Vegetative	27.26 ± 1.10^{hi}	950.0 ± 20.0^{a}	1550.0 ± 86.0^{b}
	Reproductive	52.52 ± 1.12^{d}	800.0 ± 33.0^{b}	1270.0 ± 76.0^{c}
	Post-Reproductive	33.32 ± 1.01^{g}	850.0 ± 18.0^{b}	1750.0 ± 42.0^{a}
	Positive Control (Bavistin)	68.68 ± 1.00^{c}	400.0 ± 18.0^{e}	700.0 ± 15.0^{f}

Mean values ± SD (n=3) for MIC, MFC, and percent growth inhibition, with significant differences ($p<0.01$).
The superscript letters indicate significant differences among mean values as determined by Tukey's test ($p < 0.01$). Values sharing the same letter are not significantly different, while those with different letters differ significantly.

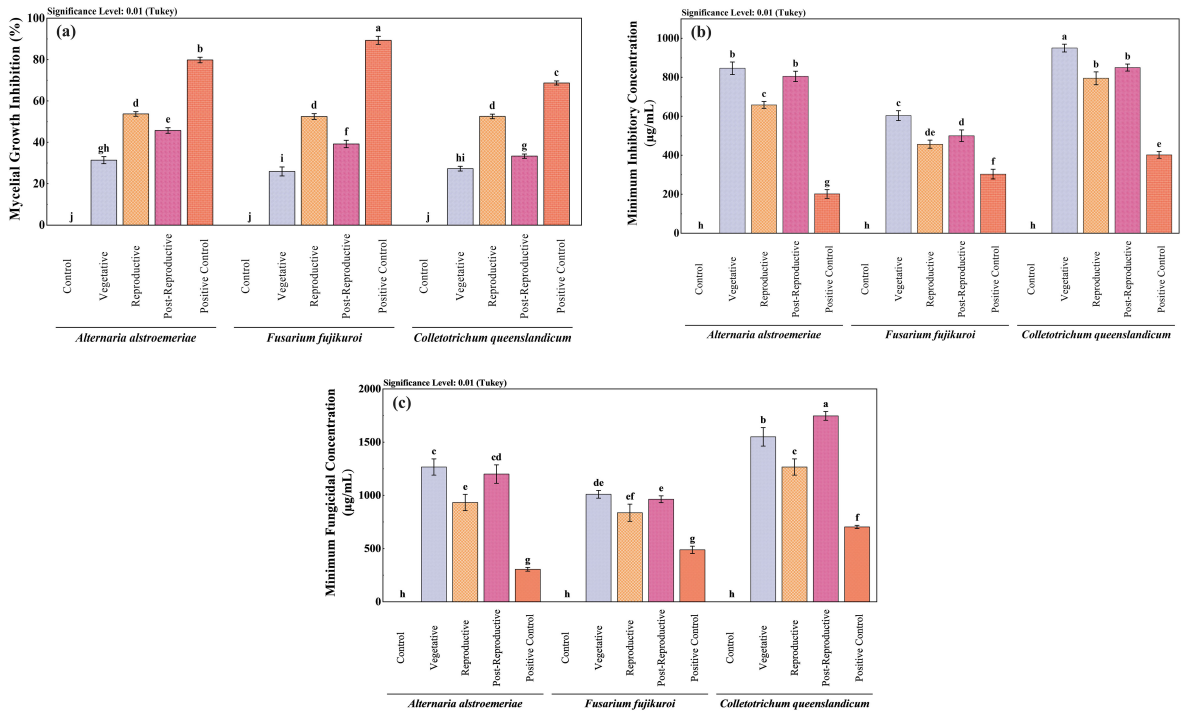

FIGURE 3
Comparative antifungal activity of *Cymbopogon martinii* essential oils from different growth stages. Bar graphs depict **(a)** Mycelial growth inhibition, **(b)** Minimum Inhibitory Concentration (MIC), and **(c)** Minimum Fungicidal Concentration (MFC). Positive control (Bavistin) was used as a reference standard for all assays. Significant differences ($p< 0.01$) illustrate variations in antifungal effectiveness of the oils as the plant matures.

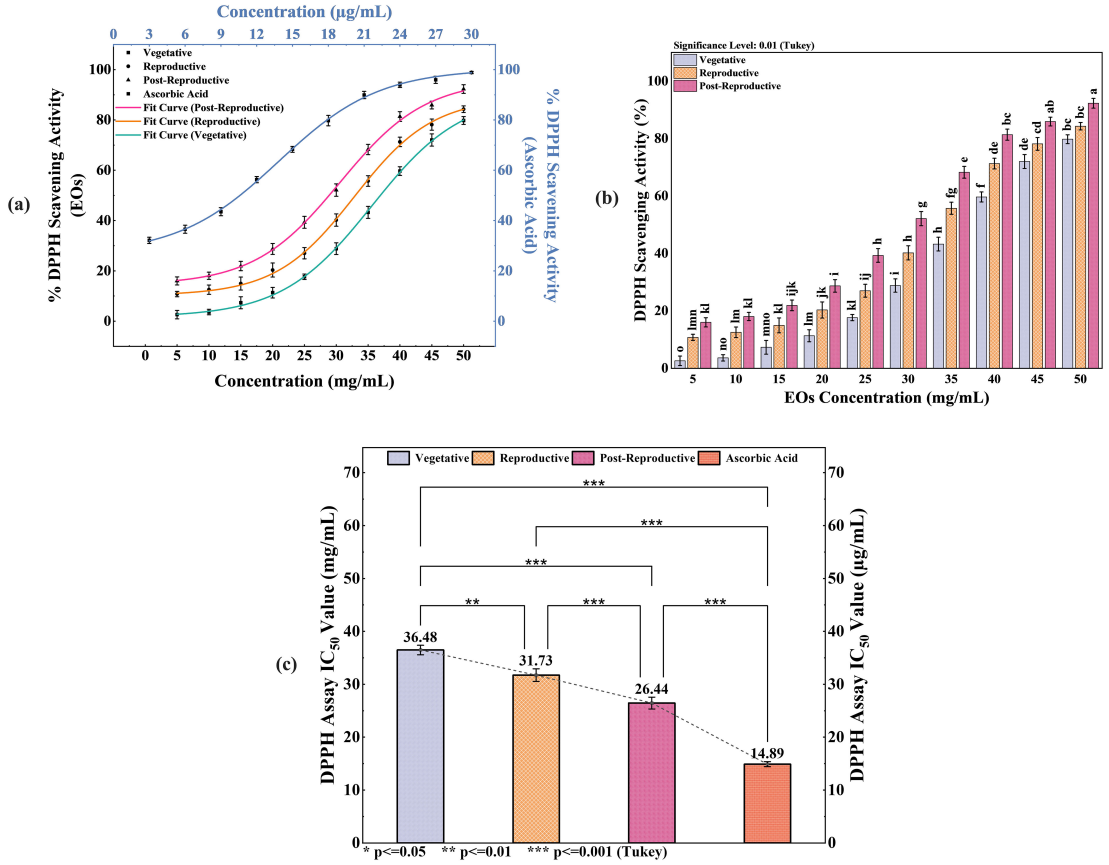

FIGURE 4
Antioxidant potential of *Cymbopogon martinii* essential oils at various growth stages via DPPH radical scavenging assay. **(a)** Dose–response curve showing % inhibition of DPPH radical by essential oils and ascorbic acid (Positive Control), used for IC_{50} calculation. **(b)** Statistical comparison of DPPH activity across growth stages (Tukey's *post-hoc* test). **(c)** IC_{50} values indicating concentration for 50% inhibition, comparing essential oils to the standard. Bars marked with the same letter indicate no significant difference ($p < 0.01$). The symbols indicate levels of statisticalsignificance: ** = $p < 0.01$, *** = $p < 0.001$.

chemical and biological variables. The loading plot (Figure 7b) further illustrates the contribution of individual variables to each principal component, supporting the interpretation of stage-specific chemical signatures and bioactivities. The associated eigenvalues were 42.61 for PC1 and 33.39 for PC2, confirming their strong explanatory power. Detailed loading values for individual compounds and activities are provided in Supplementary Table S2. Together, the PCA results underscore distinct compositional and bioactivity profiles of CMEO across growth stages, with clear separation and variable contributions effectively summarized by PC1 and PC2.

4 Discussion

4.1 Essential oil yield and compositional dynamics across growth stages

This study explored growth stage–dependent changes in the essential oil profile of wild-growing *C. martinii* and their relationship to antimicrobial and antioxidant activities. EO yield followed a bell-shaped trend, peaking during the reproductive stage, likely due to increased metabolic demand for volatiles involved in pollinator attraction, an observation consistent with other aromatic plants (Palá-Paúl et al., 2001). GC-MS analysis confirmed stage-specific quantitative variation in EO composition, particularly a broader activation of biosynthetic pathways during the reproductive phase. Such developmental modulation of EO output has been widely noted in aromatic species undergoing physiological transitions (Moghaddam and Mehdizadeh, 2017; Chrysargyris et al., 2021).

4.2 Shifts in major chemical classes: oxygenated *vs.* hydrocarbon monoterpenes

A developmental increase in oxygenated monoterpenes accompanied by a reduction in monoterpene hydrocarbons was observed, reflecting regulatory shifts in terpene metabolism. This pattern aligns with previous findings in *C. martinii* and other monoterpene-rich taxa (Rao et al., 2005; Verma et al., 2018), though past studies often overlooked stage-specific variation.

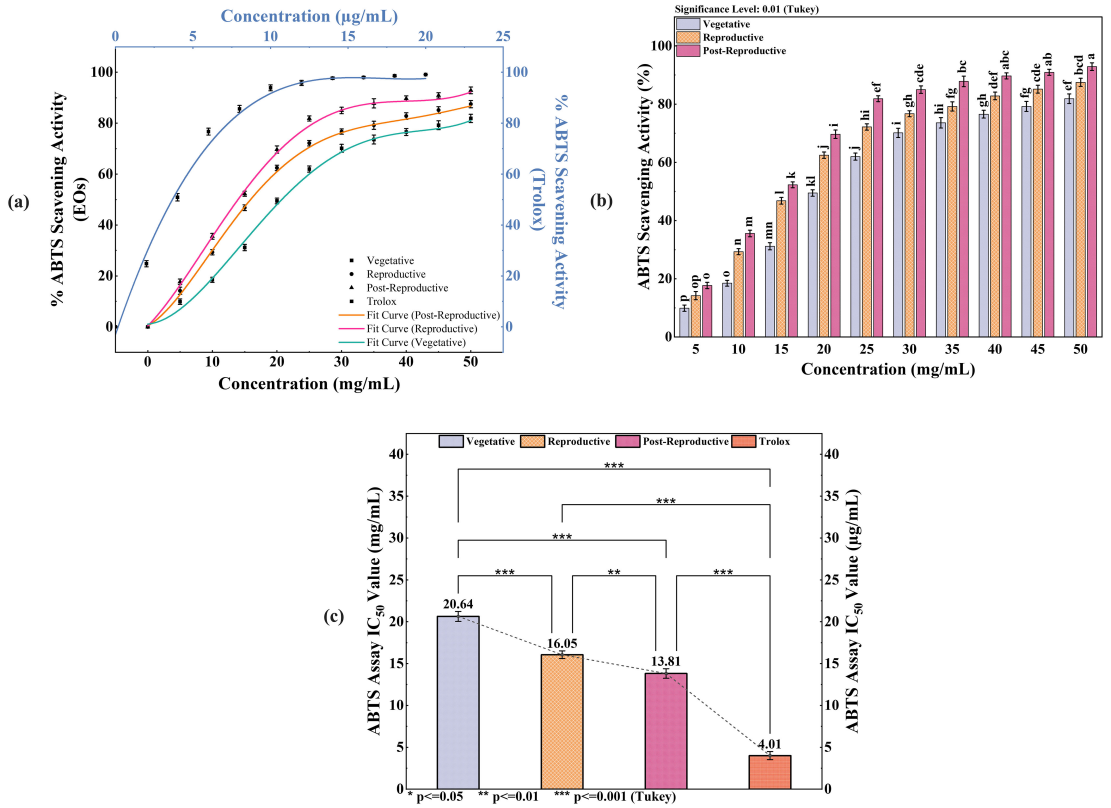

FIGURE 5
ABTS radical scavenging activity of *Cymbopogon martinii* essential oils across growth stages. **(a)** Dose–response curve showing % ABTS radical scavenging by essential oils and Trolox (Positive Control), used for IC_{50} calculation.**(b)** Comparative analysis of ABTS activity significance across growth stages (Tukey's test). **(c)** IC_{50} values indicating the concentration required for 50% inhibition, comparing essential oils to Trolox. Bars with identical letters represent no significant difference ($p < 0.01$). The symbols indicate levels of statistical significance: ** = $p < 0.01$, *** = $p < 0.001$.

The transition from carveol dominance in the vegetative phase to cis-/trans-p-mentha-1(7),8-dien-2-ol in reproductive and post-reproductive stages suggests biochemical prioritization of compounds linked to reproductive signaling and defense, similar to trends reported in other species (Chu et al., 2013; Rathore et al., 2022).

4.3 Geographic, climatic influence, and chemotypic variation

Our results resemble the profile of *C. martinii* var. *sofia* reported from Rajasthan Jain and Sharma (2017), characterized by carveol-rich chemotypes rather than the geraniol-dominant var. *motia* (Raina et al., 2003; Rao et al., 2005). This chemotypic divergence likely reflects the influence of geography and wild-growing conditions on EO biosynthesis (Jangi et al., 2022).

4.4 Functional roles of key compounds

Growth stage–specific enrichment of compounds reveals their probable ecological functions. Carveol and cis-piperitol were more abundant in the vegetative phase, supporting roles in constitutive defense. Their decline over time coincided with increased levels of trans-/cis-p-mentha-1(7),8-dien-2-ol, likely linked to reproductive signaling or adaptive protection under stress. Stable levels of trans-carveyl acetate suggest a constitutive protective function across development. Carvone, which increased in the post-reproductive stage, is a well-established antimicrobial agent and may serve in late-stage defense enhancement (Bakrim et al., 2022).

4.5 Biosynthetic basis and environmental considerations

Key monoterpenes identified in *C. martinii* including carveol, carvone, D-limonene, and p-mentha-dien-2-ol isomers are synthesized via the plastidial MEP pathway from geranyl diphosphate (GPP), with downstream modifications by terpene synthases and cytochrome P450 monooxygenases (Dudareva et al., 2013; Vranová et al., 2013; Tholl, 2015). The increased abundance of oxygenated monoterpenes during later growth stages suggests developmentally regulated biosynthesis aligned with functions like reproductive signaling and oxidative stress mitigation. Although EO biosynthesis is influenced by environmental conditions such as rainfall and temperature, our sampling across identical phenological stages in two growing

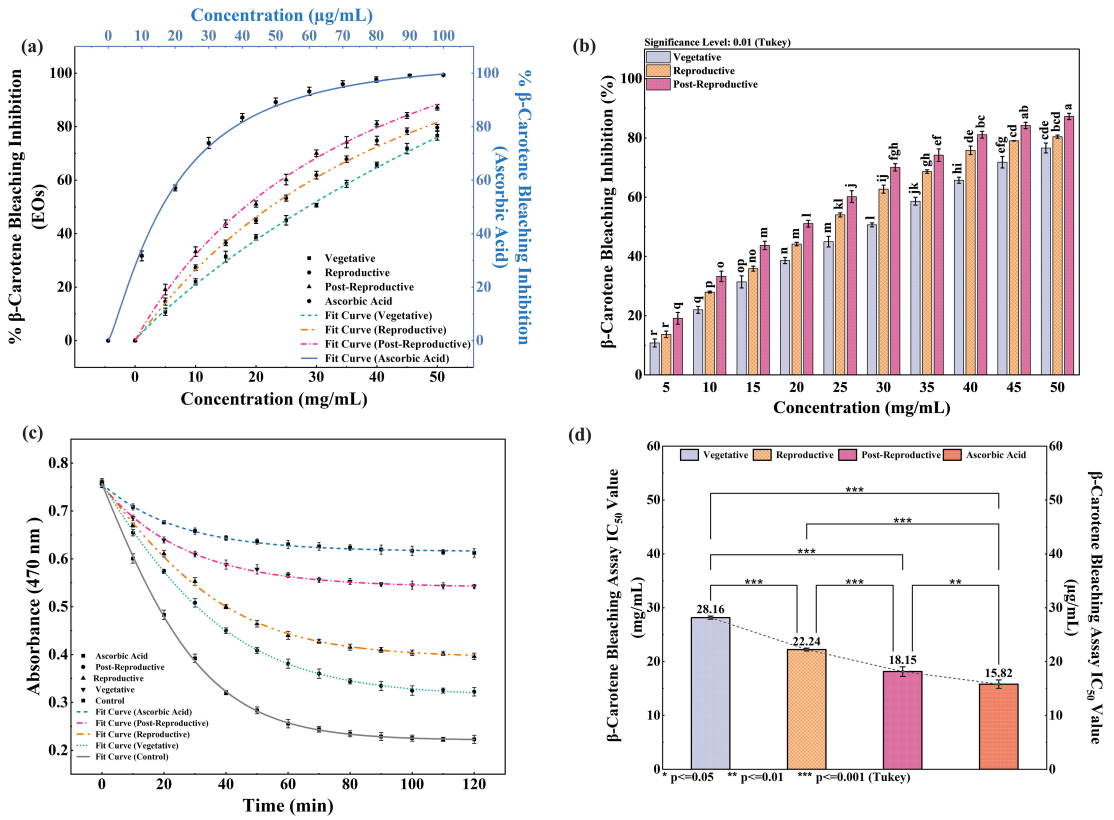

FIGURE 6
Inhibition of β-carotene degradation by *Cymbopogon martinii* essential oils at different growth stages. **(a)** Dose–response curve for % inhibition of β-carotene bleaching by essential oils and ascorbic acid (Positive Control), used for IC_{50} calculation. **(b)** Significance test across growth stages (Tukey's analysis) for bleaching inhibition activity. **(c)** Rate of β-carotene degradation in the presence of essential oils compared to control. **(d)** IC_{50} values of essential oils and standard for bleaching inhibition. Identical letters on bars indicate no significant variation ($p< 0.01$). The symbols indicate levels of statistical significance: ** = $p < 0.01$, *** = $p < 0.001$.

TABLE 4 DPPH radical scavenging activity and IC_{50} of essential oils of *Cymbopogon martinii* at different growth stage and the standard.

Concentration (mg/mL)	% DPPH Scavenging Activity at Different Growth Stages			Concentration (µg/mL)	Positive Control (Ascorbic Acid)
	Vegetative	Reproductive	Post-Reproductive		
5	2.60 ± 1.66°	10.78 ± 1.07^{lmn}	16.01 ± 1.60^{kl}	3	32.11 ± 1.26
10	3.64 ± 1.11^{no}	12.54 ± 1.84^{lm}	18.04 ± 1.42^{kl}	6	36.55 ± 1.59
15	7.32 ± 2.39^{mno}	14.95 ± 2.59^{kl}	21.91 ± 1.85^{ijk}	9	43.51 ± 1.60
20	11.34 ± 2.10^{lm}	20.32 ± 2.80^{jk}	28.70 ± 2.17^{i}	12	56.28 ± 1.25
25	17.66 ± 1.09^{kl}	27.01 ± 2.25^{ij}	39.29 ± 2.38^{h}	15	68.33 ± 1.17
30	28.81 ± 2.32^{i}	40.19 ± 2.47^{h}	52.12 ± 2.45^{g}	18	79.74 ± 2.07
35	43.26 ± 2.39^{h}	55.73 ± 2.12^{fg}	68.27 ± 2.05^{e}	21	89.93 ± 1.45
40	59.67 ± 1.73^{f}	71.29 ± 1.87^{de}	81.37 ± 1.93^{bc}	24	93.97 ± 1.05
45	72.02 ± 2.42^{de}	78.14 ± 2.21^{cd}	85.92 ± 1.53^{ab}	27	95.97 ± 1.42
50	79.77 ± 1.54^{bc}	84.29 ± 1.30^{bc}	92.29 ± 1.71^{a}	30	98.87 ± 0.45
IC_{50}	**36.48 ± 0.90^{a}**	**31.73 ± 1.19^{b}**	**26.44 ± 1.12^{c}**	**IC_{50}**	**14.89 ± 0.46^{d}**

Values represent means ± SD (n=3). The significant difference ($p<0.01$) is indicated by the letters (Tukey's test).
The bold values represent the IC_{50} values, which indicate the concentration of essential oil (or standard antioxidant) required to achieve 50% inhibition.

TABLE 5 ABTS radical scavenging activity and IC_{50} of essential oils of *Cymbopogon martinii* at different growth stages and the standard.

Concentration (mg/mL)	% ABTS Scavenging Activity at Different Growth Stages			Concentration (µg/mL)	Positive Control (Trolox)
	Vegetative	Reproductive	Post-Reproductive		
5	9.89 ± 1.09^{p}	14.19 ± 1.42^{op}	17.69 ± 1.09^{o}	2	24.81 ± 1.23
10	18.48 ± 1.00^{o}	29.30 ± 1.03^{n}	35.56 ± 1.14^{m}	4	50.90 ± 1.46
15	31.16 ± 1.23^{mn}	46.81 ± 1.15^{l}	52.28 ± 1.00^{k}	6	76.71 ± 1.36
20	49.46 ± 1.12^{kl}	62.46 ± 1.08^{j}	69.67 ± 1.43^{i}	8	85.63 ± 1.35
25	61.98 ± 1.21^{j}	72.16 ± 1.07^{hi}	81.87 ± 1.00^{ef}	10	93.91 ± 1.16
30	70.14 ± 1.58^{i}	76.72 ± 1.03^{gh}	85.00 ± 1.29^{cde}	12	95.81 ± 0.99
35	73.59 ± 1.77^{hi}	79.21 ± 1.58^{fg}	87.81 ± 1.81^{bc}	14	97.67 ± 0.44
40	76.56 ± 1.35^{gh}	82.82 ± 1.30^{def}	89.71 ± 1.03^{abc}	16	97.99 ± 0.31
45	79.21 ± 1.73^{fg}	85.16 ± 1.34^{cde}	90.94 ± 1.04^{ab}	18	98.62 ± 0.28
50	81.87 ± 1.65^{ef}	87.49 ± 1.41^{bcd}	92.90 ± 1.31^{a}	20	99.10 ± 0.06
IC_{50}	**20.64 ± 0.60^{a}**	**16.05 ± 0.46^{b}**	**13.81 ± 0.57^{c}**	**IC_{50}**	**4.01 ± 0.48^{d}**

Values represent means ± SD (n=3). The significant difference ($p<0.01$) is indicated by the letters (Tukey's test).
The bold values represent the IC_{50} values, which indicate the concentration of essential oil (or standard antioxidant) required to achieve 50% inhibition.

seasons minimized inter-annual variability. Averaged GC-MS data (mean ± SD) allowed a clearer focus on stage-specific metabolic trends. Future studies under controlled environments could further distinguish developmental effects from climatic factors.

4.6 Stage-dependent antibacterial activity

Antibacterial potency varied with growth stage, paralleling chemical composition. Reproductive-stage EOs showed the strongest activity, attributed to elevated cis- and trans-p-mentha-1(7),8-dien-2-ol, which destabilize bacterial membranes and inhibit enzymatic systems (Alitonou et al., 2012; Ambrosio et al., 2020, 2021). Post-reproductive oils, though still active, showed slightly reduced efficacy, likely due to decreased D-limonene, β-myrcene, and eugenol compounds known for disrupting bacterial respiration and membranes (Nuñez and D'Aquino, 2012; Han et al., 2020; Połeć et al., 2020; Gupta et al., 2021; Ulanowska and Olas, 2021). Their partial replacement by carvone and trans-carvyl acetate, which act through quorum sensing and enzyme inhibition (Pina

TABLE 6 β-Carotene bleaching inhibition activity and IC_{50} of essential oils of *Cymbopogon martinii* at different growth stage and the standard.

Concentration (mg/mL)	% β-Carotene Bleaching Inhibition at Different Growth Stages			Concentration (µg/mL)	Positive Control (Ascorbic Acid)
	Vegetative	Reproductive	Post-Reproductive		
5	10.78 ± 1.36^{r}	14.57 ± 1.35^{r}	19.08 ± 1.98^{q}	10	31.7 ± 1.86
10	21.95 ± 1.17^{q}	27.3 ± 1.03^{p}	33.26 ± 1.77^{o}	20	57.1 ± 1.09
15	31.39 ± 2.02^{op}	36.55 ± 1.04^{no}	43.72 ± 1.41^{m}	30	73.88 ± 2.05
20	38.61 ± 1.04^{n}	44.85 ± 1.01^{m}	51.07 ± 1.16^{l}	40	83.43 ± 1.52
25	44.99 ± 1.78^{m}	53.29 ± 1.11^{kl}	60.2 ± 1.98^{j}	50	89.22 ± 1.49
30	50.64 ± 0.67^{l}	61.86 ± 1.41^{ij}	70.07 ± 1.24^{fgh}	60	93.21 ± 1.54
35	58.62 ± 1.31^{jk}	67.85 ± 1.21^{gh}	74.19 ± 2.11^{ef}	70	95.92 ± 1.24
40	65.72 ± 1.02^{hi}	74.81 ± 1.60^{de}	81.08 ± 1.15^{bc}	80	97.64 ± 1.03
45	71.79 ± 1.94^{efg}	78.3 ± 1.23^{cd}	84.20 ± 1.09^{ab}	90	99.0 ± 0.58
50	76.6 ± 1.67^{cde}	79.64 ± 1.19^{bcd}	87.26 ± 1.07^{a}	100	99.34 ± 0.34
IC_{50}	**28.16 ± 0.30^{a}**	**22.24 ± 0.26^{b}**	**18.15 ± 0.89^{c}**	**IC_{50}**	**15.81 ± 0.79^{d}**

Values represent means ± SD (n=3). The significant difference ($p<0.01$) is indicated by the letters (Tukey's test).
The bold values represent the IC_{50} values, which indicate the concentration of essential oil (or standard antioxidant) required to achieve 50% inhibition.

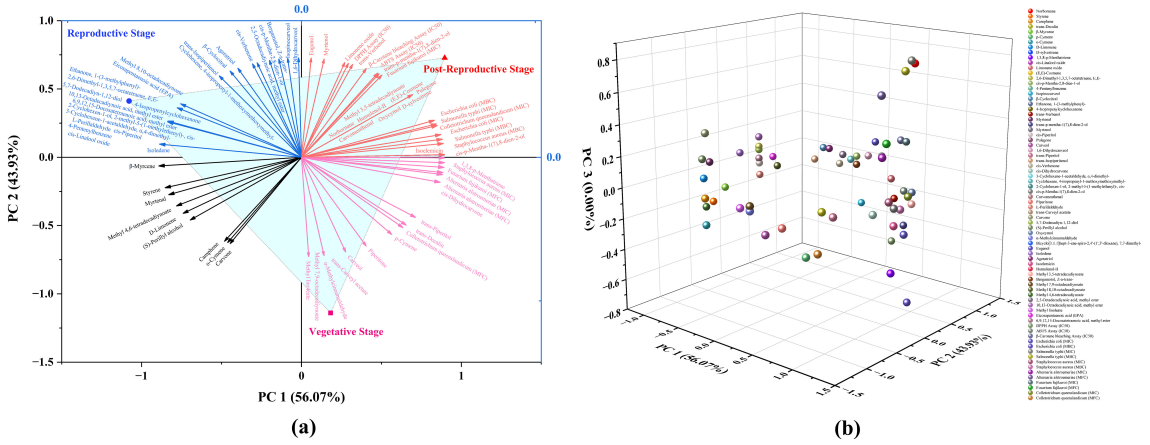

FIGURE 7
Principal Component Analysis (PCA) depicting the distribution and influence of chemical constituents and biological activities of essential oils from *Cymbopogon martinii* across three phenological stages. **(a)** Two-dimensional PCA biplot combining sample scores and variable loadings. Clear separation among vegetative, reproductive, and post-reproductive stages is evident, reflecting significant stage-specific differences in chemical composition and bioactivity. Principal Components 1 and 2 (PC1 and PC2) accounted for 56.07% and 43.93% of the total variance, respectively. **(b)** PCA loading plot illustrating the spatial distribution and contributions of individual compounds and biological activities to the principal components.

et al., 2022), may have altered overall potency. Vegetative-stage oils exhibited the weakest antibacterial action, dominated by carveol and cis-piperitol, which act on microbial enzymes but may lack strong membrane-disruptive properties (Roman et al., 2023). Additionally, limited synergism among constituents may contribute to reduced efficacy (Kamatou et al., 2008; Tamgue et al., 2011). Susceptibility varied by strain: *S. aureus* was most sensitive, likely due to its permeable Gram-positive cell wall (Oussalah et al., 2007; Galgano et al., 2022), while Gram-negative *E. coli* and *S. typhi* were more resistant due to their outer membranes (Longbottom et al., 2004; Dai et al., 2013; Rashid et al., 2013). Slightly higher sensitivity of *S. typhi* may relate to differences in membrane structure or EO interactions (Azad, 2021).

4.7 Antifungal activity: stage-specific efficacy

The antifungal potential of CMEOs showed strong dependence on plant growth stage, primarily linked to the abundance of oxygenated monoterpenes. Vegetative-phase oils exhibited the weakest activity, despite carveol's known ability to disrupt fungal membranes (Soković et al., 2006; Abbaszadeh et al., 2014). The limited efficacy may reflect insufficient synergy with other active compounds or inhibitory interactions (Boni, 2017; James and Ikani, 2023). In contrast, reproductive-stage oils demonstrated the strongest antifungal effects, coinciding with maximum concentrations of cis- and trans-p-mentha-1(7),8-dien-2-ol compounds that disrupt fungal membranes and induce cell leakage (Kostik and Bauer, 2015; Brahmi et al., 2021). Their interaction with ergosterol alters membrane fluidity and integrity (Busato de Feiria et al., 2016; Benomari et al., 2018; Soliman et al., 2022), and may also interfere with ergosterol biosynthesis (Mohamed Ibrahim et al., 2018; Scalese et al., 2024). Post-reproductive EOs retained moderate antifungal activity, supported by elevated levels of carveol, trans-carveyl acetate, and p-mentha-1(7),8-dien-2-ol isomers. These compounds likely act through multiple mechanisms, including membrane destabilization, glycolytic inhibition, and morphological disruption (Yu et al., 2022; Xiong et al., 2023). The reduced presence of D-limonene, β-myrcene, and cis-piperitol may have contributed to the slight decline in activity. Sensitivity varied by fungal strain. *A. alstroemeriae* was most susceptible, likely due to its more permeable membrane structure. *F. fujikuroi* showed intermediate response, while *C. queenslandicum* was least sensitive, possibly due to inherent resistance mechanisms like enhanced sterol biosynthesis and stress adaptation (Moutassem et al., 2019; Vasileva, 2023; Erdoğan, 2024).

4.8 Antioxidant potential and its chemical drivers

Antioxidant activity increased progressively from the vegetative to the post-reproductive stage, consistent across DPPH, ABTS, and β-carotene bleaching assays. Similar trends have been observed in other aromatic species such as *Foeniculum vulgare* and *Origanum vulgare*, where late-stage accumulation of active compounds enhances radical-scavenging potential (Salami et al., 2017; Morshedloo et al., 2018). Post-reproductive EO showed the highest antioxidant activity, attributed to elevated levels of cis- and trans-p-mentha-1(7),8-dien-2-ol, known for their radical stabilization and hydrogen-donating abilities (Sitzmann et al., 2014; Jordá Marín, 2018). Additional contributors included eugenol, D-limonene, 1,3,8-p-menthatriene, and carveol all recognized for their antioxidant efficacy (Niki, 2010; Gülçin, 2011; Mueller and Boehm, 2011; Serafim et al., 2021; Orlo et al., 2023). Trans-carveyl acetate may also enhance activity via hydrogen

donation. In contrast, vegetative-stage EO showed the lowest antioxidant effect despite high carveol content, likely due to limited synergy with other active compounds. Reproductive-stage EO displayed moderate activity, supported by cis-piperitol and p-mentha-1(7),8-dien-2-ol, though lower levels of carvone and carveol may have reduced overall potency (Duarte-Almeida et al., 2006; Olszowy and Dawidowicz, 2018; Pombal et al., 2020). The antioxidant roles of β-myrcene and cis-piperitol remain underexplored and merit further study.

4.9 Multivariate analysis confirms stage-specific clustering

Principal component analysis (PCA) clearly differentiated EO samples by phenological stage, with vegetative, reproductive, and post-reproductive oils forming distinct clusters (Figure 7a). The loading plot (Figure 7b) revealed that antimicrobial compounds were strongly associated with reproductive-stage oils, while antioxidant-rich constituents clustered with post-reproductive samples. Vegetative EO appeared chemically intermediate.

The PCA model explained 100% of the variance (PC1 = 56.07%, PC2 = 43.93%) and was supported by eigenvalue and loading data (Supplementary Tables S1, S2), confirming its robustness. These results highlight the importance of the growth stage in determining both EO composition and bioactivity, offering a framework for selecting optimal harvest times based on intended applications of *C. martinii* essential oil.

5 Conclusion

The present study clearly demonstrates that the growth stage of wild-grown *Cymbopogon martinii* (Roxb.) Wats. significantly influences the essential oil's chemical composition and bioactivity. A statistically significant shift ($P < 0.0001$) was observed from monoterpene hydrocarbons dominating the vegetative phase to an abundance of oxygenated monoterpenes in the reproductive and post-reproductive stages. These changes reflect adaptive physiological responses related to defense, reproductive signaling, and oxidative stress management. Correlation analysis identified key compounds such as carvone, D-limonene, (S)-perillyl alcohol, and α-methylcinnamaldehyde as strong contributors to enhanced antimicrobial, antifungal, and antioxidant activities. Biological assays confirmed that reproductive-stage oil was most effective against *Staphylococcus aureus* and *Alternaria alstroemeriae*, while post-reproductive oil exhibited the highest antioxidant activity. These findings underscore the importance of selecting the appropriate harvest stage to maximize essential oil quality for specific end uses. The results provide a practical framework for guiding the targeted use of *C. martinii* essential oil in pharmaceutical, cosmetic, and agricultural applications as a sustainable alternative to synthetic agents. Future work may explore cultivation practices and genotype selection to further optimize bioactive profiles for commercial exploitation.

Data availability statement

The original contributions presented in the study are included in the article/Supplementary Material. Further inquiries can be directed to the corresponding author.

Author contributions

PS: Software, Writing – original draft, Visualization, Formal analysis, Validation, Data curation, Writing – review & editing, Methodology, Conceptualization. MM: Conceptualization, Writing – review & editing, Validation, Supervision, Software, Writing – original draft, Visualization, Resources, Formal analysis.

Funding

The author(s) declare that no financial support was received for the research, and/or publication of this article.

Acknowledgments

The author, PS gratefully acknowledges the University Grants Commission (UGC) for providing financial support through a fellowship grant. The authors would like to extend their sincere appreciation to the funding agency Anusandhan National Research Foundation (ANRF), Science and Engineering Research Board (SERB), State University Research Excellence (SURE) & Empowerment and Equity Opportunities for Excellence in Science, New Delhi, India. The author MM is also highly thankful to the Ministry of Education and SPD-RUSA Rajasthan for the financial support received under the RUSA-2.0 project. All the authors acknowledge their host institute for infrastructure support. The authors are also grateful to their respective universities for providing support during the work. All the authors read and approve the content of the manuscript for publication

Conflict of interest

The authors declare that the research was conducted in the absence of any commercial or financial relationships that could be construed as a potential conflict of interest.

Generative AI statement

The author(s) declare that no Generative AI was used in the creation of this manuscript.

Any alternative text (alt text) provided alongside figures in this article has been generated by Frontiers with the support of artificial intelligence and reasonable efforts have been made to ensure

accuracy, including review by the authors wherever possible. If you identify any issues, please contact us.

Publisher's note

Supplementary material

The Supplementary Material for this article can be found online at: https://www.frontiersin.org/articles/10.3389/fpls.2025.1660363/full#supplementary-material

References

Abbaszadeh, S., Sharifzadeh, A., Shokri, H., Khosravi, A. R., and Abbaszadeh, A. (2014). Antifungal efficacy of thymol, carvacrol, eugenol and menthol as alternative agents to control the growth of food-relevant fungi. *J. Mycol. Med.* 24, e51–e56. doi: 10.1016/j.mycmed.2014.01.063

Ahn, Y., and Jun, Y. (2007). Measurement of pain-like response to various NICU stimulants for high-risk infants. *Early Hum. Dev.* 83, 255–262. doi: 10.1016/j.earlhumdev.2006.05.022

Alitonou, G., Avlessi, F., Tchobo, F., Noudogbessi, J.-P., Tonouhewa, A., Yehouenou, B., et al. (2012). Chemical composition and biological activities of essential oils from the leaves of *Cymbopogon giganteus* Chiov. and *Cymbopogon schoenanthus* (L.) Spreng (Poaceae) from Benin. *Int. J. Biol. Chem. Sci.* 6, 1819–1827. doi: 10.4314/ijbcs.v6i4.37

Ambrosio, C. M. S., Contreras-Castillo, C. J., and Da Gloria, E. M. (2020). *In vitro* mechanism of antibacterial action of a citrus essential oil on an enterotoxigenic *Escherichia coli* and *Lactobacillus rhamnosus*. *J. Appl. Microbiol.* 129, 541–553. doi: 10.1111/jam.14660

Ambrosio, C. M. S., Diaz-Arenas, G. L., Agudelo, L. P. A., Stashenko, E., Contreras-Castillo, C. J., and da Gloria, E. M. (2021). Chemical composition and antibacterial and antioxidant activity of a citrus essential oil and its fractions. *Molecules* 26, 2888. doi: 10.3390/molecules26102888

Ambrosio, C. M. S., Ikeda, N. Y., Miano, A. C., Saldaña, E., Moreno, A. M., Stashenko, E., et al. (2019). Unraveling the selective antibacterial activity and chemical composition of citrus essential oils. *Sci. Rep.* 9, 17719. doi: 10.1038/s41598-019-54084-3

Azad, S. (2021). Analysis on the antimicrobial and repellent activities of *Cymbopogon martinii* essential oil. *Biosci. Biotechnol. Res. Commun.* 14, 905–915. doi: 10.21786/bbrc/14.2.70

Bakrim, S., Benkhaira, N., Bourais, I., Benali, T., Lee, L. H., El Omari, N., et al. (2022). Health benefits and pharmacological properties of stigmasterol. *Antioxidants* 11, 1803. doi: 10.3390/antiox11101912

Balouiri, M., Sadiki, M., and Ibnsouda, S. K. (2016). Methods for *in vitro* evaluating antimicrobial activity: A review. *J. Pharm. Anal.* 6, 71–79. doi: 10.1016/j.jpha.2015.11.005

Benomari, F. Z., Andreu, V., Kotarba, J., Dib, M. E. A., Bertrand, C., Muselli, A., et al. (2018). Essential oils from Algerian species of *Mentha* as new bio-control agents against phytopathogen strains. *Environ. Sci. pollut. Res.* 25, 29889–29900. doi: 10.1007/s11356-017-9991-4

Boni, G. C. (2017). Purified bioactive compounds from *Mentha* spp. oils as a source of Candidosis treatment. A brief review. *Rev. Fitos* 11, 95–106. doi: 10.5935/2446-4775.20170009

Braca, A., De Tommasi, N., Di Bari, L., Pizza, C., Politi, M., and Morelli, I. (2001). Antioxidant principles from *Bauhinia tarapotensis*. *J. Nat. Prod.* 64, 892–895. doi: 10.1021/np0100845

Brahmi, M., Adli, D. E. H., Boufadi, M. Y., Arabi, W., Kahloula, K., and Slimani, M. (2021). Antimicrobial and antiochratoxic activities of mentha spicata essential oil. *Phytotherapie* 19, 397–403. doi: 10.3166/phyto-2021-0278

Busato de Feiria, S. N., de Laet Santana, P., Boni, G. C., Anibal, P. C., Boriollo, M. F. G., Figueira, G. R., et al. (2016). Essential oil composition of *Mentha* spp. extracted seasonally and their effects against *Candida* yeast growth and biofilm formation. *Adv. Med. Plant Res.* 4, 106–115.

Chellappandian, M., Vasantha-Srinivasan, P., Senthil-Nathan, S., Karthi, S., Thanigaivel, A., Ponsankar, A., et al. (2018). Botanical essential oils and uses as mosquitocides and repellents against dengue. *Environ. Int.* 113, 214–230. doi: 10.1016/j.envint.2017.12.038

Choudhri, H. P., Verma, D. K., Bhise, R. N., Sharma, R. S., Srivastava, R. K., and Kumar, S. (2022). Export performance of palmarosa oil in India: a growth and instability analysis. *Econ. Aff. (New Delhi)* 67 (02), 43–48. doi: 10.46852/0424-2513.2.2022.8

Chrysargyris, A., Evangelides, E., and Tzortzakis, N. (2021). Seasonal variation of antioxidant capacity, phenols, minerals and essential oil components of sage, spearmint and sideritis plants grown at different altitudes. *Agronomy* 11, 1766. doi: 10.3390/agronomy11091766

Chu, S. S., Liu, Q. Z., Jiang, G. H., and Liu, Z. L. (2013). Chemical composition and insecticidal activity of the essential oil derived from *Phlomis umbrosa* against two grain storage insects. *J. Essent. Oil-Bearing Plants* 16, 51–58. doi: 10.1080/0972060X.2013.764184

Dai, J., Zhu, L., Yang, L., and Qiu, J. (2013). Chemical composition, antioxidant and antimicrobial activities of essential oil from *Wedelia prostrata*. *EXCLI J.* 12, 479–490.

Dataintelo, (2023). *Palmarosa oil market size, trends, and forecast 2023–2032*. Available online at: https://www.dataintelo.com/report/palmarosa-oil-market (Accessed July 28, 2025).

de Alencar Filho, J. M. T., Araújo, L. D. C., Oliveira, A. P., Guimarães, A. L., Pacheco, A. G. M., Silva, F. S., et al. (2017). Chemical composition and antibacterial activity of essential oil from leaves of *Croton heliotropiifolius* in different seasons of the year. *Rev. Bras. Farmacogn.* 27, 440–444. doi: 10.1016/j.bjp.2017.02.004

Duarte-Almeida, J. M., Dos Santos, R. J., Genovese, M. I., and Lajolo, F. M. (2006). Evaluation of the antioxidant activity using the β-carotene/linoleic acid system and the DPPH scavenging method. *Cienc. e Tecnol. Aliment.* 26, 446–452. doi: 10.1590/s0101-20612006000200031

Dudareva, N., Klempien, A., Muhlemann, J. K., and Kaplan, I. (2013). Biosynthesis, function and metabolic engineering of plant volatile organic compounds. *New Phytol.* 198, 16–32. doi: 10.1111/nph.12145

Eliason, N. E. (1940). Textbook of diagnostic microbiology. *Am. Speech* 15, 310.

Enayatifard, R., Akbari, J., Babaei, A., Rostamkalaei, S. S., Hashemi, S. M. H., and Habibi, E. (2021). Anti-microbial potential of nano-emulsion form of essential oil obtained from aerial parts of *Origanum vulgare* L. as food additive. *Adv. Pharm. Bull.* 11, 327–334. doi: 10.34172/apb.2021.028

Erdoğan, O. (2024). Inhibitory effect of plant essential oils on controlling *Alternaria* species. *Int. J. Agric. Environ. Food Sci.* 8, 468–478. doi: 10.31015/jaefs.2024.2.20

Galgano, M., Capozza, P., Pellegrini, F., Cordisco, M., Sposato, A., Sblano, S., et al. (2022). Antimicrobial activity of essential oils evaluated in vitro against *Escherichia coli* and *Staphylococcus aureus*. *Antibiotics* 11, 979. doi: 10.3390/antibiotics11070979

Gülçin, I. (2011). Antioxidant activity of eugenol: A structure-activity relationship study. *J. Med. Food* 14, 975–985. doi: 10.1089/jmf.2010.0197

Gupta, A., Jeyakumar, E., and Lawrence, R. (2021). Strategic approach of multifaceted antibacterial mechanism of limonene traced in *Escherichia coli*. *Sci. Rep.* 11, 13816. doi: 10.1038/s41598-021-92843-3

Han, Y., Sun, Z., and Chen, W. (2020). Antimicrobial susceptibility and antibacterial mechanism of limonene against *Listeria monocytogenes*. *Molecules* 25, 33. doi: 10.3390/molecules25010033

Insawang, S., Pripdeevech, P., Tanapichatsakul, C., Khruengsai, S., Monggoot, S., Nakham, T., et al. (2019). Essential oil compositions and antibacterial and antioxidant activities of five *Lavandula stoechas* cultivars grown in Thailand. *Chem. Biodivers.* 16, e1900371. doi: 10.1002/cbdv.201900371

Jagadish Chandra, K. S. (1975). Cytogenetical evolution in some species of *Cymbopogon* cited in advancing frontiers in cytogenetics. *Hindustan Publ. Corp. New Delhi.*

Jain, N., and Sharma, M. (2017). Chemical composition of the leaf oil of *Cymbopogon martinii* var. *sofia* collected from Udaipur, Rajasthan and their screening against fungi causing dermatophytosis in human beings. *J. Essent. Oil-Bearing Plants* 20, 801–808. doi: 10.1080/0972060X.2017.1341344

James, S. A., and Ikani, P. E. (2023). A review of the antifungal activities of mint plant extracts against fungal isolates. *Bio-Research* 21, 2031–2057. doi: 10.4314/br.v21i2.9

Jangi, F., Ebadi, M. T., and Ayyari, M. (2022). Qualitative characteristics of hyssop (*Hyssopus officinalis* L.) under the influence of harvest time and drying methods. *Dry. Technol.* 40, 2696–2709. doi: 10.1080/07373937.2021.1955375

Jordá Marín, S. (2018). Composición química y actividad antifúngica de los aceites esenciales satureja montana y *Mentha longifolia*. *Univ. Politècnica València* 5, 59–100.

Kakaraparthi, P. S., Srinivas, K. V. N. S., Kumar, J. K., Kumar, A. N., Rajput, D. K., and Anubala, S. (2015). Changes in the essential oil content and composition of palmarosa (*Cymbopogon martini*) harvested at different stages and short intervals in two different seasons. *Ind. Crops Prod.* 69, 348–354. doi: 10.1016/j.indcrop.2015.02.020

Kamatou, G. P. P., Van Zyl, R. L., Davids, H., Van Vuuren, S. F., and Viljoen, A. M. (2008). Synergistic and antagonistic interactions of essential oils on the biological activities of the solvent extracts from three *Salvia* species. *Nat. Prod. Commun.* 3, 1111–1115. doi: 10.1177/1934578x0800300714

Kostik, V., and Bauer, B. (2015). *Antifungal activity of the essential oils of wild-growing Mentha piperita L and Mentha spicata L from the Mariovo region* (Antalya, Turkey: Republic of Macedonia). Available online at: http://eprints.ugd.edu.mk/13113/%0Ahttp://eprints.ugd.edu.mk/13113/1/final_program.pdf (Accessed July 25, 2025).

Liu, Q., Meng, X., Li, Y., Zhao, C. N., Tang, G. Y., and Li, H.B. (2017). Antibacterial and antifungal activities of spices. *Int. J. Mol. Sci.* 18, 1283. doi: 10.3390/ijms18061283

Longbottom, C. J., Carson, C. F., Hammer, K. A., Mee, B. J., and Riley, T. V. (2004). Tolerance of *Pseudomonas aeruginosa* to *Melaleuca alternifolia* (tea tree) oil is associated with the outer membrane and energy-dependent cellular processes. *J. Antimicrob. Chemother.* 54, 386–392. doi: 10.1093/jac/dkh359

Mallavarapu, G. R., Rao, B. R. R., Kaul, P. N., Ramesh, S., and Bhattacharya, A. K. (1998). Volatile constituents of the essential oils of the seeds and the herb of palmarosa (*Cymbopogon martinii* (Roxb.) Wats. var. motia Burk.). *Flavour Fragr. J.* 13, 167–169. doi: 10.1002/(SICI)1099-1026(199805/06)13:3<167::AID-FFJ719>3.0.CO;2-B

Market Report Analytics (2023). *Global and India palmarosa oil market insights and forecast*. Available online at: https://www.marketreportanalytics.com/report/global-and-India-palmarosa-oil-market (Accessed July 28, 2025).

Mkaddem Mounira, G. (2024). *Essential oils and their bioactive molecules: recent advances and new applications*. (London, UK: IntechOpen). doi: 10.5772/intechopen.113406

Moghaddam, M., and Mehdizadeh, L. (2017). "Chemistry of essential oils and factors influencing their constituents," in *Soft chemistry and food fermentation* (Academic Press, Cambridge, MA, USA: Elsevier), 379–419. doi: 10.1016/b978-0-12-811412-4.00013-8

Mohamed Ibrahim, S., Mohamed, G., Al Haidari, R., Soliman El-Kholy, A., Asfour, H., and Zayed, M. (2018). Fusaristerol A: A new cytotoxic and antifungal ergosterol fatty acid ester from the endophytic fungus *Fusarium* sp. associated with *Mentha longifolia* roots. *Pharmacogn. Mag.* 14, 308–311. doi: 10.4103/pm.pm_113_18

Morshedloo, M. R., Mumivand, H., Craker, L. E., and Maggi, F. (2018). Chemical composition and antioxidant activity of essential oils in *Origanum vulgare* subsp. gracile at different phenological stages and plant parts. *J. Food Process. Preserv.* 42, e13516. doi: 10.1111/jfpp.13516

Moutassem, D., Belabid, L., Bellik, Y., Ziouche, S., and Baali, F. (2019). Efficacy of essential oils of various aromatic plants in the biocontrol of Fusarium wilt and inducing systemic resistance in chickpea seedlings. *Plant Prot. Sci.* 55, 202–217. doi: 10.17221/134/2018-PPS

Mueller, L., and Boehm, V. (2011). Antioxidant activity of β-carotene compounds in different *in vitro* assays. *Molecules* 16, 1055–1069. doi: 10.3390/molecules16021055

Niki, E. (2010). Assessment of antioxidant capacity *in vitro* and in *vivo*. *Free Radic. Biol. Med.* 49, 503–515. doi: 10.1016/j.freeradbiomed.2010.04.016

Nuñez, L., and D'Aquino, M. (2012). Microbicide activity of clove essential oil (*Eugenia Caryophyllata*). *Braz. J. Microbiol.* 43, 1255–1260. doi: 10.1590/S1517-83822012000400003

Olszowy, M., and Dawidowicz, A. L. (2018). Is it possible to use the DPPH and ABTS methods for reliable estimation of antioxidant power of colored compounds? *Chem. Pap.* 72, 393–400. doi: 10.1007/s11696-017-0288-3

Orlo, E., Nerín, C., Lavorgna, M., Wrona, M., Russo, C., Stanzione, M., et al. (2023). Antioxidant activity of coatings containing eugenol for flexible aluminium foils to preserve food shelf-life. *Food Packag. Shelf Life* 39, 101145. doi: 10.1016/j.fpsl.2023.101145

Oussalah, M., Caillet, S., Saucier, L., and Lacroix, M. (2007). Inhibitory effects of selected plant essential oils on the growth of four pathogenic bacteria: *E. coli* O157:H7, *Salmonella typhimurium*, *Staphylococcus aureus* and *Listeria monocytogenes*. *Food Control* 18, 414–420. doi: 10.1016/j.foodcont.2005.11.009

Palá-Paúl, J., Pérez-Alonso, M. J., Velasco-Negueruela, A., Palá-Paúl, R., Sanz, J., and Conejero, F. (2001). Seasonal variation in chemical constituents of *Santolina rosmarinifolia* L. ssp. *rosmarinifolia*. *Biochem. Syst. Ecol.* 29, 663–672. doi: 10.1016/S0305-1978(01)00032-1

Pina, L. T. S., Serafini, M. R., Oliveira, M. A., Sampaio, L. A., Guimarães, J. O., and Guimarães, A. G. (2022). Carvone and its pharmacological activities: A systematic review. *Phytochemistry* 196, 113080. doi: 10.1016/j.phytochem.2021.113080

Połeć, K., Broniatowski, M., Wydro, P., and Hąc-Wydro, K. (2020). The impact of β-myrcene – the main component of the hop essential oil – on the lipid films. *J. Mol. Liq.* 308, 113028. doi: 10.1016/j.molliq.2020.113028

Pombal, S., Roncero, A. M., Tobal, I. E., García, N., Silva, L., Diez, D., et al. (2020). Antioxidant activity of new carvone derivatives. *Nat. Prod. Commun.* 15, 1934578X20908081. doi: 10.1177/1934578X20908081

Prashara, A., Hili, P., Veness, R. G., and Evans, C. S. (2003). Antimicrobial action of palmarosa oil (*Cymbopogon martinii*) on Saccharomyces cerevisiae. *Phytochemistry* 63, 569–575. doi: 10.1016/S0031-9422(03)00226-7

Raina, V. K., Srivastava, S. K., Aggarwal, K. K., Syamasundar, K. V., and Khanuja, S. P. S. (2003). Essential oil composition of *Cymbopogon martinii* from different places in India. *Flavour Fragr. J.* 18, 312–315. doi: 10.1002/ffj.1222

Rao, B. R. R., Kaul, P. N., Syamasundar, K. V., and Ramesh, S. (2005). Chemical profiles of primary and secondary essential oils of palmarosa (*Cymbopogon martinii* (Roxb.) Wats var. motia Burk.). *Ind. Crops Prod.* 21, 121–127. doi: 10.1016/j.indcrop.2004.02.002

Rashid, S., Rather, M. A., Shah, W. A., and Bhat, B. A. (2013). Chemical composition, antimicrobial, cytotoxic and antioxidant activities of the essential oil of *Artemisia indica* Willd. *Food Chem.* 138, 693–700. doi: 10.1016/j.foodchem.2012.10.102

Rastogi, S. C., Heydorn, S., Johansen, J. D., and Basketter, D. A. (2001). Fragrance chemicals in domestic and occupational products. *Contact Dermatitis* 45, 221–225. doi: 10.1034/j.1600-0536.2001.450406.x

Rathore, S., Mukhia, S., Kapoor, S., Bhatt, V., Kumar, R., and Kumar, R. (2022). Seasonal variability in essential oil composition and biological activity of *Rosmarinus officinalis* L. accessions in the western Himalaya. *Sci. Rep.* 12, 3305. doi: 10.1038/s41598-022-07298-x

Roman, H., Niculescu, A. G., Lazăr, V., and Mitache, M. M. (2023). Antibacterial efficiency of *Tanacetum vulgare* essential oil against ESKAPE pathogens and synergisms with antibiotics. *Antibiotics.* 12, 1635. doi: 10.3390/antibiotics12111635

Saeb, K., and Gholamrezaee, S. (2012). Variation of essential oil composition of *Melissa officinalis* L. leaves during different stages of plant growth. *Asian Pac. J. Trop. Biomed.* 2, S547–S549. doi: 10.1016/S2221-1691(12)60271-8

Sakkas, H., Gousia, P., Economou, V., Sakkas, V., Petsios, S., and Papadopoulou, C. (2016). *In vitro* antimicrobial activity of five essential oils on multidrug resistant Gram-negative clinical isolates. *J. Intercult. Ethnopharmacol.* 5, 212–218. doi: 10.5455/jice.20160331064446

Salami, M., Rahimmalek, M., and Ehtemam, M. H. (2017). Comprehensive research on essential oil and phenolic variation in different *Foeniculum vulgare* populations during transition from vegetative to reproductive stage. *Chem. Biodivers.* 14, e1600246. doi: 10.1002/cbdv.201600246

Scalese, G., Mosquillo, M. F., Pérez-Díaz, L., and Gambino, D. (2024). Biosynthesis of ergosterol as a relevant molecular target of metal-based antiparasitic and antifungal compounds. *Coord. Chem. Rev.* 503, 215608. doi: 10.1016/j.ccr.2023.215608

Serafim, C.A. de L., Araruna, M. E. C., Alves Júnior, E. B., Silva, L. M. O., Silva, A. O., da Silva, M. S., et al. (2021). (-)-Carveol prevents gastric ulcers via cytoprotective, antioxidant, antisecretory and immunoregulatory mechanisms in animal models. *Front. Pharmacol.* 12. doi: 10.3389/fphar.2021.736829

Sharma, P., Guarve, K., Gupta, S., Malik, G., and Wilson, K. (2023). Essential oils' Chemical characterization and investigation of some biological activities: A demanding review. *Essent. Oils Contrib. to Chem. Knowl.* 3, 101–119. doi: 10.1201/9781003226345-4

Sitzmann, J., Habegger, R., Schnitzler, W. H., and Grassmann, J. (2014). Comparative analysis of antioxidant activities of fourteen *Mentha* essential oils and their components. *Chem. Biodivers.* 11, 1978–1989. doi: 10.1002/cbdv.201400100

Soković, M. D., Glamočlija, J., Marin, P. D., Brkić, D. D., Vukojević, J., Jovanović, D., et al. (2006). Antifungal activity of the essential oil of *Mentha* x *piperita*. *Pharm. Biol.* 44, 511–515. doi: 10.1080/13880200600878700

Soliman, S. A., Hafez, E., Alkolaibe, A. M. G., Abdel Razik, E. S. S., Abd-Ellatif, S., Ibrahim, A. A., et al. (2022). Biochemical characterization, antifungal activity, and relative gene expression of two *Mentha* essential oils controlling *Fusarium oxysporum*, the causal agent of *Lycopersicon esculentum* root rot. *Plants* 11, 189. doi: 10.3390/plants11020189

Tamgue, O., Louis, B., Nguefack, J., Lekagne Do, J. B., and Daboy Dako, C. (2011). Synergism and antagonism of essential oil fractions of *Cymbopogon citratus*, *Ocimum gratissimum* and *Thymus vulgaris* against *Penicillium expansum*. *Int. J. Plant Pathol.* 2, 51–62. doi: 10.3923/ijpp.2011.51.62

Tholl, D. (2015). "Biosynthesis and biological functions of terpenoids in plants," in *Biotechnol. isoprenoids* (Cham, Switzerland: Springer), 63–106.

Tit, D. M., and Bungau, S. G. (2023). Antioxidant activity of essential oils. *Antioxidants* 12, 10835–10847. doi: 10.3390/antiox12020383

Ulanowska, M., and Olas, B. (2021). Biological properties and prospects for the application of eugenol—A review. *Int. J. Mol. Sci.* 22, 3671. doi: 10.3390/ijms22073671

Vasileva, K. (2023). Study of the influence of plant extracts on the mycelium growth of *Alternaria solani*. *Agric. Sci.* 15, 74–78. doi: 10.22620/agrisci.2023.39.008

Verma, R. S., Padalia, R. C., Goswami, P., Verma, S. K., Chauhan, A., Singh, V. R., et al. (2018). Chemical composition and antibacterial activity of p-menthane chemotype of *Cymbopogon martini* (Roxb.) W. Watson (Poaceae) from India. *J. Essent. Oil Res.* 30, 182–188. doi: 10.1080/10412905.2018.1429327

Vranová, E., Coman, D., and Gruissem, W. (2013). Network analysis of the MVA and MEP pathways for isoprenoid synthesis. *Annu. Rev. Plant Biol.* 64, 665–700. doi: 10.1146/annurev-arplant-050312-120116

Wettasinghe, M., and Shahidi, F. (1999). Evening primrose meal: A source of natural antioxidants and scavenger of hydrogen peroxide and oxygen-derived free radicals. *J. Agric. Food Chem.* 47, 1801–1812. doi: 10.1021/jf9810416

Xiong, H. B., Zhou, X. H., Xiang, W. L., Huang, M., Lin, Z. X., Tang, J., et al. (2023). Integrated transcriptome reveals that D-limonene inhibits *Candida tropicalis* by disrupting metabolism. *Lwt* 176, 114535. doi: 10.1016/j.lwt.2023.114535

Yexiao, C. H., Jiang, S. S., Yan, B. F., and Ye, M. (2020). Chemical composition and antifungal activity of essential oil from *Citrus maxima* against *Botrytis cinerea*. *Tianran Chanwu Yanjiu yu Kaifa* 32, 47–56. doi: 10.16333/j.1001-6880.2020.1.007

Yu, H., Lin, Z. X., Xiang, W. L., Huang, M., Tang, J., Lu, Y., et al. (2022). Antifungal activity and mechanism of D-limonene against foodborne opportunistic pathogen *Candida tropicalis*. *Lwt* 159, 113144. doi: 10.1016/j.lwt.2022.113144

frontiers | Frontiers in Plant Science

TYPE Original Research
PUBLISHED 12 September 2025
DOI 10.3389/fpls.2025.1590072

OPEN ACCESS

EDITED BY
Mariam Gaid,
Independent researcher, Braunschweig, Germany

REVIEWED BY
Yaxi Zhou,
Beijing Union University, China
Yanqin Yang,
Chinese Academy of Agricultural Sciences, China
Antim Maurya,
University of Mississippi, United States

*CORRESPONDENCE
Zhihui Zhao
lyzhihuizhao@126.com

RECEIVED 11 March 2025
ACCEPTED 03 June 2025
PUBLISHED 12 September 2025

CITATION
Ren P, Dao R, Wang L, Muhammad N, Sang Y, Liu M and Zhao Z (2025) HS-GC-IMS with sensory evaluation technique to analyze volatile flavor compounds of jujube flowers. *Front. Plant Sci.* 16:1590072. doi: 10.3389/fpls.2025.1590072

HS-GC-IMS with sensory evaluation technique to analyze volatile flavor compounds of jujube flowers

Peixing Ren[1,2], Ruirui Dao[1,2], Lili Wang[1,2], Noor Muhammad[1,2], Yaxin Sang[3], Mengjun Liu[1,2] and Zhihui Zhao[1,2]*

[1]College of Horticulture, Hebei Agricultural University, Baoding, Hebei, China, [2]Research Center of Chinese Jujube, Hebei Agricultural University, Baoding, Hebei, China, [3]College of Food Science and Technology, Hebei Agricultural University, Baoding, Hebei, China

The combination of headspace gas chromatography-ion mobility spectrometry (HS-GC-IMS) and sensory evaluation technique was employed to detect and analyze the volatile organic compounds (VOCs) in jujube flowers at different developmental stages across various varieties, and to compare them with other plant flowers known for their characteristic aromas. A total of 65 volatile compounds were identified in jujube flowers at different stages. The aroma fingerprint analysis revealed 24 distinct aromas, with 14 aromas increasing in intensity from the bud stage to full bloom. Varieties such as Fuxiang, Dongzao, and Xingguang exhibited significantly stronger aromas at the flowering stage compared to other varieties. Additionally, sensory evaluation indicated a preference for the fragrance of jujube flowers among men. This study offers new insights into the development of jujube flower-based spices, highlighting their considerable potential and laying a foundation for further research on plant flower spices.

KEYWORDS

jujube flowers, different periods, varieties, GC-IMS, PCA

Highlights

- The volatile fingerprints of jujube flowers in different periods were established by HS-GC-IMS.
- HS-GC-IMS combined with PCA can well differentiate the volatile differences of jujube flowers in different periods.
- Sensory evaluation showed men prefer preferred jujube aroma.
- Jujube flowers aroma has the potential to be developed into men ‘s perfume.

1 Introduction

Jujube (*Ziziphus jujuba* Mill.) belongs to the genus *Ziziphus* of the family Rhamnaceae (Gao et al., 2013). It is native to China and is cultivated in Asia, Europe and the Americas (Liu et al., 2020). China has the largest the world's largest jujube cultivation area globally, with a history over 4,000 years (Hernández et al., 2015; Li et al., 2009; Wojdyło et al., 2016). Jujube fruit contains vitamins, carbohydrates, organic acids, cAMP, and proline, making it both a medicinal and edible treasure (Choi et al., 2011; Guo et al., 2015; Li et al., 2007; Liu et al., 2015). The jujube flower is the primary source of fragrance in the jujube tree, and it is highly esteemed for its pleasant aroma and abundance. It also provides valuable nectar, making it important to investigate the fragrance attributes of jujube flowers.

Generally, Jujube flowers bloom in May and can last until July. Jujube flowers are small and numerous, exhibiting a yellow-green color as a whole, with a uniquely warm and inviting fragrance.

Flavor is an important perceptual property of foods, and it that is used in assessing their nutrition-related properties and freshness (Shi et al., 2017). Floral scents are primarily derived from VOCs synthesized within plant organs and released into the air. Generally, Jujube flowers bloom in May and can last until July. Jujube flowers are small and numerous, exhibiting a yellow-green color as a whole, with a uniquely warm and inviting fragrance. The aroma of jujube flowers serves as a signal to attract honey bees, which collect nectar to produce jujube honey after its own transformation process (Ma W. et al., 2020). Jujube flowers contain many volatile compounds, including esters, alkanes, aldehydes, and ketones, which contribute to their pleasant aroma (Xia et al., 2020). Furthermore, these flowers contain essential nutritional components, including calcium (Ca), iron (Fe), magnesium (Mg), as well as bioactive compounds such as mannose and phenols, making them a unique blend of scent and nutrition (Du et al., 2024; Fahim et al., 2014).

Volatile compounds are crucial not only for the fragrance of plants but also for their ecological interactions and potential applications in flavor, fragrance, and health-related industries. As the cultivation area of jujube continues to expand, understanding the aromatic characteristics of jujube flowers becomes increasingly important. The fragrance of jujube flowers, known for its delicate, restrained, and enduring profile, has long been appreciated, particularly in East Asian cultures, where it aligns with traditional preferences. This subtle yet distinctive aroma holds promising potential for both commercial and cultural applications. While previous studies have primarily focused on fruit aroma (Feng et al., 2022), the volatile compounds in flowers, and their dynamic changes throughout development and in different varieties, have not been systematically explored. Moreover, there is a significant gap in research comparing the volatile components of jujube within other flowers.

The study of plant aroma compounds plays a crucial role in understanding plant sensory characteristics, with aroma being a key distinguishing feature of jujube. Jujube aroma consists of a complex mixture of volatile compounds produced through various biotransformations of sugars, amino acids and other metabolites (Wang et al., 2018; Zhu and Xiao, 2018). Due to its ease of operation, enhanced sensitivity, streamlined processing, and efficient analytical speed, gas chromatography-ion mobility spectometry (GC-IMS) has become a widely used method food aroma analysis (Wang et al., 2020). Different plant tissue exhibit unique flavor profile, with flowers often having the most pronounced aromas (Ma et al., 2023). GC-IMS is a novel technique for odors detection, with IMS separating ions based on their mobility under atmospheric pressure (Li et al., 2019). Combining IMS with other analytical instruments enhances its performance and improves the accuracy of results. In recent years, headspace gas chromatography-ion mobility spectrometry (HS-GC-IMS) has been widely applied to investigate volatile compounds in food science. For example (Feng et al., 2022), used GC-IMS and sensory evaluation to characterize the volatile organic compounds (VOCs) characteristics in Molixiang grapes from different regions. In another study (Leng et al., 2021), employed GC-IMS to analyze postharvest preservation of peach fruit, finding a significant increase in esters and alcohols levels with prolonged storage. Similarly (Yao et al., 2024), examined the volatile components and aroma profiles of Yijiangzi monofloral honey and its corresponding flowers by GC-IMS, discovering that most of the compounds in honey originated from flowers. PCA is a detection method based on multivariate statistics, which is used to reduce the dimension or transform multiple indicators into several comprehensive indicators for extracting features and revealing the relationship between variables. The converted score information also can be entered into a cluster analysis and further discriminant analysis. PCA can be combined with HS-GC-IMS to detect the volatile flavor substances in plant flower. Based on these previous studies, GC-IMS appears to be a promising technique for analyzing VOCs in jujube flowers.

This study aims to fill these knowledge gaps by systematically investigating the volatile components of jujube flowers. Flowers in three development stages and eleven varieties were studied to reveal the distribution of volatile compounds and identify the characteristic components. Furthermore, jujube flowers were compared with other plant species renowned for their distinctive floral aromas, providing a comprehensive orientation towards understanding the diversity of floral fragrance profiles. The findings from this research will provide valuable insights for the development and application of jujube flower aroma and serve as a reference for future studies on the volatile compound accumulation mechanisms in jujube. This work will contribute to the broader understanding of plant volatiles and their potential in various industries.

2 Materials and methods

2.1 Plant material

All jujube flowers samples used in this study were collected from the Third Farm Branch of Hebei Agricultural University (115° 48′E, 38°85′N) in June 2023. Samples were harvested at three

developmental stages: flower bud stage, flowering stage, and late flowering stage, and immediately transported to the laboratory for analysis. Jujube flowers with uniform appearance and no physical damage were selected as experimental samples (Figure 1). The study included eleven jujube varieties: Fushuai, Fuxiang, Xingguang, Dongzao, Yueguang, Yuhong, Chenguang, Yushuai, Zanshuo, Jinsixiaozao, and Dajinsiwang. For comparative analysis, flowers of Lily bulb, Rose, Chrysanthemum, and Carnation were obtained from the Baoding Agro-ecological Park in Hebei Province (Figure 1). These four species were selected due to their widespread recognition and distinctive aromatic properties. All samples were healthy, free from pest damage, and exhibited no signs of spoilage.

2.2 Sensory evaluation

The sensory evaluation was conducted in accordance with the ethical guidelines outlined in the World Medical Association (Helsinki Declaration). A total of 20 healthy, non-smoking participants (10 men and 10 women, aged 20–42 years) were recruited from students and faculty members of our institution. Prior to the aroma evaluation, all participants underwent a one-week training program, which included more than two hours of daily sessions to familiarize them with the characteristics of plant floral aromas and the requirements for sensory evaluation. During this training, participants were introduced to the descriptive terminology used for plant floral aromas. Written informed consent was obtained from each participant before commencing the sensory evaluation.

2.3 Headspace gas chromatography-ion mobility spectrometry analysis

The volatile compounds of jujube flowers were analyzed using HS-GC-IMS flavor analyzer (Flavour Spec ®) provided by the company für Analytische Sensorysteme mb H (G.A.S., Dortmund, Germany). For the analysis, 1g of flower sample was weighed and placed in a 20ml headspace glass extraction bottle. The samples were incubated at 60°C for 15 min. Following incubation, 0.5 ml of the headspace phase was automatically injected into the sampler in a splitless injection mode with a syringe at 45°C. Volatile components were separated using an MXT-WAX capillary column (30 m × 0.53 mm ID, 1.0 µm df, RESTEK, USA) in the gas chromatography and coupled to IMS at 45°C. Nitrogen (purity of 99.999%) was used as the carrier gas. The program flow rate was as follows: 2 mL/min for the first 2 min, increasing linearly to 10 mL/min over 8 min, then increasing to 100 mL/min over the final 15 minutes, after which the flow was stopped. The analysis was conducted under normal pressure. The analyte was separated on a column maintained at 60°C and ionized in the IMS ionization chamber at 45°C. The drift gas (nitrogen) flow rate was set to 150 mL/min. Each sample was analyzed in triplicate. The retention index (RI) of volatile compounds was calculated using C4-C8 n-ketone (China National Pharmaceutical Chemical Reagents Beijing Co., Ltd.) as an external reference under the same chromatographic conditions. Volatile compounds were identified by comparing the standard drift time and RI with those in the GC-IMS libraries and NIST 2014 (National Institute of Standards and Technology, Gaithersburg, Maryland, United States).

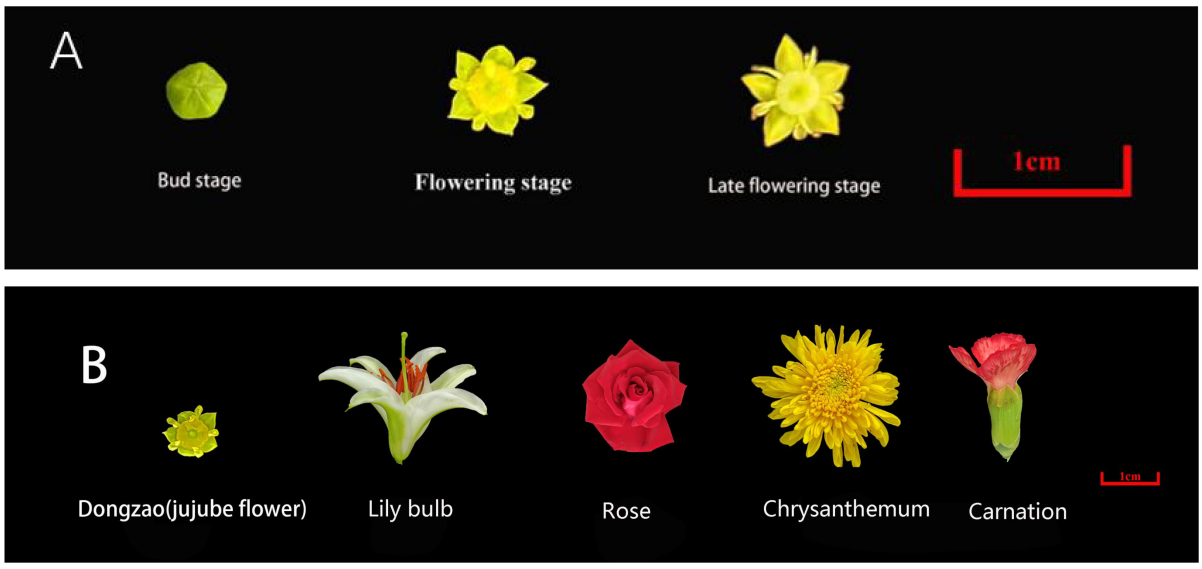

FIGURE 1
(A) Jujube flowers in three periods. **(B)** Jujube flowers and four other commonly recognized flowers.

2.4 Statistical analysis

The HS-GC-IMS data is processed using the laboratory analysis instrument Vocal and its three plug-ins, the NIST database and the IMS database. The topographic map and fingerprint of volatile compounds in jujube flowers were established by using the Reporter and Gallery Plot plug-in. Principal Component Analysis (PCA) was performed using the Dynamic PCA plug-in (g.a.s., Dortmund, Germany) to evaluate the regularity and difference between test samples. The analysis was performed using Origin software (version 2021b, USA). OPLS-DA and PLSR analyses were conducted to further evaluate the characteristics of samples using SIMCA 14.1.

3 Results and discussion

3.1 Variation of volatile flavor compounds in jujube flowers at different growth stages

3.1.1 HS-GC-IMS topographic maps of jujube flowers across different growth stage

HS-GC-IMS was employed to analyze the differences in volatile substances in jujube flowers at various growth stages. Taking the Fuxiang variety as an example, Figure 2 showed the topographic map of volatile substances, where X, Y and Z represent ion migration time, GC retention time and ion peak intensity, respectively. As illustrated in Figure 2, jujube flowers at different stages showed similar visualization patterns, with slight variations in ion peak intensity. The red-circled area in Figure 2 clearly highlights the differences in peak intensity between the various stages. Notably, the ion peak intensity during the flowering stage was significantly higher compared to the bud stage and the late flowering stage. GC-IMS separates mixtures into individual compounds through a gas chromatography column, then ionizes these compounds using ion mobility spectrometry, and further analyzes them based on the migration rates of each compound's ions under the influence of an electric field (Yang et al., 2021). This dual separation allows for the distinct identification of each compound. By analyzing the migration time and ion peak intensity of each volatile compound, the volatile profile of jujube flowers can be qualitatively analyzed.

Because the topographic map is relatively rough, the volatile substances in jujube flowers cannot be clearly displayed. To better distinguish the volatile flavor components at different stages of flowering, we normalized the ion migration time and reaction ion peak (RIP). Each point around the RIP represents a volatile substance found in jujube flowers. Most volatile substance signals appeared within a drift time of 1.0-1.75 ms and a retention time of 200-1000 s. In the visualization, the color of each point indicates the signal intensity of a single substance: red indicates a higher intensity, blue signifies lower intensity, and the color depth correlated with the intensity level. Different models were applied to distinguish the volatile components of jujube flowers across various growth stages, as shown in Figure 2. From the two-dimensional topographic plots (Figure 2), it is evident that the signal intensities within the red box are markedly higher in jujube flowers during the flowering stage compared to those at the other two developmental periods. In Figure 2, the bud stage of Fuxiang variety is used as a reference to compare the other two stages. Red indicates a higher intensity than the reference, while blue indicates a lower intensity. When the drift time was 1.0-1.5 ms and the retention time was 400-800 s, the volatile substances in both the flowering stage and the late flowering stage were significantly higher than those in the bud stage, with the flowering stage showing slightly more red than that in the late flowering stage. As jujube flowers continue to bloom, certain aroma components are continuously produced. However, during the late flowering stage, the levels of these aroma components gradually decline as a result of flower ovary pollination and the subsequent formation of fruits. To further explore the volatile substances represented by these red dots, an in-depth statistical analysis of jujube samples across different periods is necessary.

3.1.2 Qualitative analysis volatile flavor components in jujube flowers at different growth stages

In this study, the two-dimensional cross-qualitative approach, utilizing the GC-IMS Library Search, was employed to further identify the detected compounds. Figure 3 presents the results of the library search-based qualitative analysis of the sample. In Figure 3, the horizontal axis represents the drift time, while the vertical axis corresponds to the retention time. The red numbers displayed in Figure 3, denote the identified organic compounds. Table 1 provides the qualitative results of volatile components detected in jujube flowers across different growth stages. The red numbers in Figure 3, align with the compound numbers listed in Table 1. Notably, due to the enhanced proton affinity and higher concentration of dimers, their drift time is greater than that of monomers (Lantsuzskaya et al., 2015). Some compounds may produce multiple signals due to varying concentrations, such as monomers and dimers (Li et al., 2019). According to our study results, we found that a total of 31 compounds exist in the form of dimers. Ultimately, we detected 105 peaks and identified 65 volatile compounds from our samples, including 15 aldehydes, 12 esters, 11 alcohols, 11 olefins, 8 ketones, 4 ethers, and 4 other substances (1 furan, 1 pyrazine, 1 thiazole and 1 pyridine), as show in Table 1.

3.1.3 Analysis of volatile flavor components of jujube flowers in different periods

To distinguish the differences between jujube flowers in different periods, the Gallery Plot plug-in was used to generate volatile fingerprints (Figure 4). The row represents the detected volatile organic compounds, and the column showed the signal intensity of the same compound presented in different jujube flowers samples. Each point in the figure represents a volatile substance, and the depth of the color is related to the content of the volatile substance. The brighter the color, the higher the content of the substance in the sample.

As illustrated in Figure 4, the aromatic profiles of jujube flowers were compared across different growth stages. The highest diversity of aroma components was observed during the flowering stage

10.3389/fpls.2025.1590072

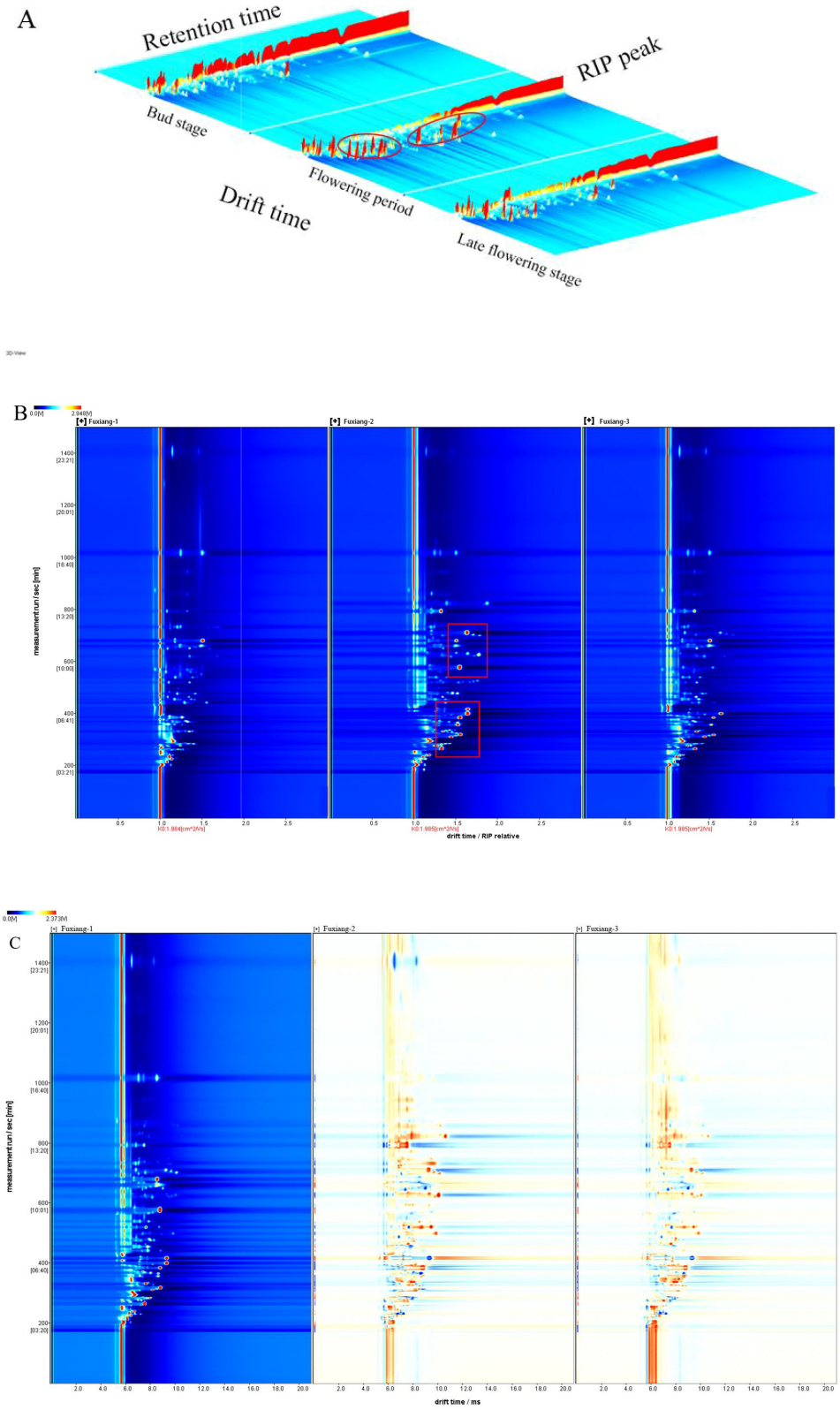

FIGURE 2
GC-IMS analysis of Fuxiang flowers in different periods. **(A)** 3D-topographic plots of Fuxiang flowers; **(B)** 2D-topographic plots of Fuxiang flowers; **(C)** The difference comparison topographic plots of Fuxiang flowers.

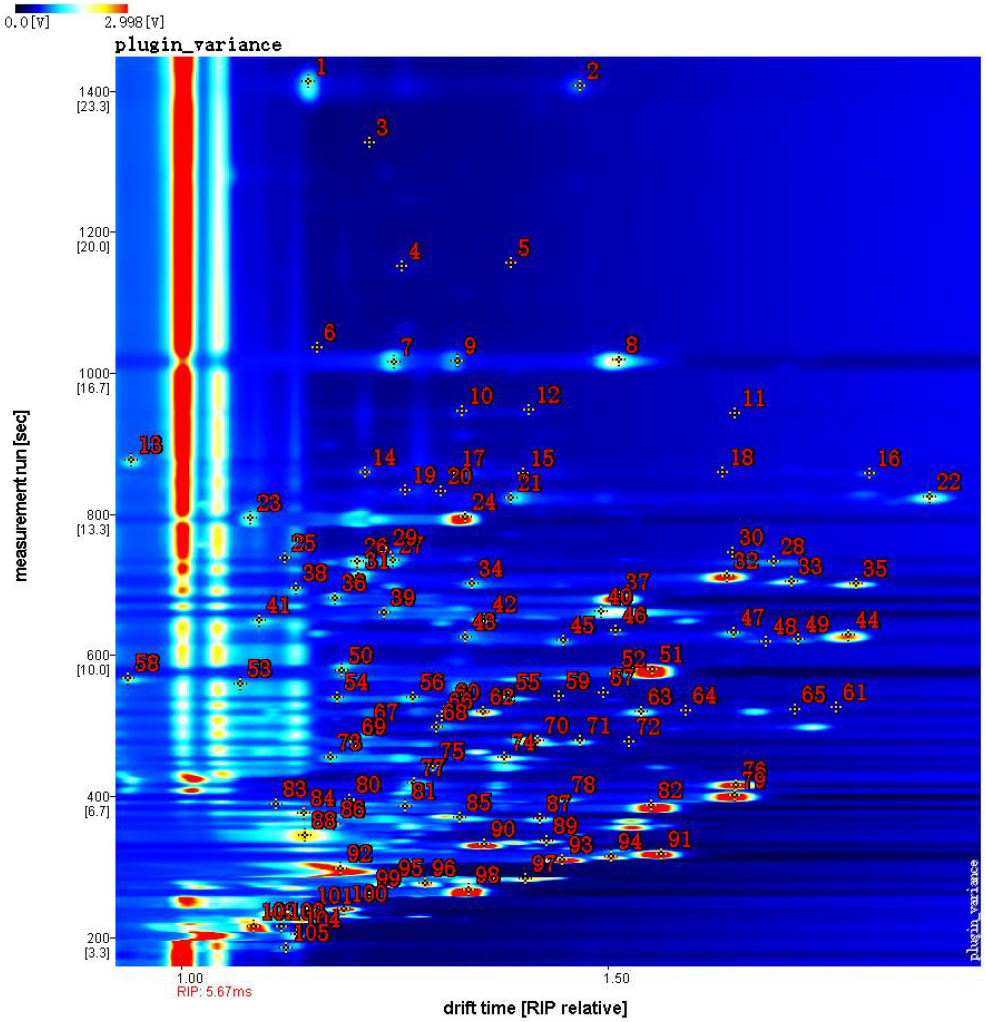

FIGURE 3
Library search qualitative analysis of jujube flowers across different periods.

TABLE 1 Detected volatile organic compounds (VOCs) in jujube flowers identified byHS-GC-IMS.

Count	Compound	Flavor description	CAS#	Formula	MW[a]	RI[b]	Rt[c]	Dt[d]	Comment
Aldehydes									
1	Benzaldehyde	sweet, almond, nutty	C100527	C7H6O	106.1	1493	1413.836	1.15015	Monomer
2	Benzaldehyde		C100527	C7H6O	106.1	1491.6	1408.328	1.46858	Dimer
3	n-Octanal	fatty, citrus, honey	C124130	C8H16O	128.2	1316.1	858.444	1.40149	Monomer
4	n-Octanal		C124130	C8H16O	128.2	1315.8	857.796	1.80804	Dimer
5	(E)-2-Heptenal	guava	C18829555	C7H12O	112.2	1266.6	746.689	1.24164	Monomer
6	(E)-2-Heptenal		C18829555	C7H12O	112.2	1266.1	745.634	1.64713	Dimer
7	Butanal	fermented, bready	C123728	C4H8O	72.1	827.3	216.273	1.08541	Monomer
8	Butanal		C123728	C4H8O	72.1	825.2	215.009	1.11821	Dimer
9	Valeraldehyde	cocoa chocolate	C110623	C5H10O	86.1	1008	360.018	1.17985	Monomer
10	Valeraldehyde		C110623	C5H10O	86.1	1017.1	369.369	1.42174	Dimer

(Continued)

TABLE 1 Continued

Count	Compound	Flavor description	CAS#	Formula	MW[a]	RI[b]	Rt[c]	Dt[d]	Comment
Aldehydes									
11	1-hexanal	green, woody, vegetative	C66251	C6H12O	100.2	1032.8	386.144	1.26358	Monomer
12	1-hexanal		C66251	C6H12O	100.2	1033.6	386.969	1.552	Dimer
13	3-Methyl-2-butenal	nutty, cherry	C107868	C5H8O	84.1	1217.3	649.704	1.09243	Monomer
14	3-Methyl-2-butenal		C107868	C5H8O	84.1	1217.8	650.577	1.35719	Dimer
15	2-Hexenal	almond, apple, plum	C505577	C6H10O	98.1	1234.1	681.148	1.18116	Monomer
16	2-Hexenal		C505577	C6H10O	98.1	1235	682.895	1.51462	Dimer
17	(E)-2-hexen-1-al	green, apple	C6728263	C6H10O	98.1	1209.6	635.728	1.51032	
18	Butyraldehyde	bready, yeasty	C123728	C4H8O	72.1	915.5	277.32	1.28767	
19	2-methylbutanal	green, fruity	C96173	C5H10O	86.1	922.3	282.722	1.40501	
20	3-Methyl butanal	peach	C590863	C5H10O	86.1	864.8	240.412	1.19159	
21	Octylaldehyde	orange	C124130	C8H16O	128.2	1351.3	948.006	1.40896	
22	Propanal	nutty	C123386	C3H6O	58.1	861.2	237.999	1.15131	
23	(E)-2-Pentenal	sharp	C1576870	C5H8O	84.1	1165.2	560.897	1.36286	
Alcohols									
24	3-heptanol	green, herbal	C589822	C7H16O	116.2	1350.9	946.885	1.32951	Monomer
25	3-heptanol		C589822	C7H16O	116.2	1349.6	943.52	1.64988	Dimer
26	3-Methylbutan-1-ol	green, fruity	C123513	C5H12O	88.1	1223.5	661.059	1.23841	Monomer
27	3-Methylbutan-1-ol		C123513	C5H12O	88.1	1224.2	662.369	1.49315	Dimer
28	1 -hexanol	peach, fruity, green, sweet	C111273	C6H14O	102.2	1316.2	858.734	1.32117	Monomer
29	1 -hexanol		C111273	C6H14O	102.2	1316.4	859.094	1.63589	Dimer
30	Butanol	fruity, green, sweet	C71363	C4H10O	74.1	1152.3	540.792	1.18445	Monomer
31	Butanol		C71363	C4H10O	74.1	1152.3	540.792	1.38521	Dimer
32	1-Pentanol	wintergreen, almond	C71410	C5H12O	88.1	1151.9	540.215	1.27273	Monomer
33	1-Pentanol		C71410	C5H12O	88.1	1156.4	547.132	1.49627	Dimer
34	3-Pentanol	sweet, nutty	C584021	C5H12O	88.1	1107.9	477.171	1.20437	Monomer
35	3-Pentanol		C584021	C5H12O	88.1	1108.9	478.546	1.41842	Dimer
36	1- butanol	butter, creamy	C71363	C4H10O	74.1	1091.6	455.72	1.17545	Monomer
37	1- butanol		C71363	C4H10O	74.1	1092	456.27	1.37988	Dimer
38	2-butanol	fruit, green	C78922	C4H10O	74.1	1024.6	377.344	1.14496	Monomer
39	2-butanol		C78922	C4H10O	74.1	1017.6	369.919	1.32754	Dimer
40	Propanol	camphor	C71238	C3H8O	60.1	1035.6	389.169	1.11239	
41	Linalool	citrus, rose, woody, green	C78706	C10H18O	154.3	1470.7	1327.537	1.22144	
42	1 -heptanol	onion, sweet, corn, green	C111706	C7H16O	116.2	1421.8	1156.775	1.38779	
Alkenes									
43	(E)-3-hexen-1-ol	green, cherry	C928972	C6H12O	100.2	1376	1016.412	1.25006	Monomer
44	(E)-3-hexen-1-ol		C928972	C6H12O	100.2	1376.8	1018.655	1.51404	Dimer
45	beta-ocimene	green, woody	C13877913	C10H16	136.2	1260.4	733.663	1.20741	Monomer

(Continued)

TABLE 1 Continued

Count	Compound	Flavor description	CAS#	Formula	MW[a]	RI[b]	Rt[c]	Dt[d]	Comment
Alkenes									
46	beta-ocimene		C13877913	C10H16	136.2	1260.7	734.33	1.24923	Dimer
47	beta-ocimene		C13877913	C10H16	136.2	1260.1	732.996	1.69536	Trimer
48	Limonene	lemon, fruity	C138863	C10H16	136.2	1249.9	712.156	1.20836	Monomer
49	Limonene		C138863	C10H16	136.2	1250.3	713.03	1.64056	Dimer
50	Limonene		C138863	C10H16	136.2	1245.9	704.295	1.71641	
51	3-carene	orange, fruity	C13466789	C10H16	136.2	1207.6	632.234	1.64914	Monomer
52	3-carene		C13466789	C10H16	136.2	1200.5	619.569	1.68635	Dimer
53	3-carene		C13466789	C10H16	136.2	1202.1	622.512	1.72438	Trimer
54	myrcene	peach, fruity, green	C123353	C10H16	136.2	1139.9	522.271	1.59313	Monomer
55	myrcene		C123353	C10H16	136.2	1140.8	523.646	1.7204	Dimer
56	(Z)-2-pentenol	fruity, green	C1576950	C5H10O	86.1	1323.4	876.236	0.94252	
57	alpha-terpinolene	sweet, floral, plastic	C586629	C10H16	136.2	1316.6	859.74	1.21715	
58	2-methyl-2-propenal	fruity, green, sweet	C78853	C4H6O	70.1	897.3	263.507	1.22167	
59	1-Penten-3-ol	fruity, green	C616251	C5H10O	86.1	1169.2	567.306	0.93813	
60	beta-Pinene	woody, camphor	C127913	C10H16	136.2	1082	443.62	1.29614	
61	1,4-dimethylbenzene	pungent, fruity	C106423	C8H10	106.2	1164.5	559.813	1.07054	
Ester									
62	Hexanoic acid propyl ester	fruity	C626777	C9H18O2	158.2	1301.5	823.858	1.38732	Monomer
63	Hexanoic acid propyl ester		C626777	C9H18O2	158.2	1301.7	824.218	1.87885	Dimer
64	amyl acetate	banana, pear	C628637	C7H14O2	130.2	1142.7	526.396	1.31429	Monomer
65	amyl acetate		C628637	C7H14O2	130.2	1143.1	526.946	1.769	Dimer
66	Ethyl 2-methy lpropionate	sweet, floral	C97621	C6H12O2	116.2	940.8	297.847	1.18835	Monomer
67	Ethyl 2-methy lpropionate		C97621	C6H12O2	116.2	964.3	318.281	1.5639	Dimer
68	isoamyl formate	wine, fruity	C110452	C6H12O2	116.2	1061.7	418.87	1.27405	Monomer
69	Isoamyl formate		C110452	C6H12O2	116.2	1059.3	416.12	1.65201	Dimer
70	ethyl (E)-2-butenoate	spicy, sweet, garlicy	C623701	C6H10O2	114.1	1176	578.258	1.18872	Monomer
71	ethyl (E)-2-butenoate		C623701	C6H10O2	114.1	1177.4	580.564	1.55322	Dimer
72	Methyl butyrate	fruity, green	C623427	C5H10O2	102.1	993.4	345.526	1.14632	Monomer
73	Methyl butyrate		C623427	C5H10O2	102.1	985	337.405	1.42968	Dimer
74	2-Methyl butanoic acid ethyl ester	apple, fruity	C7452791	C7H14O2	130.2	1046.7	401.544	1.64969	
75	isovaleric acid, methyl ester	fruity, celery	C556241	C6H12O2	116.2	1042	396.319	1.19845	
76	(E)-Ethyl-2-hexenoate	fruity, vegetable	C27829727	C8H14O2	142.2	1376.4	1017.533	1.32439	
77	Ethyl propanoate	sweet, rum, fruit, grape, pineapple	C105373	C5H10O2	102.1	956	310.946	1.4473	
78	3-methylbutyl propanoate	fruity, green	C105680	C8H16O2	144.2	1138.8	520.621	1.35478	
79	Acetic acid ethyl ester	fruity, nutty	C141786	C4H8O2	88.1	902.4	267.314	1.33738	

(Continued)

10.3389/fpls.2025.1590072

TABLE 1 Continued

Count	Compound	Flavor description	CAS#	Formula	MW[a]	RI[b]	Rt[c]	Dt[d]	Comment
Ketone									
80	2,3-Pentanedione	spicy, butter, creamy	C600146	C5H8O2	100.1	1122.9	497.796	1.21941	Monomer
81	2,3-Pentanedione		C600146	C5H8O2	100.1	1123.5	498.621	1.3004	Dimer
82	Isovalerone	green, fruity, sweet	C108838	C9H18O	142.2	1244.4	701.238	1.34145	Monomer
83	Isovalerone		C108838	C9H18O	142.2	1244.8	702.112	1.79226	Dimer
84	2,6-dimethyl-4-heptanone	oily, woody, lemon, herbal	C108838	C9H18O	142.2	1204.4	626.557	1.33429	Monomer
85	2,6-dimethyl-4-heptanone		C108838	C9H18O	142.2	1205.7	628.74	1.78367	Dimer
86	6-methyl-5-hepten-2-one	citrus, fruity	C110930	C8H14O	126.2	1383	1036.597	1.16036	
87	2-Butanone	green, clover, honey, sweet	C78933	C4H8O	72.1	914.2	276.366	1.24801	
88	Hexan-2-one	fruity, green, nutty	C591786	C6H12O	100.2	1173.5	574.223	1.50908	
89	3-penten-2-one, 4-methyl	Mint, honey	C141797	C6H10O	98.1	1153.4	542.548	1.44335	
90	2-propanone	oily, woody, lemon, herbal	C67641	C3H6O	58.1	772.6	185.353	1.12322	
Others									
91	2-Ethoxyethanol	sweet, minty	C110805	C4H10O2	90.1	1288.7	794.555	1.08235	Monomer
92	2-Ethoxyethanol		C110805	C4H10O2	90.1	1289.3	795.993	1.33379	Dimer
93	diethyl disulfide	onion	C110816	C4H10S2	122.2	1241.3	695.124	1.13537	
94	Dimethyl trisulfide	minty, herbal, eucalyptus	C3658808	C2H6S3	126.3	1305.2	832.487	1.30528	
95	Dipropyl disulfide		C629196	C6H14S2	150.3	1420.2	1151.266	1.25947	
96	2-ethylpyrazine	peanuts, nuts, roasted cocoa, woody	C13925003	C6H8N2	108.1	1262.6	738.332	1.12221	
97	2,6-Lutidine	nuts, amines, wood, bread	C108485	C7H9N	107.2	1201.2	620.879	1.44879	
98	tetrahydrothiophene	pungent, fruity	C110010	C4H8S	88.2	1134.1	513.746	1.30619	
99	2,5-Dimethylfuran	green, sweet	C625865	C6H8O	96.1	978.9	331.642	1.35647	
Unknowns									
100	1		unidentified	*	*	1138.6	520.346	1.53991	
101	2		unidentified	*	*	1109.5	479.371	1.46817	
102	3		unidentified	*	*	1108.5	477.996	1.52602	
103	4		unidentified	*	*	1041.8	396.044	1.45082	
104	5		unidentified	*	*	960.2	314.614	1.5056	
105	6		unidentified	*	*	806.3	203.859	1.13657	

[a]Represents the molecular mass.
[b]Represents the retention index calculated using n-ketones C4–C8 as external standard on MXT-WAX column.
[c]Represents the retention time in the capillary GC column.
[d]Represents the drift time in the drift tube.

(Figure 4, red box B), while the bud stage exhibited the least variety (Figure 4, red box A). Common to all samples were compounds such as methyl butyrate, 1-butanol, 3-pentanol, 2,6-dimethyl-4-heptanone, ethyl 2-methylpropionate, 2-ethoxyethanol, and 3-methylbutan-1-ol (Figure 4, red box D). During the bud stage, the aroma profile was predominantly characterized by a higher presence of alcohols and aldehydes (Figure 4, red box A). Notably, compounds like 3-heptanol, 3-methylbutan-1-ol, n-octanal, benzaldehyde, 2-butanol, butyraldehyde, 2-methylbutanal, and 3-methylbutanal were found in higher concentrations, imparting grassy, nutty, and jasmine-like scents to the jujube flowers. As the flower buds developed and accumulated nutrients, the aromatic intensity of the flowers gradually increased.

The flowering stage marked a significant divergence in aroma composition compared to the other stages, with an increase in 14 distinct aroma substances, including valeraldehyde, (E)-2-hexen-1-al, octylaldehyde, limonene, 3-carene, myrcene, terpinolene, hexanoic acid propyl ester, isoamyl formate, ethyl (E)-2-

10.3389/fpls.2025.1590072

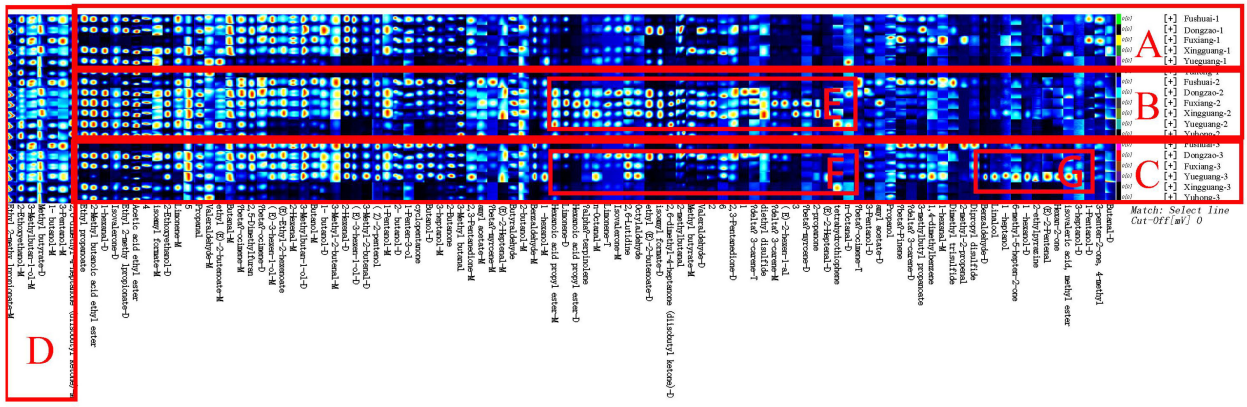

FIGURE 4
Fingerprint comparison of volatile organic compounds (VOCs) in jujube flowers samples determined by HS-GC-IMS.

butenoate, 2,3-pentanedione, 2,6-dimethyl-4-heptanone, 2-propanone, and diethyl disulfide (Figure 4, red box E). These newly emerged compounds were primarily esters and alkenes. Substances such as myrcene, terpinolene, 2-nonanone, 2,3-pentadione, and phellandrene, which are yellow liquids under standard conditions, contribute to the yellow coloration of the nectar disc and enhance the flowers' robust fragrance.

During the late flowering stage, some of the aroma components that increased during the flowering stage may have oxidized due to prolonged exposure to air. Consequently, the newly formed aroma components from the flowering period were largely absent in the late flowering stage (Figure 4, red box F). However, as indicated in Figure 4, red box G, eight additional aroma components were identified in the late flowering stage, including dipropyl disulfide, 2-methylbutanal, linalool, 6-methyl-5-hepten-2-one, 1-heptanol, (E)-2-pentenal, isovaleric acid, and methyl ester. Similar compounds, such as Benzaldehyde, (E) -2-Heptenal, and Butanal, have also been found in jujube fruit (Yang et al., 2019).

Similarly, aldehydes were found to be the most abundant across all three stages, followed by esters, alkenes, alcohols, and ketones (Figure 5). Notably, the levels of esters and alkenes during the flowering stage were significantly higher compared to the other two stages, serving as the primary factor contributing to the differences observed across the periods. In contrast, ketones and aldehydes exhibited minimal changes during the flowering stage, suggesting that they have a limited influence on the aroma profile of jujube

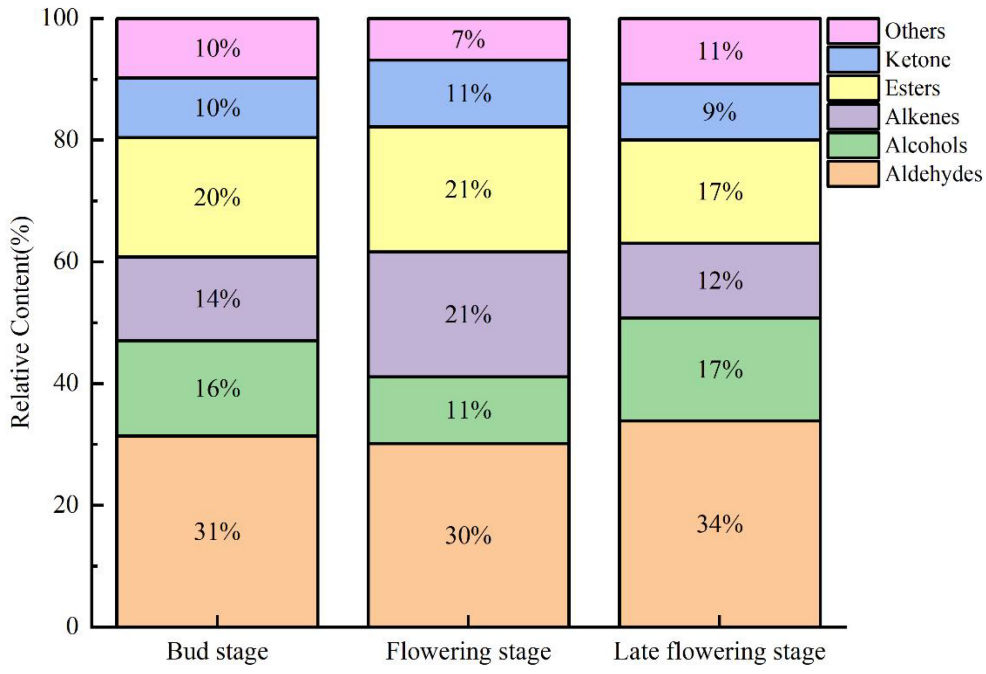

FIGURE 5
Relative contents of volatile components in different periods of jujube flowers.

flowers. During the flowering bud stage, a higher concentration of aldehydes and alcohols was formed, which were subsequently transformed into esters and alkenes during the flowering stage, thereby enhancing the aromatic profile of jujube flowers. The disappearance of certain compounds in the late flowering stage may be attributed to factors such as bee pollination, flower ovary fertilization, and oxidation due to prolonged exposure to air. Comparable findings have been reported in studies on truffles, red peppers, green peppers, and tea (Korkmaz et al., 2023; Shao et al., 2023; Yue et al., 2023).

3.1.4 PCA of volatile flavor components in jujube flowers across different developmental stages

Principal Component Analysis (PCA) is a widely utilized unsupervised analytical tool for the analysis of volatile compounds. In a PCA plot, samples with similar expression profiles exhibit a higher degree of clustering, while those with greater differences are positioned farther apart (Ma Q. et al., 2020). To better distinguish and comprehensively analyze the variations in volatile compounds across different stages of jujube flowers, we applied principal component analysis. As shown in Figure 6, the combined contribution of PC1 and PC2 for jujube flowers across different stages exceeds 60%, which is sufficient to highlight the distinctions among the stages. The aroma profile of jujube flowers at the flowering stage is notably distant from those at the bud stage and the late flowering stage, indicating a significant difference between the flowering stage and the other two periods. This finding is consistent with the results derived from the fingerprint analysis, as previously discussed.

3.2 Volatile flavor components variations among different jujube flowers varieties at the flowering stage

Based on the analysis of aroma profiles in jujube flowers across different growth stages, the flowering period was identified as the phase with the highest concentration of aromatic compounds. To identify cultivars with the most abundant aromatic profiles, we conducted a comparative study of 11 major jujube varieties during their flowering stage, representing nearly all principal cultivars currently cultivated. The analysis revealed that Fuxiang, Dongzao, and Xingguang exhibited the richest composition of aromatic compounds during flowering (Figure 7, red box A), whereas Yushuai, Zanshuo, Jinsixiaozao, and Dajinsiwang showed the lowest concentrations of these compounds (Figure 7, red box B). These findings suggest that Fuxiang, Dongzao, and Xingguang represent the most suitable varieties for the extraction of aromatic compounds from jujube flowers.

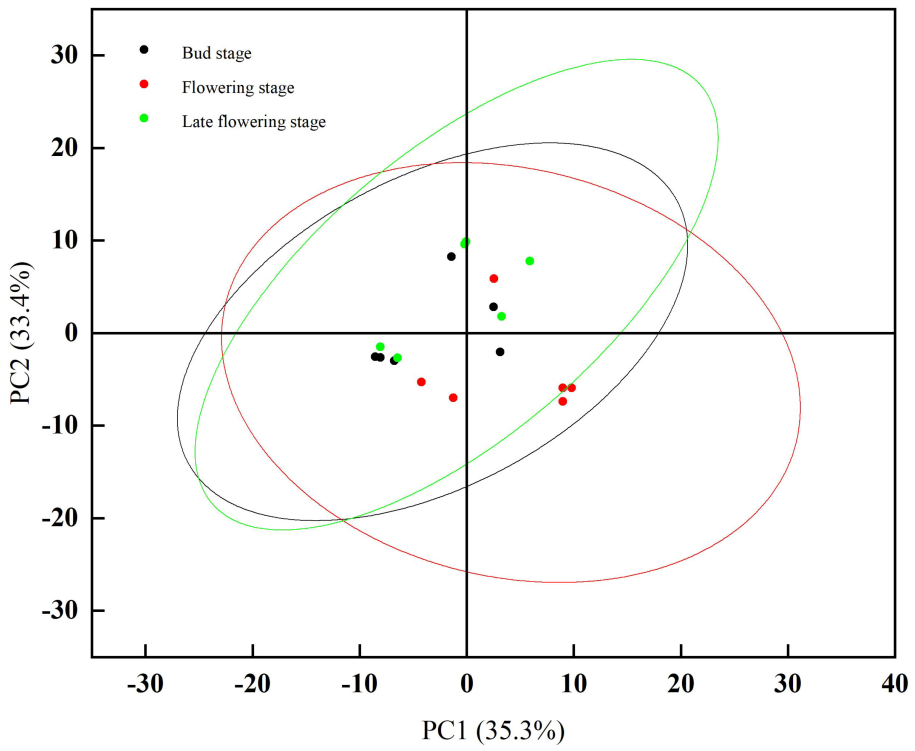

FIGURE 6
PCA analysis results of volatile components of jujube flowers in different periods.

10.3389/fpls.2025.1590072

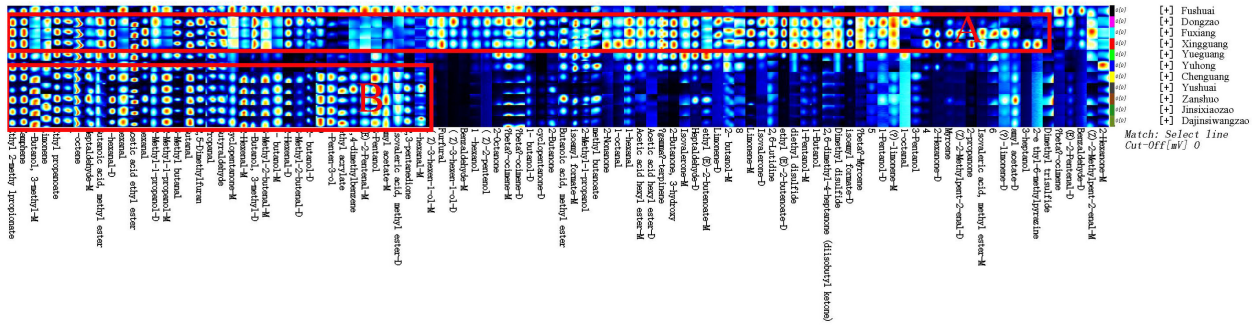

FIGURE 7
Volatile differences of different varieties of jujube flowers.

3.3 Differences in volatile flavor components between jujube flowers and other plant flowers

3.3.1 Qualitative analysis of jujube flowers and other plant flowers in volatile flavor components

Table 2 presents the qualitative analysis of volatile components in different plant flowers. A total of 102 signal peaks were detected, with 61 compounds successfully identified. These compounds were categorized as follows: 10 alcohols, 12 esters, 9 olefins, 11 aldehydes, 11 ketones, and 8 other substances, including 2 furans, 2 pyrazines, 1 aromatic hydrocarbon, 1 alkane, 1 acid, 1 amine and 8 substances unidentified.

3.3.2 Analysis of volatile flavor components of different plant flowers

As shown in Figure 8, the aroma profile of jujube flowers exhibits significant differences compared to the other four plant

TABLE 2 VOCs information of jujube flowers and other plant flowers detected by HS-GC-IMS.

Count	Compound	Flavor description	CAS#	Formula	MW[a]	RI[b]	Rt [sec][c]	Dt [a.u][d]	Comment
Alcohols									
1	(Z)-3-hexen-1-ol	woody, green	C928961	C6H12O	100.2	1408.5	970.643	1.24305	Monomer
2	(Z)-3-hexen-1-ol		C928961	C6H12O	100.2	1408.1	969.771	1.50963	Dimer
3	1-pentanol-4-methyl	fruity, green, nutty	C626891	C6H14O	102.2	1374.5	907.58	1.32286	Monomer
4	1-pentanol-4-methyl		C626891	C6H14O	102.2	1372.9	904.824	1.63624	Dimer
5	(E)-3-hexen-1-ol	green, cherry	C928972	C6H12O	100.2	1434.1	1020.711	1.24887	Monomer
6	(E)-3-hexen-1-ol		C928972	C6H12O	100.2	1432.5	1017.547	1.50653	Dimer
7	3-Pentanol	sweet, nutty	C584021	C5H12O	88.1	1107.3	478.13	1.40947	Monomer
8	3-Pentanol		C584021	C5H12O	88.1	1110.5	483.574	1.2089	Dimer
9	2-Methyl-1-propanol	pine, woody, camphor	C78831	C4H10O	74.1	1095.2	458.281	1.17063	Monomer
10	2-Methyl-1-propanol		C78831	C4H10O	74.1	1096	459.488	1.37312	Dimer
11	1-Butanol, 3-methyl	tea, nutty	C123513	C5H12O	88.1	1213.2	660.507	1.24244	Monomer
12	1-Butanol, 3-methyl		C123513	C5H12O	88.1	1213.3	660.744	1.48814	Dimer
13	Butanol	fruity, green, sweet	C71363	C4H10O	74.1	1142.1	540.484	1.18678	Monomer
14	Butanol		C71363	C4H10O	74.1	1141.1	538.505	1.39325	Dimer
15	1-Hexanol	fruity, green, sweet	C111273	C6H14O	102.2	1433.3	1019.129	1.31693	
16	1-Propanol, 2-methyl-	musty, pungent	C78831	C4H10O	74.1	1084.8	442.59	1.38605	
17	1-Penten-3-ol	fruity, green,	C616251	C5H10O	86.1	1159.6	574.631	0.93902	

(Continued)

10.3389/fpls.2025.1590072

TABLE 2 Continued

Count	Compound	Flavor description	CAS#	Formula	MW[a]	RI[b]	Rt [sec][c]	Dt [a.u][d]	Comment
Esters									
18	(E)-Ethyl-2-hexenoate	fruity, vegetable	C27829727	C8H14O2	142.2	1328.8	829.473	1.33273	Monomer
19	(E)-Ethyl-2-hexenoate		C27829727	C8H14O2	142.2	1331.1	833.232	1.81108	Dimer
20	isoamyl formate	wine, fruity	C110452	C6H12O2	116.2	1040.6	389.485	1.25895	Monomer
21	isoamyl formate		C110452	C6H12O2	116.2	1049.9	400.046	1.64025	Dimer
22	Methyl butyrate	fruity, green	C623427	C5H10O2	102.1	999.9	346.239	1.14681	Monomer
23	Methyl butyrate		C623427	C5H10O2	102.1	994.6	340.899	1.43606	Dimer
24	butyl 2-methylbutanoate	fruity, green, woody	C15706737	C9H18O2	158.2	1283.3	758.374	1.38831	Monomer
25	butyl 2-methylbutanoate		C15706737	C9H18O2	158.2	1282.2	756.772	1.8953	Dimer
26	Linalyl acetate	orange, lemon and pear	C115957	C12H20O2	196.3	1503.4	1170.136	1.2167	
27	Isobutyl 3-methylbutyrate	sweet, fruity	C589593	C9H18O2	158.2	1159.3	574.136	1.38587	
28	Ethyl 2-methy lpropionate	sweet, floral	C97621	C6H12O2	116.2	967.6	317.891	1.56062	
29	Butanoicacid propyl ester	fruity, green	C105668	C7H14O2	130.2	1142.1	540.484	1.27379	
30	2-methylbutanoic acid ethyl ester	apple, green	C7452791	C7H14O2	130.2	1025.4	372.67	1.6685	
31	Acetic acid ethyl ester	fruity, nutty	C141786	C4H8O2	88.1	898	267.419	1.33822	
32	Isovaleric acid, methyl ester	fruity, celery	C556241	C6H12O2	116.2	1023.1	370.268	1.52645	
33	Citronellyl formate	lemon, cucumber, scented, rose	C105851	C11H20O2	184.3	1569.9	1333.925	1.35067	
Alkenes									
34	myrcene	peach, fruity, green	C123353	C10H16	136.2	1193.7	635.631	1.15676	Monomer
35	myrcene		C123353	C10H16	136.2	1185.3	625.207	1.2878	Dimer
36	myrcene		C123353	C10H16	136.2	1187.6	628.05	1.59271	Trimer
37	Pinene	woody, camphor	C127913	C10H16	136.2	1159.6	574.631	1.21332	Monomer
38	Pinene		C127913	C10H16	136.2	1159.8	575.125	1.29296	Dimer
39	Pinene		C127913	C10H16	136.2	1158.3	572.156	1.71032	Trimer
40	3-Carene	orange, fruity	C13466789	C10H16	136.2	1184.7	624.496	1.66957	Monomer
41	3-Carene		C13466789	C10H16	136.2	1182.4	621.684	1.72612	Dimer
42	3-carene		C13466789	C10H16	136.2	1191	632.32	1.64607	Trimer
43	Terpinolene	sweet, floral, plastic	C586629	C10H16	136.2	1306.1	793.201	1.20996	Monomer
44	Terpinolene		C586629	C10H16	136.2	1306.6	794.001	1.32886	Dimer
45	Limonene	lemon, fruity	C138863	C10H16	136.2	1242.2	699.458	1.21107	Monomer
46	Limonene		C138863	C10H16	136.2	1242.2	699.458	1.28961	Dimer
47	Styrene	sweet, floral, plastic	C100425	C8H8	104.2	1193.1	634.92	1.51208	Monomer
48	Styrene		C100425	C8H8	104.2	1187	627.339	1.78171	Dimer
49	Camphene	camphor	C79925	C10H16	136.2	1061.9	414.227	1.21156	Monomer
50	Camphene		C79925	C10H16	136.2	1064.4	417.245	1.64671	Dimer
51	1-octene	oily, woody, lemon	C111660	C8H16	112.2	855.4	240.599	1.15205	
52	Dipentene	green, orange	C138863	C10H16	136.2	1250.1	710.413	1.63813	

(Continued)

TABLE 2 Continued

Count	Compound	Flavor description	CAS#	Formula	MW[a]	RI[b]	Rt [sec][c]	Dt [a.u][d]	Comment
Aldehydes									
53	2-Hexenal	almond, apple, plum	C505577	C6H10O	98.1	1230.9	683.961	1.17692	Monomer
54	2-Hexenal		C505577	C6H10O	98.1	1228.2	680.407	1.51334	Dimer
55	2-methyl-2-propenal	fruity, green, sweet	C78853	C4H6O	70.1	875.1	252.636	1.05846	Monomer
56	2-methyl-2-propenal		C78853	C4H6O	70.1	896.4	266.363	1.22148	Dimer
57	Heptaldehyde	fruity, pineapple, sweet	C111717	C7H14O	114.2	1243.2	700.745	1.3408	Monomer
58	Heptaldehyde		C111717	C7H14O	114.2	1246.4	705.242	1.7144	Dimer
59	Butanal	fermented, bready	C123728	C4H8O	72.1	848.3	236.375	1.1138	Monomer
60	Butanal		C123728	C4H8O	72.1	843.2	233.418	1.28086	Dimer
61	3-Methyl-2-butenal	nutty, cherry	C107868	C5H8O	84.1	1205.3	650.319	1.35584	
62	3-methylbutanal	chocolate, peach	C590863	C5H10O	86.1	858.6	242.499	1.19029	
63	Propanal	nutty	C123386	C3H6O	58.1	833.3	227.716	1.14198	
64	Butyraldehyde	bready, yeasty	C123728	C4H8O	72.1	912.1	276.922	1.2879	
65	Hexanal	green, woody, vegetative	C66251	C6H12O	100.2	1162.2	580.074	1.55547	
66	acrolein	butter, creamy	C107028	C3H4O	56.1	821.1	220.943	0.95984	
67	beta-ocimene	green, woody	C13877913	C10H16	136.2	1266.5	733.681	1.24493	
Ketones									
68	3-Hydroxy-2-butanone	cream, sweet	C513860	C4H8O2	88.1	1295.2	776.388	1.07785	Monomer
69	3-Hydroxy-2-butanone		C513860	C4H8O2	88.1	1294.4	775.187	1.33051	Dimer
70	2-Nonanone	fruity, oils, herbs	C821556	C9H18O	142.2	1326.2	825.226	1.39327	Monomer
71	2-Nonanone		C821556	C9H18O	142.2	1325.2	823.624	1.87879	Dimer
72	3-methyl-2-pentanone	fruity, pineapple, sweet	C565617	C6H12O	100.2	1016.6	363.343	1.17661	Monomer
73	3-methyl-2-pentanone		C565617	C6H12O	100.2	1023.2	370.288	1.47133	Dimer
74	3-Octanone	fruity, sweet	C106683	C8H16O	128.2	1205.3	650.319	1.30166	Monomer
75	3-Octanone		C106683	C8H16O	128.2	1206	651.267	1.71493	Dimer
76	2,3-pentadione	spicy, butter, creamy	C600146	C5H8O2	100.1	1024.8	372.034	1.31433	
77	Isovalerone	fruity, green, sweet	C108838	C9H18O	142.2	1243.7	701.52	1.78996	
78	3-Pentanone	minty, herbal, eucalyptus	C96220	C5H10O	86.1	984.3	331.288	1.35213	
79	2-propanone	sweet, green	C67641	C3H6O	58.1	815.9	218.102	1.12149	
80	Phellandrene	terpenes, spicy	C99832	C10H16	136.2	1132.1	521.679	1.67935	
81	2,3-Pentanedione	spicy, butter, creamy	C600146	C5H8O2	100.1	1102.8	470.707	1.30181	
82	Isomenthone	musty, herbal	C491076	C10H18O	154.3	1516.8	1201.261	1.34069	
Others									
83	methyl 2-furoate	fruity, mushroom	C611132	C6H6O3	126.1	1598.2	1410.462	1.15399	
84	Linalool oxide	green, sweet	C60047178	C10H18O2	170.3	1538.3	1253.306	1.2623	Monomer
85	Linalool oxide		C60047178	C10H18O2	170.3	1528.3	1228.814	1.81103	Dimer
86	3-Isopropyl-2-methoxypyrazine	green beans	C25773404	C8H12N2O	152.2	1478	1112.867	1.2397	

(Continued)

10.3389/fpls.2025.1590072

TABLE 2 Continued

Count	Compound	Flavor description	CAS#	Formula	MW[a]	RI[b]	Rt [sec][c]	Dt [a.u][d]	Comment
Others									
87	2,3-dimethyl-5-ethylpyrazine	fruity, pineapple, sweet	C15707343	C8H12N2	136.2	1538.3	1253.306	1.2281	
88	p-Cymene	fruity, sweet	C99876	C10H14	134.2	1265.3	731.953	1.20831	Monomer
89	p-Cymene		C99876	C10H14	134.2	1262.5	727.95	1.30574	Dimer
90	2,2,4,6,6-Pentamethylheptane	sweet, almond, fruity, green	C13475826	C12H26	170.3	918.5	281.357	1.31608	Monomer
91	2,2,4,6,6-Pentamethylheptane		C13475826	C12H26	170.3	926.3	286.847	1.40061	Dimer
92	2-Methylbutanoic acid	nutty, grassy	C116530	C5H10O2	102.1	1575.1	1347.701	1.20672	Monomer
93	2-Methylbutanoic acid		C116530	C5H10O2	102.1	1576.9	1352.294	1.44901	Dimer
94	Dibutylamine	wintergreen, almond, cherry	C111922	C8H19N	129.2	1120.8	501.389	1.74129	
Unknowns									
95	1		unidentified	*	*	1607	1434.954	1.33072	
96	2		unidentified	*	*	1131	519.699	1.54072	
97	3		unidentified	*	*	1106.5	476.895	1.46969	
98	4		unidentified	*	*	1046.5	396.123	1.45283	
99	5		unidentified	*	*	990.3	336.76	1.38932	
100	6		unidentified	*	*	962.8	314.09	1.50326	
101	7		unidentified	*	*	817.9	219.168	1.08806	
102	8		unidentified	*	*	787.9	203.461	1.13843	

[a]Represents the molecular mass.
[b]Represents the retention index calculated using n-ketones C4–C8 as external standard on MXT-WAX column.
[c]Represents the retention time in the capillary GC column.
[d]Represents the drift time in the drift tube.

species. Common volatile compounds detected across all plant flower samples include methyl butyrate, 1-octene, butanol, acetic acid ethyl ester, 3-methyl-2-butenal, 3-pentanol, propanal, 2-hexenal, and 1-butanol, 3-methyl (Figure 9, red box B). Notably, jujube flowers contain 24 unique aroma components and 4 unidentified compounds (Figure 8, red box A). The clustering heat map analysis further confirmed that these 24 volatile compounds effectively distinguish jujube flowers from other samples (Figure 9).

Several key compounds contribute to the distinctive aroma and functional properties of jujube flowers. For instance, (E)-3-hexen-1-ol, 3-pentanol, 1-hexanol, 1-propanol, 2-methyl-, (E)-ethyl-2-

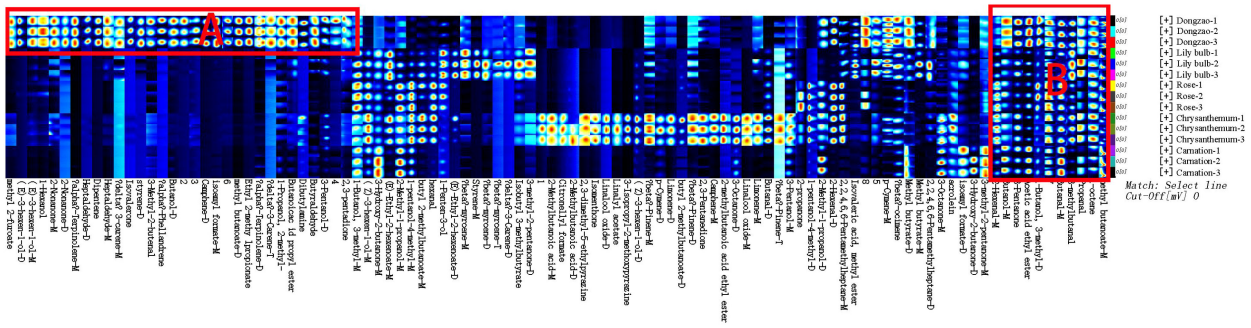

FIGURE 8
Comparison of HS-GC-IMS fingerprints of volatile organic compounds (VOCs) in jujube flowers and other plant flowers samples.

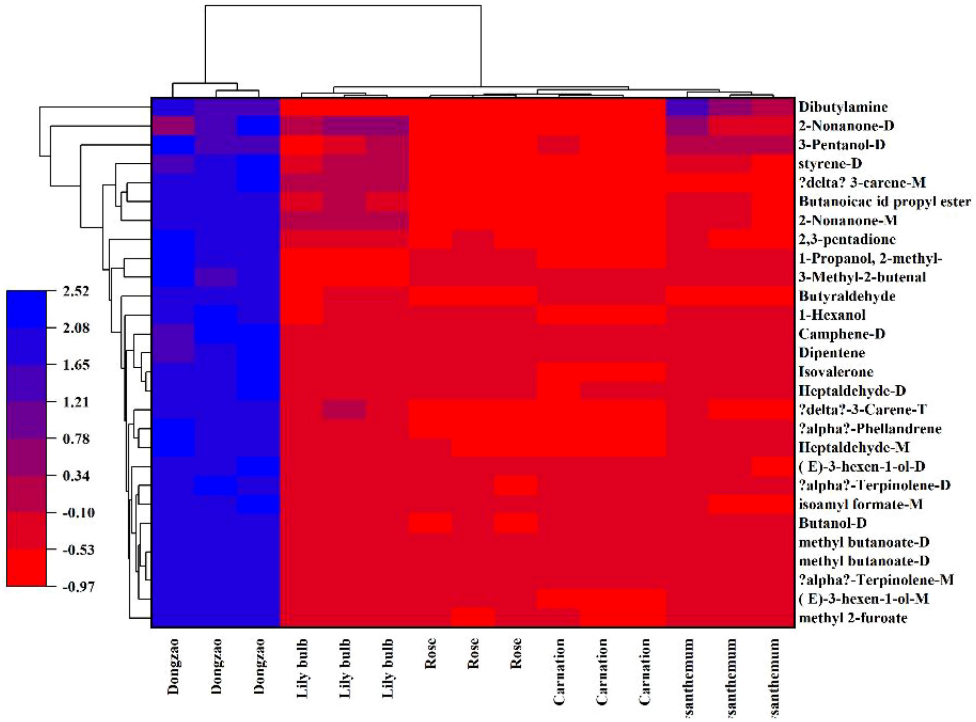

FIGURE 9
Screening of differential volatile components in jujube flowers.

hexenoate, isoamyl formate, isobutyl 3-methylbutyrate, butanoic acid propyl ester, phellandrene, 2,3-pentadione, 2-nonanone, heptaldehyde, and dipentene impart fruity, nutty, and creamy aromas to jujube flowers. Additionally, terpinolene and α-phellandrene exhibit anti-inflammatory and antioxidant activities, which are beneficial for *in vitro* wound healing (de Christo Scherer et al., 2019). Camphene, commonly found in vegetables and herbs (Tiwari and Kakkar, 2009), is also present in jujube flowers. Isoamyl formate, a colorless oily liquid with a distinctive plum and black currant aroma, possesses antimicrobial properties that inhibit or kill bacteria, yeast, filamentous fungi, and oomycetes, thereby promoting plant health (Hummadi et al., 2022). These compounds collectively protect jujube flowers from pests and diseases during their development. Ketones, which are key products of the Maillard reaction and precursors to many flavor compounds (Smuda and Glomb, 2013),are also prominent in jujube flowers. For example, 2-nonanone, a colorless to light yellow liquid with an herbal aroma, can be utilized in active packaging systems to preserve fruit freshness post-harvest and prevent flavor degradation caused by high volatile content (Almenar et al., 2009). Terpinolene, 2-nonanone, 2,3-pentadione, and phellandrene are major components of the yellow liquid in jujube nectar. Furthermore, 3-carene, 3-pentanol, and isoamyl formate in jujube flowers contribute to pathogen resistance, underscoring the dual medicinal and nutritional value of jujube fruit (Shu et al., 2020; Song et al., 2015).These findings highlight the unique aromatic and functional characteristics of jujube flowers, which are integral to their role in both ecological and agricultural contexts.

3.3.3 Jujube flowers and other plant flowers PCA of volatile flavor components

Principal Component Analysis (PCA) of the fragrance profiles of jujube flowers and four other plant species revealed a total contribution rate of 70.5% for the principal components, with PC1 accounting for 43.7% and PC2 for 26.8% of the cumulative variance. This level of contribution is sufficient to effectively capture the differences in fragrance between jujube flowers and the other plant species (Figure 10). The significant spatial separation observed between jujube flowers and the other four plant species in the PCA plot further underscores the distinctiveness of jujube flower fragrance. These findings align well with the results presented in the fingerprint analysis (Figure 8), reinforcing the conclusion that jujube flowers possess a unique aromatic profile compared to the other plants studied.

3.3.4 Similarity analysis of 24 characteristic volatile organic compounds of jujube flowers

A PCA model was constructed to analyze the 24 characteristic aroma compounds of jujube flowers and other plant species. The results revealed that jujube flowers were predominantly located in the first and fourth quadrants, demonstrating a clear distinction from the other four plant species (Figure 11). In this study, the model exhibited excellent fit and predictability, as indicated by R2X, R2Y, and Q2 values approaching 1. Figure 11 further illustrates that the aroma profile of jujube flowers is distributed across the first and fourth quadrants, consistent with the PCA results. To ensure the robustness of the model and avoid overfitting, a permutation test was conducted. As shown in Figure 11, after 200 cross-validations,

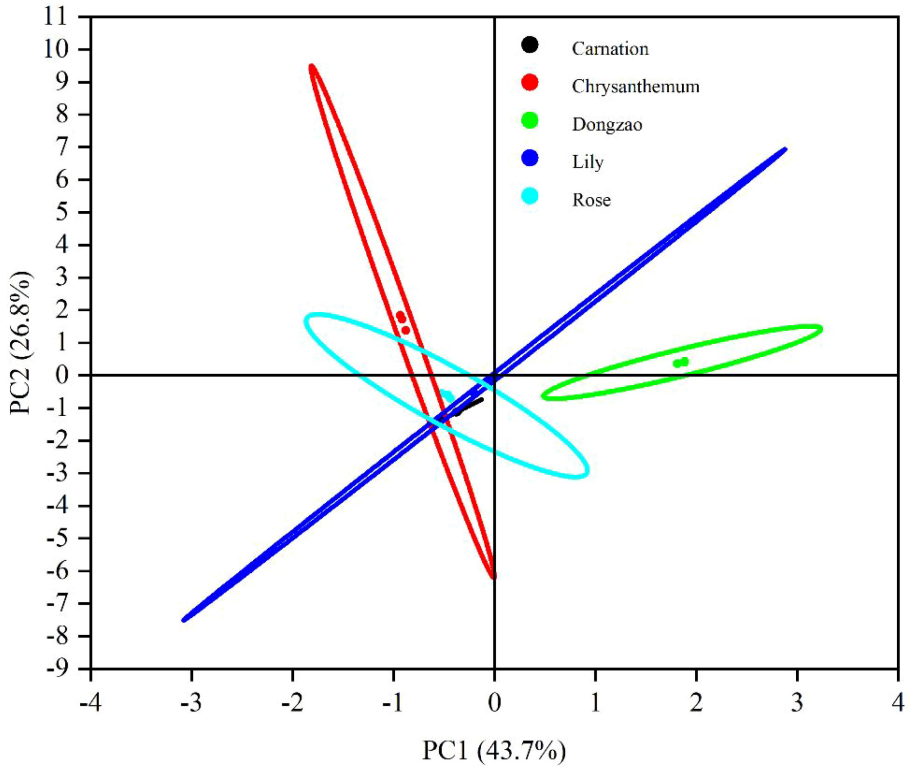

FIGURE 10
PCA analysis results of volatile components of jujube flowers and other plant flowers.

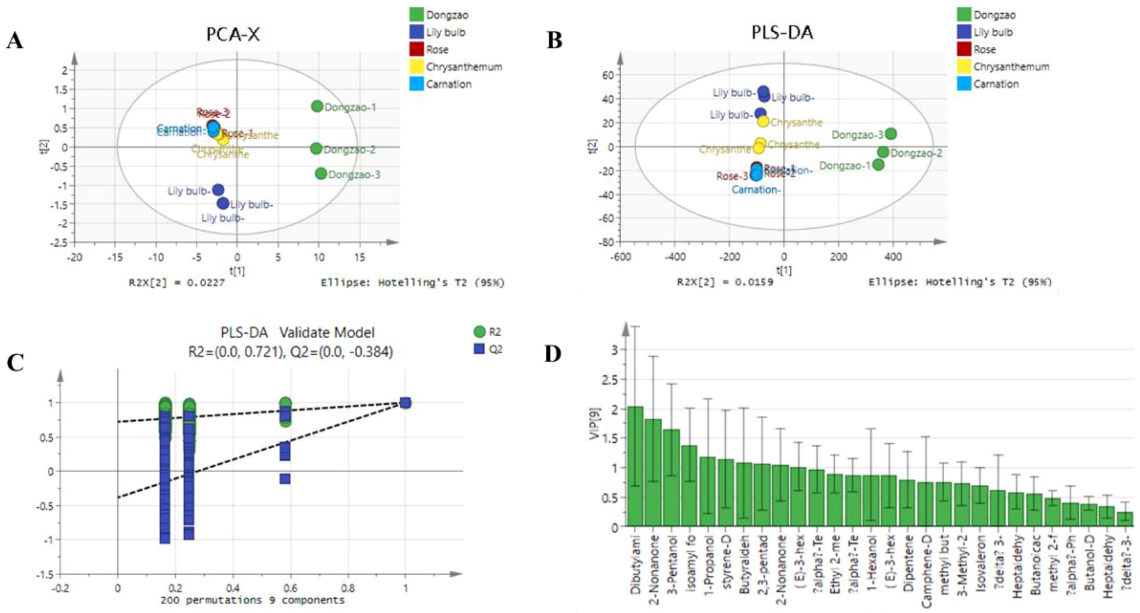

FIGURE 11
PCA analysis of 24 characteristic aroma compounds of jujube flowers and other plant species. **(A)** PCA-X score plot showing clustering of Dongzao, Lily bulb, Rose, Chrysanthemum, and Carnation samples. **(B)** PLS- DA score plot with similar groupings. **(C)** PLS-DA validation model displaying R2 and Q2values across permutations. **(D)** Bar chart of variable importance in projection (VIP) scores for different chemical compounds, with Dibutylam and 2-Nonanone as top compounds.

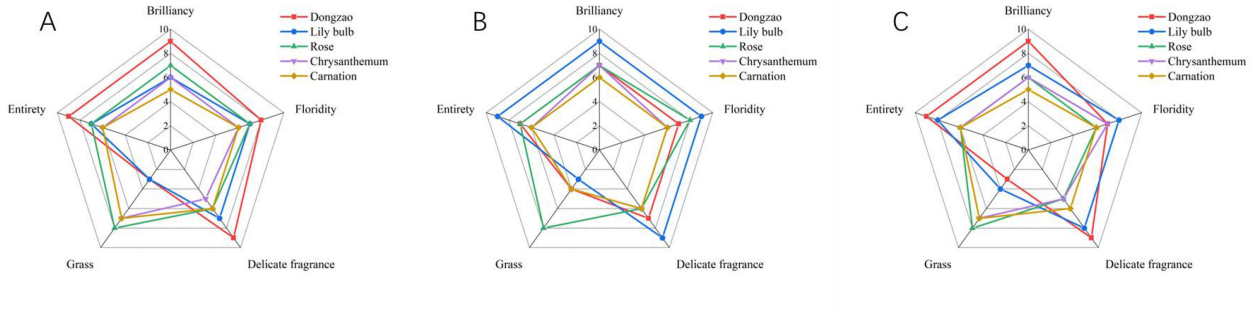

FIGURE 12
The sensory evaluation map of different plant floral fragrances. **(A)** Men's sensory evaluation score. **(B)** Women's sensory evaluation score. **(C)** Comprehensive sensory evaluation score.

the Q and abscissa intercepts were negative, and the R2 and Q2 values remained below the original values, confirming that the model did not overfit the data.

The contribution of individual aroma compounds to the overall profile of jujube flowers was evaluated using VIP (Variable Importance in Projection) values. As depicted in Figure 11, nine aroma components with VIP values greater than 1 were identified as significant contributors: dibutylamine, 2-nonanone, 3-pentanol, isoamyl formate, 1-propanol, 2-methyl-, styrene, butyraldehyde, 2,3-pentadione, and (E)-3-hexen-1-ol. These compounds are considered the primary volatile substances responsible for the distinctive aroma of jujube flowers.

3.4 Sensory evaluation of jujube flowers and other plant flowers volatile flavor components

For sensory evaluation, we recruited a panel of 10 male and 10 female participants, which revealed significant gender-based differences in fragrance preferences. Most male participants expressed a preference for the fragrance of jujube flowers, describing it as pleasant and unique compared to the aromas of the other flowers (Figure 12). In contrast, female participants tended to favor more vibrant and fragrant flowers, with Lily bulb receiving the highest score among them (Figure 12). These results highlight the differing aromatic preferences between men and women, with jujube flowers and Lily bulb representing the favored choices of each group, respectively (Figure 12).

Based on the positive feedback from male evaluators regarding the fragrance of jujube flowers (Dongzao), there is potential to extract and utilize its pleasant aroma for the development of male-oriented fragrances or air fresheners in the future. This approach aligns with the sensory preferences identified in the study and offers a promising avenue for product innovation.

4 Conclusion

Aroma is a critical factor in evaluating jujube flowers. In this study, we employed GC-IMS combined with fingerprint analysis and PCA to identify the primary aroma components in jujube flowers. The results revealed that the flowering stage contains the highest concentration of aroma components, with 14 specific compounds showing a significant increase from the bud stage to the flowering stage. Further analysis using clustering heat maps and PLS-DA highlighted 24 characteristic aroma components in jujube flowers, among which 9 were identified as the dominant contributors to their fragrance. Dongzao, Fuxiang, and Xingguang were identified as the three jujube varieties with the most abundant and distinctive aromatic profiles. These findings confirm that GC-IMS combined with fingerprint and PCA analysis is an efficient and reliable method for studying jujube flower aromas. Additionally, sensory evaluation revealed that male participants exhibited a stronger preference for the fragrance of jujube flowers, describing it as pleasant and appealing. This suggests potential applications for jujube flower aroma in the development of men's perfumes, air fresheners, aromatherapy products, and more. In conclusion, the analytical methods employed in this study provide valuable insights into the flavor substances of jujube flowers and offer a foundation for further research and product development.

Data availability statement

The original contributions presented in the study are included in the article/Supplementary Material, further inquiries can be directed to the corresponding author/s.

Ethics statement

The studies involving humans were approved by The sensory evaluation was conducted in accordance with The Code of Ethics of the World Medical Association (Helsinki Declaration). The studies were conducted in accordance with the local legislation and institutional requirements. The participants provided their written informed consent to participate in this study. Written informed consent was obtained from the individual(s) for the publication of any potentially identifiable images or data included in this article.

Author contributions

PR: Conceptualization, Methodology, Validation, Writing – original draft, Writing – review & editing. RD: Resources, Writing – review & editing. LW: Writing – review & editing. NM: Writing – review & editing. YS: Methodology, Writing – review & editing. ML: Resources, Writing – review & editing. ZZ: Writing – review & editing.

Funding

The author(s) declare financial support was received for the research and/or publication of this article. This research was financially supported by the Key R&D Projects of Ministry of Science and Technology of the People's Republic of China (2022YFD1600403).

Conflict of interest

The authors declare that the research was conducted in the absence of any commercial or financial relationships that could be construed as a potential conflict of interest.

Generative AI statement

The author(s) declare that no Generative AI was used in the creation of this manuscript.

Publisher's note

Supplementary material

The Supplementary Material for this article can be found online at: https://www.frontiersin.org/articles/10.3389/fpls.2025.1590072/full#supplementary-material

References

Almenar, E., Catala, R., Hernandez-Muñoz, P., and Gavara, R. (2009). Optimization of an active package for wild strawberries based on the release of 2-nonanone. *LWT-Food Sci. Technol.* 42, 587–593. doi: 10.1016/j.lwt.2008.09.009

Choi, S.-H., Ahn, J.-B., Kozukue, N., Levin, C. E., and Friedman, M. (2011). Distribution of free amino acids, flavonoids, total phenolics, and antioxidative activities of jujube (Ziziphus jujuba) fruits and seeds harvested from plants grown in Korea. *J. Agric. Food Chem.* 59, 6594–6604. doi: 10.1021/jf200371r

de Christo Scherer, M. M., Marques, F. M., Figueira, M. M., Peisino, M. C. O., Schmitt, E. F. P., Kondratyuk, T. P., et al. (2019). Wound healing activity of terpinolene and α-phellandrene by attenuating inflammation and oxidative stress in *vitro*. *J. Tissue viability* 28, 94–99. doi: 10.1016/j.jtv.2019.02.003

Du, Y., Xu, K., Zhao, H., Wu, Y., Jiang, H., He, J., et al. (2024). Preliminary Study on the Pathogenic Mechanism of Jujube Flower Disease in Honeybees (Apis mellifera ligustica) Based on Midgut Transcriptomics. *Genes* 15, 533. doi: 10.3390/genes15050533

Fahim, H., Dasti, J. I., Ali, I., Ahmed, S., and Nadeem, M. (2014). Physico-chemical analysis and antimicrobial potential of A pis dorsata, A pis mellifera and Z iziphus jujube honey samples from Pakistan. *Asian Pacific J. Trop. biomedicine* 4, 633–641. doi: 10.12980/APJTB.4.2014APJTB-2014-0095

Feng, T., Sun, J., Song, S., Wang, H., Yao, L., Sun, M., et al. (2022). Geographical differentiation of Molixiang table grapes grown in China based on volatile compounds analysis by HS-GC-IMS coupled with PCA and sensory evaluation of the grapes. *Food Chemistry: X* 15, 100423. doi: 10.1016/j.fochx.2022.100423

Gao, Q.-H., Wu, C.-S., and Wang, M. (2013). The jujube (Ziziphus jujuba Mill.) fruit: a review of current knowledge of fruit composition and health benefits. *J. Agric. Food Chem.* 61, 3351–3363. doi: 10.1021/jf4007032

Guo, S., Duan, J.-A., Zhang, Y., Qian, D., Tang, Y., Zhu, Z., et al. (2015). Contents changes of triterpenic acids, nucleosides, nucleobases, and saccharides in jujube (Ziziphus jujuba) fruit during the drying and steaming process. *Molecules* 20, 22329–22340. doi: 10.3390/molecules201219852

Hernández, F., Legua, P., Melgarejo, P., Martínez, R., and Martínez, J. (2015). Phenological growth stages of jujube tree (Ziziphus jujube): codification and description according to the BBCH scale. *Ann. Appl. Biol.* 166, 136–142. doi: 10.1111/aab.12169

Hummadi, E. H., Cetin, Y., Demirbek, M., Kardar, N. M., Khan, S., Coates, C. J., et al. (2022). Antimicrobial volatiles of the insect pathogen Metarhizium brunneum. *J. Fungi* 8, 326. doi: 10.3390/jof8040326

Korkmaz, C., Hellal, K., Taş Küçükaydın, M., Çayan, F., Küçükaydın, S., and Duru, M. E. (2023). Volatile compound profiling of seven tuber species using HS-SPME-GC-MS and classification by a chemometric approach. *ACS omega* 8, 34111–34119. doi: 10.1016/j.ijbiomac.2015.01.061

Lantsuzskaya, E., Krisilov, A., and Levina, A. (2015). Structure of the cluster ions of ketones in the gas phase according to ion mobility spectrometry and ab initio calculations. *Russian J. Phys. Chem. A* 89, 1838–1842. doi: 10.1134/S0036024415100179

Leng, P., Hu, H.-W., Cui, A.-H., Tang, H.-J., and Liu, Y.-G. (2021). HS-GC-IMS with PCA to analyze volatile flavor compounds of honey peach packaged with different preservation methods during storage. *Lwt* 149, 111963. doi: 10.1016/j.lwt.2021.111963

Li, J.-W., Fan, L.-P., Ding, S.-D., and Ding, X.-L. (2007). Nutritional composition of five cultivars of Chinese jujube. *Food Chem.* 103, 454–460. doi: 10.1016/j.foodchem.2006.08.016

Li, H., Li, F., Wang, L., Sheng, J., Xin, Z., Zhao, L., et al. (2009). Effect of nano-packing on preservation quality of Chinese jujube (Ziziphus jujuba Mill. var. inermis (Bunge) Rehd). *Food Chem.* 114, 547–552. doi: 10.1016/j.foodchem.2008.09.085

Li, M., Yang, R., Zhang, H., Wang, S., Chen, D., and Lin, S. (2019). Development of a flavor fingerprint by HS-GC–IMS with PCA for volatile compounds of Tricholoma matsutake Singer. *Food Chem.* 290, 32–39. doi: 10.1016/j.foodchem.2019.03.124

Liu, G., Liu, X., Zhang, Y., Zhang, F., Wei, T., Yang, M., et al. (2015). Hepatoprotective effects of polysaccharides extracted from Zizyphus jujube cv. Huanghetanzao. *Int. J. Biol. macromolecules* 76, 169–175. doi: 10.1016/j.ijbiomac.2015.01.061

Liu, M., Wang, J., Wang, L., Liu, P., Zhao, J., Zhao, Z., et al. (2020). The historical and current research progress on jujube–a superfruit for the future. *Horticulture Res.* 7. doi: 10.1038/s41438-020-00346-5

Ma, Q., Chen, X., Zhang, K., Yao, D., Yang, L., Wang, H., et al. (2020). Chemical fingerprint analysis for discovering markers and identifying Saussurea involucrata by HPLC coupled with OPLS-DA. *J. analytical Methods Chem* 2020. doi: 10.1155/2020/7560710

Ma, Y., Yin, J., Wang, J., Liu, X., He, J., Zhang, R., et al. (2023). Selenium speciation and volatile flavor compound profiles in the edible flowers, stems, and leaves of selenium-hyperaccumulating vegetable Cardamine violifolia. *Food Chem.* 427, 136710. doi: 10.1016/j.foodchem.2023.136710

Ma, W., Zheng, X., Li, L., Shen, J., Li, W., and Gao, Y. (2020). Changes in the gut microbiota of honey bees associated with jujube flower disease. *Ecotoxicology Environ. Saf.* 198, 110616. doi: 10.1016/j.ecoenv.2020.110616

Shao, Y., Liu, X., Zhang, Z., Wang, P., Li, K., and Li, C. (2023). Comparison and discrimination of the terpenoids in 48 species of huajiao according to variety and geographical origin by E-nose coupled with HS-SPME-GC-MS. *Food Res. Int.* 167, 112629. doi: 10.1016/j.foodres.2023.112629

Shi, X., Lv, Y., and Guo, S. (2017). Effects of heat treatment and β-cyclodextrin addition on soymilk flavor. *Trans. Chin. Soc. Agric. Eng* 33, 293–300. doi: 10.11975/j.issn.1002-6819.2017.08.039

Shu, H., Zhang, W., Yun, Y., Chen, W., Zhong, Q., Hu, Y., et al. (2020). Metabolomics study on revealing the inhibition and metabolic dysregulation in Pseudomonas fluorescens induced by 3-carene. *Food Chem.* 329, 127220. doi: 10.1016/j.foodchem.2020.127220

Smuda, M., and Glomb, M. A. (2013). Fragmentation pathways during Maillard-induced carbohydrate degradation. *J. Agric. Food Chem.* 61, 10198–10208. doi: 10.1021/jf305117s

Song, G. C., Choi, H. K., and Ryu, C.-M. (2015). Gaseous 3-pentanol primes plant immunity against a bacterial speck pathogen, Pseudomonas syringae pv. tomato via salicylic acid and jasmonic acid-dependent signaling pathways in Arabidopsis. *Front. Plant Sci.* 6. doi: 10.3389/fpls.2015.00821

Tiwari, M., and Kakkar, P. (2009). Plant derived antioxidants–geraniol and camphene protect rat alveolar macrophages against t-BHP induced oxidative stress. *Toxicol. Vitro* 23, 295–301. doi: 10.1016/j.tiv.2008.12.014. Get rights and content.

Wang, S., Chen, H., and Sun, B. (2020). Recent progress in food flavor analysis using gas chromatography–ion mobility spectrometry (GC–IMS). *Food Chem.* 315, 126158. doi: 10.1016/j.foodchem.2019.126158

Wang, L., Zhu, J., Wang, Y., Wang, X., Chen, F., and Wang, X. (2018). Characterization of aroma-impact compounds in dry jujubes (Ziziphus jujube Mill.) by aroma extract dilution analysis (AEDA) and gas chromatography-mass spectrometer (GC-MS). *Int. J. Food properties* 21, 1844–1853. doi: 10.1080/10942912.2016.1273234

Wojdyło, A., Carbonell-BarraChina, Á.A., Legua, P., and Hernández, F. (2016). Phenolic composition, ascorbic acid content, and antioxidant capacity of Spanish jujube (Ziziphus jujube Mill.) fruits. *Food Chem.* 201, 307–314. doi: 10.1016/j.foodchem.2016.01.090

Xia, Y., Liu, Y., Wang, J., and Shuang, Q. (2020). Assessment of key aroma compounds in fresh jujube brandy by GC-O-MS and odor activity value. *J. Food Process. Preservation* 44, e14494. doi: 10.1111/jfpp.14494

Yang, L., Liu, J., Wang, X., Wang, R., Ren, F., Zhang, Q., et al. (2019). Characterization of volatile component changes in jujube fruits during cold storage by using headspace-gas chromatography-ion mobility spectrometry. *Molecules* 24 (21) 3904. doi: 10.3390/molecules24213904

Yang, Y., Wang, B., Fu, Y., Shi, Y.-G., Chen, F.-L., Guan, H.-N., et al. (2021). HS-GC-IMS with PCA to analyze volatile flavor compounds across different production stages of fermented soybean whey tofu. *Food Chem.* 346, 128880. doi: 10.1016/j.foodchem.2020.128880

Yao, L., Cai, R., Wang, H., Yu, C., Tong, C., He, Z., et al. (2024). The volatile composition, aroma profile and antioxidant capacity of Yijiangzi (Aatragalus sinicus L.) monofloral honey and its correlation with the flower. *Lwt* 205, 116565. doi: 10.1016/j.lwt.2024.116565

Yue, C., Cao, H., Zhang, S., Hao, Z., Wu, Z., Luo, L., et al. (2023). Aroma characteristics of Wuyi rock tea prepared from 16 different tea plant varieties. *Food Chemistry: X* 17, 100586. doi: 10.1016/j.fochx.2023.100586

Zhu, J., and Xiao, Z. (2018). Characterization of the major odor-active compounds in dry jujube cultivars by application of gas chromatography–olfactometry and odor activity value. *J. Agric. Food Chem.* 66, 7722–7734. doi: 10.1021/acs.jafc.8b01366

Frontiers in
Plant Science

Cultivates the science of plant biology and its applications

The most cited plant science journal, which advances our understanding of plant biology for sustainable food security, functional ecosystems and human health.

Discover the latest Research Topics

See more →

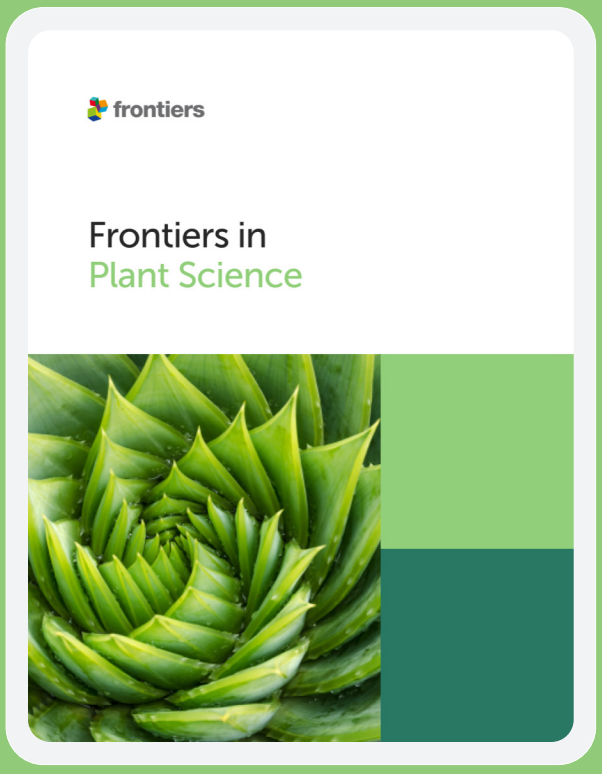

Frontiers

Avenue du Tribunal-Fédéral 34
1005 Lausanne, Switzerland
frontiersin.org

Contact us

+41 (0)21 510 17 00
frontiersin.org/about/contact